Biological and Medical Physics, Biomedical Engineering

Dong Soo Lee *Editor*

Radionanomedicine

Combined Nuclear and Nanomedicine

Springer

Biological and Medical Physics, Biomedical Engineering

More information about this series at http://www.springer.com/series/3740

BIOLOGICAL AND MEDICAL PHYSICS, BIOMEDICAL ENGINEERING

The fields of biological and medical physics and biomedical engineering are broad, multidisciplinary and dynamic. They lie at the crossroads of frontier research in physics, biology, chemistry, and medicine. The Biological and Medical Physics, Biomedical Engineering Series is intended to be comprehensive, covering a broad range of topics important to the study of the physical, chemical and biological sciences. Its goal is to provide scientists and engineers with textbooks, monographs, and reference works to address the growing need for information.

Books in the series emphasize established and emergent areas of science including molecular, membrane, and mathematical biophysics; photosynthetic energy harvesting and conversion; information processing; physical principles of genetics; sensory communications; automata networks, neural networks, and cellular automata. Equally important will be coverage of applied aspects of biological and medical physics and biomedical engineering such as molecular electronic components and devices, biosensors, medicine, imaging, physical principles of renewable energy production, advanced prostheses, and environmental control and engineering.

Dong Soo Lee
Editor

Radionanomedicine

Combined Nuclear and Nanomedicine

Springer

Editor
Dong Soo Lee
Department of Nuclear Medicine
Seoul National University
Seoul
Republic of Korea

ISSN 1618-7210 ISSN 2197-5647 (electronic)
Biological and Medical Physics, Biomedical Engineering
ISBN 978-3-319-67719-4 ISBN 978-3-319-67720-0 (eBook)
https://doi.org/10.1007/978-3-319-67720-0

Library of Congress Control Number: 2018938352

Printed on acid-free paper

This Springer imprint is published by the registered company Springer International Publishing AG part of Springer Nature
The registered company address is: Gewerbestrasse 11, 6330 Cham, Switzerland

Foreword

Nanotechnology is the manipulation of matter with at least one dimension sized from 1 to 100 nanometers. Nanotechnology as defined by size is naturally very broad, including fields of science as diverse as surface science, organic chemistry, molecular biology, semiconductor physics, energy storage, microfabrication, molecular engineering, etc. The associated research and applications are equally diverse, ranging from extensions of conventional device physics to completely new approaches based upon molecular self-assembly, from developing new materials with dimensions on the nanoscale to direct control of matter on the atomic scale.

Scientists currently debate about the future implications of nanotechnology which may be able to create many new materials and devices with a vast range of applications. On the other hand, nanotechnology raises many of the same issues as any new technology, including concerns about the toxicity and environmental impact of nanomaterials, and their potential effects on global economics, as well as speculation about various doomsday scenarios. These concerns have led to a debate among advocacy groups and governments on whether special regulation of nanotechnology is warranted.

Nanomedicine can be defined as medical application of nanotechnology. Nanomedicine ranges from the medical applications of nanomaterials and biological devices, nanoelectronic devices and biosensors and possible future applications of molecular nanotechnology. Nanomaterials can be functionalized to interface with biological molecules and structures as the size of nanomaterials is comparable to most biological molecules and structures. Nanomaterials can be useful for both in vivo and in vitro biomedical research and applications and integration of nanomaterials with biology has led to the development of advanced diagnostic devices, physical therapy applications, analytical tools, contrast agents, and drug delivery vehicles. The expansion of nanomedicine is a radionanomedicine which relies on the labeling of radionuclides onto nanomaterials. The key advantage of radionanomedicine is a possibility of using low amount of nanomaterials for theragnosis. Nanotheranostics, the merger of diagnostic and therapeutic function as a system using the benefits of nanotechnology. Since treating cancer is not similar in all cases, it requires therapy to be adapted to the patient's specific biomolecules.

It helps identifying biomarkers to gain better understanding of the diagnosis and in turn treating the specific disorder based on the precise diagnosis. By mostly utilizing the unique properties of nanoparticles to achieve biomarker identification and drug delivery, nanotheranostics can be applied to noninvasively discover and target image biomarkers and further deliver treatment based on the biomarker distribution.

Nanomedicine strives for delivering valuable set of research tools and clinically useful devices and its industry sales reached $16 billion in 2015, with an average of $3.8 billion investment in nanotechnology R&D every year and increase of 45% per year global funding for emerging nanotechnology. Global funding for nanotechnology increased by 45% per year in recent years, with product sales exceeding $1 trillion in 2013. As the nanomedicine industry continues to grow, it is expected to have a significant impact on the economy.

Nanomedicine affects almost all the aspects of healthcare. Nanomedicine helps to engineer novel and advanced tools for the treatment of various diseases and the improvement of human biosystems using molecular nanotechnology. Cardiovascular diseases, neurodegenerative disorders, cancer, diabetes, infectious diseases, and HIV/AIDS are the main diseases whose treatment can be benefitted by using nanomedicine. Nanoparticles are directly injected into the tumor and are activated to produce heat and destroy the cells of the tumor either by x-ray, light, or magnetic field. Gold nanorods are being used to carry chemotherapy drugs into the tumor and locally excite it by infrared rays. The heat induced is helpful to destroy cells of tumor as well as encapsulate drugs. In recent years, the intercrossing of nanotechnology in stem cell biology and biomedicine has led to an emerging new research field, known as stem cell nanotechnology. Stem cell nanotechnology is defined as the application of nanotechnology in stem cells research and development, and it is characterized as highly rapid in development, highly interdisciplinary, and highly controversial. During the last decade, I have seen a number of successful applications of nanotechnology methods to basic neuroscience and to medical practice. It is expected that the development of novel nanotechnologies will result in important insights on the brain mechanisms, and eventually provide better medical care to patients.

Pharmaceutical nanotechnology for drug delivery using nanotechnology plays a major role in the future of pharmaceutical research. Interestingly, pharmaceutical sciences are using nanoparticles to reduce toxicity and side effects of drugs and up to recently did not realize that carrier systems themselves may impose risks to the patient. Nanochemistry is the combination of chemistry and nanoscience. Nanochemistry is related by synthesis of building blocks which are dependent on size, surface, shape, and defect properties. Nanochemistry is being used in chemical, physical, and materials science as well as engineering, biological, and medical applications. Nanochemistry and other nanoscience fields have the same core concepts but the usages of those concepts are different. Nanoconstruct synthesis is dependent on how the surface, size, and shape will lead to self-assembly of the building blocks into the functional structures; they probably have functional defects and might be useful for photonic, electronic, medical, or bioanalytical problems.

I have been fortunate to observe and witness the superb activities of nuclear and molecular imaging research at the Seoul National University under the direction of Prof. Dong Soo Lee as a visiting professor since 2010. His biology, chemistry, and physics groups have dedicated to innovate, radiolabel nanomaterials and image animals for the pharmacokinetic studies. I am very proud of them for the production of the first book on radionanomedicine which helps scientists and physicians in the field of nanomedicine as well as nanoengineering. I am sure that this book stimulates research workers in nanomedicine to improve studies in the arrangement, characterization, and abuse of nanoparticles, nanowires, nanotubes, nanorods, nanocrystals, nanounits, and their congregations as well as applying radionanomedicine in clinical practice in the following decade.

Irvine, USA E. Edmund Kim, M.D., M.S.
Professor of Radiological Sciences, University of California, Irvine
Professor of Molecular Medicine and Biopharmaceutical Sciences
Seoul National University, Korea
Professor of Oncology, Kyunghee University, Korea

Preface

I designed this book to suit the needs of the scientists and the physicians in the field of nanomedicine and nuclear medicine. Nanomedicine is about application of nanomaterials for medical purposes and includes all the endeavors of in vivo and in vitro application for clinical use, and is mostly done by scientists and engineers and nuclear medicine is practiced everyday in the clinic by many nuclear medicine physicians in collaboration with radiopharmaceutical scientists and nuclear medicine physicists. Radionanomedicine is combined efforts of these people to solve the unsolved problems in the current practice of medicine, which ranges from oncology, infection/inflammation, heart and brain diseases, and others.

Scientists in nanomedicine and nuclear medicine would like very much to understand how to coordinate the lessons/know-hows to implement the current understanding of nanomaterials and their behavior in the human body to be useful for therapeutic/ theranostic purposes. I, as a nuclear medicine physician, recognize that the inherent principles in nuclear medicine, tracer technology, shall solve the issues with which nanomedicine are confronted now. Clinical application of radionanomedicines, i.e., radiolabeled nanopharmaceuticals or radionanodrugs, will enable imaging simultaneously with therapy in everyday routines and we will open these entirely new opportunities by looking into the disciplines about both fields of science/medicine in more depth now.

I envisioned that simple endeavor to synthesize the knowledge which are being produced and established everyday in nanomedicine and nuclear medicine will help myself, my colleagues in nuclear medicine, radiochemistry, and nanomedicine to be enlightened with eureka in scientific comprehension. After reading the manuscript for editing/proofreading, I experienced this joyous enlightenment in this book and am now very much eager to share this feeling with the future readers of this book. I am going to explain to my fellow scientists and physicians how to achieve this goal using this book.

This book was weaved with two crossing lines in horizontals and verticals, the former of which is the synthesis of nuclear and nanomedicines and the latter of which are ranged from the materials used as exogenous inorganic or organic or endogenous (of exosomes), how to modify the surface with radiolabeling

capability, how to make materials authentic using click and robust manufacturing, and how to finally use the materials for targeted delivery and/or imaging while understanding essences of bodily response, either physiologic or immune, considering all the factors affecting the host–material interactions. The entire possibility of using radionanomedicines for clinical molecular imaging and/or therapeutic/theranostic use is highly expected to be learned by the readers as far as they take efforts to read any chapters of this book. You will find complementarity and planned redundancy in chapters and sections, guidance of which was introduced by myself at each of the seven sections. I wish the readers full of future prospects of radionanomedicine.

The integrity of making this book depended on chapter authors and indispensable works of Dr. Minseok Suh. I appreciate his efforts in helping to edit.

Seoul, Republic of Korea Dong Soo Lee

Contents

Contributors

Amr S. Abu Lila Department of Pharmacokinetics and Biopharmaceutics, Institute of Medical Biosciences, Tokushima University, Sho-Machi, Tokushima, Japan; Department of Pharmaceutics and Industrial Pharmacy, Faculty of Pharmacy, Zagazig University, Zagazig, Egypt; Department of Pharmaceutics, College of Pharmacy, Hail University, Hail, Saudi Arabia

Weibo Cai Department of Biomedical Engineering, Department of Materials Science and Engineering, Departments of Radiology and Medical Physics, University of Wisconsin-Madison, Madison, WI, USA; University of Wisconsin Carbone Cancer Center, Madison, WI, USA

Daiqin Chen Department of Radiology, Center for Molecular Imaging, University of Michigan, Ann Arbor, MI, USA

Feng Chen Department of Radiology, Sloan Kettering Institute for Cancer Research, New York, NY, USA

Gi Jeong Cheon Department of Nuclear Medicine, Seoul National University College of Medicine, Seoul, Korea

Hongyoon Choi Department of Nuclear Medicine, Seoul National University College of Medicine, Seoul, Republic of Korea; Department of Molecular Medicine and Biopharmaceutical Sciences, Graduate School of Convergence Science and Technology, College of Medicine or College of Pharmacy, Seoul National University, Seoul, Republic of Korea

Bart Cornelissen Department of Oncology, CR-UK/MRC Oxford Institute for Radiation Oncology, University of Oxford, Oxford, UK

Carolina A. Ferreira Department of Biomedical Engineering, University of Wisconsin-Madison, Madison, WI, USA

Yong Song Gho Department of Life Sciences, Pohang University of Science and Technology (POSTECH), Pohang, Republic of Korea; The Krefting Research Centre, Institute of Medicine, University of Gothenburg, Gothenburg, Sweden; Exosome BioSciences Inc., Pohang, Republic of Korea

Sanjana Ghosh Department of Biomedical Engineering, University at Buffalo, State University of New York, Buffalo, NY, USA

Shreya Goel Department of Materials Science and Engineering, University of Wisconsin-Madison, Madison, WI, USA

Seunggyun Ha Department of Nuclear Medicine, Seoul National University College of Medicine, Seoul, Republic of Korea; Department of Molecular Medicine and Biopharmaceutical Sciences, Graduate School of Convergence Science and Technology, Seoul National University, Seoul, Republic of Korea

Byung Hee Hong Department of Chemistry, College of Natural Science, Seoul National University, Seoul, Republic of Korea; Program in Nano Science and Technology, Graduate School of Convergence Science and Technology, Seoul National University, Seoul, Republic of Korea

Hao Hong Department of Radiology, Center for Molecular Imaging, University of Michigan, Ann Arbor, MI, USA

Do Won Hwang Department of Nuclear Medicine, Seoul National University College of Medicine, Seoul, Republic of Korea; Department of Molecular Medicine and Biopharmaceutical Sciences, Graduate School of Convergence Science and Technology, College of Medicine or College of Pharmacy, Seoul National University, Seoul, Republic of Korea

Hyung-Jun Im Department of Transdisciplinary Studies, Graduate School of Convergence Science and Technology, Seoul National University, Seoul, Korea

Tatsuhiro Ishida Department of Pharmacokinetics and Biopharmaceutics, Institute of Medical Biosciences, Tokushima University, Sho-Machi, Tokushima, Japan

Keon Wook Kang Department of Nuclear Medicine, Seoul National University College of Medicine, Seoul, Republic of Korea; Cancer Research Institute, Seoul National University, Seoul, Republic of Korea

Dong Wook Kim Department of Chemistry, Inha University, Nam-gu, Incheon, Korea

Yong-il Kim Department of Nuclear Medicine, Asan Medical Center, University of Ulsan College of Medicine, Seoul, Republic of Korea

James C. Knight Department of Oncology, CR-UK/MRC Oxford Institute for Radiation Oncology, University of Oxford, Oxford, UK

Changjin Lee Department of Life Sciences, Pohang University of Science and Technology (POSTECH), Pohang, Republic of Korea

Dong Soo Lee Department of Nuclear Medicine, Seoul National University College of Medicine, Seoul, Republic of Korea; Department of Molecular Medicine and Biopharmaceutical Sciences, Graduate School of Convergence Science and Technology, Seoul National University, Seoul, Republic of Korea; Korea Brain Research Institute, Daegu, Republic of Korea

Jae Sung Lee Department of Nuclear Medicine, Seoul National University College of Medicine, Seoul, Republic of Korea; Department of Biomedical Sciences, Seoul National University College of Medicine, Seoul, Republic of Korea

Yun-Sang Lee Department of Nuclear Medicine, Seoul National University College of Medicine, Seoul, Republic of Korea; Department of Molecular Medicine and Biopharmaceutical Sciences, Graduate School of Convergence Science and Technology, Seoul National University, Seoul, Republic of Korea

Jonathan F. Lovell Department of Biomedical Engineering, University at Buffalo, State University of New York, Buffalo, NY, USA

So Won Oh Department of Nuclear Medicine, Seoul National University College of Medicine, Seoul, Republic of Korea; Department of Nuclear Medicine, Seoul National University Boramae Medical Center, Seoul, Republic of Korea

Venugopal Rajendiran Department of Biomedical Engineering, University at Buffalo, State University of New York, Buffalo, NY, USA; Department of Chemistry, School of Basic and Applied Sciences, Central University of Tamil Nadu, Thiruvarur, India

Seongho Seo Department of Neuroscience, College of Medicine, Gachon University, Incheon, Republic of Korea

Young Kee Shin Department of Molecular Medicine and Biopharmaceutical Sciences, Graduate School of Convergence Science and Technology, Seoul National University, Seoul, Republic of Korea; The Center for Anti-Cancer Companion Diagnostics, Bio-MAX/N-Bio, Seoul National University, Seoul, Republic of Korea; Laboratory of Molecular Pathology and Cancer Genomics, College of Pharmacy, Seoul National University, Seoul, Republic of Korea

Myung Geun Song Department of Nuclear Medicine, Seoul National University College of Medicine, Seoul, Republic of Korea; Cancer Research Institute, Seoul National University, Seoul, Republic of Korea; Biomedical Research Institute, Seoul National University Hospital, Seoul, Republic of Korea

Minseok Suh Department of Nuclear Medicine, Seoul National University College of Medicine, Seoul, Republic of Korea; Department of Molecular Medicine and Biopharmaceutical Sciences, Graduate School of Convergence Science and Technology, Seoul National University, Seoul, Republic of Korea

Lingyi Sun Department of Medicine, University of Pittsburgh School of Medicine, Pittsburgh, PA, USA

Je Min Yoo Department of Chemistry, College of Natural Science, Seoul National University, Seoul, Republic of Korea

Dexing Zeng Department of Medicine, University of Pittsburgh School of Medicine, Pittsburgh, PA, USA; Department of Radiology, University of Pittsburgh School of Medicine, Pittsburgh, PA, USA

Chapter 1
Introduction

Dong Soo Lee

Abstract Radionanomedicine is a novel discipline of combined nuclear and nanomedicine. Nuclear medicine has an almost one century of history since its birth and has been successfully applied for clinical application. Clinical nuclear medicine ranges from therapy with imaging theranostic to hybrid imaging such as positron emission tomography/computed tomography (PET/CT), PET/magnetic resonance imaging (PET/MRI), single photon emission computed tomography (SPECT)/CT or gamma camera imaging. Theranostic application of nuclear medicine is recently emphasized by the urgent needs raised by individualized or personalized medicine.

Radionanomedicine is a novel discipline of combined nuclear and nanomedicine. Nuclear medicine has an almost one century of history since its birth and has been successfully applied for clinical application. Clinical nuclear medicine ranges from therapy with imaging theranostic to hybrid imaging such as positron emission tomography/computed tomography (PET/CT), PET/magnetic resonance imaging (PET/MRI), single photon emission computed tomography (SPECT)/CT or gamma camera imaging. Theranostic application of nuclear medicine is recently emphasized by the urgent needs raised by individualized or personalized medicine.

Nuclear medicine is based on the tracer principle or tracer technology, which enabled the birth of clinical nuclear medicine despite radiation hazard of radionuclides for therapy and especially imaging. Very small amount of radionuclides or radioisotopes are used for clinical human use and this makes the use of trace amount of pharmaceuticals which does not raise any concern of pharmacologic effect. According to the regulations widely accepted by drug agencies, microdosing

D. S. Lee (✉)
Department of Nuclear Medicine, Seoul National University College of Medicine, Seoul 03080, Republic of Korea
e-mail: dsl@snu.ac.kr

D. S. Lee
Department of Molecular Medicine and Biopharmaceutical Sciences, Graduate School of Convergence Science and Technology, Seoul National University, Seoul 03080, Republic of Korea

D. S. Lee (ed.), *Radionanomedicine*, Biological and Medical Physics, Biomedical Engineering, https://doi.org/10.1007/978-3-319-67720-0_1

studies are allowed for less than 100 ng amount of radiopharmaceuticals. This amount can be given to human volunteers without preclinical studies in animals. The allowance is because of two issues; there should be the difference between human being and animals either large or small, and this amount per humans with normal body weight must not cause any problem with experimental systemic injection. The other way of knowing the distribution of novel drug with this amount is injecting it and doing mass spectrometry. Radiolabeling of a novel radiopharmaceutical shall allow tracing the tracks of injected radiolabeled radiopharmaceuticals in the human body and this is the basis of tracer technology of nuclear medicine.

Nanomedicine is recently coined term which indicates the emerging field of medicine using nanomaterials. Nanomaterials are the composite chemicals having nanometer-sized superstructures larger than biomacromolecules. Peptides or antibodies have the dimension of a few nanometers to tens of nanometers in their long diameters but are not called as nanomaterials. Living organisms are using those biological materials for running bodily chemical or physiological functions and we call them biologics. In contrast, nanomaterials were first named based on their unique ingenuity of fabrication to make a homogeneous artefactual superstructures made of inorganic materials. Now nanomaterials consist of inorganic to organic materials, which implies that as well as we could fabricate new larger nanomaterials we could understand their behaviors in biological milieu. Thus, the term nanomedicine immediately implies that people started to use nanomaterials for human being for diagnostic or therapeutic purposes. Systemic injection of nanomaterials should be without any toxicity and with desired biological effects. Even the combination of biologics and nanomaterials are very often proposed for clinical and human use.

The barrier of nanomedicine against popular clinical human use is the concerns about the possible toxicity of nanomaterials. Or in other words, the possible toxicity is in fact the lack of knowledge about the behavior of nanomaterials in vivo. We already know that cadmium is toxic in certain amount but we don't know the perpetual effect of cadmium of CdSe quantum dots if injected in vivo or in humans. Possible toxicity can be prevented by not using the nanomaterials of interest; however, lack of knowledge does not let us advance or withdraw attractive novel nanomaterials. Sometimes, the side effects of nanomaterials are easily unraveled even with its plausible mechanism of toxicity. Carbon nanotubes are examples, in that the shape of carbon nanotubes were toxic to the alveolar epithelial cells because of the shape, which immediately reminded medical doctors of the toxicity of asbestos and silica. Textbook knowledge leads us to be concerned about pneumoconiosis, which almost thwarted the hype of fancy possibility of using carbon nanotubes in humans for clinical purposes.

However, many other nanomaterials are not composed of frankly toxic substances such as iron oxides, carbons (graphenes), silica and other inert-looking substances. The only concern is the amount of these nanomaterials and again the lack of understanding the fates of these nanomaterials in vivo or in humans after systemic injection. Targeted delivery is always hoped and proven by animal

experiments and proposed with great potentials for human and clinical utility. Problem was always that investigators could not reveal the distribution of these nanomaterials repeatedly after systemic administration. Development of how to measure silica or graphene was not an easy task and only the measurement of high molecular weight metals was possible with inductively coupled plasma mass spectrometry (ICP-MS) but with limited success to predict the whereabouts or kinetics of the nanomaterials. The substance themselves can be toxic or does betray the expectation that they will reach targets in vivo but we did not have very good methods to trace or track the trails.

Trace amount use and tracer capability of nuclear medicine are the two beauties of its fundamental advantage, which enabled its use for so many clinical situations. Globally, for example in 2015, 20 million procedures (imaging and therapy) in North America, 10 million in European Union and the vicinity and 5 million in Far East Asia were performed. Globally up to 40 million procedures are taking advantage of the trace amount of radionuclides and radiopharmaceuticals for use and tracer capability for imaging and targeted delivery. We could now see the chance of using the advantages of nuclear medicine to be refined for use with nanomedicines. Here nanomedicines are the generic name for nanodrugs, collectively called as a group. If nanomedicines are radiolabeled, they are now radionanomedicines. In contrast, radionanomedicine is the combined nuclear and nanomedicine. Radionanomedicine is using radionanomedicines for in vivo imaging, targeted delivery and hopefully therapy. Recently, combined therapy and diagnostics came to be called as theranostics. And the ultimate feature of radionanomedicine is radionanomedical theranostics. The emphasis on theranostics instead of diagnostic imaging is due to the realization that there are full of many variations of too many imaging entries in clinical use and that the therapy is off the point that it is not personalized nor individualized. Recent emphasis on precision medicine is one example of this collective awareness. Useless and harmful biologics or small molecules are delivered to the patients carelessly, and post-hoc decision is reached that the treatment regimen was not helpful to most of the patients.

Radionanomedicine can rescue the dilemma of the novel therapeutic drugs composed of nanomaterials, or nanomedicines. Regulations about biologics are going to be applied similarly to the nanomedicines. The only difference is that we do not know well but also cannot predict easily the perpetual fates of nanomedicines in vivo after systemic administration in humans. By labeling radionuclides to these nanomaterials or nanomedicines, we can trace the biodistribution in vivo after systemic administration and begin predicting the fates of those radionanomedicines in vivo. This eventually will individualize the choice of patients in whom we expect the biological or radiation effect upon the disease of interest such as cancers. For cancers, so many tyrosine kinase (TK) inhibitors or monoclonal antibodies had been developed and clinically in use, but shotgun type of therapy is so prevalent to result in the patients' agony and pharmaceutical company's profit. Elucidation methods of bodily fates of small chemicals and biologics are well established and metabolomics are the newest name for that

endeavor, and now nanomedicines are going to be understood in detail so as to enable the investigators predict easily the fate, success of targeted delivery and side effect.

Tracer kinetic analysis is now well established in nuclear medicine and individualized dosimetry upon this kinetic understanding is underway. Every new small molecular radiopharmaceutical or biologics used to go through the elucidation procedures of biodistribution and radiation absorbed dose distribution and expected administered radiation to the target of interest. Nuclear medicine can easily adopt the nanomaterials and do the same way to reveal the possible advantage of using nanomaterials instead of biologics. It is an easy expansion of the discipline's principle, nevertheless the exploration of new opportunity. Nuclear medicine will discard immediately the radionanomedicines if the adopted nanomaterials are toxic or do not behave as we expected or too cumbersome to handle. Compounding radiopharmaceutical with radionuclides at bedside is a common practice in nuclear medicine and even the production of the nanomedicines and compounding procedure using radionuclides at bedside are prolonged, then again nuclear medicine will not adopt the radionanomedicines.

As time goes by, chemistry and chemical engineering come to be more and more versatile to fabricate nanomedicines in good manufacturing practice (GMP) and supply radionanomedicine precursors to the clinic, and then nuclear medicine physicians will be glad to use them after an easy labeling for theranostic, therapeutic or diagnostic imaging purpose. Individual radiation dosimetry and determination of the appropriate dose to the patients and optimal time schedules are going to be devised soon. That is the way how radionanomedicine shall enter the clinical arena. Clinical radionanomedicine is the next discipline when several successful radionanomedicines are approved and compounding procedures come to be popular in clinical practice. Platform technology is to be developed for realization of this expected clinical future.

Radionanomedicine is the ultimate future of nanomedicine. Nanomedicines are not going to be adopted easily in clinical medicine with so many unknowns. Radionanomedicines, if successfully meet the criteria of approval for biologics, will soon appear at the clinic, and nuclear medicine physicians are going to accommodate the procedures and get very much familiar in using them, then again nanomedicines might come back on their own to become independent drugs for clinical use. The trap of lack of knowledge will be overcome by radionanomedicine. We need to take efforts to make things practical and understand the details and always vigilant for the possible human and clinical use of these huge pools of materials that humankind never encountered in their long history of evolution.

With the themes passionately explained above, keeping in mind the advantage or beauty of radionanomedicine, I edited this book as follows. This was extended endeavor I and my colleagues published the first review article in 2015 in Nanomedicine, nanotechnology, biology and medicine [1]. After that, the concept was refined again and again in many presentations at global congresses and conferences of either nuclear medicine society or nanomedicine society. Systematic description of the problems which have been solved and more problems which need

to be solved were the first trial of this new book about a novel discipline. The only remaining thing after this fully-equipped book was published is that in the era of in vitro companion diagnostics, whether radionanomedicine will also need to be with in vitro companion diagnostics or radionanomedicine will act as an option of in vivo companion diagnostics for the novel therapeutics which will be developed and approved for any clinical use. In vivo companion diagnostics are going to be explained in another book in due time, and now is the time to enjoy the well-dispersed problems and solutions and moreover the expanded imaginations to comprehend the reason for success or failure of novel theranostics, therapeutics and diagnostic imaging in vivo in this book.

Here the book was composed of several sections. Each section contained several chapters written by different authors. The chapters are mutually complimentary and not exclusive but a little redundant. The redundancy was intentional and went through a meticulous editing by myself and my young colleague radiochemists and nuclear medicine physicians. Here follows the details.

Radionanomedicine can be classified to the one which use exogenous radionanomedicines, i.e. radiolabeled nanomedicines or nanomaterials and another which use endogenous radionanomedicine. This is quite a convenient classification to understand the bodily response to the administered nanomaterials while body responds to the exogenous materials in one way and the endogenous materials in another way. The response of bodily immune system can change biodistribution and even cause adverse reaction to the exogenous materials but the response of immune response to the endogenous materials might be more sophisticated. Understanding of the resulting fate of exogenous or endogenous materials should depend on different way of reasoning.

Among the exogenous materials, iron oxide, gold, quantum dots, silica or other materials have been the majority since the dates of the advent of nanomedicine but most recently, emphasizing in vivo usability, new materials came to be the focus of attention. Graphenes and porphysomes were the examples and we detailed the explanation. In the chapters of inorganic nanomaterials, theranostic porphysomes and organic nanomaterials, one can meet the comprehensive review of the progress of hope to use these radiolabeled nanomedicines for possible human and clinical use. Radiolabeled iron oxides, radiolabeled gold, radiolabeled quantum dots, or radiolabeled silica and others are going to make a path to clinical translation one day and their preliminary application to small animals in vivo are to be found in this section. The theranostic applicability of porphysome of photodynamic and beta ray-emitting radionuclides will be understood by reading the special chapter of porphyrin and phthalocyanine radiolabeling. One will be able to understand how many radionuclides can be easily chelated with porphyrin which will later be the constituent making nanoparticles for simultaneous beta-radiation and photodynamic therapy.

In the following chapter of graphene, the great but still unexplored possibility of using graphene oxide or radiographene was explained in great abstraction from the recent developments and trials to use these novel materials for biomedical purposes. Every detail will cast a concern of lack of knowledge and at the same time a hope of

using these materials for imaging tools as well as for therapeutics. Final fate of graphene or radiographene was unexpectedly amusing that living body can handle it metabolically. Organic nanomaterials are bodily ones but made of extrinsic materials mostly polymers or liposomes/micelles. Scientific and pharmaceutical community already cumulated lots of long-term experiences of using these classical nanomaterials. Radiolabeling of these nanomedicines might expand their use and thus looking back the successful use of drug-loaded nanomedicines will help the readers to imagine and draw a picture of future of using radiolabeled organic nanomaterials even including albumin. Understanding the role of albumin is still underway. How to use radiolabeled organic nanomedicines for theranostic purposes are to be investigated further.

Interestingly recently, we came to know that there are endogenous counterparts of liposomes. Almost all of a sudden, these lipid bilayered extracellular vesicles or exosomes produced endogenously by every kind of cells are circulating in the body in health and diseases, and the exosomes are to find their appropriate position to explain their roles in physiology. Extracellular vesicles, if they have the chances to be used as carriers of familiar biomolecules from one cell to another, shall have capability of being used as therapeutic or theranostic nanomedicines. What remains to be understood is the whereabouts of these exosomes in the body after systemic injection. The chapter of 'extracellular vesicles', a great synopsis with assuring promise to the understanding the reason of existence of extracellular vesicles in body are followed by technical details of new methods of radiolabeling of extracellular vesicles, the facts revealed about biodistribution elucidated using these methods and the consequent prediction of the future use of these exosomes for therapy and theranostics. In the strict description of the literature reports which tried to figure out the distribution of systemically administered exosomes, one should find the revelation that fluorescent dyes are not appropriate for finding or quantifying the distribution of exosomes. We still don't know whether the membrane labeling of intact exosomes or intracellular labeling of exosomes is appropriate method to make us be able to estimate the biological effects when we injected therapeutics-loaded exosomes. Notwithstanding validation of therapeutic potential, the quantitative and/or qualitative distribution of endogenous or administered exosomes should now be investigated. After long years of struggle to understand the physiology or pathophysiology of exosomes and their subsets, and hopefully before so long, the exosomes, either radiolabeled or not, will find a way to contribute to clinical nanomedicine.

It is well known that surface characteristics are crucial in determining the in vivo behavior of nanomedicines. And there have been so many improvement of the surface modification technology so far. The next move to the future facile use of nanomedicines depends upon the optimization of surface modification of exosomes. Along the surface modification one can also bind chelator which later chelates radionuclides, which will yield radionanomedicines. These radionanomedicines are going to be used for further characterization of biodistribution, quantification of successful targeted delivery and clearance from the body. Investigators feel really curious of the consequences of the surface modification or even radiolabeling in

terms of in vivo behavior of radionanomedicines. Readers are going to enjoy the comprehensive summary of the existing methods using a variety of gamma, beta and even alpha emitting radionuclides. Further concern to modify surface to let the nanomedicines to reach the target using further modification or binding targeting ligands led us to adopt earlier the click chemistry. Click chemistry is once overviewed here because it is the critical finishing stroke to modify the surface of radionanomedicines. This click chemistry technology and its importance were going to be further elaborated in the next section.

The next section was entitled 'Targeted delivery with Click chemistry'. We have clinically-proven technology called nuclear medicine, where we are able to use trace amount of radionanomedicines and image and quantify the radionanomedicines in every organs and tissues using tracer kinetic on PET or SPECT associated with CT or MRI. What remains is to make radionanomedicines properly for clinical use. Targeting molecules are a lot, ranging from small molecules such as mannose or galactose, via biomacromolecules such as monoclonal antibodies, affibody, avibody, nanobody, aptamer, aptide, and natural or non-natural peptides. These molecules are going to endow radionanomedicines the superb targeting capacity if they are bound on the surface of nanomedicines upright and robustly. And thus preservation of ligand functionality, that is to say, targeting capability using click chemistry was detailed again. Readers can refer to this chapter to browse the copper-dependent or copper-free methods of click reaction to bind ligands upon nanomedicines to choose one the most suitable for their purpose. Bioorthogonal reaction is recently coined term which explains the existence of desired chemical reaction which is totally ignored by the body and physiology. If we use bioorthogonal reaction between two parts of radionanomedicines, even the binding reaction can be done in vivo after administration of parts separately. This orthogonality in theory sounds very attractive and the readers will find the reality and progress of applying this technology in the following chapter. Finally for easy and successful clinical application, we need platform technology and this nano-platform technology, while guaranteeing their consistency in producing the final product even up to GMP grades.

As was mentioned above, tracer principle of radionanomedicine allow us to trace in vivo biodistribution of radionanomedicines after injection systemically via many chosen routes using whole body imaging and quantification. Introduction of relevant and available instruments and their principles were detailed in preclinical PET/CT, SPECT/CT and PET/MRI. One can easily survey their choices even though he or she is not familiar with nuclear medicine technologies. Tracer kinetic analysis will enable us to discover the mechanism of targeting and excretion and sort out the better fabrication, modification and multiplexed binding of ligands and chelators afterwards. This imaging and quantification on PET and SPECT supplies a great opportunity to facilitate the discovery of the clinically most desired composition of radionanomedicines.

Now in the next two sections entitled 'Factors Affecting Biodistribution and their Consequences' and 'Immune Responses to Nanomaterials', the readers can estimate the best guess of the behaviors of nanomedicines or radionanomedicines in vivo

considering the best knowledge of the factors and their consequences and bodily responses to the parameterized characteristics of nanomedicines and radionanomedicines. The contents in the chapters would be a description of the efforts to understand the in vivo behavior of nanomaterials from the different perspectives. People used to develop new nanomaterials first and feel happy with the implication of these nanomaterials which might be used in humans for clinical purposes. And they are frustrated with the general dis-knowledge of our field of the behavior of nanomaterials in vivo. The accumulation of the reports in the literature should have been understood in reasonable way and readers can encounter the description meticulously prepared. Size and shape was critical for the clinical application of a type of silica nanoparticles and the radiating tracks of novel endeavor to develop other nanomedicines were supposed to take place based on this knowledge. PEGylation or newer zwitterionic modification is now popular practice to make nanomaterials biocompatible, more specifically hydrophilic, hiding from the trapping or immune responses of the body. The stealth effect of these modifications was once coined to exaggerate the hope to deceive the bodily non-immune or immune surveillance system. This idea is going through reality testing and the readers can get the summary of the progress including the most recent achievements. Nanomaterials were not inert in systemic circulation and recent proteomic analysis even enabled fingerprinting of the constitution of wrapping plasma proteins around nanomedicines. In our long tradition of developing new radiopharmaceuticals using small molecules or biomacromolecules, it was customary to add the biodistribution data made of histograms associated with representative, gamma camera, SPECT or PET images of the small animals. For nanomedicines and radionanomedicines, the same customs are repeatedly exercised by many investigators; however, in the chapter 'Excretion and Clearance', readers can now learn the framework regarding how to comprehend the behavior of novel nanomedicines and radionanomedicines in vivo. Caveat was that we should not automatically assume that liver uptake is the clearance by mononuclear phagocytic system. Hepatobiliary clearance was repeatedly reported in the literature but without proper emphasis on their significance. Renal or other peripheral clearance by non-phagocytic cells should be kept in mind to correctly interpret the excretion and clearance.

Immune response to the exogenous or endogenous nanomaterials must be explained with the best knowledge of versatility of diverse immune surveillance system of human as well as animals. Doxorubicin-containing liposomes had been clinically used for more than 2 decades now and taught the scientific and medical community very well, and thus we understand the details of the immune response to the challenges by exogenous drug-containing liposomes systemically administered to patients. Interestingly, first-line of response was non-specific reactions including complement and other cascade protein system in the plasma. This was followed by less-specific humoral immune response of IgM. We now know the first encounter can elicit mild to serious even fatal reaction to the similar kind of liposomal constructs and second injection will meet humoral or other well-known adaptive immunity of the body. In the meantime, most recently, the understanding of innate immunity and adaptive immunity and their differentiation was totally changed.

Innate immunity could have been trained, i.e. enhanced response to the second encounter by innate immune cells. Beside this, the important Kupffer cells were repositioned as resident macrophages and circulating monocytes are no more the exclusive supplier of macrophages in tissues. The imaginary scenario on which nanomedicines and radionanomedicines will meet bodily immune system was included in the chapter 'Innate Immunity'. I wish readers might learn the framework of how readers should estimate the nanomaterial-immune interaction and do their own thought-experiments about the disposition of radionanomedicines in vivo.

Molecular imaging is struggling to find a way to the clinical use during the 15 years since its composition of independent society and scientific activity. This field had achieved the goal that we now have every instrument for small animal imaging. Currently clinically used molecular imaging are the ones already available when the discipline of molecular imaging was formulated in 2002, i.e. neurotransmitter receptor or transporter imaging or abnormal protein imaging such as amyloid or tau. Thus, molecular imaging, in narrow sense, imaging of the cellular and molecular processes elucidated by molecular biology technologies. Engineered fluorescent proteins contributed a lot to the advancement of molecular biology and molecular imaging and in vivo translation was tried every time to study important molecular processes. Bioluminescent proteins followed and now application and adoption of nanomaterials for similar purposes became prevalent. The most popular ones are those using quantum dots, surface enhanced Raman scattering dots, upconversion nanoparticles and graphenes. In vitro, ex vivo or topical application of these nanomaterials is popular and promising but for systemic application, we need to make these nanomaterials as multimodal with radiolabeling or choosing magnetic particles. This was detailed in the chapter of 'Molecular Imaging'.

Last chapter is the highlight entitled 'Theranostic Use'. In fact, our eternal goal is to intervene in the bad pathophysiological processes of the diseases in humans. Imaging or diagnostic tools are already saturated and the introduction of nanomaterials and their clinical and human use was applauded by the experts and the public expecting better therapeutics even forcing us to take the risks of using these materials to humans. Therapeutic use of radionanomedicines labeled with DNA-breaking or cell-killing beta or alpha ray emitting radioisotope mandates the understanding of individualized radiation dosimetry and dose-biologic effect relationship. Thus in the last chapter, the authors described the current knowledge of nuclear medicine therapy which is also called molecular radiation therapy. The readers can have lessons and be equipped with the rounded knowledge acquired from trials-and-errors in the fields of radiation therapy and nuclear medicine therapy. Based on this whether the final goal of better treatment customized for individual patients will be achieved or not adopting radionanomaterials should now be determined. The conclusion taking shapes in everyone's mind might all be different regarding this matter, however, the task or contribution of this book is supplying the bases to contemplate the possibility and the obstacles inherently borne in this discipline and not admonishing or feeding the conclusion. The future of radionanomedicine depends on the many following investigators' hands and brains. I now add the final comment, here, the success of one field called ~medicine, in

our case radionanomedicine, relies on the successful clinical human application to help people. Not on the exotic, unusual, fancy, fantastic novel materials with impetuous prospects.

Reference

1. D.S. Lee, H.J. Im, Y.S. Lee, Radionanomedicine: widened perspectives of molecular theragnosis. Nanomedicine **11**(4), 795–810 (2015)

Part I
Exogenous Radionanomedicine

Exogenous radionanomedicine is the simplified phrase representing radionanomedicine using exogenous nanomaterials. Nanomaterials used to be exogenous in that they were fabricated in laboratories not by nature. In vivo use of exogenous nanomaterials requires their cleanliness without any toxic substances, nor pathogenic infectious agents nor pyrogenic materials. Among exogenous nanomaterials, organic ones already began to be used two decades ago with doxorubicin containing liposomes (Doxil®) and currently this went public with the cease of patent-ship. Albumin joined, dendrimer, or other polymers are struggling to enter into the success in application to clinical use. In the meanwhile, very small silica nanoparticle, with the encouraging characteristics of inertness with rapid renal excretion, called C-dots are in clinical trial for treating brain tumors now. Other inorganic materials such as iron oxide, gold, and various forms of particles not made of any frank toxic substances such as lanthanide-doped upconversion nanoparticles or surface-enhanced Raman scattering dots are sincerely being investigated but yet without any tangible roles in clinics. Radiolabeled inorganic nanoparticles such as iron oxide or gold or even CdSe quantum dots might be able to be used in vivo when they were used in trace amount (10^{16} particles or less) according to the regulatory guidance of microdosing test for first in humans. And this can be a breakthrough for any nanomaterials reported to be implied for their potential for clinical utility. This spectrum of exogenous nanomaterials was described in Chaps. 2 and 5 with the selected reports in the literature so that the readers can feel the progress of the discipline of nanomaterials sciences.

Porphyrin and porphysomes and their cousin phthalocyanines have a unique position in that porphyrin is a component to constitute endogenous substance of heme. And interestingly, it makes a complex to yield sizable nanomaterials. The labeling of porphysomes with radionuclides and their implied use for in vivo delivery of radionuclides are detailed in Chap. 3. The readers are recommended to pay attention to the theranostic capability of these materials. In addition, recent introduction of graphenes and radiographenes raised great hope for the possible use as drug carrier or radionuclide carrier. Explicit understanding of in vivo behavior of graphene oxides having inherent heterogeneity of size and shape and contents of functional carboxyl or hydroxyl residues requires much further investigation. Radiolabeling of these materials shall elucidate the potential of graphenes in vivo in human and possibly in clinics. Surveying all these nanomaterials in this part is supposed to help clarify the significance of the old and new exogenous nanomaterials, which leads to the following parts.

Chapter 2
Exogenous Radionanomedicine: Inorganic Nanomaterials

Carolina A. Ferreira, Shreya Goel and Weibo Cai

Abstract Roles of nuclear medicine and molecular imaging in cancer diagnosis and therapy are constantly evolving. Single-photon emission computed tomography (SPECT) and positron emission tomography (PET) imaging allows the investigation of not only morphological but also functional characteristics of tumor tissues and possess distinct advantageous characteristics, such as high specificity and sensitivity, excellent quantifiability and virtually no tissue penetration limit. Nanoparticles, as multifunctional materials, hold the potential of being surface-engineered, conjugated to numerous targeting agents while carrying therapeutic or diagnostic agents and, thus, can provide the platforms needed for enhancing imaging and therapy efficacy and specificity; hence a large number of nanocarriers have been radiolabeled with a vast array of SPECT and PET agents for preclinical studies. In this context, radiolabeled nanoparticles hold the potential to deeply impact the science of clinical practice, from disease diagnosis to patient management. This chapter provides a comprehensive overview of the methods of synthesis, radiolabeling and further applications of the most commonly used nanoparticles in radionanomedicine.

C. A. Ferreira · W. Cai (✉)
Department of Biomedical Engineering, University of Wisconsin-Madison, Madison, WI 53705, USA
e-mail: wcai@uwhealth.org

C. A. Ferreira
e-mail: cferreira2@wisc.edu

S. Goel (✉) · W. Cai
Department of Materials Science and Engineering, University of Wisconsin-Madison, Madison, WI 53705, USA
e-mail: shreya.goel.shreya@gmail.com

W. Cai
Departments of Radiology and Medical Physics, University of Wisconsin-Madison, Madison, WI 53705, USA

W. Cai
University of Wisconsin Carbone Cancer Center, Madison, WI 53792, USA

D. S. Lee (ed.), *Radionanomedicine*, Biological and Medical Physics, Biomedical Engineering, https://doi.org/10.1007/978-3-319-67720-0_2

2.1 Introduction

Molecular imaging and the development of molecular agents aimed at the visualization of in vivo intracellular events without any molecular or cellular disturbance can be excellent tools to study disease mechanisms as well as in vivo pharmacokinetics of targeted therapeutic and imaging probes. Nuclear medicine, including nuclear imaging and treatment of diseases with radiolabeled tracers, has been well-established in preclinical and clinical settings for decades [1]. Currently available targeting strategies for cancer therapy and imaging usually rely on the use of monoclonal antibodies and peptides, which are often limited by insufficient delivery to tumor tissue, due to heterogeneous expression levels of tumor cells receptors, as well as dose-limiting off-target side-effects. To ensure that toxicity levels are low but the therapeutic effect remains maximized, it is essential to deliver the desired agents to the correct site, at the appropriate concentration at the right time [2].

Nanocarrier systems (NS) could serve as the platforms needed for enhancing the delivery of imaging probes and therapeutics to the tumor sites, thus enhancing imaging and therapeutic efficacy. Nanoparticles (NPs) are structures, nanometers in size [3] and, as such, can extravasate from the endothelial cell layers to the tumor site, while carrying large therapeutic and diagnostic cargos such as small molecule drugs and radioisotopes [4]. Multifunctionality is the key advantage of nanoparticles since nanomaterials, in contrast to traditional agents, have an extremely high surface-to-volume ratio that provides chemically active sites and easily tailorable surface bioengineering to achieve enhanced biological outcomes, such as increased blood circulation time, target specificity, reticuloendothelial system (RES) evasion and therapeutic delivery [5]. Also, NPs can be constructed to have tunable properties (optical, electronic, magnetic, and biological), sizes, shapes and chemical compositions. By integrating a variety of functional components such as imaging agents, targeting ligands and therapeutic compounds into the nanomaterials, they can be precisely tailored for personalized targeted theranostics of diseases [6]. Thus, the combination of an ideal size range with an ability to be conjugated with distinctive targeting ligands makes nanosystems excellent candidates to break the physiological barriers and access different diseased tissues in a controlled manner [7].

It is worth mentioning that a NS can accumulate at certain tissue sites through two different targeting mechanisms: passive and active. Passive targeting relies on enhanced permeability and retention (EPR) effect arising from the anatomical differences between healthy and non-healthy tissues. The EPR effect exploits (i) leaky tumor vasculature for greater extravasation and accumulation of nanoparticles at the tumor site, as well as (ii) inefficient lymphatic drainage at those sites to allow prolonged retention of such molecules in the targeted tissue [7]. This type of targeting enables non-specific accumulation of molecules and can occur in other diseases besides cancer, such as infection and/or inflammation [8]. In contrast,

enhanced accumulation and retention of the NPs at the diseased site via active targeting mechanism relies on specific ligand-receptor or antibody-receptor interactions. Several studies reporting NPs modified with specific ligands such as monoclonal antibodies [9] folic acid and peptides [10–12] as well as aptamers [13] have been reported to date. Successful targeting depends on the selection of the right targeting moiety, considerations for which include the expression level of receptors, its affinity and specificity for the receptor, and ease of conjugation to the nanoplatform. Despite the advantages gained from NP utilization, there are still challenges that need to be addressed, such as, the uptake of NPs by the RES, in which NPs are rapidly removed from the circulation through the liver or spleen, thereby raising concerns about NP toxicity in these tissues. Furthermore, NP aggregation can cause them to be trapped in the liver or lungs due to capillary blockage [14]. Polyethylene glycol (PEG) modification of NP surface can alleviate many of these limitations and, thus, this approach has been extensively used for a variety of material types. An excellent review on NP PEGylation for imaging and therapy has been published elsewhere [15].

While a great variety of materials have been proposed in the development of NS, different imaging techniques have also been used for imaging NP-based tracers, including magnetic resonance imaging (MRI), as well as optical and nuclear imaging modalities techniques such as fluorescence and bioluminescence, single photon emission computed tomography (SPECT) and positron emission tomography (PET) [1]. In this context, nanomaterials have been extensively explored to be used as carriers for therapeutic and/or diagnostic radioisotopes. A radiolabeled nanoplatform must be designed to incorporate high radiostability and high specific activity in the final product. For that, a radiolabeling method must, ideally, be quick, safe and efficient, with minimal effect on the intrinsic properties and pharmacokinetics of the NP vector [16]. The most commonly used radiolabeling methods rely on the use of exogenous chelators, such as 1,4,7,10-tetraazacyclododecane-1,4,7,10-tetraacetic acid (DOTA), 1,4,7-triazacyclononane-1,4,7-triacetic acid (NOTA), p-isothiocyanatobenzyl-desferrioxamine (Df-Bz-NCS) and diethylene triamine pentaacetic acid (DTPA), which establish stable complexes with the radioisotopes through coordination. Since the coordination chemistry is different for every isotope, the selection of proper chelator is crucial [17]. It is important to mention, however, that the conjugation of the chelator into the NPs could potentially alter one or more in vivo parameter, such as biodistribution, elimination pathway, absorption and metabolism of the final nanoconstruct [18]. Also, concerns about a possible detachment of the isotope in vivo have compelled the need for developing improved radiolabeling techniques. Hence, chelator-free radiolabeling has been proposed, in which intrinsically radiolabeled NPs are synthesized using different methods, such as specific trapping, cation exchange, proton beam activation and synthesis using hot-plus-cold precursors [19]. Intrinsic radiolabeling of NPs has been shown to be an attractive alternative for an easier and more realiable radiolabeling of nanomaterials [18–21].

Among the different materials that have been developed, inorganic NPs have many favorable properties such as easy fabrication, tunable size, generation of heat or reactive oxygen species (ROS), X-ray absorption, and energy transfer properties [22]. Herein, we will provide a brief review on the types of inorganic NPs that are being studied for radionanomedicine applications.

2.2 Magnetic Nanoparticles

Magnetic NPs (MNPs) comprises a class of extensively studied nanomaterials that have been used in a diverse range of biomedical applications, such as imaging, drug delivery, cancer therapy (hyperthermia) and cell labeling [23]. The advantages of MNPs are based on their large availability and unique combination of physical and chemical properties, including facile synthesis methods, easily-modified surface chemistry, and magnetic responsiveness. MNPs are also advantageous due to their established good biocompatibility in comparison to other multifunctional nanomaterials with low degradability and in vivo elimination rate [24]. Furthermore, the ability to enhance proton relaxation of specific tissues, enable their detectability by MRI, an imaging technique that allows acquisition of morphological and anatomical data without tissue penetration limitation [25]. Most importantly, if the ability to respond to a magnetic field is explored, MNPs can be useful theranostics tools [26].

Depending on the constituents of the contrast agents, magnetic NPs can be categorized into (i) superparamagnetic iron oxide NPs (SPIONs) based T2 contrast agents, and (ii) paramagnetic gadolinium (Gd) or manganese (Mn) based T1 contrast agents [16]. The three main categories of biologically suitable iron oxide NPs (IONPs); magnetite (Fe_3O_4), maghemite (γ-Fe_2O_3) and hematite (α-Fe_2O_3), can be further classified as standard superparamagnetic iron oxide (SSPIO) ($\sim$60–150 nm) or ultra-small superparamagnetic iron oxide (USPIO; approximately 5–40 nm) NPs [27]. Size parameters not only determine their biological behavior but are known to affect their magnetization capacity, dispersibility, and stability in solution. To be useful for theranostic purposes, IONPs must be monodispersed, with high magnetization, large susceptibility and small hydrodynamic size to avoid the mononuclear phagocytic system, but still large enough to not affect its magnetic properties [28]. Since IONPs tend to agglomerate in solution, the strategy of using coating materials such as organic polymers (PEG, chitosan, polysorbate, polyaniline), or surfactants (sodium oleate and dodecylamine), and others (liposomes, inorganic metals) have been successfully to date, resulting in improved in vivo behavior [26].

Different SPION formulations are currently approved for clinical use such as the Ferridex I.V.® or Endorem® for spleen and liver imaging [29], Ferumoxytol® for iron replacement therapy, and Combidex® for imaging lymph node metastases [30], as well as Gastromark®, Resovist® and Sinerem® as MRI contrast agents [31]. PET/MRI is a rising hybrid imaging technology that combines excellent soft tissue

contrast and excellent resolution provided by MR with high sensitivity and quantification of radiotracer metabolism provided by PET. Also, unlike the conventional PET/CT where imaging information is acquired in sequence, PET/MRI allows simultaneous image acquisition [32], leading to largely improved diagnostic outcomes. Moreover, PET/MRI systems have been successfully conceived for small-animal imaging [33, 34], accelerating the research for novel bimodal magnetic radiotracers [32, 35]. In this context, radiolabeled magnetic NPs have gained much attention lately as dual-modality imaging agents due to their ability to act not only as imaging tracers for PET or SPECT but also as MRI contrast agent [33]. Approaches involving chelator-free and chelator-based radiolabeling have been reported in an array of differently designed and surface-functionalized IONPs with different radioisotopes, suited for both SPECT and PET.

To date, IONPs have been radiolabeled with various types of suitable radionuclides for SPECT imaging. Technetium-99 m (^{99m}Tc), the most commonly used radioisotope in SPECT in its reduced form ($^{99m}TcO_2$), can react with electron donor groups and can, be linked to IONPs through the $–COO^-$ group of chelating agents DTPA and NOTA or $–NH_2$ group of chitosan and modified PEG [36]. Madru et al. [36] developed ^{99m}Tc-labeled IONPs (radiolabeling yield $\sim$ 99%) for SPECT/MRI imaging of sentinel lymph nodes, by conjugating the reduced state of $^{99m}TcO^{4-}$ to the functionalized PEG coating on the IONP surface. An impressive uptake value of 200%ID/g (percentage of injected dose per gram of tissue) was found for ^{99m}Tc-IONPs SLN tissue, whereas less than 2%ID/g was found in the liver and spleen. IONPs have also been labeled with multiple other radioisotopes for SPECT, such as ^{125}I [37], ^{131}I [38, 39], ^{111}In [40, 41] and ^{188}Re [42] and further review can be found elsewhere [43].

The increasing availability of PET imaging isotopes together with the optimization of the radiolabeling methods, as well as its greater sensitivity when compared to SPECT, have contributed to the greater success of PET imaging in clinical and preclinical settings. In this context, several PET radioisotopes have been used to radiolabel iron oxide NPs, such as ^{64}Cu [44–46], ^{68}Ga [47], ^{18}F [48], ^{11}C [33], ^{89}Zr [49], ^{69}Ge [50]. For example, ^{64}Cu-labeled SPIONS conjugated with DOX and functionalized with cRGD were developed for targeted theranostic purposes [45]. The targeted NPs had significantly higher tumor accumulation when compared to non-targeted SPIONs. The MRI r_2 relaxivity of the SPIO nanocarriers was measured to be similar to that of the Ferridex®; an FDA approved SPIO-based MRI contrast agent. De Rosales et al. [46] directly radiolabeled SPIONs with a dithiocarbamate bisphosphonate (DTCBP) that binds to both ^{64}Cu and the NP, leaving the nanosystem polymeric coating (dextran) unaffected. Using the lymphatic system as in vivo model, the popliteal lymph nodes of a C57BL/6 mouse were located using T2*-weighted MR images (Fig. 2.1a). PET imaging confirmed the uptake of NPs in both popliteal and iliac lymph nodes (Fig. 2.1b, c). Hence, [^{64}Cu(DTCBP)$_2$]–Endorem was a successful PET–MR dual-modality imaging agent that accumulated in draining lymph nodes.

Following the emerging concept of intrinsically radiolabeled NPs, in a study by Boros et al. [49] IONPS were successfully chelator-free radiolabeled with

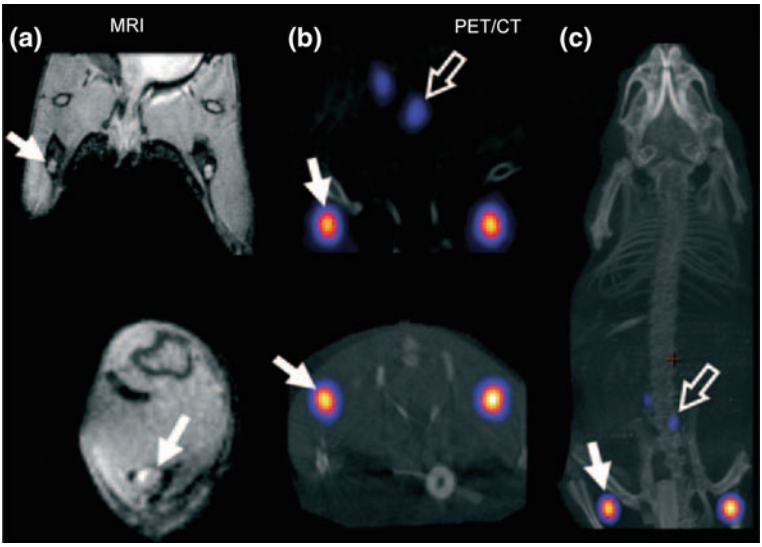

Fig. 2.1 In vivo PET/MR imaging studies with [^{64}Cu(DTCBP)$_2$]– Endorem in a mouse. **a** Coronal (top) and short axis (bottom) MR images of the lower abdominal area and upper hind legs showing the popliteal lymph nodes (solid arrows). PET/CT images showing the uptake of the radiolabeled nanosystem in **b** the popliteal (solid arrow) and iliac lymph nodes (hollow arrow) that can also be identified in **c** whole-body images. Adapted with permission [46]

^{89}Zr through iron bonding and heat-induced methods. Thermodynamically and kinetically stable ^{89}Zr–USPION were studied in vivo in a subcutaneous acute phase response inflammation model, and results validated the potential of ^{89}Zr–USPION as a PET/CT tracer of tissues enriched with activated macrophages. In the same manner, through a chelator-free radiolabeling method, Cui et al. [51] took advantage of the high affinity between $Al(OH)_3$ and fluoride anions and labeled $Al(OH)_3$ coated IONPs with ^{18}F. High radiolabeling efficiency of 97% was achieved and, after tail vein injection, a rapid accumulation of the radiolabeled IONPS was found in the spleen and liver as confirmed by in vivo PET/CT and PET/MR imaging. However, due to the unstable $Al(OH)_3$ shell, [^{18}F]-fluoride was progressively released from NPs in vivo, resulting in a considerable bone accumulation demonstrating suboptimal radiolabeling stability. Our group further demonstrated the feasibility of chelator-free radiolabeling of SPIONs with Germanium-69 (^{69}Ge) [50] and Arsenic-72 (^{72}As) [52]. Water-soluble poly(acrylic acid) (PAA) modified PEGylated SPION was used for both studies. While the high affinity of germanium for metal oxides was explored for the ^{69}Ge labeling, ^{72}As labeling involved occupation of vacant FeO_4 tetrahedral sites in magnetite NPs by $As^{III}O_3$ trigonal pyramids and $As^{V}O_4$ tetrahedra, yielding highly stable complexes in both scenarios. PET/MRI lymph node mapping in vivo was demonstrated with ^{72}As-SPION and ^{69}Ge-SPION, as can be seen in Fig. 2.2. Accumulation of ^{69}Ge-SPION@PEG in the popliteal lymph node is evident at 0.5, 2, and 20 h p.i. (Fig. 2.2a, marked by

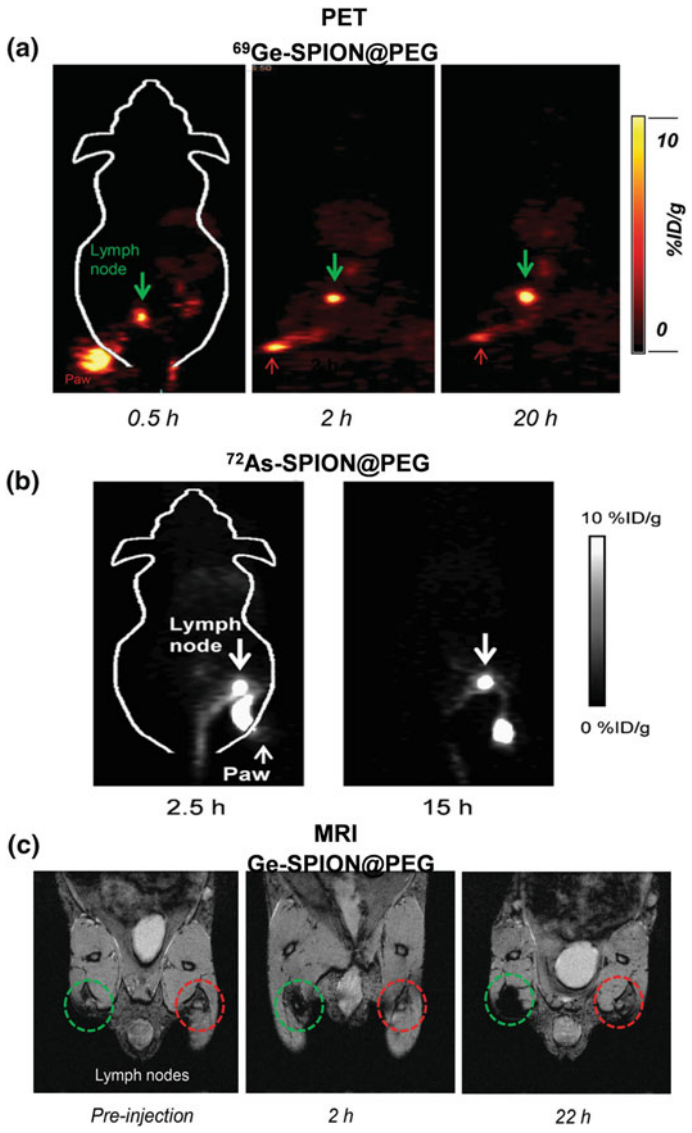

Fig. 2.2 In vivo lymph node imaging with PET after subcutaneous injection of **a** ^{69}Ge-SPION@PEG or **b** ^{72}As-SPION@PEG into left footpad of the mouse. **c** In vivo lymph node mapping with MRI before and after injection of Ge-SPION@PEG. Adapted with permission [50, 52]

green arrows), with uptake found to be 7.5 ± 2.5, 12.5 ± 3.1 and 28.0 ± 5.2%ID/g, respectively [50]. At 2.5 and 15 h p.i., lymph node uptake of ^{72}As-SPION@PEG is seen with values of 12.5 and 13.2%ID/g, respectively (Fig. 2.2b) [52]. PET observations were further confirmed by MRI, as demonstrated in Fig. 2.2c that

shows the darkening of the lymph nodes after injection of cold Ge-SPION@PEG. It is possible to affirm, thus, that radiolabeled IONPs have emerged as imaging systems with a clear capacity of allowing non-invasive quantitative imaging results with the great advantage of supporting simultaneously multi-modality imaging.

2.3 Gold Nanoparticles

Gold NPs (AuNPs), or colloidal gold, can be defined as suspension gold metal particles, in the nanometer scale suspended in a fluid, usually aqueous medium that can be synthesized to have between 3 and 200 nm in diameter. In the molecular imaging field, AuNPs have been extensively applied due to their unique optical and electronic properties, as well as its high stability and biological compatibility. AuNPs can also be easily surface-modified, synthesized with a controllable morphology and are considered bio-inert and nontoxic [53]. Many subtypes of gold NPs, classified according to their size, shape, and physical properties, including gold nanorods, nanospheres, nanoshells, nanocages as well as gold surface-enhanced Raman scattering (SERS) NPs have been developed and preclinically investigated for molecular imaging [54].

The most commonly used method of AuNPs synthesis, the cluster beam method, was developed more than 50 years ago and involves citrate reduction of $HAuCl_4$, as suggested by Turkevich et al. [55]. The dissolution of Au(III) salt or Au(I) complex to Au(0) by a reducing agent, in the presence of Lewis base ligands, usually results in monodispersed particles with controlled average diameters of 10–60 nm. For smaller AuNPs ($\sim$5 nm), other types of reducing agents can be used [56] while for larger particles, a method described by Goia and Matijevic [57] used. Other methods of synthesis and optimization protocols, including electrochemical oxidation/reduction procedure and two-step seed-mediated surfactant-assisted protocol have been proposed [58].

It is important to highlight the significance of the optical properties of AuNPs, considering that their absorption and emission are within the visible range of light. Because the light scattered from AuNPs is in the visible portion of the electromagnetic spectrum in accordance with their plasmon bands, an effect known as "localized surface plasmon resonance" (LSPR) that happens when an electromagnetic wave passes through, it is possible to optically track the position of individual NPs, paving the way for imaging applications [59] and, thus, AuNPs have shown potential as contrast agents for optoacoustic cancer imaging [60]. Furthermore, since SPR peaks of gold nanostructures can be easily tuned between visible and NIR windows by simply changing the shape and size of AuNPs, they have been variously harnessed for fluorescence (FL), photoacoustic (PA) and Raman imaging, as well as for photothermal therapy (PTT) [61–63]. The biggest advantage of AuNPs in imaging lies in their multiplexing ability. The inherent optical properties and high X-ray absorption coefficient allow their use as multimodal contrast agents, with widespread applications in optical, MR, CT and radionuclide imaging [27].

To this end, AuNPs have been radiolabeled with a number of isotopes for use with SPECT or PET, and more in-depth information regarding the application of radiolabeled AuNPs can be found in recently published review papers [1, 16, 64, 65].

Macrocyclic chelating ligands are usually used for the labeling of AuNPs with a SPECT or PET radionuclide [1]. Ocampo-Garcia et al. [66] evaluated the potential of ^{99m}Tc-labelled gold NPs (~20 nm) with good radiolabeling yield (>95%) and good stability in human serum, conjugated to the HYNIC-Gly-Gly-Cys-NH_2 (HYNIC-GGC) peptide and thiol-mannose, as agent for sentinel lymph node (SLN) identification. Biodistribution studies and in vivo SPECT/CT images of Wistar rats demonstrated a clear lymph node uptake (11.58 ± 1.98%ID at 1 h) that remained constant for 24 h with low accumulation in the kidneys (0.98 ± 0.10% ID) and insignificant uptake in all other organs. AuNPs have also been labeled with PET isotopes through chelator-based methods [67]. For example, Xie et al. [68], reported gold nanoshells coated with PEG_{2k}-DOTA radiolabeled with ^{64}Cu for tumor diagnosis. The radiolabeling efficiency was 81.3%, and PET imaging demonstrated that AuNPs showed higher accumulation at the tumor site, mainly at 20 and 44 h p.i. [68]. In an interesting study performed by Chen et al. [69], the kinetics of renal clearable Au NPs were analyzed by dynamic PET imaging of ultrasmall (~3 nm) ^{64}Cu–NOTA–Au–GSH. It is possible to observe, in the PET/CT image (Fig. 2.3a), a predominant uptake of NPs in the bladder (yellow arrow) and kidneys (red arrows). The NPs demonstrated rapid renal clearance (≈75%ID, 24 h p.i.) and drastically reduced hepatic uptake. The elimination half-life of ~6 min was found to be over 130-times shorter than previously reported for similar NPs [70], thereby indicating the superiority of PET in accurately assessing the in vivo pharmacokinetics of intravenously injected NPs [69]. In another study [71], AuNPs conjugated with Cetuximab (a specific antibody against EGFR) were radiolabeled with ^{89}Zr using desferrol as a chelator agent. The nanoprobe predominantly accumulated in the liver (red arrows) and in the A431 tumors implanted in both legs (green arrows), as shown in Fig. 2.3b. Maximum tumor uptake was observed at 48 h p.i., with a 12.0 ± 2.3 tumor-to-background ratio. The radiolabeled NPs proved to be a successful PET imaging agent and a potentially therapeutic alternative approach [71].

Nuclear bombardment, radiochemical synthesis, and post-synthetic radiolabeling are some chelator-free approaches that have been proposed for AuNPs radiolabeling [72]. Using the hot-plus-cold method, trace levels of radioactive (hot) precursor $^{64}CuCl_2$ were mixed with non-radioactive (cold) gold chloride copper acetylacetonate precursors during the synthesis [73] to yield ^{64}Cu-alloyed AuNP (^{64}CuAuNPs). This strategy resulted in a good radiolabeling stability, without any degradation or transchelation in mouse serum up to 48 h, as well as improved in vivo stability when compared with ^{64}Cu-DOTA. Mice bearing EMT-6 tumors were used to assess the passive targeting capability of ^{64}CuAuNPs and tumor metabolism was also evaluated in comparison to ^{18}F-fluorodeoxyglucose (^{18}F-FDG) (Fig. 2.4). ^{64}CuAuNPs demonstrated similar tumor accumulation (4.93 ± 0.32%ID/g) as that of ^{18}F-FDG (4.59 ± 0.43%ID/g). Additionally, enhanced tumor-to-muscle (T/M) ratios were observed (3.99 ± 0.89, 11.9 ± 2.08

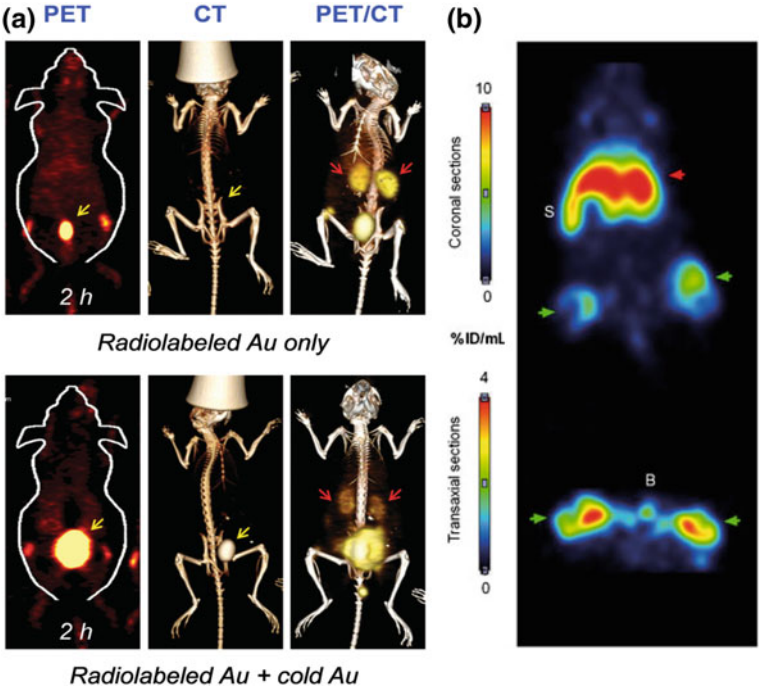

Fig. 2.3 **a** In vivo PET/CT imaging of ^{64}Cu-NOTA-Au-GSH and cold NOTA-Au-GSH at 2 h p.i. Yellow arrows indicate the bladder and red arrows mark the kidneys. **b** A431-bearing nude mice, 48 h p.i. of ^{89}Zr -AuNPs–PPAA–Cetuximab–showing coronal (upper) and transaxial (lower) PET images Color scales, expressed as %ID/ml, indicate radioactivity uptake levels in tumors (green arrows) and liver (red arrows). The bladder is indicated by 'B' and the spleen with 'S.' Adapted with permission [69, 71]

and 16.2 ± 1.07%ID/g at 1, 24 and 48 h p.i.) [73]. Similarly, Zhou et al. [70] demonstrated a one-step thermal reduction synthesis of NIR-emitting ultrasmall radioactive glutathione (GS)-coated luminescent [^{198}Au]Au NPs, with rapid and effective renal clearance, as visualized through two different imaging modalities (SPECT and optical imaging) [70].

As discussed in this section, a large number of studies support the use of radioactive gold NPs as potential theranostic agents. However, a few limitations regarding their use in biological applications have been found, such as low stability in vivo [22] and lack of active tumor targeting [74]. In order to solve this problem, PEG [74] coating of AuNPs and surface functionalization with different types of biomolecules and ligands, such as peptides [75], DNA [76], RNA [77], antibodies [78] has been extensively undertaken [74]. A thorough review covering all aspects of bioconjugation of AuNP and their in vitro and in vivo characteristics can be found elsewhere [79]. Perhaps the biggest challenge in using AuNPs for in vivo purposes is their slow kinetics of elimination and considerable accumulation in the liver and spleen. This potential concern with the use of AuNPs is evident

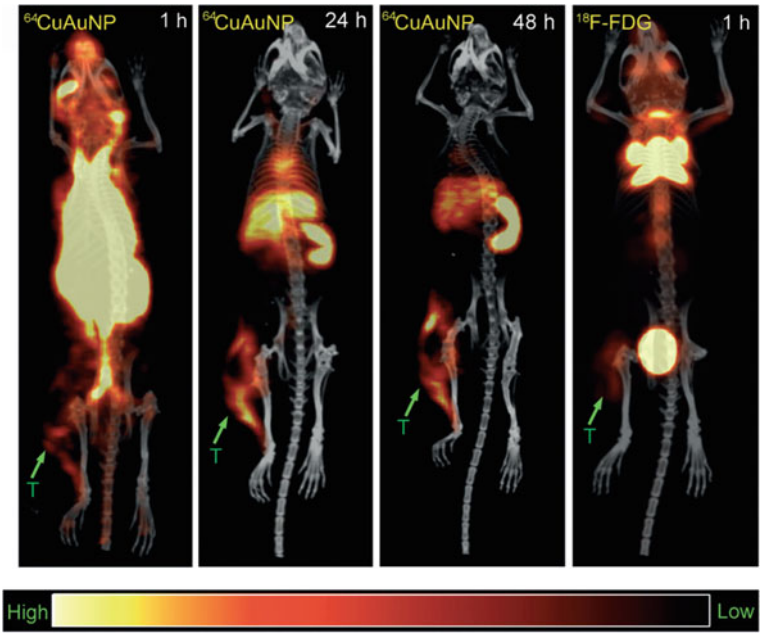

Fig. 2.4 **a** Representative PET/CT images at 1, 24 and 48 h p.i. of alloyed ^{64}CuAuNPs, and ^{18}F-FDG at 1 h in EMT-6 tumor-bearing mice (green arrow T: tumor). Reproduced with permission [73]

in the study performed by Sadauskas et al. [80] reporting only a 9% decrease in the amount of gold present in the liver up to 6 months after AuNPs (~40 nm) were intravenously injected. Another report has demonstrated inflammatory and apoptotic responses in the liver after administration of AuNPs [81]. Nephrotoxicity is always a concern upon AuNP administration, since AuNPs have been shown to enter renal cells and accumulate in the kidney tissue [82]. Therefore, despite their promising potential in molecular theranostics, in-depth evaluation of their pharmacokinetic profiles and long-term toxicities in vivo, is warranted.

2.4 Quantum Dots

Semiconductor quantum dots (QDs) have attracted much attention in the last two decades due to their unique optical and electronic properties, which are not observed in either isolated molecules or bulk materials [83]. QDs often described as "artificial atoms" or "particles with physical dimensions smaller than the exciton Bohr radius", are semiconductor crystals of nanometer size (2–10 nm) composed of groups II–VI or III–V elements [84]. Virtually any semiconductor metal (e.g., CdS, CdSe, CdTe, ZnS, PbS), as well as alloys and other metals (e.g. Au) can be

employed to make a quantum dots [85]. Structurally, QDs are comprised of a shell-coated semiconductor core, and a capping agent to improve water solubility. The QDs core, usually made from cadmium selenide (CdSe), absorbs incident photons generating electron-hole pairs that rapidly recombine emitting a photon of less energy [86]. The quantum confinement, or physical confinement of excitons, presents QDs with many unique features that favor their biological use over conventional fluorophores for fluorescence imaging [87]. Conventional dye molecules, such as organic dyes or fluorescent proteins, present major limitations, including poor photostability that can result in photobleaching, as well as phototoxicity through the production of toxic radicals that prevents long-term visualization of labeled compounds in living cells [88]. Photostable QDs, on the other hand, are advantageous for having size- and composition-tunable emission from visible to infrared wavelengths, large absorption coefficients and high levels of brightness [84]. Moreover, QDs can be used for combinatorial optical encoding [89], a technique that makes use of a large amount of fluorophores that are combine to encode several molecules at the same time; or multiplex imaging, in which QD is targeted to specific tissues that can be imaged at the same time, since (i) a single wavelength of excitation can be used to concurrently excite multiple probes of different emissions (ii) size and composition can be tuned to make QDs with a wide range of absorption and emission wavelengths from the visible to NIR regions [87, 89, 90]. The QDs size can be tuned by various methods; for example, through the Ostwald ripening process in which the growth rate is dependent on both the temperature and the amount of limiting reagent [91]. The shape of QDs can also be controlled, and more information about synthesis parameters can be found in the literature [92]. For more information about the types and applications of QDs as biological imaging agents, including for optical imaging technology, please refer to literature [93–96].

To make QDs water soluble, which is important when considering biological applications, QDs are often encapsulated by amphiphilic molecules, such as PEG, triblock copolymers, octylamine-modified polyacrylic acid, oligomeric phosphine and copolymers of alkyl monomers and anhydrides [97]. Functionalization of QDs with several molecules, such as nucleic acids, peptides, proteins, antibodies, and enzymes have been reported [23]. Detailed information regarding QDs' surface modification and conjugation with biomolecules can be found here [23, 98, 99].

Since optical imaging is mainly limited by poor tissue penetration even in the NIR (700- 900 nm) window, QD-based materials have been explored as potential imaging agents for both SPECT and PET. Felber et al. [100] attempted to radiolabel QDs with $[^{99m}Tc(OH_2)_3(CO)_3]^+$ using a new coating ligand containing a terminal thiol group, a PEG linker and 2,3-diaminopropionic acid (DAP) chelator (HS-PEG-DAP) and although the radiolabeling yield was high ($\geq 95\%$), the complex was unstable in serum and coating ligand detachment was found, in which the quantum yield decreased from 10 to 7% after one week. In contrast, Park et al. [101] investigated the possibility of radioiodination of QDs using Bolton-hunter reagent. The authors were able to successfully radiolabeled QDs using

^{125}I-sulfo-SHPP and biodistribution results from gamma counting and SPECT/CT imaging were in agreement with previously published papers [101].

Following a research trend, several studies have been reported indicating that QDs can provide a multifunctional nanoplatform for multimodality imaging and therapy that is especially suitable for synergistic optical/PET imaging combining the sensitivity, quantification and limitless tissue penetration of PET with high resolution and specificity of optical methods [102]. Cai et al. [103] reported the first targeted dual-modality fluorescence/PET probe based on QDs. QDs and RGD-functionalized QDs (RGD-QD) radiolabeled with ^{64}Cu via DOTA, with labeling yields greater than 90% for both. With small-animal PET and NIRF imaging in athymic nude mice, it was possible to observe a relatively high uptake of QDs in the liver, spleen, lymph nodes, and bone marrow. The tumor uptake of the two QD compounds was significantly different at all time points studied, except at 1 h p.i. (Fig. 2.5a). ^{64}Cu–DOTA–QD showed an uptake less than 1%ID/g in the tumor tissue, suggesting low EPR effect, while active targeting (^{64}Cu–DOTA–QD–RGD) lead to a significantly higher tumor uptake (2.2 ± 0.3, 4.0 ± 1.0, and 4.3 ± 0.5%ID/g at 5, 18, and 25 h after injection, respectively) [103]. From that point forward, several other studies have demonstrated the use of radiolabeled QDs for tumor-targeted PET imaging as well as for multi-modality purposes [97, 104–109].

Although the majority of studies make use of chelators, the stability of chelator-based radiolabeled moieties in living animals can be a problem. For example, in the study by Cai et al. [103], PET and NIR fluorescence imaging data of mice injected with ^{64}Cu-labeled NIR QDs, were in good agreement with each other at earlier time points of investigation, after which the distribution of ^{64}Cu (PET) and the QDs (optical imaging) showed significant differences [103, 105]. Therefore, efforts have been made in order to achieve a chelator-free QD radiolabeling strategy. Intrinsic radiolabeling allows a variety of radionuclides to be incorporated into the QDs, such as those of ^{64}Cu, ^{111}In, ^{59}Zn, ^{81}Se and others [18]. Sun et al. [110] designed self-illuminating chelator-free ^{64}Cu radiolabeled QDs, and evaluated their Cerenkov luminescence and PET imaging capability in vivo. Ion exchange between $^{64}Cu^{+}$ and the original cation was used to trap ^{64}Cu into ionic QDs, and nearly 100% radiolabeling yield and high radiostability were achieved. In vivo PET imaging studies in U87MG tumor-bearing mice showed ~5% ID/g uptake in the tumor (1 h p.i.) that increased and peaked to 12.7% ID/g at 17 h p.i and over 10%ID/g remained in the tumor tissue at the 42 h time point. Cerenkov resonance energy transfer (CRET) imaging showed similar pattern with high tumor uptake, suggesting the feasibility of using ^{64}Cu-doped QDs for both CRET and PET imaging (Fig. 2.5b, c). Other papers on intrinsically radiolabeled QDs have been published [18, 20, 111, 112].

While CdSe-based QDs have been widely investigated, their use in the clinical settings is hampered by limitations such as toxicity of Cd ions in the core of QDs, heterogeneous biodistribution profiles and concerns about the metabolism and clearance behavior of the QDs [93]. An interesting paper regarding renal clearance

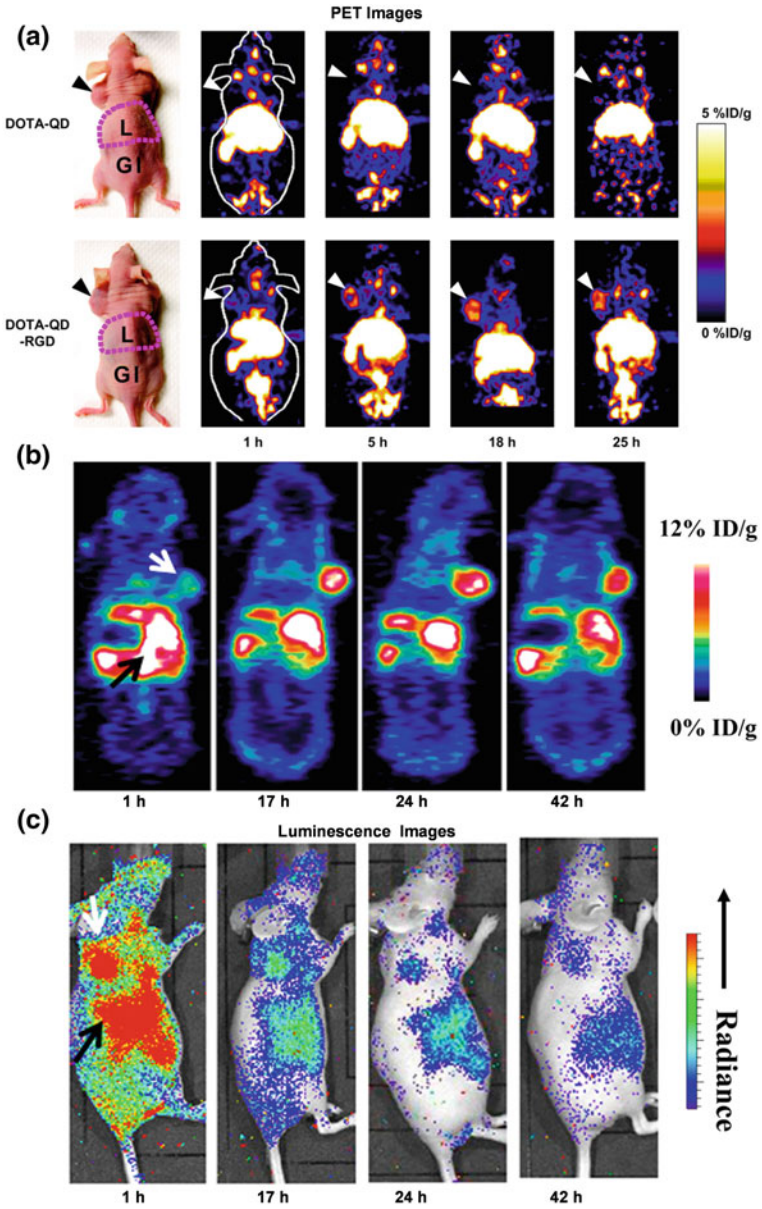

Fig. 2.5 **a** Whole-body coronal PET images of mice at 1, 5, 18, and 25 h after injection of 7–14 MBq of ^{64}Cu- DOTA–QD or DOTA–QD–RGD. **b** Whole-body coronal PET images of U87MG tumor-bearing mice at 1, 17, 24, and 42 h after intravenous injection of 250 μCi of ^{64}Cu-doped QD580. **c** Whole-body luminescence images of U87MG tumor-bearing mice at 1, 17, 24, and 42 h p.i. of 250 μCi of ^{64}Cu-doped QD580 (Ex: Closed; Em: Open). Arrowheads indicate tumors. Adapted with permission [103, 110]

and biocompatibility of QDs has been reported by Choi et al. [113]. Development of biocompatible QDs together with a reduction in QD toxicity can thus accelerate the use of these NPs in tumor imaging improve the possibility of clinical translation.

2.5 Silica Nanoparticles

Since the first report of the use of silica in biological applications [114], silica particles have attracted increasing interest due to their remarkable potential as nanoplatforms for imaging, therapy or both. In fact, Therasphere®, a system composed of silica microspheres associated with Yttrium-90 has been successfully used in the clinic as a therapeutic agent for hepatocellular carcinoma and colon metastasis derived from hepatic cancer [115–117]. More recently, dye-doped ultrasmall silica NPs (SiNPs), called Cornell dots (or C-dots), were approved by the United States Food and Drug Administration (FDA) as an investigational new drug (IND) and have entered clinical investigation in melanoma patients [118]. The C-dots, of around 7 nm in size contain the Cy5 dye enclosed in its interior and the cyclic cRGDY peptide ligands, as well as the isotope ^{124}I attached to its surface. This type of SiNP has shown excellent biological properties such as specific accumulation in tumor tissues with high affinity and avidity in $\alpha_v\beta_3$ integrin-expressing melanomas and the capacity of being renal clearable with relatively high efficiency [118]. In a micro-dosing clinical trial, these Cy5 dye-loaded C dots were labeled with ^{124}I for PET/CT imaging of integrin-expressing lesions. The tracers were well tolerated, exhibited good in vivo stability, reproducible pharmacokinetic signatures consistent with renal clearance, and preferential accumulation at the target site [119].

Unlike many other nanomaterials, SiNPs do not possess a novel property, except for the increase in surface area that is natural to every nanomaterial. SiNPs also do not have any special optical or magnetic properties, such as light absorption or magnetic field interference. However, SiNPs present a major advantage of having very well-defined and easily tunable properties such as crystallinity, size, morphology, and porosity [120]. In addition, chemical groups on the surface of SiNPs allow various well-established functionalization steps granting precise control of drug or chemical loading, PEGylation, conjugation with active targets and, consequently, the modulation of in vivo behavior [121]. Other features including easy and inexpensive synthesis, water dispersibility, high stability and biocompatibility, scalable synthetic availability, large pore volume for efficient and enhanced immobilization/encapsulation of drug molecules or biomolecules makes silica NPs particularly suitable for a diverse range of biological applications [122]. Also, silica is “generally recognized as safe” (ID Code: 14808–60–7) for oral administration by the FDA since 2010, which improves the chances of clinical translation of any SiNP formulation [123].

There are two major types of SiNPs: solid SiNPs (SSiNPs), and mesoporous silica NPs (MSNs) with interior channels and an exterior particle surface, which can

be advantageous over solely solid NPs [124]. These NPs can be synthesized through well-established procedures to produce particles within a narrow size range and nearly uniform composition. More information regarding silica synthesis, parameters control and characterization methods can be found in the literature [121, 125, 126].

Kumar et al. [127] designed SSiNPs conjugated with a near-infrared fluorophore (DY776) and ^{124}I for PET and optical imaging in vivo. The injected NPs showed high sequestration in the spleen (~58%ID/g within 5 min p.i., increasing to 61% ID/g at 24 h), liver (46%ID/g), lungs (from 9.6% to 4.7%ID/g) and kidney (1.93–1.22%ID/g at 24 h p.i.). The clearance studies of the injected NPs indicated that almost all (100%) of the NPs were eliminated via the hepatobiliary pathway by day 15, without any sign of toxicity [127]. Tang et al. [128] reported a simple method to synthesize monodisperse and size-controlled SiNPs for dual modality lymph node imaging. The group showed that when the size of conjugates is as small as 20 nm (ultra-small silica NPs [USSiNPs]), they are rapidly taken by lymph nodes in vivo and investigations of the lymphatic trafficking were carried out using ^{64}Cu-labeled NPs for PET/CT imaging in normal C57BL/6 mice. In the PET/CT images, it is possible to clearly visualize the left popliteal lymph nodes (P-LN) in as early as 12 min p.i..The signal increased rapidly in the left P-LN from 3.5 to 9.8%ID/g at 12 and 62 min p.i. respectively, indicating efficient lymphatic draining of the NPs. The group further demonstrated that the SiNPs could be actively targeted to the lymphatic metastases by being conjugated with a DNA aptamer (AS1411), validating the potential role of SiNPs in the noninvasive tumor staging field [128].

Further improvement in the morphology of SiNPs was achieved by designing hollow MSNs (HMSNs) with a large interstitial cavity and a mesoporous shell [16]. Chen et al. [129], reported the in vivo tumor-targeted PET/NIR fluorescence (NIRF) dual-modality imaging and enhanced drug delivery of HMSNs. As-synthesized HMSNs could load up to 1129.2 mg doxorubicin per gram of HMSN, which was 3–15 times higher previously reported for MSNs. The NPs were radiolabeled with ^{64}Cu using NOTA as a chelator, conjugated with NIR fluorophore ZW800, PEGylated and further conjugated with TRC105, a chimeric monoclonal antibody against CD105, for targeted delivery to CD105 overexpressed on tumor vasculature. Through PET imaging of 4T1 tumor-bearing mice injected with ^{64}Cu-HMSN-ZW800-TRC105, rapid and high tumor accumulation (8.5 ± 1.1%ID/g at 0.5 h p.i.) was observed that peaked at 9.9 ± 0.9%ID/g at 4 h p.i., demonstrating enhanced specific tumor accumulation (Fig. 2.6a) [129]. In contrast, the tumor uptake in mice injected with untargeted tracer (^{64}Cu-HMSN-ZW800) was found to be only one third of the tracer containing TRC105 (Fig. 2.6b) at all the time points examined, suggesting that well-chosen targeting ligands could indeed enhance tumor accumulation of NPs. These data were further confirmed by blocking studies results (Fig. 2.6c) [129].

Schaffer et al. [130] validated the ability of SiNPs to be intrinsically radiolabeled to a vast array of radioisotopes (^{89}Zr, ^{68}Ga, ^{111}In, ^{90}Y, ^{177}Lu, ^{64}Cu), at pH = 7.3, 70 °C and incubation times of up to 1 h. Labeling yields of more than 99% could be obtained, with the labeling characteristics and stability of the binding depending on the oxophilicity and hardness of the radioisotope, respectively [130]. However,

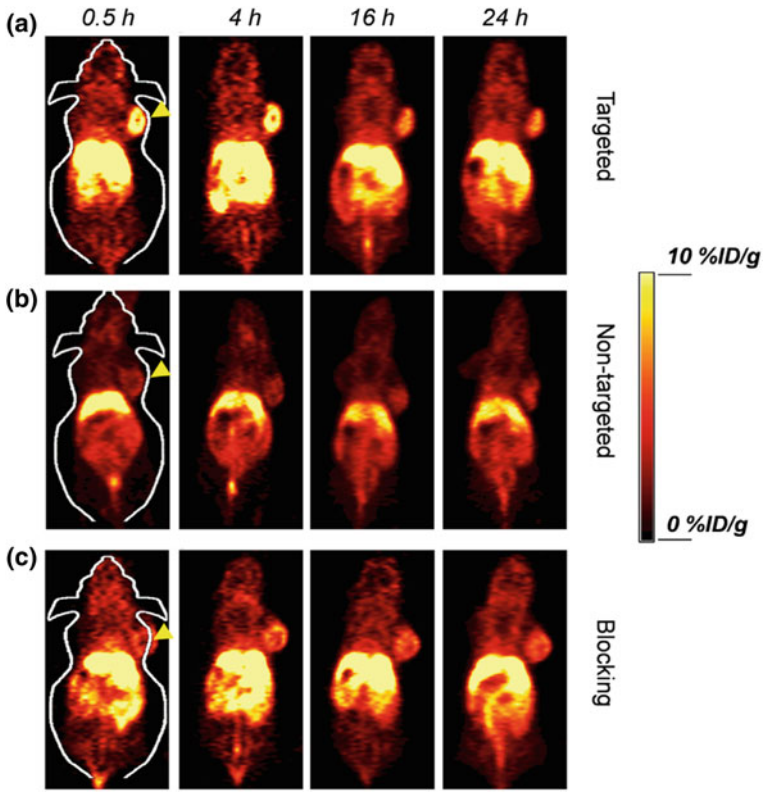

Fig. 2.6 In vivo tumor-targeted PET imaging. Serial coronal PET images of 4T1 tumor-bearing mice at different time-points post-injection of **a** targeted group: ^{64}Cu–NOTA–HMSN–ZW800–TRC105, **b** non-targeted group: ^{64}Cu–NOTA–HMSN–ZW800, or **c** blocking group: ^{64}Cu–NOTA–HMSN–ZW800–TRC105 with a blocking dose (1 mg/mouse) of free TRC105. Tumors are indicated by yellow arrowheads. Reproduced with permission [129]

Chen et al. [131] reported, through in vivo radiostability tests, that chelator-free ^{89}Zr binding to non-porous SiNPs was weak and the isotope detached from the NPs within a day of intravenous administration, with images showing relatively high accumulation in the bones ("free" ^{89}Zr is an osteophile). Interestingly, in the same paper, the authors demonstrated that MSNs, since the mesochannels protected the isotope from transmetallation by intrinsic protein chelators in the body, could be a more reliable platform for radiolabeling oxophilic radiometals when compared to dense SiNPs [131]. The same group synthesized CD105-targeted, dendritic, biodegradable mesoporous silica NPs (bMSNs) with hierarchically organized, spoke-like porous network, that could self-degrade over time [21]. Intrinsic ^{89}Zr labeling demonstrated excellent yields (≈94.7% and 98.6% for CD105-targeted and non-targeted MSNs, respectively). In vivo biodistribution studies in mice with 4T1 xenografts showed a quick accumulation of the the NPs in the targeted group, with

an uptake value of 4.5 ± 0.6%ID/g at 0.5 h p.i that peaked at 6 h p.i. (11.4 ± 2.1% ID/g) and remained in the tumor tissue for up to 48 h p.i. In contrast, the NP tumor uptake based solely on the EPR effect (passive targeting) was approximately three times lower (peaking at 3.6 ± 0.3%ID/g) [21]. Further review on nonporous silica NPs [132], USSiNPs [122] and HMSNs [133] for nanomedicine application can be found elsewhere.

2.6 Other Nanomaterials

2.6.1 Carbon Nanotubes

Carbon nanotubes (CNTs) are hollow-structured nanomaterials made of graphite arranged and ordered in a very precise manner, conferring them with a variety of properties such as ultra-light weight and high aspect ratio. Every carbon atom on the NP surface can serve as a conjugation site for a range of ligands, which can be explored for multifunctionalized biological applications [134]. For that, these nanomaterials, ranging between 1 nm-1 μm, have been employed as optical imaging probes, therapeutic agents and drug nanocarriers [135]. Furthermore, the strong absorption in NIR and far NIR (NIR II) windows (750–1000 and 1000–1700 nm, respectively), allows deep tissue imaging with high resolution, enhanced contrast and minimized autofluorescence and photobleaching, leading to widespread applications in optical and photoacoustic imaging, photothermal imaging and therapy [16]. In addition, CNTs are suitable Raman probes for biological sensing and imaging, owing to their extremely large scattering cross-sections, allowing strong resonance Raman scattering [136]. Wang et al. [137] were the first use a radioisotope (^{125}I) to investigate the biodistribution of CNTs in vivo. Since then, CNTs has been radiolabeled with several radioisotopes such as ^{14}C [138], ^{111}In [139], ^{99m}Tc [140], ^{86}Y [141] and ^{64}Cu [142]. For example, Liu et al. [142] developed ^{64}Cu-DOTA-labeled single-wall carbon nanotubes (^{64}Cu-DOTA-SWNTs) functionalized with PEG and cRGDyk peptide. Results indicated a longer blood circulation, superior hydrophilicity and reduced RES uptake when compared with previously reported studies [143]. Conjugation with the peptide conferred integrin $\alpha_v\beta_3$ specific uptake in U87MG glioblastoma xenografts ($\sim$13% ID/g) (Fig. 2.7a), attributed to the multivalency effect of SWNTs, which was further confirmed by the unique Raman signatures of the nanoprobes [142]. Chelator-free radiolabeling has also been reported, in which alpha-emitters ($^{225}Ac^{3+}$) [144] and positron-emitters ($^{64}Cu^{2+}$) [145] were loaded and confined inside the carbon nanotubes by simple sonication. This radiolabeling method could have the advantage of preventing radioisotope translocation and leakage, by protecting the radioisotopes from transmetallation, and consequent off-target toxicity in vivo. Despite the fact that several groups reported the use of radiolabeled CNTs, the progress in CNT-based probes for nuclear imaging has relatively slowed down in the last few

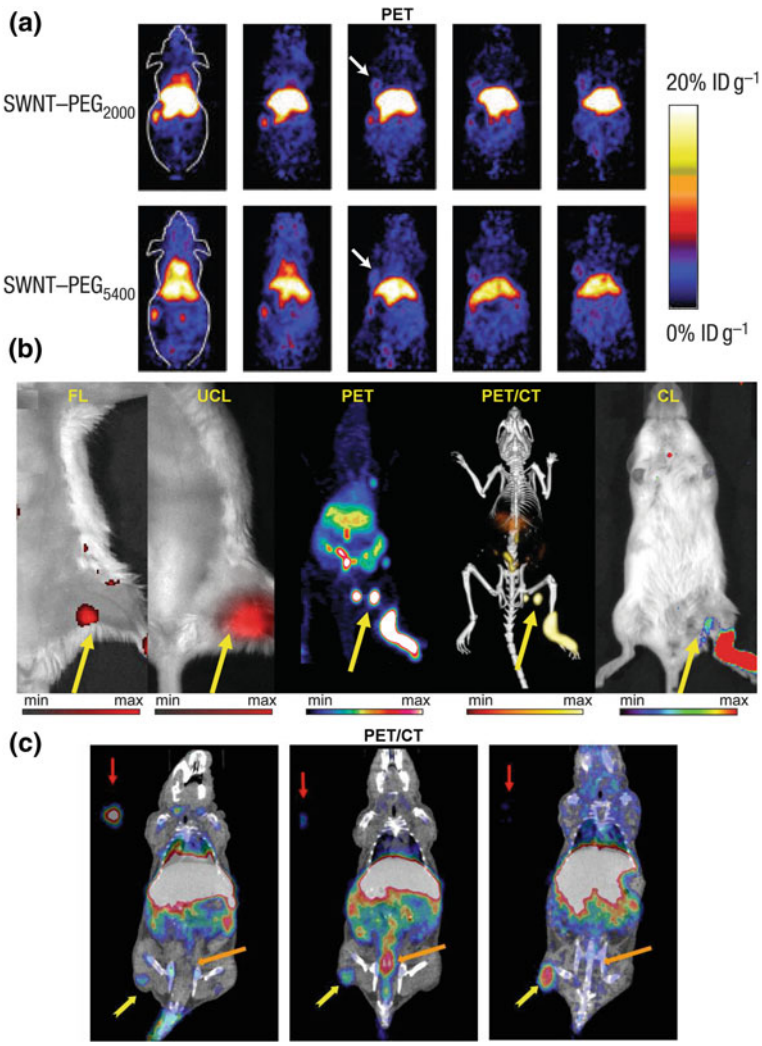

Fig. 2.7 **a** Micro PET images of U87MG tumor-bearing mice post tail-vein injection of ^{64}Cu-labeled SWNT-PEG$_{2000}$ and SWNT-PEG$_{5400}$, respectively. The white arrows point to the tumors. **b** Hexamodal *in vivo* lymphatic imaging using PoP–UCNPs in mice via FL, UCL, PET, PET/CT and Cerenkov luminescence (CL) imaging (photoacoustic imaging not shown). Yellow arrows indicate the location of the lymph nodes (C) Micro-PET/CT images of nude mice-bearing U87MG glioma xenografts acquired at 1, 6, and 24 h after i.v. injection of PEG-[^{64}Cu]CuS NPs. Yellow arrow: tumor; orange arrow: bladder; Red arrow: standard. Adapted with permission [142, 158, 162]

years, attributed possibly to the potential toxicity of carbon nanomaterials over long-term. Nonetheless the development of CNT-based imaging agents still has room to grow when it comes to multimodality nuclear imaging applications [136].

2.6.2 Upconversion Nanoparticles

Upconversion NPs (UCNPs) are a relatively new class of nanomaterials that have been studied for biological applications. UCNPs have numerous features that make them well-suited for therapeutic and diagnostic applications. First, their unprecedented frequency conversion capability is commonly absent in traditional fluorophores [146]. During the upconversion process, the trivalent lanthanide ions, when embedded in a proper inorganic host lattice, sequentially absorb multiple photons in order to produce higher energy anti-Stokes luminescence [147]. In a simpler manner, when UCNPs are excited by a NIR source (e.g., 980 nm), they emit higher-energy photons in the ultraviolet (UV) to NIR range. Furthermore, they present other several advantages such as negligible autofluorescence background, high resistance to photo-bleaching, deeper tissue penetration and less light scattering [148]. The basic structure of UCNPs consists of an inorganic host matrix (fluorides, oxides, heavy halides etc.), a sensitizer (to enhance UCL efficiency; Yb^{3+}) and an emitter (Er^{3+}, Tm^{3+} and Ho^{3+} dopant ions). Doping is a commonly used method to incorporate different functional lanthanide (Ln) ions in the NPs to achieve multifunctional properties. UCNPs doped with Gd is an example of a tracer agent that has been used both for MRI and optical imaging [149]. Moreover, another theranostic application of UCNPs relies on the combination of photoluminescence (PL) imaging with other imaging modalities besides MRI, such as computed tomography (CT) [150], SPECT [151] and PET [152]. Although only a few studies have been reported so far, UCNPs have been radiolabeled with ^{68}Ga [153], ^{64}Cu [154] and ^{124}I [155] through a chelator-based method and with ^{153}Sm [156] and ^{18}F [157] through a chelator-free radiolabeling strategy. In an interesting study, Rieffel et al. [158], demonstrated the ability of UCNPs as multiplexing imaging agents, in which a hexamodal porphyrin-phospholipid-coated UCNP (PoP-UCNP) system was developed. A simple incubation post-labeling method was carried out by making use of the high affinity of copper for porphyrins resulting in >80% labeling yield. ^{64}Cu radiolabeled PEGylated PoP-UCNPs could then be used for fluorescence, NIR-to-NIR UCL, PET, CT, Cerenkov luminescence, and photoacoustic tomography (PAT) for in vivo lymphatic mapping (Fig. 2.7b). Altogether, these studies show the vastly improved imaging potential of simple yet higher-order upconversion NPs for multimodality imaging [158].

2.6.3 Copper Sulfide Nanoparticles

With different types of inorganic nanomaterials available, copper sulfide (CuS) NPs have become an appealing choice because of their good biocompatibility, low toxicity and reasonable price. In addition, unlike the Au-mediated materials, the p-type semiconductor CuS possesses a d-d transition band showing NIR absorption (700–1100 nm) and, thus, does not depend on the dielectric constant

of the surrounding medium [159]. With this inherent characteristic, CuS NPs are able to absorb light in the NIR region and directly convert it to thermal energy to be used in thermal ablation of tumor cells. Recently, CuS NPs, with advantages of high stability and high photothermal conversion efficiency, are being highlighted as promising multifunctional agents that can integrate both imaging and therapy [160]. More specifically for nuclear imaging, a prudent approach to utilize low specific activity ^{64}Cu for PET imaging is to synthesize intrinsically radiolabeled NPs using a radioactive precursor ($^{64}CuCl_2$ solution). Adopting this strategy, ^{64}Cu atoms are built inside the crystal lattice of the normal nanocrystals, resulting in high radiochemical stability. Intrinsically radiolabeled ^{64}CuS NPs are one such class of nanoplatforms, which can easily be prepared by metathesis reaction of $^{64}CuCl_2$ and Na_2S. The simplicity of the procedure allows synthesis of clinically relevant doses of the radioactive ^{64}CuS NPs in an adequately shielded facility with minimum radiation exposure to the personnel involved [161]. Zhou et al. [162], for instance, synthesized ~11 nm diameter [^{64}Cu]CuS NPs to be used not only for PET/CT imaging but also for photothermal ablation purposes. PEGylated [^{64}Cu]CuS NPs, exhibited high radiolabeling efficiency and stability, even without the use of any chelators. A high tumor uptake was found for these NPs in a U87MG human glioblastoma tumor model, as a result of passive targeting (Fig. 2.7c). Signs of hyperthermia-induced necrosis (e.g., loss of nucleus, cell shrinkage etc.) were seen in tumor tissue as a consequence to NIR laser irradiation. In general, this proof-of-concept study revealed the potential of CuS NPs to act as a promising multifunctional moiety for image-guided photothermal ablation of cancer [162].

2.6.4 Others

Zinc oxide (ZnO) NPs of a wide variety of nanostructures and miscellaneous semiconducting, optical, and piezoelectric properties, have also been used for biomedical purposes, especially due its the low toxicity and biodegradability property, as Zn^{2+} itself is an intrinsic element in a healthy adult involved in various involved in various aspects of metabolism [163]. Owing to its intrinsic fluorescence, ZnO NPs have been used for not only optical imaging [164], but also for bioimaging techniques such as MRI [165] and PET [166]. Novel red fluorescent ZnO NPs were developed by Hong et al. [166] followed by successful conjugation of ^{64}Cu and TRC105 to these ZnO NPs. PET scans following the injection of [^{64}Cu] NOTA-–ZnO–PEG–TRC105 in 4T1 tumor-bearing mice revealed a high radioactivity accumulation in the tumor, liver, and the abdominal area. However, other tissues exhibited negligible accumulation leading to good tumor imaging contrast [166].

Recently, a few groups have found that atomically thin transitional metal dichalcogenides (TMDCs) nanosheets are also promising in the biomedical field [167]. Chou et al. discovered that sulfur-terminated molecules could be used to modify MoS_2 nanosheets to acquire better physiological stability and

biocompatibility [168]. Applying their high absorbance in the NIR region, MoS_2 [167], WS_2 [169], and Bi_2Se_3 [170] nanosheets have been utilized in photothermal therapy of cancers. In a noteworthy study performed by Cheng et al. [171], $FeSe_2$-decorated Bi_2Se_3 nanosheets were developed for theranostic purposes, combining four imaging modalities together with photothermal and radiotherapeutic properties. $FeSe_2$ NPs were gradually converted into Bi_2Se_3 nanosheets, with the addition of $Bi(NO_3)_3$ and further functionalized with PEG. ^{64}Cu labeling was straightforwardly executed by mixing $^{64}CuCl_2$ with $FeSe_2/Bi2Se_3$–PEG at 37 °C for 1 h under constant shaking, resulting in a labeling yield of 95%. Taking advantage of the increased r_2 relaxivity of $FeSe_2$, the X-ray attenuation capability of Bi_2Se_3 and its NIR optical absorbance, together with the chelator-free radiolabeling with ^{64}Cu, in vivo multimodal imaging using four different imaging modalities (MR/CT/PA/PET) was performed showing efficient tumor uptake of the nanosystem. Similarly, a tetramodal (PET/MR/PAT/PTT), ^{64}Cu labeled theranostic agent based on iron oxide decorated self-assembled MoS_2 nanosheets was developed by the same group, in which strong PAT signals and clear darkening effects in T_2 weighted MR images indicated passive tumor retention of the nanoconstructs. PET imaging was also carried out demonstrating the feasibility of visualizing in vivo tumor (approximately 6%ID/g accumulation) with this moiety. Furthermore, after 14 days of i.v. injection of the nanosystem and irradiation with 808 nm laser, complete tumor resection was observed [172]. These studies emphasize the potential of using transitional metal dichalcogenides for multimodal image-guided cancer therapy.

Another emerging example of novel NPs for molecular imaging was reported by Ai et al. [173] and Zhan et al. [174], utilizing Gd_2O_2S:Eu nanophosphors for dual-modality imaging. Radioluminescent lanthanide-doped nanophosphors (RLNPs), such as the Eu^{3+} doped gadolinium oxysulfides used in these reports, have gained increased attention in the biological imaging field due to their unique properties such as high photochemical stability, adjustable fluorescence emission, low photobleaching and large Stokes shift [175]. $Gd_2O_2S:Eu^{3+}$ NPs are strongly UV or X-rays absorbers, and because of their re-emission of red light with a high quantum yield, they are suitable to be used as optical luminescent and radioluminescent (RL) agents [176]. This type of nanomaterial can also be used as an MRI contrast agent due to strong transverse relaxivity of Gd [177]. With that in mind, in the study performed by Ai et al173], Gd_2O_2S:Eu NPs of approximately 13 nm in size were synthesized and chelator free radiolabeled with ^{89}Zr, by taking advantage of the oxophilic nature of the isotope and the plenty O_2^- donors on the NP surface leading to a NP concentration, pH and temperature dependent labeling yield of ~43% at pH 7–8 and ~76% at pH 9–10. A proximity between the scintillation source and the emitter allowed an improved in vivo RL efficiency. The study results underline the ability in using these nanophosphors in integrated multimodal PET/RL/MR studies.

A summary of the NPs and references can be found in Table 2.1. For a complete and in-depth review of multifunctional radiolabeled NPs for imaging or therapy, please refer to the following papers [2, 22, 27, 178–182].

Table 2.1 Summary of radiolabeled inorganic nanoparticles employed for in vivo molecular imaging

Type of nanoparticle	Radioisotope	Labeling method	Imaging modality	References
Iron oxide NPs	^{99m}Tc	Chelator-based	SPECT/MRI	[36]
	^{125}I		SPECT	[37]
	^{131}I			[38, 39]
	^{111}In			[40, 41]
	^{188}Re			[42]
	^{64}Cu		PET/CT/MRI	[44, 45, 46]
	^{68}Ga		PET/MRI	[47]
	^{18}F		PET/CT/MRI/FL	[48]
	^{89}Zr	Chelator-free	PET/CT	[49]
	^{69}Ge		PET/MRI	[50]
	^{72}As		PET/MRI	[52]
	^{51}Cr		SPECT	[183]
Gold NPs	^{99m}Tc	Chelator-based	SPECT/CT	[66]
	^{89}Zr		PET	[71]
	^{64}Cu		PET/CT	[69, 70]
		Chelator-free	PET/CT	[68, 73]
	^{198}Au		SPECT/FL	[70]
	^{111}In		SPECT/CT	[184]
Quantum dots	^{99m}Tc	Chelator-based	SPECT	[100]
	^{125}I		SPECT/CT	[101]
	^{64}Cu		PET/FL	[103]
	^{18}F			[104]
	^{64}Cu	Chelator-free	PET/CL	[110]
	^{65}Zn		SPECT	[183]
	^{111}In		SPECT/FL	[185]
	^{109}Cd			[18]
	^{125m}Te		SPECT/CT/FL	[186]
Silica NPs	^{124}I	Chelator-based	PET/CT	[119]
	^{64}Cu			[128, 129]
		Chelator-free		[130]
	^{68}Ga			[130]
	^{89}Zr			[130, 131, 21]
	^{111}In			[130]
	^{90}Y			[115–117, 130]

(continued)

Table 2.1 (continued)

Type of nanoparticle	Radioisotope	Labeling method	Imaging modality	References
Carbon nanotubes	^{125}I	Chelator-based	SPECT/CT	[137]
	^{99m}Tc			[138]
	^{111}In			[139]
	^{14}C		PET/CT	[140]
	^{86}Y			[141]
	^{64}Cu			[142]
		Chelator-free		[145]
	^{225}Ac			[144]
Upconversion NPs	^{68}Ga	Chelator-based	PET/CT	[153]
	^{64}Cu			[154]
	^{124}I			[155]
	^{18}F	Chelator-free		[157]
	^{64}Cu		PET/CT/FL/Cerenkov Luminescence/PAT	[158]
	^{153}Sm		SPECT/CT	[156]
				[151]
CuS NPs	^{64}Cu		PET/CT	[162]
ZnO NPs		Chelator-based	PET/CT/FL	[166]
MoS_2/$FeSe_2$/Bi_2Se_3		Chelator-free	PET/CT/MRI/PAT	[171, 172]
Gd_2O_2S:Eu NPs	^{89}Zr		PET/CT/RL/MRI	[173, 174]

2.7 Conclusion and Future Perspectives

In a broad sense, it is possible to ascertain the major role of nuclear molecular imaging, specifically PET and SPECT, in the diagnosis and management of tumor processes at the molecular and cellular levels. It also allows noninvasive visualization and monitoring of therapeutic responses and disease progression. Furthermore, molecular imaging has the advantage of allowing in vivo characterization of the genetic changes involved oncogenesis, holding a predictive capability for selection of optimal molecular therapeutic regimes, promising the best outcomes, on a per-case basis (i.e., personalized medicine). In both SPECT and PET, the intensity of the imaging signal is proportional to the amount of the tracer and the ability to image physiological and functional processes, guided by the pharmacokinetics and biodistribution of the radiotracer, which provides vital information not available from conventional imaging techniques. However, insufficient signal intensity, lack of stability, nonspecific interactions, and low circulation half-life are still limitations that must be overcome. With that in mind, NPs may serve as the

carriers needed for enhancing the delivery of radionuclides, as well as therapeutic agents to the tumor sites, thus enhancing imaging and therapeutic efficacy. Inorganic NPs, more specifically, offer unique sizes, high surface-to-volume ratio and physiochemical properties that allow the conjugation of several therapeutic and diagnostic agents, including radiotracers, through distinct synthetic strategies. Their controllably designed surface chemistry can also enhance its targeting to disease sites using a wide variety of probes as well as its tailorability to be adapted for multipurpose applications.

Indubitably, the radiotracer plays a major role in the success of diagnostic accuracy optimization. An ideal nanosystem must have no toxicity, be targeted with optimal selectivity and specifically accumulate in the desired tissue with a high signal-to-noise ratio, must have improved in vivo pharmacokinetics with negligible accumulation in the RES organs and rapid and complete clearance from the body. For that, the selection of both the isotope and the targeted carrier are of major importance. In addition to a large amount of types of NPs being employed for this purpose, a wide range of radioisotopes and labeling methods have also been developed. Although, in the early years of development of molecular imaging agents using NPs, SPECT radioisotopes, such as ^{99m}Tc, seemed to be the choice of a majority of the reports, this pattern is rapidly changing due to a larger availability of PET isotopes and established radiolabeling procedures, which coordinates with the tendency, of migrating to PET in the clinical settings, because of its superior sensitivity and resolution of PET when compared to SPECT technique. Despite the advances in the last decades, clinical translation of NP-based systems is still challenging, especially due to the intrinsic heterogeneity of human tumors, both genetically and phenotypically, as well as the fact that intra-tumoral distribution of NPs is influenced by several different factors such as interstitial fluid pressure, blood flow, diffusion and stroma thickness, which leads to variable and unpredictable tumor permeability. Thus, efforts from the scientific community, as well as funding and regulatory authorities, must be undertaken to harness the full potential of nanotheranostic moieties in the clinical settings.

Acknowledgements This work was supported, in part, by the University of Wisconsin — Madison, the National Institutes of Health (NIBIB/NCI 1R01CA169365, 1R01EB021336, P30CA014520), the American Cancer Society (125246-RSG-13-099-01-CCE) and CNPq (Brazilian National Council for Scientific and Technological Development).

References

1. S. Same, A. Aghanejad, S. Akbari Nakhjavani, J. Barar, Y. Omidi, Radiolabeled theranostics: magnetic and gold nanoparticles. Bioimpacts **6**, 169–181 (2016)
2. G. Ting, C.H. Chang, H.E. Wang, T.W. Lee, Nanotargeted radionuclides for cancer nuclear imaging and internal radiotherapy. J. Biomed. Biotechnol. (2010)
3. S.M. Moghimi, A.C. Hunter, J.C. Murray, Nanomedicine: current status and future prospects. FASEB J. **19**, 311–330 (2005)

4. V. Mailander, K. Landfester, Interaction of nanoparticles with cells. Biomacromol **10**, 2379–2400 (2009)
5. C. Fang, M. Zhang, Multifunctional magnetic nanoparticles for medical imaging applications. J. Mater. Chem. **19**, 6258–6266 (2009)
6. A.B. de Barros, A. Tsourkas, B. Saboury, V.N. Cardoso, A. Alavi, Emerging role of radiolabeled nanoparticles as an effective diagnostic technique. EJNMMI Res. **2**, 39 (2012)
7. S. Parveen, R. Misra, S.K. Sahoo, Nanoparticles: a boon to drug delivery, therapeutics, diagnostics and imaging. Nanomedicine **8**, 147–166 (2012)
8. H. Nehoff, N.N. Parayath, L. Domanovitch, S. Taurin, K. Greish, Nanomedicine for drug targeting: strategies beyond the enhanced permeability and retention effect. Int. J. Nanomed. **9**, 2539–2555 (2014)
9. S.L. Bellis, Biomaterials Advantages of RGD peptides for directing cell association with biomaterials. Biomaterials **32**, 4205–4210 (2011)
10. A.L. de Barros, L.G. das Mota, C.A. de Ferreira, M.C. de Oliveira, A.M. de Goes, Cardoso VN. Bombesin derivative radiolabeled with technetium-99 m as agent for tumor identification. Bioorg. Med. Chem. Lett. **20**, 6182–6184
11. A.L. Daugherty, R.J. Mrsny, Formulation and delivery issues for monoclonal antibody therapeutics. Adv. Drug Deliv. Rev. **58**, 686–706 (2006)
12. A. Garcia-Bennett, M. Nees, B. Fadeel, In search of the holy grail: Folate-targeted nanoparticles for cancer therapy. Biochem. Pharmacol. **81**, 976–984 (2011)
13. J.H. Lee, M.V. Yigit, D. Mazumdar, Y. Lu, Molecular diagnostic and drug delivery agents based on aptamer-nanomaterial conjugates. Adv. Drug Deliv. Rev. **62**, 592–605 (2010)
14. K. Knop, R. Hoogenboom, D. Fischer, U.S. Schubert, Poly(ethylene glycol) in drug delivery: pros and cons as well as potential alternatives. Angew. Chem. Int. Ed. Engl. **49**, 6288–6308 (2010)
15. J.V. Jokerst, T. Lobovkina, R.N. Zare, S.S. Gambhir, Nanoparticle PEGylation for imaging and therapy. Nanomedicine (London) **6**, 715–728 (2011)
16. S. Goel, C.G. England, F. Chen, W. Cai, Positron emission tomography and nanotechnology: a dynamic duo for cancer theranostics. Adv. Drug Deliv. Rev. **113**, 157–176 (2016)
17. D. Sarko, M. Eisenhut, U. Haberkorn, W. Mier, Bifunctional chelators in the design and application of radiopharmaceuticals for oncological diseases. Curr. Med. Chem. **19**, 2667–2688 (2012)
18. M. Sun, D. Hoffman, G. Sundaresan, L. Yang, N. Lamichhane, J. Zweit, Synthesis and characterization of intrinsically radiolabeled quantum dots for bimodal detection. Am. J. Nucl. Med. Mol. Imaging **2**, 122–135 (2012)
19. S. Goel, F. Chen, E.B. Ehlerding, W. Cai, Intrinsically radiolabeled nanoparticles: an emerging paradigm. Small **10**, 3825–3830 (2014)
20. W. Cai, H. Hong, In a "nutshell": intrinsically radio-labeled quantum dots. Am. J. Nucl. Med. Mol. Imaging **2**, 136–140 (2012)
21. S. Goel, F. Chen, S. Luan, H.F. Valdovinos, S. Shi, S.A. Graves et al., Engineering intrinsically zirconium-89 radiolabeled self-destructing mesoporous silica nanostructures for in vivo biodistribution and tumor targeting studies. Adv. Sci. **3**, 1600122 (2016)
22. H.Y. Yoon, S. Jeon, D.G. You, J.H. Park, I.C. Kwon, H. Koo et al., Inorganic nanoparticles for image-guided therapy. Bioconjug. Chem. **28**(1), 124–134 (2017)
23. J. Conde, J.T. Dias, V. Grazú, M. Moros, P.V. Baptista, J.M. de la Fuente, Revisiting 30 years of biofunctionalization and surface chemistry of inorganic nanoparticles for nanomedicine. Front. Chem. **2**, 48 (2014)
24. M. Longmire, P.L. Choyke, H. Kobayashi, Clearance properties of nano-sized particles and molecules as imaging agents: considerations and caveats. Nanomedicine (London) **3**, 703–717 (2008)
25. T.F. Massoud, S.S. Gambhir, Molecular imaging in living subjects: seeing fundamental biological processes in a new light. Genes Dev. **17**, 545–580 (2003)

26. V.I. Shubayev, T.R. Pisanic 2nd, S. Jin, Magnetic nanoparticles for theragnostics. Adv. Drug Deliv. Rev. **61**, 467–477 (2009)
27. Y. Xing, J. Zhao, P.S. Conti, K. Chen, Radiolabeled nanoparticles for multimodality tumor imaging. Theranostics **4**(3), 290–306 (2014)
28. P. Bouziotis, D. Psimadas, T. Tsotakos, D. Stamopoulos, C. Tsoukalas, Radiolabeled iron oxide nanoparticles as dual-modality SPECT/MRI and PET/MRI agents. Curr. Top. Med. Chem. **12**, 2694–2702 (2012)
29. Y.-X.J. Wang, Superparamagnetic iron oxide based MRI contrast agents: Curr. Status Clin Appl. Quant Imaging Med. Surg. **1**, 35–40 (2011)
30. M.G. Harisinghani, J. Barentsz, P.F. Hahn, W.M. Deserno, S. Tabatabaei, C.H. van de Kaa et al., Noninvasive detection of clinically occult lymph-node metastases in prostate cancer. N. Engl. J. Med. **348**, 2491–2499 (2003)
31. F.M. Kievit, M. Zhang, Surface engineering of iron oxide nanoparticles for targeted cancer therapy. Acc. Chem. Res. **44**, 853–862 (2011)
32. M.S. Judenhofer, H.F. Wehrl, D.F. Newport, C. Catana, S.B. Siegel, M. Becker et al., Simultaneous PET-MRI: a new approach for functional and morphological imaging. Nat. Med. **14**, 459–465 (2008)
33. F. Ai, C.A. Ferreira, F. Chen, W. Cai, Engineering of radiolabeled iron oxide nanoparticles for dual-modality imaging. Wiley Interdiscip Rev Nanomed Nanobiotechnol. **8**(4), 619–630 (2016)
34. M.S. Judenhofer, S.R. Cherry, Applications for preclinical PET/MRI. Semin. Nucl. Med. **43**, 19–29 (2013)
35. H. Zaidi, A. Del Guerra, An outlook on future design of hybrid PET/MRI systems. Med. Phys. **38**, 5667–5689 (2011)
36. R. Madru, P. Kjellman, F. Olsson, K. Wingardh, C. Ingvar, F. Stahlberg et al., ^{99m}Tc-labeled superparamagnetic iron oxide nanoparticles for multimodality SPECT/MRI of sentinel lymph nodes. J. Nucl. Med. **53**, 459–463 (2012)
37. Y. Tang, C. Zhang, J. Wang, X. Lin, L. Zhang, Y. Yang et al., MRI/SPECT/Fluorescent tri-Modal probe for evaluating the homing and therapeutic efficacy of transplanted mesenchymal stem cells in a rat ischemic stroke model. Adv. Funct. Mater. **25**, 1024–1034 (2015)
38. J. Chen, S. Zhu, L. Tong, J. Li, F. Chen, Y. Han et al., Superparamagnetic iron oxide nanoparticles mediated ^{131}I-hVEGF siRNA inhibits hepatocellular carcinoma tumor growth in nude mice. BMC Cancer **14**, 114 (2014)
39. S.I. Park, B.J. Kwon, J.H. Park, H. Jung, K.H. Yu, Synthesis and characterization of 3-[^{131}I] iodo-L-tyrosine grafted Fe_3O_4@SiO_2 nanocomposite for single photon emission computed tomography (SPECT) and magnetic resonance imaging (MRI). J. Nanosci. Nanotechnol. **11**, 1818–1821 (2011)
40. H. Zolata, F. Abbasi Davani, H. Afarideh, Synthesis, characterization and theranostic evaluation of Indium-111 labeled multifunctional superparamagnetic iron oxide nanoparticles. Nucl. Med. Biol. **42**, 164–170 (2015)
41. H. Wang, R. Kumar, D. Nagesha, R.I. Duclos, S. Sridhar, S.J. Gatley, Integrity of ^{111}In-radiolabeled superparamagnetic iron oxide nanoparticles in the mouse. Nucl. Med. Biol. **42**, 65–70 (2015)
42. J. Cao, Y. Wang, J. Yu, J. Xia, C. Zhang, D. Yin et al., Preparation and radiolabeling of surface-modified magnetic nanoparticles with rhenium-188 for magnetic targeted radiotherapy. J. Magn. Mater. **277**, 165–174 (2004)
43. R. Thomas, I.-K. Park, Y. Jeong, Magnetic iron oxide nanoparticles for multimodal imaging and therapy of cancer. Int. J. Mol. Sci. **14**, 15910–15930 (2013)
44. B.R. Jarrett, B. Gustafsson, D.L. Kukis, A.Y. Louie, Synthesis of ^{64}Cu-labeled magnetic nanoparticles for multimodal imaging. Bioconjug. Chem. **19**, 1496–1504 (2008)

45. X. Yang, H. Hong, J.J. Grailer, I.J. Rowland, A. Javadi, S.A. Hurley et al., cRGD-functionalized, DOX-conjugated, and ^{64}Cu-labeled superparamagnetic iron oxide nanoparticles for targeted anticancer drug delivery and PET/MR imaging. Biomaterials **32**, 4151–4160 (2011)
46. R.T.M. de Rosales, R. Tavaré, R.L. Paul, M. Jauregui-Osoro, A. Protti, A. Glaria et al., Synthesis of ^{64}Cu(II)–Bis(dithiocarbamatebisphosphonate) and its conjugation with superparamagnetic iron oxide nanoparticles: In vivo evaluation as dual-modality PET–MRI agent. Angew. Chem. Int. Ed. Engl. **50**, 5509–5513 (2011)
47. S. Kim, M.K. Chae, M.S. Yim, I.H. Jeong, J. Cho, C. Lee et al., Hybrid PET/MR imaging of tumors using an oleanolic acid-conjugated nanoparticle. Biomaterials **34**, 8114–8121 (2013)
48. N.K. Devaraj, E.J. Keliher, G.M. Thurber, M. Nahrendorf, R. Weissleder, ^{18}F labeled nanoparticles for in vivo PET-CT imaging. Bioconjug. Chem. **20**, 397–401 (2009)
49. E. Boros, A.M. Bowen, L. Josephson, N. Vasdev, J.P. Holland, Chelate-free metal ion binding and heat-induced radiolabeling of iron oxide nanoparticles. Chem Sci. **6**, 225–236 (2015)
50. R. Chakravarty, H.F. Valdovinos, F. Chen, C.M. Lewis, P.A. Ellison, H. Luo et al., Intrinsically germanium-69-labeled iron oxide nanoparticles: synthesis and in-vivo dual-modality PET/MR zimaging. Adv. Mater. **26**, 5119–5123 (2014)
51. X. Cui, S. Belo, D. Kruger, Y. Yan, R.T.M. de Rosales, M. Jauregui-Osoro et al., Aluminium hydroxide stabilised $MnFe_2O_4$ and Fe_3O_4 nanoparticles as dual-modality contrasts agent for MRI and PET imaging. Biomaterials **35**, 5840–5846 (2014)
52. F. Chen, P.A. Ellison, C.M. Lewis, H. Hong, Y. Zhang, S. Shi et al., Chelator-free synthesis of a dual-modality PET/MRI agent. Angew. Chem. Int. Ed. Engl. **52**, 13319–13323 (2013)
53. R.A. Sperling, P. Rivera Gil, F. Zhang, M. Zanella, W.J. Parak, Biological applications of gold nanoparticles. Chem. Soc. Rev. **37**, 1896–1908 (2008)
54. W. Cai, T. Gao, H. Hong, J. Sun, Applications of gold nanoparticles in cancer nanotechnology. Nanotechnol. Sci. Appl. **1**, 17–32 (2008)
55. J. Turkevich, P.C. Stevenson, J. Hillier, A study of the nucleation and growth processes in the synthesis of colloidal gold. Discuss. Faraday Soc. **11**, 55–75 (1951)
56. N. Khlebtsov, L. Dykman, Biodistribution and toxicity of engineered gold nanoparticles: a review of in vitro and in vivo studies. Chem. Soc. Rev. **40**, 1647–1671 (2011)
57. D. Goia, E. Matijević, Tailoring the particle size of monodispersed colloidal gold. Colloids Surf. Physicochem. Eng. Asp. **146**, 139–152 (1999)
58. R. Herizchi, E. Abbasi, M. Milani, A. Akbarzadeh, Current methods for synthesis of gold nanoparticles. Artif. Cells Nanomed. Biotechnol. **44**, 596–602 (2016)
59. C.J. Murphy, A.M. Gole, J.W. Stone, P.N. Sisco, A.M. Alkilany, E.C. Goldsmith et al., Gold nanoparticles in biology: beyond toxicity to cellular imaging. Acc. Chem. Res. **41**, 1721–1730 (2008)
60. S. Mallidi, T. Larson, J. Aaron, K. Sokolov, S. Emelianov, Molecular specific optoacoustic imaging with plasmonic nanoparticles. Opt. Express **15**, 6583–6588 (2007)
61. J.K. Young, E.R. Figueroa, R.A. Drezek, Tunable nanostructures as photothermal theranostic agents. Ann. Biomed. Eng. **40**, 438–459 (2012)
62. X. Huang, M.A. El-Sayed, Gold nanoparticles: Optical properties and implementations in cancer diagnosis and photothermal therapy. J. Adv. Res. **1**, 13–28 (2010)
63. X. Huang, P.K. Jain, I.H. El-Sayed, M.A. El-Sayed, Plasmonic photothermal therapy (PPTT) using gold nanoparticles. Lasers Med. Sci. **23**, 217 (2007)
64. N. Zhao, Y. Pan, Z. Cheng, H. Liu, Gold nanoparticles for cancer theranostics: a brief update. J. Innov. Opt. Health Sci. **9**, 1–10 (2016)
65. M. Das, K.H. Shim, S.S.A. An, D.K. Yi, Review on gold nanoparticles and their applications. Toxicol. Environ. Health Sci. **3**, 193–205 (2011)
66. B.E. Ocampo-García, F.M. de Ramírez, G. Ferro-Flores, L.M. De León-Rodríguez, C.L. Santos-Cuevas, E. Morales-Avila et al., ^{99m}Tc-labeled gold nanoparticles capped with HYNIC-peptide/mannose for sentinel lymph node detection. Nucl. Med. Biol. **38**, 1–11 (2011)

67. Y. Xing, J. Zhao, X. Shi, P.S. Conti, K. Chen, Recent development of radiolabeled nanoparticles for PET imaging. Austin J. Nanomed. Nanotechnol. **2**, 1016 (2014)
68. H. Xie, Z.J. Wang, A. Bao, B. Goins, W.T. Phillips, In vivo PET imaging and biodistribution of radiolabeled gold nanoshells in rats with tumor xenografts. Int. J. Pharm. **395**, 324–330 (2010)
69. F. Chen, S. Goel, R. Hernandez, S.A. Graves, S. Shi, R.J. Nickles et al., Dynamic positron emission tomography imaging of renal clearable gold nanoparticles. Small **12**, 2775–2782 (2016)
70. C. Zhou, G. Hao, P. Thomas, J. Liu, M. Yu, S. Sun et al., Near-infrared emitting radioactive gold nanoparticles with molecular pharmacokinetics. Angew. Chem. Int. Ed. Engl. **51**, 10118–10122 (2012)
71. L. Karmani, D. Labar, V. Valembois, V. Bouchat, P.G. Nagaswaran, A. Bol et al., Antibody-functionalized nanoparticles for imaging cancer: influence of conjugation to gold nanoparticles on the biodistribution of ^{89}Zr-labeled cetuximab in mice. Contrast Media Mol. Imaging **8**, 402–408 (2013)
72. T. Aweda, D. Sultan, Y. Liu, Radio-labeled nanoparticles for biomedical imaging, in *Nanotechnology for Biomedical Imaging and Diagnostics*, ed. by Y. Mikhail (Wiley, New York, 2014), pp. 193–221
73. Y. Zhao, D. Sultan, L. Detering, S. Cho, G. Sun, R. Pierce et al., Copper-64-alloyed gold nanoparticles for cancer imaging: Improved radiolabel stability and diagnostic accuracy. Angew. Chem. Int. Ed. Engl. **53**, 156–159 (2014)
74. J. Lipka, M. Semmler-Behnke, R.A. Sperling, A. Wenk, S. Takenaka, C. Schleh et al., Biodistribution of PEG-modified gold nanoparticles following intratracheal instillation and intravenous injection. Biomaterials **31**, 6574–6581 (2010)
75. L. Sun, D. Liu, Z. Wang, Functional gold nanoparticle − peptide Complexes as cell-targeting agents. Langmuir **24**, 10293–10297 (2008)
76. D.J. Javier, N. Nitin, M. Levy, A. Ellington, R. Richards-Kortum, Aptamer-targeted gold nanoparticles as molecular-specific contrast agents for reflectance imaging. Bioconjug. Chem. **19**, 1309–1312 (2008)
77. D.A. Giljohann, D.S. Seferos, A.E. Prigodich, P.C. Patel, C.A. Mirkin, Gene regulation with polyvalent siRNA-nanoparticle conjugates. J. Am. Chem. Soc. **131**, 2072–2073 (2009)
78. R. Marega, L. Karmani, L. Flamant, P.G. Nageswaran, V. Valembois, B. Masereel et al., Antibody-functionalized polymer-coated gold nanoparticles targeting cancer cells: an in vitro and in vivo study. J. Mater. Chem. **22**, 21305–21312 (2012)
79. P.M. Tiwari, K. Vig, V. Dennis, S.R. Singh, Functionalized gold nanoparticles and their biomedical applications. Nanomaterials **1**, 31–63
80. E. Sadauskas, G. Danscher, M. Stoltenberg, U. Vogel, A. Larsen, H. Wallin, Protracted elimination of gold nanoparticles from mouse liver. Nanomedicine **5**, 162–169 (2009)
81. W.-S. Cho, M. Cho, J. Jeong, M. Choi, H.-Y. Cho, B.S. Han et al., Acute toxicity and pharmacokinetics of 13 nm-sized PEG-coated gold nanoparticles. Toxicol. Appl. Pharmacol. **236**, 16–24 (2009)
82. J.F. Dorsey, L. Sun, D.Y. Joh, A. Witztum, G.D. Kao, M. Alonso-Basanta et al., Gold nanoparticles in radiation research: potential applications for imaging and radiosensitization. Transl. Cancer Res. **2**, 280–291 (2013)
83. X. Gao, L. Yang, J.A. Petros, F.F. Marshall, J.W. Simons, S. Nie, In vivo molecular and cellular imaging with quantum dots. Curr. Opin. Biotechnol. **16**, 63–72 (2005)
84. W.C.W. Chan, D.J. Maxwell, X. Gao, R.E. Bailey, M. Han, S. Nie, Luminescent quantum dots for multiplexed biological detection and imaging. Curr. Opin. Biotechnol. **13**, 40–46 (2002)
85. Y. Ghasemi, P. Peymani, S. Afifi, Quantum dot: magic nanoparticle for imaging, detection and targeting. Acta Biomed. **80**, 156–165 (2009)
86. M.J. Bruchez, M. Moronne, P. Gin, S. Weiss, A.P. Alivisatos, Semiconductor nanocrystals as fluorescent biological labels. Science **281**, 2013–2016 (1998)

87. K.-H. Lee, Quantum dots: a quantum jump for molecular imaging? J. Nucl. Med. **48**, 1408–1410 (2007)
88. L.A. Bentolila, X. Michalet, F.F. Pinaud, J.M. Tsay, S. Doose, J.J. Li et al., Quantum dots for molecular imaging and cancer medicine. Discov. Med. **5**, 213–218 (2005)
89. J.K. Jaiswal, H. Mattoussi, J.M. Mauro, S.M. Simon, Long-term multiple color imaging of live cells using quantum dot bioconjugates. Nat. Biotechnol. **21**, 47–51 (2003)
90. I.L. Medintz, H.T. Uyeda, E.R. Goldman, H. Mattoussi, Quantum dot bioconjugates for imaging, labelling and sensing. Nat. Mater. **4**, 435–446 (2005)
91. X. Peng, J. Wickham, A.P. Alivisatos, Kinetics of II-VI and III-V colloidal semiconductor nanocrystal growth: "Focusing" of size distributions. J. Am. Chem. Soc. **120**, 5343–5344 (1998)
92. X. Peng, L. Manna, W. Yang, J. Wickham, E. Scher, A. Kadavanich et al., Shape control of CdSe nanocrystals. Nature **404**, 59–61 (2000)
93. H.-C. Huang, S. Barua, G. Sharma, S.K. Dey, K. Rege, Inorganic nanoparticles for cancer imaging and therapy. J. Control Release **155**, 344–357 (2011)
94. S. Jin, Y. Hu, Z. Gu, L. Liu, H.-C. Wu, Application of quantum dots in biological imaging. J. Nanomater. **2011**, 1–13 (2011)
95. P. Pericleous, M. Gazouli, A. Lyberopoulou, S. Rizos, N. Nikiteas, E.P. Efstathopoulos, Quantum dots hold promise for early cancer imaging and detection. Int. J. Cancer **131**, 519–528 (2012)
96. M. Fang, C.-W. Peng, D.-W. Pang, Y. Li, Quantum dots for cancer research: current status, remaining issues, and future perspectives. Cancer Biol. Med. **9**, 151–163 (2012)
97. H. Zhang, D. Yee, C. Wang, Quantum dots for cancer diagnosis and therapy: biological and clinical perspectives. Nanomedicine (London) **3**, 83–91 (2008)
98. Y. Zhu, H. Hong, Z.P. Xu, Z. Li, W. Cai, Quantum dot-based nanoprobes for in vivo targeted imaging. Curr. Mol. Med. **13**, 1549–1567 (2013)
99. R. Dey, S. Mazumder, M.K. Mitra, S. Mukherjee, G.C. Das, Review: Biofunctionalized quantum dots in biology and medicine. J. Nanomater. **2009**, 1–17 (2009)
100. M. Felber, M. Bauwens, J.M. Mateos, S. Imstepf, F.M. Mottaghy, R. Alberto, ^{99m}Tc radiolabeling and biological evaluation of nanoparticles functionalized with a versatile coating ligand. Chemistry **21**, 6090–6099 (2015)
101. J.J. Park, T.S. Lee, J.H. Kang, E.J. Kim, R.J. Yoo, G.S. Woo et al., SPECT/CT imaging of radiolabeled quantum dots, in *Proceedings of KNS Autumn Meet* (2010), pp. 793–794
102. S. Yang, S. Goel, W. Cai, In vivo molecular imaging with quantum dots: toward multimodality and theranostics, in *Biological and Pharmaceutical Applications of Nanomaterials*, ed. by P. Prokopovich (CRC Press, New York, 2015), pp. 319–346
103. W. Cai, K. Chen, Z.-B. Li, S.S. Gambhir, X. Chen, Dual-function probe for PET and near-infrared fluorescence imaging of tumor vasculature. J. Nucl. Med. **48**, 1862–1870 (2007)
104. F. Ducongé, T. Pons, C. Pestourie, L. Hérin, B. Thézé, K. Gombert et al., Fluorine-18-labeled phospholipid quantum dot micelles for in vivo multimodal imaging from whole body to cellular scales. Bioconjug. Chem. **19**, 1921–1926 (2008)
105. K. Chen, Z.-B. Li, H. Wang, W. Cai, X. Chen, Dual-modality optical and positron emission tomography imaging of vascular endothelial growth factor receptor on tumor vasculature using quantum dots. Eur. J. Nucl. Med. Mol. Imaging **35**, 2235–2244 (2008)
106. C. Tu, X. Ma, A. House, S.M. Kauzlarich, A.Y. Louie, PET imaging and biodistribution of silicon quantum dots in mice. ACS Med. Chem. Lett. **2**, 285–288 (2011)
107. K. Hu, H. Wang, G. Tang, T. Huang, X. Tang, X. Liang et al., In vivo cancer dual-targeting and dual-modality imaging with functionalized quantum dots. J. Nucl. Med. **56**, 1278–1284 (2015)
108. M.L. Schipper, G. Iyer, A.L. Koh, Z. Cheng, Y. Ebenstein, A. Aharoni et al., Particle size, surface coating, and PEGylation influence the biodistribution of quantum dots in living mice. Small **5**, 126–134 (2009)

109. M.L. Schipper, Z. Cheng, S.-W. Lee, L.A. Bentolila, G. Iyer, J. Rao et al., microPET-based biodistribution of quantum dots in living mice. J. Nucl. Med. **48**, 1511–1518 (2007)
110. X. Sun, X. Huang, J. Guo, W. Zhu, Y. Ding, G. Niu et al., Self-illuminating ^{64}Cu-doped CdSe/ZnS nanocrystals for in vivo tumor imaging. J. Am. Chem. Soc. **136**, 1706–1709 (2014)
111. S.J. Kennel, J.D. Woodward, A.J. Rondinone, J. Wall, Y. Huang, S. Mirzadeh, The fate of MAb-targeted Cd^{125m}Te/ZnS nanoparticles in vivo. Nucl. Med. Biol. **35**, 501–514 (2008)
112. S.J. Kennel, J.D. Woodward, A.J. Rondinone, J. Wall, Y. Huang, S. Mirzadeh, The fate of MAb-targeted Cd^{125m}Te/ZnS nanoparticles in vivo. Nucl. Med. Biol. **35**, 501–514 (2008)
113. H.S. Choi, W. Liu, P. Misra, E. Tanaka, J.P. Zimmer, B.I. Ipe et al., Renal clearance of quantum dots. Nat. Biotechnol. **25**, 1165–1170 (2007)
114. M. Vallet-Regi, A. Rámila, R.P. del Real, J. Pérez-Pariente, A new property of MCM-41: drug delivery system. Chem. Mater. **13**, 308–311 (2001)
115. D.M. Coldwell, A.S. Kennedy, C.W. Nutting, Use of yttrium-90 microspheres in the treatment of unresectable hepatic metastases from breast cancer. Int. J. Radiat. Oncol. Biol. Phys. **69**, 800–804 (2007)
116. R. Salem, R.J. Lewandowski, B. Atassi, S.C. Gordon, V.L. Gates, O. Barakat et al., Treatment of unresectable hepatocellular carcinoma with use of ^{90}Y microspheres (TheraSphere): safety, tumor response, and survival. J. Vasc. Interv. Radiol. **16**, 1627–1639 (2005)
117. R.J. Lewandowski, K.G. Thurston, J.E. Goin, C.O. Wong, V.L. Gates, Buskirk M. Van et al., 90Y microsphere (TheraSphere) treatment for unresectable colorectal cancer metastases of the liver: Response to treatment at targeted doses of 135–150 Gy as Measured by [18F] Fluorodeoxyglucose positron emission tomography and Computed Tomographic Imaging. J. Vasc. Interv. Radiol. **16**, 1641–1651 (2005)
118. M. Benezra, O. Penate-medina, P.B. Zanzonico, D. Schaer, H. Ow, A. Burns et al., Multimodal silica nanoparticles are effective cancer-targeted probes in a model of human melanoma. J. Clin. Invest. **121**, 2768–2780 (2011)
119. E. Phillips, O. Penate-Medina, P.B. Zanzonico, R.D. Carvajal, P. Mohan, Y. Ye et al., Clinical translation of an ultrasmall inorganic optical-PET imaging nanoparticle probe. Sci. Transl. Med. **6**, 260ra149 (2014)
120. I.I. Slowing, J.L. Vivero-Escoto, C.-W. Wu, Lin VS-Y. Mesoporous silica nanoparticles as controlled release drug delivery and gene transfection carriers. Adv. Drug Deliv. Rev. **60**, 1278–1288 (2008)
121. A. Liberman, N. Mendez, W.C. Trogler, A.C. Kummel, Synthesis and surface functionalization of silica nanoparticles for nanomedicine. Surf. Sci. Rep. **69**, 132–158 (2014)
122. K. Zarschler, L. Rocks, N. Licciardello, L. Boselli, E. Polo, K.P. Garcia et al., Ultrasmall inorganic nanoparticles: State-of-the-art and perspectives for biomedical applications. Nanomedicine **12**, 1663–1701 (2016)
123. E.B. Ehlerding, F. Chen, W. Cai, Biodegradable and renal clearable inorganic nanoparticles. Adv. Sci. (Weinh) **3** (2016)
124. J.L. Vivero-Escoto, R.C. Huxford-Phillips, W. Lin, Silica-based nanoprobes for biomedical imaging and theranostic applications. Chem. Soc. Rev. **41**, 2673–2685 (2012)
125. B.G. Trewyn, I.I. Slowing, S. Giri, H.-T. Chen, V.S.-Y. Lin, Synthesis and functionalization of a mesoporous silica nanoparticle based on the sol-gel process and applications in controlled release. Acc. Chem. Res. **40**, 846–853 (2007)
126. C. Barbé, J. Bartlett, L. Kong, K. Finnie, H.Q. Lin, M. Larkin et al., Silica particles: a novel drug-delivery system. Adv. Mater. **16**, 1959–1966 (2004)
127. R. Kumar, I. Roy, T.Y. Ohulchanskky, L.A. Vathy, E.J. Bergey, M. Sajjad et al., In vivo biodistribution and clearance studies using multimodal organically modified silica nanoparticles. ACS Nano **4**, 699–708 (2010)

128. L. Tang, X. Yang, L.W. Dobrucki, I. Chaudhury, Q. Yin, C. Yao et al., Aptamer-functionalized, ultra-small, monodisperse silica nanoconjugates for targeted dual-modal imaging of lymph nodes with metastatictTumors. Angew. Chem. Int. Ed. Engl. **51**, 12721–12726 (2012)
129. F. Chen, H. Hong, S. Shi, S. Goel, H.F. Valdovinos, R. Hernandez et al., Engineering of hollow mesoporous silica nanoparticles for remarkably enhanced tumor active targeting efficacy. Sci Rep. **4**, 5080 (2014)
130. T.M. Shaffer, M.A. Wall, S. Harmsen, V.A. Longo, C.M. Drain, M.F. Kircher et al., Silica nanoparticles as substrates for chelator-free labeling of oxophilic radioisotopes. Nano Lett. **15**, 864–868 (2015)
131. F. Chen, S. Goel, H.F. Valdovinos, H. Luo, R. Hernandez, T.E. Barnhart et al., In vivo integrity and biological fate of chelator-free zirconium-89-labeled mesoporous silica nanoparticles. ACS Nano **9**, 7950–7959 (2015)
132. L. Tang, J. Cheng, Nonporous silica nanoparticles for nanomedicine application. Nano Today **8**, 290–312 (2013)
133. S. Shi, F. Chen, W. Cai, Biomedical applications of functionalized hollow mesoporous silica nanoparticles: focusing on molecular imaging. Nanomedicine (London) **8**, 2027–2039 (2013)
134. R. Alshehri, A.M. Ilyas, A. Hasan, A. Arnaout, F. Ahmed, A. Memic, Carbon nanotubes in biomedical applications: factors, mechanisms, and remedies of toxicity. J. Med. Chem. **59**, 8149–8167 (2016)
135. W. Yang, P. Thordarson, J.J. Gooding, S.P. Ringer, F. Braet, Carbon nanotubes for biological and biomedical applications. Nanotechnology **18**, 412001 (2007)
136. H. Gong, R. Peng, Z. Liu, Carbon nanotubes for biomedical imaging: the recent advances. Adv. Drug Deliv. Rev. **65**, 1951–1963 (2013)
137. H. Wang, J. Wang, X. Deng, H. Sun, Z. Shi, Z. Gu et al., Biodistribution of carbon single-wall carbon nanotubes in mice. J. Nanosci. Nanotechnol. **4**, 1019–1024 (2004)
138. X. Deng, S. Yang, H. Nie, H. Wang, Y. Liu, A generally adoptable radiotracing method for tracking carbon nanotubes in animals. Nanotechnology **19**, 75101 (2008)
139. L. Lacerda, A. Soundararajan, R. Singh, G. Pastorin, K.T. Al-Jamal, J. Turton et al., Dynamic imaging of functionalized multi-walled carbon nanotube systemic circulation and urinary vxcretion. Adv. Mater. **20**, 225–230 (2008)
140. J. Guo, X. Zhang, Q. Li, W. Li, Biodistribution of functionalized multiwall carbon nanotubes in mice. Nucl. Med. Biol. **34**, 579–583 (2007)
141. M.R. McDevitt, D. Chattopadhyay, J.S. Jaggi, R.D. Finn, P.B. Zanzonico, C. Villa et al., PET imaging of soluble yttrium-86-labeled carbon nanotubes in mice. PLoS ONE **2**, e907 (2007)
142. Z. Liu, W. Cai, L. He, N. Nakayama, K. Chen, X. Sun et al., In vivo biodistribution and highly efficient tumour targeting of carbon nanotubes in mice. Nat. Nanotechnol. **2**, 47–52 (2007)
143. B. Czarny, D. Georgin, F. Berthon, G. Plastow, M. Pinault, G. Patriarche et al., Carbon nanotube translocation to distant organs after pulmonary exposure: insights from in situ ^{14}C-radiolabeling and tissue radioimaging. ACS Nano **8**, 5715–5724 (2014)
144. M.L. Matson, C.H. Villa, J.S. Ananta, J.J. Law, D.A. Scheinberg, L.J. Wilson, Encapsulation of alpha-particle-emitting ^{225}Ac3 + ions within carbon nanotubes. J. Nucl. Med. **56**, 897–900 (2015)
145. B.T. Cisneros, J.J. Law, M.L. Matson, A. Azhdarinia, E.M. Sevick-Muraca, L.J. Wilson, Stable confinement of positron emission tomography and magnetic resonance agents within carbon nanotubes for bimodal imaging. Nanomedicine (London) **9**, 2499–2509 (2014)
146. G. Chen, H. Qiu, P.N. Prasad, X. Chen, Upconversion nanoparticles: design, nanochemistry, and applications in theranostics. Chem. Rev. **114**, 5161–5214 (2014)
147. F. Auzel, Upconversion and anti-Stokes processes with f and d ions in solids. Chem. Rev. **104**, 139–173 (2004)

148. J. Shen, L. Zhao, G. Han, Lanthanide-doped upconverting luminescent nanoparticle platforms for optical imaging-guided drug delivery and therapy. Adv. Drug Deliv. Rev. **65**, 744–755 (2013)
149. Z. Gu, L. Yan, G. Tian, S. Li, Z. Chai, Y. Zhao, Recent advances in design and fabrication of upconversion nanoparticles and their safe theranostic applications. Adv. Mater. **25**, 3758–3779 (2013)
150. H. Xing, W. Bu, S. Zhang, X. Zheng, M. Li, F. Chen et al., Multifunctional nanoprobes for upconversion fluorescence. MR and CT trimodal imaging. Biomaterials **33**, 1079–1089 (2012)
151. Y. Yang, Y. Sun, T. Cao, J. Peng, Y. Liu, Y. Wu et al., Hydrothermal synthesis of NaLuF4:153Sm, Yb, Tm nanoparticles and their application in dual-modality upconversion luminescence and SPECT bioimaging. Biomaterials **34**, 774–783 (2013)
152. Y. Sun, M. Yu, S. Liang, Y. Zhang, C. Li, T. Mou et al., Fluorine-18 labeled rare-earth nanoparticles for positron emission tomography (PET) imaging of sentinel lymph node. Biomaterials **32**, 2999–3007 (2011)
153. J. Gallo, I.S. Alam, J. Jin, Y.-J. Gu, E.O. Aboagye, W.-T. Wong et al., PET imaging with multimodal upconversion nanoparticles. Dalton Trans. **43**, 5535–5545 (2014)
154. H.J. Seo, S.H. Nam, H.-J. Im, J.-Y. Park, J.Y. Lee, B. Yoo et al., Rapid hepatobiliary excretion of micelle-encapsulated/radiolabeled upconverting nanoparticles as an integrated form. Sci Rep. **5**, 15685 (2015)
155. J. Lee, T.S. Lee, J. Ryu, S. Hong, M. Kang, K. Im et al., RGD peptide-conjugated multimodal NaGdF4:Yb^{3+}/Er^{3+} nanophosphors for upconversion luminescence, MR, and PET imaging of tumor angiogenesis. J. Nucl. Med. **54**, 96–103 (2013)
156. T. Cao, Y. Yang, Y. Sun, Y. Wu, Y. Gao, W. Feng et al., Biodistribution of sub-10 nm PEG-modified radioactive/upconversion nanoparticles. Biomaterials **34**, 7127–7134 (2013)
157. Q. Liu, M. Chen, Y. Sun, G. Chen, T. Yang, Y. Gao et al., Multifunctional rare-earth self-assembled nanosystem for tri-modal upconversion luminescence/fluorescence/positron emission tomography imaging. Biomaterials **32**, 8243–8253 (2011)
158. J. Rieffel, F. Chen, J. Kim, G. Chen, W. Shao, S. Shao et al., Hexamodal imaging with porphyrin-phospholipid-coated upconversion nanoparticles. Adv. Mater. **27**, 1785–1790 (2015)
159. L. Wang, Synthetic methods of CuS nanoparticles and their applications for imaging and cancer therapy. RSC Adv. **6**, 82596–82615 (2016)
160. S. Goel, F. Chen, W. Cai, Synthesis and biomedical applications of copper sulfide nanoparticles: from sensors to theranostics. Small **10**, 631–645 (2014)
161. R. Chakravarty, S. Chakraborty, R.S. Ningthoujam, K.V. Vimalnath Nair, K.S. Sharma, A. Ballal et al., Industrial-scale synthesis of intrinsically radiolabeled ^{64}CuS nanoparticles for use in positron emission tomography (PET) imaging of cancer. Ind. Eng. Chem. Res. **55**, 12407–12419 (2016)
162. M. Zhou, R. Zhang, M. Huang, W. Lu, S. Song, M.P. Melancon et al., A chelator-free multifunctional [^{64}Cu]CuS nanoparticle platform for simultaneous micro-PET/CT imaging and photothermal ablation therapy. J. Am. Chem. Soc. **132**, 15351–15358 (2010)
163. Y. Zhang, T.R. Nayak, H. Hong, W. Cai, Biomedical applications of zinc oxide nanomaterials. Curr. Mol. Med. **13**, 1633–1645 (2013)
164. W.-Q. Zhang, Y. Lu, T.-K. Zhang, W. Xu, M. Zhang, S.-H. Yu, Controlled synthesis and biocompatibility of water-soluble ZnO nanorods/Au nanocomposites with tunable UV and visible emission intensity. J. Phys. Chem. C **112**, 19872–19877 (2008)
165. Y. Liu, K. Ai, Q. Yuan, L. Lu, Fluorescence-enhanced gadolinium-doped zinc oxide quantum dots for magnetic resonance and fluorescence imaging. Biomaterials **32**, 1185–1192 (2011)
166. H. Hong, F. Wang, Y. Zhang, S.A. Graves, S.B.Z. Eddine, Y. Yang et al., Red fluorescent zinc oxide nanoparticle: A novel platform for cancer targeting. ACS Appl. Mater. **7**, 3373–3381 (2015)

167. S.S. Chou, B. Kaehr, J. Kim, B.M. Foley, M. De, P.E. Hopkins et al., Chemically exfoliated MoS2 as near-infrared photothermal agents. Angew. Chem. Int. Ed. Engl. **52**, 4160–4164 (2013)
168. S.S. Chou, M. De, J. Kim, S. Byun, C. Dykstra, J. Yu et al., Ligand conjugation of chemically exfoliated MoS2. J. Am. Chem. Soc. **135**, 4584–4587 (2013)
169. L. Cheng, J. Liu, X. Gu, H. Gong, X. Shi, T. Liu et al., PEGylated WS(2) nanosheets as a multifunctional theranostic agent for in vivo dual-modal CT/photoacoustic imaging guided photothermal therapy. Adv. Mater. **26**, 1886–1893 (2014)
170. J. Li, F. Jiang, B. Yang, X.-R. Song, Y. Liu, H.-H. Yang et al., Topological insulator bismuth selenide as a theranostic platform for simultaneous cancer imaging and therapy. Sci. Rep. **3**, 1998 (2013)
171. L. Cheng, S. Shen, S. Shi, Y. Yi, X. Wang, G. Song et al., $FeSe_2$-decorated Bi_2Se_3 nanosheets fabricated via cation exchange for chelator-free ^{64}Cu-labeling and multimodal image-guided photothermal-radiation therapy. Adv. Funct. Mater. **26**, 2185–2197 (2016)
172. T. Liu, S. Shi, C. Liang, S. Shen, L. Cheng, C. Wang et al., Iron oxide decorated MoS2 nanosheets with double PEGylation for chelator-free radiolabeling and multimodal imaging guided photothermal therapy. ACS Nano **9**, 950–960 (2015)
173. F. Ai, S. Goel, Y. Zhan, H.F. Valdovinos, F. Chen, T.E. Barnhart et al., Intrinsically 89Zr-labeled Gd2O2S: Eu nanophosphors with high in vivo stability for dual-modality imaging. Am. J. Transl. Res. **8**, 5591–5600 (2016)
174. Y. Zhan, F. Ai, F. Chen, H.F. Valdovinos, H. Orbay, H. Sun et al., Intrinsically zirconium-89 labeled Gd2O2S: Eu nanoprobes for in vivo positron emission tomography and gamma-ray-induced radioluminescence imaging. Small **12**, 2872–2876 (2016)
175. C. Sun, G. Pratx, C.M. Carpenter, H. Liu, Z. Cheng, S. Sam Gambhir et al., Synthesis and radioluminescence of PEGylated Eu^{3+}-doped nanophosphors as bioimaging probes. Adv. Mater. **23**, H195–H199 (2011)
176. Y. Song, H. You, Y. Huang, M. Yang, Y. Zheng, L. Zhang et al., Highly uniform and monodisperse $Gd_2O_2S:Ln^{3+}$ (Ln = Eu, Tb) submicrospheres: Solvothermal synthesis and luminescence properties. Inorg. Chem. **49**, 11499–11504 (2010)
177. S.A. Osseni, S. Lechevallier, M. Verelst, P. Perriat, J. Dexpert-Ghys, D. Neumeyer et al., Gadolinium oxysulfide nanoparticles as multimodal imaging agents for T2-weighted MR{,} X-ray tomography and photoluminescence. Nanoscale **6**, 555–564 (2014)
178. E. Morales-Avila, G. Ferro-Flores, B.E. Ocampo-García, de María Ramírez, F, Radiolabeled nanoparticles for molecular imaging, in ed. by B. Schaller (Molecular Imaging. Intech. 2012)
179. I. Ojea-Jimenez, J. Comenge, L. Garcia-Fernandez, Z.A. Megson, E. Casals, V.F. Puntes, Engineered inorganic nanoparticles for drug delivery applications. Curr. Drug Metab. **14**, 518–530 (2013)
180. K. Stockhofe, J.M. Postema, H. Schieferstein, T.L. Ross, Radiolabeling of nanoparticles and polymers for PET imaging. Pharmaceuticals (Basel). **7**, 392–418 (2014)
181. G. Ferro-Flores, B.E. Ocampo-García, C.L. Santos-Cuevas, E. Morales-Avila, E. Azorín-Vega, Multifunctional radiolabeled nanoparticles for targeted therapy. Curr. Med. Chem. **21**, 124–138 (2014)
182. J. Xie, S. Lee, X. Chen, Nanoparticle-based theranostic agents. Adv. Drug Deliv. Rev. **62**, 1064–1079 (2010)
183. D. Bargheer, A. Giemsa, B. Freund, M. Heine, C. Waurisch, G.M. Stachowski et al., The distribution and degradation of radiolabeled superparamagnetic iron oxide nanoparticles and quantum dots in mice. Beilstein J. Nanotechnol. **6**, 111–123 (2015)
184. Q.K.T. Ng, C.I. Olariu, M. Yaffee, V.F. Taelman, N. Marincek, T. Krause et al., Indium-111 labeled gold nanoparticles for in-vivo molecular targeting. Biomaterials **35**, 7050–7057 (2014)

185. M. Sun, G. Sundaresan, P. Jose, L. Yang, D. Hoffman, N. Lamichhane et al., Highly stable intrinsically radiolabeled indium-111 quantum dots with multidentate zwitterionic surface coating: dual modality tool for biological imaging. J. Mater Chem. B **2**, 4456–4466 (2014)
186. J.D. Woodward, S.J. Kennel, S. Mirzadeh, S. Dai, J.S. Wall, T. Richey et al., In vivo SPECT/CT imaging and biodistribution using radioactive $Cd^{125m}Te$/ZnS nanoparticles. Nanotechnology **18**, 175103 (2007)

Chapter 3
Porphyrin and Phthalocyanine Radiolabeling

Venugopal Rajendiran, Sanjana Ghosh and Jonathan F. Lovell

Abstract There have been substantial improvements in radiopharmaceutical chemistry with respect to designing new diagnostic and therapeutic agents for combatting diseases. Porphyrin and phthalocyanine derivatives have been explored in this field because they possess unique photophysical properties, can accumulate in human and animal tumors, and their metal complexes are both thermodynamically and kinetically stable. A wide variety of radiolabeled metalloporphyrins and metallo phthalocyanines can be prepared that are stable in biological media. Radiolabeled compounds have been employed in preclinical applications for nuclear imaging, biodistribution studies, and photodynamic therapy. This chapter provides an overview of radiopharmaceutical applications of porphyins and phthalocyanines including small molecule and nanoparticle-based approaches.

3.1 Introduction

3.1.1 Background on Porphyrins and Phthalocyanines

Porphyrins are a class of intensely colored naturally occurring compounds that play a vital role in numerous biological functions like photosynthesis and oxygen transport, to name just two. The term *porphyrin* is derived from the Greek word

V. Rajendiran · S. Ghosh · J. F. Lovell (✉)
Department of Biomedical Engineering, University at Buffalo,
State University of New York, Buffalo, NY 14260, USA
e-mail: jflovell@buffalo.edu

S. Ghosh
e-mail: sghosh22@buffalo.edu

V. Rajendiran
Department of Chemistry, School of Basic and Applied Sciences,
Central University of Tamil Nadu, Thiruvarur 610005, India
e-mail: rajendiran@cutn.ac.in

D. S. Lee (ed.), *Radionanomedicine*, Biological and Medical Physics,
Biomedical Engineering, https://doi.org/10.1007/978-3-319-67720-0_3

porphura, which means 'purple'. The basic tetrapyrrole skeleton is found in natural pigments like hemin, chlorophyll and bacteriochlorophyll. The structure of porphyrin consists of a heterocyclic macrocycle made from four pyrrole subunits interconnected via methine bridges (=CH–). The simplest form of porphyrin molecules is porphyrin itself (Fig. 3.1a).

The tetradentate porphyrin core provides space for metal coordination with a diameter of up to 0.37 nm. When metal atoms coordinate, deprotonation of pyrrole nitrogens occurs that results in two negative charges. The macrocyclic ring system of porphyrins exhibits aromatic character and is highly stable, as are their transition metal ion coordination complexes. For example, the stability constant of ZnTPP (tetraphenylporphyrin) is 10^{29} [1]. Porphyrins can form complexes with almost all metals. There has been much recent activity in the use of porphyrins for tumor

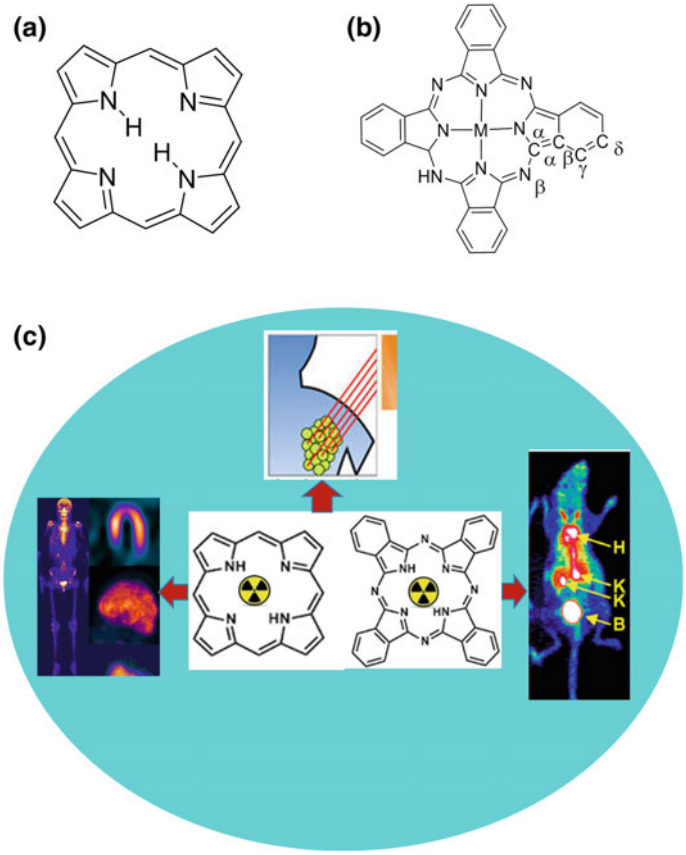

Fig. 3.1 **a** Porphyrin macrocyclic system. **b** The structure and labelling scheme for simple metallophthalocyanines. **c** Schematic illustrations of various biomedical applications of radiolabeled metalloporphyrin and metallopthalocyanines

imaging and therapy [2, 3]. The advantageous photophysical properties of porphyrin derivatives have led to roles in many biomedical applications, particularly in photodynamic therapy (PDT) and molecular imaging. The characteristic of some tetrapyrroles to accumulate in tumors is used for these applications [4].

The history of porphyrins in PDT has been described in the literature [5–7]. In 1912, Meyer-Betz observed the photodynamic effect by injecting himself with hematoporphyrin and subsequently exposing small regions of skin to light. In 1924, Policard observed natural porphyrin fluorescence in experimental tissue. In 1961, the tumor-localizing properties of a hematoporphyrin derivative (HPD) and its detection by fluorescence were discovered by Lipson and photosensitization of porphyrins for eradication of experimental tumors in animals was reported later. The preparation of HPD as reported by Lipson was the basis for the subsequent use of Photofrin® for PDT.

Phthalocyanines (Pcs) are structurally related to porphyrins but do not occur naturally. The term was coined in 1933, by Sir Reginald Linstead, who also determined the structure [8]. The structure of Pc is similar to that of porphyrins and Fig. 3.1b shows the structure for simple metal-Pcs [9]. Pcs have found numerous applications from colorants to catalysts. Pc derivatives of different charge and lipophilicity can be prepared by the addition of the appropriate substituents on the benzene rings of the macrocycle [10]. One application of note for Pcs is the use of tetrasulfonated phthalocyanine (PcS_4) which has been used clinically as Photosens [11]. Recently, Pcs have been explored in numerous theranostic application [12].

Porphyrins and Pcs have been used extensively for photosensitizers and radiolabeling [13]. Cu-phthalocyanine was described as a ^{64}Cu chelator that accumulated in rodent brain tumors as early as 1951 [14]. These molecules are useful for use as radiochelators, for image-guided PDT, and for building more complex structures with imaging capabilities for disease detection.

3.1.2 *Radionuclides for Labeling Porphyrins and Phthalocyanines*

The radioactive decomposition of radionuclides into subatomic particles or protons allows for sensitive imaging and tracking. With nuclear medicine technology such as positron emission tomography (PET) and single photon emission tomography (SPECT), compounds labeled with γ or positron emitting radionuclides are viable for whole body in vivo imaging [5] (Fig. 3.1c). Radiolabeling can enable quantitative whole body imaging of compound distribution. Various techniques for radiolabeling are illustrated in Fig. 3.2a the radionuclide is attached to a nanoparticle surface by an exogenous chelator; (B) the radionuclide is entrapped in an enclosed compartment; or (C) nanoparticles are manufactured from pre-radiolabeled building blocks [15]. The specific localization and sensitizing ability of porphyrins for tumor imaging and biodistribution studies are generally

maintained with radiolabeling. Radiolabeled porphyrins can thus provide a non-invasive means for deep tumor detection and image-guided PDT.

Hematoporphyrin, one of the most common photosensitizers, has been explored for radiolabeling. ^{99m}Tc pertechnetate and stannous chloride were used to radiolabel hematoporphyrin and derivatives and it was thought that the radiolabeling occurs at the carboxylic chains of the porphyrin. The ^{99m}Tc-labeled species was stable in biological conditions. Hematoporphyrin labeled with ^{57}Co and ^{64}Cu coordinated in

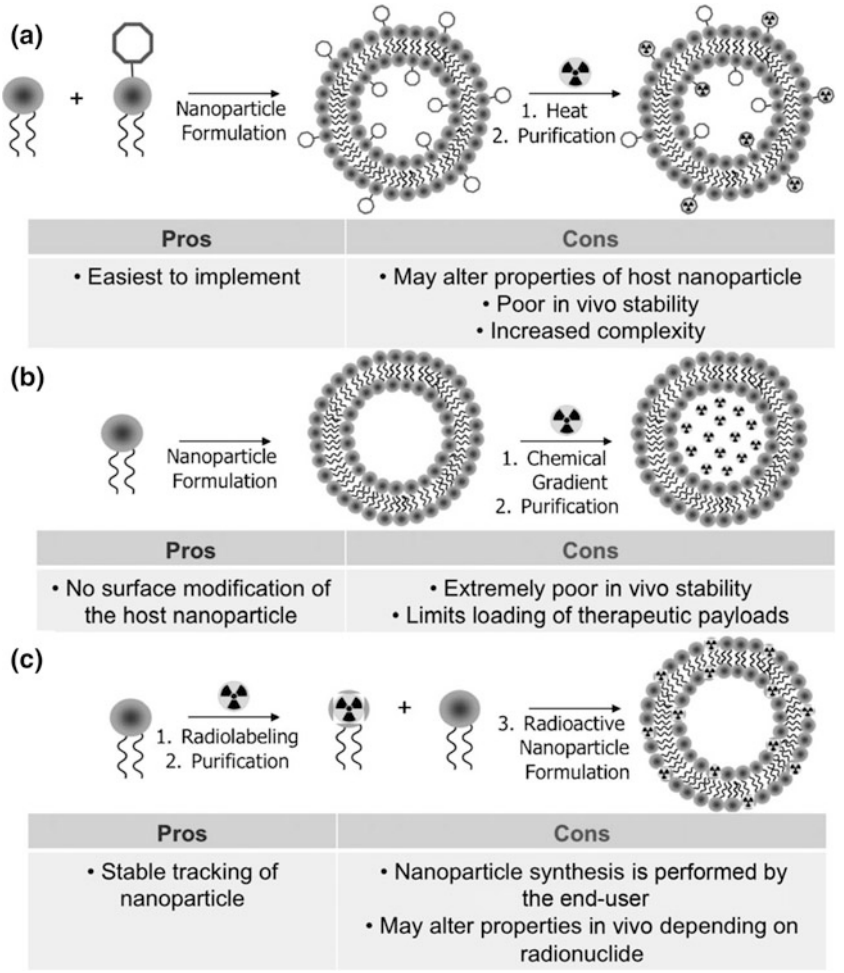

Fig. 3.2 The various techniques for radiolabeling of nanoparticles are illustrated. **a** An exogenous chelator is incorporated into the nanoparticle formulation and subsequently radiolabeled. **b** The radioisotope is entrapped into an enclosed compartment within the nanoparticle. **c** The building blocks are radiolabeled and subsequently the nanoparticle is synthesized. Permission obtained from [15]. Copyright (2012) by Wiley-VCH Verlag GmbH & Co. KGaA, Weinheim

the tetrapyrrole core lacked significant tumor localization, whereas hematoporphyrin labeled with ^{109}Pd was shown to accumulate in the tumor [16]. Sulfonated metallophthalocyanines were studied as potential radiopharmaceuticals for tumor imaging and later as candidate drugs for tumor PDT [17]. Table 3.1 shows applications of derivatives of porphyrin and Pc radiolabeled by different metallic radioisotopes.

3.2 Coordination Chemistry of Metalloporphyrins and Metallophthalocyanines

Many naturally occurring porphyrins are metal-bound and do not show toxicity towards living organisms in the presence of light. Also, it was observed that the introduction of a metal into the porphyrin molecule does not destroy the tendency of the porphyrin to concentrate in tumors [18]. Understanding coordination chemistry of metalloporphyrins and metallopthalocyanines is important for their use in radiolabeling for biological applications. Porphyrin and many derivatives readily form complexes with a variety of metals by deprotonation of one or two, of the pyrrole NH protons and the resulting metal complexes are thermodynamically and kinetically stable [19]. Usually, it tends to form a planar four-coordinated complexes with square-planar geometry. In addition to this, it has a tendency to form some 5–8 higher coordination geometries during the course of addition of extra ligands. Amongst all, the most studied complexes are four coordinated square-planar, five coordinated square-pyramidal and six coordinated octahedral metalloporphyrins [20]. Scheldt studied the influence of occupied or unoccupied $3d^{22}_{x-y}$ and $3d^{2}_{z}$ orbitals on the bond lengths of metal-porphyrin nitrogen (M-N) and metal-axial ligand (M-L) [20]. Detailed discussion on stable oxidation states of metal ions in metalloporphyrins and optical absorption spectra of metalloporphyrins were reported by Dolphin et al. [21]. Like porphyrins, the coordination chemistry of metallophthalocyanines also received attention and have similar structures as metalloporphyrins [22].

3.3 Porphyrin Radiolabeling

3.3.1 Cobalt-57

Transition metals often play a major role in designing metalloporphyrin PET imaging agents. ^{57}Co, with a half-life of 271.8 days, was chelated in porphyrins and employed to detect tumors in vivo over thirty years ago [23]. Two ^{57}Co porphyrins, Co(III)-Corproporphyrin (CoCorp) and Co(III)-Uroporphyrin (CoUro) were used as tumor specific agents. Tumor distribution of CoCorp and CoUro showed that the

Table 3.1 Applications of derivatives of porphyrin and phthalocyanine labeled with different metallic radioisotopes

Compound	Radioisotope	Half-life	Application	References
Porphyrin	^{57}Co	271.8 days	Tumor detection	[24]
Porphyrin	^{64}Cu	12.7 h	PET/CT	[15]
Porphyrin	^{64}Cu	12.7 h	Tumor detection	[27]
Porphyrin	^{64}Cu	12.7 h	PET	[31]
Porphyrin	^{64}Cu	12.7 h	Synthesis of bimodal imaging agents	[85]
Porphyrin	^{64}Cu	12.7 h	PET	[32]
Phthalocyanine	^{64}Cu	12.7 h	PET	[80]
Phthalocyanine	^{64}Cu	12.7 h	PET	[17]
Porphyrin	^{188}Re	16.98 h	Radionuclide therapy	[79]
Porphyrin	^{10}B	(known to be stable)	Boron neutron capture therapy (BNCT)	[86]
Porphyrin	^{111}In	2.80 days	Tumor imaging	[87]
Porphyrin	^{111}In	2.80 days	Cancer detection	[88]
Porphyrin	^{111}In	2.80 days	Labeling HPD	[89]
Porphyrin	^{111}In	2.80 days	Tumor detection	[65]
Porphyrin	^{111}In	2.80 days	Tumor detection	[67]
Porphyrin	^{111}In	2.80 days	Imaging of lymph nodes	[66]
Porphyrin	^{111}In	2.80 days	Monoclonal antibody labelling	[69]
Porphyrin	$^{186/188}$Re	^{186}Re($t_{1/2}$ = 90 h), ^{188}Re($t_{1/2}$ = 16.9 h)	Tumor radiotherapy	[76]
Porphyrin	^{67}Ga	78.26 h	SPECT	[45]
Porphyrin	^{68}Ga	271 days	PET	[47]
Porphyrin	^{68}Ga	271 days	PET	[48]
Porphyrin	^{68}Ga	271 days	SPECT	[45]
Porphyrin	^{67}Ga	78.26 h	Human melanoma detection	[90]
Phthalocyanine	^{67}Ga	78.26 h	PDT	[10]
Porphyrin	^{99m}Tc	6 h	Tumor imaging	[57]
Porphyrin	^{99m}Tc	6 h	Fluorescent imaging for tumor detection	[60]
Porphyrin	^{99m}Tc	6 h	Tumor localization	[55]
Porphyrin	^{99m}Tc	6 h	Tumor imaging and diagnosis	[59]
Porphyrin	^{99m}Tc	6 h	Tumor imaging	[59]
Porphyrin	^{140}Nd	3.37 days	Tumor therapy; PET	[71]
Porphyrin	^{18}F	109.77 min	Tumor detection	[91]
Porphyrin	^{18}F	109.77 min	PDT/PET	[92]
Phthalocyanine	^{65}Zn	244.26 days	PDT	[82]

(continued)

Table 3.1 (continued)

Compound	Radioisotope	Half-life	Application	References
Porphyrin	^{166}Ho	26.8 h	SPECT; Biodistribution studies	[72]
Porphyrin	^{177}Lu	6.647 days	Tumor therapy	[93]
Porphyrin	^{177}Lu	6.647 days	Cancer Radiotherapy	[73]

CoCorp had 7% uptake, comparable to the 9% found for a ^{67}Ga citrate approach. In another approach, ^{57}Co labeled hematoporphyrin **1** was developed and examined for biodistribution studies in BWI0232 adenocarcinoma-bearing mice [24]. In vivo distribution studies indicated that 24 h after intravenous administration, the ratios of tumor-to-blood and tumor-to-muscle could discriminate tumorous tissues.

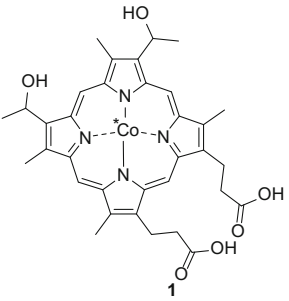

1

3.3.2 Copper-64 for Porphyrin and Porphysome

Copper radionuclides have received attention in the field of radiopharmaceutical research because of their favorable physical properties and availability [25]. Decades ago, attempts were made at tumor localization in mice bearing varieties of tumors by using several ^{64}Cu labeled porphyrins [26, 27]. The biodistribution of ^{67}Cu radiolabeled 5,10,15,20-tetrakis(4-carboxyphenyl)porphinato(^{67}Cu) (^{67}Cu-TCPP) was examined in rat lymph nodes, surrounding muscle, fat and blood [28]. Later, synthetic porphyrins such as N-benzyl-5,10,15,20-tetrakis (4-carboxyphenyl)porphine (NbzHTCPP) **2** and N-4-nitrobenzyl-5-(4-carboxyphenyl)-10,15,20-tris(4-sulfophenyl)porphine (N-bzHCS$_3$P) **3** were employed with radiocopper for antibody-mediated delivery [29, 30]. An anti-renal cell carcinoma (RCC) antibody and A6H conjugated copper-67 labeled N-bzHCS$_3$P was used for biodistribution analysis in human RCC xenograft-bearing nude mice. ^{67}CuCS$_3$P-A6H exhibited a tumor-to-blood ratio of over 16 after 45 h. Fluoro substitution impacted pharmacokinetics of ^{64}Cu labeled 5,10,15,20-tetrakis(penta fluoro phenyl) porphyrin ((^{64}Cu)-TFPP) **4** and this compound was used for PET

imaging 4 h after injection in rats [31]. Pharmacokinetic studies indicated that the (^{64}Cu)-TFPP (**4**) were mostly washed out from the circulation through kidneys and liver.

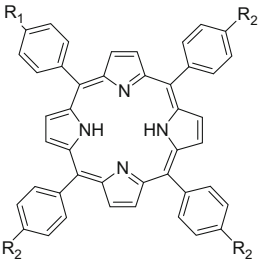

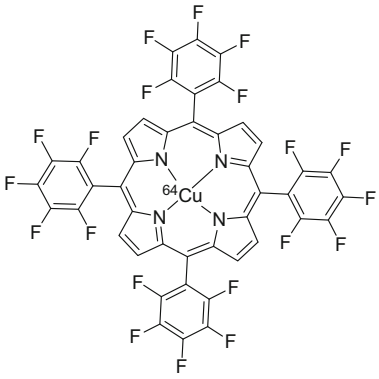

4

Name	R	R1	R2
2	p-nitrobenzyl	CO_2	SO_3
3	Benzyl	CO2	CO_2

As shown in Fig. 3.3a, Zheng et al. modified a folate receptor (FR) targeting fluorescent/PDT agent as a ^{64}Cu radiolabeled porphyrin-peptide-folate (PPF) probe [32] for PET imaging of cancer (Fig. 3.3b). The resulting ^{64}Cu-PPF exhibited selective uptake in FR-positive tumors in small animals on PET with a high tumor-to-muscle ratio after 24 h (8.9). FR-mediated tracer uptake by the tumor was further confirmed by competitive blocking studies (Fig. 3.3c).

There has been interest in developing nanoparticle-based ^{64}Cu-labeled PET imaging agents. Emerging nanoparticle approaches have potential for theranostic and translational research [33–36]. Zheng and his co-workers developed multifunctional ^{64}Cu-labeled porphysome nanoparticles as radiotracers through a post-labeling method for PET imaging [37]. ^{64}Cu-porphysomes successfully visualized tumors in an orthotopic prostate cancer model. The same group further developed multimodal imaging with porphysomes capable of both nuclear and optical delineation of macro- and the microscopic tumors. These ^{64}Cu-porphysomes had the ability to detect small (<2 mm) prostate-derived metastases (Fig. 3.4) [38]. Such multimodal approaches are gaining popularity for next generation diagnostic imaging [39].

Recently, a porphyrin mesh polymer was chelated with ^{64}Cu (Fig. 3.5a) to show rapid renal clearance on dynamic whole body PET [40]. Experimental data indicates that small porphyrin-polyethylene glycol (PEG) polymers can serve as an effective multimodal marker of renal function (Fig. 3.5b–d). In addition to porphyrin mesh, surfactant-stripped ^{64}Cu-labeled frozen pheophytin micelles for

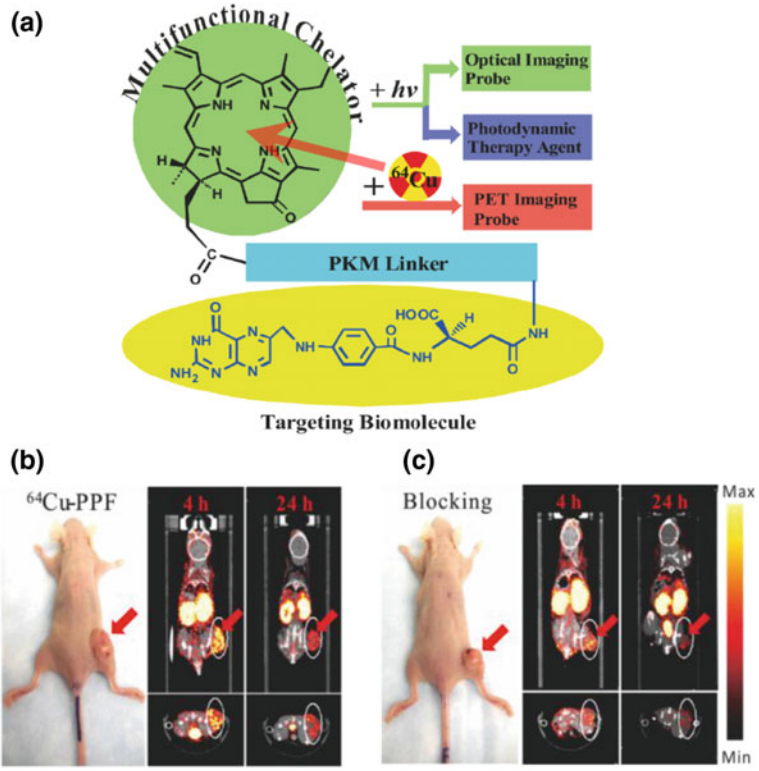

Fig. 3.3 **a** The structure design of the PPF (Pyro-PKM linker-Folate, molecular weight of 1800 g/mol). Here the PKM linker (pharmacokinetics modifying linker) is the peptide sequence, GDEVDGSGK. **b** Representative MicroPET/CT images (coronal images (top) and single transverse slices passing through the tumors (bottom)) of KB tumor-bearing mice at 4, 24 h after intravenous injection of ^{64}Cu-PPF. **c** Images, including coronal images (top) and single transverse slices passing through the tumors (bottom), obtained with pre-injection (0.5 h earlier) of 500-fold excess folic acid for blockade. Permission obtained from [32]. Copyright (2011) by IVYSPRING International Publisher

multimodal gut imaging was described [41]. This oral contrast agent passed through the intestine harmlessly. Furthermore, multimodal nanoparticles using porphyrin-phospholipid (PoP)-coated upconversion nanoparticles can seamlessly labeled with ^{64}Cu (Fig. 3.6) and be employed for PET imaging in a mouse model simultaneously with five other small animal imaging modalities [42].

Li et al. developed all-in-one multifunctional nanoparticles with combined diagnostic and therapeutic functions. This porphyrin-based organic nanoconstruct termed nanoporphyrin was produced by using a single organic building block; a porphyrin/cholic acid hybrid (Fig. 3.7a) [43]. The agent could be used for PET imaging (Fig. 3.7b). To increase the sensitivity of this imaging agent, dual-modality

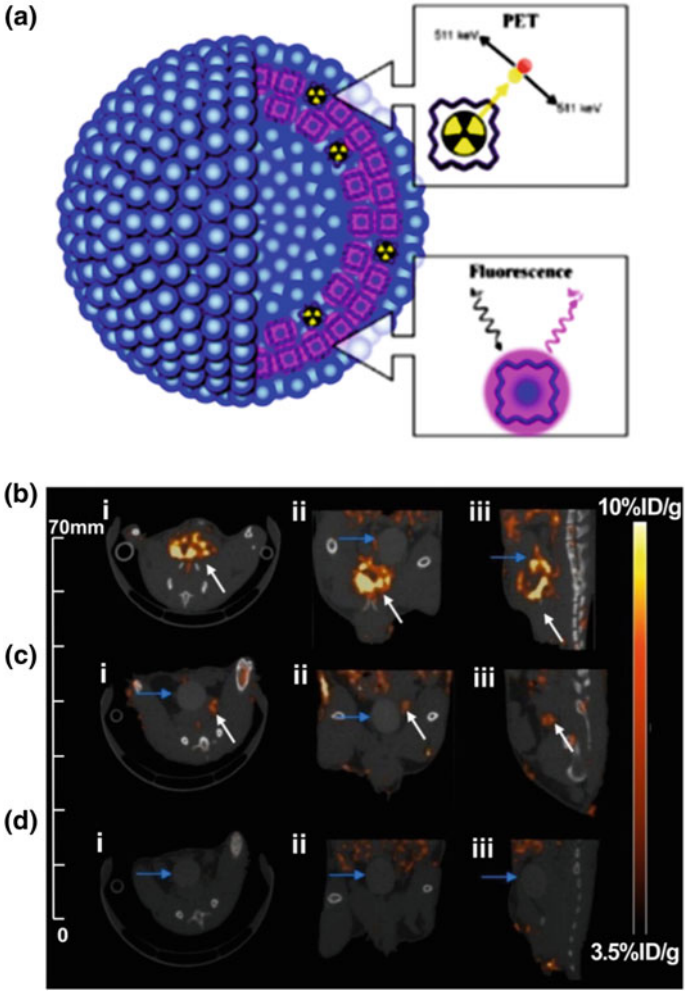

Fig. 3.4 ^{64}Cu-porphysomes as a PET agent. **a** Schematic diagram of the multimodal properties of ^{64}Cu-porphysomes as a result of direct radiolabeling a fraction of the porphyrin-lipid bilayer of preformed photonic porphysomes creating intrinsic multimodal nanoparticles. ^{64}Cu-porphysome selectivity in orthotopic prostate tumor models. Representative MicroPET/CT images of (i) axial, (ii) coronal, and (iii) sagittal single slices through, **b** orthotopic PC3 tumor, **c** orthotopic 22RV1 tumor, and **d** healthy male mice at 24 h after i.v. injection of ^{64}Cu-porphysomes. White arrows depict prostate tumor; blue arrows depict bladder. Permission obtained from [38]. Copyright (2013) by American Chemical Society

nanoprobes for PET and MRI was constructed via nanoporphyrin chelation with both ^{64}Cu(II) and Gd(III) (Fig. 3.7c) [43].

Cai and co-workers developed a liposome-based sequentially activated nanotheranostic system [44]. This was prepared by encapsulating the hydrophobic

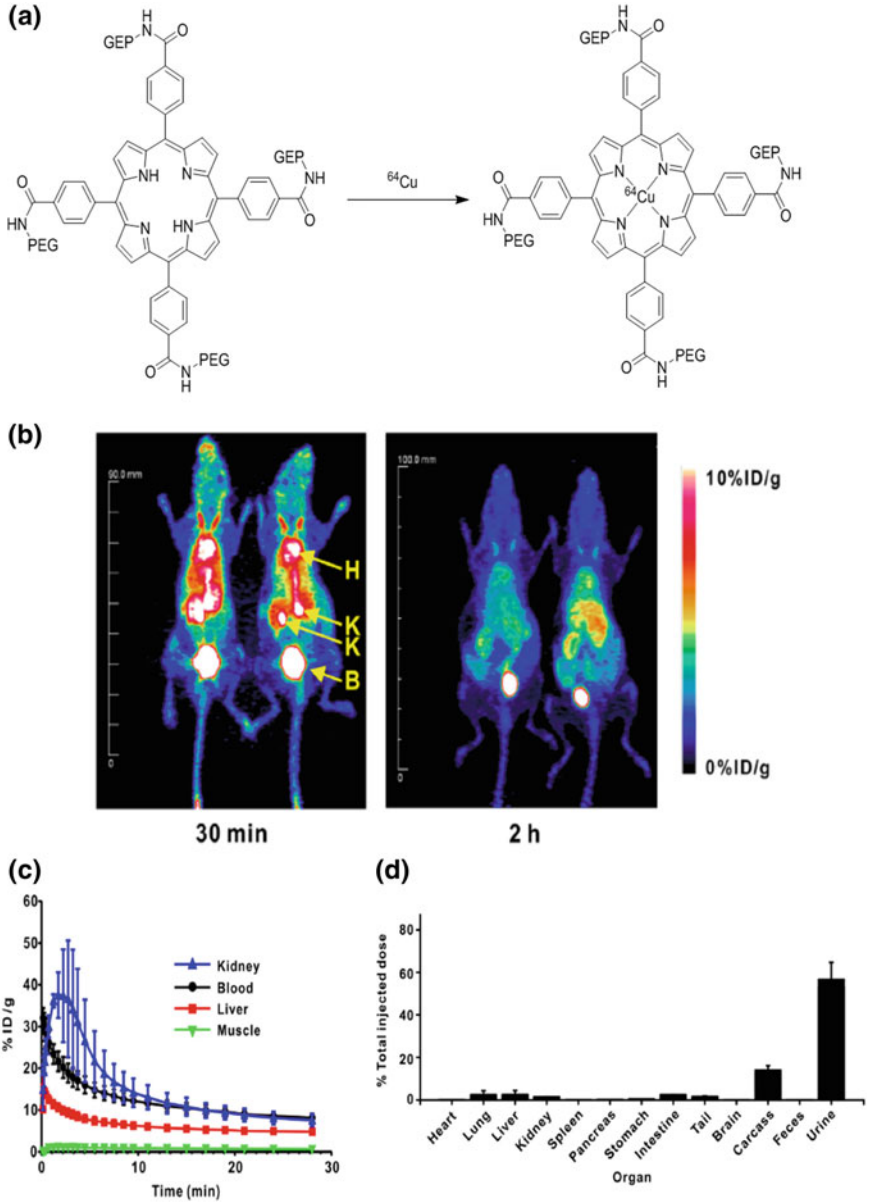

Fig. 3.5 **a** Facile post-chelation strategy for inserting ^{64}Cu into the porphyrin mesh. **b** Representative PET images of mice 30 min and 2 h post intravenous injection of ^{64}Cu-porphyrin-PEG mesh. Heart (H), Kidneys (K) and bladder (B) are indicated. **c** Dynamic PET imaging reveals ^{64}Cu distribution in indicated organs (mean ± std. dev. for n = 4 mice). **d** ^{64}Cu biodistribution of extracted organs 4 h after intravenous injection of ^{64}Cu-porphyrin mesh (mean ± std. dev. for n = 3 mice). Permission obtained from [40]. Copyright (2016) by Elsevier Ltd.

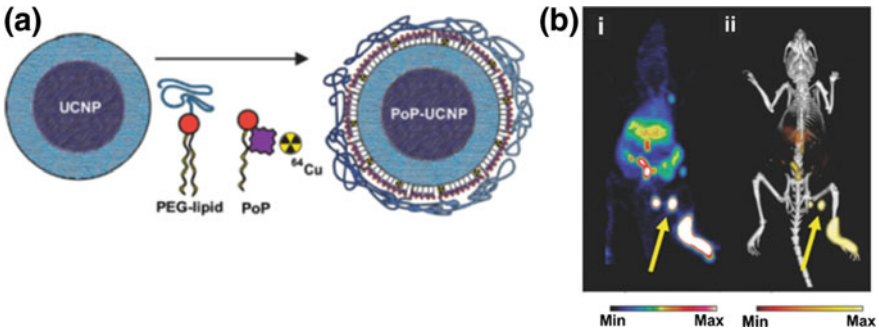

Fig. 3.6 ^{64}Cu-PoP coated UCNPs as multifunctional imaging agent. **a** Schematic diagram of the PoP-UCNP structure. Core-shell UCNPs were transferred to the aqueous phase by lipid coating with PEG-lipid and PoP. Radioactive ^{64}Cu can seamlessly be chelated inside the nanostructure. **b** Accumulation of PoP-UCNPs in the first draining lymph node is indicated with yellow arrows on PET (left) and merged PET/CT (right). Permission obtained from [42]. Copyright (2015) by Wiley-VCH Verlag GmbH & Co. KGaA, Weinheim

photosensitizer chlorin e6 (hCe6) into the hydrophobic bilayers and the hydrophilic hypoxia-activated prodrug AQ4 N into the aqueous cavity of PEG-shelled liposomes. The AQ4 N-hCe6-liposome showed hypoxia-dependent cytotoxicity and effective photodynamic cell killing. ^{64}Cu chelation was carried out with AQ4 N-hCe6-liposome for theranostic PET imaging. Tumor accumulation of AQ4 N-^{64}Cu-hCe6-liposome was measured to be 4.7% injected dose per gram (%ID/g).

3.3.3 Gallium-67 and 68

Porphyrins radiolabeled with Gallium-67 and 68 have been employed in various radiopharmaceutical applications. ^{67}Ga labeled tetraphenyl porphyrin (^{67}Ga-TPP) **5** was employed for biodistribution studies and SPECT imaging in rats [45]. Pharmacokinetic data revealed that most of the complex washed out through kidneys with low liver uptake. In another study, tissue distribution of 7,12-bis (1-decyloxyethyl)-Ga(III)-3,8,13,17-tetramethylporphyrin-2,18-dipropionyldiaspartic acid (ATX-70) **6** was examined in tumor-bearing mice [46]. Roughly 24 h after administration, high tumor-to-skin and tumor-to-muscle concentration ratios were observed.

^{68}Ga-labeled, fluorine substituted 5,10,15,20-tetrakis(pentafluoro-13 phenyl) porphyrin (^{68}Ga-TFPP) **7** was prepared and examined in Swiss mice bearing fibrosarcoma with biodistribution and SPECT imaging studies (Fig. 3.7d) [47]. The complex was mostly washed out from circulation through kidneys and liver,

and exhibited enhanced target-to-nontarget ratio. A set of five porphyrin derivatives (**7**–**12**) was labeled with ^{68}Ga for PET imaging in tumor-bearing rats and exhibited clear tumor visualization [48].

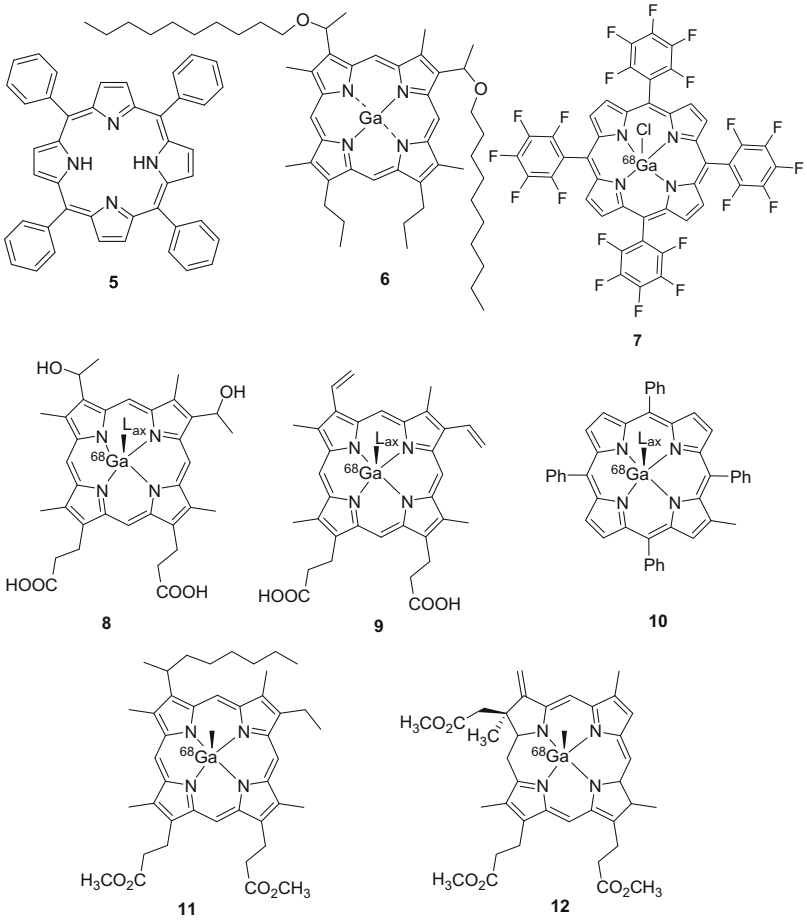

3.3.4 Technetium-99m

Technetium-99m complexes are extensively used in nuclear medicine in the diagnosis of many cancers and non-cancer diseases because ^{99m}Tc radionuclide has favorable nuclear properties (140 keV, γ emitters; $t_{1/2}$ = 6:01 h), low cost and ready availability [49, 50]. ^{99m}Tc-labeled simple porphin and hematoporphyrin were employed for in vivo biodistribution studies [51, 52]. Later, various modified ^{99m}Tc labeled porphyrins were developed. On injecting ^{99m}Tc labeled

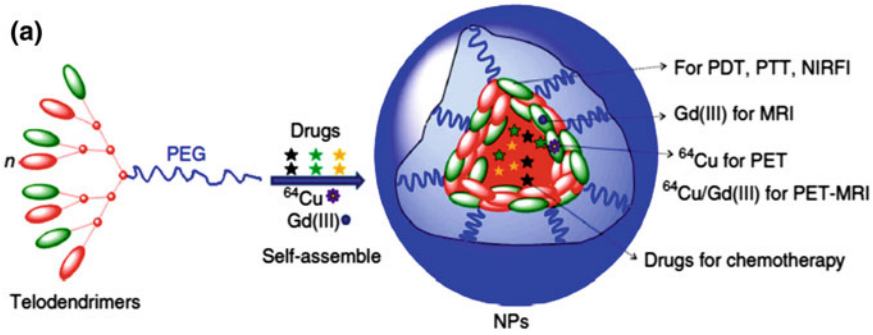
(a)
n
PEG
Telodendrimers
Drugs
64Cu
Gd(III)
Self-assemble
NPs
For PDT, PTT, NIRFI
Gd(III) for MRI
64Cu for PET
64Cu/Gd(III) for PET-MRI
Drugs for chemotherapy

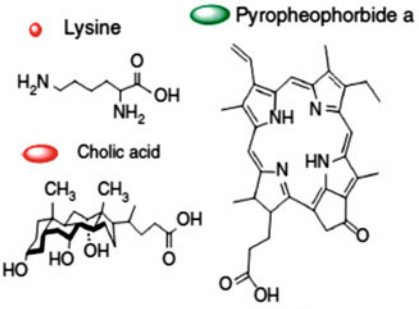
Lysine
Pyropheophorbide a
Cholic acid

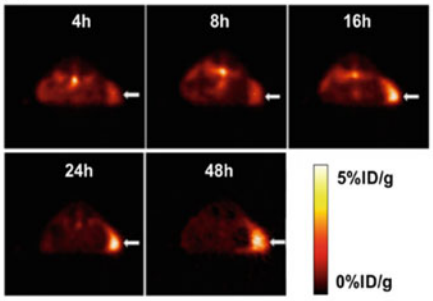
(b)
4h
8h
16h
24h
48h
5%ID/g
0%ID/g

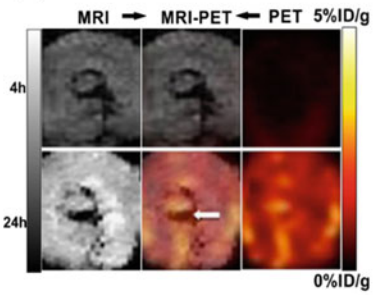
(c)
MRI
MRI-PET
PET
5%ID/g
4h
24h
0%ID/g


(d)
Tumor

◂**Fig. 3.7** Self-assembled multifunctional NP. **a** Schematic illustration of a multifunctional NP self-assembled by a representative porphyrin–telodendrimer, PEG5 k-Por4-CA4, composed of four pyropheophorbide-a molecules and four cholic acids attached to the terminal end of a linear PEG chain. **b** PET image of nude mice bearing SKOV3 ovarian cancer xenografts at 4, 8, 16, 24 and 48 h post injection of ^{64}Cu-labeled NPs (150–200 ml, ^{64}Cu dose: 0.6–0.8 mCi). The white arrow points to the tumor site. **c** PET-MR images of tumor slices of nude mice bearing A549 lung cancer xenograft at 4 or 24 h post injection of dual-labeled NPs. White arrow points to the necrotic area in the center of the tumor. Permission obtained from [43]. Copyright (2014) by Springer Nature. (D) SPECT images of ^{68}Ga-TFPP (90 MBq, 22 μCi) in Swiss mice bearing fibrosarcoma tumors 1 h post injection. Permission obtained from [47]. Copyright (2012) by Springer

meso-5,10,15,20-tetrakis(3,4-bis(carboxymethyleneoxy)phenyl)porphyrin **13** (T3,48CPP) in tumor-bearing Swiss mice, the compound accumulated in the abdominal tumor [53].

Chatterjee et al. reported ^{99m}Tc labeled *meso*-Tetrakis(4-(carboxymethyleneoxy) phenyl)porphyrin and injected this into mammary-tumor-bearing rats, resulting in tumor accumulation [54]. Siegler et al. described ^{99m}Tc-labeled hematoporphyrin derivative for localizing neoplasms in tumor-bearing animal [55]. The scintigrams and tissue distribution data demonstrated favorable tumor-to-organ ratios sufficiently high for tumor detection. Porphyrin**-**phospholipid liposomes have been labeled with ^{99m}Tc [56].

A water-soluble ^{99m}Tc labeled cyclam acid porphyrin (CAP), 5,10,15,20-tetrakis (4-(4′,8′,11′-tris(carboxymethyl)-1′-(1′,4′,8′,11′-tetraazacyclotetradecane)amido-methyleneoxy)-phenyl) porphyrin (**14 a, b**) was developed for tumor imaging [57]. In vivo distribution studies and scintigram imaging were performed in C6-gliomas and N-nitroso-N-methylurea (NMU) induced mammary tumor bearing rats. These compounds had high tumor-to-muscle ratios compared with ^{99m}Tc(V)-DMSA, ^{99m}Tc-Citrate and ^{201}TlCl, suggesting that ^{99m}Tc-CAP has potential for cancer detection. The same group reported water soluble dendritic porphyrins, termed **15a** and **15b** successfully radiolabeled with ^{99m}Tc [58]. These were administered them to Wistar rats bearing C6-glioma for scintigram imaging and biodistribution studies. Tumor to muscle ratios of **15a** and **15b** were 8.0 and 9.7, respectively.

^{99m}Tc labeled 5,10,15,20-tetrakis(3,4-bis(carboxymethyleneoxy)phenyl) porphyrin (T3,4BCPP) **16** was developed for tumor imaging [59]. It is noteworthy that in this compound ^{99m}Tc binds at the periphery of the porphyrin, a free-base porphyrin without metal substitution in the porphyrin core. By using this water-soluble compound, biodistribution and imaging studies were carried out in C6-gliomas and mammary tumor-bearing animals. T3,4BCPP showed higher tumor-to-muscle ratio in both C6-gliomas, C3H/J mammary tumors and NMU-induced mammary tumors compared with already reported chelates. Chu et al. reported an amino acid histidine-coupled hematoporphyrin (His-Hp) **17** radiolabeled with (^{99m}Tc $(CO)_3(H_2O)_3)^+$ [60]. This was employed for biodistribution studies in mice bearing S180 tumors and tumor uptake was observed.

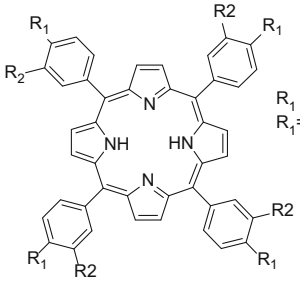

R_1 = OCH2COOH, R_2 = H(T4CPP)
R_1=R_2 = OCH_2COOH (T3, 4BCPP)

13

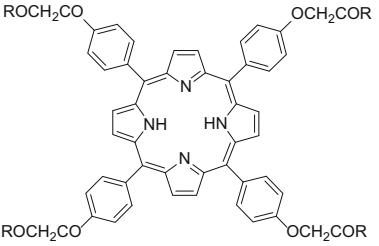

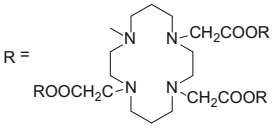

R = CH_2CH_3(**14a**)
R = H (**14b**)

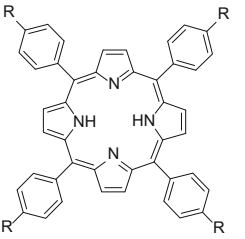

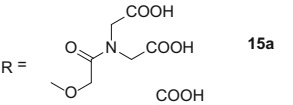

15a

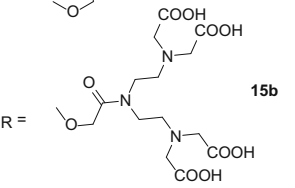

15b

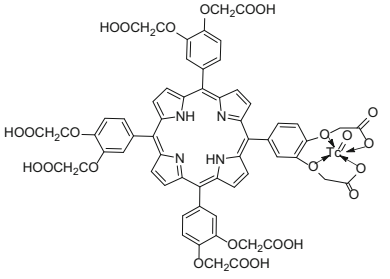

16

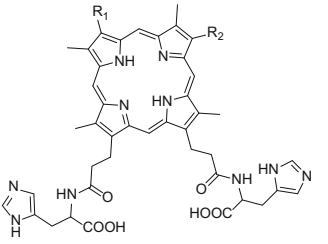

R_1, R_2 = $CH=CH_2$, $CH(OH)CH_3$

17

3.3.5 *Paladium-109*

Beta-emitting ^{109}Pd labeled porphyrins have been used for various radiopharmaceutical applications [61]. ^{109}Pd-hematoporphyrin or ^{100}Pd-protoporphyrin were explored in homograft rejection studies [62]. Water soluble ^{109}Pd porphyrins were also employed for biodistribution studies in mice bearing various types of tumors [27]. Banerji's group prepared a water soluble 5,10,15,20-tetrakis(3,4-bis(carboxymethyleneoxy)phenyl)porphyrin radiolabeled **18** labeled with ^{109}Pd [63]. Biodistribution revealed high tumor-to-blood and tumor-to-muscle ratios (4.4 and 38 at 24 h post-injection). Moreover, the complex showed predominant renal clearance (89%, 24 h post-injection). The same group developed ^{109}Pd labeled 5,10,15,20-tetrakis(3,4-bis(carboethoxymethyleneoxy)phenyl)-porphyrin **19** [64] and biodistribution data revealed efficient tumor uptake in Swiss mice bearing fibrosarcomas.

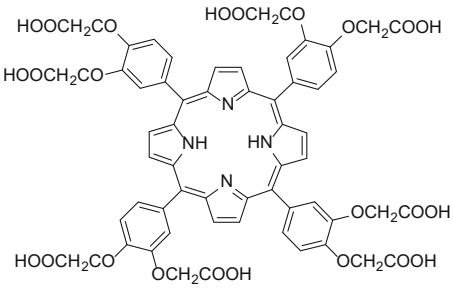

18

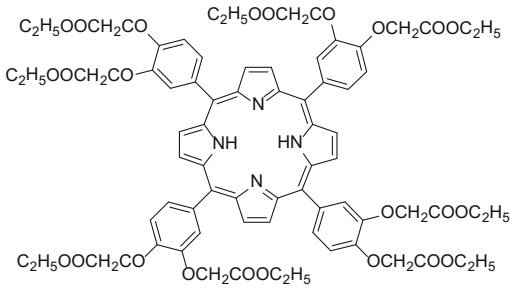

19

3.3.6 Indium-111

^{111}In has received attention in radionanomedicine and has a physical half-life of 2.83 days [65]. An indium labeled water-soluble tetra-4-N-methylpyridyl porphyrin tosylate (^{111}In-T4NMPYP) **20** was prepared and evaluated for selective localization in melanoma [66]. However, tumor uptake was low compared to ^{67}Ga-citrate at 48 h. Indium-111-(^{111}ln) was labeled tetra (N,N,N-trimethylanilinium) porphyrin (TTAP) **21a**, tetra(4-sulfonatophenyl)porphyrin (T4SPP) **21b** and tetra(*N*-methyl-4-pyridyl)porphyrin (TMPyP) **21c** [66, 67]. Lymph node uptake was examined and in rats, (^{111}In)TTAP showed a maximum lymph node to muscle ratio [66]. Lymph nodes in rabbits were visualized by gamma scintigraphy 48 h after intravenous injection of labeled TTAP. Tumor uptake on nuclear scintigraphy imaging of ^{111}ln-labeled HPD was investigated in murine mammary adenocarcinomas and breast tumors in Sprague- Dawley female rats [65]. ^{111}ln-HPD selective uptake was observed in breast tumors.

Nakajima et al. reported a bimodal tumor imaging agent, ^{111}In-labeled metalloporphyrin (^{111}In-ATN-10) **22.** It has both a non-radioactive manganese complex in the porphyrin core and a chelating group attached in its side chain to coordinate with radioactive ^{111}In [68]. Three kinds of tumors were imaged with ^{111}In-ATN-10 and tumors were well-visualized compared to ^{67}Ga-citrate. Bedel-Cloutour et al. reported five different monoclonal antibody labeled with hydrosoluble monosubstituted aryl porphyrins **23** [69]. The conjugates exhibited good mAb-labeling efficiency, as well as preservation of immunoreactivity.

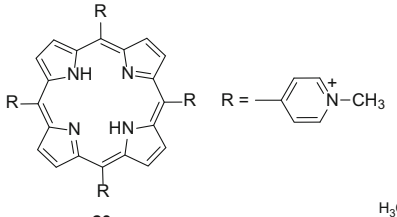

20

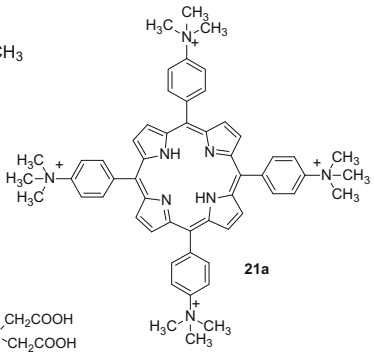

21a

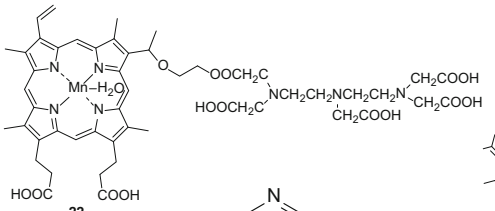

22

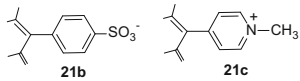

21b

21c

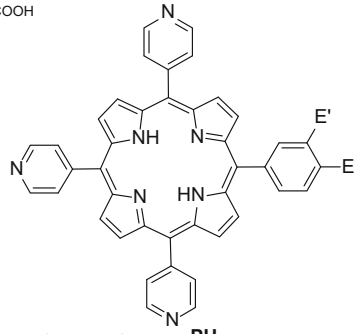

[(3-E'-4-E)-P]Py$_3$ PH$_2$

1- E' = NO_2 E = F
2- E' = H E = F
3- E' = H E = $O(CH_2)_4NH_2$
4- E' = H E = OCH_2COOH
5- E' = H E = OCH_2-COO 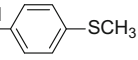

23

3.3.7 Neodymium-140

The β-emitting and $t_{1/2}$ = 3.37 days and availability of neodymium-140 make it an interesting radionuclide for porphyrin labeling [70]. The biodistribution report of the ^{140}Nd-labeled 5,10,15,20-tetraphenylporphyrin ((^{140}Nd)-TPP) **24** [71] compound in vital organs of Swiss mice bearing fibrosarcoma showed that the complex is mostly excreted through liver and kidneys.

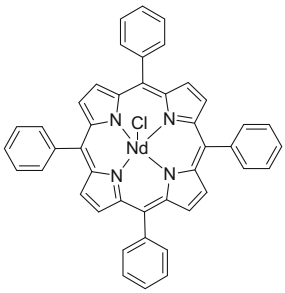

24

3.3.8 Holmium-166

β emitting with a 26.8 h half-life, ^{166}Ho radionuclide is an interesting radionuclide for targeted therapies [72]. ^{166}Ho-labeled 5,10,15,20-tetrakis(phenyl)porphyrin ((^{166}Ho)-TPP) [72] was administered to rats for biodistribution studies. The complex was mostly cleared from the circulation through kidneys and the liver to a lesser extent.

3.3.9 Lutetium-177

5,10,15,20-tetrakis(4-carboxymethyleneoxyphenyl)porphyrin **25** was synthesized and coupled with a macrocyclic bi-functional chelating agent, p-amino-benzyl-1,4,7,10-tetraazacyclododecane-1,4,7,10-tetraacetic acid [73]. The porphyrin-BFCA conjugate was labeled with ^{177}Lu for biodistribution and imaging in Swiss mice bearing either fibrosarcoma or thymic lymphoma tumors. **25** exhibited specific affinity towards thymic lymphoma compared to fibrosarcoma.

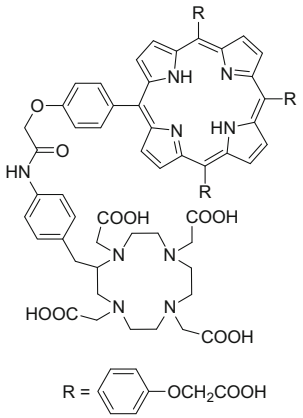

25

3.3.10 Rhenium-186 and 188

^{188}Re generally exhibits the same chelation and radiolabeling chemistry as ^{99m}Tc [74]. Gamma ray-emitting ^{188}Re ($t_{1/2}$ = 16.9 h, β = 2.1 meV, γ = 155 keV 15%) is suitable for imaging and β emitting ^{186}Re ($t_{1/2}$ = 90 h, β = 1.07 meV, γ = 137 keV) offer potential for local radiotherapy [75]. A novel water-soluble porphyrin, meso-tetrakis(3,4-bis(carboxymethyleneoxy)phenyl)porphyrin, **26** was developed with dicarboxylic acid groups as aromatic substituents in the periphery [76, 77]. This β emitting $^{186/188}$Re compound was employed for biodistribution studies in Swiss mice bearing fibrosarcomas and thymic lymphoma. Radionuclide complex showed selectivity towards thymic lymphoma compared to fibrosarcoma. Deng et al. reported a novel ^{188}Re-labeled meso-tetrakis(4-sulfophenyl) porphyrin (TPPS4) **27** [78] as well as a meso-tetrakis(3,4-bis(carboxymethyleneoxy)phenyl) porphyrin (T3,4CPP) **28** [79]. These were evaluated after intravenous injection in tumor-bearing mice. Both compounds exhibited good tumor affinity.

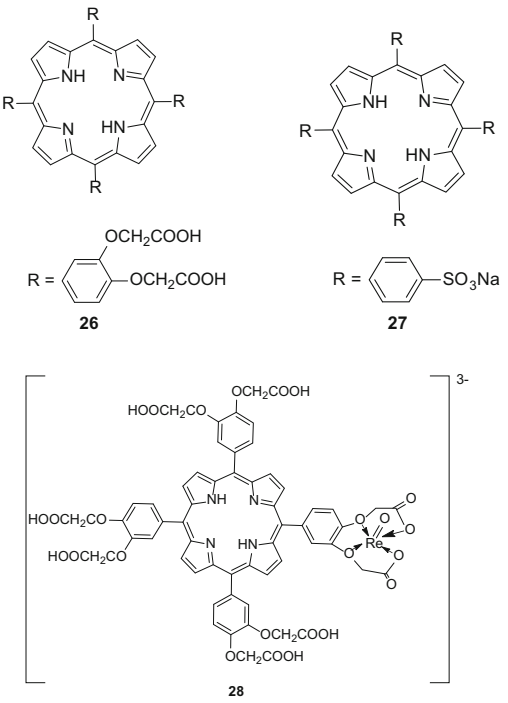

3.4 Phthalocyanine Radiolabeling

3.4.1 Copper-64

^{64}Cu labeled phthalocyanines (Pcs) have been employed for PET imaging agents. ^{64}Cu labeled sulfonated metallophthalocyanines (PcS), ^{64}CuPcS **29,** was employed for biodistribution studies in tumor-bearing rats using PET imaging [17]. Biodistribution results showed that tumor uptake was low (0.2%ID/g) and most ^{64}Cu was taken up by the kidneys and liver (20 and 12%ID/g, respectively). Guérin et al. reported various modified ^{64}Cu labeled sulfonated metallophthalocyanines (^{64}CuPcS$_n$) **30a-d** and their biodistribution studies [80]. The amphiphilic derivatives ^{64}CuPcS$_2$ and ^{64}CuPcS$_3$C$_6$ (1–1.5% injected dose per gram, respectively) exhibited the highest tumor-to-background ratios.

^{64}Cu-labeled frozen micellar naphthalocyanines (nanonaps) were used for whole-body PET imaging of the gastrointestinal tract [81]. Labeling was achieved in just 30 min with over 65% radiolabeling when nanonaps were incubated with ^{64}Cu in aqueous solution (Fig. 3.8a). The movement of the nanonaps through the GI tract was monitored by using PET imaging (Fig. 3.8b). Serial whole-body consecutive coronal images of the mouse are shown in Fig. 3.8c.

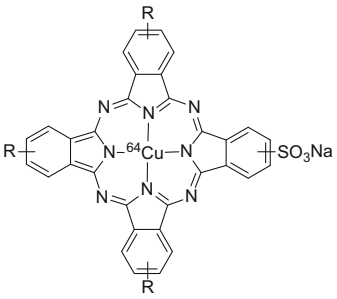

29

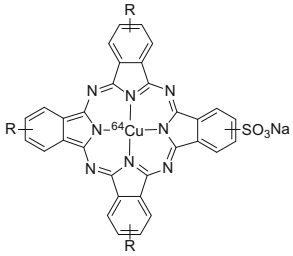

30a: $R^1 = R^2 = R^3 = R^4 = SO_3Na$;
30b: $R^1 = R^2 = R^3 = SO_3Na$ $R^4 = H$;
30c: $R^1 = R^2 = SO_3Na$ $R^3 = R^4 = H$;
$R^1 = R^3 = SO_3Na$ $R^2 = R^4 = H$;
30d:$R^1 = R^2 = R^3 = SO_3Na$ $R^4 = C_6H_{11}$

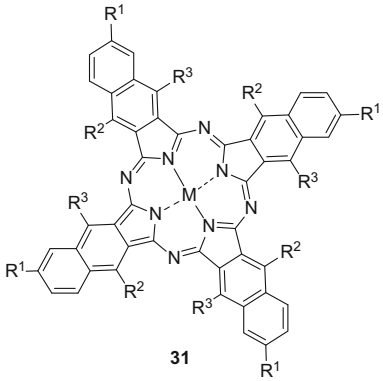

31

Chemical structure of napthalocyanines used. BNc: M= 2H; R^1 = t-Bu; R^2,R^3=H. VBNc: M=VO; R^1 = t-Bu; R^2,R^3=H. ZnBNc: M=Zn;R^1 = t-Bu; R^2,R^3=H. ONc: M=2H; R^1=H; R^2,R^3=O-$(CH_2)_3CH_3$. Phthalocyanines contain single outer benzenes. BPc: M= 2H; R^1 = t-Bu; R^2,R^3=H. VBPc:M=VO; R^1 = t-Bu; R^2=$N(CH_3)_2$; R_3=H.

3.4.2 Zinc-65

Lier et al. reported the effect of human serum components on the photodynamic activity of radiolabeled zinc phthalocyanine (ZnPc) toward Chinese hamster fibroblasts [82]. The association of ^{65}ZnPc with serum low density lipoproteins (LDL) and human serum albumin appeared to enhance the photodynamic effect of this sensitizer.

3.4.3 Gallium-67

Scasnar et al. prepared a series of sulfophthalocyanines (PcS) labeled with ^{67}Ga and studied the effect of the degree of sulfonation on biodistribution [10]. They suggested that lesser sulfonated ^{67}GaPcS, which had significant binding with the various lipoprotein fractions, should be explored for PDT for cancer, whereas increased sulfonation favored association to albumin and suitable for tumor imaging. The same group studied the biodistribution and tumor uptake of ^{67}Ga-labeled lipophilic Ga-TOPc and amphiphilic Ga-TOPcS in tumor bearing C3H mice [83]. The amphiphilic ^{67}Ga-TOPcS exhibited promising tumor uptake and tissue distribution pattern compared to the highly lipophilic ^{67}Ga-TOPc.

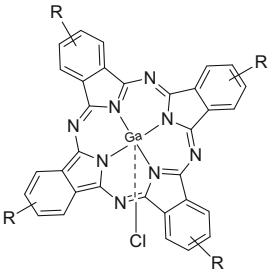

R = $OC_{18}H_{37}$

32a

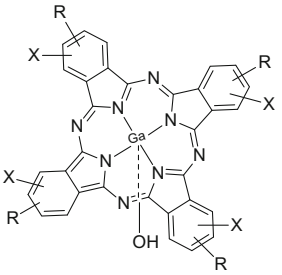

R = $OC_{18}H_{37}$, X = H or SO_3^-

32b

3.4.4 Technetium-99m

The biodistribution of ^{99}Tc-labeled-tetrasulfophthalocyanine **33** was evaluated in tumor-bearing rats. Most of the radioactivity accumulated in the liver, kidneys, ovaries and uterus while tumor uptake was mainly in the exterior cell layers [84].

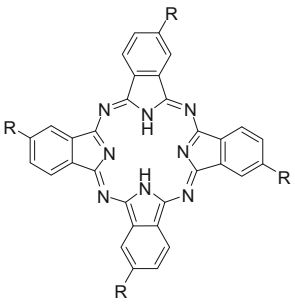

R =H; R= SO_3^-

33

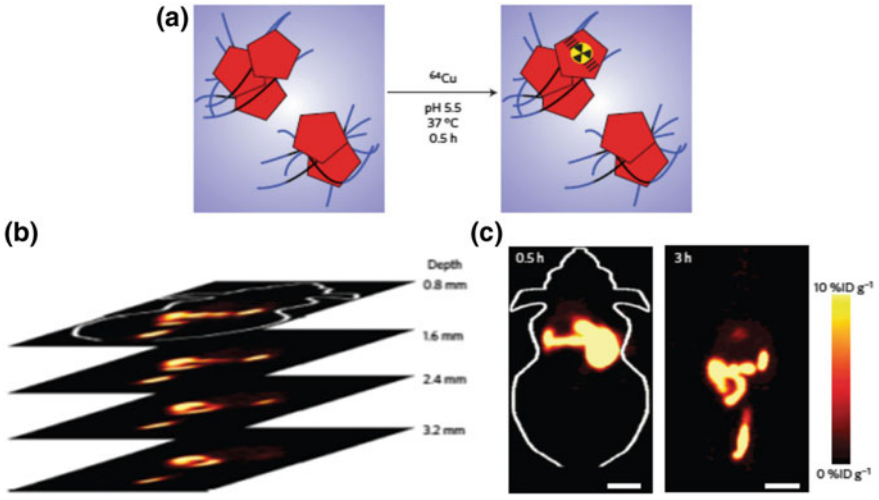

Fig. 3.8 **a** Nanonap labelling using ^{64}Cu. **b** Representative PET imaging of nanonaps. ^{64}Cu-labeled ONc nanonaps were gavaged and mice were imaged at the indicated time points. Scale bars, 1 cm. **c** Representative 0.8-mm-thick coronal slices through the mouse, 3 h after gavage. Permission obtained from [81]. Copyright (2014) by Macmillan Publishers Limited

3.5 Conclusion

Numerous radiolabeled porphyrins and phthalocyanines and their radiopharmaceutical applications such as biodistribution, tumor uptake, PET/SPECT imaging and PDT have been summarized in this chapter. Tumor accumulation depends on many factors including the characteristics of the tumor, the porphyrin or PC, the type of targeting groups and the choice of radioisotopes. Many radiolabeled porphyrins exhibit high tumor uptake that hold potential to be translated into imaging or therapeutic agents for cancer applications.

References

1. M. Biesaga, K. Pyrzyńska, M. Trojanowicz, Porphyrins in analytical chemistry. A review. Talanta **51**(2), 209–224 (2000)
2. H. Huang, W. Song, J. Rieffel, J.F. Lovell, Emerging applications of porphyrins in photomedicine. Front Phys. **3**, 23 (2015)
3. Y. Zhang, J.F. Lovell, Porphyrins as theranostic agents from prehistoric to modern times. Theranostics **2**(9), 905–915 (2012)
4. D. Kessel, Hematoporphyrin and HPD: photophysics, photochemistry and phototherapy. Photochem. Photobiol. **39**(s1), 851–859 (1984)
5. K.M. Smith, K.M. Kadish, R. Guilard, *Handbook of Porphyrin Science: With Applications to Chemistry, Physics, Materials Science, Engineering, Biology and Medicine*, vol 3, (World Scientific, 2012)

6. T.J. Dougherty, A brief history of clinical photodynamic therapy development at Roswell Park Cancer Institute. J. Clin. Laser Med. Surg. **14**(5), 219–221 (1996)
7. R. Ackroyd, C. Kelty, N. Brown, M. Reed, The history of photodetection and photodynamic therapy. Photochem. Photobiol. **74**(5), 656–669 (2001)
8. C.M. Allen, W.M. Sharman, J.E. Van Lier, Current status of phthalocyanines in the photodynamic therapy of cancer. J. Porphyr. Phthalocyannines **5**(2), 161–169 (2001)
9. D.R. Tackley, G. Dent, W.E. Smith, Phthalocyanines: structure and vibrations. Phys. Chem. Chem. Phys. **3**(8), 1419–1426 (2001)
10. V. Ščasnár, Lier J.E. Van, Biological activities of phthalocyanines—XV. Radiolabeling of the differently sulfonated ^{67}Ga-phthalocyanines for photodynamic therapy and tumor imaging. Nucl. Med. Biol. **20**(3), 257–262 (1993)
11. N. Sekkat, H. van den Bergh, T. Nyokong, N. Lange, Like a bolt from the blue: phthalocyanines in biomedical optics. Molecules **17**(1), 98 (2012)
12. Y. Zhang, J.F. Lovell, Recent applications of phthalocyanines and naphthalocyanines for imaging and therapy. Wiley Interdiscip. Rev. Nanomed. Nanobiotechnol. **9**(1), e1420 (2017)
13. H. Ali, J.E. van Lier, Metal Complexes as photo- and radiosensitizers. Chem. Rev. **99**(9), 2379–2450 (1999)
14. F.R. Wrenn, M.L. Good, P. Handler, The use of positron-emitting radioisotopes for the localization of brain tumors. Science **113**(2940), 525–527 (1951)
15. T.W. Liu, T.D. MacDonald, J. Shi, B.C. Wilson, G. Zheng, Intrinsically copper-64-labeled organic nanoparticles as radiotracers. Angew. Chem. Int. Ed. Engl. **51**(52), 13128–13131 (2012)
16. P.A. Waghorn, Radiolabelled porphyrins in nuclear medicine. J. Label. Comp. Radiopharm. **57**(4), 304–309 (2014)
17. A. Soucy-Faulkner, J.A. Rousseau, R. Langlois, V. Berard, R. Lecomte, F. Bénard et al., Copper-64 labeled sulfophthalocyanines for positron emission tomography (PET) imaging in tumor-bearing rats. J. Porphyr. Phthalocyanines **12**(01), 49–53 (2008)
18. F.H. Figge, G.S. Weiland, L.O. Manganiello, Cancer detection and therapy. Affinity of neoplastic, embryonic, and traumatized tissues for porphyrins and metalloporphyrins. Proc. Soc. Exp. Biol. Med. **68**(3), 640–641 (1948)
19. K.M. Smith, *Porphyrins and Metalloporphyrins* (Elsevier, Amsterdam, 1975)
20. W.R. Scheidt, Trends in metalloporphyrin stereochemistry. Acc. Chem. Res. **10**(9), 339–345 (1977)
21. D. Dolphin, *The Porphyrins*, vol. 1 (Academic Press, New York, 1979)
22. K. Kasuga, M. Tsutsuo, Some new developments in the chemistry of metallophthalocyanines. Coord. Chem. Rev. **32**(1), 67–95 (1980)
23. P. Hambright, J. Smart, J. McRae, M. Nohr, Y. Yano, P. Chu et al., Tumor imaging with ^{57}cobalt (III)-sandwich complexes and ^{57}cobalt (III)-porphyrins. Inorg. Nucl. Chem. Lett. **12**(2), 217–222 (1976)
24. L. Anghileri, M. Heidbreder, R. Mathes, ^{57}Co-hematoporphyrin accumulation by experimental tumors. Nuklearmedizin **15**(4), 183 (1976)
25. M. Michael, C. Redvanly, *Handbook of Radiopharmaceuticals* (Wiley, England, 2003)
26. R. Bases, S.S. Brodie, S. Rubenfeld, Attempts at tumor localization using Cu^{64}-labeled copper porphyrins. Cancer **11**(2), 259–263 (1958)
27. P. Hambright, R. Fawwaz, P. Valk, J. McRae, A. Bearden, The distribution of various water soluble radioactive metalloporphyrins in tumor bearing mice. Bioinorg. Chem. **5**(1), 87–92 (1975)
28. D. Cole, J. Mercer-Smith, S. Schreyer, J. Norman, D. Lavallee, The biological characteristics of a water soluble porphyrin in rat lymph nodes. Int. J. Rad. Appl. Instrum. B. **17**(5), 457–464 (1990)
29. M.K. Bhalgat, J.C. Roberts, J.A. Mercer-Smith, B.D. Knotts, R.L. Vessella, D.K. Lavallee, Preparation and biodistribution of copper-67-labeled porphyrins and porphyrin-A6H immunoconjugates. Nucl. Med. Biol. **24**(2), 179–185 (1997)

30. J.C. Roberts, S.L. Newmyer, J.A. Mercer-Smith, S.A. Schreyer, D.K. Lavallee, Labeling antibodies with copper radionuclides using N-4-nitrobenzyl-5-(4-carboxyphenyl)-10, 15, 20-tris (4-sulfophenyl) porphine. Int. J. Rad. Appl. Instrum. A. **40**(9), 775–781 (1989)
31. Y. Fazaeli, A.R. Jalilian, M.M. Amini, M. Aboudzadeh, S. Feizi, A. Rahiminezhad et al., Preparation, nano purification, quality control and labeling optimization of (^{64}Cu)-5, 10, 15, 20-tetrakis (penta fluoro phenyl) porphyrin complex as a possible imaging agent. J. Radioanal. Nucl. Chem. **295**(1), 255–263 (2013)
32. J. Shi, T. Liu, J. Chen, D. Green, D. Jaffray, B.C. Wilson et al., Transforming a targeted porphyrin theranostic agent into a PET imaging probe for cancer. Theranostics **1**, 363–370 (2011)
33. H. Huang, J.F. Lovell, Advanced functional nanomaterials for theranostics. Adv. Funct. Mater. **27**(2), 1603524 (2017)
34. D. Luo, K.A. Carter, J.F. Lovell, Nanomedical engineering: shaping future nanomedicines. Wiley Interdiscip. Rev. Nanomed. Nanobiotechnol. **7**(2), 169–188 (2015)
35. S.M. Janib, A.S. Moses, J.A. MacKay, Imaging and drug delivery using theranostic nanoparticles. Adv. Drug Deliv. Rev. **62**(11), 1052–1063 (2010)
36. X. Ma, Y. Zhao, X.-J. Liang, Theranostic nanoparticles engineered for clinic and pharmaceutics. Acc. Chem. Res. **44**(10), 1114–1122 (2011)
37. T.W. Liu, T.D. MacDonald, J. Shi, B.C. Wilson, G. Zheng, Intrinsically copper-64-labeled organic nanoparticles as radiotracers. Angew. Chem. Intl. Ed. Engl. **51**(52), 13128–13131 (2012)
38. T.W. Liu, T.D. MacDonald, C.S. Jin, J.M. Gold, R.G. Bristow, B.C. Wilson et al., Inherently multimodal nanoparticle-driven tracking and real-time delineation of orthotopic prostate tumors and micrometastases. ACS Nano **7**(5), 4221–4232 (2013)
39. J. Rieffel, U. Chitgupi, J.F. Lovell, Recent advances in higher-order, multimodal, biomedical imaging agents. Small **11**(35), 4445–4461 (2015)
40. H. Huang, R. Hernandez, J. Geng, H. Sun, W. Song, F. Chen et al., A porphyrin-PEG polymer with rapid renal clearance. Biomaterials **76**, 25–32 (2016)
41. Y. Zhang, D. Wang, S. Goel, B. Sun, U. Chitgupi, J. Geng et al., Surfactant-stripped frozen pheophytin micelles for multimodal gut imaging. Adv. Mater. **28**(38), 8524–8530 (2016)
42. J. Rieffel, F. Chen, J. Kim, G. Chen, W. Shao, S. Shao et al., Hexamodal imaging with porphyrin-phospholipid-coated upconversion nanoparticles. Adv. Mater. **27**(10), 1785–1790 (2015)
43. Y. Li, Lin T-y, Y. Luo, Q. Liu, W. Xiao, W. Guo et al., A smart and versatile theranostic nanomedicine platform based on nanoporphyrin. Nat. Commun. **5**, 4712 (2014)
44. L. Feng, L. Cheng, Z. Dong, D. Tao, T.E. Barnhart, W. Cai et al., Theranostic liposomes with hypoxia-activated prodrug to effectively destruct hypoxic tumors post photodynamic therapy. ACS Nano. (2016)
45. Y. Fazaeli, A.R. Jalilian, M.M. Amini, A. Rahiminejad-kisomi, S. Rajabifar, F. Bolourinovin et al., Preparation and preliminary evaluation of (^{67}Ga)-tetra phenyl porphyrin complexes as possible imaging agents. J. Radioanal. Nucl. Chem. **288**(1), 17–24 (2011)
46. K. Sasaki, N. Yumita, R. Nishigaki, I. Sakata, S. Nakajima, Umemura Si. Pharmacokinetic study of a gallium-porphyrin photo- and sono-sensitizer, ATX-70, in tumor-bearing mice. Cancer Sci. **92**(9), 989–995 (2001)
47. Y. Fazaeli, A.R. Jalilian, M.M. Amini, K. Ardaneh, A. Rahiminejad, F. Bolourinovin et al., Development of a ^{68}Ga-fluorinated porphyrin complex as a possible PET imaging agent. Nucl. Med. Mol. Imaging **46**(1), 20–26 (2012)
48. F. Zoller, P.J. Riss, F.-P. Montforts, D.K. Kelleher, E. Eppard, F. Rösch, Radiolabelling and preliminary evaluation of 68 Ga-tetrapyrrole derivatives as potential tracers for PET. Nucl. Med. Biol. **40**(2), 280–288 (2013)
49. S. Jurisson, D. Berning, W. Jia, D. Ma, Coordination compounds in nuclear medicine. Chem. Rev. (U. S.) **93**(3), 11371156 (1993)

50. S.S. Jurisson, J.D. Lydon, Potential technetium small molecule radiopharmaceuticals. Chem. Rev. (U. S.) **99**(9), 2205–2218 (1999)
51. D.W. Wong, A. Mandal, I.C. Reese, J. Brown, R. Siegler, In vivo assessment of ^{99m}Tc-labeled hematoporphyrin derivative in tumor-bearing animals. Int. J. Nucle. Med. Biol. **10**(4), 211–218 (1983)
52. A.-Y. Wang, J.-L. Lin, W.-C. Lin, Studies on the porphine labeled with 99 mTc–pertechnetate. J. Radioanal. Nucl. Chem. **284**(1), 21–28 (2010)
53. S. Shetty, S. Murugesan, S. Chatterjee, S. Banerjee, T. Srivastava, O.P. Noronha et al., A new ^{99m}Tc labeled porphyrin for specific imaging of Sarcoma 120: Synthesis and biological study in a Swiss mouse model. J. Label. Comp. Radiopharm. **38**(5), 411–418 (1996)
54. S.R. Chatterjee, S. Murugesan, J. Kamat, S. Shetty, T. Srivastava, O. Noronha et al., Photodynamic effects induced by meso-tetrakis (4-(carboxymethyleneoxy) phenyl) porphyrin using rat hepatic microsomes as model membranes. Arch. Biochem. Biophys. **339**(1), 242–249 (1997)
55. D.W. Wong, A. Mandal, I.C. Reese, J. Brown, R. Siegler, In vivo assessment of ^{99m}Tc-labeled hematoporphyrin derivative in tumor-bearing animals. Int. J. Nucl. Med. Biol. **10**(4), 211–218 (1983)
56. J.-H. Lee, S. Shao, K.T. Cheng, J.F. Lovell, C.H. Paik, ^{99m}Tc-labeled porphyrin–lipid nanovesicles. J. Liposome Res. **25**(2), 101–106 (2015)
57. S. Murugesan, S. Shetty, T. Srivastava, O. Noronha, A. Samuel, A technetium-99m-labelled cyclam acid porphyrin (CAP) for tumour imaging. Appl. Radiat. Isot. **55**(5), 641–646 (2001)
58. M. Subbarayan, S.J. Shetty, T.S. Srivastava, O.P. Noronha, A.M. Samuel, H. Mukhtar, Water-soluble ^{99m}Tc-labeled dendritic novel porphyrins tumor imaging and diagnosis. Biochem. Biophys. Res. Commun. **281**(1), 32–36 (2001)
59. M. Subbarayan, S. Shetty, T. Srivastava, O. Noronha, A. Samuel, Evaluation studies of technetium-99m-porphyrin (T3, 4BCPP) for tumor imaging. J. Porphyr. Phthalocyanines. **5** (12), 824–828 (2001)
60. Y. Liu, B. Shen, F. Liu, B. Zhang, T. Chu, J. Bai et al., Synthesis, radiolabeling, biodistribution and fluorescent imaging of histidine-coupled hematoporphyrin. Nucl. Med. Biol. **39**(4), 579–585 (2012)
61. R.A. Fawwaz, W. Hemphill, H. Winchell, Potential use of ^{109}Pd-porphyrin complexes for selective lymphatic ablation. J. Nucl. Med. **12**(5), 231–236 (1971)
62. R. Fawwaz, F. Frye, W. Loughman, W. Hemphill, Survival of skin homografts in dogs injected with ^{109}Pd-protoporphyrin. J. Nucl. Med. **15**(11), 997–1002 (1974)
63. S. Chakraborty, T. Das, S. Banerjee, H. Sarma, M. Venkatesh, Preparation and preliminary biological evaluation of a novel ^{109}Pd labeled porphyrin derivative for possible use in targeted tumor therapy. Q. J. Nucl. Med. Mol. Imaging **51**(1), 16 (2007)
64. T. Das, S. Chakraborty, H. Sarma, S. Banerjee, A novel (^{109}Pd) palladium labeled porphyrin for possible use in targeted radiotherapy. Radiochim. Acta **96**(7), 427–433 (2008)
65. D.W. Wong, A. Mandal, J. Brown, I.C. Reese, R. Siegler, S. Hyman, In vivo assessment of ^{111}In-labeled hematoporphyrin derivative in breast tumor-bearing animals. Int. J. Rad. Appl. Instrum. B. **16**(3), 269–281 (1989)
66. G. Robinson Jr., A. Alavi, R. Vaum, M. Staum, Imaging of lymph node uptake after intravenous administration. J. Nucl. Med. **27**, 239 (1986)
67. C. Ljungquist, Delineation of a transplanted malignant melanoma with indium-111-labeled porphyrin. J. Nucl. Med. **26**, 756–760 (1985)
68. S. Nakajima, H. Yamauchi, I. Sakata, H. Hayashi, K. Yamazaki, T. Maeda et al., ^{111}In-labeled Mn-metalloporphyrin for tumor imaging. Nucl. Med. Biol. **20**(2), 231–237 (1993)
69. C.H. Bedel-Cloutour, L. Mauclaire, A. Saux, M. Pereyre, Syntheses of functionalized indium porphyrins for monoclonal antibody labeling. Bioconjug. Chem. **7**(6), 617–627 (1996)
70. R. Firestone, V. Shirley, C. Baglin, S. Chu, J. Zipkin, *Table of Isotopes* (A Wiley-Interscience Publication. Wiley, New York, 1996)

71. M. Aboudzadeh, Y. Fazaeli, H. Khodaverdi, H. Afarideh, Production, nano-purification, radiolabeling and biodistribution study of (^{140}Nd) 5, 10, 15, 20-tetraphenylporphyrin complex as a possible imaging agent. J. Radioanal. Nucl. Chem. **295**(1), 105–113 (2013)
72. N. Vahidfar, A.R. Jalilian, Y. Fazaeli, A. Bahrami-Samani, D. Beiki, A. Khalaj, Development and evaluation of a ^{166}holmium labelled porphyrin complex as a possible therapeutic agent. J. Radioanal. Nucl. Chem. **295**(2), 979–986 (2013)
73. H.D. Sarma, T. Das, S. Banerjee, M. Venkatesh, P.B. Vidyasagar, K.P. Mishra, Studies on efficacy of a novel ^{177}Lu-labeled porphyrin derivative in regression of tumors in mouse model. Curr. Radiopharm. **4**(2), 150–160 (2011)
74. J. Crudo, M. Edreira, E. Obenaus, S. de Castiglia, Labeling of the anti-melanoma 14f7 monoclonal antibody with rhenium-188-MAG3 chelate: conjugation optimization, in vitro stability and animal studies. J. Radioanal. Nucl. Chem. **261**(2), 337–342 (2004)
75. K.M. Kadish, K.M. Smith, R. Guilard, *Handbook of Porphyrin Science* (World Scientific, Singapore, 2010), pp. 1–35 2014
76. S. Banerjee, T. Das, G. Samuel, H. Sarma, M. Venkatesh, M. Pillai, A novel ($^{186/188}$Re)-labelled porphyrin for targeted radiotherapy. Nucl. Med. Commun. **22**(10), 1101–1107 (2001)
77. H.D. Sarma, T. Das, S. Banerjee, M. Venkatesh, P.B. Vidyasagar, K.P. Mishra, Biologic evaluation of a novel ^{188}Re-labeled porphyrin in mice tumor model. Cancer Biother. Radiopharm. **25**(1), 47–54 (2010)
78. Z. Jia, H. Deng, M. Pu, Synthesis and preliminary biological studies of the novel conjugate ^{188}Re-labeled meso-tetrakis (4-sulfophenyl) porphyrin in mice. Nucl. Med. Biol. **34**(6), 643–649 (2007)
79. Jia Z-y, Pu Deng H-f, Luo S-z M-f, Rhenium-188 labelled meso-tetrakis (3, 4-bis (carboxymethyleneoxy) phenyl) porphyrin for targeted radiotherapy: preliminary biological evaluation in mice. Eur. J. Nucl. Med. Mol. Imaging **35**(4), 734–742 (2008)
80. E.R. Ranyuk, N. Cauchon, H. Ali, R. Lecomte, B. Guérin, J.E. van Lier, PET imaging using ^{64}Cu-labeled sulfophthalocyanines: synthesis and biodistribution. Bioorg. Med. Chem. Lett. **21**(24), 7470–7473 (2011)
81. Y. Zhang, M. Jeon, L.J. Rich, H. Hong, J. Geng, Y. Zhang et al., Non-invasive multimodal functional imaging of the intestine with frozen micellar naphthalocyanines. Nat. Nanotechnol. **9**(8), 631–638 (2014)
82. M. Obochi, R. Boyle, Lier J. Van, Biological activities of phthalocyanines. XIII. The effects of human serum components on the in vitro uptake and photodynamic activity of zinc phthalocyanine. Photochem. Photobiol. **57**(4), 634–640 (1993)
83. J. Rousseau, R. Boyle, A. MacLennan, T. Truscott, J. Van Lier, Biodistribution and tumor uptake of (^{67}Ga) chlorogallium-tetraoctadecyloxy phthalocyanine and its sulfonation products in tumor bearing C3H mice. Int. J. Rad. Appl. Instrum. B. **18**(7), 777–782 (1991)
84. J. Rousseau, D. Autenrieth, J.E. Van Lier, Synthesis, tissue distribution and tumor uptake of (^{99}Tc) tetrasulfophthalocyanine. Int. J. Appl. Radiat. Isot. **34**(3), 571–579 (1983)
85. C.P. Gros, A. Eggenspiller, A. Nonat, J.-M. Barbe, F. Denat, New potential bimodal imaging contrast agents based on DOTA-like and porphyrin macrocycles. Med. Chem. Commun. **2**(2), 119–125 (2011)
86. B. Laster, S. Kahl, J. Kalef-Ezra, E. Popenoe, R.G. Fairchild, *Biological Efficacy of a Boronated Porphyrin as Measured in Cell Culture* (Brookhaven National Lab, Upton, NY (USA), 1987)
87. F. Benard, S. Kudrevich, J. Rousseau, J. van Lier, Radiolabeled phthalocyanines as tumor imaging agents. Clin. Nucl. Med. **21**(6), 512 (1996)
88. D.K. Lavallee, R. Fawwaz, The synthesis and characterization of 111 in hematoporphyrin derivative. Int. J. Rad. Appl. Instrum. B **13**(6), 639–641 (1986)
89. D.W. Wong, A simple and efficient method of labeling hematoporphyrin derivative with ^{111}In. Appl. Radiat. Isot. **35**(7), 691–692 (1984)

90. N. Maric, S.M. Chan, P.B. Hoffer, P. Duray, Radiolabeled porphyrin vs gallium-67 citrate for the detection of human melanoma in athymic mice. Int. J. Rad. Appl. Instrum. B. **15**(5), 543–551 (1988)
91. R.R. Kavali, B. Chul Lee, B. Seok Moon, S. Dae Yang, K. Soo Chun, C. Woon Choi et al., Efficient methods for the synthesis of 5-(4-(18F) fluorophenyl)-10, 15, 20-tris (3-methoxyphenyl) porphyrin as a potential imaging agent for tumor. J. Label. Comp Radiopharm. **48**(10), 749–758 (2005)
92. G.M. Entract, F. Bryden, J. Domarkas, H. Savoie, L. Allott, S.J. Archibald et al., Development of PDT/PET theranostics: Synthesis and biological evaluation of an ^{18}F-radiolabeled water-soluble porphyrin. Mol. Pharm. **12**(12), 4414–4423 (2015)
93. T. Das, S. Chakraborty, H.D. Sarma, S. Banerjee, M. Venakatesh, A novel ^{177} Lu-labeled porphyrin for possible use in targeted tumor therapy. Nucl. Med. Biol. **37**(5), 655–663 (2010)

Chapter 4
Graphene-Based Nanomaterials

Je Min Yoo, Do Won Hwang and Byung Hee Hong

Abstract Graphenes are unique nanomaterials which was recently made compatible for physiological milieu, and thus find a way to be used as nanocarriers. The surface engineering abilities of nano-graphene oxides (nano-GOs) or graphene quantum dots (GQDs) in their own outstanding photoluminescence property have made it possible to be used for imaging or drug delivery. Though many successes were not reported in the application of GQDs in vivo, toxicity and safety of GOs in vitro and in vivo are being investigated. Interestingly, GOs are found to be degraded in vivo. In addition to much effort to use GOs as drug carriers, there have been recent trials to apply GOs for magnetic resonance imaging (MRI) and positron emission tomography (PET) or even multiplexed imaging with MRI/fluorescence or MRI/PET. The product has the composition of chelator-conjugated GOs loaded with iron oxide nanoparticles, and a variety of radionuclides such as ^{68}Ga, ^{64}Cu or ^{125}I and ^{131}I and ^{177}Lu were used for PET or SPECT imaging and for radionuclide

J. M. Yoo · B. H. Hong (✉)
Department of Chemistry, College of Natural Science,
Seoul National University, Seoul, Republic of Korea
e-mail: byunghee@snu.ac.kr

J. M. Yoo
e-mail: jyoo1130@snu.ac.kr

B. H. Hong
Program in Nano Science and Technology, Graduate School of Convergence
Science and Technology, Seoul National University, Seoul, Republic of Korea

D. W. Hwang
Department of Nuclear Medicine, Seoul National University
College of Medicine, Seoul, Republic of Korea
e-mail: hdw6592@snu.ac.kr

D. W. Hwang
Department of Molecular Medicine and Biopharmaceutical Sciences,
Graduate School of Convergence Science and Technology,
College of Medicine or College of Pharmacy,
Seoul National University, Seoul, Republic of Korea

D. S. Lee (ed.), *Radionanomedicine*, Biological and Medical Physics,
Biomedical Engineering, https://doi.org/10.1007/978-3-319-67720-0_4

therapy, respectively. Multiplexed imaging or theranostics will enable targeted delivery, imaging in vivo with PET/SPECT and/or MRI and ex vivo confirmation of the tissues in preclinical studies.

4.1 Introduction

Although scientific breakthroughs have brought advances in radionanomedicine to enable nanoparticle-assisted magnetic resonance imaging (MRI) and radionanoparticle-using positron emission tomography (PET), challenges including the real-time imaging with respectable temporal/ spatial resolutions and the discovery of less toxic probes with adequate stability still remain to be solved. To that end, researchers continuously endeavor to discover novel candidates that can further improve the techniques. Since its first historical discovery in 2004, graphene has continually gained attention of scientists across diverse disciplines due to many of its extraordinary properties. While the major research foci have been exploration of graphenes' electrical, mechanical, physical and chemical characteristics, recent investigations are done on its optical properties along with the non-toxic and environment-friendly nature. Especially, these unique characteristics have drawn researchers' interests in the field of biomedicine. In addition to the therapeutic utility of graphene as carrier of drug delivery or near-infrared (NIR) laser-mediated cancer ablation, a few recent studies have also suggested the potential role of graphene-based nanomaterials as exogenous probes for molecular imaging taking advantage of its unique feature. In this chapter, we will discuss the preparation, toxicity and a few recent applications of graphene-based nanomaterials in radionanomedicine.

4.2 Preparation of Graphene-Based Nanomaterials for Biomedical Applications

Due to many of its unprecedented properties, the first historical discovery of graphene by Andrei Geim and Konstantin Novoselov immediately drew significant attention of scientists [1]. As it is an atomically thin material with unusual electrical and physical characteristics, the initial focus of graphene research was on the replacement of indium tin oxide for transparent electrodes, which can provide flexibility to them as well.

In the meantime, researchers in the field of biomedicine have taken notice of other important aspects of graphene: its environment-friendly and non-toxic nature, as well as the outstanding optical properties [2, 3]. Above all, it should be noted that dispersed graphene-based nanomaterials including graphene oxides (GOs), graphene quantum dots (GQDs), and reduced graphene oxides (rGOs) are more

frequently employed for biomedical applications while the term graphene refers to a two-dimensional atomic film. GOs and GQDs are especially broadly utilized for biomedical applications due to their high dispersibility and low cytotoxicity. Briefly, GOs are synthesized through the Hummer's method and GQDs can be obtained by thermo-oxidative cutting of carbon precursors including GOs. Notably, GOs and GQDs have various functional groups available for further modifications, which can be utilized for specialized purposes and further enhance their dispersibility. Table 4.1 summarizes characteristic features of graphene-based nanomaterials for imaging applications [2]. The following sections will introduce a few modification approaches of graphene-based nanomaterials.

Table 4.1 Characteristic features of graphene derivatives for bioimaging

Types	Structure	Optical properties	Toxicity	Imaging applications
GOs	Sub-10 nm to micrometer size range Disrupted sp^2 domain with hydrophilic oxygenated group	Intrinsic photo-luminescence emission with UV excitation, and tunable emission wavelength located at the range of UV–Vis	Typically more toxic than GQDs, and cell-line dependent toxicity but no significant toxicity for both in vitro and in vivo levels at low doses	Fluorescence (Intrinsic and extrinsic) and Raman imaging, Photoacoustic imaging (Extrinsic)
GQDs	Few nanometer (2–5 nm) small sp^2 domain size and oxygenated groups at edge		Generally, non-toxic (up to 1 mg ml^{-1}). Excretion through both renal and fecal clearance. No significant toxicity based on in vitro and in vivo studies	Fluorescence imaging (Intrinsic)
rGOs	Large connected sp^2 domains than GOs, with few hydrophilic group	A high photoluminescence quenching effect with enhanced absorption cross-section in NIR range	More toxic than hydrophilic graphene derivatives. Not-readily biodegradable without functional moieties	Fluorescence (Extrinsic) and Photoacoustic imaging (Intrinsic)

Yoo et al. [2], Copyright 2015

4.2.1 Enhancing the Dispersibility and Stability Under Physiological Conditions

In general, GOs are well-dispersed in water for several months without much aggregation. In physiological conditions, however, they are more prone to aggregate owing to the presence of ionic salts. To enhance the stability under these conditions, modification with biocompatible polymers and nano-sized GOs are employed [4–8]. Among many modification methods, grafting of polyethylene glycol (PEG) is the most frequently used. Many reports have shown that PEG grafting can improve the dispersibility and stability of GOs in biological buffers and highly concentrated salts. PEGs can be grafted on the edges of GOs by the reactions with carboxylic acid and epoxy groups. Other polymers such as polyacrylic acid (PAA), polyamido amine (PAMAM), and dextran can be also conjugated on GOs by the same reactions [4–6]. While as-synthesized GOs show a wide range of sizes, reduction of the average size can be simply achieved by sonication. Many reports show that high energy sonication can break down large GO flakes into nanometer scale particles, as small as 10 nm, which show greater dispersibility in many solvents including biological buffers [7, 8].

4.2.2 Graphene as Nanocarriers

Although micrometer-scale GOs are known to be toxic, their large hydrophobic basal plane and oxygen-containing functional groups on the edges are advantageous for both covalent and non-covalent chemical modifications with other molecules including fluorescent organic dyes.

In 2010, Peng et al. employed fluorescein-labeled GOs for intracellular imaging studies [9]. To prevent the fluorescence quenching and improve dispersibility, PEGs were grafted to grant enough space between GOs and fluorescein. They successfully utilized GOs–PEG-fluorescein system for intracellular imaging without much toxicity. Similarly, Yang et al. utilized cyanine 7 (Cy7)-labeled GOs for in vivo fluorescence imaging, which also could target tumor [10]. In addition, active targeting of tumor cells could be done by introducing cancer targeting moieties on the edges (Fig. 4.1a–c). As folate receptors are overexpressed on tumor cells, folic acid can be employed as the targeting moiety. Through a simple Ethyl dimethylaminopropyl carbodiimide (EDC) coupling reaction, folic acid can be covalently bonded to the carboxyl groups of GOs. Amine group-containing antibodies including Herceptin and transferrin can be also easily conjugated with GOs through the same reactions, thus enabling antibody-based targeting. Other molecules such as vascular endothelial growth factor (VEGF), anti-endoglin antibody (TRC105), β-cyclodextrin, and hyaluronic acid have also been employed on graphene-based nanomaterials for active targeting imaging studies [11–13]. It should be also noted that these systems successfully targeted tumor cells without significant toxicity.

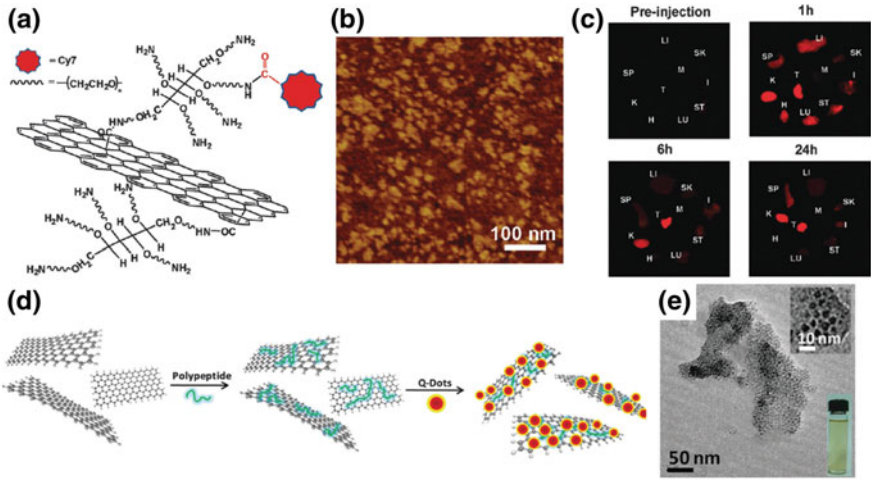

Fig. 4.1 Covalent modification and Non-covalent modification of graphene. **a** A scheme of a nano-graphene sheet (NGS) with PEG functionalization and labeled by Cy7. **b** An AFM image of NGS–PEG. **c** Spectrally resolved ex vivo fluorescence images of organs before injection and 1, 6, and 24 h after injection of NGS–PEG–Cy7. **d** A scheme of sequential peptides and QDs adsorption on rGO sheets. **e** TEM image of the QD–rGO. QD: quantum dot, rGO: reduced graphene oxide. Adapted with permission [10]

In addition to aforementioned covalent modifications, non-covalent methods have also been frequently employed to incorporate different molecules on graphene-based nanomaterials. In 2012, Hu et al. grafted inorganic quantum dots (QDs) on rGOs. [14] Foremost, amphiphilic poly (L-lysine) layer was introduced by π–π interactions, followed by the electrostatic interactions with 11-mercaptoundecanoic acid capped-CdSe/ZnS QDs (Fig. 4.1d, e). Similarly, Chen et al. reported the grafting of bovine serum albumin (BSA) capped-QDs on rGOs with polyethylenimine layer [15]. Both systems successfully showed decent intracellular imaging abilities without appreciable toxicity.

4.2.3 Reduction of GOs to Make rGO

Although rGOs generally exhibit poor solubility and non-negligible toxicity, their high absorption in the NIR region makes them well-suited for photoacoustic imaging and photothermal therapies. rGOs can be prepared by chemical, electrochemical, or photothermal reduction of GOs, where chemical reduction is regarded to be the most facile method to obtain rGOs [16–18]. In 2007, Stankovich et al. reported the use of hydrazine-assisted reduction of GOs in aqueous conditions [18]. Although the insolubility of rGOs and the toxicity of hydrazine often require further modifications for more practical applications, hydrazine is still the most widely

used reducing agent to produce rGOs. As rGOs feature a negligible amount of oxygen-containing—epoxy, hydroxyl, and carboxyl—functional groups, surface modifications on rGOs are performed through non-covalent interactions between aromatic ring molecules and rGOs' basal plane. Namely, Shi et al. reported in 2013 the grafting of hydrophobic alkyl chain-terminated PEGs on rGOs to achieve higher dispersibility [19].

Recently, several groups utilized proteins as novel reducing agents, which can assure better stability and biocompatibility as well. In 2011, Liu et al. utilized gelatin as the reducing agent, which yielded well-dispersed rGOs in physiological conditions [20]. Gelatin-rGO composite was employed as a novel in vitro imaging agent, which was successfully internalized in cells without significant toxicity. In 2013, Sheng et al. reported BSA-assisted reduction of GOs, where BSA functions as a surfactant as well [21]. Resulting BSA–rGOs was employed as in vivo imaging probes as it exhibited great solubility in physiological conditions.

4.2.4 Photoluminescent Nano-GOs and GQDs

While GOs are known for their ability to quench fluorescence in close proximity, GQDs exhibit faint, yet non-negligible photoluminescence. Typically, the quantum yields (QYs) of solvothermally synthesized GQDs (5–10 nm) are below 20% [22–24]. In 2011, Zhu et al. synthesized GQDs by solvothermally cut GOs in dimethylformamide [23]. The resulting GQDs showed great dispersibility in physiological conditions, with an average size of 5.3 nm and distinct green fluorescence with 11.4% QY. The authors employed these GQDs for bio-imaging studies without any significant toxicity. In 2012, Zhang et al. reported an electrochemical oxidation of graphite to produce GQDs [24]. Electrolysis of graphite under alkaline conditions and subsequent treatment with hydrazine yielded GQDs with green photoluminescence, with 14% QY. They also utilized GQDs for bio-imaging studies on various types of stem cells without any appreciable toxicity.

Interestingly, the optical properties of GQDs can be modulated by various surface modifications. In 2012, Li et al. reported microwave-assisted method to produce GQDs, with subsequent reduction using $NaBH_4$ [25]. Initially, as-synthesized GQDs exhibited green-yellow fluorescence with 11.7% QY. On the other hand, reduced GQDs showed blue fluorescence with an increased QY of 22.9%. Photoluminescence was found to be altered by either reduction or grafting of exogenous molecules [25, 26]. They showed that both $NaBH_4$ –assisted reduction of GQDs and grafting of alkylamines yielded blue-shifted emission, with increased QYs. In 2013, Wu et al. synthesized nitrogen-doped GQDs via bottom-up method from L-glutamic acid as the precursor, yielding about 5 nm-sized GQDs [27]. The authors employed the n-doped GQDs as an effective in vitro and in vivo imaging agent with a QY reaching 54.5%.

4.3 Toxicity of Graphene-Based Nanomaterials

A number of different carbon allotropes including carbon nanotubes (CNTs), fullerenes, and graphene-based nanomaterials have been considered in various biomedical applications. Nevertheless, previous studies consistently reported toxicity entirely different according to the types of materials, allotropes, despite their similarities in the chemical compositions. While CNTs exhibit relatively high levels of toxicity in many studies, recent investigations showed that most graphene-based materials show negligible toxicities [28, 29].

4.3.1 In Vitro Toxicity

Regarding GOs and GQDs applied in biomedicine, several groups recently investigated their in vitro toxicity and cellular uptake on different cell types. The studies generally agreed on the lack of significance toxicity despite internalization in the cells, which make graphene-based nanomaterials candidates for diverse biological studies [30–35]. On the contrary, studies suggested that certain forms of GOs and GQDs can be damaging seriously to the cells [34, 35]. Micrometer-sized GOs were found severely toxic on a number of different cell lines on a thorough cytotoxicity screening study [36]. Large GOs and GO-based nanoplatelets induced significant cytotoxicity and thereby could cause lung diseases [37, 38]. The toxicity of graphene-based nanomaterials was believed to depend strongly on the particle size and nano-sized GOs and GQDs was without significant toxicity [35, 38, 39]. Akhavan et al., however, proposed an entirely different mechanism of toxicity. The authors suggested that the direct interaction between the edges of these graphene-based nanomaterials and the cell membranes led to the cytotoxicity, which was independent of the particle size and thus even nano-sized GOs and GQDs could also induce lethal damages to cells [40, 41]. In addition, the toxicity studies of other nanoparticles suggested that cellular internalization and cytotoxicity also depended on the shape as well [42, 43]. To sum up, the mechanism of cytotoxicity of graphene-based nanomaterials still remains unclear and further studies are warranted.

The effects of edge functionalization on cytotoxicity and membrane permeability have also been investigated thoroughly. Edge modification with PEG and other hydrophilic polymers have been the most widely employed technique to improve biocompatibility in physiological conditions while reducing the cytotoxic effects [7]. In 2014, Yuan et al. and Kong et al. modified GQDs with various functional groups including PEG, NH_2, COOH, and $CO–N(CH_3)_2$ and explored the effects on their cytotoxicity and membrane permeability [33, 44]. Although their membrane permeability differed among these GQDs variants by displaying 8, 13, and 19% permeability respectively for GQDs with PEG, OH/COOH, and NH_2 groups,

all these variants showed only negligible cytotoxicity. Sasidharan et al. reported the importance of functional groups in attenuating potential toxicity induced by graphene-based nanomaterials without any functional groups [31]. They suggested that hydrophobic interactions between the basal planes of graphene-based nanomaterials with the cell membrane likely provoke toxicity including apoptosis triggered by elevated intracellular reactive oxygen species and the cell membrane deformation. In the presence of functional groups, however, the hydrophobic interactions can be hindered to some extent, thus preventing subsequent toxicity. The presence of functional groups also plays a role in enzyme-catalyzed biodegradation of large graphene-based nanomaterials, which will be highlighted later in detail.

4.3.2 In Vivo Toxicity

For biomedical applications, in vivo toxicology and biodistribution of graphene-based nanomaterials have been explored recently. In 2010, Yang et al. studied the long-term in vivo biodistribution and pharmacokinetics of PEGylated ^{125}I-nanographene sheets with (NGS) [45]. With systemic toxicology examination, the authors confirmed the radioactivity of NGS in the blood and various organs after intravenous (i.v.) injection. Notably, radioactive NGS decreased persistently in most organs, which were presumably excreted by fecal or renal routes. On hematology and blood biochemistry examination to investigate long-term in vivo effect, NGS injection (20 mg/kg) did not show any significant damages in the mice until 3 months. In 2013, the same researchers carried out similar investigations with functionalized nano-GOs through two other major administration routes: intraperitoneal (i.p.) injection and oral uptake [30]. Interestingly, while oral feeding did not induce any notable accumulation of nano-GOs in tissues, i.p. injected mice exhibited highly accumulated nano-GOs in the mononuclear phagocytic (reticuloendothelial) system. Nevertheless, both did not induce any severe toxicity in mice. More recently, Nurunnabi et al. carried out long-term in vivo toxicology and biodistribution studies on mice treated with carboxylated GQDs through i.v. injection [46]. The in vivo and ex vivo images showed that GQDs were distributed mainly in the kidney, liver, spleen, lung, and tumor sites (Fig. 4.2). And these accumulations did not elicit any organ lesions or damages, confirmed by further analyses on mice administered with 5 or 10 mg/kg GQDs at 21 days. Although some reports argue that high doses of large GOs can evoke severe damages in cells [36], most studies have confirmed that nano-GOs and GQDs exhibit respectable biocompatibility which can presumably be cleared out through kidneys without significant accumulation.

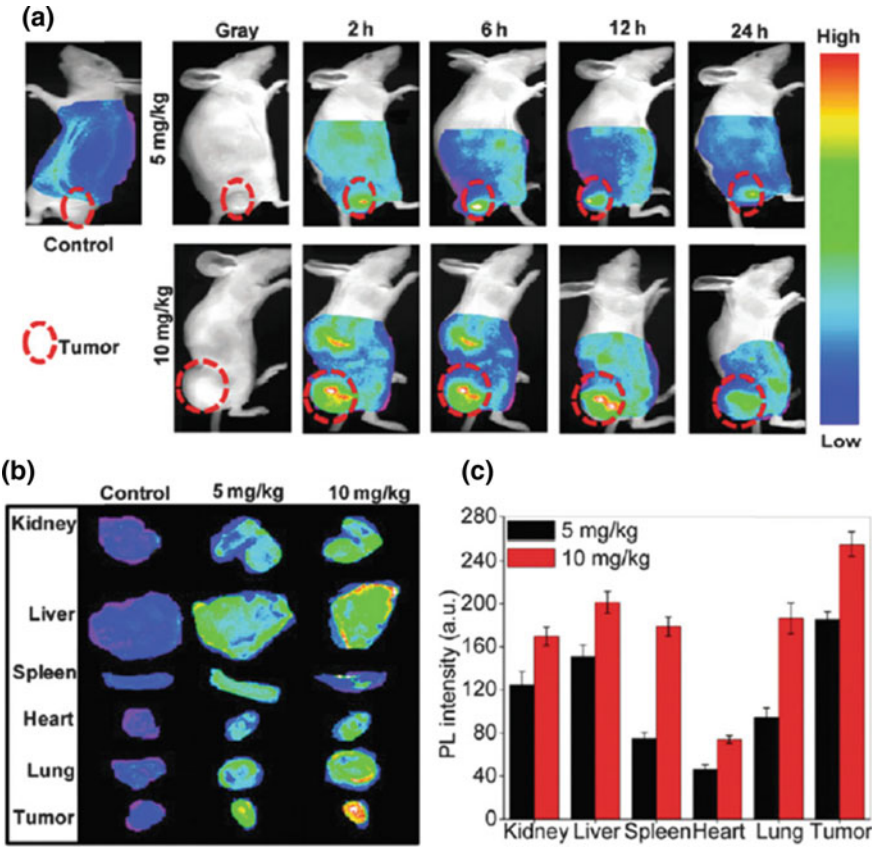

Fig. 4.2 In vivo imaging and biodistribution of the carboxylated GQDs. **a** The in vivo imaging of KB tumor bearing mice after intravenous injection of GQDs (5 and 10 mg kg^{-1}). **b** and **c** ex vivo images and quantitative distribution of isolated organs of mice at 24 h after injection. GQD: graphene quantum dot. Adapted with permission [46]

4.3.3 Biodegradation

In addition to various in vitro/in vivo toxicity studies, some researches devoted special attention to potential oxidative biodegradation of graphene-based nanomaterials by intracellular enzymes. In 2011 and 2012, Kotchey et al. reported two studies on enzyme-catalyzed degradation of graphene-based nanomaterials. Foremost, the authors utilized low concentrations of horseradish peroxidase (HRP) to verify their effects on GOs and rGOs [47]. Obtained atomic force microscopy (AFM) and transmission electron microscopy images as well as Raman spectra concordantly showed that HRP caused the generation of holey GOs, which resulted in debris of oxidized GO flakes in the end. Contrarily, HRP did not induce any structural changes on rGOs, which implied that the presence of functional

groups was the key for enzymatic oxidation. Indeed, the authors discussed that GOs' oxygenated functional groups promote weaker binding with HRP and thus enabled it to be more dynamic, which ultimately brought its catalytic heme site in proximity of GOs to induce oxidative degradation (Fig. 4.3). In 2012, the authors performed similar studies with similar outcomes using myeloperoxidase (MPO), which has a human analogue as human MPO [48]. The report encourages the use of functionalized graphene-based nanomaterials for in vivo studies as they can be readily degraded by peroxidase-related intracellular enzymes. However, experiments must be carried out in a cautious manner as these in vitro outcomes may turn out to be entirely irrelevant to the actual biodegradation processes in the body. Besides the fact that oxidative debris of GOs can also be lethal to cells, the levels of intracellular enzymes may be more dilute in physiological milieu in vivo.

4.4 Graphene-Based Nanomaterials for Biomedical Applications

4.4.1 Therapeutic Applications

Graphene-based nanomaterials are known to exhibit high absorbance in the NIR region, which gave rise to novel approaches for NIR laser-triggered selective ablation of cancer cells [49, 50]. With appropriate modifications with targeting moieties, graphene-based nanomaterials can specifically target malignant tumor cells without damaging the healthy ones. Interestingly, graphene-based nanomaterials' hydrophobic basal plane can be exploited for various synergistic therapies. Some groups attended to the fact that hydrophobic anti-cancer drugs and photodynamic agents could be easily loaded onto the basal plane of graphene-based materials through π–π interactions. By combining the photothermal ablation with either chemotherapies or photodynamic therapies, therapeutic effects came to be higher [51, 52]. NIR-responsive hyperthermia was not only utilized for the direct ablation of cells, but also employed as an external cue for controlled drug/gene delivery by disorganizing a drug-loading matrix or endocytosed vesicles by NIR laser [53–55]. Moreover, some groups also discovered unusual stem cell growth and differentiation patterns on graphene substrates, which can be possibly employed in stem cell engineering and/or stem cell-based therapy [56, 57].

4.4.2 Fluorescence Sensing and Imaging

In addition to the therapeutic applications, people have utilized graphene oxides (GOs) for bio-sensing studies by exploiting their ability to quench fluorescence. For the first time in 2009, Lu et al. reported the detection of fluorophore-labeled DNA

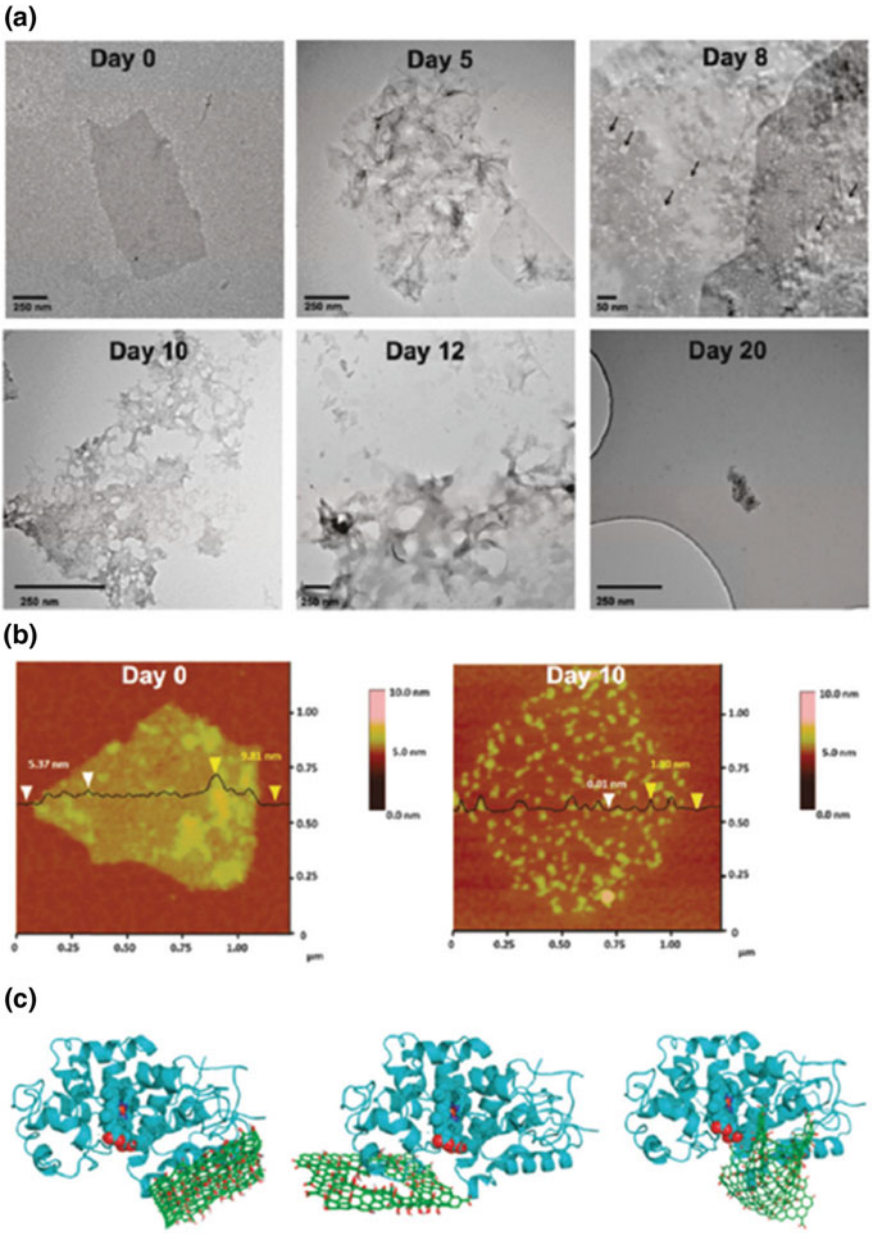

Fig. 4.3 Enzymatic oxidation of GO. **a** TEM images of GOs incubated with horse radish peroxidase (HRP). **b** AFM images with GOs incubated with HRP. **c** Simulated docking between GO and HRP. AFM: atomic force microscopy. Adapted with permission [47]

with GOs; the fluorescence of fluorophore-labeled single-stranded DNA is quenched by GOs, where it can be instantly recovered by adding its complementary sequence [58]. With further surface modifications on GOs, other groups also reported the detection of other small biological molecules including protein kinases, neurotransmitters, and metabolites with phosphates [59–62]. Rationally designed GOs were also employed in the discrimination of Fe^{2+} and Fe^{3+} in living cells based on the level of fluorescence quenching [63].

A number of studies focused on the graphene-based nanomaterials' outstanding optical properties for various imaging applications. As mentioned, GQDs exhibit respectably high photoluminescence without the issue of serious toxicity or photobleaching, which can also be tuned by appropriate size/edge modifications. Recently, many groups exploited these properties in various photothermal therapy and drug delivery systems to yield in situ imaging upon therapies. Nahain et al. used 20 nm-sized GQDs to track the successful targeting of overexpressed CD44 receptors in cancer cells [64]. The authors prepared GQDs-hyaluronic acid (HA) conjugate to target the receptors, where their localization in the tumor tissue could be monitored with GQDs' intrinsic fluorescence both in vitro and in vivo (Fig. 4.4). Anti-cancer treatment was subsequently achieved by loading doxorubicin on the plane of GQDs, which was immediately released under acidic conditions. In 2014, Ge et al. demonstrated more advanced photodynamic anti-cancer therapy with a few nanometer-sized GQDs [65]. Notably, the synthesized GQDs exhibited a broad absorption range with distinct emission at 680 nm. The authors exploited these optical properties and utilized them as novel photodynamic agents, which can generate singlet oxygen with respectable pH-and photostability in both in vivo and in vitro trials. Moreover, they could simultaneously track the whole process with fluorescence imaging.

In 2013, Zheng et al. utilized GQDs as a novel fluorophore to reveal unknown biological functions [66]. In this study, the authors specifically labeled and tracked the dynamic movements of insulin receptors in adipocytes with GQDs' fluorescence to confirm the specific biological roles of a few neighboring proteins (Fig. 4.5). Through the dynamic tracking, they found that two distinct proteins regulate insulin receptor's internalization and recycling in an opposite manner: while TNF α improves the insulin resistance, apelin enhances the insulin sensitivity. Although this study alone cannot bring momentous changes in diabetes treatments, the report is remarkable as they utilized GQDs' fluorescence to divulge unknown cellular functions while previous researchers exploited GQDs' fluorescence merely on tracking drug delivery by monitoring successful targeting.

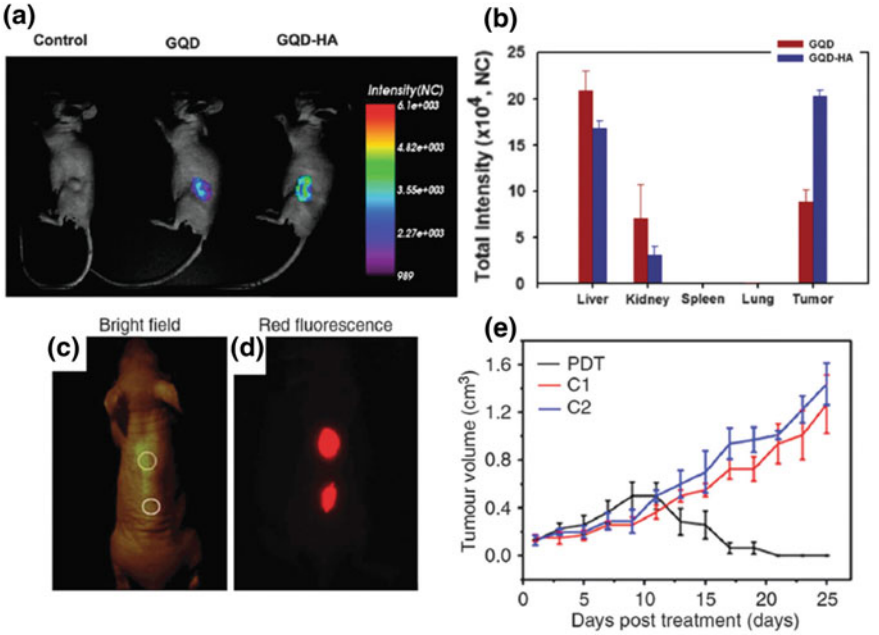

Fig. 4.4 Graphene based in vivo targeting imaging agents. **a** In vivo fluorescence images of GQD–HA in mice after tail vein injection. **b** Fluorescence intensity from dissected organs. **c** and **d** Bright field image and in vivo fluorescence image after GQD injection. **e** Time-dependent tumor growth curves. HA: hyaluronic acid. Adapted with permission [64]

4.5 Recent Applications of Graphene-Based Nanomaterials in Magnetic Resonance Imaging

MRI is the most powerful technique for imaging tumors, the cardiac and nervous systems as it enables high-resolution imaging in a non-invasive manner [67]. However, when a diseased lesion do not show distinct change in relaxation times, MRI imaging does not help discover the diseased areas. MRI contrast agents are employed to maximize the difference in relaxation time. Currently, most of the commercial contrast agents are paramagnetic nanoparticles and metal ion complexes [68]. Graphene-based nanomaterials do not exhibit intrinsic paramagnetism and is not a candidate as a novel MRI contrast agent. However, functionalized graphene-based nanomaterial possess oxygenated functional groups and cavities that can load various drugs with conventional MRI contrast agents. In addition, appropriate edge modifications can enable efficient targeting to specific regions. Moreover, docking MRI contrast agents inside graphene-based nanomaterials can also alleviate the toxicity concerns of heavy metal ions by decreasing the release rate.

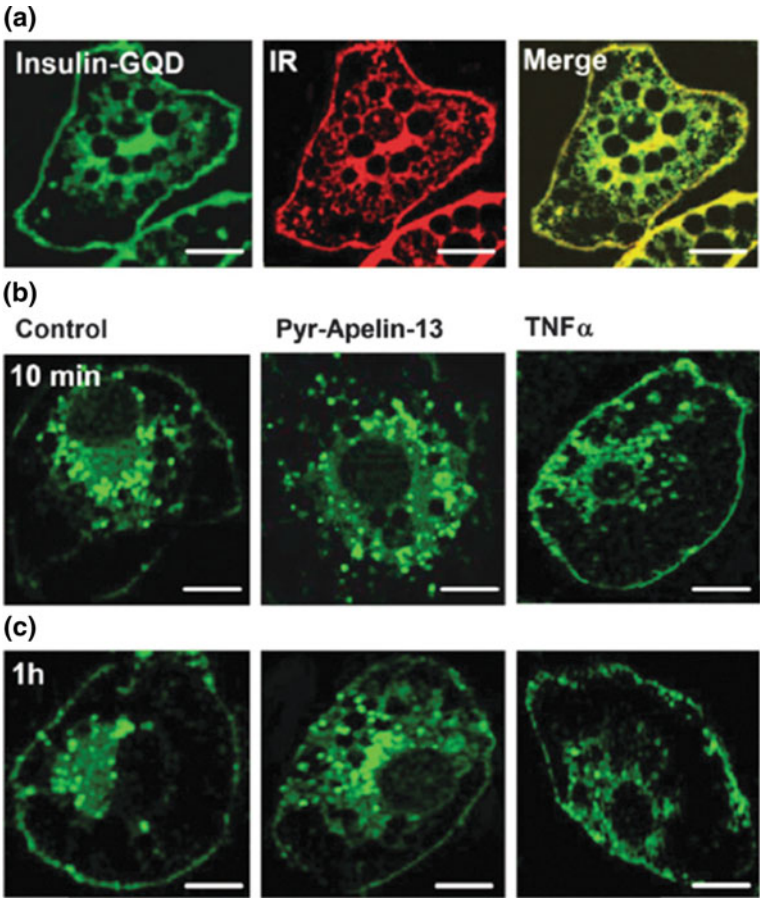

Fig. 4.5 Dynamic tracking of protein of interest. **a** Confocal fluorescence images of insulin conjugated GQDs (green, left) or with antibodies against insulin receptor (IR) (red, middle). **b** and **c** Cellular distribution of insulin receptors after (**b**) 10 min or (**c**) 1 h incubation with insulin-GQDs. Scale bar = 10 μm. Adapted with permission [66]

4.5.1 Paramagnetic Ions Coordinated Graphene

Iron (Fe), manganese (Mn), and gadolinium (Gd) are representative paramagnetic metal ions with high magnetic moments. When these ions coordinate surrounding water molecules, the spin-lattice relaxation (T1) efficiently occurs. Since the T1 contrast depends on the net magnetization with respect to time, these ions can be employed as adequate T1 contrast agents [69]. Nevertheless, as highly paramagnetic metal ions typically exhibit high toxicity owing to the random coordination with biomolecules, these ions are mostly used as chelated forms [68]. To that end, functionalized graphene derivatives with cavities and oxygenated functional groups

can be decent candidates for chelating or burying the metal ions to decrease potential toxicity.

In 2013, Kanakia et al. reported the use of dextran-coated graphene nanoplatelets (GNP–Dex) with Mn^{2+} ions as enhanced T_1-weighted MRI contrast agents [70]. The preparation of such complex was simply achieved by intercalating Mn^{2+} ions in GNP–Dex, which was stable in the physiological conditions. Remarkably, the r_1 relaxivity of GNP–Dex–Mn^{2+} system was 92 mM^{-1} s^{-1} (per Mn^{2+} ion), which greatly exceeds that of clinical Mn^{2+}-based contrast agents. In addition, the T_1-weighted phantom imaging also showed marked contrast enhancement.

In 2014, Gizzatov et al. employed functionalized graphene nanoribbons (GNRs) to coordinate Gd^{3+} ion [71]. Highly carboxyphenylated GNRs were produced by reductively cutting multi-walled carbon nanotubes (MWCNTs) using K/Na alloy, which were subsequently functionalized with p-carboxyphenyldiazonium to yield carboxyphenyl GNRs (average width 125–280 nm, average thickness 7–15 nm). Obtained GNRs were successfully coordinated with Gd^{3+} ions to form Gd–GNRs complex without additional surfactants. Notably, Gd–GNRs composite significantly enhanced the relaxation rates of T1 and T2 (spin-spin relaxation) at 1.41 T, by displaying r_1 and r_2 values of 70 ± 6 and 108 ± 9 Mm^{-1} s^{-1} respectively. The T_1- and T_2-weighted phantom images further confirmed that the use of Gd–GNRs composite results in better MRI contrasts, which greatly exceeds those of GNRs or H_2O-based images.

4.5.2 Paramagnetic Nanoparticles-Decorated Graphene

Currently, most of the commercial nanoparticle-based MRI contrast agents utilize magnetic iron oxides (i.e. superparamagnetic iron oxide—SPIO) [72]. In general, the mechanism of relaxation of superparamagnetic agents is different from that for paramagnetic ion-based agents. Paramagnetic nanoparticles' large magnetic field leads to water molecule spin dephasing around the nanoparticle, producing transverse relaxation T_2 contrast. As graphene derivatives can be used as a template for the growth of nanoparticles or efficiently conjugated with capped ligands, graphene derivatives-paramagnetic nanoparticles can be easily prepared as T_2 contrast-enhancing agents [73].

In 2011, Chen et al. reported the first attempt to employ graphene-based nanomaterial as a novel T_2 contrast agent [74]. In the study, Fe_3O_4–GOs composite was prepared by coating Fe_3O_4 nanoparticles with dimercaptosuccinic acid (DMSA), which were subsequently conjugated with aminodextran (AMD). Finally, Fe_3O_4–DMSA–AMD and GOs were covalently grafted by EDC coupling, which yielded the final composite with an average size of 174.4 nm. Remarkably, the T_2 relaxation rate of Fe_3O_4–GOs (per Fe concentration) was significantly enhanced by exhibiting r_2 = 76 Mm^{-1} s^{-1}, which greatly exceeded those of other composites without GOs; 24 and 21 Mm^{-1} s^{-1}, respectively for DMSA–Fe_3O_4 and AMD–Fe_3O_4.

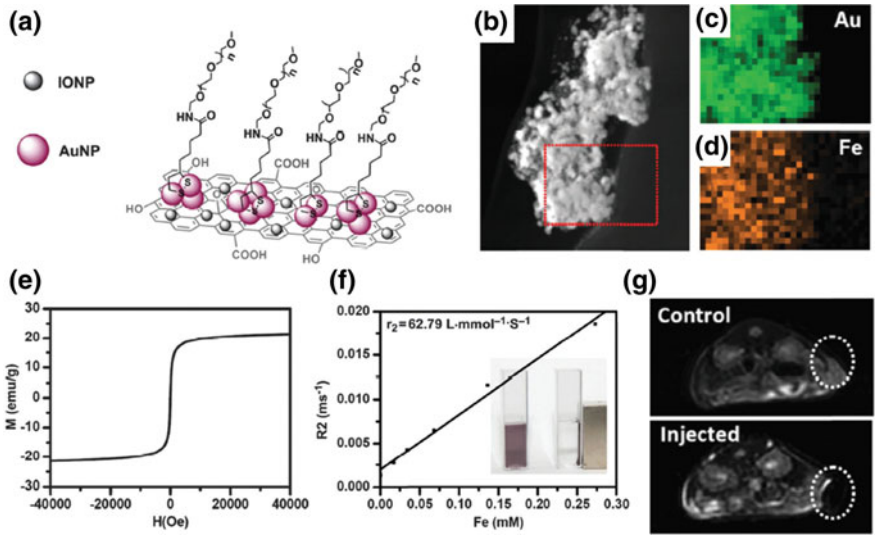

Fig. 4.6 Graphene based MRI imaging. **a** Schematic representation of paramagnetic nanoparticle coordinated GO (GO–IONP–Au). **b** Scanning tunneling electron microscope (STEM) image, and **c**, **d** energy dispersive X-ray spectroscopy (EDS) images of GO–IONP–Au. **e** Magnetization loops, and **f** T2 relaxation rates with Fe concentration. **g** T2-weighted magnetic resonance images of 4T1 tumor-bearing mice before and after intratumoral injection of a graphene based contrast agent. Adapted with permission [75]

After two years, Shi et al. demonstrated the use of iron oxide nanoparticle (IONPs)–GOs–gold nanoparticle (AuNP) composite for similar studies (Fig. 4.6) [75]. The complex was prepared by the adsorption of IONPs on the surface of GOs, followed by the growth of AuNP and subsequent PEGylation. Owing to the complicated preparation steps, the complex exhibited wide distribution of size between 200 and 600 nm. Originated from IONPs, the graphene-based complex showed strong paramagnetic characteristics, which was confirmed from clear T_2-weighted image in the tumor region. Using similar methods, other groups produced different types of paramagnetic nanoparticles in combination with GOs. Peng et al. used manganese ferrite ($MnFe_2O_4$) nanoparticle-GOs complex that showed very high T_2 relaxation rate, r_2 = 256.2 Fe Mm^{-1} s^{-1} [76]. The result was exceeded by Chen et al., who utilized needle-shaped β-FeOOH nanorods-GOs composite to yield the higher T_2 relaxation rate, r_2 = Fe 303.82 Mm^{-1} s^{-1} [77].

4.5.3 Graphene-Based Multifunctional MRI Contrast Agents

Development of multifunctional MRI contrast agents that could enable simultaneous targeting, imaging, and curing has gained significant attention of researchers as

such materials may facilitate improved therapeutic efficiency. As functionalized graphene derivatives are amphiphilic, they are structurally advantageous to play such versatile roles. While their functional edges are available for molecular conjugation with metal contrast agents or targeting moieties, the basal plane is capable of loading various hydrophobic drugs at the same time.

In 2014, Wang et al. reported mesoporous silica nanosheets–Fe_3O_4–GOs complex as a multifunctional MRI agent [78]. The complex was prepared by coating Fe_3O_4–GOs composite with aminopropyltriethoxysilane and tetraethyl orthosilicate to form mesoporous silica nanosheets–Fe_3O_4–GOs. The complex was further modified with interleukin-13-based peptide (IP) loaded with doxorubicin for efficient targeting and chemotherapy. After i.v. injection of the complex, T_2-weighted image clearly visualized that the targeting was successfully done by IP moiety. The doxorubicin was released by photothermal heating of GOs, which immediately weakened the hydrophobic and electrostatic interactions between GOs due to the presence of highly concentrated hydrogen ions. Similarly, by another group an analogous multifunctional complex was loaded with 5-FU, a different type of anticancer drug on Fe_3O_4–GOs composite [79].

Based on these progress in developing MRI contrast agents for imaging and therapy, the use of radiolabeled multimodal graphenes will be detailed in the following section.

4.6 In Vivo Radionuclide Imaging of Radiolabeled Graphene

Current various imaging modalities have their own unique properties in terms of sensitivity and resolution, which has been taking advantage of being fit for relevant experimental purposes. Although MRI provides definite soft tissue structural information enabling high-resolution images, the low sensitivity in the detection of interested tissue area still remains inherent limitation of MRI. Also, as for the fluorescence imaging, fluorescence imaging has been extensively applied in examining a variety of exquisite biological events with microscopic resolution. However, the light absorption/scattering in biological tissues of fluorescence imaging creates high auto-fluorescence background, leading to low target to background ratio obliterating image quality and data misinterpretation.

Radionuclide imaging, has played crucial roles in practical application including disease diagnosis, providing high sensitivity in the clinical as well as preclinical areas. Moreover, greater biological and clinical accuracy are achieved through quantitative and tomographic imaging, taking radioactivity's advantage of depth imaging [80]. Radio-graphene was recently named in a review article, which focused on the broad usability of radiolabeled graphenes (GOs and GQDs) for targeted delivery and therapy [81]. Many available functional groups exposed at the edge of GO has enabled the easy radiolabeling of GOs for in vivo use. Bifunctional

chelating agents such as isothiocyanatobenzyl-1,4,7-triazacyclononane-triacetic acid (SCN–NOTA) can be simply conjugated on the carboxylate group of the surface of GOs which will be used later to label radionuclides such as ^{68}Ga or ^{64}Cu [82, 83]. It also has the ability to chelate other radionuclide, ^{177}Lu for cancer theranostic approach exploiting its emission of gamma ray and beta ray.

As another labeling method, click chemistry has been successfully adopted for a simple and rapid labeling of GOs or GQDs in mild condition, showing that the reaction between clickable moieties of esop and its corresponding azadibenzocyclooctyne group occurs within several minutes at room temperature [84–86]. Through this simple reaction, the well-defined and simple click reaction for modification of GOs shall aid in the development of a variety of radionuclide-labeled graphene nanosheets capable of decorating multifunctional theranostic biomolecules.

To date, researchers have attempted to develop graphene-based in vivo active tumor targeting by incorporating specific ligands together with radioisotope labeling [87, 88]. Cai and his group used the ^{64}Cu-labeled GOs on PET imaging and achieved successful cancer targeting [87]. ^{64}Cu–GOs labeled with monoclonal antibody against proliferating endothelial marker, TRC105 (^{64}Cu–NOTA–GO–TRC105), showed specific targeting to the 4T1 breast cancers inoculated in the mouse. A parallel study of tumor targeting used ^{66}Ga-labeled nano GO (nGO)-PEG for PET imaging [88]. Other reports followed to show again efficient tumor targeting of GOs conjugated with monoclonal antibody (mAb) against follicle stimulating hormone receptor (FSHR), which is ubiquitously expressed in tumor vasculature. ^{64}Cu–NOTA–GO–FSHR–mAb accumulated persistently in metastatic breast cancer nodules in the lungs on PET imaging [89]. In addition, vascular endothelial growth factor 121 ($VEGF_{121}$) was conjugated with GOs by Shi et al. for targeting VEGF receptor and could enhance the targeting efficiency of GOs to the tumor [90]. Serial whole body PET images of ^{64}Cu–GO–$VEGF_{121}$ showed rapid accumulation of graphene in U87MG tumor-bearing mice within 30 min. The same group also used ^{64}Cu–NOTA–RGO–IONP–PEG, finding that radiolabeled-GOs cumulated passively in peripheral ischemic area. A reinjection of ^{64}Cu–RGO–IONP–PEG revealed accelerated blood clearance, and IgM against PEG was the cause of this shortening of circulation [91, 92].

SPECT is approximately ten times less sensitive than PET. However, concurrent imaging of multiple radionuclides of different energies is an advantage of SPECT. Additionally, SPECT is widely available in clinics unlike PET's dependence on the availability of cyclotron, and SPECT radionuclides are simpler to prepare and usually have a longer half-life than PET radionuclides. Cornelissen et al. explored feasibility of targeting the HER2-overproducing breast cancer using anti-HER2 antibody-conjugated nGO, radiolabeled with ^{111}In-benzyl-diethylenetriaminepentaacetic acid via π–π stacking on SPECT [93]. The pharmacokinetics of radiolabeled nGO-trastuzumab conjugates were better when compared to radiolabeled trastuzumab without NGO, clearing from circulation at a faster rate. Fazaeli et al. investigated in vivo targeting and SPECT imaging of tumors with ^{198,199}AU@AF–GO

nanostructure, and found that ^{198,199}Au@AF–GO had effective tumor targeting/imaging as well as rapid clearance from the body [94].

The radioisotope ^{125}I has a long half-life of 60 days, which enables to trace long-term biodistribution and potential toxicity and was used labeling PEG–GO [95]. There was an exponential decrease of the activity of ^{125}I–PEG–GO administered in mice. Over the course of 60 days, this ^{125}I–PEG–GO was gradually excreted from the liver and spleen. While it would be possible that ^{125}I would be detached from ^{125}I–PEG–GO, ^{125}I–PEG–GO remained stable in plasma until 15 days and radioactivity of the thyroid radioactivity did not rise. Thus, radioactivity was supposed to indicate where the GO was located. Further investigation is necessary to determine the exact mechanism of graphene sheet clearance in vivo. Nevertheless, those findings could provide great insight into advancement of GO in drug deliver application.

One significant advantage of using radio-graphene is the ability to use very small amounts of radioactive materials for in vivo radionuclide imaging, successfully overcoming the dose-dependent toxicity issue. In contrast to MRI, which has a low sensitivity, highly sensitive radionuclide imaging uses lower doses and can utilizes least amounts of nanoparticles, leading to apparently lower toxicity [96].

The functionalization of graphene surfaces and graphene itself present many opportunities for combined cancer treatment. In a recent study, a combination approach was done, with rGO-gold nanorod functionalized with anticancer chemotherapy drug. It successfully enhanced therapeutic effects, in addition to dramatically regressing the tumor with amplified photothermal effects [97]. Ideal candidates for combination therapy can be selected among antisense oligonucleotides, chemical drugs, photothermal/photodynamic agents, and therapeutic radionuclides [98, 99]. Furthermore, augmented therapy targeting DNA using combination of doxorubicin and alpha particle could be made possible by graphene's capability of easy penetration of cell membranes [100, 101].

The localization and kinetics of GO can be traced in small animals or in humans by radionuclide imaging especially using PET so as to elucidate targeting ability and other organ distribution. Photothermal capability of GO combined with therapeutic radioisotope such as ^{131}I or ^{177}Lu will synergize and this combination enhance the effects of GO-based therapeutics in any disease of interest. ^{131}I-labeled rGO induced effective photothermal heating and cancer killing by high energy beta ray emitted from ^{131}I (Fig. 4.7) [102].

Radionuclide imaging is recognized as a more accurate and reliable imaging modality than optical imaging, at least in terms of quantitation capability and human application. These advantages will further enhance the advancement of radio-graphene approaches in clinical application, and because radiolabeling of graphene is simple and quick, harnessing radio-graphene platform for the targeted cancer theranostics will be rapidly growing. Current lack of detailed knowledge regarding in vivo characteristics will surely call for further studies using radio-graphenes for in vivo tracking of GO-based therapeutic drugs. Radio-graphene has

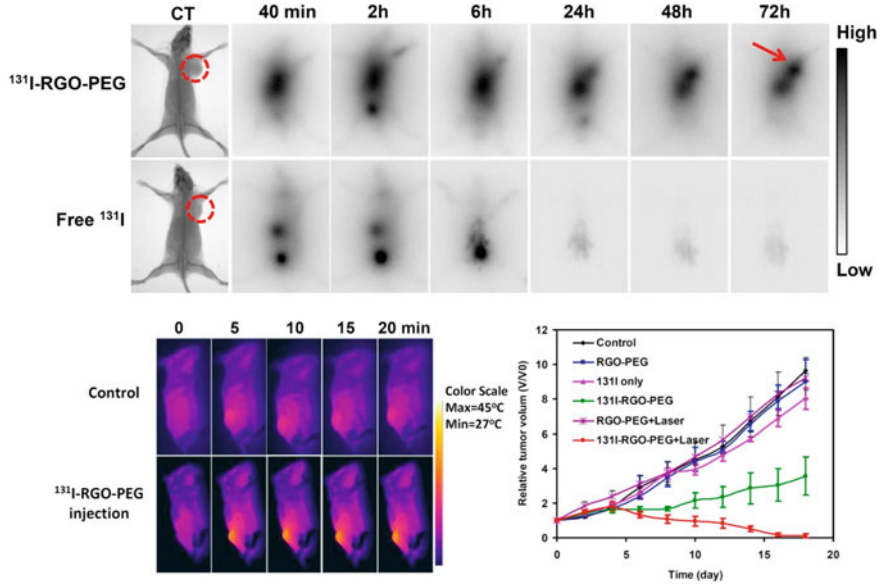

Fig. 4.7 Combination cancer therapy of ^{131}I-labeled reduced graphene oxide nanosheets. ^{131}I–RGO–PEG passively targeted 4T1 tumor area by EPR effect in mice after intravenous injection. ^{131}I radioactivity was clearly found at tumor site until 72 h (upper panel). An IR thermal images were obtained in 48 h post inoculation, and temperature changes were monitored during 808 nm laser irradiation (left lower panel). The combination cancer therapy including radionuclide and photothermal therapy was conducted until 18 days. ^{131}I–RGO–PEG with laser irradiation revealed the improved cancer therapeutic efficiency with tumor growth inhibition (right lower panel). Adapted with permission [102]

far-reaching applications and high multi-functionality versatile within biomedical imaging purposes and provides new nanoplatforms for in vivo drug delivery and therapy.

References

1. K.S. Novoselov, A.K. Geim, S.V. Morozov, D. Jiang, Y. Zhang, S.V. Dubonos et al., Electric field effect in atomically thin carbon films. Science **306**(5696), 666–669 (2004)
2. J.M. Yoo, J.H. Kang, B.H. Hong, Graphene-based nanomaterials for versatile imaging studies. Chem. Soc. Rev. **44**(14), 4835–4852 (2015)
3. D. Bitounis, H. Ali-Boucetta, B.H. Hong, D.H. Min, K. Kostarelos, Prospects and challenges of graphene in biomedical applications. Adv. Mater. **25**(16), 2258–2268 (2013)
4. S. Zhu, H. Zhen, Y. Li, P. Wang, X. Huang, P. Shi, PEGylated graphene oxide as a nanocarrier for podophyllotoxin. J. Nanopart. Res. **16**(8), 2530 (2014)

5. P.S. Wate, S.S. Banerjee, A. Jalota-Badhwar, R.R. Mascarenhas, K.R. Zope, J. Khandare et al., Cellular imaging using biocompatible dendrimer-functionalized graphene oxide-based fluorescent probe anchored with magnetic nanoparticles. Nanotechnology **23**(41), 415101 (2012)
6. G. Gollavelli, Y.C. Ling, Multi-functional graphene as an in vitro and in vivo imaging probe. Biomaterials **33**(8), 2532–2545 (2012)
7. X. Sun, Z. Liu, K. Welsher, J.T. Robinson, A. Goodwin, S. Zaric et al., Nano-graphene oxide for cellular imaging and drug delivery. Nano Res. **1**(3), 203–212 (2008)
8. J. Liu, J.T. Robinson, X. Sun, H. Dai, PEGylated nanographene oxide for delivery of water-insoluble cancer drugs. J. Am. Chem. Soc. **130**(33), 10876–10877 (2008)
9. C. Peng, W. Hu, Y. Zhou, C. Fan, Q. Huang, Intracellular imaging with a graphene-based fluorescent probe. Small **6**(15), 1686–1692 (2010)
10. K. Yang, S. Zhang, G. Zhang, X. Sun, S.T. Lee, Z. Liu, Graphene in mice: ultrahigh in vivo tumor uptake and efficient photothermal therapy. Nano Lett. **10**(9), 3318–3323 (2010)
11. Z. Sun, P. Huang, G. Tong, J. Lin, A. Jin, P. Rong et al., VEGF-loaded graphene oxide as theranostics for multi-modality imaging-monitored targeting therapeutic angiogenesis of ischemic muscle. Nanoscale **5**(15), 6857–6866 (2013)
12. H. Hong, K. Yang, Y. Zhang, J.W. Engle, L. Feng, Y. Yang et al., In vivo targeting and imaging of tumor vasculature with radiolabeled, antibody-conjugated nanographene. ACS Nano. **6**(3), 2361–2370 (2012)
13. X. Mao, H. Li, Chiral imaging in living cells with functionalized graphene oxide. J. Mater. Chem. B Mater. Biol. Med. **1**(34), 4267 (2013)
14. S.H. Hu, Y.W. Chen, W.T. Hung, I.W. Chen, S.Y. Chen, Quantum-dot-tagged reduced graphene oxide nanocomposites for bright fluorescence bioimaging and photothermal therapy monitored in situ. Adv. Mater. **24**(13), 1748–1754 (2012)
15. M.L. Chen, J.W. Liu, B. Hu, M.L. Chen, J.H. Wang, Conjugation of quantum dots with graphene for fluorescence imaging of live cells. Analyst **136**(20), 4277–4283 (2011)
16. L.J. Cote, R. Cruz-Silva, J. Huang, Flash reduction and patterning of graphite oxide and its polymer composite. J. Am. Chem. Soc. **131**(31), 11027–11032 (2009)
17. G.K. Ramesha, S. Sampath, Electrochemical reduction of oriented graphene oxide films: an in situ Raman spectroelectrochemical study. J. Phys. Chem. C **113**(19), 7985–7989 (2009)
18. S. Stankovich, D.A. Dikin, R.D. Piner, K.A. Kohlhaas, A. Kleinhammes, Y. Jia et al., Synthesis of graphene-based nanosheets via chemical reduction of exfoliated graphite oxide. Carbon **45**(7), 1558–1565 (2007)
19. S. Shi, K. Yang, H. Hong, H.F. Valdovinos, T.R. Nayak, Y. Zhang et al., Tumor vasculature targeting and imaging in living mice with reduced graphene oxide. Biomaterials **34**(12), 3002–3009 (2013)
20. K. Liu, J.-J. Zhang, F.-F. Cheng, T.-T. Zheng, C. Wang, J.-J. Zhu, Green and facile synthesis of highly biocompatible graphene nanosheets and its application for cellular imaging and drug delivery. J. Mater. Chem. **21**(32), 12034 (2011)
21. Z. Sheng, L. Song, J. Zheng, D. Hu, M. He, M. Zheng et al., Protein-assisted fabrication of nano-reduced graphene oxide for combined in vivo photoacoustic imaging and photothermal therapy. Biomaterials **34**(21), 5236–5243 (2013)
22. L. Zhang, Y. Xing, N. He, Y. Zhang, Z. Lu, J. Zhang et al., Preparation of graphene quantum dots for bioimaging application. J. Nanosci. Nanotechnol. **12**(3), 2924–2928 (2012)
23. S. Zhu, J. Zhang, C. Qiao, S. Tang, Y. Li, W. Yuan et al., Strongly green-photoluminescent graphene quantum dots for bioimaging applications. Chem. Commun. **47**(24), 6858–6860 (2011)
24. M. Zhang, L. Bai, W. Shang, W. Xie, H. Ma, Y. Fu et al., Facile synthesis of water-soluble, highly fluorescent graphene quantum dots as a robust biological label for stem cells. J. Mater. Chem. **22**(15), 7461 (2012)
25. Q. Liu, K. Wang, J. Huan, G. Zhu, J. Qian, H. Mao et al., Graphene quantum dots enhanced electrochemiluminescence of cadmium sulfide nanocrystals for ultrasensitive determination of pentachlorophenol. Analyst **139**(11), 2912–2918 (2014)

26. S. Zhu, J. Zhang, S. Tang, C. Qiao, L. Wang, H. Wang et al., Surface chemistry routes to modulate the photoluminescence of graphene quantum dots: from fluorescence mechanism to up-conversion bioimaging applications. Adv. Funct. Mater. **22**(22), 4732–4740 (2012)
27. X. Wu, F. Tian, W. Wang, J. Chen, M. Wu, J.X. Zhao, Fabrication of highly fluorescent graphene quantum dots using L-glutamic acid for in vitro/in vivo imaging and sensing. J. Mater. Chem. C Mater. Opt. Electron Devices **1**(31), 4676–4684 (2013)
28. A.M. Jastrzebska, P. Kurtycz, A.R. Olszyna, Recent advances in graphene family materials toxicity investigations. J. Nanopart. Res. **14**(12), 1320 (2012)
29. C. Fisher, A.E. Rider, Z. Jun Han, S. Kumar, I. Levchenko, K. Ostrikov, Applications and nanotoxicity of carbon nanotubes and graphene in biomedicine. J. Nanomater. **2012**, 1–19 (2012)
30. K. Yang, H. Gong, X. Shi, J. Wan, Y. Zhang, Z. Liu, In vivo biodistribution and toxicology of functionalized nano-graphene oxide in mice after oral and intraperitoneal administration. Biomaterials **34**(11), 2787–2795 (2013)
31. A. Sasidharan, L.S. Panchakarla, P. Chandran, D. Menon, S. Nair, C.N. Rao et al., Differential nano-bio interactions and toxicity effects of pristine versus functionalized graphene. Nanoscale **3**(6), 2461–2464 (2011)
32. C. Wu, C. Wang, T. Han, X. Zhou, S. Guo, J. Zhang, Insight into the cellular internalization and cytotoxicity of graphene quantum dots. Adv Healthc Mater. **2**(12), 1613–1619 (2013)
33. X. Yuan, Z. Liu, Z. Guo, Y. Ji, M. Jin, X. Wang, Cellular distribution and cytotoxicity of graphene quantum dots with different functional groups. Nanoscale Res. Lett. **9**(108) (2014)
34. Y. Chong, Y. Ma, H. Shen, X. Tu, X. Zhou, J. Xu et al., The in vitro and in vivo toxicity of graphene quantum dots. Biomaterials **35**(19), 5041–5048 (2014)
35. H. Zhang, C. Peng, J. Yang, M. Lv, R. Liu, D. He et al., Uniform ultrasmall graphene oxide nanosheets with low cytotoxicity and high cellular uptake. ACS Appl. Mater. Interfaces **5**(5), 1761–1767 (2013)
36. S.M. Chowdhury, G. Lalwani, K. Zhang, J.Y. Yang, K. Neville, B. Sitharaman, Cell specific cytotoxicity and uptake of graphene nanoribbons. Biomaterials **34**(1), 283–293 (2013)
37. K. Wang, J. Ruan, H. Song, J. Zhang, Y. Wo, S. Guo et al., Biocompatibility of graphene oxide. Nanoscale Res. Lett. **6**(1), 8 (2011)
38. A. Schinwald, F.A. Murphy, A. Jones, W. MacNee, K. Donaldson, Graphene-based nanoplatelets: a new risk to the respiratory system as a consequence of their unusual aerodynamic properties. ACS Nano. **6**(1), 736–746 (2012)
39. R.G. Mendes, B. Koch, A. Bachmatiuk, X. Ma, S. Sanchez, C. Damm et al., A size dependent evaluation of the cytotoxicity and uptake of nanographene oxide. J. Mater. Chem. B Mater. Biol. Med. **3**(12), 2522–2529 (2015)
40. O. Akhavan, E. Ghaderi, A. Akhavan, Size-dependent genotoxicity of graphene nanoplatelets in human stem cells. Biomaterials **33**(32), 8017–8025 (2012)
41. O. Akhavan, E. Ghaderi, Graphene nanomesh promises extremely efficient in vivo photothermal therapy. Small **9**(21), 3593–3601 (2013)
42. R. Agarwal, V. Singh, P. Jurney, L. Shi, S.V. Sreenivasan, K. Roy, Mammalian cells preferentially internalize hydrogel nanodiscs over nanorods and use shape-specific uptake mechanisms. Proc. Natl. Acad. Sci. U. S. A. **110**(43), 17247–17252 (2013)
43. A. Albanese, P.S. Tang, W.C. Chan, The effect of nanoparticle size, shape, and surface chemistry on biological systems. Annu. Rev. Biomed. Eng. **14**, 1–16 (2012)
44. W. Kong, J. Liu, R. Liu, H. Li, Y. Liu, H. Huang et al., Quantitative and real-time effects of carbon quantum dots on single living HeLa cell membrane permeability. Nanoscale **6**(10), 5116–5120 (2014)
45. K. Yang, J. Wan, S. Zhang, Y. Zhang, S.T. Lee, Z. Liu, In vivo pharmacokinetics, long-term biodistribution, and toxicology of PEGylated graphene in mice. ACS Nano. **5**(1), 516–522 (2011)
46. M. Nurunnabi, Z. Khatun, K.M. Huh, S.Y. Park, D.Y. Lee, K.J. Cho et al., In vivo biodistribution and toxicology of carboxylated graphene quantum dots. ACS Nano. **7**(8), 6858–6867 (2013)

47. G.P. Kotchey, S.A. Hasan, A.A. Kapralov, S.H. Ha, K. Kim, A.A. Shvedova et al., A natural vanishing act: the enzyme-catalyzed degradation of carbon nanomaterials. Acc. Chem. Res. **45**(10), 1770–1781 (2012)
48. G.P. Kotchey, B.L. Allen, H. Vedala, N. Yanamala, A.A. Kapralov, Y.Y. Tyurina et al., The enzymatic oxidation of graphene oxide. ACS Nano. **5**(3), 2098–2108 (2011)
49. J.T. Robinson, S.M. Tabakman, Y. Liang, H. Wang, H.S. Casalongue, D. Vinh et al., Ultrasmall reduced graphene oxide with high near-infrared absorbance for photothermal therapy. J. Am. Chem. Soc. **133**(17), 6825–6831 (2011)
50. B. Tian, C. Wang, S. Zhang, L. Feng, Z. Liu, Photothermally enhanced photodynamic therapy delivered by nano-graphene oxide. ACS Nano. **5**(9), 7000–7009 (2011)
51. C. Jang, J.H. Lee, A. Sahu, G. Tae, The synergistic effect of folate and RGD dual ligand of nanographene oxide on tumor targeting and photothermal therapy in vivo. Nanoscale **7**(44), 18584–18594 (2015)
52. L. Zhou, L. Zhou, S. Wei, X. Ge, J. Zhou, H. Jiang et al., Combination of chemotherapy and photodynamic therapy using graphene oxide as drug delivery system. J. Photochem. Photobiol. B **135**, 7–16 (2014)
53. H. Kim, W.J. Kim, Photothermally controlled gene delivery by reduced graphene oxide-polyethylenimine nanocomposite. Small **10**(1), 117–126 (2014)
54. P. Matteini, F. Tatini, L. Cavigli, S. Ottaviano, G. Ghini, R. Pini, Graphene as a photothermal switch for controlled drug release. Nanoscale **6**(14), 7947 (2014)
55. V. Shanmugam, S. Selvakumar, C.-S. Yeh, Near-infrared light-responsive nanomaterials in cancer therapeutics. Chem. Soc. Rev. **43**(17), 6254 (2014)
56. W.C. Lee, C.H.Y.X. Lim, H. Shi, L.A.L. Tang, Y. Wang, C.T. Lim et al., Origin of enhanced stem cell growth and differentiation on graphene and graphene oxide. ACS Nano. **5**(9), 7334–7341 (2011)
57. S.Y. Park, J. Park, S.H. Sim, M.G. Sung, K.S. Kim, B.H. Hong et al., Enhanced differentiation of human neural stem cells into neurons on graphene. Adv. Mater. **23**(36), H263–H267 (2011)
58. C.H. Lu, H.H. Yang, C.L. Zhu, X. Chen, G.N. Chen, A graphene platform for sensing biomolecules. Angew. Chem. Int. Ed. Engl. **48**(26), 4785–4787 (2009)
59. X. Li, S. Zhu, B. Xu, K. Ma, J. Zhang, B. Yang et al., Self-assembled graphene quantum dots induced by cytochrome c: a novel biosensor for trypsin with remarkable fluorescence enhancement. Nanoscale **5**(17), 7776–7779 (2013)
60. S.J. Jeon, S.Y. Kwak, D. Yim, J.M. Ju, J.H. Kim, Chemically-modulated photoluminescence of graphene oxide for selective detection of neurotransmitter by "turn-on" response. J. Am. Chem. Soc. **136**(31), 10842–10845 (2014)
61. Y. Wang, J.T. Chen, X.P. Yan, Fabrication of transferrin functionalized gold nanoclusters/graphene oxide nanocomposite for turn-on near-infrared fluorescent bioimaging of cancer cells and small animals. Anal. Chem. **85**(4), 2529–2535 (2013)
62. J.J. Liu, X.L. Zhang, Z.X. Cong, Z.T. Chen, H.H. Yang, G.N. Chen, Glutathione-functionalized graphene quantum dots as selective fluorescent probes for phosphate-containing metabolites. Nanoscale **5**(5), 1810–1815 (2013)
63. Q. Mei, C. Jiang, G. Guan, K. Zhang, B. Liu, R. Liu et al., Fluorescent graphene oxide logic gates for discrimination of iron (3+) and iron (2+) in living cells by imaging. Chem. Commun. **48**(60), 7468–7470 (2012)
64. A.A. Nahain, J.E. Lee, I. In, H. Lee, K.D. Lee, J.H. Jeong et al., Target delivery and cell imaging using hyaluronic acid-functionalized graphene quantum dots. Mol. Pharm. **10**(10), 3736–3744 (2013)
65. J. Ge, M. Lan, B. Zhou, W. Liu, L. Guo, H. Wang et al., A graphene quantum dot photodynamic therapy agent with high singlet oxygen generation. Nat. Commun. **5**, 4596 (2014)
66. X.T. Zheng, A. Than, A. Ananthanaraya, D.H. Kim, P. Chen, Graphene quantum dots as universal fluorophores and their use in revealing regulated trafficking of insulin receptors in adipocytes. ACS Nano. **7**(7), 6278–6286 (2013)

67. P. Mansfield, Snapshot magnetic resonance imaging (nobel lecture). Angew. Chem. Int. Ed. Engl. **43**(41), 5456–5464 (2004)
68. P.E.J. Caravan, T.J. McMurry, R.B. Lauffer, Gadolinium(III) chelates as MRI contrast agents: structure, dynamics, and applications. Chem. Rev. **99**(9), 2293–2352 (1999)
69. G.J.M.W. Strijkers, G.A. van Tilborg, K. Nicolay, MRI contrast agents: current status and future perspectives. Anticancer Agents Med. Chem. **7**(3), 291–305 (2007)
70. S. Kanakia, J.D. Toussaint, S.M. Chowdhury, G. Lalwani, T. Tembulkar, T. Button et al., Physicochemical characterization of a novel graphene-based magnetic resonance imaging contrast agent. Int J Nanomedicine. **8**, 2821–2833 (2013)
71. A. Gizzatov, V. Keshishian, A. Guven, A.M. Dimiev, F. Qu, R. Muthupillai et al., Enhanced MRI relaxivity of aquated $Gd3^+$ ions by carboxyphenylated water-dispersed graphene nanoribbons. Nanoscale **6**(6), 3059–3063 (2014)
72. H.B. Na, I.C. Song, T. Hyeon, Inorganic nanoparticles for MRI contrast aAgents. Adv. Mater. **21**(21), 2133–2148 (2009)
73. H. Li, J.M. Melnyczuk, L.I. Lewis, S. Palchoudhury, J. Wu, P. Nagappan et al., Selectively self-assembling graphene nanoribbons with shaped iron oxide nanoparticles. RSC Adv. **4** (62), 33127 (2014)
74. W. Chen, P. Yi, Y. Zhang, L. Zhang, Z. Deng, Z. Zhang, Composites of aminodextran-coated Fe_3O_4 nanoparticles and graphene oxide for cellular magnetic resonance imaging. ACS Appl. Mater. Interfaces **3**(10), 4085–4091 (2011)
75. X. Shi, H. Gong, Y. Li, C. Wang, L. Cheng, Z. Liu, Graphene-based magnetic plasmonic nanocomposite for dual bioimaging and photothermal therapy. Biomaterials **34**(20), 4786–4793 (2013)
76. E. Peng, E.S.G. Choo, P. Chandrasekharan, C.-T. Yang, J. Ding, K.-H. Chuang et al., Synthesis of manganese ferrite/graphene oxide nanocomposites for biomedical applications. Small **8**(23), 3620–3630 (2012)
77. M.L. Chen, L.M. Shen, S. Chen, H. Wang, X.W. Chen, J.H. Wang, In situ growth of β-FeOOH nanorods on graphene oxide with ultra-high relaxivity for in vivo magnetic resonance imaging and cancer therapy. J. Mater. Chem. B Biol. Med. **1**, 2582–2589 (2013)
78. Y. Wang, R. Huang, G. Liang, Z. Zhang, P. Zhang, S. Yu et al., MRI-visualized, dual-targeting, combined tumor therapy using magnetic graphene-based mesoporous silica. Small **10**(1), 109–116 (2014)
79. K. Dey, A. Ghosh, P. Modak, A. Indra, S. Majumdar, S. Giri, Tuning of multiferroic orders correlated to oxygen stoichiometry in magnetite films. Appl. Phys. Lett. **105**(14), 142905 (2014)
80. J. Lin, X. Chen, P. Huang, Graphene-based nanomaterials for bioimaging. Adv. Drug Deliv. Rev. **105**, 242–254 (2016)
81. D.W. Hwang, Radio-graphene in theranostic perspectives. Nucl. Med. Mol. Imaging. *51*, 1–5 (2016)
82. J.M. Craft, R.A. De Silva, K.A. Lears, R. Andrews, K. Liang, S. Achilefu et al., In vitro and in vivo evaluation of a ^{64}Cu-labeled NOTA-Bn-SCN-Aoc-bombesin analogue in gastrin-releasing peptide receptor expressing prostate cancer. Nucl. Med. Biol. **39**, 609–616 (2012)
83. C.M. Kang, S.M. Kim, H.J. Koo, M.S. Yim, K.H. Lee, E.K. Ryu et al., In vivo characterization of ^{68}Ga-NOTA-VEGF 121 for the imaging of VEGF receptor expression in U87MG tumor xenograft models. Eur. J. Nucl. Med. Mol. Imaging **40**, 198–206 (2013)
84. C.J. Choy, X. Ling, J.J. Geruntho, S.K. Beyer, J.D. Latoche, B. Langton-Webster et al., ^{177}Lu-labeled phosphoramidate-based PSMA inhibitors: the effect of an albumin binder on biodistribution and therapeutic efficacy in prostate tumor-bearing mice. Theranostics **7**, 1928–1939 (2017)
85. J.P. Meyer, P. Adumeau, J.S. Lewis, B.M. Zeglis, Click chemistry and radiochemistry: the first 10 years. Bioconjug. Chem. **27**, 2791–2807 (2016)

86. D. Prim, F. Rebeaud, V. Cosandey, R. Marti, P. Passeraub, M.E. Pfeifer, ADIBO-based "click" chemistry for diagnostic peptide micro-array fabrication: physicochemical and assay characteristics. Molecules **18**, 9833–9849 (2013)
87. H. Hong, K. Yang, Y. Zhang, J.W. Engle, L. Feng, Y. Yang et al., In vivo targeting and imaging of tumor vasculature with radiolabeled, antibody-conjugated nanographene. ACS Nano. **6**, 2361–2370 (2012)
88. H. Hong, Y. Zhang, J.W. Engle, T.R. Nayak, C.P. Theuer, R.J. Nickles et al., In vivo targeting and positron emission tomography imaging of tumor vasculature with ^{66}Ga-labeled nano-graphene. Biomaterials **33**, 4147–4156 (2012)
89. D. Yang, L. Feng, C.A. Dougherty, K.E. Luker, D. Chen, M.A. Cauble et al., In vivo targeting of metastatic breast cancer via tumor vasculature-specific nano-graphene oxide. Biomaterials **104**, 361–371 (2016)
90. S. Shi, K. Yang, H. Hong, F. Chen, H.F. Valdovinos, S. Goel et al., VEGFR targeting leads to significantly enhanced tumor uptake of nanographene oxide in vivo. Biomaterials **39**, 39–46 (2015)
91. H.J. Im, C.G. England, L.Z. Feng, S.A. Graves, R. Hernandez, R.J. Nickles et al., Accelerated blood clearance phenomenon reduces the passive targeting of PEGylated nanoparticles in peripheral arterial disease. ACS Appl. Mater. Interfaces **8**, 17955–17963 (2016)
92. C.G. England, H.J. Im, L.Z. Feng et al., Re-assessing the enhanced permeability and retention effect in peripheral arterial disease using radiolabeled long circulating nanoparticles. Biomaterials **100**, 101–109 (2016)
93. B. Cornelissen, S. Able, V. Kersemans, P.A. Waghorn, S. Myhra, K. Jurkshat et al., Nanographene oxide-based radioimmunoconstructs for in vivo targeting and SPECT imaging of HER2-positive tumors. Biomaterials **34**, 1146–1154 (2013)
94. Y. Fazaeli, O. Akhavan, R. Rahighi, M.R. Aboudzadeh, E. Karimi, H. Afarideh, In vivo SPECT imaging of tumors by ^{198,199}Au-labeled graphene oxide nanostructures. Mater. Sci. Eng. C Mater. Biol. Appl. **45**, 196–204 (2014)
95. K. Yang, J.M. Wan, S.A. Zhang, Y.J. Zhang, S.T. Lee, Z.A. Liu, In vivo pharmacokinetics, long-term biodistribution, and toxicology of PEGylated graphene in mice. ACS Nano. **5**, 516–522 (2011)
96. F.M. Lu, Z. Yuan, PET/SPECT molecular imaging in clinical neuroscience: recent advances in the investigation of CNS diseases. Quant. Imaging Med. Surg. **5**, 433–447 (2015)
97. J. Song, X. Yang, O. Jacobson, L. Lin, P. Huang, G. Niu et al., Sequential drug release and enhanced photothermal and photoacoustic effect of hybrid reduced graphene oxide-loaded ultrasmall gold nanorod vesicles for cancer therapy. ACS Nano. **9**, 9199–9209 (2015)
98. T.H. Tran, H.T. Nguyen, T.T. Pham, J.Y. Choi, H.G. Choi, C.S. Yong et al., Development of a graphene oxide nanocarrier for dual-drug chemo-phototherapy to overcome drug resistance in cancer. ACS Appl. Mater. Interfaces **7**, 28647–28655 (2015)
99. L. Zhou, L. Zhou, S. Wei, X. Ge, J. Zhou, H. Jiang et al., Combination of chemotherapy and photodynamic therapy using graphene oxide as drug delivery system. J. Photochem. Photobiol. B **5**(135), 7–16 (2014)
100. B. Lewis, E. Chalhoub, C. Chalouhy, O. Sartor, Radium-223 in bone-metastatic prostate cancer: current data and future prospects. Oncology **29**, 483–488 (2015)
101. D.A. Scheinberg, M.R. McDevitt, Actinium-225 in targeted alpha-particle therapeutic applications. Curr. Radiopharm. **4**, 306–320 (2011)
102. L. Chen, X. Zhong, X. Yi, M. Huang, P. Ning, T. Liu et al., Radionuclide ^{131}I labeled reduced graphene oxide for nuclear imaging guided combined radio- and photothermal therapy of cancer. Biomaterials **66**, 21–28 (2015)

Chapter 5
Organic Nanomaterials: Liposomes, Albumin, Dendrimer, Polymeric Nanoparticles

Keon Wook Kang and Myung Geun Song

Abstract Organic nanoparticles (NPs) as a drug delivery system have a relative long history of development and many of them are now approved for commercial use. The nano-carrier used for drug delivery should be eliminated from the body, either by degradation or by excretion. While many inorganic nano-carriers are very stable and difficult to metabolize, many of organic NPs are biodegradable. Radiolabeling of biomolecules enables tracing these molecules in vivo. Biodistribution and autoradiography studies validate tissue distribution of the nano-carriers in animals. Nuclear medicine imaging such as single photon emission computed tomography (SPECT) or positron emission tomography (PET) allows non-invasive longitudinal monitoring of the in vivo pharmacokinetics and tissue distribution of the nano-carriers even in human subjects. In vivo tracking of nano-carriers using radionuclide imaging techniques enables a theranostic approach as well, not just being a drug carrier. The combination of diagnostic and therapeutic capabilities in a single drug delivery system can be used for precision personalized therapies. In this chapter, we dealt with four different groups of biodegradable organic NPs and their radiolabeled forms: liposomes, albumin-based nanoparticles, dendrimers, and polymeric nanoparticles.

K. W. Kang (✉) · M. G. Song
Department of Nuclear Medicine, Seoul National University
College of Medicine, Seoul 03080, Republic of Korea
e-mail: kangkw@snu.ac.kr

K. W. Kang · M. G. Song
Cancer Research Institute, Seoul National University,
Seoul, Republic of Korea

M. G. Song
Biomedical Research Institute, Seoul National University Hospital,
Seoul 03082, Republic of Korea
e-mail: mgsong0310@snu.ac.kr

D. S. Lee (ed.), *Radionanomedicine*, Biological and Medical Physics,
Biomedical Engineering, https://doi.org/10.1007/978-3-319-67720-0_5

5.1 Introduction

Organic nanoparticles (NPs) are made of organic molecules. Natural organic molecules may exist in 1–1000 nm in diameter which are proteins aggregates, lipid bodies, milk emulsions, viruses, antibodies, albumin and etc. Organic NPs are also produced as a form of food, cosmetics and pharmaceuticals. Pharmaceutical formulations are including liposomes, albumin, dendrimer, polymers and their conjugate forms [1].

Organic NPs as a drug delivery system have a relative long history of development and many of them are now approved for commercial use. The nano-carrier used for drug delivery should be eliminated from the body, either by degradation or by excretion. Many inorganic nano-carriers are very stable and difficult to metabolize, so they could be deposited in the body for long time [2]. Thus, biodegradable nanomaterials are preferred for drug delivery which needs to improve solubility, extend the half-life, and reduce toxicity. In this chapter, we dealt with four different groups of biodegradable organic NPs as nano drugs: liposomes, albumin-based NPs, dendrimers, and polymeric NPs.

Radiolabeling of biomolecules enables tracing these molecules in vivo. Biodistribution and autoradiography studies validate tissue distribution of the nano-carriers in animals. Nuclear medicine imaging such as single photon emission computed tomography (SPECT) or positron emission tomography (PET) allows non-invasive longitudinal monitoring of the in vivo pharmacokinetics and tissue distribution of the nano-carriers even in human subjects.

In vivo tracking of nano-carriers using radionuclide imaging techniques enables a theranostic approach as well, not just being a drug carrier. The combination of diagnostic and therapeutic capabilities in a single drug delivery system can be used for personalized precision therapies. In vivo imaging of radiolabeled NPs prior to therapy has a function of companion diagnostics to predict accumulation of NPs at target sites. This predicts the potential therapeutic response and enable to select appropriate patients and to determine the dose to obtain an optimal therapeutic response. The therapeutic NPs can be administered, if the radiolabeled NPs are accumulated in the target tissues sufficiently determined by prior in vivo imaging. Biodistribution of tracing dose of drug is not always the same as that of therapeutic dose. During the radioiodine therapy of thyroid cancer, sometimes imaging after therapeutic dose shows more metastatic lesions than diagnostic imaging. So, drug-loaded NPs can also be radiolabeled to verify their delivery to the tissue of interest for monitoring in the initial or following occasions of treatment. Insufficient accumulation of the NPs on the target could explain a lack of therapeutic response. Increased accumulation of the NPs on the normal organs predict the adverse effects. Thus, radionuclide imaging of NPs can play an important role in the management of the individual patients in each session of treatment.

Nano-drug delivery system has the long biologic half-lives, typically in the order of days. It is essential to select radioisotopes with long half-life for following-up imaging to evaluate the effective therapy. For nuclear medicine planar imaging or

SPECT imaging, γ-ray emitting radionuclides, such as ^{99m}Tc (t½ = 6 h) and ^{111}In (t½ = 2.8 d) are used. For PET imaging, ^{64}Cu (t½ = 12.7 h) or ^{89}Zr (t½ = 3.3 d) is preferred over ^{18}F (t½ = 110 min) or ^{68}Ga (t½ = 68 min). Some radionuclides such as ^{166}Ho, ^{177}Lu, ^{131}I, and ^{188}Re emit both gamma and beta ray at the same time. NPs labeled with these radionuclides can be used for simultaneous imaging and therapy, so called radio-theranostics. Radionuclides emitting beta (^{90}Y) or alpha ray (^{225}Ac or ^{213}Bi) can be used for targeted radionuclide therapy.

5.2 Liposomes

Liposomes are spherical vesicles organized as the phospholipid bilayer resembling cell membranes. Ever since their discovery in 1965, liposomes have been extensively studied exploring their potential for diagnostic and therapeutic purposes [3]. The targeting property of liposomes is based on the enhanced permeability and retention (EPR) effect, which is the increased vascular permeability found in tumors or inflamed tissues [4]. Targeting efficacy and biodistribution are dependent on factors such as size, composition, charge, and surface modification [5]. The size of the liposomes is one of the key factor of affecting biodistribution. Liposomes are primarily taken up by the liver when smaller than 70 nm, while taken up by the spleen when larger than 200 nm [6]. Liposomes with a diameter of 100–200 nm showed up-to fourfold higher uptake rate in the tumor compared to larger or smaller vesicles due to increased circulation time [7]. Composition of the liposomes is related with the in vivo stability. The addition of cholesterol to the phospholipids results in increased rigidity and chemical stability of liposomes in physiological conditions6. When conventional liposomes are administered intravenously, they will be coated with plasma proteins and organized into the protein corona. The protein corona covering liposomes acts as opsonins. Opsonins are circulating host defense serum molecules which are attached to the surface of microbes or foreign bodies, promoting their clearance by phagocytic pathways. Liposomes coated by opsonins are recognized by the mononuclear phagocyte system and rapidly cleared from the blood circulation [8]. Polyethylene glycol (PEG) can be coated on the surface of liposomes to interfere opsonization. The first U.S. Food and Drug Administration (FDA) approved liposomal formulation was PEGylated liposomal doxorubicin (Doxil®). It was approved in 1995 [9].

Radiolabeled liposomes can be used to determine the biodistribution of liposomal drugs and provide theranostic opportunity in combination with therapeutic and diagnostic agents [10]. Vescan®, the first liposomal-based radiotracer formulation was developed as an imaging agent [11]. ^{111}In-based ionophore was loaded within the micellar structure of the liposomes. Although Vescan® was not approved by the FDA for commercial use, clinical trials provided a good understanding of the patient's liposome clearance rate and imaging in various tumors.

Various strategies have been developed for the radiolabeling of liposomes [12, 13]. The four major strategies are passive encapsulation [14], membrane labeling

[15], surface chelation [16] and remote loading [17] (Fig. 5.1). Passive encapsulation incorporates the radioisotopes within the liposomes during the formation of their structure. This method is rarely used nowadays because of the low infusion efficiency (<10%) of the radiolabeled compound into the liposomes. Membrane labeling is a method that liposome membranes are labeled with radionuclides before forming liposomes. The radioactive compound can be either covalently bound to the membrane surface of the liposome or located inside of the membrane if radionuclide containing molecules is hydrophobic. The main drawback of this method is a tedious and laborious purification process. Radiolabeled lipid derivatives can be formed into liposomes like the passive loading. Notably, noncovalent loading of radionuclides can be released in vivo and then radioactivities represent freed radionuclides as well as labeled ones. Thus this method might provide false estimates of location of liposomes in the body.

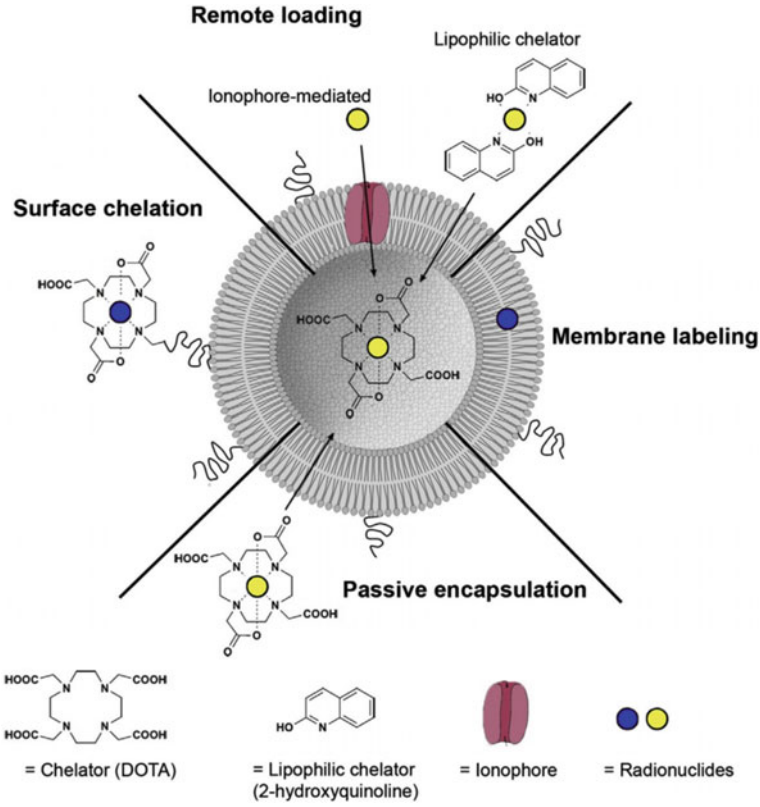

Fig. 5.1 Schematic diagram of passive encapsulation, membrane labeling, surface chelation, and remote loading methods for preparing radioactive liposomes. Reprinted from [13] with permission from Elsevier

The surface chelation and stepped remote loading approaches are featuring high radiolabeling efficiency and retention. Surface chelation uses chelators that are incorporated into the hydrophobic membrane surface of the liposomes during their formation. This method has high-efficiency loading of the liposomes (>90%). In vivo stability of radionuclides labeled on the surface of liposomes is dependent on the radionuclide–chelator binding constant. When the radionuclides are exposed to biomolecules in the blood, it might be released from the chelator if the biding is not tight enough. The remote loading method is active loading and concentrating of radionuclides into the internal aqueous compartment of the liposomes. It provides both high loading efficiencies (>90%) and high in vivo stability because the radionuclides are located inside of liposome.

During the development of liposomal drugs, ^{99m}Tc and ^{111}In were popularly used to monitor the fate of liposomes in vivo using tissue biodistribution studies and scintigraphic imaging in earlier days, since their physical half-life is similar to the biologic half time of liposomes [18–20]. Clinical studies provided insights in the in vivo behavior of liposomes in cancer patients and guided the development of liposomal drugs. Planar scan and SPECT imaging of PEG-coated and ^{111}In-labeled liposomes succeeded in visualizing tumor lesions in different types of locally advanced cancer [21]. Clinical studies with this companion diagnostic imaging showed that liposomes were well tolerated in all patients and accumulated in the tumor in 15 of 17 patients (4 of 5 breast, 5 of 5 head and neck, 3 of 4 bronchus, 2 of 2 glioma, and 1 of 1 cervix cancer). The tumor uptake of liposomes were 0.5–3.5% of the injected dose at 72 h which was estimated from regions of interest on gamma camera images. The highest uptake were observed in the patients with head and neck cancers [33.0 ± 15.8%ID/kg (percentage of injected dose/kg)]. Radiolabeled PEGylated liposomes accumulate in solid tumors and remain there according to the imaging findings at 7 days after injection. In addition, significant localization of the liposomes was found in the tissues of the mononuclear phagocytic system (MPS a.k.a. RES; reticuloendothelial system) such as liver, spleen, and bone marrow. Due to the low sensitivity (∼70%) for detecting tumors, no radiolabeled liposomes were approved for diagnostic agents by the FDA.

Since liposomes localize in inflamed tissues, gamma camera imaging with radiolabeled liposomes was also applied to image infectious or inflammatory lesions. PEGylated liposomal formulation was used to detect inflammatory foci in patients. ^{99m}Tc-PEG liposome scintigraphy were directly compared with those of ^{111}In-immunoglobulin G (lgG) scintigraphy in patients with soft-tissue infection (n = 3), septic arthritis (n = 3), autoimmune polyarthritis (n = 2), infected hip prosthesis (n = 1), infected osteosynthesis (n = 1), spondylodiscitis (n = 1), infected aortic prosthesis (n = 1), colitis (n = 1), abdominal abscess (n = 1), and pneumonia (n = 1). Of the 16 proven lesions, 15 were detected by ^{99m}Tc-PEG liposome scan which is similar to ^{111}In-IgG imaging [22]. Radiolabeled liposomes were also used to image inflamed foci in patients with rheumatoid arthritis. ^{99m}Tc labeled negatively charged liposomes were injected to 6 patients with rheumatoid arthritis intravenously [23]. All clinically involved joints could be visualized on scan 20–22 h later exception of the small interphalangeal joints. These studies

showed that scintigraphic imaging of infection and inflammation using radiolabeled liposomes is safe, sensitive and specific.

PET imaging with radiolabeled liposomes has only been carried out in animal models. ^{18}F and ^{68}Ga have been used to radiolabel liposomes and to image different types of cancers. However, the short half-life of these radionuclides (110 and 68 min, respectively) is not optimal. Radionuclides with longer half-lives, like ^{64}Cu ($t_{1/2}$ = 12.7 h) and ^{89}Zr ($t_{1/2}$ = 78.4 h) are needed to image the accumulation of liposomes in tumors at later time points. PEGylated liposomes labeled with ^{64}Cu were used to evaluate PET imaging of cancer. Biodistribution studies were done using two different molar level of PEG (5 and 10 mol%) on the surface of PEGylated liposomes with remote loaded ^{64}Cu in a xenograft mouse model with human neuroendocrine tumor cells (NCI-H727). A significantly higher liposomal uptake (%ID/g) was observed in small tumors compared to large tumors at the 24 h ($P < 0.001$) and 48 h ($P < 0.001$) time points.

^{89}Zr can track liposomes over a week after injection. To quantify in vivo pharmacokinetics of liposomal NPs, liposome was labeled with ^{89}Zr efficiently using a method based on a rapid ligand exchange reaction between the membrane-permeable ^{89}Zr(8-hydroxyquinolinate)4 complex and the hydrophilic liposomal cavity-encapsulated deferoxamine (DFO) [24]. These ^{89}Zr-labeled liposomal NPs showed remarkable stability in phosphate-buffered saline and serum without leakage of radioactivity. Radiolabel retention of them in fresh rat serum at 37 °C for 24 and 48 h was 95 and 94%, respectively. In the PET images, the KB tumor xenografts were visible at 6 h, and became clearer at 24 h, and then the signals became weaker at 48 h due to washing out of radio-activity in the endocytosed liposomes degraded over time. The pharmacokinetic analysis from the PET images indicated that the radioactivity, at last, was gradually and in parts washed out from the kidney and liver, or remainders were deposited in the bone over time. The catabolism of the liposome-encapsulated ^{89}Zr-DFO in the liver caused release of ^{89}Zr into the circulation, leading to its accumulation in bone.

Radiolabeling of drug-loaded liposomes enables a theranostic strategy which allows monitoring the liposomes and their contents during therapy using radionuclide imaging. The combination of chemotherapy and radionuclide therapy will also be possible, if the liposomes are loaded with chemotherapeutic drugs and also labeled with beta emitting radionuclides, such as ^{90}Y, ^{131}I, ^{166}Ho, ^{177}Lu, and ^{188}Re or with alpha-emitters, such as ^{213}Bi or ^{225}Ac. Some radionuclides such as ^{131}I, ^{166}Ho, ^{177}Lu, and ^{188}Re, emits both beta particles and gamma photons at the same time. Since beta ray can destroy nearby cells, and gamma ray can escape from the body and be captured by gamma cameras, radiolabeling of liposomes with these radionuclides will enable theranostic on their own.

^{188}Re is a theranostic radionuclide because it emits both gamma rays and high energy of beta particles (2.12 meV). Since its atomic radius and gamma energy (155 keV) is similar to ^{99m}Tc, both radionuclides can be labeled with the same chemical methods and are optimal for gamma camera imaging. Moreover, ^{188}Re can be conveniently produced by ^{188}W/^{188}Re generator systems. ^{188}Re has been embedded in PEGylated liposomal particles via N,N-bis(2-mercaptoethyl)- N′,N′-

diethylethylenediamine (BMEDA) chelator for the treatment of human non–small cell lung cancer cells (NCI-H292) in a xenograft tumor model [25]. The pharmacokinetics and the dosimetry of ^{188}Re-BMEDA and ^{188}Re-PEG-liposome were revealed by SPECT/CT imaging and the concurrent biodistribution analysis. Compared with ^{188}Re-BMEDA, ^{188}Re-PEG-liposome showed a longer mean residence time, larger maximal concentration, and a slower pace of clearance. The accumulation of ^{188}Re-PEG-liposome at the tumor site remained detectable up to 48 h. The maximal absorbed dose to the liver, spleen and subcutaneous tumor (300 mm3) was estimated at 4 Sv, 17 Sv, and 70 Gy, respectively. When the tumor growth was monitored up to 21 d, only ^{188}Re-PEG-liposome suppressed tumor growth and extended life span of tumor bearing mice.

The high killing efficacy of alpha particles arises from the high linear energy transfer (LET). LET is the amount of energy deposited per unit distance traveled. Due to high LET, alpha particles therapy is independent of the cellular oxygenation or cell cycle. The range of alpha particles in the tissues is short as 50–100 μm. So their irradiation are well localized to the target cells, while surrounding healthy tissues are minimally exposed. Immuno-liposomes labeled with alpha emitters, ^{213}Bi ($t_{1/2}$ = 46 min) were injected in mice with breast cancer metastases induced by intra-cardiac injection of rat HER-2/neu expressing syngeneic tumor cells [26]. ^{213}Bi and the rat HER2/neu antibody was conjugated to a 100 nm diameter liposome. Median survival times were similar to those obtained with antibody conjugated with ^{213}Bi.

5.3 Albumin

Albumin is the most abundant plasma protein which is synthesized in the liver and constitutes approximately 60% of total plasma protein. Its distribution is primarily intravascular and its plasma half-life is 19 days [27]. Its molecular weight is 66.5 kDa and small enough to filter out through glomerulus in the kidney. Like antibodies, albumin binds to the neonatal Fc receptor (FcRn) which is expressed in proximal tubular cells, and is reabsorbed [28]. Albumin is a carrier protein for steroids, thyroid hormone, retinoid, other lipophilic hormones, and lipophilic drugs (Fig. 5.2).

When Evans blue-albumin complex was injected into tumor bearing mice via a tail vein, it gradually accumulated in the tumor [29]. When Evans blue-albumin complex was injected into the solid tumor, it was retained in the tumor for a long period. This phenomenon is now called the EPR effect on the tumor. Many nano-drug delivery systems, including liposome, use this strategy for the passive targeting of tumors. Abraxane® is a NP albumin-bound paclitaxel (PTX) and became the first albumin based antineoplastic agent approved by the FDA.

Radiolabeled human serum albumin (HSA) was used for the detection of protein losing enteropathy [30]. ^{99m}Tc-HSA scan showed blood pool imaging reflecting its intravascular distribution. In patients with protein losing enteropathy, radioactivity

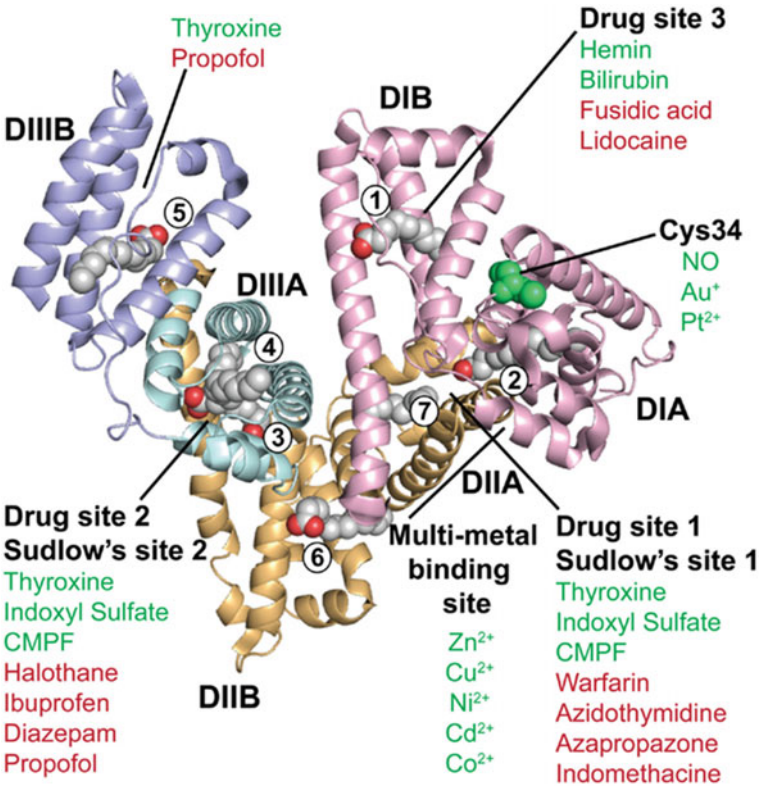

Fig. 5.2 The crystal structure of human albumin depicts multiple binding sites of hormones, drugs, and metals. Reprinted from [28] with permission

accumulated in the abdomen and migrated distally (Fig. 5.3). When ^{99m}Tc-HSA was injected in a tumor bearing mouse, radioactivity accumulated slowly in the tumor. It has not yet been elucidated why albumin accumulates in the tumor. Some mechanism other than the EPR effect is suggested. GP60, a 60 kDa glycoprotein, which is expressed on the plasma membrane of endothelial cells binds albumin and enhances penetration of Abraxane® by endothelial transcytosis [31]. A secreted protein, acidic and rich in cysteine (SPARC) is highly expressed in malignant cells and secreted into interstitial space. Since albumin has an affinity to SPARC, SPARC may play a role in albumin accumulation in the tumor [32].

^{99m}Tc micro-aggregated HSA has been used for bone marrow scan, since <80 nm sized particles preferentially are taken up by macrophages in the bone marrow, while bigger sized particles (200–400 nm) tend to accumulated more in the Kupffer cell of liver [33]. Bone marrow scan help to diagnosis of bony metastasis or osteomyelitis revealing defects in bone marrow which are replaced by tumors or leukocytes. Recently ^{99m}Tc HSA nanocolloids are more frequently used for sentinel lymph node (SLN) detection. Mapping lymph nodes on tumor drainage pathway

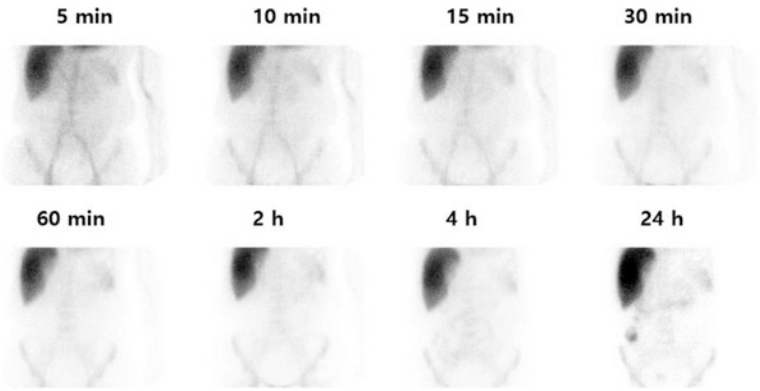

Fig. 5.3 A serial ^{99m}Tc-HSA scans in a patient with protein losing enteropathy. Until 4 h, radioactivity is within blood pool. At 24 h radioactivity accumulated in the right lower quadrant of abdomen and migrated distally

can guide minimal invasive surgery in cancers with early stage such as breast cancer, melanoma, and etc. ^{99m}Tc nanocolloidal albumin was approved in Europe for lymphoscintigraphy, bone marrow scintigraphy and visualization of inflammatory processes. Manufacturers declare in the technical leaflet that more than 95% of the particles of nanocolloidal albumin are smaller than 80 nm. Three commercially available ^{99m}Tc HSA nanocolloids (Nanoalbumon®, Nanocoll® and Nanotop®) were compared for their size and radioactivity distribution [34]. The ranges of particle diameter were 6.5–68 nm for Nanocoll®, 5.6–79 nm for Nanotop®, and 12–122 nm for Nanoalbumon®. The size and radioactivity distribution are similar between Nanotop® and Nanocoll®, and those of Nanoalbumon® is bigger than the others. Smallest particles can pass SLNs, and more node tiers are visualized, decreasing the accuracy of SLN mapping.

Combination of chemotherapy and radionuclide therapy based on albumin NPs was tried to show synergistic treatment effect in a mouse model bearing murine breast cancer 4T1 tumor [35]. HSA was labeled with radionuclide ^{131}I through a standard chloramine-T oxidation method, and then were added with PTX to prepare ^{131}I-HSA-PTX NPs. ^{131}I-HSA-PTX showed obvious tumor accumulation on gamma imaging 24 h after intravenous injection. Compared to radionuclide therapy (^{131}I-HSA) or chemotherapy (HSA-PTX) alone group, the combination therapy by ^{131}I-HSA-PTX was significantly more effective to decrease the tumor volumes.

Strategies labeling innate albumin in vivo were also tried using albumin binding molecules [36]. Evans Blue (EB), an albumin binding dye, displays reversible binding to serum albumin with IC_{50} in the micromolar range. A truncated EB was labeled with ^{68}Ga through 1,4,7-triazacyclononane-N,N′,N″-triacetic acid (NOTA) chelator (^{68}Ga-NEB). ^{68}Ga-NEB was retained in the blood circulation and cleared slowly but steadily from the blood in healthy volunteers. As a blood volume imaging agent, ^{68}Ga-NEB imaging clearly differentiated hepatic hemangioma from

other benign or malignant focal hepatic lesions. The radiolabeled EB was also evaluated as a radiotherapeutic agent in a mouse model of glioblastoma. Two injections of 7.4 MBq of ^{90}Y-1,4,7,10-tetra-azacyclododecanetetra-acetic acid (DOTA)-EB-RGD peptide eliminated the tumor xenografts.

5.4 Dendrimers

Dendrimers are a group of highly branched spherical synthetic polymers. Tomalia and his colleagues described the stepwise synthesis of dendrimers in 1980s, and coined the name of dendrimer meaning dendritic polymer [37]. They consist of a core and several layers with active terminal groups. These layers are formed by repetition of the polymer. The core is generation 0 (G0) and each layer will be G1, G2, G3, and so on. Due to the high loading capacity of payloads and the capability to control the polymer structure, dendrimers are favorable platforms for drug and gene delivery. Through the modification of cores, interiors, and surface groups of dendrimer, the properties of dendrimer can be optimized to reach favorable physical characteristics, biodistribution, receptor-mediated targeting, and controlled release of the payloads (Fig. 5.4) [38]. It can specifically target tumor cells by incorporating tumor-affine molecules. Dendrimers can carry gadolinium or radionuclides for magnetic resonance imaging (MRI) or nuclear medicine imaging and therapy.

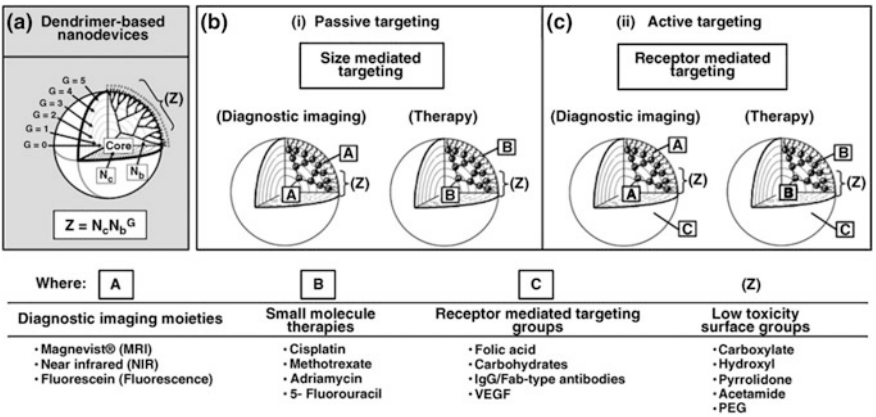

Fig. 5.4 Dendrimer architecture and targeting modalities. **a** Illustration of general dendrimer architectural topology with the three architectural components: (i) core, (ii) interior and (iii) terminal surface groups (Z). **b** Passive size-mediated targeting: dendrimer-based diagnostic imaging and therapy delivery nanodevices involving (A) imaging moieties, (B) small-molecule therapy components and (Z) low-toxicity terminal surface groups. **c** Active receptor-mediated targeting: dendrimer based diagnostic imaging and therapy delivery nanodevices involving (A) imaging moieties, (B) small-molecule therapy components, (C) receptor-mediated targeting groups and (Z) low-toxicity surface groups. Reprinted from [38] with permission from Elsevier

SPL7013 Gel (VivaGel®), dendrimers made from poly-L-lysine is in phase 3 clinical trials for prevention of sexual transmitted infections, such as HIV and genital herpes [39]. It blocks viruses by making biofilm when it is topically applied to vagina. For the drug delivery, docetaxel linked on PEGylated dendrimers (DEP™ docetaxel) is in Phase 1 clinical trials for advanced or metastatic cancer.

The size, surface charge and solubility of dendrimers can be precisely controlled by alteration of both the core and surface repeating units. There are different types of dendrimers, such as polyamidoamine (PAMAM), polypropylene imine (PPI) and poly-L-lysine. Among them, PAMAM dendrimers are the most intensively investigated for their biomedical applications. SuperFect® (Qiagen), well-known gene transfection agent for cell lines is PAMAM dendrimers.

Biodistribution of dendrimers has been studied by administration of radiolabeled dendrimers in animals. Charge has a crucial role affecting the biodistribution and toxicity of dendrimers. The body distribution of ^{125}I-labelled cationic PAMAM dendrimers (G3 and G4) and ^{125}I-labelled anionic ones (G2.5, G3.5 and G5.5) was investigated after intraperitoneal or intravenous administration to rats [40]. Cationic PAMAM was cleared very rapidly from circulation. Only 0.1–1% was detected in blood just 1 h after administration due to accumulation of dendrimers (60–90%) in the liver. Anionic PAMAM showed longer circulation times. Substantial amount (15–40%) of injected dose still remained in the blood 1 h after injection. However significant amount (25–70%) of anionic dendrimers accumulated in the liver as well. The cationic dendrimers were cytotoxic at the concentration of 0.05 mg/ml while anionic dendrimers were not cytotoxic up to concentrations of 1 mg/ml after 72 h of incubation with B16F10 cells. The toxic effects induced by cationic dendrimers could be related with membrane disruption due to interactions with negatively charged cell membranes [41].

The preclinical pharmacokinetics of G1 and G4 PAMAM were compared after ^{111}In labeling via DOTA like chelator (pyridine-N-oxide DOTA) [42]. The G1 was cleared fast from the blood, with only 0.51 ± 0.07% administered dose remaining in the blood 2 h after injection. A high radioactivity uptake in the kidney at 5 min rapidly decreased at 1 h after dosing. This rapid decreasing of radioactivity in the short time intervals is related with elimination of the agent to urine. G4 revealed a slower decrease of blood radioactivity over time. Two hours after administration, 4.33 ± 0.70% of the administered activity was still in the blood. G4 administration led to significant and long-term radioactivity in the liver (20.56 ± 2.59%) and kidneys (5.85 ± 0.58%) at 48 h post-injection.

The impact of PEGylation on the pharmacokinetics and biodistribution was investigated after intravenous administration of 3H-labeled poly L-lysine dendrimers to rats [43]. The larger dendrimer constructs (i.e. >30 kDa) were poorly cleared through kidneys and showed extended elimination half-lives (t½ 1–3 d) when compared to the smaller dendrimers (i.e. < 20 kDa) which were rapidly cleared from the plasma into the urine (t½ 1–10 h). The larger dendrimers concentrated in the organs of the MPS (RES) such as liver and spleen later on.

Radiolabeled dendrimers can be used for imaging diagnostics. ^{64}Cu-labeled LyP 1-dendrimer designed for PET imaging of atherosclerotic plaque [44]. LyP-1 is

a cyclic 9-amino acid peptide and binds to p32 proteins on activated macrophages [45]. Yet, the in vivo plaque accumulation of monomeric [^{18}F]FBA-LyP-1 was low (0.31 ± 0.05%ID/g). Multivalent peptides increase the binding avidity of targeting biomarker [46]. To increase the avidity of LyP-1 constructs to p32, dendritic form of LyP-1 ((LyP-1)4-dendrimer) was synthesized. ^{64}Cu was labeled via chelator 6-BAT (6-[p-(bromoacetamido)benzyl]-1,4,8,11-tetraazacyclotetradecane-N,N,N′, N″,N‴-tetraacetic acid) on (LyP-1)4-dendrimer for PET/CT imaging. Radioactivity of the LyP-1-dendrimer was 1.1 ± 0.26%ID/g in the aorta of ApoE-null mice having developed atherosclerosis on a high fat diet for 6 months.

Radionuclide-based theranostic strategy have been investigated by radiolabeling of dendrimers with radionuclides emitting both beta and gamma ray simultaneously such as ^{177}Lu, ^{131}I, and ^{188}Re. Dendrimers were radiolabeled with ^{177}Lu after conjugation with DOTA [47]. Biodistribution studies of ^{177}Lu-DOTA-dendrimers in C57BL/6 melanoma-bearing mice showed a high uptake in liver (20%ID/g), and spleen (18%ID/g). The blood activity decreased by half in 4 h through renal system. The tumor uptake was 5%ID/g and remained constant over 24 h.

Chlorotoxin (CTX)-conjugated multifunctional dendrimers labeled with radionuclide ^{131}I were synthesized and utilized for targeted SPECT imaging and radiotherapy of cancer [48]. Amine-terminated PAMAM dendrimers of G5 were used as a platform. The dendrimers was conjugated with PEG, CTX, and 3-(4′-hydroxyphenyl)propionic acid-OSu (HPAO). CTX selectively interacts with matrix metallopeptidase 2 (MMP-2) which are specifically upregulated in gliomas. The hydrodynamic size of them were 233.5 nm and the surface potential of the G5. NHAc-HPAO-(PEG-CTX)-(mPEG) dendrimers was +25.9 mV. The dendrimer platform was labeled with ^{131}I using the chloramine-T method through the phenol group of HPAO moiety. This theranostic dendrimer platform had an ability for targeted SPECT imaging and radiotherapy of an MMP-2 overexpressing C6 glioma mouse model.

G4 poly-L-lysine dendrimer was radiolabeled with ^{188}Re via nitro-imidazole chelating ligand (ImDendrim) [49]. Nude mice bearing hepatocellular carcinoma HepG2 xenograft tumors were treated with a 0.1 ml of ^{188}Re-ImDendrim at doses of 37, 74, 92.5 and 111 MBq by a single intratumoral injection. After 3 and 24 h post in situ administration of ^{188}Re-ImDendrim, SPECT/CT imaging was done. At 24 h post injection of ^{188}Re-ImDendrim, almost total administered radioactivity was retained locally in the injection site. There were no significant diffusion outside the injection area and no significant uptake in various organs including lungs, heart, liver, kidneys and brain (Fig. 5.5). The cationic poly-L-lysine groups of dendrimer limit its diffusion rate and showed high retention in the site of injection. ^{188}Re-ImDendrim treated group showed significant anti-tumor property even with the lowest dose of 37 MBq per mouse. In comparison, injection of nonradioactive ImDendrim or free ^{188}Re did not result in any anti-tumor effect. In situ introduction of ^{188}Re-ImDendrim is in phase 1 clinical trial for treatment of inoperable liver cancers which are non-responding to conventional therapy.

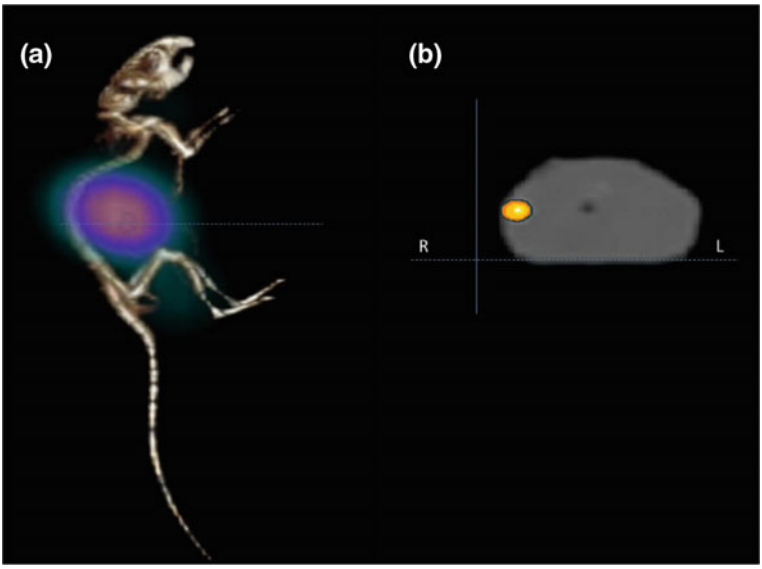

Fig. 5.5 SPECT/CT images of tumor-bearing mice after in situ injection of ^{188}Re-ImDendrim. Reprinted from [49] with permission

5.5 Polymeric Nanoparticles

Polymeric NPs are defined as submicron-sized solid polymer particles with matrix type structure, in which a cargo can be encapsulated within the polymer matrix or absorbed in the surface [50]. Their biocompatibility and biodegradability makes them suitable for various biomedical applications. These applications include drug and gene delivery, tissue engineering, medical supplies like sutures or wound dressings, imaging agents, cosmetics, food and beverage. The most common synthetic polymers are polyesters like polylactic acid (PLA), polyglycolic acid (PGA) or their copolymer poly(lactic-co-glycolic acid) (PLGA).

Paclitaxel loaded polymeric micelle (Genexol PM) was approved for the treatment of breast cancer, non-small cell lung cancer, and ovarian cancer in Korea. Genexol PM consists of biodegradable di-block copolymers, methoxy poly(ethylene glycol)-poly(DL-lactic acid) (mPEG-PDLLA). The copolymer residue increases the water-solubility of paclitaxel and allows delivery of higher doses than those achievable with paclitaxel alone [51].

PLGA is a particularly interesting material for the development of clinically relevant drug delivery systems, due to its long history of safety in humans. PLGA is biodegradable and undergoes hydrolysis in the body to produce the original monomers, lactic acid and glycolic acid. Microparticle formulations of PLGA are clinically approved for use in humans for direct injection. NPs composed of PLGA

(BIND-014) is in phase 2 clinical trials for targeted delivery of docetaxel to prostate-specific membrane antigen (PSMA) in metastatic prostate cancer [52].

PEG is a highly biocompatible polyether. It has been frequently used as a surface modifier of NPs to reduce their cytotoxicity. Biodistribution studies of polymeric NPs have shown that they are normally opsonized and removed from the bloodstream by macrophages in reticuloendothelial system (RES) such as liver and spleen very rapidly [53]. When they are PEGylated (attachment of PEG to molecules or macrostructures), their half-time become longer and they migrate preferentially to the spleen, while smaller particles concentrate in bone marrow. The length effect of PEG was studied using biodistribution in rats and PET imaging in mice. Various lengths of PEG chains (1.1, 2.0, and 5.0 kDa) was grafted to poly (methyl methacrylate-co-methacryloxysuccinimide) (PMMA-co-PMASI) [54]. After preparation of polymeric micelles, DOTA ligand was introduced to polymer terminal as a chelator for ^{64}Cu. Diameters of the micelles with PEG of 1.1, 2.0, and 5.0 kDa were 9.7 ± 1.1, 17 ± 2, and 20 ± 3 nm, respectively. Biodistribution studies and PET imaging was done after injection of ^{64}Cu labeled polymeric micelles. The 5.0 kDa PEG micelle showed a slow blood clearance, and 31 ± 2% of the dose was still in blood at 48 h after injection. It was almost ten times higher than that of 1.1 kDa PEG micelles and twice higher than that of 2.0 kDa ones. Liver uptake of 1.1, 2.0, and 5.0 kDa PEG micelles at 24 h from the injection was decreased in this order and to be about 4.0, 2.8, and 1.2%ID/g, respectively. Excretion profiles showed that the urine activity of 1.1 kDa PEG NP exhibited a significantly higher than that of the 5.0 kDa PEG derivative. This study showed a trend that longer PEG lengths correlates with longer blood circulation lifetimes and lower uptake in the liver.

Polymeric NPs has been studied for vaccine adjuvants replacing aluminum salts. Radiolabeling can reveal the fate of subcutaneously administered polymeric NPs. ^{125}I was labeled with poly(γ-PGA-Phe), consisted of hydrophilic poly(γ-glutamic acid) and hydrophobic phenylalanine after adding tyrosine (Tyr)-residues for radioiodination [55]. These NPs were 200 nm in diameter and had a negative zeta-potential. ^{125}I has a relatively long physical half-life of 60 days and enables monitoring a long process of excretion of NPs. Gamma scintigraphic images and biodistribution study were followed up until 11 d post injection to the mice. The amount of γ-PGA-Phe-Tyr(^{125}I) NPs at the site of injection (SOI) gradually decreased over a week. About 3% of injection doses were remained at SOI, and little was detected in the organs and blood all the time. At 11 d post-injection, NPs were detected from the excretion 14 ± 4 and 59 ± 1% from feces and urine, respectively.

Radiolabeled polymeric NPs was studied for chemoradiation therapy. Core-crosslinked polymeric micelles (CCPM) was prepared from self-assembly and cross-linking of poly[oligo(ethylene glycol) methyl ether methacrylate]30-b-poly(2-(methacryloyloxy)ethyl 4-oxo-4-(3-(triethoxysilyl)propylamino)butanoate) [56]. ^{177}Lu was conjugated via a chelator complex, DTPA-bz-SCN which was introduce to CCPM. ^{177}Lu emits beta ray for treating tumors. In addition, ^{177}Lu can be used for scintigraphy and dosimetry because it emits gamma ray. On the other hand,

cyclopamine (CPA) which is a radio-sensitizer, encapsulated in liquid–lipid NPs (CPA-LLP) for intravenous injection. The size of CCPM-^{177}Lu was 33.1 ± 1.2 nm, and that of CPA-LLP was 48.2 ± 3.1 nm. For the combination therapy, CPA-LLP was injected via tail vein, and CCPM-^{177}Lu was injected intratumorally in 4T1 murine breast cancer and Miapaca-2 human pancreatic adenocarcinoma mice models. The combination of CPA-LLP and CCPM-^{177}Lu delayed tumor growth more than either monotherapy did alone.

The natural polymeric NPs are made of chitosan, hyaluronic acid, and etc. Chitosan is a natural biodegradable cationic polysaccharide consisting of D-glucosamine and N-acetyl-D-glucosamine. It is prepared by the deacetylation of natural biopolymer chitin which is found in the exoskeleton of crustaceans. Chitosan derivatives have been actively studied because of high viscosity, low toxicity, superior mucoadhesive properties, and biocompatibility [57]. They are suitable for drug delivery vehicle as well as biomaterials for tissue engineering. Chitosan has been approved by the FDA for wound dressing, because it achieves hemostasis and induces normal tissue regeneration [58].

About 300 nm sized glycol chitosan NPs (CNPs) were labeled with ^{64}Cu to monitor in vivo biodistribution of NPs [59]. A strained cyclooctyne derivative, dibenzyl cyclooctyne (DBCO) conjugated with a DOTA chelator. Azide (N3) group was introduce to CNPs. ^{64}Cu-radiolabeled CNPs was synthesized via copper-free click reaction between ^{64}Cu-DOTA-Lys-PEG4-DBCO and CNP-N3. ^{64}Cu-CNPs (0.25 mCi, 200 μg) were administered to SCC7 tumor-bearing mice. Radioactivity in the tumor region gradually increased from 6.1 ± 1.3%ID/g at 2 h post-injection up to 11.3 ± 1.25%ID/g at 50 h post-injection (Fig. 5.6). Liver and

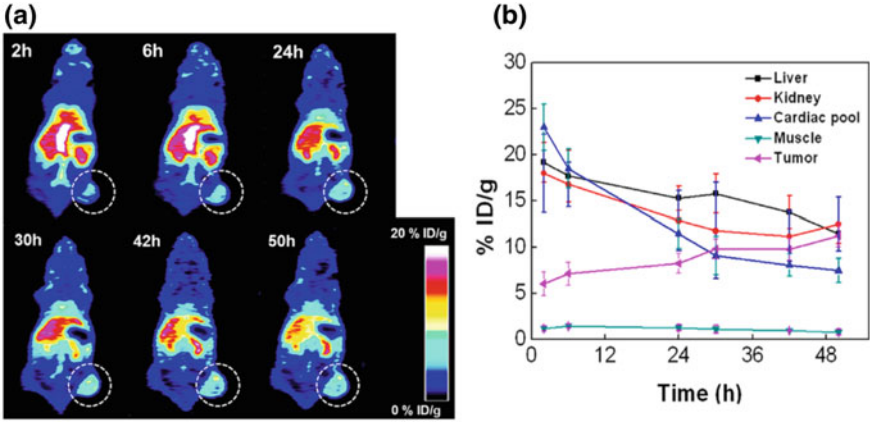

Fig. 5.6 PET images (A) and quantitative analysis (B) of intravenously administered ^{64}Cu-CNPs in tumor-bearing mice. White circles denote the tumor. Quantitative analysis (%ID/g) for tumor, liver, kidney, cardiac pool, and muscle based on ROI analysis of PET data. Error bars represent mean ± standard deviation (n = 7). Reprinted from [59] with permission from American Chemical Society

kidney were organs of major CNP accumulation. The blood half-life for the ^{64}Cu-CNPs can be estimated as 27 h by monitoring radioactivity obtained from the cardiac pool of each experimental tumor-bearing mouse over time.

References

1. G. Romero, S. Moya, Synthesis of organic nanoparticles, in *Nanobiotechnology: Inorganic Nanoparticles vs Organic Nanoparticles*, ed. by J. de la Fuente, V. Grazu (Elsevier, Amsterdam, 2012), pp. 115–141
2. M. Li, K.T. Al-Jamal, K. Kostarelos, J. Reineke, Physiologically based pharma-cokinetic modeling of nanoparticles. ACS Nano **4**, 6303–6317 (2010)
3. A.D. Bangham, M.M. Standish, J.C. Watkins, Diffusion of univalent ions across the lamellae of swollen phospholipids. J. Mol. Biol. **13**, 238–252 (1965)
4. K. Maruyama, Intracellular targeting delivery of liposomal drugs to solid tumors based on EPR effects. Adv. Drug Deliv. Rev. **63**, 161–169 (2011)
5. L. Sercombe, T. Veerati, F. Moheimani, S.Y. Wu, A.K. Sood, S. Hua, Advances and challenges of liposome assisted drug delivery. Front Pharmacol. **6**, 286 (2015)
6. T. van der Geest, P. Laverman, J.M. Metselaar, G. Storm, O.C. Boerman, Radionuclide imaging of liposomal drug delivery. Expert Opin. Drug Deliv. **13**(9), 1231–1242 (2016)
7. D. Liu, A. Mori, L. Huang, Role of liposome size and RES blockade in controlling biodistribution and tumor uptake of GM1-containing liposomes. Biochim. Biophys. Acta **1104**, 95–101 (1992)
8. X. Yan, G.L. Scherphof, J.A. Kamps, Liposome opsonization. J. Liposome Res. **15**(1–2), 109–139 (2005)
9. Y. Barenholz, Doxil®–the first FDA-approved nano-drug: lessons learned. J. Control Release. **160**(2), 117–134 (2012)
10. W.T. Phillips, B.A. Goins, A. Bao, Radioactive liposomes. Wiley Interdiscip. Rev. Nanomed. Nanobiotechnol. **1**(1), 69–83 (2009)
11. G.M. Jensen, T.H. Bunch, Conventional liposome performance and evaluation: lessons from the development of Vescan. J. Liposome Res. **17**, 121–137 (2007)
12. A. Srivatsan, X. Chen, Recent advances in nanoparticle-based nuclear imaging of cancers. Adv. Cancer Res. **124**, 83–129 (2014)
13. A.L. Petersen, A.E. Hansen, A. Gabizon, T.L. Andresen, Liposome imaging agents in personalized medicine. Adv. Drug Deliv. Rev. **64**(13), 1417–1435 (2012)
14. A. Gabizon, R. Chisin, S. Amselem, S. Druckmann, R. Cohen, D. Goren et al., Pharmacokinetic and imaging studies in patients receiving a formulation of liposome-associated adriamycin. Br. J. Cancer **64**(6), 1125–1132 (1991)
15. J.R. Morgan, K.E. Williams, R.L. Davies, K. Leach, M. Thomson, L.A. Williams, Localisation of experimental staphylococcal abscesses by ^{99m}Tc-technetium-labelled liposomes. J. Med. Microbiol. **14**(2), 213–217 (1981)
16. E. Andreozzi, J.W. Seo, K. Ferrara, A. Louie, Novel method to label solid lipid nanoparticles with ^{64}Cu for positron emission tomography imaging. Bioconjug. Chem. **22**(4), 808–818 (2011)
17. A.L. Petersen, T. Binderup, P. Rasmussen, J.R. Henriksen, D.R. Elema, A. Kjær et al., ^{64}Cu loaded liposomes as positron emission tomography imaging agents. Biomaterials **32**(9), 2334–2341 (2011)
18. R.T. Proffitt, L.E. Williams, C.A. Presant, G.W. Tin, J.A. Uliana, R.C. Gamble et al., Tumor-imaging potential of liposomes loaded with In-111-NTA: biodistribution in mice. J. Nucl. Med. **24**(1), 45–51 (1983)

19. L.G. Espinola, J. Beaucaire, A. Gottschalk, V.J. Caride, Radiolabeled liposomes as metabolic and scanning tracers in mice. II. In-111 oxine compared with Tc-99 m DTPA, entrapped in multilamellar lipid vesicles. J. Nucl. Med. **20**(5), 434–440 (1979)
20. A.F. Turner, C.A. Presant, R.T. Proffitt, L.E. Williams, D.W. Winsor, J.L. Werner, In-111-labeled liposomes: dosimetry and tumor depiction. Radiology **166**(3), 761–765 (1988)
21. K.J. Harrington, S. Mohammadtaghi, P.S. Uster, D. Glass, A.M. Peters, R.G. Vile et al., Effective targeting of solid tumors in patients with locally advanced cancers by radiolabeled PEGylated liposomes. Clin. Cancer Res. **7**(2), 243–254 (2001)
22. E.T. Dams, W.J. Oyen, O.C. Boerman, G. Storm, P. Laverman, P.J. Kok et al., ^{99m}Tc-PEG liposomes for the scintigraphic detection of infection and inflammation: clinical evaluation. J. Nucl. Med. **41**(4), 622–630 (2000)
23. B.D. Williams, M.M. O'Sullivan, G.S. Saggu, K.E. Williams, L.A. Williams, J.R. Morgan, Synovial accumulation of technetium labelled liposomes in rheumatoid arthritis. Ann. Rheum. Dis. **46**(4), 314–318 (1987)
24. N. Li, Z. Yu, T.T. Pham, P.J. Blower, R. Yan, A generic ^{89}Zr labeling method to quantify the in vivo pharmacokinetics of liposomal nanoparticles with positron emission tomography. Int. J. Nanomedicine. **12**, 3281–3294 (2017)
25. L.T. Lin, C.H. Chang, H.L. Yu, R.S. Liu, H.E. Wang, S.J. Chiu et al., Evaluation of the therapeutic and diagnostic effects of PEGylated liposome-embedded ^{188}Re on human non-small cell lung cancer using an orthotopic small-animal model. J. Nucl. Med. **55**(11), 1864–1870 (2014)
26. M. Lingappa, H. Song, S. Thompson, F. Bruchertseifer, A. Morgenstern, G. Sgouros, Immunoliposomal delivery of ^{213}Bi for alpha-emitter targeting of metastatic breast cancer. Cancer Res. **70**(17), 6815–6823 (2010)
27. P.J. Theodore, *All About Albumin* (Elsevier, Amsterdam, 1995)
28. K.M. Sand, M. Bern, J. Nilsen, H.T. Noordzij, I. Sandlie, J.T. Andersen, Unrav-eling the interaction between FcRn and albumin: opportunities for design of albumin-based therapeutics. Front. Immunol. **5**, 682 (2015)
29. Y. Matsumura, H. Maeda, A new concept for macromolecular therapeutics in cancer chemotherapy: mechanism of tumoritropic accumulation of proteins and the antitumor agent smancs. Cancer Res. **46**, 6387–6392 (1986)
30. C.R. Divgi, N.M. Lisann, S.D. Yeh, R.S. Benua, Technetium-99m albumin scintigraphy in the diagnosis of protein-losing enteropathy. J. Nucl. Med. **27**(11), 1710–2 (1986)
31. D.W. Nyman, K.J. Campbell, E. Hersh, K. Long, K. Richardson, V. Trieu, N. Desai, M. J. Hawkins, D.D. Von Hoff, Phase I and pharmacokinetics trial of ABI-007, a novel nanoparticle formulation of paclitaxel in patients with advanced non-hematologic malignancies. J. Clin. Oncol. **23**(31), 7785–7793 (2005)
32. A.M. Merlot, D.S. Kalinowski, D.R. Richardson, Unraveling the mysteries of serum albumin-more than just a serum protein. Front Physiol. **5**, 299 (2014)
33. R. Kloiber, B. Damtew, L. Rosenthall, A crossover study comparing the effect of particle size on the distribution of radiocolloid in patients. Clin. Nucl. Med. **6**(5), 204–206 (1981)
34. M.G. Persico, L. Lodola, F.E. Buroni, M. Morandotti, P. Pallavicini, C. Aprile, ^{99m}Tc-human serum albumin nanocolloids: particle sizing and radioactivity distribution. J. Label. Comp. Radiopharm. **58**(9), 376–382 (2015)
35. L. Tian, Q. Chen, X. Yi, G. Wang, J. Chen, P. Ning et al., Radionuclide I-131 labeled Albumin-Paclitaxel nanoparticles for synergistic combined chemo-radioisotope therapy of cancer. Theranostics **7**(3), 614–623 (2017)
36. O. Jacobson, D.O. Kiesewetter, X. Chen, Albumin-binding Evans Blue derivatives for diagnostic imaging and production of long-acting therapeutics. Bioconjug. Chem. **27**, 2239–2247 (2016)
37. D.A. Tomalia, H. Baker, J.R. Dewald, M. Hall, G. Kallos, S. Martin, A new class of polymers: starburst-dendritic macromolecules. Polym. J. **9**(1), 117–132 (1985)
38. A.R. Menjoge, R.M. Kannan, D.A. Tomalia, Dendrimer-based drug and imaging conjugates: design considerations for nanomedical applications. Drug Discov. Today. **15**, 171–185 (2010)

39. C.F. Price, D. Tyssen, S. Sonza, A. Davie, S. Evans, G.R. Lewis et al., SPL7013 Gel (VivaGel®) retains potent HIV-1 and HSV-2 inhibitory activity following vaginal administration in humans. PLoS ONE **6**(9), e24095 (2011)
40. N. Malik, R. Wiwattanapatapee, R. Klopsch, K. Lorenz, H. Frey, J.W. Weener et al., Dendrimers: relationship between structure and biocompatibility in vitro, and preliminary studies on the biodistribution of 125I-labelled polyamidoamine dendrimers in vivo. J. Control Release. **65**, 133–148 (2000)
41. K. Jain, P. Kesharwani, U. Gupta, N.K. Jain, Dendrimer toxicity: let's meet the challenge. Int. J. Pharm. **394**, 122–142 (2010)
42. V. Biricová, A. Lázničková, M. Lázníček, M. Polášek, P. Hermann, Radio-labeling of PAMAM dendrimers conjugated to a pyridine-N-oxide DOTA analog with ^{111}In: optimization of reaction conditions and biodistribution. J. Pharm. Biomed. Anal. **56**(3), 505–512 (2011)
43. L.M. Kaminskas, B.J. Boyd, P. Karellas, G.Y. Krippner, R. Lessene, B. Kelly, C.J. Porter, The impact of molecular weight and PEG chain length on the systemic pharmacokinetics of PEGylated poly l-lysine dendrimers. Mol. Pharm. **5**(3), 449–463 (2008)
44. J.W. Seo, H. Baek, L.M. Mahakian, J. Kusunose, J. Hamzah, E. Ruoslahti et al., ^{64}Cu-labeled LyP-1-dendrimer for PET-CT imaging of atherosclerotic plaque. Bioconjug. Chem. **25**(2), 231–239 (2014)
45. J. Hamzah, V.R. Kotamraju, J.W. Seo, L. Agemy, V. Fogal, L.M. Mahakian et al., Specific penetration and accumulation of a homing peptide within atherosclerotic plaques of apolipo-protein E-deficient mice. Proc. Natl. Acad. Sci. U S A. **108**(17), 7154–7159 (2011)
46. B.P. Gray, S. Li, K.C. Brown, From phage display to nanoparticle delivery: functionalizing liposomes with multivalent peptides improves targeting to a cancer biomarker. Bioconjug. Chem. **24**(1), 85–96 (2013)
47. L. Kovacs, M. Tassano, M. Cabrera, C.B. Zamboni, M. Fernández, R.M. Anjos et al., Development of ^{177}Lu-DOTA-dendrimer and determination of its effect on metal and ion levels in tumor tissue. Cancer Biother. Radiopharm. **30**(10), 405–409 (2015)
48. L. Zhao, J. Zhu, Y. Cheng, Z. Xiong, Y. Tang, L. Guo et al., Chlorotoxin-conjugated multifunctional dendrimers labeled with radionuclide ^{131}I for single photon emission computed tomography imaging and radiotherapy of gliomas. ACS Appl. Mater. Interfaces. **7**(35), 19798–19808 (2015)
49. G. Yang, N. Sadeg, H. Belhadj-Tahar, New potential in situ anticancer agent derived from [^{188}Re]rhenium nitro-imidazole ligand loaded 5th generation poly-L-lysine dendrimer for treatment of transplanted human liver carcinoma in nude mice. Drug Des. **6**, 144 (2017)
50. C.P. Reis, R.J. Neufeld, A.J. Ribeiro, F. Veiga, Nanoencapsulation I. Methods for preparation of drug-loaded polymeric nanoparticles. Nanomedicine **2**, 8 (2006)
51. I.H. Park, J.H. Sohn, S.B. Kim, K.S. Lee, J.S. Chung, S.H. Lee et al., An open-label, randomized, parallel, phase III trial evaluating the efficacy and safety of polymeric micelle-formulated paclitaxel compared to conventional Cremophor EL-based paclitaxel for recurrent or metastatic HER2-negative breast cancer. Cancer Res. Treat. **49**(3), 569–577 (2017)
52. J. Shi, P.W. Kantoff, R. Wooster, O.C. Farokhzad, Cancer nanomedicine: progress, challenges and opportunities. Nat. Rev. Cancer **17**(1), 20–37 (2017)
53. D.E. Owens 3rd, N.A. Peppas, Opsonization, biodistribution, and pharmaco-kinetics of polymeric nanoparticles. Int. J. Pharm. **307**(1), 93–102 (2006)
54. E.D. Pressly, R. Rossin, A. Hagooly, K. Fukukawa, B.W. Messmore, M.J. Welch et al., Structural effects on the biodistribution and positron emission tomography (PET) imaging of well-defined ^{64}Cu-labeled nanoparticles comprised of amphiphilic block graft copolymers. Biomacromol **8**(10), 3126–3134 (2007)
55. R. Toita, Y. Kanai, H. Watabe, K. Nakao, S. Yamamoto, J. Hatazawa et al., Biodistribution of ^{125}I-labeled polymeric vaccine carriers after subcutaneous injection. Bioorg. Med. Chem. **21**(17), 5310–5315 (2013)

56. J. You, J. Zhao, X. Wen, C. Wu, Q. Huang, F. Guan et al., Chemoradiation therapy using cyclopamine-loaded liquid-lipid nanoparticles and lutetium-177-labeled core-crosslinked polymeric micelles. J. Control Release. **202**, 40–48 (2015)
57. B. Fonseca-Santos, M. Chorilli, An overview of carboxymethyl derivatives of chitosan: their use as biomaterials and drug delivery systems. Mater. Sci. Eng. C Mater. Biol. Appl. **77**, 1349–1362 (2017)
58. I. Wedmore, J.G. McManus, A.E. Pusateri, J.B. Holcomb, J. Trauma, A special report on the chitosan-based hemostatic dressing: experience in current combat operations. J. Trauma **60** (3), 655–658 (2006)
59. D.E. Lee, J.H. Na, S. Lee, C.M. Kang, H.N. Kim, S.J. Han et al., Facile method to radiolabel glycol chitosan nanoparticles with ^{64}Cu via copper-free click chemistry for microPET imaging. Mol. Pharm. **10**(6), 2190–8 (2013)

Part II
Endogenous Radionanomedicine

Chapter 6: Endogenous Radionanomedicine: Extracellular Vesicles
Chapter 7: Endogenous Radionanomedicine: Radiolabeling
Chapter 8: Endogenous Radionanomedicine: Biodistribution and Imaging
Chapter 9: Endogenous Radionanomedicine: Validation of Therapeutic Potential

This interesting part deals only with extracellular vesicles. The findings of the existence of extracellular vesicles are already decades old but the lack of analytical methods prevented understanding the meaning of these endogenous structures in various physiological processes. There is an explosion of the new revelations of the important roles done by extracellular vesicles, their genesis, transfer, auto- or paracrine/ endocrine effects, fates in vivo, and contribution to the pathology. To indicate a few among many, the feasibility of using extracellular vesicles as drug delivery vehicles or as alternatives of therapeutic cells are examples. The correct understanding of the roles of extracellular vesicles in physiology and pathology will be facilitated by tracing the whereabouts of extracellular vesicles using their radiolabeled counterparts in vivo and even quantify the biodistribution repeatedly in vivo without sacrificing animals in preclinical setting and using tomographic imaging in humans.

For this purpose, investigators needed to develop ingenious or simplest methods to label extracellular vesicles with radionuclides and these are detailed in Chap. 7 and again the simplicity of the newly developed method of radiolabeling will lead to earlier translation of therapeutic use of extracellular vesicles to clinical use. The readers are recommended to find out the limitations of the popular fluorescent dye labeling method for tracing the fates of exogenously prepared extracellular vesicles in vivo in animal experiments, and the advantage of using radiolabeling. They are also encouraged to understand further the limitations of using radiolabeled extracellular vesicles for their biological roles after injection for intended therapeutic roles for destroying cancers or regenerating the damaged tissues. Surface and intraluminal labelings are all possible and the ambiguity is supposed to lie in the

current lack of knowledge about whether pharmacological effects are served by the lipid–protein bilayers or the intra-vesicular contents or both. After browsing the recent findings in the literature about biodistribution and imaging in Chap. 8, the readers can now enter into the meditation of the possible use of extracellular vesicles as therapeutics. How we validate the therapeutic success and how to realize the therapeutic potential of extracellular vesicles, if any, follow. In Chap. 9, the readers will meet the similar thoughts and realizations through experiments, impetuous or meticulous, but based on so much curiosity.

Endogenous nanomedicine was coined by myself to name the entire pursuit to this direction and endogenous radionanomedicine is the subdiscipline of using radiolabeled nanomedicines. As was introduced in Chap. 1, endogenous radionanomedicine is using endogenous radionanomedicines, i.e., radiolabeled endogenous nanomedicines, again, i.e., radiolabeled extracellular vesicles for therapeutic/ theranostic purposes.

Chapter 6
Endogenous Radionanomedicine: Extracellular Vesicles

Changjin Lee, Do Won Hwang and Yong Song Gho

Abstract Extracellular vesicles are bilayered proteolipids ranging from 30 to 1000 nm in diameter. All cells of three domains of life on earth actively shed extracellular vesicles to the surrounding environments including various biological body fluids. Moreover, extracellular vesicles harbor specific subsets of cellular bioactive molecules including proteins, lipids, mRNAs, miRNAs, and metabolites. During last decade, explosively growing evidences are supporting the emerging roles of these complex extracellular organelles as endogenous and environmental nanocarriers by carrying specific subsets of bioactive cargos: extracellular vesicle-mediated intercellular communication is evolutionarily conserved phenomenon. Furthermore, extracellular vesicles are novel targets for diagnostics and therapeutics. Thus, a future comprehensive understanding of extracellular vesicle-mediated intercellular communication including their complex pathophysiological functions is critical to decode the secrets of life and to develop novel extracellular vesicle-based diagnostics and therapeutics against hard-to-cure diseases such as cancer. Here, we briefly review history, biogenesis, pathophysiological

C. Lee · Y. S. Gho (✉)
Department of Life Sciences, Pohang University of Science and Technology (POSTECH), Pohang 37673, Republic of Korea
e-mail: ysgho@postech.ac.kr

D. W. Hwang
Department of Nuclear Medicine, Seoul National University College of Medicine, Seoul, Republic of Korea

D. W. Hwang
Department of Molecular Medicine and Biopharmaceutical Sciences, Graduate School of Convergence Science and Technology, College of Medicine or College of Pharmacy, Seoul National University, Seoul, Republic of Korea

Y. S. Gho
The Krefting Research Centre, Institute of Medicine, University of Gothenburg, Gothenburg, Sweden

Y. S. Gho
Exosome BioSciences Inc., Pohang, Republic of Korea

D. S. Lee (ed.), *Radionanomedicine*, Biological and Medical Physics, Biomedical Engineering, https://doi.org/10.1007/978-3-319-67720-0_6

function, and biomedical application of mammalian extracellular vesicles that are categorized into exosomes and ectosomes (also known as microvesicles). We also discuss on perspectives for a future comprehensive understanding of extracellular vesicle-mediated pathophysiological functions, decoding the secrets of life, as well as developing novel extracellular vesicle-based diagnostics and therapeutics against hard-to-cure diseases: isolation of extracellular vesicles, extracellular vesicle-mimetic nanovesicles as novel alternatives to extracellular vesicle-based therapeutics, and a holistic systems biology approach based on the concept of emergent properties.

6.1 Introduction

Extracellular vesicles (EVs) are nano-sized bilayered spherical proteolipids encapsulating various cellular components [1–11]. Cells of all domains of life on earth actively release these vesicles to the extracellular environment including various biological fluids. EVs are endogenous and environmental nanocarriers of specific subsets of cellular bioactive molecules including proteins, lipids, mRNAs, miRNAs, and metabolites (Fig. 6.1). Growing evidence in this emerging field has shown that EVs are involved in intercellular, inter-species and inter-kingdom communications: collectively, EV-mediated communication is evolutionarily conserved phenomenon.

Despite recent explosively increased interest regarding their components, biogenesis, and pathophysiological functions as well as biomedical application (Fig. 6.2), EVs are first observed, in the middle of 20th century, without recognition of their physiological roles and evolutionally conserved cell biological properties. Briefly, in 1946, platelet-derived particles were first observed from normal human plasma [12] and designated them as “platelet dust” [13]. Later on, other investigators independently observed EVs and referred them differently such as matrix vesicles during calcification process [14] and prostasomes present in seminal plasma [15, 16]. In 1981, Dvorak and colleagues reported that cancer cells shed plasma membrane vesicles that carry procoagulant activity [17].

In 1983, studies on the biogenesis and physiological functions of EVs were reported and detailed ultrastructural studies showed that vesicles formed in multivesicular bodies are released by fusion of multivesicular bodies with the cell membrane during the maturation of red blood cells [18, 19]. In 1996, these types of EVs known as exosomes isolated from B lymphocytes exhibited their antigen-presenting function in T cell responses [20]. Moreover, in 2002, Kim and colleagues reported, for the first time, that sphingomyelin present in cancer cell-derived EVs plays a critical role in angiogenesis, the new blood vessel formation from pre-existing vasculature [21].

In 2007, discovery of EV-mediated lateral gene transfer, where mRNA in EVs from donor cells were translated in recipient cells [22], have led intensive studies focusing on EVs as genetic carriers able to modulate pathophysiological status of

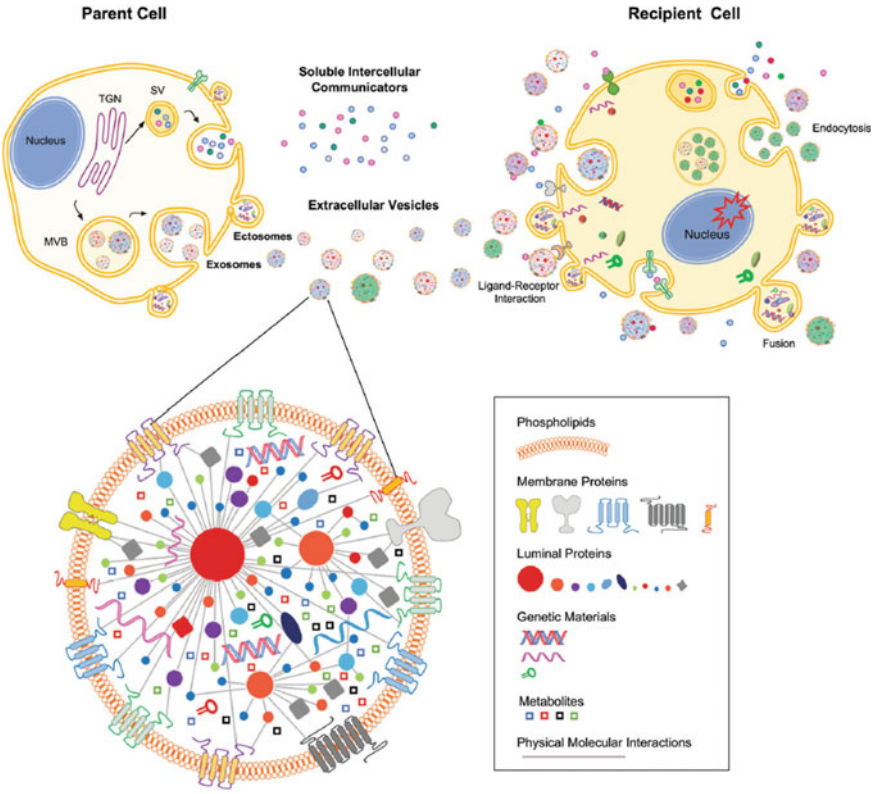

Fig. 6.1 EV-mediated intercellular communication is evolutionarily conserved. In addition to soluble intercellular communicators, mammalian cells release two different types of EVs, known as exosomes and ectosomes, for intercellular communication. Cargo proteins of EVs are physically and functionally interconnected each other to form complex nano-sized extracellular organelles [1]. Reprinted with permission from [1]

recipient cells. After this discovery, the presence of nucleic acids including miRNAs and other noncoding RNAs in EVs and their influences on recipient cells were also identified in various types of cells including cancer and stem cells [23–27]. From the recent multiomics studies with conjunction of bioinformatics approaches, a huge number of vesicular cargos including proteins, lipids, mRNAs, miRNAs, and metabolites have been catalogued, which leads better understanding of these complex extracellular organelles [9]. All these vesicular components identified by multiomics studies have been deposited in a community web portal database for EV research, EVpedia at http://evpedia.info [9–11].

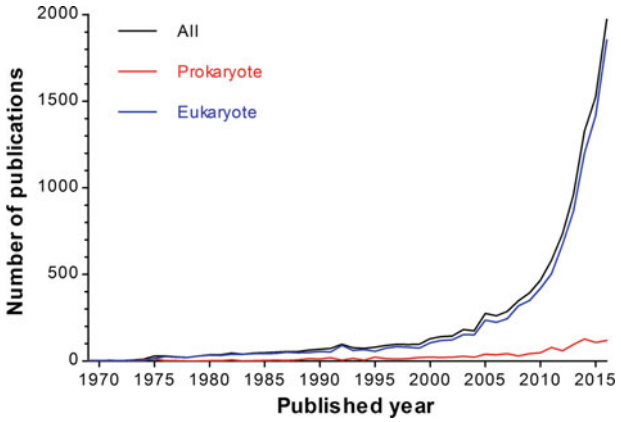

Fig. 6.2 EV-related publication trend. Number of publication on EV research explosively grows during the last decade, showing that EVs are emerging biology filed. EVpedia (http://evpedia.info), Copyright 2017

6.2 Classification and Biogenesis of EVs

EVs are lipid bilayer-limited nano-sized vesicles, ranging from 30 to 1000 nm in diameter [4, 5]. Although diverse nomenclatures represent for EVs derived from three domains of life (archaea, bacteria, and eukarya) as reported in EVpedia at http://evpedia.info (Fig. 6.3), mammalian EVs are generally categorized into exosomes and ectosomes based on their biogenesis mechanisms: exosomes (30–100 nm in diameter) that are released to the extracellular space after fusion of multivesicular bodies with the plasma membrane, and ectosomes (100–1000 nm in

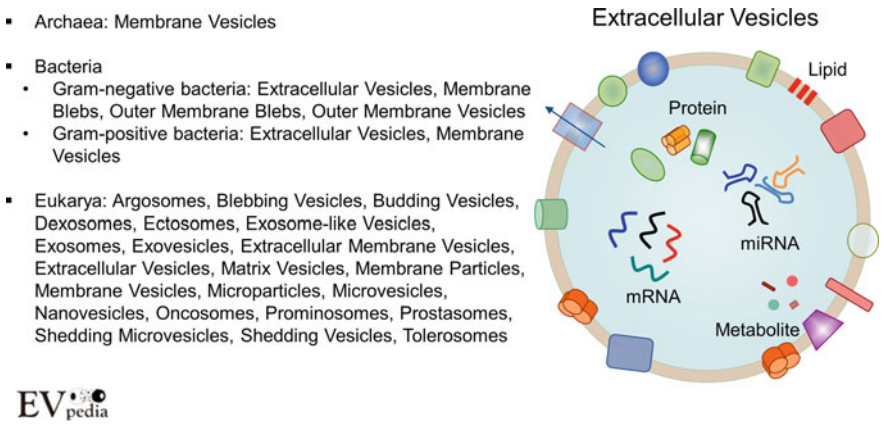

Fig. 6.3 Diverse nomenclatures represent for EVs derived from three domains of life (archaea, bacteria, and eukarya). EVpedia (http://evpedia.info), Copyright 2017

diameter), also known as microvesicles, that are secreted via shedding of plasma membrane fraction (Fig. 6.4).

Exosomes carry various cytosolic proteins associated with endolysosomal pathways due to their cytoplasmic origin while their cargos of ectosomes are similar to the plasma membrane components of their parental cells due to their biogenesis mechanism [28]. Exosomes, defined as a density of 1.13–1.19 g/ml, contain plasma membrane and endosomal proteins: tetraspanins (CD9, CD63, and CD81), Alix, and TSG101, which are commonly used as their marker proteins [29, 30]. However, ectosomes, unlike exosomes, their density and specific markers are not well defined [31, 32]. Since exosomes and ectosomes share various common physical and chemical properties such as density, size, morphology, and cargos which results in difficulties in isolating them separately, therefore, issues regarding different subtypes, cargos, and functions of each type of EVs remain to be solved. In the past few years, use of less strict term EVs has been recommended for any type of vesicles found in conditioned medium of cultured cells and biological fluids unless methods clearly separate these two main types of EVs [33].

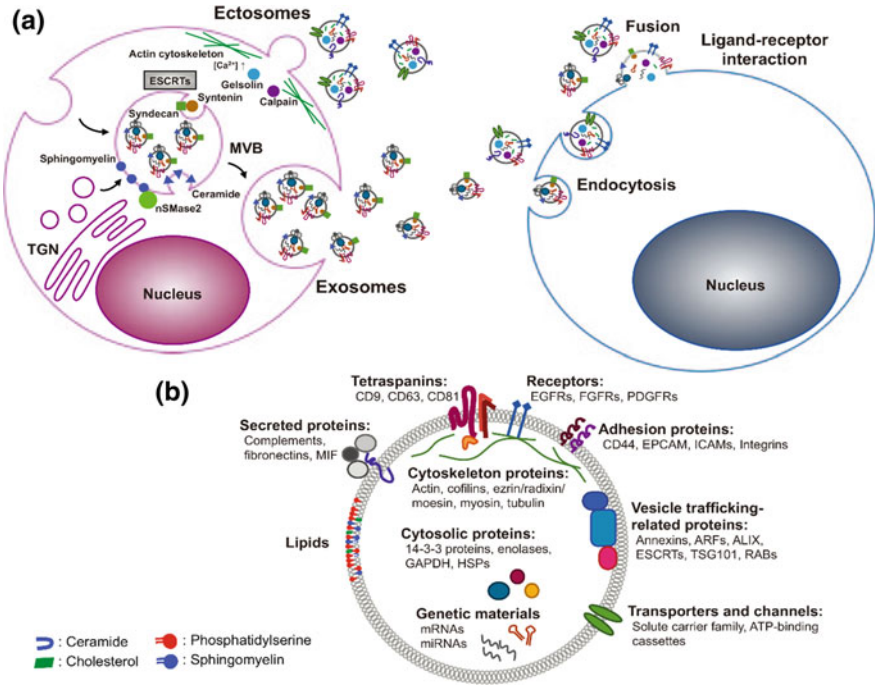

Fig. 6.4 Exosomes and ectosomes, the two major types of EVs secreted by mammalian cells, are generated by similar mechanisms (**a**) whereby their enriched components including proteins, lipids, and genetic materials are deposited on specific local domain of membrane that undergo internal or outward budding then pinching off (**b**). Reprinted with permission from [5]

Electron microscopic approaches have been preferred for direct observation of the morphology and size of EVs [20]. Transmission electron microscopic analysis of EVs deposited on grids displays their broad sizes around 30–1000 nm in diameter and cup-shaped morphological features [19, 20], although the shape is now considered as an artifact induced by fixation and dehydration during the specimen preparation. Indeed, they exhibited spherical shape when observed by cryo-EM [28, 34]. Another important defining character of membrane-enclosed vesicles is their floatation feature in density gradient analysis, although exact densities of exosomes and ectosomes were not yet clearly identified [27, 31]. Analysis for these features of EVs derived from conditioned medium of cultured cells and biological fluids must be validated to confirm the purified EV entities.

6.3 Biological Function of EVs

Although there is a long way to decode a comprehensive understanding of EV-mediated complex pathophysiological functions, explosively growing evidences are supporting the emerging roles of EVs as critical mechanisms for intercellular communication in various biological events. Although their complex diverse pathophysiological roles have been investigated in the field of cardiovascular, diabetic, inflammatory, and neurodegenerative diseases, EVs have been most intensively studied in cancer biology by far.

Cancer cell-derived EVs have played a significant role in cancer development, progression, and metastasis in complex tumor tissue microenvironment. First of all, cancer EVs are involved in angiogenic process to support the growth of primary and metastasized tumors as well as to facilitate the complicate metastatic processes [2, 21]. Furthermore, to promote tumor progression, cancerous cells have smart way to evade the host immune system. Cancer EVs are enriched with immunoregulatory factors so that their roles are escaping immune system. Cancer EVs can deliver immune-suppressive cargos as a form of mRNA and miRNA to immune cells to reprogram the condition of immune-related cells as supporters of tumor progression [35, 36]. Vesicular cargos that induce apoptotic signals are directly delivered to the activated immune cells or indirectly induces the proliferation of regulatory T cells and immune suppressor cells. For instance, cancer EVs can directly transfer inhibitory signals to cognate receptors on immune cells: negative signaling induced by cancer EVs results in an abortive immune response [37]. Additionally, cancer EVs downregulate the activation level of natural killer (NK) cells by NKG2D, activating receptor for NK cells, and as a result, the cytotoxic capability of NK cells is suppressed [38]. Cancer patients with downregulated antitumor immunity have high level of cancer cell-derived EVs in their body fluid. Their cargos acquired from parent cancer cells facilitates tumor growth by modification of surrounding environment and interference of antitumor immunotherapies. Cancer EVs also play a

role in downregulating the function of T effector cells: vesicular CD39 and CD73 are responsible for ATP-dependent adenosine production which results in negative immune modulation of T effector cells [39, 40].

In addition, EVs also can manipulate the microenvironment locally to form a pro-tumorigenic niche. Especially, vesicular miRNAs are involved in every step from initiation to metastasis of cancer. For example, miR-200 family present in breast cancer EVs plays crucial role in promotion of mesenchymal-to-epithelial transition by transfer of miR-200 to non-metastatic cancer cells [41]. In addition, the angiogenic miR-210 present in cancer EVs is targeted to the endothelial cells, which resulting in promoting angiogenesis [42]. Moreover, oncogenic receptor or proteins including mutant EGFR or KRAS are exchanged via EVs between cancer cells to activate genes responsible for anti-apoptotic function in recipient cancer cells [43]. In order to promote their survival and proliferation, cancer cells continuously communicate with their stromal cells and develop the appropriate cancer-prone microenvironments. Cancer EVs activate fibroblast cells, which degrades extracellular matrix and promote cancer-promoting cytokine secretion [44, 45]. Furthermore, cancer EVs regulate the neovascularization for tumor growth and thrive [2, 21]. Because hypoxic condition around tumor requires provision of oxygen and nutrition, cancer cells release EVs containing angiogenic signaling molecules and stimulate angiogenesis by activating endothelial and stromal cells [21, 46, 47]. EV-associated miR-9 secreted by cancer cells was taken up by endothelial cells, which effectively suppressed SOCS5 expression, resulting in activation of JAK-STAT signaling cascade involved in promoting tumor angiogenesis [48]. Moreover, recent studies have demonstrated that EVs act as a key player to drive a pre-metastatic niche formation by communicating with stromal cells [49]. Different subtype integrin in cancer EVs was capable of determining organ tropism, showing that $\alpha_6\beta_4$ integrin EVs preferentially induce lung metastasis. The similar interesting study suggested that highly metastatic pancreatic ductal adenocarcinomas (PDACs)-derived EVs were preferentially accumulated in liver tissue before PDAC liver metastasis and established liver pre-metastatic niche [50]. These EVs were selectively taken up by Kupffer cells to secrete TGF-β and to produce fibronectin from hepatic stellate cells, leading to forming fibrotic environment and macrophage recruitment to eventually support metastasis in liver tissue.

In summary, cancer EVs have played critical roles in regulating tumor survival and fate ranging from tumor initiation to tumor metastasis by activating tumor angiogenesis, and creating immunosuppressive and tumor-supporting niche environments. Thus, the deep investigation of EVs or further controlling cancer-associated EVs in cancer research could help understand the mode of action on tumor development and progression.

6.4 Biomedical Application of EVs

Over the past decades, there have been extensive researches carried out on EVs as a potential diagnostic biomarker discovery and a therapeutic development [51–53]. Disease-associated EVs are known to shuttle disease specific biomolecules such as abnormal RNAs and oncoproteins to the recipient cells, leading to the reprogramming of recipient target cells. Since abnormal cells continuously release the EVs which circulate in the blood stream, EVs that are likely to contain disease-related markers can be simply isolated from the biofluids such as blood and urine: EVs isolated from biofluids are harnessed as promising circulating diagnostic biomarkers without invasive manner. In tumor development and progress, cells require multistage process of tumorigenesis: EVs as intercellular communicators, facilitate tumorigenesis by transferring their chemokine receptors, oncogenes, and oncoproteins. Recent studies demonstrated that differences between their vesicular protein and nucleic acid cargos of cancer EVs and normal cell-derived EVs make possible for EV-based cancer diagnostics [54–56]. It is becoming increasingly clear that EV-associated miRNAs are potential diagnostic and prognostic indicators against many different types of cancer by providing evidence that vesicular miRNAs are positively correlated with the advanced cancer stages [57, 58].

EVs hold the great promise in wide range of therapeutic application in alternative regenerative medicine, drug delivery system, and biosensing platform including radionanomedicine. More details on EV-based therapeutic potential are reviewed in the following Chap. 9, “Validation of Therapeutic Potential”. As for the harnessing of EVs as drug delivery carrier, because original job of EVs is to deliver the bioactive molecules to relevant target recipient cells in our body, EVs can be used as drug delivery conveyor by loading exogenous chemical or nucleic acid drugs into the EVs. When compared with other drug delivery systems, EV-based drug delivery conveyer has substantial advantages such as the drug loading capacity to vesicular lumen, long half-life in blood stream, membrane penetration ability, intrinsic homing capability, and feasible membrane modification to increase blood half-life and targeting capacity. The short interfering RNA (siRNA)-loaded EVs are effective to induce cancer cell death via post-transcriptional gene silencing [59, 60]. Therapeutic functions of EVs have been reported predominantly in stem cells, which exhibit the ability to induce angiogenic programs in quiescent endothelial cells [61, 62], suppress apoptosis and stimulate cell proliferation [63, 64], deliver immunomodulatory signals, as well as recruit and/or reprogram cells that are required for tissue regeneration [24]. Stem cell-based therapy has also been intensively investigated in its potential use for the treatment of degenerative diseases. However, many challenges, such as undesirable cancer formation and ethical issues still remains as unsolved risk factors. Because stem cell-derived EVs harbor the biofunctional molecules of stem cells, those EVs have been considered as alternative therapeutic drug to stem cell therapeutics. Especially, the therapeutic

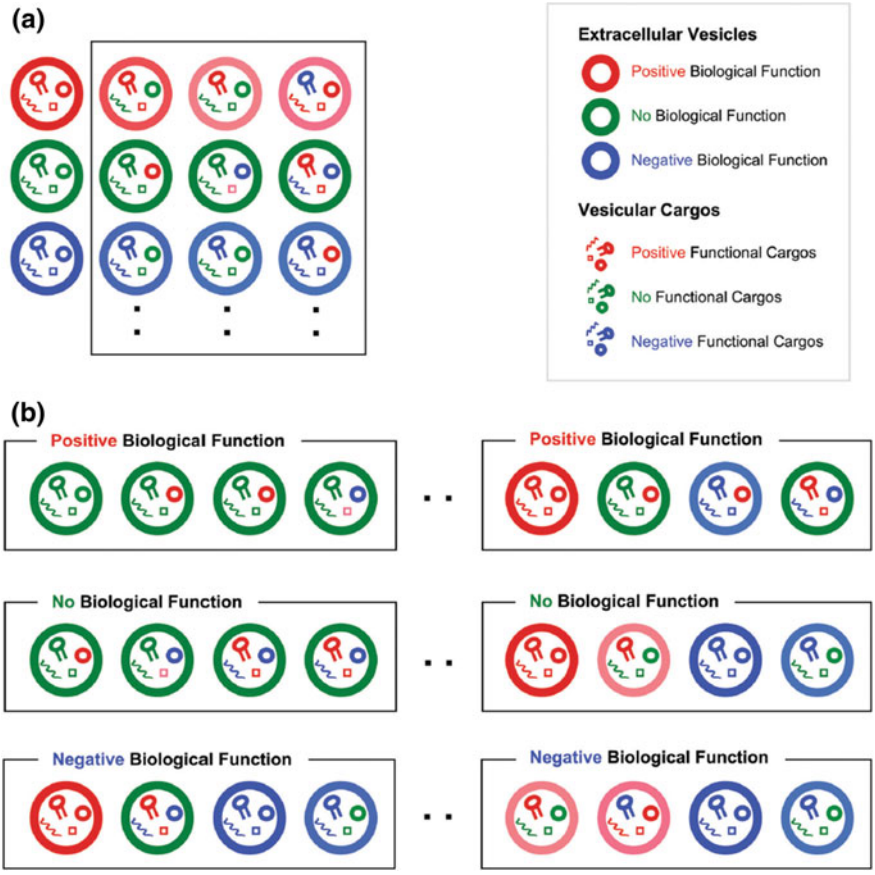

Fig. 6.5 Emergent property of EVs at a single vesicle level (**a**) or at a systems level as a whole (**b**). A holistic systems biology approach based on the concept of emergent properties of EVs is critical to elucidate the complex pathological functions of EVs, to decode the secrets of life as well as to develop novel EV-based diagnostics and therapeutics against hard-to-cure diseases [1]. Reprinted with permission from [1]

potential of mesenchymal stem cell-derived EVs have been widely investigated in the fields such as pulmonary hypertension [65], myocardial infarction injury [66], and acute kidney injury [67].

6.5 Perspectives and Conclusion

Over the past decades, there have been extensive researches carried out on cargos, biogenesis, pathophysiological function, and biomedical application of mammalian extracellular vesicles (also known as exosomes and ectosomes). Although a

progress in this emerging extracellular vesicle biology help us to understand the complexity of intercellular communication networks, following issues are remaining to be solved in more detail.

First of all, to facilitate the basic EV research and biomedical application of EVs, it is critical that EVs should be specifically isolated from cellular debris and other interfering components. The need for standard procedure to purify EVs is widely recognized, however, ultracentrifugation-based techniques are still employed at most, although other alternative procedures such as gel filtration, polymer-based precipitation, and immunoaffinity-based chromatography techniques are currently developed. Second, to overcome the major drawbacks for clinical use of EVs such as low production yield and potential toxicity of naturally secreted vesicles, EV-mimetic nanovesicle technologies should be further developed as novel alternatives to extracellular vesicle-based therapeutics, theranostics, drug delivery, and vaccines [8, 68–76]. Lastly, EVs are too complex themselves in terms of their structures, components, and biological functions. Furthermore, single cells produce several different subtypes of EVs, suggesting that our body and environments are full of a heterogeneous colloidal solution of complex diverse subtypes of EVs [1]. Thus, a holistic systems biology approach based on the concept of emergent properties of EVs (Fig. 6.5) is critical to elucidate the complex pathological functions of EVs, to decode the secrets of life as well as to develop novel EV-based diagnostics and therapeutics against hard-to-cure diseases [1].

References

1. Y.S. Gho, C. Lee, Emergent properties of extracellular vesicles: a holistic approach to decode the complexity of intercellular communication networks. Mol. BioSyst. **13**(7), 1291–1296 (2017)
2. Y.J. Yoon, O.Y. Kim, Y.S. Gho, Extracellular vesicles as emerging intercellular communicasomes. BMB Rep. **47**(10), 531–539 (2014)
3. M. Yanez-Mo, P.R. Siljander, Z. Andreu, A.B. Zavec, F.E. Borras, E.I. Buzas et al., Biological properties of extracellular vesicles and their physiological functions. J. Extracell Vesicles. **4**, 27066 (2015)
4. D.S. Choi, D.K. Kim, Y.K. Kim, Y.S. Gho, Proteomics, transcriptomics and lipidomics of exosomes and ectosomes. Proteomics **13**(10–11), 1554–1571 (2013)
5. D.S. Choi, D.K. Kim, Y.K. Kim, Y.S. Gho, Proteomics of extracellular vesicles: exosomes and ectosomes. Mass Spectrom. Rev. **34**(4), 474–490 (2015)
6. E.Y. Lee, D.S. Choi, K.P. Kim, Y.S. Gho, Proteomics in gram-negative bacterial outer membrane vesicles. Mass Spectrom. Rev. **27**(6), 535–555 (2008)
7. J.H. Kim, J. Lee, J. Park, Y.S. Gho, Gram-negative and gram-positive bacterial extracellular vesicles. Semin. Cell Dev. Biol. **40**, 97–104 (2015)
8. O.Y. Kim, J. Lee, Y.S. Gho, Extracellular vesicle mimetics: novel alternatives to extracellular vesicle-based theranostics, drug delivery, and vaccines. Semin. Cell Dev. Biol. **67**, 74–82 (2017)
9. D.K. Kim, J. Lee, R.J. Simpson, J. Lotvall, Y.S. Gho, EVpedia: a community web resource for prokaryotic and eukaryotic extracellular vesicles research. Semin. Cell Dev. Biol. **40**, 4–7 (2015)

10. D.K. Kim, B. Kang, O.Y. Kim, D.S. Choi, J. Lee, S.R. Kim et al. EVpedia: an integrated database of high-throughput data for systemic analyses of extracellular vesicles. J. Extracell Vesicles **2** (2013)
11. D.K. Kim, J. Lee, S.R. Kim, D.S. Choi, Y.J. Yoon, J.H. Kim et al., EVpedia: a community web portal for extracellular vesicles research. Bioinformatics **31**(6), 933–939 (2015)
12. E. Chargaff, R. West, The biological significance of the thromboplastic protein of blood. J. Biol. Chem. **166**(1), 189–197 (1946)
13. P. Wolf, The nature and significance of platelet products in human plasma. Br. J. Haematol. **13**(3), 269–288 (1967)
14. H.C. Anderson, Vesicles associated with calcification in the matrix of epiphyseal cartilage. J. Cell Biol. **41**(1), 59–72 (1969)
15. B. Stegmayr, G. Ronquist, Promotive effect on human sperm progressive motility by prostasomes. Urol. Res. **10**(5), 253–257 (1982)
16. G. Ronquist, I. Brody, A. Gottfries, B. Stegmayr, An Mg^{2+} and Ca^{2+}—stimulated adenosine triphosphatase in human prostatic fluid–part II. Andrologia **10**(6), 427–433 (1978)
17. H.F. Dvorak, S.C. Quay, N.S. Orenstein, A.M. Dvorak, P. Hahn, A.M. Bitzer et al., Tumor shedding and coagulation. Science **212**(4497), 923–924 (1981)
18. C. Harding, J. Heuser, P. Stahl, Endocytosis and intracellular processing of transferrin and colloidal gold-transferrin in rat reticulocytes: demonstration of a pathway for receptor shedding. Eur. J. Cell Biol. **35**(2), 256–263 (1984)
19. R.M. Johnstone, M. Adam, J.R. Hammond, L. Orr, C. Turbide, Vesicle formation during reticulocyte maturation. Association of plasma membrane activities with released vesicles (exosomes). J. Biol. Chem. **262**(19), 9412–9420 (1987)
20. G. Raposo, H.W. Nijman, W. Stoorvogel, R. Liejendekker, C.V. Harding, C.J. Melief et al., B lymphocytes secrete antigen-presenting vesicles. J. Exp. Med. **183**(3), 1161–1172 (1996)
21. C.W. Kim, H.M. Lee, T.H. Lee, C. Kang, H.K. Kleinman, Y.S. Gho, Extracellular membrane vesicles from tumor cells promote angiogenesis via sphingomyelin. Cancer Res. **62**(21), 6312–6317 (2002)
22. H. Valadi, K. Ekstrom, A. Bossios, M. Sjostrand, J.J. Lee, J.O. Lotvall, Exosome-mediated transfer of mRNAs and microRNAs is a novel mechanism of genetic exchange between cells. Nat. Cell Biol. **9**(6), 654–659 (2007)
23. M.P. Hunter, N. Ismail, X. Zhang, B.D. Aguda, E.J. Lee, L. Yu et al., Detection of microRNA expression in human peripheral blood microvesicles. PLoS One **3**(11), e3694 (2008)
24. J. Ratajczak, K. Miekus, M. Kucia, J. Zhang, R. Reca, P. Dvorak et al., Embryonic stem cell-derived microvesicles reprogram hematopoietic progenitors: evidence for horizontal transfer of mRNA and protein delivery. Leukemia **20**(5), 847–856 (2006)
25. J. Skog, T. Wurdinger, S. van Rijn, D.H. Meijer, L. Gainche, M. Sena-Esteves et al., Glioblastoma microvesicles transport RNA and proteins that promote tumour growth and provide diagnostic biomarkers. Nat. Cell Biol. **10**(12), 1470–1476 (2008)
26. E.N. Nolte-'t Hoen, M. Waasdorp, W. Stoorvogel, M.H. Wauben, P.A. t Hoen, Deep sequencing of RNA from immune cell-derived vesicles uncovers the selective incorporation of small non-coding RNA biotypes with potential regulatory functions. Nucleic Acids Res. **40** (18), 9272–9285 (2012)
27. M. Colombo, G. Raposo, C. Thery, Biogenesis, secretion, and intercellular interactions of exosomes and other extracellular vesicles. Annu. Rev. Cell Dev. Biol. **30**, 255–289 (2014)
28. G. Raposo, W. Stoorvogel, Extracellular vesicles: exosomes, microvesicles, and friends. J. Cell Biol. **200**(4), 373–383 (2013)
29. M. Simons, G. Raposo, Exosomes–vesicular carriers for intercellular communication. Curr. Opin. Cell Biol. **21**(4), 575–581 (2009)
30. R.J. Simpson, S.S. Jensen, J.W. Lim, Proteomic profiling of exosomes: current perspectives. Proteomics **8**(19), 4083–4099 (2008)
31. C. Thery, M. Ostrowski, E. Segura, Membrane vesicles as conveyors of immune responses. Nat. Rev. Immunol. **9**(8), 581–593 (2009)

32. V. Muralidharan-Chari, J.W. Clancy, A. Sedgwick, C. D'Souza-Schorey, Microvesicles: mediators of extracellular communication during cancer progression. J. Cell Sci. **123**(Pt 10), 1603–1611 (2010)
33. S.J. Gould, G. Raposo, As we wait: coping with an imperfect nomenclature for extracellular vesicles. J. Extracell Vesicles. **2**, 20389 (2013)
34. J. Conde-Vancells, E. Rodriguez-Suarez, N. Embade, D. Gil, R. Matthiesen, M. Valle et al., Characterization and comprehensive proteome profiling of exosomes secreted by hepatocytes. J. Proteome Res. **7**(12), 5157–5166 (2008)
35. T.L. Whiteside, Exosomes and tumor-mediated immune suppression. J. Clin. Invest. **126**(4), 1216–1223 (2016)
36. C. Ciardiello, L. Cavallini, C. Spinelli, J. Yang, M. Reis-Sobreiro, P. de Candia et al., Focus on extracellular vesicles: new frontiers of cell-to-cell communication in cancer. Int. J. Mol. Sci. **17**(2), 175 (2016)
37. M. Szajnik, M. Czystowska, M.J. Szczepanski, M. Mandapathil, T.L. Whiteside, Tumor-derived microvesicles induce, expand and up-regulate biological activities of human regulatory T cells (Treg). PLoS One **5**(7), e11469 (2010)
38. A. Clayton, J.P. Mitchell, J. Court, S. Linnane, M.D. Mason, Z. Tabi, Human tumor-derived exosomes down-modulate NKG2D expression. J Immunol. **180**(11), 7249–7258 (2008)
39. A. Clayton, S. Al-Taei, J. Webber, M.D. Mason, Z. Tabi, Cancer exosomes express CD39 and CD73, which suppress T cells through adenosine production. J. Immunol. **187**(2), 676–683 (2011)
40. P.J. Schuler, Z. Saze, C.S. Hong, L. Muller, D.G. Gillespie, D. Cheng et al., Human CD4 + CD39 + regulatory T cells produce adenosine upon co-expression of surface CD73 or contact with CD73 + exosomes or CD73 + cells. Clin. Exp. Immunol. **177**(2), 531–543 (2014)
41. M.T. Le, P. Hamar, C. Guo, E. Basar, R. Perdigao-Henriques, L. Balaj et al., miR-200-containing extracellular vesicles promote breast cancer cell metastasis. J. Clin. Invest. **124**(12), 5109–5128 (2014)
42. N. Kosaka, H. Iguchi, K. Hagiwara, Y. Yoshioka, F. Takeshita, T. Ochiya, Neutral sphingomyelinase 2 (nSMase2)-dependent exosomal transfer of angiogenic microRNAs regulate cancer cell metastasis. J. Biol. Chem. **288**(15), 10849–10859 (2013)
43. M. Demory Beckler, J.N. Higginbotham, J.L. Franklin, A.J. Ham, P.J. Halvey, I.E. Imasuen et al., Proteomic analysis of exosomes from mutant KRAS colon cancer cells identifies intercellular transfer of mutant KRAS. Mol. Cell. Proteomics **12**(2), 343–355 (2013)
44. J. Webber, R. Steadman, M.D. Mason, Z. Tabi, A. Clayton, Cancer exosomes trigger fibroblast to myofibroblast differentiation. Cancer Res. **70**(23), 9621–9630 (2010)
45. M. Tomasetti, W. Lee, L. Santarelli, J. Neuzil, Exosome-derived microRNAs in cancer metabolism: possible implications in cancer diagnostics and therapy. Exp. Mol. Med. **49**(1), e285 (2017)
46. X. Zhang, X. Yuan, H. Shi, L. Wu, H. Qian, W. Xu, Exosomes in cancer: small particle, big player. J. Hematol. Oncol. **8**, 83 (2015)
47. B.M. Lopes-Bastos, W.G. Jiang, J. Cai, Tumour-endothelial cell communications: important and indispensable mediators of tumour angiogenesis. Anticancer Res. **36**(3), 1119–1126 (2016)
48. G. Zhuang, X. Wu, Z. Jiang, I. Kasman, J. Yao, Y. Guan et al., Tumour-secreted miR-9 promotes endothelial cell migration and angiogenesis by activating the JAK-STAT pathway. EMBO J. **31**(17), 3513–3523 (2012)
49. A. Hoshino, B. Costa-Silva, T.L. Shen, G. Rodrigues, A. Hashimoto, M. Tesic Mark et al., Tumour exosome integrins determine organotropic metastasis. Nature **527**(7578), 329–335 (2015)
50. B. Costa-Silva, N.M. Aiello, A.J. Ocean, S. Singh, H. Zhang, B.K. Thakur et al., Pancreatic cancer exosomes initiate pre-metastatic niche formation in the liver. Nat. Cell Biol. **17**(6), 816–826 (2015)

51. P. Vader, X.O. Breakefield, M.J. Wood, Extracellular vesicles: emerging targets for cancer therapy. Trends Mol. Med. **20**(7), 385–393 (2014)
52. A. Thind, C. Wilson, Exosomal miRNAs as cancer biomarkers and therapeutic targets. J. Extracell Vesicles. **5**, 31292 (2016)
53. A. Sharma, Z. Khatun, A. Shiras, Tumor exosomes: cellular postmen of cancer diagnosis and personalized therapy. Nanomedicine Lond. **11**(4), 421–437 (2016)
54. M. Hosseini, S. Khatamianfar, S.M. Hassanian, R. Nedaeinia, M. Shafiee, M. Maftouh et al., Exosome-encapsulated microRNAs as potential circulating biomarkers in colon cancer. Curr. Pharm. Des. **23**(11), 1705–1709 (2017)
55. S.N. Hurwitz, M.A. Rider, J.L. Bundy, X. Liu, R.K. Singh, D.G. Meckes Jr., Proteomic profiling of NCI-60 extracellular vesicles uncovers common protein cargo and cancer type-specific biomarkers. Oncotarget **7**(52), 86999–87015 (2016)
56. X. Zhou, W. Wen, X. Shan, W. Zhu, J. Xu, R. Guo et al., A six-microRNA panel in plasma was identified as a potential biomarker for lung adenocarcinoma diagnosis. Oncotarget **8**(4), 6513–6525 (2017)
57. Y. Tanaka, H. Kamohara, K. Kinoshita, J. Kurashige, T. Ishimoto, M. Iwatsuki et al., Clinical impact of serum exosomal microRNA-21 as a clinical biomarker in human esophageal squamous cell carcinoma. Cancer **119**(6), 1159–1167 (2013)
58. M. Verma, T.K. Lam, E. Hebert, R.L. Divi, Extracellular vesicles: potential applications in cancer diagnosis, prognosis, and epidemiology. BMC Clin. Pathol. **15**, 6 (2015)
59. L. Alvarez-Erviti, Y. Seow, H. Yin, C. Betts, S. Lakhal, M.J. Wood, Delivery of siRNA to the mouse brain by systemic injection of targeted exosomes. Nat. Biotechnol. **29**(4), 341–345 (2011)
60. T.A. Shtam, R.A. Kovalev, E.Y. Varfolomeeva, E.M. Makarov, Y.V. Kil, M.V. Filatov, Exosomes are natural carriers of exogenous siRNA to human cells in vitro. Cell Commun. Signal. **11**, 88 (2013)
61. M.C. Deregibus, V. Cantaluppi, R. Calogero, M. Lo Iacono, C. Tetta, L. Biancone et al., Endothelial progenitor cell derived microvesicles activate an angiogenic program in endothelial cells by a horizontal transfer of mRNA. Blood **110**(7), 2440–2448 (2007)
62. S. Ela, I. Mager, X.O. Breakefield, M.J. Wood, Extracellular vesicles: biology and emerging therapeutic opportunities. Nat. Rev. Drug Discov. **12**(5), 347–357 (2013)
63. S. Gatti, S. Bruno, M.C. Deregibus, A. Sordi, V. Cantaluppi, C. Tetta et al., Microvesicles derived from human adult mesenchymal stem cells protect against ischaemia-reperfusion-induced acute and chronic kidney injury. Nephrol. Dial. Transplant. **26**(5), 1474–1483 (2011)
64. M.B. Herrera, V. Fonsato, S. Gatti, M.C. Deregibus, A. Sordi, D. Cantarella et al., Human liver stem cell-derived microvesicles accelerate hepatic regeneration in hepatectomized rats. J. Cell Mol. Med. **14**(6B), 1605–1618 (2010)
65. C. Lee, S.A. Mitsialis, M. Aslam, S.H. Vitali, E. Vergadi, G. Konstantinou et al., Exosomes mediate the cytoprotective action of mesenchymal stromal cells on hypoxia-induced pulmonary hypertension. Circulation **126**(22), 2601–2611 (2012)
66. R.C. Lai, F. Arslan, M.M. Lee, N.S. Sze, A. Choo, T.S. Chen et al., Exosome secreted by MSC reduces myocardial ischemia/reperfusion injury. Stem Cell Res. **4**(3), 214–222 (2010)
67. S. Bruno, C. Grange, M.C. Deregibus, R.A. Calogero, S. Saviozzi, F. Collino et al., Mesenchymal stem cell-derived microvesicles protect against acute tubular injury. J. Am. Soc. Nephrol. **20**(5), 1053–1067 (2009)
68. J. Kim, C. Han, W. Jo, S. Kang, S. Cho, D. Jeong et al., Cell-engineered nanovesicle as a surrogate inducer of contact-dependent stimuli. Adv. Healthc. Mater. **6**(17) (2017)
69. S.C. Jang, O.Y. Kim, C.M. Yoon, D.S. Choi, T.Y. Roh, J. Park et al., Bioinspired exosome-mimetic nanovesicles for targeted delivery of chemotherapeutics to malignant tumors. ACS Nano. **7**(9), 7698–7710 (2013)
70. S.C. Jang, Y.S. Gho, Could bioengineered exosome-mimetic nanovesicles be an efficient strategy for the delivery of chemotherapeutics? Nanomed. Lond. **9**(2), 177–180 (2014)

71. D. Jeong, W. Jo, J. Yoon, J. Kim, S. Gianchandani, Y.S. Gho et al., Nanovesicles engineered from ES cells for enhanced cell proliferation. Biomaterials **35**(34), 9302–9310 (2014)
72. O.Y. Kim, S.J. Choi, S.C. Jang, K.S. Park, S.R. Kim, J.P. Choi et al., Bacterial protoplast-derived nanovesicles as vaccine delivery system against bacterial infection. Nano. Lett. **15**(1), 266–274 (2015)
73. K. Oh, S.R. Kim, D.K. Kim, M.W. Seo, C. Lee, H.M. Lee et al., In vivo differentiation of therapeutic insulin-producing cells from bone marrow cells via extracellular vesicle-mimetic nanovesicles. ACS Nano. **9**(12), 11718–11727 (2015)
74. T.R. Lunavat, S.C. Jang, L. Nilsson, H.T. Park, G. Repiska, C. Lasser et al., RNAi delivery by exosome-mimetic nanovesicles—implications for targeting c-Myc in cancer. Biomaterials **102**, 231–238 (2016)
75. O.Y. Kim, N.T. Dinh, H.T. Park, S.J. Choi, K. Hong, Y.S. Gho, Bacterial protoplast-derived nanovesicles for tumor targeted delivery of chemotherapeutics. Biomaterials **113**, 68–79 (2017)
76. D.W. Hwang, H. Choi, S.C. Jang, M.Y. Yoo, J.Y. Park, N.E. Choi et al., Noninvasive imaging of radiolabeled exosome-mimetic nanovesicle using ^{99m}Tc-HMPAO. Sci. Rep. **5**, 15636 (2015)

Chapter 7
Endogenous Radionanomedicine: Radiolabeling

Hongyoon Choi and Do Won Hwang

Abstract Recently, extracellular vesicles have received much attention as potential therapeutics in a variety of fields ranging from cancer targeted delivery to regenerative medicine. In spite of promising results of therapeutic usage of extracellular vesicles reported in various studies from small animals and in vitro investigations, the basic physiology of administered extracellular vesicles in vivo have not yet been fully understood. This issue limits clinical application of extracellular vesicles. Recently developed imaging techniques of extracellular vesicles have provided useful information including organ distribution and clearance of the injected extracellular vesicles over time in vivo. Among several imaging techniques, radionuclide imaging modality capable of tracing the radiolabeled extracellular vesicles in vivo are promising in terms of clinical application, deep organ imaging and quantitative biodistribution analyses. Here, we review the specific methods of radiolabeling of extracellular vesicles and their initial results. We also discuss how radiolabeling facilitates clinical translation of extracellular vesicles.

7.1 Introduction

Endogenous nanoparticles for the therapeutic delivery and diagnostic tracking are mostly based on extracellular vesicles (EVs) [1, 2]. EVs, as naturally occurring vesicles, convey various bioactive molecules and change the biological properties of recipient cells [3]. And thus, their clinical application as therapeutics has

H. Choi (✉) · D. W. Hwang
Department of Nuclear Medicine, Seoul National University College of Medicine, Seoul, Republic of Korea
e-mail: chy1000@snu.ac.kr

H. Choi · D. W. Hwang (✉)
Department of Molecular Medicine and Biopharmaceutical Sciences, Graduate School of Convergence Science and Technology, College of Medicine or College of Pharmacy, Seoul National University, Seoul, Republic of Korea
e-mail: hdw6592@snu.ac.kr

D. S. Lee (ed.), *Radionanomedicine*, Biological and Medical Physics, Biomedical Engineering, https://doi.org/10.1007/978-3-319-67720-0_7

received great attention. Increasing evidences demonstrated that EVs can be as a drug-carrier used in cancer therapy [4, 5] as well as biomolecules-carrier in regenerative medicine for diseases accompanied by tissue loss [6]. Furthermore, they transport genetic materials such as microRNAs and proteins for therapeutic purposes [4, 7, 8]. Although these promising therapeutic effects reported in earlier proof-of-concept studies [4], most studies did not fully demonstrate the systemic properties of EVs after in vivo administration [9, 10]. Limited knowledge on this biodistribution of EVs is one of the obstacles in clinical translation of EVs as carrier of targeted delivery.

Noninvasive imaging can provide valuable information on in vivo distribution and kinetics of administered EVs. After in vivo administration of several types of nanoparticles, various metabolic and clearance processes take place. This variability in the processes of biological and physiological actions make clinical translation more difficult, which mandates extensive studies of EVs' biodistribution and kinetics in a diverse situations. While the knowledge about physiology of EVs is fundamental to successful therapeutic application, in vitro results do not always reflect biological/physiological fates of administered EVs in vivo. For example, as an essential and elementary study to predict the fate of in vivo administered nanoparticles, serum stability test is usually performed in vitro. However, the in vitro observations cannot be directly translated into the in vivo ones, i.e. stability is vicarious. That is because clearance of nanoparticles in vivo mainly depends upon the status of biological milieu at the time of injection as well as the milieu difference between in vitro and in vivo [11, 12]. Understanding biodistribution of EVs based on in vivo imaging of EVs is more than welcome to predict the role of EVs as a novel drug-carrier [13–15].

In addition to bioapplication of EVs as drug carriers, stem cell-derived EVs have attracted considerable attention as promising alternatives to stem cells considering that EVs contain many biomolecules involved in tissue regeneration. EVs derived from mesenchymal stem cells (MSC) or hematopoietic stem cells have facilitated translational researches overcoming previous limitations of stem cell researches [16]. Initial pioneering studies of stem cell transplantation showed regenerative effects of transplanted stem cells for disease-associated extensive cell death such as myocardial infarct [17–19]. Stem cell therapy was supposed to be due to the plausible phenomena that stem cells differentiate into specific cell types in the infarcted tissue for successful regeneration. However, despite this initial wishful speculation, several following studies revealed that the therapeutic effects on regeneration were mediated not by direct cellular trans-differentiation and regeneration but by paracrine effects of the transplanted cells [20–23]. Paracrine effects are mediated by various factors secreted by stem cells, including cytokines, chemokines, growth factors, and various biomolecules such as proteins and nucleic acids [23]. EVs recently joined this group of factors or molecules. Even though a variety of factors related to paracrine effects of stem cells have been elucidated, it is not yet known which factors are essential and others are not; whether a factor affects critically the tissue regeneration [24]. In tissue regeneration, EVs are also known to affect cellular differentiation and modulation, and thus EVs are considered to be a

good candidate for regenerative therapy [16]. Radiolabeled EVs derived from stem cells will visualize clearly the localization and duration of stay at the target site and the consequent reparative effect even at, for example, neurodegenerative lesion of the brain.

For this future application and new therapeutic development, understanding the physiology of administered EVs is crucial. EVs are originated from cells and thus they have much less concerns of toxicity compared with other organic and inorganic exogenous nanomaterials. Using any visualization or imaging methods, EVs' biological action, metabolism and excretion is to be understood. These in vivo physiological studies will be initially in small animals, and human-specific physiology is beyond reach again as there are definitive difference between species. To facilitate achieving this final goal of clinical translation, clinically applicable imaging methods are desired. Radionuclide imaging is one of the most widely used functional imaging techniques in the clinical setting, and it enables to investigate kinetics to elucidate in vivo fate of EVs. We will review the advantages and expectations of imaging of radiolabeled EVs in vivo and introduce currently reported radiolabeled EVs.

7.2 Facilitating Clinical Use of EVs: Radionuclide Imaging of EVs

To realize promises of clinical application of EVs, a better understanding of biodistribution and systemic feature of administered EVs is needed [25]. Recently, several methods have been introduced to reveal the physiology of EVs. One of the most commonly used methods is direct labeling using lipophilic fluorescence dye intercalated in lipid bilayers [26–29]. The overview of imaging methods including optical imaging is described in another chapter. However, fluorescence imaging has substantial limitation in light penetration depth. Thus, it is hard to visualize biodistribution in deep organs as well as to accurately quantify the distribution of specific organs. Most fluorescence imaging methods are not free from toxicity issues. In terms of translation into clinical trials, another noninvasive imaging technique would be needed to overcome these shortcomings.

A feasible method for human imaging for EVs is to image the radionuclide-labeled EVs and MR imaging. Among them, by virtue of its superb sensitivity, radiolabeling requires very low dose of EVs for image acquisition, which could be a definitive advantage in facilitating clinical imaging. The usage of trace amount of EVs for imaging is important also regarding safety issues. Even though cellular originated EVs are relatively free from toxicity mediated by innate immune response which produces reactive oxygen species [30], biocompatible nanomaterials such as liposomes also have concerns of cellular toxicity due to surface ligands and/or the accompanying phagocytosis and degradation [31]. Degraded products from EVs, though not intact EVs themselves, might become the target recognized

by the bodily immune responses. Radiolabeled EVs requires trace amounts of nanomaterials, much less than pharmacologic amounts, and therefore, in vivo effects of radiolabeled EVs will be negligible and different from chemical and biological properties of physiological amount of EVs [2, 32].

Radionuclide imaging for monitoring biodistribution and in vivo fate of EVs could have facilitated more clinical trials for EVs as a drug-carrier and regenerative therapeutics. Aforementioned concept of using just trace amount of EVs for identifying kinetics and distribution is closely related to phase 0 clinical trial. The clinical trial platform requires in vivo evaluation on drug effects and pharmacokinetics for proper target drug selection in drug developments [33]. Radiolabeled EVs could be applied to this phase 0 model to select appropriate candidates among so many subtypes of EVs for further trials. The physiology of EVs could be different according to the cell origin, extraction methods and environmental conditions. Among various subtypes of EVs, radiolabeled EVs could help select appropriate subtypes of EVs for further therapeutic usage [34]. In order to reveal in vivo kinetics and fate of EVs precisely, robust methods for radiolabeling is required. Strategy for radiolabeling and proper selection of radionuclides in accordance with purposes is needed.

7.3 Radiolabeling Methods for Extracellular Vesicles

7.3.1 Radiolabeling Using Streptavidin

Most of the EV imaging studies employed optical probes of fluorescence or bioluminescence. Applying previous bioluminescence labeling methods to radionuclide labeling, Morishita et al. reported ^{125}I-labeled EVs [35]. Previously, they developed bioluminescence reporter system for imaging EVs using Gaussia luciferase (gLuc), a reporter protein that emits chemiluminescence, and lactadherin located on the outer surface of EVs [36]. They applied this reporter system to radiolabel EVs by employing the streptavidin and biotin. As these two molecules are strongly bound to each other, they designed EVs with a fusion protein of streptavidin and lactadherin. The fusion protein was made by replacing the epidermal growth factor-like domain of lactadherin with streptavidin. The product vector was transfected into the B16BL6 murine melanoma cells and from these cells, EVs were collected that have the fusion protein in their outer membrane. For radiolabeling, they incubated ^{125}I-iodobenzoyl norbiotinamide with EVs and then ^{125}I-labeled biotin was bound with streptavidin of EVs (Fig. 7.1). As radiolabel is located at the membrane of EVs, it could trace the fate of EVs even after their vesicle forms were degraded. Multimodal imaging can also be done if biotin is combined either with luciferases, nanoparticles as well as radionuclides [37]. Other radioiodine such as ^{123}I and ^{124}I could also be used for SPECT and PET imaging, respectively. However, this method requires protein modification and vector insertion and per se cannot be used in humans or in clinical applications.

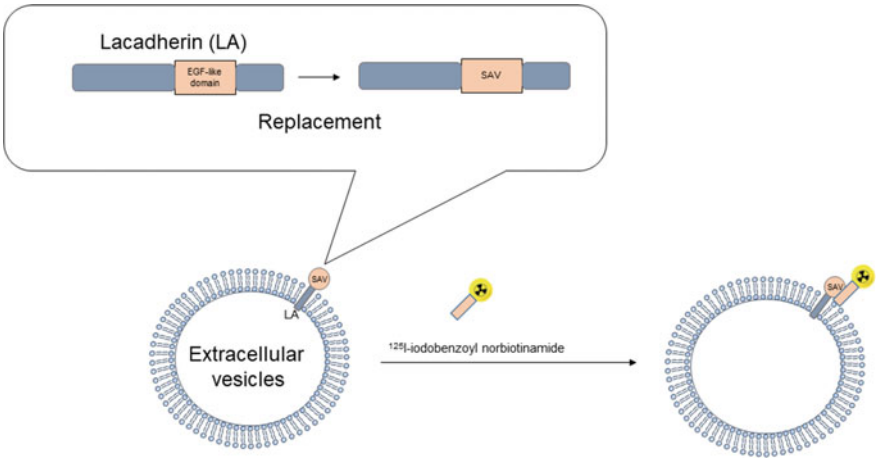

Fig. 7.1 Radiolabeled EVs using ^{125}I-labeled biotin. EVs were extracted from murine melanoma cells which expressed a fusion protein. It was made by replacing the epidermal growth factor-like domain of lactadherin (LA) with streptavidin (SAV). ^{125}I-iodobenzoyl norbiotinamide (Biotin) was incubated with EVs expressing the fusion protein, which produced ^{125}I-labeled EVs. Adapted from [35] with permission

7.3.2 ^{99m}Tc Radiolabeled EVs

As another simple labeling method without protein modification, the labeling based on radionuclide trapping in EVs was developed [38]. The radiolabeling was performed by ^{99m}Tc-hexamethylpropyleneamineoxime (HMPAO) under physiologic condition. Because ^{99m}Tc is one of the most commonly used tracers in nuclear medicine, it has merits in facilitating future clinical translation. The authors used exosome-mimetic nanovesicles collected from murine macrophage cell lines, which yielded much larger amount than the pristine EVs [13]. Purified EVs were simply incubated with ^{99m}Tc-HMPAO under room temperature for 1 h (Fig. 7.2). To remove free ^{99m}Tc-HMPAO and its metabolites, either a size-exclusion column, PD-10, or exosome exclusive spin column with centrifugation was applied. The ^{99m}Tc-HMPAO-labeled EVs were used for the biodistribution study as well as SPECT imaging. The method is based on previously well-known labeling methods clinically used for WBC labeling [39, 40]. The highly lipophilic HMPAO penetrate easily the lipid bilayers of the cellular membranes and be trapped by reaction with glutathione which contains sulfhydryl groups. By this reaction, HMPAO is converted to hydrophilic metabolites that cannot go out of the lipid bilayers. As the study also revealed that EVs had glutathione as cells did, labeling of EVs with ^{99m}Tc-HMPAO was supposed to be stable until the integrity of the lipid bilayers are maintained. Serial SPECT images acquired from this study are represented in Fig. 7.3. SPECT imaging revealed high accumulation of EVs in the liver and spleen and radioactivity increased in intestine as time lapsed. Interestingly, one could see

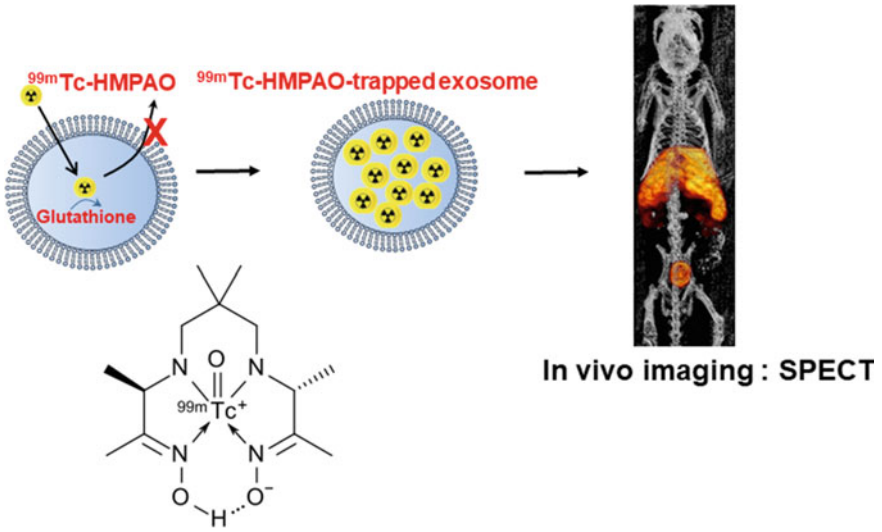

Fig. 7.2 Radiolabeling strategy for EVs using ^{99m}Tc-HMPAO. ^{99m}Tc-HMPAO has been widely used for cell labeling as it is converted into hydrophilic metabolites in cytosol and trapped in lipid bilayers. This principle was similarly applied to the radiolabeling of EVs. By incubating ^{99m}Tc-HMPAO and extracted EVs under physiologic condition, EVs trapping ^{99m}Tc could be acquired. This radiolabeled EVs could be used for in vivo SPECT imaging. Adapted from [38] with permission

the lymph node radioactivity, which was supposed to the homing of EVs derived from macrophage cell lines. In contrast, EVs derived from neural stem cells did not show any radioactivity in lymph nodes, which is added in the Supplementary materials in the paper [38].

Another ^{99m}Tc radiolabeling was reported using ^{99m}Tc-tricarbonyl [41]. ^{99m}Tc-tricarbonyl has been used for various radiolabeled biomolecules including peptides and liposomes [42, 43]. It has a feature of nonspecific binding to amino acids including histidine, methionine and cysteine. As EVs have various surface proteins, the simple mixing them with ^{99m}Tc-tricarbonyl can easily produce ^{99m}Tc-radiolabeled EVs. The method was similar with ^{99m}Tc-HMPAO labeling. They extracted EVs from erythrocytes by ultracentrifugation. Extracted EVs were incubated with ^{99m}Tc-tricarbonyl complex solution at room temperature. After the labeling, free ^{99m}Tc-tricarbonyl was removed by a desalting column. Using this labeling method, SPECT imaging was successfully done and high accumulation of EVs was found in liver and spleen. The distribution pattern was similar to ^{99m}Tc-HMPAO labeled EVs.

So far, the above two methods have been reported to radiolabel EVs with using ^{99m}Tc. Both methods were simple and radiolabeling was performed under

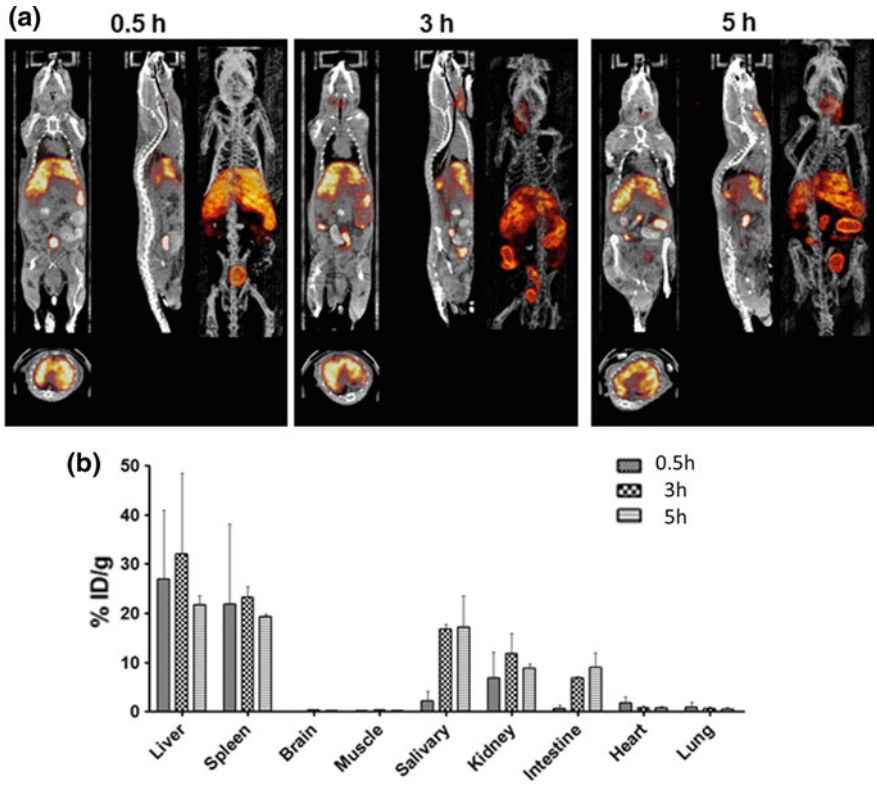

Fig. 7.3 SPECT images of ^{99m}Tc-labeled EVs. ^{99m}Tc-HMPAO labeled EVs were used for SPECT imaging. **a** After the administration of the radiolabeled EVs, SPECT images were serially acquired. EVs were mainly accumulated in the liver and spleen. The intestinal activity was gradually increased for 5 h. **b** Quantification of radioactivity could provide in vivo biodistribution information. Volume-of-interests were drawn on the serially acquired SPECT images and the accumulation of EVs were estimated. EVs were mainly accumulated in the liver and spleen. Salivary gland uptake was increased for 5 h after the administration. Adapted from [38] with permission

physiologic condition. Furthermore, ^{99m}Tc imaging is one of the most widely using SPECT images. However, despite these advantages, the question still remains that ^{99m}Tc-HMPAO compounds could circulate and be excreted from the body when EVs were metabolized and/or degraded. There is no guarantee that the radioactivity we are observing is coming from the intact EVs administered. Relatively short half-life of ^{99m}Tc of 6 h limited long-term monitoring of EVs and if EVs accumulated slowly in the target tissues such as tumor, radionuclides with long half-life would be required.

7.3.3 *Multifunctional Radionuclide Labeling Methods Using Click Chemistry*

Radiolabeling using a chelator combined with radionuclide under physiologic conditions was also suggested [44]. The method was based on click chemistry [45, 46]. As EVs have surface proteins, there are free amine groups presented on their surface. This functional amine moiety can be taken advantage of simple clickable radiolabeling of EVs under mild physiologic condition. To label bifunctional chelator which can react easily with corresponding radionuclide, EVs were treated with N-hydroxysuccinimide-azadibenzocyclooctyne (NHS-ADIBO). N3-introduced chelators including NOTA(1,4,7-triazacyclononane-1,4,7-triacetic acid), DOTA(1,4,7,10-tetraazacyclododecane-1,4,7,10-tetraacetic acid) or TETA (1,4,8,11-tetraazacyclotetradecane-1,4,8,11-tetraacetic acid) can react with ADIBO-conjugated EVs based on cycloaddition reaction of click chemistry. The important advantages of this method is that we are able to use various chelators and positron emitting radionuclides such as ^{68}Ga, ^{64}Cu, and ^{89}Zr. The appropriate radionuclides can be simply selected according to the research purposes. For instance, to monitor long-term biodistribution, radionuclides with longer half-life such as ^{111}In can be chosen for radiolabeling. In addition, therapeutic radionuclides such as ^{67}Cu, ^{177}Lu, ^{90}Y and ^{188}Re can be labeled on the EVs. Labeling of these therapeutic radionuclides will enable therapeutic usage of EVs in cancer treatment. The only problem is that most of the EVs systemically administered localized in the liver and the spleen and only a small amount of EVs seemed to localize at the target sites. However, this problem of EVs, endogenous radionanomedicines, is not worse than the problem with other exogenous radionanomedicines, either inorganic or organic.

Recent studies revealed that EVs could play a role as drug carrier and some showed effects on tumor suppression by transferring microRNAs or therapeutic drugs [47–49]. Based on these pioneering proof-of-concept studies, we could just hope that EVs would play a role in cancer treatment by combining radionuclide therapy and drug carriers carrying therapeutic drugs as cargos while monitoring by radionuclide imaging. We still don't know that this wish is volatile or solid and the follow-up studies will be very much enlightening. Radiolabeling of EVs are the prerequisites to understand and predict the future of clinically usable EVs as a multifunctional multiplex platform.

7.4 Conclusion

Radionuclide imaging of EVs was recently introduced. Since in vivo monitoring of EVs is crucial to understand in vivo fate of EVs as well as to apply EVs to possible clinical therapeutics. So far, even though various studies using optical imaging system reported in vivo biodistribution of systemically administered EVs, it has

substantial limitations of light penetration in deep tissue. Even in small animals, quantification of accumulated EVs in deep organs cannot be done using optical imaging method. As radionuclide imaging is a noninvasive imaging method already clinically widely used, radiolabeled EVs will play an important role in understanding the therapeutic EVs which is expected to be applied to clinical situation.

The firstly reported radiolabeling method was streptavidin-based radiolabeling system. ^{125}I was successfully labeled to EVs and biodistribution study was performed. However, it required EVs extracted from the modified cells to express a designed vector transfected. SPECT images of EVs were firstly reported by radiolabeling with ^{99m}Tc-HMPAO. The method was simple as it only mixed EVs with clinically used ^{99m}Tc-HMPAO under physiologic condition. Another simple method for SPECT imaging using ^{99m}Tc-tricarbonyl was also reported. As EVs have various areas of potential therapeutic uses including regenerative medicine, cancer, inflammation and neurological disorders, flexible radiolabeling in various biomedical application is needed. Radiolabeling based on click chemistry could provide a simple, rapid, and multifunctional platform for the radiolabeling. Appropriate chelators and combined radionuclides can be chosen according to the purpose: SPECT, PET imaging or therapeutic/theranostic use.

In the future, EVs as multifunctional nanoparticles will be used in various fields. As the application of EVs has gradually expanded, the need of quantitative imaging will increase. EVs are highly diverse as they are originated from various cells and conditions [50, 51]. The physiology of EVs will be different when they are administered in vivo. Personalized tracking of EVs will be needed due to the diversity of EVs. The flexible imaging platforms to trace EVs in vivo is required. Efficient production of EVs combined with simple radiolabeling platforms under physiologic conditions will facilitate theranostic application of EVs.

References

1. H. Choi, Y.-S. Lee, D.W. Hwang, D.S. Lee, Translational radionanomedicine: a clinical perspective. Eur. J. Nanomed. **8**(2), 71–84 (2016)
2. D.S. Lee, H.J. Im, Y.S. Lee, Radionanomedicine: widened perspectives of molecular theragnosis. Nanomedicine **11**(4), 795–810 (2015)
3. P. Vader, X.O. Breakefield, M.J. Wood, Extracellular vesicles: emerging targets for cancer therapy. Trends Mol. Med. **20**(7), 385–393 (2014)
4. S.M. van Dommelen, P. Vader, S. Lakhal, S.A. Kooijmans, W.W. van Solinge, M.J. Wood et al., Microvesicles and exosomes: opportunities for cell-derived membrane vesicles in drug delivery. J. Control Release **161**(2), 635–644 (2012)
5. S. Ohno, M. Takanashi, K. Sudo, S. Ueda, A. Ishikawa, N. Matsuyama et al., Systemically injected exosomes targeted to EGFR deliver antitumor microRNA to breast cancer cells. Mol. Ther. **21**(1), 185–191 (2013)
6. L. Biancone, S. Bruno, M.C. Deregibus, C. Tetta, G. Camussi, Therapeutic potential of mesenchymal stem cell-derived microvesicles. Nephrol. Dial. Transplant. **27**(8), 3037–3042 (2012)

7. L. Alvarez-Erviti, Y. Seow, H. Yin, C. Betts, S. Lakhal, M.J. Wood, Delivery of siRNA to the mouse brain by systemic injection of targeted exosomes. Nat. Biotechnol. **29**(4), 341–345 (2011)
8. D. Sun, X. Zhuang, X. Xiang, Y. Liu, S. Zhang, C. Liu et al., A novel nanoparticle drug delivery system: the anti-inflammatory activity of curcumin is enhanced when encapsulated in exosomes. Mol. Ther. **18**(9), 1606–1614 (2010)
9. K. Hagiwara, T. Ochiya, N. Kosaka, A paradigm shift for extracellular vesicles as small RNA carriers: from cellular waste elimination to therapeutic applications. Drug Deliv. Transl. Res. **4**(1), 31–37 (2014)
10. L. Barile, V. Lionetti, E. Cervio, M. Matteucci, M. Gherghiceanu, L.M. Popescu et al., Extracellular vesicles from human cardiac progenitor cells inhibit cardiomyocyte apoptosis and improve cardiac function after myocardial infarction. Cardiovasc. Res. **103**(4), 530–541 (2014)
11. F. Alexis, E. Pridgen, L.K. Molnar, O.C. Farokhzad, Factors affecting the clearance and biodistribution of polymeric nanoparticles. Mol. Pharm. **5**(4), 505–515 (2008)
12. T.K. Jain, M.K. Reddy, M.A. Morales, D.L. Leslie-Pelecky, V. Labhasetwar, Biodistribution, clearance, and biocompatibility of iron oxide magnetic nanoparticles in rats. Mol. Pharm. **5** (2), 316–327 (2008)
13. S.C. Jang, O.Y. Kim, C.M. Yoon, D.S. Choi, T.Y. Roh, J. Park et al., Bioinspired exosome-mimetic nanovesicles for targeted delivery of chemotherapeutics to malignant tumors. ACS Nano **7**(9), 7698–7710 (2013)
14. C.P. Lai, E.Y. Kim, C.E. Badr, R. Weissleder, T.R. Mempel, B.A. Tannous et al., Visualization and tracking of tumour extracellular vesicle delivery and RNA translation using multiplexed reporters. Nat. Commun. **6**, 7029 (2015)
15. C.P. Lai, O. Mardini, M. Ericsson, S. Prabhakar, C.A. Maguire, J.W. Chen et al., Dynamic biodistribution of extracellular vesicles in vivo using a multimodal imaging reporter. ACS Nano **8**(1), 483–494 (2014)
16. O.G. De Jong, B.W. Van Balkom, R.M. Schiffelers, C.V. Bouten, M.C. Verhaar, Extracellular vesicles: potential roles in regenerative medicine. Front. Immunol. **5**, 608 (2014)
17. D. Orlic, J. Kajstura, S. Chimenti, I. Jakoniuk, S.M. Anderson, B. Li et al., Bone marrow cells regenerate infarcted myocardium. Nature **410**(6829), 701–705 (2001)
18. C. Stamm, B. Westphal, H.-D. Kleine, M. Petzsch, C. Kittner, H. Klinge et al., Autologous bone-marrow stem-cell transplantation for myocardial regeneration. Lancet **361**(9351), 45–46 (2003)
19. J.G. Shake, P.J. Gruber, W.A. Baumgartner, G. Senechal, J. Meyers, J.M. Redmond et al., Mesenchymal stem cell implantation in a swine myocardial infarct model: engraftment and functional effects. Ann. Thorac. Surg. **73**(6), 1919–1926 (2002)
20. P.R. Baraniak, T.C. McDevitt, Stem cell paracrine actions and tissue regeneration. Regen. Med. **5**(1), 121–143 (2010)
21. T.J. Burdon, A. Paul, N. Noiseux, S. Prakash, D. Shum-Tim, Bone marrow stem cell derived paracrine factors for regenerative medicine: current perspectives and therapeutic potential. Bone Marrow. Res. **2011**, 207326 (2011)
22. M. Mirotsou, T.M. Jayawardena, J. Schmeckpeper, M. Gnecchi, V.J. Dzau, Paracrine mechanisms of stem cell reparative and regenerative actions in the heart. J. Mol. Cell. Cardiol. **50**(2), 280–289 (2011)
23. M. Gnecchi, Z. Zhang, A. Ni, V.J. Dzau, Paracrine mechanisms in adult stem cell signaling and therapy. Circ. Res. **103**(11), 1204–1219 (2008)
24. J.R. Lavoie, M. Rosu-Myles, Uncovering the secretes of mesenchymal stem cells. Biochimie **95**(12), 2212–2221 (2013)
25. T. Lener, M. Gimona, L. Aigner, V. Börger, E. Buzas, G. Camussi et al., Applying extracellular vesicles based therapeutics in clinical trials–an ISEV position paper. J. Extracell. Vesicles. **4**, 30087 (2015)
26. J.L. Hood, R.S. San, S.A. Wickline, Exosomes released by melanoma cells prepare sentinel lymph nodes for tumor metastasis. Cancer Res. **71**(11), 3792–3801 (2011)

27. S.I. Ohno, M. Takanashi, K. Sudo, S. Ueda, A. Ishikawa, N. Matsuyama et al., Systemically injected exosomes targeted to EGFR deliver antitumor microRNA to breast cancer cells. Mol. Ther. **21**(1), 185–191 (2013)
28. H.C. Christianson, K.J. Svensson, T.H. van Kuppevelt, J.P. Li, M. Belting, Cancer cell exosomes depend on cell-surface heparan sulfate proteoglycans for their internalization and functional activity. Proc. Natl. Acad. Sci. U S A. **110**(43), 17380–17385 (2013)
29. T. Tian, Y.L. Zhu, F.H. Hu, Y.Y. Wang, N.P. Huang, Z.D. Xiao, Dynamics of exosome internalization and trafficking. J. Cell. Physiol. **228**(7), 1487–1495 (2013)
30. T. Xia, M. Kovochich, J. Brant, M. Hotze, J. Sempf, T. Oberley et al., Comparison of the abilities of ambient and manufactured nanoparticles to induce cellular toxicity according to an oxidative stress paradigm. Nano Lett. **6**(8), 1794–1807 (2006)
31. K.B. Knudsen, H. Northeved, P.E. Kumar, A. Permin, T. Gjetting, T.L. Andresen et al., In vivo toxicity of cationic micelles and liposomes. Nanomedicine **11**(2), 467–477 (2015)
32. Y.S. Lee, Y.I. Kim, D.S. Lee, Future perspectives of radionanomedicine using the novel micelle-encapsulation method for surface modification. Nucl. Med. Mol. Imaging **49**(3), 170–173 (2015)
33. R. Kinders, R.E. Parchment, J. Ji, S. Kummar, A.J. Murgo, M. Gutierrez et al., Phase 0 clinical trials in cancer drug development: from FDA guidance to clinical practice. Mol. Interv. **7**(6), 325–334 (2007)
34. O.P. Wiklander, J.Z. Nordin, A. O'Loughlin, Y. Gustafsson, G. Corso, I. Mäger et al., Extracellular vesicle in vivo biodistribution is determined by cell source, route of administration and targeting. J. Extracell. Vesicles **4**(1), 26316 (2015)
35. M. Morishita, Y. Takahashi, M. Nishikawa, K. Sano, K. Kato, T. Yamashita et al., Quantitative analysis of tissue distribution of the B16BL6-derived exosomes using a streptavidin-lactadherin fusion protein and iodine-125-labeled biotin derivative after intravenous injection in mice. J. Pharm. Sci. **104**(2), 705–713 (2015)
36. Y. Takahashi, M. Nishikawa, H. Shinotsuka, Y. Matsui, S. Ohara, T. Imai et al., Visualization and in vivo tracking of the exosomes of murine melanoma B16-BL6 cells in mice after intravenous injection. J. Biotechnol. **165**(2), 77–84 (2013)
37. H.P. Lesch, M.U. Kaikkonen, J.T. Pikkarainen, S. Ylä-Herttuala, Avidin-biotin technology in targeted therapy. Expert Opin. Drug Deliv. **7**(5), 551–564 (2010)
38. D.W. Hwang, H. Choi, S.C. Jang, M.Y. Yoo, J.Y. Park, N.E. Choi et al., Noninvasive imaging of radiolabeled exosome-mimetic nanovesicle using ^{99m}Tc-HMPAO. Sci. Rep. **5**, 15636 (2015)
39. A.M. Peters, The utility of [^{99m}Tc] HMPAO-leukocytes for imaging infection. Semin. Nucl. Med. **24**(2), 110–127 (1994)
40. L. Filippi, O. Schillaci, Usefulness of hybrid SPECT/CT in ^{99m}Tc-HMPAO-labeled leukocyte scintigraphy for bone and joint infections. J. Nucl. Med. **47**(12), 1908–1913 (2006)
41. Z. Varga, I. Gyurkó, K. Pálóczi, E.I. Buzás, I. Horváth, N. Hegedűs et al., Radiolabeling of extracellular vesicles with 99mTc for quantitative in vivo imaging studies. Cancer Biother. Radiopharm. **31**(5), 168–173 (2016)
42. A. Helbok, C. Decristoforo, G. Dobrozemsky, C. Rangger, E. Diederen, B. Stark et al., Radiolabeling of lipid-based nanoparticles for diagnostics and therapeutic applications: a comparison using different radiometals. J. Liposome Res. **20**(3), 219–227 (2010)
43. R. Schibli, A.P. Schubiger, Current use and future potential of organometallic radiopharmaceuticals. Eur. J. Nucl. Med. Mol. Imaging **29**(11), 1529–1542 (2002)
44. D.S. Lee, D.W. Hwang, H. Choi, Y.S. Lee, J.M. Jeong, Y.S. Gho et al., Method for labeling exosomes with radioactive substance and use thereof. Google Patents (2017)
45. H.C. Kolb, M. Finn, K.B. Sharpless, Click chemistry: diverse chemical function from a few good reactions. Angew. Chem. Int. Ed. Engl. **40**(11), 2004–2021 (2001)
46. J.M. Jeong, Y.J. Kim, Y.S. Lee, D.S. Lee, J.K. Chung, M.C. Lee, Radiolabeling of NOTA and DOTA with positron emitting ^{68}Ga and investigation of in vitro properties. Nucl. Med. Mol. Imaging **43**(4), 330–336 (2009)

47. R. van der Meel, M.H. Fens, P. Vader, W.W. van Solinge, O. Eniola-Adefeso, R.M. Schiffelers, Extracellular vesicles as drug delivery systems: lessons from the liposome field. J. Control Release **195**, 72–85 (2014)
48. A. Bronisz, Y. Wang, M.O. Nowicki, P. Peruzzi, K.I. Ansari, D. Ogawa et al., Extracellular vesicles modulate the glioblastoma microenvironment via a tumor suppression signaling network directed by miR-1. Cancer Res. **74**(3), 738–750 (2014)
49. S. El Andaloussi, I. Mäger, X.O. Breakefield, M.J. Wood, Extracellular vesicles: biology and emerging therapeutic opportunities. Nat. Rev. Drug Discov. **12**(5), 347 (2013)
50. M. Mittelbrunn, F. Sánchez-Madrid, Intercellular communication: diverse structures for exchange of genetic information. Nat. Rev. Mol. Cell Biol. **13**(5), 328 (2012)
51. A. Bobrie, M. Colombo, S. Krumeich, G. Raposo, C. Théry, Diverse subpopulations of vesicles secreted by different intracellular mechanisms are present in exosome preparations obtained by differential ultracentrifugation. J. Extracell. Vesicles **1**(1), 18397 (2012)

Chapter 8
Endogenous Radionanomedicine: Biodistribution and Imaging

Hongyoon Choi and Dong Soo Lee

Abstract In vivo distribution of extracellular vesicles (EVs) are important in clinical application. Recently, tracking methods have been developed to monitor EVs in vivo. It ranged from fluorescence imaging to clinically available radionuclide imaging or magnetic resonance imaging. Each method has pros and cons in terms of capability of quantification, penetration depth, availability and clinical translatability. We introduce currently available labeling methods for imaging and their advantages and disadvantages. These imaging methods have elucidated the in vivo biodistribution of EVs. However, technical factors such as isolation, labeling methods and administration methods as well as biological factors including cell sources have resulted in variability of biodistribution patterns. We also review biodistribution results of EVs and what impacts on biodistribution.

8.1 Methods for Imaging Extracellular Vesicles

8.1.1 Overall Strategy for the Labeling

For the clinical application of extracellular vesicles (EVs), in vivo tracking methods are crucial as their physiologic properties could determine therapeutic efficacy and potential toxicity. A better understanding of biodistribution of EVs upon systemic

H. Choi (✉) · D. S. Lee
Department of Nuclear Medicine, Seoul National University
College of Medicine, Seoul 03080, Republic of Korea
e-mail: chy1000@snu.ac.kr

D. S. Lee
e-mail: dsl@snu.ac.kr

H. Choi · D. S. Lee
Department of Molecular Medicine and Biopharmaceutical Sciences,
Graduate School of Convergence Science and Technology,
College of Medicine or College of Pharmacy, Seoul National University,
Seoul 03080, Republic of Korea

D. S. Lee (ed.), *Radionanomedicine*, Biological and Medical Physics,
Biomedical Engineering, https://doi.org/10.1007/978-3-319-67720-0_8

administration is urgently needed for the therapeutic application of EVs [1–3]. Thus, several noninvasive imaging methods have been developed for tracking EVs. They basically employed labeling exogenous tracers which generate signals ranged from visible light to radiation as EVs could be loaded with various bioactive materials including tracers as well as drugs, nanoparticles, genetic materials such as microRNAs [4, 5].

The loading methods of tracers can be roughly classified into two categories: (1) A strategy that parent cells load tracers so that the later-secreted EVs carry the targeted materials and (2) another strategy of direct labeling and decorating EVs. Using the first strategy, several hybrid EVs loading magnetic, fluorescent and therapeutic nanoparticles can be produced [6–8]. In addition, genetic modification of the parent cells allows to produce sustainably the EVs that inherit fluorescence proteins [9, 10]. In contrast, the second strategy is more flexible and simple for the labeling as the direct labeling is feasible regardless of types of EVs obtained from various cell types and conditions. Because several lipophilic drugs may interact directly with lipid bilayers of EVs, the labeling can be performed under physiologic condition by incubating lipophilic tracers and EVs.

Various labeling methods have been developed for tracking in vivo distribution and fate of EVs. The ideal method of labeling EVs should be specific and stable in in vivo environment. Deep organ imaging and quantification are required for clinical application and accurately estimating biodistribution. However, the

Table 8.1 Pros and cons of labeling methods

Labeling methods	Pros	Cons
Fluorescent dye	Simple and easy highly available for imaging modality Microscopic imaging	Limits in clinical application Unable to visualize deep organs Autofluorescence Persistent signals after degradation of EVs
Reporter protein for fluorescence/bioluminescence	Highly stable Enabling cell-type specific labeling Highly sensitive (bioluminescence)	Limits in clinical application Hard to visualize deep organs Preparation of genetically modified cells
Radiolabeling	Sensitive Feasibility of clinical application Quantitative analysis	Radiation safety issues Specialized imaging modality is required
Magnetic resonance imaging	Feasibility of clinical application Deep organ imaging and high resolution No radiation hazard	Relatively low sensitivity Limited in quantification Specialized imaging modality is required

methods currently developed have some limitations. Pros and cons of each method is summarized in Table 8.1.

8.1.2 Fluorescence Labeling

Direct fluorescent-dye labeling have been most widely used for the labeling of EVs. Fluorescence labeling enables whole body imaging of small animals using highly sensitive optical cameras and fluorescence microscopic imaging. Lipophilic dyes such as PKH, DiI and DiR can be used for fluorescence emitting EVs [11–16]. This simple labeling method can visualize cellular-level interactions. For example, live-cell imaging showed internalizing EVs through endocytosis pathway and recycling of EVs [15]. However, fluorescence dye imaging is limited to exogenous EVs. Furthermore, it is unable to acquire deep organ imaging. In terms of in vivo imaging, among lipophilic dyes, near-infrared (NIR) dyes are more ideal for in vivo imaging than general fluorescence dye as NIR could provide higher signal-to-noise ratio and relatively higher penetration depth. For example, a report used lipophilic NIR dye, IRDye800, for whole body biodistribution study [17]. Nonetheless, the method has inherent limitation against direct clinical translation. In addition, recently, issues with regard to tracking biodistribution using lipophilic dyes in preclinical studies have been raised. EVs can be metabolized and degraded in in vivo, however, dyes persist in tissues and emit signals, which results in misleading results of biodistribution. Lipophilic dyes could be integrated with intact lipid bilayers as well as degraded lipids and other lipophilic compounds during circulation [9]. Furthermore, lipophilic dyes may cause aggregation of EVs and hinder accurate imaging and trafficking of EVs [18].

As aforementioned, reporter system can be used for fluorescence imaging of EVs. Protein markers of EVs, such as CD63, were used to design reporter conjugated to fluorescent proteins [19, 20]. This labeling strategy allows to generate a cell line that continuously produce EVs containing the reporter proteins. In spite of the stability, the signal intensity depends on the amount of protein expression of EVs, which could be heterogeneous in population of EVs. Subpopulation of EVs without specific reporter protein cannot be monitored by this specific protein-targeted reporter system [21]. Another reporter method based on palmitoylation signal provided membrane of EVs expressing fluorescence signals [9]. While lipophilic dyes can be nonspecifically bound to lipid entities as well as EVs, the reporter system has specific and selective imaging of EVs. This property allows for live-cell imaging of EVs from specific cell types which showed exchanging EVs between different cell populations [22]. However, they need genetically engineered cells which limit in clinical application as well as flexible labeling for various types of EVs. Whole body imaging instead of microscopic cellular level imaging using this method is difficult due to relatively low yield of fluorescence-labeled EVs from reporter system.

8.1.3 Bioluminescence Reporter System

The bioluminescence reporters have advantages in high sensitivity particularly compared with fluorescence-based imaging. Bioluminescence imaging of EVs employs luciferase enzymes as imaging reporters. In particular, one of the most commonly used luciferase enzymes, Gaussia luciferase (gLuc), was reported to be much brighter than the firefly or Renilla luciferases. But the tissue penetration of the emission photon makes the advantage of gLuc over firefly or Renilla luciferases. Luciferases in common, they are free from autofluorescence problems due to absent bioluminescence signals due to absence of any bioluminescence proteins reacting with substrates we inject to these small animals. Thus, this approach is more useful than fluorescence-based imaging for whole body imaging as a biodistribution study.

As a reporter being expressed solely in EVs, a group used a fusion protein which consists of gLuc enzyme combined with transmembrane domain of lactadherin [10]. This bioluminescence reporter overcomes the issue of recirculating and persistent fluorescence signals. Thus, EVs using this fusion protein, gLuc-lactadherin, was used for serial whole body imaging to quantitatively monitor the clearance of intravenously injected EVs [23]. A similar bioluminescence reporter system was reported by Lai et al. using membrane-bound variant of the gLuc reporter and a biotin acceptor peptide [9]. This reporter system allowed multimodal imaging of bioluminescence and fluorescence in vivo as fluorescence combined with streptavidin could provide fluorescence-mediated tomography imaging simultaneously.

Bioluminescence reporter system has several merits in small animal imaging due to high sensitivity, specificity for EVs as well as enabling multimodal imaging as aforementioned. However, this system has an inherent shortcomings that luminescence signals are attenuated in deep organs and that no substrates of luciferin or coelenterazine for these luciferases are allowed for the administration to humans. Moreover, relatively complicated labeling method compared with lipophilic dyes limits the high throughput in vivo kinetics study of various EVs extracted from different cell types.

Furthermore, similarly to fluorescence reporter imaging, the bioluminescent signal depends on the reporter protein expression [7, 15]. These labeling procedures are complicated compared to those of fluorescence dyes, which limits the study of biodistribution and fate of EVs in various cells under different conditions in vivo.

8.1.4 Radionuclide Imaging

Briefly, radionuclide imaging of EVs is sensitive and feasible to be extended to the human and clinical applications. Details of radiolabeled EVs are introduced in previous chapter. Recently developed ^{99m}Tc-labeled EVs used ^{99m}Tc-HMPAO and ^{99m}Tc-tricarbonyl. They used direct labeling of EVs [24, 25]. Another ^{125}I-labeled EVs employed a reporter system. EVs with a fusion protein of streptavidin and

lactadherin was labeled by ^{125}I-iodobenzoyl norbiotinamide [23]. In spite of advantages of radionuclide imaging of EVs in noninvasive imaging and biodistribution studies, the relative expensiveness of these specialized instruments—SPECT and PET—limited its wide use for small animal imaging in many research centers. Furthermore, for clinical translation, compared with magnetic resonance imaging, radiation hazard should be considered especially with longer half-life radionuclides with higher energies.

8.1.5 Magnetic Resonance Imaging

Another clinically feasible approach for imaging EVs is labeling with superparamagnetic iron oxide nanoparticles for magnetic resonance imaging [26, 27]. To load magnetic nanoparticles, a facilitating method for EV loading was required as they were different from lipophilic dyes which easily passed EV membrane. Hu et al. employed electroporation of EVs with superparamagnetic iron oxide nanoparticles to produce nanoparticle-laden EVs [26]. The electroporation for EV loading has been used for facilitating EV loading of biomaterials such as siRNA [28]. Superparamagnetic iron oxide nanoparticles were labeled to melanoma producing EVs and they were imaged in vitro and in vivo using magnetic resonance imaging. However, electric pulse can temporarily disturb the lipid bilayer structure which may alter the composition of EVs that eventually affect the function. In this regard, Busato et al. suggested an optimal magnetic nanoparticle labeling method without electroporation and under physiologic condition [27]. Their strategy was not based on direct labeling of EVs. Instead, they employed the strategy that parent cells load ultrasmall superparamagnetic iron oxide nanoparticles.

Magnetic resonance imaging is also clinically applicable and even more, free from radiation hazard. However, due to limitation in sensitivity and thus they needed to administer much larger amount of EVs, current in vivo magnetic resonance images were only obtained after intramuscular injection [26, 27]. Though locally accumulated EVs at injection sites could produce discernable magnetic resonance signal intensity change, systemic biodistribution and accumulation in target tissues such as cancer and inflammation require higher sensitivity. Thus, increasing sensitivity for tracking of systemically administered magnetic nanoparticle-labeled EVs is required to avoid the necessity to administer too large amount of EVs to yield sufficient signal-to-noise ratio. The quantitative analysis is also limited in magnetic resonance imaging compared with radionuclide imaging.

8.2 Variability of Biodistribution of EVs

8.2.1 Challenging in Tissue Targeting: Tropism of EVs

One of the important features of EVs that raise the promises for their application as drug carriers and therapeutics is their tissue-homing characteristics. Because of various surface proteins of EVs which can interact with recipient cells, EVs have initially received great attention for tissue-targeting endogenous nanomaterials [5]. Initial pilot studies which aimed at regenerative therapeutics as EVs showed that mesenchymal stem cell-derived EVs had therapeutic effects on myocardial ischemic tissue injuries or renal tissue loss by tissue homing effect of EVs [18, 29–33]. Moreover, tumor-derived EVs were reported to be accumulated in the lymph nodes which suggested pre-metastatic behavior [34] implying EVs' tropism that could be applied to tissue targeting.

Unfortunately, this tissue targeting capacity and in vivo distribution of EVs is highly affected by the physiological state of EVs as well as their extraction and administration methods [35]. So far, many studies using various imaging techniques reported too much variability regarding in vivo distribution of EVs. As those studies used different cell type-derived EVs as well as different techniques for acquisition of EVs, the in vivo distribution results should have been so variable. This variety of in vivo biodistribution are determined by technical, intrinsic and biological factors of EVs. The factors that have impact on biodistribution are summarized in Table 8.2. For the successful, if ever, application of EVs as therapeutics and drug carriers, we should consider these factors to achieve desirable tissue targeting.

8.2.2 Technical Factors

Firstly, technical factors of EVs affect physiology of EVs. The isolation methods of EVs are not standardized and their effects on the in vivo distribution are not yet elucidated well. There have been various methods of EVs' isolation including

Table 8.2 Factors affecting biodistribution of EVs

	Specific factors
Technical factor	Isolation method Loading method Administration dose Administration route Labeling method
Intrinsic factor	Definition of EVs Size of EVs
Biological factor	Originated cell types Variety of EVs in single cells

size-exclusion chromatography, centrifugation and ultrafiltration [36–38]. As EVs isolated by ultracentrifugation tended to be aggregated more [39], in vivo distribution of EVs isolated using this method should be different from those obtained using other methods. Furthermore, different drug/biomaterial loading methods of EVs would have also changed the physiology of EVs [40]. As aforementioned in the previous section, loading methods can be roughly divided into two categories: manipulating parent cells followed by isolating EVs and isolation of EVs followed by loading materials. Drug-loaded EVs prepared by these two different methods would have resulted in the differences of the characteristics of EVs even though they were derived from the same cell sources [40]. Direct comparison between these two methods was performed [18]. Directly labeled EVs with fluorescence dye showed higher accumulation in the liver, while EVs collected from fluorescence-labeled parent cells showed higher accumulation in the injured tissue. When electroporation was used to load nucleic acids in EVs [28, 41], electroporation itself cause aggregation of EVs [28]. Thus, the results of EVs' biodistribution using this labeling method for magnetic nanoparticles should be carefully interpreted and even we need to suspect that labeled EVs cannot represent the physiology of unlabeled EVs [26].

In vivo administration methods also influence the biodistribution as well as the amount of the administered dose of EVs. Wiklander et al. investigated systemically the effects of administration routes, cell source and targeting on the biodistribution pattern [35]. For example, intravenously administered EVs resulted in dose-dependent decrease in the accumulation in the liver and increase in the accumulation in the bowel. Saturation of the mononuclear phagocyte system of the liver was proposed as the mechanism. This dose-dependence in biodistribution pattern is important when we try to use imaging to trace the EVs' biodistribution to represent the biodistribution of therapeutic dose of EVs, as a preliminary imaging study using tracer amount of EVs may not represent biodistribution of later use of therapeutic dose of EVs. Keeping this in mind, one can try the simultaneous imaging and therapeutic trial of using EVs [42]. In this so-called theranostic approach, we mix (radio-)labeled tracer EVs with therapeutic amount of EVs and inject them and trace the biodistribution. Of course the labeling should be done in very mild and physiologic condition minimizing the effect of labeling procedure not to change the characteristics of EVs.

Another factor affecting the in vivo biodistribution is the administration route. EVs derived from melanoma cells of different studies showed distinctive accumulation patterns according to the administration route [43]. Subcutaneously injected melanoma-derived EVs accumulated in the lymph nodes [11, 26], while intravenously injected melanoma-derived EVs mainly accumulated in bone marrow and lungs [34]. Or another study showed that the major accumulated organ of the melanoma-derived EVs was liver and spleen when they were injected intravenously [10]. Head-to-head comparison of EVs derived from the same cell line (HEK293T) was investigated later. When the three administration routes, intravenous, intraperitoneal and subcutaneous administration, were compared, intraperitoneal and subcutaneous injection resulted in lower accumulation in the liver and spleen

but higher accumulation in the pancreas and bowel than intravenous administration of the same EVs [35].

The important technical factor which affects biodistribution is the labeling method. As lipophilic fluorescent dye itself has long half-life in vivo, it remained in the tissues even after the degradation of EVs [22]. Reporter system based on surface proteins or lipid bilayers could show different biodistribution patterns from other methods. Simultaneous labeling of fluorescence dye and radionuclide ^{99m}Tc-HMPAO revealed that fluorescence signals and radioactivity had different kinetics patterns [43]. As labeling process may hamper integrity of EVs and cause composition changes, optimized labeling process under physiologic condition will again be very important for accurate monitoring of biodistribution. Furthermore, multimodal imaging using various labeling methods can help understand accurate biodistribution of administered EVs.

8.2.3 Intrinsic Factors

According to the earlier findings of the in vivo distribution of liposomes, size of liposomes was already known to be a determinant factor of major uptake sites. The liposomes were commonly accumulated in the organs of mononuclear phagocyte system including liver, spleen and the lungs. When they were injected intravenously, they were generally taken up by macrophages in liver or spleen [44, 45]. The size of the nanoparticles including liposomes affected the sites of clearance among mononuclear phagocytic system organs of liver, spleen and bone marrow. Very small nanoparticles (<80 nm) tended to be cleared by bone marrow [46]. Around 100 nm sized nanoparticles can penetrate the hepatic sinusoidal endothelium, which results in increased hepatic accumulation [47, 48]. Larger nanoparticles including liposomes are prone to higher chances of opsonization and accumulate more in the spleen.

Current reports of in vivo biodistribution study of EVs showed that the major accumulation of EVs were similar with liposomes. Mostly, EVs were accumulated in the liver and spleen [43]. This pattern is similar to various nanoparticles including liposomes. Moreover, a study showed that liposomes with similar size of EVs and liposomes synthesized by lipid extracts of EVs have very similar biodistribution patterns [14]. It suggested the distribution of EVs could be mainly determined by intrinsic physiologic factors such as size.

Nonetheless, the definition of EVs include a broad spectrum of vesicles secreted by several types of cells [5, 49, 50]. Thus, size of EVs is varied according to the definition of EVs among different studies. In general, EVs include exosomes and microvesicles. Exosomes are small (30–100 nm) vesicles derived from the endosomal pathway. The microvesicles relatively larger than exosomes (50–1000 nm) and they are generated by budding of the plasma membrane [50]. The broad spectrum of size of EVs could affect various biodistribution results. EVs are not a single entity and include a group of vesicles which have been called exosomes,

ectosomes, microvesicles, oncosomes and so on. As a future work, the isolation of subpopulation of EVs should be warranted to investigate their physiological characteristics and implications. Furthermore, standardized definition of EVs and their spectrum is required.

8.2.4 Biological Factors

Given the tropism of EVs, cell-type specific biodistribution can be an important factor for the possible application of EVs for therapeutic purposes. In spite of the expectation of tropism effects according to cell types, a direct comparison between EVs originated from different cell sources (muscle, melanoma and immature bone marrow) showed similar accumulation in the liver and spleen regardless of the sources [35]. However, the differential pattern of accumulation was also observed. Muscle-derived EVs showed higher accumulation in the liver than the others and immature bone marrow-derived EVs showed higher accumulation in the spleen. Melanoma-derived EVs were accumulated more in the gastrointestinal tract and the lungs. This differential accumulation in the liver, lungs and spleen, was not explained by the size of EVs as the size of EVs originated from different cell types were similar. Though the size was a critical factor determining in vivo distribution as aforementioned, different composition of EVs associated with cell sources was another factor affecting biodistribution. This idea was also supported by the studies that the tailored EVs having modified molecular composition showed different biodistribution [51–53]. Composition change of exosomal-tetraspanin complex affected capability of EVs in their in vivo targeting and showed more accumulation in the pancreas [51]. Ohno et al. synthesized EVs to target epidermal growth factor receptor positive breast cancer and showed the tumor accumulation while the most of the EVs accumulated in liver and spleen [12]. These findings suggested that the accumulation sites of EVs was mainly mononuclear phagocyte system (or reticuloendothelial system; RES) including liver and spleen, however, the degree of accumulation and target tissue accumulation could be influenced by molecular composition of EVs. Contrary to the results of the effect of molecular composition on in vivo biodistribution, some reports showed that the EVs' composition effect was negligible compared with the EVs' size effect. Intravenously injected EVs were rapidly cleared and showed minimal tumor accumulation like liposomes and liposomes generated by exosome compounds [14]. Despite this rapid clearance, the authors found that intratumorally delivered EVs remained longer than liposomes which could partly support the potential use of EVs as drug carrier and therapeutics.

The underlying mechanism of differential accumulation patterns of EVs compared with liposomes or micelles remains unknown. Although many studies suggested that molecular composition and tailored EVs could have differential distribution patterns and enhanced target tissue accumulation, how these molecules change the physiologic property of EVs has not yet been studied. More importantly, recent study revealed that EVs isolated from a single cell source have variable

molecular composition [54]. Proteomic analysis revealed that mesenchymal stem cells secreted at least 3 types of EVs, which suggested that cells secreted many types of EVs in terms of their molecular composition. This implies the mechanistic understanding of biodistribution more complex and difficult. The composition of EVs secreted by a cell can be changed by cellular condition at one time and, even more, EVs secreted at one time from a single cell have subpopulation groups.

8.2.5 Future Direction for Biodistribution Analysis and Its Application

Various factors affect biodistribution results of EVs. It resulted in variable biodistribution results between different studies: some reported exaggerated tissue homing effects and others emphasized on mononuclear phagocyte system (RES) uptake only. Nonetheless, the important fact is that there are various types of EVs. The broad spectrum of EVs have different physiologic characters. In vivo distribution of EVs may be changed according to all the different in vivo conditions of each living subject as well. Because of this complexity, simultaneous tracking of EVs during usage of therapeutic purposes is required as a future work. Standardized procedures for the isolation and purification of EVs and multimodal labeling process will be needed as well.

Imaging of EVs is essential to understand the biodistribution of EVs. It also allows direct monitoring of EVs whether they targeted the specific tissue when we used EVs for therapeutic purposes. However, each imaging method has limitations in terms of feasibility of clinical application, capability of quantitation and easy availability. That is why we should concentrate on multimodal imaging of EVs. As EVs have various biomolecules in their surface and we can load drugs and biologic or nano therapeutics into them, EVs could work as a multifunctional endogenous nano-platform. Various feasible tailoring methods including surface modification, reporter system and loading therapeutic radionuclides could facilitate clinical application of EVs.

References

1. A.V. Vlassov, S. Magdaleno, R. Setterquist, R. Conrad, Exosomes: current knowledge of their composition, biological functions, and diagnostic and therapeutic potentials. Biochim. Biophys. Acta **1820**(7), 940–948 (2012)
2. Y. Lee, S. El Andaloussi, M.J. Wood, Exosomes and microvesicles: extracellular vesicles for genetic information transfer and gene therapy. Hum. Mol. Genet. **21**(R1), R125–R134 (2012)
3. Y. Sun, J. Liu, Potential of cancer cell-derived exosomes in clinical application: a review of recent research advances. Clin. Ther. **36**(6), 863–872 (2014)

4. D. Sun, X. Zhuang, S. Zhang, Z.-B. Deng, W. Grizzle, D. Miller et al., Exosomes are endogenous nanoparticles that can deliver biological information between cells. Adv. Drug Deliv. Rev. **65**(3), 342–347 (2013)
5. M. Colombo, G. Raposo, C. Thery, Biogenesis, secretion, and intercellular interactions of exosomes and other extracellular vesicles. Annu. Rev. Cell Dev. Biol. **30**, 255–289 (2014)
6. A.K.A. Silva, R. Di Corato, T. Pellegrino, S. Chat, G. Pugliese, N. Luciani et al., Cell-derived vesicles as a bioplatform for the encapsulation of theranostic nanomaterials. Nanoscale **5**(23), 11374–11384 (2013)
7. A.K. Silva, N. Luciani, F. Gazeau, K. Aubertin, S. Bonneau, C. Chauvierre et al., Combining magnetic nanoparticles with cell derived microvesicles for drug loading and targeting. Nanomedicine **11**(3), 645–655 (2015)
8. A.K. Silva, J. Kolosnjaj-Tabi, S. Bonneau, I. Marangon, N. Boggetto, K. Aubertin et al., Magnetic and photoresponsive theranosomes: translating cell-released vesicles into smart nanovectors for cancer therapy. ACS Nano. **7**(6), 4954–4966 (2013)
9. C.P. Lai, O. Mardini, M. Ericsson, S. Prabhakar, C.A. Maguire, J.W. Chen et al., Dynamic biodistribution of extracellular vesicles in vivo using a multimodal imaging reporter. ACS Nano. **8**(1), 483–494 (2014)
10. Y. Takahashi, M. Nishikawa, H. Shinotsuka, Y. Matsui, S. Ohara, T. Imai et al., Visualization and in vivo tracking of the exosomes of murine melanoma B16-BL6 cells in mice after intravenous injection. J. Biotechnol. **165**(2), 77–84 (2013)
11. J.L. Hood, R.S. San, S.A. Wickline, Exosomes released by melanoma cells prepare sentinel lymph nodes for tumor metastasis. Cancer Res. **71**(11), 3792–3801 (2011)
12. S. Ohno, M. Takanashi, K. Sudo, S. Ueda, A. Ishikawa, N. Matsuyama et al., Systemically injected exosomes targeted to EGFR deliver antitumor microRNA to breast cancer cells. Mol. Ther. **21**(1), 185–191 (2013)
13. T. Tian, Y.L. Zhu, F.H. Hu, Y.Y. Wang, N.P. Huang, Z.D. Xiao, Dynamics of exosome internalization and trafficking. J. Cell. Physiol. **228**(7), 1487–1495 (2013)
14. T. Smyth, M. Kullberg, N. Malik, P. Smith-Jones, M.W. Graner, T.J. Anchordoquy, Biodistribution and delivery efficiency of unmodified tumor-derived exosomes. J. Control Release. **199**, 145–155 (2015)
15. T. Tian, Y. Wang, H. Wang, Z. Zhu, Z. Xiao, Visualizing of the cellular uptake and intracellular trafficking of exosomes by live-cell microscopy. J. Cell. Biochem. **111**(2), 488–496 (2010)
16. K. Laulagnier, H. Vincent-Schneider, S. Hamdi, C. Subra, D. Lankar, M. Record, Characterization of exosome subpopulations from RBL-2H3 cells using fluorescent lipids. Blood Cells Mol. Dis. **35**(2), 116–121 (2005)
17. D. Sun, X. Zhuang, X. Xiang, Y. Liu, S. Zhang, C. Liu et al., A novel nanoparticle drug delivery system: the anti-inflammatory activity of curcumin is enhanced when encapsulated in exosomes. Mol. Ther. **18**(9), 1606–1614 (2010)
18. C. Grange, M. Tapparo, S. Bruno, D. Chatterjee, P.J. Quesenberry, C. Tetta et al., Biodistribution of mesenchymal stem cell-derived extracellular vesicles in a model of acute kidney injury monitored by optical imaging. Int. J. Mol. Med. **33**(5), 1055–1063 (2014)
19. M. Mittelbrunn, C. Gutierrez-Vazquez, C. Villarroya-Beltri, S. Gonzalez, F. Sanchez-Cabo, M.A. Gonzalez et al., Unidirectional transfer of microRNA-loaded exosomes from T cells to antigen-presenting cells. Nat. Commun. **2**, 282 (2011)
20. A. Suetsugu, K. Honma, S. Saji, H. Moriwaki, T. Ochiya, R.M. Hoffman, Imaging exosome transfer from breast cancer cells to stroma at metastatic sites in orthotopic nude-mouse models. Adv. Drug Deliv. Rev. **65**(3), 383–390 (2013)
21. C.P.-K. Lai, X.O. Breakefield, Role of exosomes/microvesicles in the nervous system and use in emerging therapies. Front Physiol. **3**, 228–242 (2012)
22. C.P. Lai, E.Y. Kim, C.E. Badr, R. Weissleder, T.R. Mempel, B.A. Tannous et al., Visualization and tracking of tumour extracellular vesicle delivery and RNA translation using multiplexed reporters. Nat. Commun. **6**, 7029 (2015)

23. M. Morishita, Y. Takahashi, M. Nishikawa, K. Sano, K. Kato, T. Yamashita et al., Quantitative analysis of tissue distribution of the B16BL6-derived exosomes using a streptavidin-lactadherin fusion protein and iodine-125-labeled biotin derivative after intravenous injection in mice. J. Pharm. Sci. **104**(2), 705–713 (2015)
24. H. Choi, S.C. Jang, M.Y. Yoo, J.Y. Park, N.E. Choi, H.J. Oh et al., Noninvasive imaging of radiolabeled exosome-mimetic nanovesicle using ^{99m}Tc-HMPAO. Sci. Rep. **5**, 15636 (2015)
25. Z. Varga, I. Gyurkó, K. Pálóczi, E.I. Buzás, I. Horváth, N. Hegedűs et al., Radiolabeling of extracellular vesicles with ^{99m}Tc for quantitative in vivo imaging studies. Cancer Biother. Radiopharm. **31**(5), 168–173 (2016)
26. L. Hu, S.A. Wickline, J.L. Hood, Magnetic resonance imaging of melanoma exosomes in lymph nodes. Magn. Reson. Med. **74**(1), 266–271 (2015)
27. A. Busato, R. Bonafede, P. Bontempi, I. Scambi, L. Schiaffino, D. Benati et al., Magnetic resonance imaging of ultrasmall superparamagnetic iron oxide-labeled exosomes from stem cells: a new method to obtain labeled exosomes. Int. J. Nanomedicine **11**, 2481 (2016)
28. S.A. Kooijmans, S. Stremersch, K. Braeckmans, S.C. de Smedt, A. Hendrix, M.J. Wood et al., Electroporation-induced siRNA precipitation obscures the efficiency of siRNA loading into extracellular vesicles. J. Control Release. **172**(1), 229–238 (2013)
29. R.C. Lai, T.S. Chen, S.K. Lim, Mesenchymal stem cell exosome: a novel stem cell-based therapy for cardiovascular disease. Regen. Med. **6**(4), 481–492 (2011)
30. L. Timmers, S.K. Lim, I.E. Hoefer, F. Arslan, R.C. Lai, A.A. van Oorschot et al., Human mesenchymal stem cell-conditioned medium improves cardiac function following myocardial infarction. Stem Cell Res. **6**(3), 206–214 (2011)
31. S. Gatti, S. Bruno, M.C. Deregibus, A. Sordi, V. Cantaluppi, C. Tetta et al., Microvesicles derived from human adult mesenchymal stem cells protect against ischaemia-reperfusion-induced acute and chronic kidney injury. Nephrol. Dial. Transplant. **26**(5), 1474–1483 (2011)
32. S. Bian, L. Zhang, L. Duan, X. Wang, Y. Min, H. Yu, Extracellular vesicles derived from human bone marrow mesenchymal stem cells promote angiogenesis in a rat myocardial infarction model. J. Mol. Med. Berl. **92**(4), 387–397 (2014)
33. L. Kilpinen, U. Impola, L. Sankkila, I. Ritamo, M. Aatonen, S. Kilpinen et al., Extracellular membrane vesicles from umbilical cord blood-derived MSC protect against ischemic acute kidney injury, a feature that is lost after inflammatory conditioning. J. Extracell. Vesicles **2**(1), 21927 (2013)
34. H. Peinado, M. Alečković, S. Lavotshkin, I. Matei, B. Costa-Silva, G. Moreno-Bueno et al., Melanoma exosomes educate bone marrow progenitor cells toward a pro-metastatic phenotype through MET. Nat. Med. **18**(6), 883–891 (2012)
35. O.P. Wiklander, J.Z. Nordin, A. O'Loughlin, Y. Gustafsson, G. Corso, I. Mäger et al., Extracellular vesicle in vivo biodistribution is determined by cell source, route of administration and targeting. J. Extracell. Vesicles **4**(1), 26316 (2015)
36. K.W. Witwer, E.I. Buzas, L.T. Bemis, A. Bora, C. Lässer, J. Lötvall et al., Standardization of sample collection, isolation and analysis methods in extracellular vesicle research. J. Extracell. Vesicles **2**(1), 20360 (2013)
37. A.N. Böing, E. Van Der Pol, A.E. Grootemaat, F.A. Coumans, A. Sturk, R. Nieuwland, Single-step isolation of extracellular vesicles by size-exclusion chromatography. J. Extracell. Vesicles **3**(1), 23430 (2014)
38. J.Z. Nordin, Y. Lee, P. Vader, I. Mäger, H.J. Johansson, W. Heusermann et al., Ultrafiltration with size-exclusion liquid chromatography for high yield isolation of extracellular vesicles preserving intact biophysical and functional properties. Nanomedicine **11**(4), 879–883 (2015)
39. R. Linares, S. Tan, C. Gounou, N. Arraud, A.R. Brisson, High-speed centrifugation induces aggregation of extracellular vesicles. J. Extracell. Vesicles **4**(1), 29509 (2015)
40. R. van der Meel, M.H. Fens, P. Vader, W.W. van Solinge, O. Eniola-Adefeso, R.M. Schiffelers, Extracellular vesicles as drug delivery systems: lessons from the liposome field. J. Control Release. **195**, 72–85 (2014)

41. T.A. Shtam, R.A. Kovalev, E.Y. Varfolomeeva, E.M. Makarov, Y.V. Kil, M.V. Filatov, Exosomes are natural carriers of exogenous siRNA to human cells in vitro. Cell Commun. Signal. **11**(1), 88 (2013)
42. H. Choi, Y.-S. Lee, D.W. Hwang, D.S. Lee, Translational radionanomedicine: a clinical perspective. Eur. J. Nanomed. **8**(2), 71–84 (2016)
43. H. Choi, D.S. Lee, Illuminating the physiology of extracellular vesicles. Stem Cell Res. Ther. **7**(1), 55 (2016)
44. S.M. Moghimi, A.C. Hunter, J.C. Murray, Long-circulating and target-specific nanoparticles: theory to practice. Pharmacol. Rev. **53**(2), 283–318 (2001)
45. S.-D. Li, L. Huang, Pharmacokinetics and biodistribution of nanoparticles. Mol. Pharm. **5**(4), 496–504 (2008)
46. S. Reske, Recent advances in bone marrow scanning. Eur. J. Nucl. Med. Mol. Imaging **18**(3), 203–221 (1991)
47. H. Sarin, Physiologic upper limits of pore size of different blood capillary types and another perspective on the dual pore theory of microvascular permeability. J. Angiogenes Res. **2**(1), 14 (2010)
48. M.C. Garnett, P. Kallinteri, Nanomedicines and nanotoxicology: some physiological principles. Occup. Med. Lond. **56**(5), 307–311 (2006)
49. S.J. Gould, G. Raposo, As we wait: coping with an imperfect nomenclature for extracellular vesicles. J. Extracell. Vesicles **2**(1), 20389 (2013)
50. S. El Andaloussi, I. Mäger, X.O. Breakefield, M.J. Wood, Extracellular vesicles: biology and emerging therapeutic opportunities. Nat. Rev. Drug Discov. **12**(5), 347 (2013)
51. S. Rana, S. Yue, D. Stadel, M. Zoller, Toward tailored exosomes: the exosomal tetraspanin web contributes to target cell selection. Int. J. Biochem. Cell Biol. **44**(9), 1574–1584 (2012)
52. S. Rana, M. Zöller, Exosome target cell selection and the importance of exosomal tetraspanins: a hypothesis. Biochem. Soc. Trans. **39**(2), 559–562 (2011)
53. L. Lattanzi, M. Federico, A strategy of antigen incorporation into exosomes: comparing cross-presentation levels of antigens delivered by engineered exosomes and by lentiviral virus-like particles. Vaccine **30**(50), 7229–7237 (2012)
54. R.C. Lai, S.S. Tan, R.W.Y. Yeo, A.B.H. Choo, A.T. Reiner, Y. Su et al., MSC secretes at least 3 EV types each with a unique permutation of membrane lipid, protein and RNA. J. Extracell. Vesicles **5**(1), 29828 (2016)

Chapter 9
Endogenous Radionanomedicine: Validation of Therapeutic Potential

Seunggyun Ha and Dong Soo Lee

Abstract Exosomes have features to be able to promise therapeutic opportunities, which are exosomes-mediated pathogenesis in certain diseases, and thus their inherent therapeutic potential, and again possibility of use of exosomes as drug carriers. There have been increasing interests in this therapeutic potential of exosomes owing to the recent reports in regenerative medicine, tumor management, infection, and organ transplantation. Radionanomedicines i.e. radiolabeled exosomes provide advantages of non-invasive, less toxic, highly penetrable, highly sensitive, and quantification-enabling characteristic of radioactivity for validation of therapeutic potentials of exosomes. Radiolabeled exosomes are expected to allow their theranostic use even in clinical settings. However, there remain the issues to overcome the low yields of exosomes, release of free radioisotope after degradation of exosomes, and yet unveiled dosimetry of therapeutic radiolabeled exosomes. This chapter reviews current evidences of therapeutic applications of exosomes in regenerative medicine and tumor management and discusses radiolabeled exosomes or exosome-mimetic nanovesicles as well as remaining issues in endogenous radionanomedicines regarding the desired therapeutic potentials of radiolabeled or unlabeled exosomes.

S. Ha (✉) · D. S. Lee
Department of Nuclear Medicine, Seoul National University
College of Medicine, Seoul 03080, Republic of Korea
e-mail: gyuriha@snu.ac.kr

S. Ha · D. S. Lee
Department of Molecular Medicine and Biopharmaceutical Sciences,
Graduate School of Convergence Science and Technology, Seoul National University,
Seoul 03080, Republic of Korea

D. S. Lee
Korea Brain Research Institute, Daegu, Republic of Korea
e-mail: dsl@snu.ac.kr

D. S. Lee (ed.), *Radionanomedicine*, Biological and Medical Physics,
Biomedical Engineering, https://doi.org/10.1007/978-3-319-67720-0_9

9.1 Introduction

Exosomes are a kind of extracellular cell-derived vesicles which have a size in a range of 30–100 μm and contain various molecules of miRNAs, mRNAs, and proteins in their spherical structure. Lots of things about characteristics of exosomes have been unveiled and it is established that exosomes regard to cell-to-cell communication via delivery of their contents to the recipient cells. There are many reports that diseases are related to specific types of exosomes which can be used as diagnostic markers. Additionally, the interest in the therapeutic potential of exosomes continues to rise, and the evidence has been accumulated over the last few years.

There are three important features of exosomes for therapeutic opportunities (Fig. 9.1) [1]. First one is exosome-mediated disease pathogenesis which implies the possibility of using exosomes as therapeutic target. Several strategies including inhibition of exosome-biogenesis, release, cell uptake and targeting of specific extracellular vesicle components are potentially applicable to block exosome-mediated pathogenesis. Next one is exosomes themselves having inherent therapeutic potential such as their involvement of antigen presentation, immune modulation, and tissue repair. Another feature of exosomes for therapeutic potential is their capability to be used as drug cargo. The spherical feature endogenously encapsulated by lipid bilayer with various surface proteins enables exosomes to contain drugs within them and consequent action for specific delivery of the materials within them. The therapeutic potentials of exosomes have been established in various areas like regenerative medicine, tumor, infection, and organ transplantation [2].

Imaging and tracking of exosomes are important to understand biodistribution of exosomes and successful targeted delivery to specific tissue, non-invasively. Different imaging strategies using fluorescence imaging, bioluminescence reporter system, magnetic resonance imaging (MRI), and radionuclide imaging have been applied for tracking of exosomes in vivo [3]. Optical imaging using direct lipophilic fluorescence dye labeling provides simple methods to observe cell-to-cell communications via exosome transferring [4–7]. Reporter imaging scheme using fluorescence or bioluminescence provides more specific imaging to exosomes compared to direct fluorescence dye labeling. Bioluminescence imaging is free from any false positive signals from retained or freely circulating fluorescent dye after exosome degradation. However, reporter imaging needs genetic engineering and has relatively inconsistent signal intensity which depends on the expression of reporter proteins. Furthermore, optical imaging systems using fluorescence or bioluminescence has inherent shortcomings of attenuation of signals due to shallow depth of photon penetration and low availability in clinical field. Superparamagnetic iron oxide nanoparticles-laden exosomes can be used for MRI for exosome-tracking [8, 9]. However, this approach needs large amounts of exosomes because of the relatively lower sensitivity of MRI compared with optical imaging or radionuclide imaging, which further complicates the problem related to

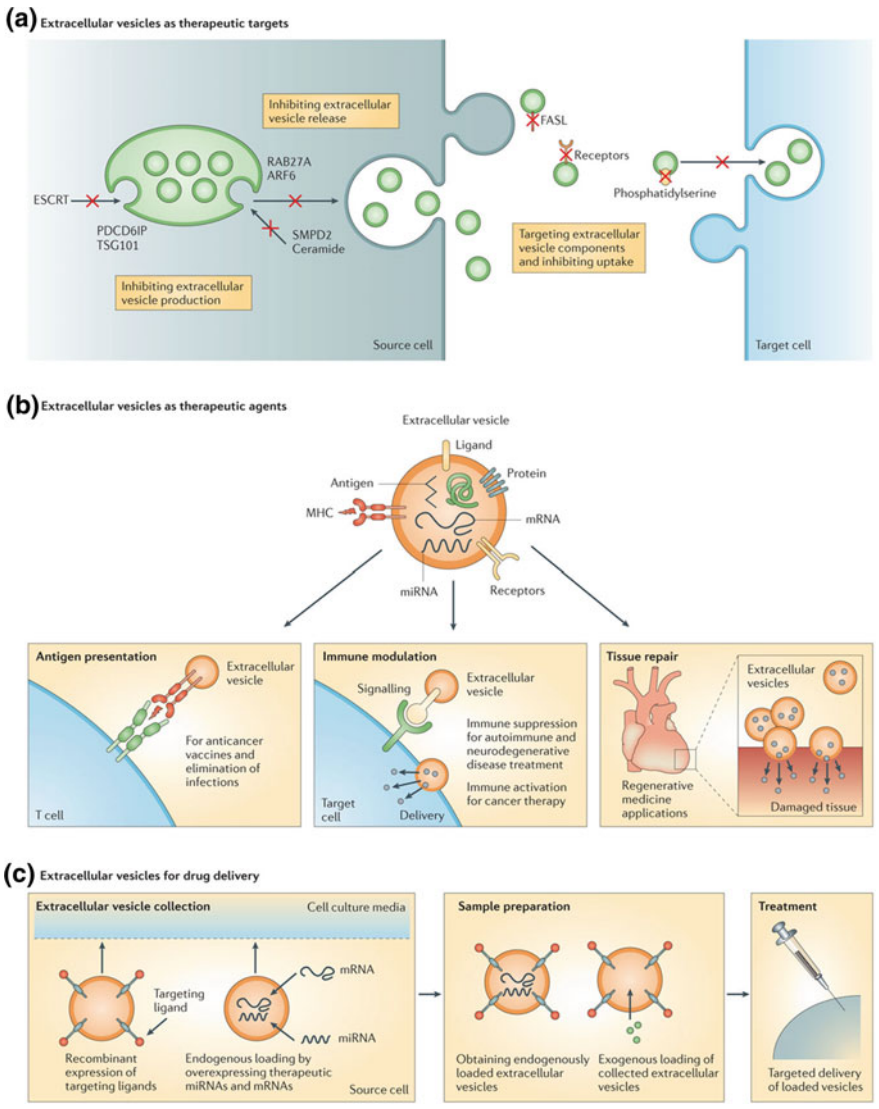

Fig. 9.1 Therapeutic strategies regarding exosomes. Exosomal therapeutic approaches are available via 3 ways that **a** regarding as therapeutic target, **b** application of innate therapeutic ability, and **c** utilization as drug cargo. Adapted from [1] with permission

lower yields of exosomes. Radiolabeling of exosomes, using gamma rays or positrons emitting particles, enables highly sensitive and less-attenuated image acquisition, and thus this can be translated to clinical application [10–13].

This chapter introduces the current states of art of evaluating the therapeutic potentials of exosomes in various fields including regenerative medicine and tumor management and discusses the role of radionanomedicine in validation of therapeutic potentials of exosomes.

9.2 Regenerative Medicine

The aim of regenerative medicine is to restore the function of damaged or lost tissues. The major strategies of regenerative medicine are related with cell-based therapies, classical tissue engineering, and biodegradable materials-based approaches [14]. Traditionally, cell-based therapies directly administer cells to damaged tissues to directly repair or support tissue repair via paracrine effect. However, there is difficulty to control the directly administered cells, which is related to safety issue of stem cell transplantation. Recently, exosomes have been evaluated as one of the cell-free approaches focusing on the paracrine hypothesis via exosomes in regenerative medicine. Exosomes in regenerative medicine may have roles in angiogenesis, suppressing apoptosis, stimulating cell proliferation, immune regulation, and extracellular matrix remodeling, which would be useful in tissue engineering.

9.2.1 Nervous System

Nerve regeneration has been a major challenge in regenerative medicine because nervous system usually lacks the capability of self-regeneration. With the rapid development of cell-based therapies, recent researches have focused on what makes neurological disorders improve via paracrine effect from cell-based therapies. Exosomes from multiple cell types including multipotent mesenchymal stem cells (MSCs), and dendritic cells (DCs) have shown to help repair nervous injury. Transfer of miRNA-133b via exosomes with green fluorescent protein-tagged CD63 from MSCs to astrocytes and neurons induce increased axonal plasticity and neurite remodeling in ischemic boundary zone, which subsequently lead to functional recovery in stroke models of rodents [15]. Exosomes with GFP-Tagged CD63 derived from Schwann cells also markedly increase axonal regeneration in vitro and in vivo [16]. Gamma-interferon (IFNγ) -stimulated DCs exosomes with CD63 conjugated to quantum dots (QD, 24 nm in size, fluoresce at 620 nm) helped remyelination of acutely damaged nerves, and nasal delivery of IFNγ-stimulated DCs exosomes coupled to QD increased central nervous system (CNS) myelination in vivo [17]. In addition, nasal administration of the IFNγ-stimulated DCs exosomes enriched with miR-219 to aging rats also showed enhancement of myelination. In the field of Alzheimer's Disease (AD), fluorescence dye (PKH26)-labeled exosomes with abundant of glycosphingolipids, derived from wild-type

neuroblastoma or primary neurons in the hippocampus improved amyloid plaque burden by clearing them by microglia [18]. These results provide the evidence of exosomes' potential for non-invasive therapeutic use of exosomes in neurological disorders including CNS demyelinating disease like multiple sclerosis and neurodegenerative disease like AD.

9.2.2 Cardiovascular System

Heart and cardiovascular system work for blood circulation under the highly synchronized regulation of myocardial contraction. Cardiomyocytes, smooth muscle cells, endothelial cells, fibroblasts and cardiac stem cells contribute to the organization and maintenance of the system. For the well-regulated circulation, cell-to-cell communication is really important. Traditionally, paracrine effect via growth-factor, endocrine effect via adiponectin, direct cell-to-cell contact via gap junction, and adhesion molecules like integrin have been regarded as important players for this effective cell-to-cell communication. Recently, exosomes have been implicated as another mediator of cell-to-cell communication in myocardial system in either physiology or pathological condition such as reperfusion injury. Paracrine effect of pluripotent cells like MSC or cardiac progenitor cells (CPC) via exosomal delivery to ischemic injured myocardium has been tested in several studies in vivo.

Intravenously injected MSC-derived exosomes reduced infarct size in mice model of cardiac ischemic reperfusion injury [19], which was mediated by transfer of glycolytic enzymes enriched in MSC-derived exosomes that enhanced glycolytic flux and adenosine triphosphate (ATP) production by complementation of depleted energetic enzymes in reperfused myocardium [20]. Additionally, membrane-bound CD73 on MSC-derived exosomes hydrolyzed adenosine monophosphate degraded from ATPs and adenosine diphosphates in injured cardiomyocytes, to adenosine, and subsequently interrupted activation of reperfusion injury salvage kinase (RISK) pathway participating in apoptosis of reperfused myocardium [21]. Meanwhile, CPC-derived exosomes which are highly enriched in miRNAs including miR-451, miR-210, miR-132, and miR-146a-3p protected ischemic myocardium via inhibition of apoptosis of cardiomyoblasts in mice model of acute ischemic reperfusion injury [22, 23]. Cardioprotective effect of exosomes was also mediated by heat shock protein (HSP) 70 on exosomes by activation of a pathway downstream of toll-like receptor 4—extracellular signal regulated protein kinases (ERK) 1/2—p38 mitogen-activated protein kinase (p38MAPK)—phosphorylation of HSP27 [24]. A recent meta-analysis study proved the therapeutic and protective effect of MSC-derived exosomes on cardiac ischemic reperfusion injury [25].

9.2.3 Acute Kidney Injury

Acute kidney injury (AKI) is a disease which is characterized by acute tubular injury inducing rapid loss of renal function mainly caused by ischemic reperfusion injury [26]. Several animal studies showed that MSCs have treatment effect to AKI [27, 28]. Recent evidence has suggested that the effect of MSCs on AKI recovery relies on paracrine mechanism rather than transdifferentiation of MSCs [29–33]. Exosomes derived from MSCs stimulated proliferation and enhanced resistance of tubular cells to apoptosis in vitro [34]. In vivo study proved treatment effect of MSC-derived exosomes on the recovery of AKI via RNA-dependent paracrine effect [34, 35]. Injection of MSC-derived exosomes into kidney repaired cisplatin-induced AKI in mice by ameliorating apoptosis by suppressing activation of the p38MAPK pathway, promoting cell proliferation via activation of the ERK 1/2 pathway [36]. A meta-analysis concluded that cell-free treatment using MSC-derived exosomes was better than MSC-conditioned media [37]. Not only MSC-derived exosomes, endothelial colony-forming cells (ECFC)-derived exosomes also had a protective effect on AKI in mice [38]. PTEN/Akt pathway in endothelial cells was targeted by miR-486-5p transferred from human cord blood ECFC via exosomes, which induced the protective effect against AKI [39].

9.3 Tumor

Exosomes participate in intercellular communication even in cancer cells. Exosomes carry various molecules of nucleic acid, lipid, and protein, and affect pathological pathways of cancer cells including tumorigenesis, tumor growth, angiogenesis, metastasis, drug resistance, immune escape, tumor-stroma interaction, and tumor thrombosis [40]. Various molecules of proteins and nucleic acids contained in exosomes have been evaluated to develop novel diagnostic and prognostic marker for various types of cancer. The idea to use exosomes as anti-tumor vaccines or drug cargo for targeted drug delivery has been evaluated even in clinical trials (Table 9.1, modified from Lener et al. J Extracellular Vesicles 2015) [41].

9.3.1 Anti-tumor Vaccination

Extracellular vesicles derived from antigen presenting cells contain MHC-peptide complexes stimulated immune response [42]. Safety, feasibility, and efficacy of vaccination of autologous DC-derived exosomes loaded with tumor antigens were tested in patients with non-small cell lung cancer (NSCLC) or melanoma in phase I clinical trials [43, 44]. In phase II clinical trials, administration of autologous

Table 9.1 Current and past NIH registered clinical trials investigating EV-based therapeutics (modified from [41] with permission)

Disease number of patients clinical trial (CT) phase	Source cell-type/ application route	Modified/unmodified vesicle type	Results	References
Melanoma Stage III/IV, metastatic n = 15 CT Phase I, open label	Autologous monocyte-derived Dendritic cell EVs s.c. inj.	MAGE3 loaded DC-EVs	Proof of feasibility and safety; toxicity < grade II Maximum tolerated dose not reached, 1 partial, 1 minor, 1 mixed response and 2 stable disease	Escudier et al. [15]
Non-small cell lung cancer Stage IIIb, n = 4 Stage IV, n = 9 CT Phase I, open label	Autologous monocyte-derived Dendritic cell EVs s.c. and intradermal inj.	Peptide loaded	Feasibility and safety; toxicity < grade I–II, 9/13 Completed therapy, DTH against MAGE peptides In 3/9, specific T cell response in 1/3, NK lytic Activity increased in 2/4	Morse et al. [16]
Colon Cancer Stage III or IV, n = 40 CT Phase I, open label	Autologous ascites-derived EVs (Aex) s.c. inj.	Unmodified ± GM-CSF	Feasibility & Safety, Toxicity Grade I-II, TU-specific Cytotoxic T Cell Response in Aex + GM-CSF group (n = 2)	Dai et al. [30]
Colon Cancer n = 35 (estimated enrolment) CT Phase I, open label	Plant nanovesicles Not mentioned in NCT registry: Route of application	Curcumin, exogenous loading		NCT01294072

(continued)

Table 9.1 (continued)

Disease number of patients clinical trial (CT) phase	Source cell-type/ application route	Modified/unmodified vesicle type	Results	References
Type I Diabetes n = 20 (estimated enrolment) CT Phase I, open label	Umbilical cord blood (allogeneic) MSC-EVs Not mentioned in NCT registry: Route of application	Unmodified		NCT02138331
Non-small cell lung cancer n = 22 CT Phase II, open label	Autologous IFN-g matured Monocyte-derived dendritic cell EVs Intradermal inj.	Peptide loaded	One patient exhibited a grade 3 hepatotoxicity. Seven patients (32%) experienced stabilization of > 4 months: the primary endpoint ($\geq$ 50% patients > 4 months) was not reached. No induction of T cell responses, but an increase in NKp30-dependent NK cell functions were evidenced in a fraction of these NSCLC patients presenting with defective NKp30 expression	NCT01159288 Besse et al. [45]
Malignant Pleural Effusion n = 30 (estimated enrolment) CT Phase II, open label	Tumor cell-derived microparticles used as vectors for chemotherapeutic drugs Pleural or peritoneal cavity	Chemotherapeutic drugs, exogenous loading		NCT01854866

Abbreviations: *CT* clinical trials; *DC* dendritic cells; *DTH* delayed type hypersensitivity; *GM-CSF* granulocyte-macrophage colony-stimulating factor; *NIH*, National Institute of Health; *NK* natural killer; *MAGE* melanoma antigen; *TU* tumor

peptide-loaded exosomes from mature DC with IFNγ stimulation was tested as maintenance immunotherapy after the first line chemotherapy in 22 patients with advanced NSCLC, which have shown that DC exosomes with IFNγ activated antitumor immunity [45]. Meanwhile, tumor-driven exosomes also have been considered for tumor antigen source for immune-stimulation [46]. However, given that tumor exosomes inherently induce immune suppressive effect via delivery of immunomodulatory factor [47], administration of native tumor exosome for tumor treatment was not sufficient for immune stimulatory anti-tumor therapy [48]. To overcome the immune suppressive effect of tumor-derived exosomes, a combination of tumor exosomes with immune stimulatory adjuvant treatment had been developed and successfully improved the anti-tumor response of immune effector cells [49]. A phase I clinical trial proved the feasibility and safety of tumor-derived exosomes for anti-tumor immunotherapy [50]. In addition, exosomes derived from human NK cells were also shown to stimulate the anti-tumor immune response in vitro [51].

9.3.2 Targeted Drug Delivery

There have been many studies to develop and validate various drug delivery systems in different types of cancer [52, 53]. Encapsulating anticancer drugs within synthetic biomaterials such as liposomes showed advantages of increased efficacy, biocompatibility, and reduced toxicity, but it also had disadvantages of immunogenicity, low solubility, short half-life, and high cost [54]. Toxicity of synthetic biomaterials was associated even with synthetic biomaterials themselves, i.e., micelles, and liposomes [55]. Recently, exosomes emerged as a new drug-delivery system with inherent advantages of natural targeting property, less toxicity, less immunogenicity, and highly efficient internalization by target cells compared to synthetic liposomes of extrinsic drug cargos [56]. However, the problems of exosomes like low yield, low solubility, non-specific targeting, and short half-life in the circulation should be overcome to use exosomes practically as drug-delivery vehicle in clinical situation.

Exosomes are released only in small amounts from mammalian cells, and thus harvesting exosomes which were naturally released from cells are generally cost-ineffective and time-consuming, which results in a low yield [57]. Exosome-mimetic nanovesicles which were produced by serial extrusion through diminishing pore-sized filters (10, 5, 1 μm) was suggested to obtain a higher yield of nanovesicles [58]. The doxorubicin loaded exosome-mimetic nanovesicles obtained from U937 human monocytes or Raw 264.7 murine macrophages showed 100-fold higher production yield and similar in vivo antitumor effect compared to those of the doxorubicin loaded exosomes. The exosome-mimetic vesicles inherit the character of monocytes or macrophages, which recognize endothelial cell adhesion molecules (CAM) for extravasation. Tumors grow rapidly with abnormal angiogenesis, therefore rapidly growing endothelial cells expressing CAMs is a

representative target for targeted therapy. Meanwhile, even though exosomes may have natural targeting properties, engineering of exosome surface is necessary to enhance specific delivery of contained anti-tumor drugs to a tumor. Doxorubin-loaded mouse immature DCs (imDCs) which were engineered to express an exosomal membrane protein Lamp2b fused to αv integrin-specific iRGD peptide (iRGD-Lamp2b) showed highly efficient targeting and antitumor-effect to αv integrin-positive breast cancer cell lines (MDA-MB-231 and MCF-7) in vitro and MDA-MB-231 tumor in vivo [59]. The targeted drug-delivery strategies using exosomes were used not only for cancer therapeutics but also for inflammatory disease management [60].

9.4 Radionanomedicine for Validation of Therapeutic Potential of Exosomes

9.4.1 Exosomes and Radionanomedicine

As we have reviewed above, there has been increasing evidence that exosomes have therapeutic potential as well as pathophysiologic roles in diseases. Most of the results have been limited in preclinical experiments in vitro and in vivo, and only a few studies have been conducted in clinical trials [41, 43, 44, 50]. To apply exosomes to the clinical situation as therapeutics successfully, confirmation of specific targeting of exosomes is mandatory and monitoring of this specific targeting is critical. To understand the behavior of administered exosomes in vivo, imaging-based studies are needed. Given the properties of radionuclide imaging modality and its successful application to clinical nuclear medicine, imaging of radiolabeled exosomes may be the most promising tracking method to follow the administered exosomes in human bodies. Radionuclide imaging has characteristics of non-invasiveness, less toxicity, high penetration, high sensitivity, and easy quantification. The combination of imaging via radiolabeling and therapeutic application of exosomes is expected to permit theranostic approaches [61].

9.4.2 Radiolabeling with Various Radioisotopes

Regardless of its potential, only a few studies used radiolabeled exosomes and their focus was limited mainly on radiolabeling methods and biodistribution in animals. Radiolabeling with ^{125}I using streptavidin-biotin system was initially applied for evaluation of ex vivo biodistribution of intravenously administered B16BL6 murine melanoma cell-derived exosomes in mice, which needed genetic modification of B16BL6 cells to produce streptavidin [12]. Radiolabeling with ^{131}I of 4775-LuT breast cancer cell-derived exosomes was also reported [62]. In addition, direct

labeling of ^{111}In-oxide to various tumor-derived exosomes (4T1 and MCF-7 breast cancer cells, and PC3 prostate cancer cell) was accomplished [10]. More recently, ^{99m}Tc-HMPAO labeling of exosomes derived from Raw 264.7 murine macrophages was reported, in which ^{99m}Tc-HMPAO, which was converted into hydrophilic form, consequently trapped within exosomes by their glutathione which are enriched in exosomes [11]. ^{99m}Tc labeling of erythrocyte-derived exosomes was also established for quantitative in vivo single-photon emission computed tomography (SPECT) imaging [13]. Most of the established exosomal radiolabeling methods are using gamma-emitting radioisotopes, so SPECT has been commonly used for imaging, which provided relatively low spatial resolution and difficulties in quantification. Positron emission tomography (PET) imaging provides better spatial resolution and quantitative information about exosomal biodistribution compared to SPECT imaging. A few methods were proposed to use radioisotope labeled exosomes for PET imaging, and now the validation studies are needed [63, 64].

9.4.3 Remaining Issues

Several issues should be taken care of to apply radiolabeled exosomes for validation of the therapeutic potential of exosomes in vivo.

Given that only small amount of exosomes are naturally released from cells, so the low yield of exosomes is one of the major hurdles in preclinical and clinical uses of exosomes especially for therapeutic application. Further, preparation of exosomes needs multiple steps of isolation and purification. Labeling of imaging materials including radiolabeling needs one more step for exosome preparation, and it causes additional burden. Exosome-mimetic nanovesicles was recently proposed as a solution for the problem of low yield, and further study especially for establishing standardized protocols are needed [58]. Considering SPECT and/or PET imaging with superior detection sensitivity, radiolabeling exosomes for tracking in vivo minimizes the technical problem of the low yield of exosomes.

Signals from free radioisotope after degradation of exosomes could interfere the interpretation of the biodistribution of radiolabeled exosomes. The degradation of exosomes happens not only during circulation but also after uptake by target cells or immune cells in the mononuclear phagocytic system (MPS). According to the studies of biodistribution using radiolabeled exosomes, exosomes were taken up and cleared by the liver and/or spleen in early phase associated with initial rapid blood clearance after intravenous injection [10–12]. The rapid clearance of systemically administered exosomes is mainly due to the macrophages of MPS [65, 66]. Radiolabeling of exosomes with ^{99m}Tc-HMPAO solved the issue of labeling only the intact exosomes since ^{99m}Tc-HMPAO is trapped only within intact exosome after the cell uptake. This hydrophilic ^{99m}Tc-HMPAO will be released after degradation in blood or in MPS [11]. Thus, the ^{99m}Tc-HMPAO activity at least at later period after systemic administration of exosomes are convoluted activity of

both ^{99m}Tc-HMPAO of intact exosomes and ^{99m}Tc-HMPAO released from degraded exosomes. This should be discriminated.

Considering the trace amount of nanoparticles for imaging used in radionanomedicine, direct radiation toxicity by imaging of radiolabeled exosomes may not be higher than that of general nuclear medicine imaging procedures in clinics. Less immunogenicity is anticipated to the self-derived exosomes [61]. Further, the phospholipid bilayers of exosomes enable direct fusion with the cell membrane of target tissue, which results in less activation of inflammatory process due to bypass of the endosomal-lysosomal pathway [67]. Meanwhile, internal radiation dosimetry assessment is required for clinical translation of radiolabeled exosomes. Biodistribution of exosomes is mainly dependent on the character of cells of exosomes origination, which is called homing ability [68]. Due to the complexity and diversity of the biodistribution of exosomes, imaging with radiolabeled exosomes should be routinely performed as theranostics before the establishment of therapeutic application.

9.5 Conclusion

The therapeutic potential of exosomes has been increasingly reported in various clinical applications including regenerative medicine and tumor management. To reduce toxicity and enhance the efficacy of treatment, specific targeting strategies using exosomes were developed and regarded as one of the promising biomaterials. Therefore, validation of specific targeting became very important. For clinical translation, radionanomedicine is an appropriate method to visualize in vivo distribution of exosomes. The use of theranostic endogenous radionanomedicine using exosomes will help achieve the goal of the therapeutic use of exosomes sooner in the clinics.

References

1. S.E. Andaloussi, I. Mäger, X.O. Breakefield, M.J. Wood, Extracellular vesicles: biology and emerging therapeutic opportunities. Nat. Rev. Drug Discov. **12**(5), 347–357 (2013)
2. A.M. Merino, M.J. Hoogduijn, F.E. Borras, M. Franquesa, Therapeutic potential of extracellular vesicles. Front. Immunol. **5**, 658 (2014)
3. H. Choi, D.S. Lee, Illuminating the physiology of extracellular vesicles. Stem Cell Res. Ther. **7**(1), 55 (2016)
4. J.L. Hood, R.S. San, S.A. Wickline, Exosomes released by melanoma cells prepare sentinel lymph nodes for tumor metastasis. Cancer Res. **71**(11), 3792–3801 (2011)
5. Ohno S-i, M. Takanashi, K. Sudo, S. Ueda, A. Ishikawa, N. Matsuyama et al., Systemically injected exosomes targeted to EGFR deliver antitumor microRNA to breast cancer cells. Mol. Ther. **21**(1), 185–191 (2013)

6. H.C. Christianson, K.J. Svensson, T.H. van Kuppevelt, J.-P. Li, M. Belting, Cancer cell exosomes depend on cell-surface heparan sulfate proteoglycans for their internalization and functional activity. Proc. Natl. Acad. Sci. U S A. **110**(43), 17380–17385 (2013)
7. T. Tian, Y.L. Zhu, F.H. Hu, Y.Y. Wang, N.P. Huang, Z.D. Xiao, Dynamics of exosome internalization and trafficking. J. Cell. Physiol. **228**(7), 1487–1495 (2013)
8. H. De La Peña, J. Madrigal, S. Rusakiewicz, M. Bencsik, G.W. Cave, A. Selman et al., Artificial exosomes as tools for basic and clinical immunology. J. Immunol. Methods **344**(2), 121–132 (2009)
9. L. Hu, S.A. Wickline, J.L. Hood, Magnetic resonance imaging of melanoma exosomes in lymph nodes. Magn. Reson. Med. **74**(1), 266–271 (2015)
10. T. Smyth, M. Kullberg, N. Malik, P. Smith-Jones, M.W. Graner, T.J. Anchordoquy, Biodistribution and delivery efficiency of unmodified tumor-derived exosomes. J. Control Release. **199**, 145–155 (2015)
11. H. Choi, S.C. Jang, M.Y. Yoo, J.Y. Park, N.E. Choi, H.J. Oh et al., Noninvasive imaging of radiolabeled exosome-mimetic nanovesicle using ^{99m}Tc-HMPAO. Sci. Rep. **5**, 15636 (2015)
12. M. Morishita, Y. Takahashi, M. Nishikawa, K. Sano, K. Kato, T. Yamashita et al., Quantitative analysis of tissue distribution of the B16BL6-derived exosomes using a streptavidin–lactadherin fusion protein and iodine-125-labeled biotin derivative after intravenous injection in mice. J. Pharm. Sci. **104**(2), 705–713 (2015)
13. Z. Varga, I. Gyurkó, K. Pálóczi, E.I. Buzás, I. Horváth, N. Hegedűs et al., Radiolabeling of extracellular vesicles with ^{99m}Tc for quantitative in vivo imaging studies. Cancer Biother. Radiopharm. **31**(5), 168–173 (2016)
14. O.G. De Jong, B.W. Van Balkom, R.M. Schiffelers, C.V. Bouten, M.C. Verhaar, Extracellular vesicles: potential roles in regenerative medicine. Front. Immunol. **5**, 608 (2014)
15. H. Xin, Y. Li, Z. Liu, X. Wang, X. Shang, Y. Cui et al., MiR-133b promotes neural plasticity and functional recovery after treatment of stroke with multipotent mesenchymal stromal cells in rats via transfer of exosome-enriched extracellular particles. Stem Cells **31**(12), 2737–2746 (2013)
16. M.A. Lopez-Verrilli, F. Picou, F.A. Court, Schwann cell-derived exosomes enhance axonal regeneration in the peripheral nervous system. Glia **61**(11), 1795–1806 (2013)
17. A.D. Pusic, K.M. Pusic, B.L. Clayton, R.P. Kraig, IFNγ-stimulated dendritic cell exosomes as a potential therapeutic for remyelination. J. Neuroimmunol. **266**(1), 12–23 (2014)
18. K. Yuyama, H. Sun, S. Sakai, S. Mitsutake, M. Okada, H. Tahara et al., Decreased amyloid-β pathologies by intracerebral loading of glycosphingolipid-enriched exosomes in Alzheimer model mice. J. Biol. Chem. **289**(35), 24488–24498 (2014)
19. R.C. Lai, F. Arslan, M.M. Lee, N.S.K. Sze, A. Choo, T.S. Chen et al., Exosome secreted by MSC reduces myocardial ischemia/reperfusion injury. Stem Cell Res. **4**(3), 214–222 (2010)
20. F. Arslan, R.C. Lai, M.B. Smeets, L. Akeroyd, A. Choo, E.N. Aguor et al., Mesenchymal stem cell-derived exosomes increase ATP levels, decrease oxidative stress and activate PI3K/Akt pathway to enhance myocardial viability and prevent adverse remodeling after myocardial ischemia/reperfusion injury. Stem Cell Res. **10**(3), 301–312 (2013)
21. R.C. Lai, R.W.Y. Yeo, K.H. Tan, S.K. Lim, Mesenchymal stem cell exosome ameliorates reperfusion injury through proteomic complementation. Regen. Med. **8**(2), 197–209 (2013)
22. L. Chen, Y. Wang, Y. Pan, L. Zhang, C. Shen, G. Qin et al., Cardiac progenitor-derived exosomes protect ischemic myocardium from acute ischemia/reperfusion injury. Biochem. Biophys. Res. Commun. **431**(3), 566–571 (2013)
23. L. Barile, V. Lionetti, E. Cervio, M. Matteucci, M. Gherghiceanu, L.M. Popescu et al., Extracellular vesicles from human cardiac progenitor cells inhibit cardiomyocyte apoptosis and improve cardiac function after myocardial infarction. Cardiovasc. Res. **103**(4), 530–541 (2014)
24. J.M. Vicencio, D.M. Yellon, V. Sivaraman, D. Das, C. Boi-Doku, S. Arjun et al., Plasma exosomes protect the myocardium from ischemia-reperfusion injury. J. Am. Coll. Cardiol. **65**(15), 1525–1536 (2015)

25. H. Zhang, M. Xiang, D. Meng, N. Sun, S. Chen, Inhibition of myocardial ischemia/reperfusion injury by exosomes secreted from mesenchymal stem cells. Stem Cells Int. **2016**, 8 (2016)
26. H. Gomez, C. Ince, D. De Backer, P. Pickkers, D. Payen, J. Hotchkiss et al., A unified theory of sepsis-induced acute kidney injury: inflammation, microcirculatory dysfunction, bioenergetics and the tubular cell adaptation to injury. Shock **41**(1), 3 (2014)
27. M. Morigi, B. Imberti, C. Zoja, D. Corna, S. Tomasoni, M. Abbate et al., Mesenchymal stem cells are renotropic, helping to repair the kidney and improve function in acute renal failure. J. Am. Soc. Nephrol. **15**(7), 1794–1804 (2004)
28. M. Morigi, M. Introna, B. Imberti, D. Corna, M. Abbate, C. Rota et al., Human bone marrow mesenchymal stem cells accelerate recovery of acute renal injury and prolong survival in mice. Stem Cells **26**(8), 2075–2082 (2008)
29. F. Tögel, K. Weiss, Y. Yang, Z. Hu, P. Zhang, C. Westenfelder, Vasculotropic, paracrine actions of infused mesenchymal stem cells are important to the recovery from acute kidney injury. Am. J. Physiol. Renal. Physiol. **292**(5), F1626–F1635 (2007)
30. B. Bi, R. Schmitt, M. Israilova, H. Nishio, L.G. Cantley, Stromal cells protect against acute tubular injury via an endocrine effect. J. Am. Soc. Nephrol. **18**(9), 2486–2496 (2007)
31. B. Imberti, M. Morigi, S. Tomasoni, C. Rota, D. Corna, L. Longaretti et al., Insulin-like growth factor-1 sustains stem cell–mediated renal repair. J. Am. Soc. Nephrol. **18**(11), 2921–2928 (2007)
32. V. Cantaluppi, L. Biancone, G.M. Romanazzi, F. Figliolini, S. Beltramo, F. Galimi et al., Macrophage stimulating protein may promote tubular regeneration after acute injury. J. Am. Soc. Nephrol. **19**(10), 1904–1918 (2008)
33. A. Ranghino, S. Bruno, B. Bussolati, A. Moggio, V. Dimuccio, M. Tapparo et al., The effects of glomerular and tubular renal progenitors and derived extracellular vesicles on recovery from acute kidney injury. Stem Cell Res. Ther. **8**(1), 24 (2017)
34. S. Bruno, C. Grange, M.C. Deregibus, R.A. Calogero, S. Saviozzi, F. Collino et al., Mesenchymal stem cell-derived microvesicles protect against acute tubular injury. J. Am. Soc. Nephrol. **20**(5), 1053–1067 (2009)
35. S. Gatti, S. Bruno, M.C. Deregibus, A. Sordi, V. Cantaluppi, C. Tetta et al., Microvesicles derived from human adult mesenchymal stem cells protect against ischaemia–reperfusion-induced acute and chronic kidney injury. Nephrol. Dial. Transplant. **26**, 1474–1483 (2011)
36. Y. Zhou, H. Xu, W. Xu, B. Wang, H. Wu, Y. Tao et al., Exosomes released by human umbilical cord mesenchymal stem cells protect against cisplatin-induced renal oxidative stress and apoptosis in vivo and in vitro. Stem Cell Res. Ther. **4**(2), 34 (2013)
37. G. Zhang, D. Wang, S. Miao, X. Zou, G. Liu, Y. Zhu, Extracellular vesicles derived from mesenchymal stromal cells may possess increased therapeutic potential for acute kidney injury compared with conditioned medium in rodent models: A meta-analysis. Exp. Ther. Med. **11**(4), 1519–1525 (2016)
38. D. Burger, J.L. Viñas, S. Akbari, H. Dehak, W. Knoll, A. Gutsol et al., Human endothelial colony-forming cells protect against acute kidney injury: role of exosomes. Am. J. Pathol. **185**(8), 2309–2323 (2015)
39. J.L. Viñas, D. Burger, J. Zimpelmann, R. Haneef, W. Knoll, P. Campbell et al., Transfer of microRNA-486-5p from human endothelial colony forming cell–derived exosomes reduces ischemic kidney injury. Kidney Int. **90**(6), 1238–1250 (2016)
40. X. Zhang, X. Yuan, H. Shi, L. Wu, H. Qian, W. Xu, Exosomes in cancer: small particle, big player. J. Hematol. Oncol. **8**(1), 83 (2015)
41. T. Lener, M. Gimona, L. Aigner, V. Börger, E. Buzas, G. Camussi et al., Applying extracellular vesicles based therapeutics in clinical trials–an ISEV position paper. J. Extracell Vesicles **4**(1), 30087 (2015)
42. G. Raposo, H.W. Nijman, W. Stoorvogel, R. Liejendekker, C.V. Harding, C.J. Melief et al., B lymphocytes secrete antigen-presenting vesicles. J. Exp. Med. **183**(3), 1161–1172 (1996)

43. M.A. Morse, J. Garst, T. Osada, S. Khan, A. Hobeika, T.M. Clay et al., A phase I study of dexosome immunotherapy in patients with advanced non-small cell lung cancer. J. Transl. Med. **3**(1), 1 (2005)
44. B. Escudier, T. Dorval, N. Chaput, F. André, M.-P. Caby, S. Novault et al., Vaccination of metastatic melanoma patients with autologous dendritic cell (DC) derived-exosomes: results of the first phase I clinical trial. J. Transl. Med. **3**(1), 1 (2005)
45. B. Besse, M. Charrier, V. Lapierre, E. Dansin, O. Lantz, D. Planchard et al., Dendritic cell-derived exosomes as maintenance immunotherapy after first line chemotherapy in NSCLC. Oncoimmunology **5**(4), e1071008 (2016)
46. J. Wolfers, A. Lozier, G. Raposo, A. Regnault, C. Théry, C. Masurier et al., Tumor-derived exosomes are a source of shared tumor rejection antigens for CTL cross-priming. Nat. Med. **7** (3), 297–303 (2001)
47. E.J. Ekström, C. Bergenfelz, V. von Bülow, F. Serifler, E. Carlemalm, G. Jönsson et al., WNT5A induces release of exosomes containing pro-angiogenic and immunosuppressive factors from malignant melanoma cells. Mol. Cancer **13**(1), 88 (2014)
48. P. Altevogt, N.P. Bretz, J. Ridinger, J. Utikal, V. Umansky, Novel insights into exosome-induced, tumor-associated inflammation and immunomodulation. Semin Cancer Biol. **28**, 51–57 (2014)
49. M. Adams, H. Navabi, D. Croston, S. Coleman, Z. Tabi, A. Clayton et al., The rationale for combined chemo/immunotherapy using a Toll-like receptor 3 (TLR3) agonist and tumour-derived exosomes in advanced ovarian cancer. Vaccine **23**(17), 2374–2378 (2005)
50. S. Dai, D. Wei, Z. Wu, X. Zhou, X. Wei, H. Huang et al., Phase I clinical trial of autologous ascites-derived exosomes combined with GM-CSF for colorectal cancer. Mol. Ther. **16**(4), 782–790 (2008)
51. L. Lugini, S. Cecchetti, V. Huber, F. Luciani, G. Macchia, F. Spadaro et al., Immune surveillance properties of human NK cell-derived exosomes. J. Immunol. **189**(6), 2833–2842 (2012)
52. T. Ishida, H. Kiwada, Accelerated blood clearance (ABC) phenomenon upon repeated injection of PEGylated liposomes. Int. J. Pharm. **354**(1), 56–62 (2008)
53. X. Xu, W. Ho, X. Zhang, N. Bertrand, O. Farokhzad, Cancer nanomedicine: from targeted delivery to combination therapy. Trends. Mol. Med. **21**(4), 223–232 (2015)
54. A. Akbarzadeh, R. Rezaei-Sadabady, S. Davaran, S.W. Joo, N. Zarghami, Y. Hanifehpour et al., Liposome: classification, preparation, and applications. Nanoscale Res. Lett. **8**(1), 102 (2013)
55. K.B. Knudsen, H. Northeved, P.K. Ek, A. Permin, T. Gjetting, T.L. Andresen et al., In vivo toxicity of cationic micelles and liposomes. Nanomedicine **11**(2), 467–477 (2015)
56. K.B. Johnsen, J.M. Gudbergsson, M.N. Skov, L. Pilgaard, T. Moos, M. Duroux, A comprehensive overview of exosomes as drug delivery vehicles—endogenous nanocarriers for targeted cancer therapy. Biochim. Biophys. Acta **1846**(1), 75–87 (2014)
57. S.M. van Dommelen, P. Vader, S. Lakhal, S. Kooijmans, W.W. van Solinge, M.J. Wood et al., Microvesicles and exosomes: opportunities for cell-derived membrane vesicles in drug delivery. J. Control Release. **161**(2), 635–644 (2012)
58. S.C. Jang, O.Y. Kim, C.M. Yoon, D.-S. Choi, T.-Y. Roh, J. Park et al., Bioinspired exosome-mimetic nanovesicles for targeted delivery of chemotherapeutics to malignant tumors. ACS Nano. **7**(9), 7698–7710 (2013)
59. Y. Tian, S. Li, J. Song, T. Ji, M. Zhu, G.J. Anderson et al., A doxorubicin delivery platform using engineered natural membrane vesicle exosomes for targeted tumor therapy. Biomaterials **35**(7), 2383–2390 (2014)
60. X. Zhuang, X. Xiang, W. Grizzle, D. Sun, S. Zhang, R.C. Axtell et al., Treatment of brain inflammatory diseases by delivering exosome encapsulated anti-inflammatory drugs from the nasal region to the brain. Mol. Ther. **19**(10), 1769–1779 (2011)
61. H. Choi, Y.-S. Lee, D.W. Hwang, D.S. Lee, Translational radionanomedicine: a clinical perspective. Eur. J. Nanomed. **8**(2), 71–84 (2016)

62. A. Nikolopoulou, A. Amor-Coarasa, T. Wuestemann, I. Matei, A. Hoshino, S. DiMagno et al., Tumor exosomes as molecular probes to detect breast cancer pre-metastatic niches: radiolabeling with I-131 and tissue uptake studies in "naïve" nude mice. J. Nucl. Med. **57** (supplement 2), 524 (2016)
63. S. Vallabhajosula, D. Lyden, H.P. Selgas, A. Nikolopoulou, Radiolabeled exosomes for the early detection of metastases and to predict breast cancer premetastatic niche: Annual rept. 1 Aug 2014–31 Jul 2015 Cornell University Medical Coll
64. D.S. Lee, C. Hongyoon, Y.S. Lee, J.M. Jeong, Y.S Gho, S.C. Jang SC, Method for labeling exosomes with radioactive substance and use thereof. Google Patents, 2015
65. Y. Takahashi, M. Nishikawa, H. Shinotsuka, Y. Matsui, S. Ohara, T. Imai et al., Visualization and in vivo tracking of the exosomes of murine melanoma B16-BL6 cells in mice after intravenous injection. J. Biotechnol. **165**(2), 77–84 (2013)
66. T. Imai, Y. Takahashi, M. Nishikawa, K. Kato, M. Morishita, T. Yamashita et al., Macrophage-dependent clearance of systemically administered B16BL6-derived exosomes from the blood circulation in mice. J. Extracell Vesicles **4**(1), 26238 (2015)
67. V. Hornung, F. Bauernfeind, A. Halle, E.O. Samstad, H. Kono, K.L. Rock et al., Silica crystals and aluminum salts activate the NALP3 inflammasome through phagosomal destabilization. Nat. Immunol. **9**(8), 847–856 (2008)
68. O.P. Wiklander, J.Z. Nordin, A. O'Loughlin, Y. Gustafsson, G. Corso, I. Mäger et al., Extracellular vesicle in vivo biodistribution is determined by cell source, route of administration and targeting. Extracell Vesicles **4**(1), 26316 (2015)

Part III
Surface Modification and Radiolabeling

In this part, the readers will browse the general concept of surface modification of nanomaterials. One of the modification will be the chelator conjugation on the surface of nanomaterials for later radiolabeling. In the later radiolabeling, radionuclides such as ^{68}Ga, ^{64}Cu, ^{89}Zr, ^{111}In, ^{90}Y, ^{177}Lu, and ^{188}Re are chelated and thus chelators join the group of surface modifiers. Surface should be modified at first with hydrophilizer, targeting ligands and chelator and thus we need at least three different modifiers conjugated with the surface of the nanomaterials. Chelator will add one step more and chemical conjugation was tried but not with such high yield and the optimization of modification reaction was found to be difficult. Solutions for this problem were pursued in various ways, such as trying core labeling or sincere optimization of the chemical stepped procedures of modification. Physical labeling methods were introduced and cast a great prospect of simultaneous multiplex labeling. Simply speaking, the composition of proper micelle was the critical step and the following violent mixing and separation was an easy addition to finalize the radiolabeling.

By understanding the desired procedures which should be optimized for each nanomaterials and radionuclides, physical labeling is recommended and the readers are recommended to see that there are disadvantages in devising the meticulous and laborious sequential labeling methods for surface modification as well as radiolabeling and understanding what procedures are being developed as template procedures of choice. Further optimization is to be validated and the further investigations are warranted.

Chapter 10
Surface Modification of Radionanomedicine

Daiqin Chen and Hao Hong

Abstract Various radioactive nanomaterials (radionanomaterials) have been successfully utilized as radionanomedicines, particularly in the field of nuclear imaging and radiation therapy. Surface modification is one of the most critical steps during the fabrication of radionanomedicines. Proper surface modification can bring multiple benefits to radioisotopes-loaded nanomaterials, which include, but not limited to, material disparity/stability improvement, in vivo pharmacokinetics optimization, adjustment of interactions with biomolecules, incorporation of diagnostic or tissue targeting moieties, addition of new material property (e.g. stimuli responsiveness), among many others. In this chapter, we tried to give a brief illustration on how various surface modification strategies can be accomplished for specific nanomaterials, and provide comments on the advantages and limitations of each strategy. By the most straightforward categorization, the surface modification can be achieved via either chemical reactions (covalent coupling) or physical interactions (usually forming noncovalent binding). Each surface modification method can work synergistically with each other to generate theranostic radionanomaterials with more attractive characteristics. In the end, different previous representative research reports were given as examples to confirm how these strategies could be used in surface modification of nanomaterials from different categories.

D. Chen · H. Hong (✉)
Department of Radiology, Center for Molecular Imaging, University of Michigan, Ann Arbor, MI 48109-2200, USA
e-mail: hahong@med.umich.edu

D. Chen
e-mail: chendychin@gmail.com

D. S. Lee (ed.), *Radionanomedicine*, Biological and Medical Physics, Biomedical Engineering, https://doi.org/10.1007/978-3-319-67720-0_10

10.1 General Comments on Surface Modification

Surface modification is extremely important for radionanomedicine. In order for radionanomaterials to be used as effective 'nanomedicines' in vivo, various surface modification strategies were taken with three primary purposes: improving their stability (and biocompatibility), optimizing in vivo pharmacokinetics, and incorporating extra diagnostic and/or disease-targeting moieties (Fig. 10.1).

Since quite some nanomaterials (especially inorganic nanomaterials) were originally dispersed in organic solvents (e.g. hexadecane) post direct synthesis [1], surface modification with various surfactants will be necessary before they can be transferred into an aqueous phase for further applications. Without proper surface coating, most nanomaterials (especially those with pristine hydrophobic surfaces) tend to agglomerate into large clusters from the hydrophobic interactions or Van der Vaals force [2]. Even for nanomaterials with good inherent aqueous dispersity (mostly organic nanomaterials), surface engineering can be beneficial for maintaining their structural integrity. Popular candidates for surface coating of nanomaterials include synthetic polymeric molecules [e.g. polyethylene glycol (PEG)] [3], small molecules [4], and various macromolecules such as proteins [5], lipids [6], or polysaccharides [7]. Another popular approach is to form an extra nano-sized layer (e.g. with silica or noble metals [8]) outside the original material core

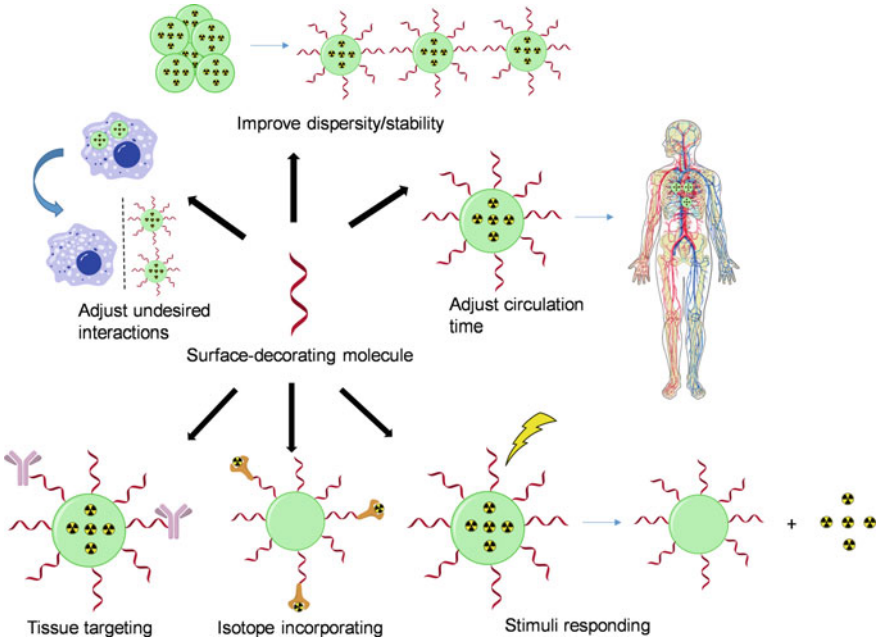

Fig. 10.1 Example goals of radionanomaterial surface modification

(core-shell structure). More specifically for radionanomaterials, surface modification can stabilize the radioisotope cargo(s) loaded on the given nanomaterial [9].

Surface coating can also determine how radionanomaterials interact with biological environments [10]. After administration in vivo, radionanomaterials usually face the interaction and adsorption of encountered molecules, including ions, lipids, saccharides, and particularly proteins [11], all of which can form 'corona' on the surface of radionanomaterials [12]. This 're-coating' of radionanomaterials is mediated by electrostatic interactions, hydrogen bonding, hydrophobic interactions, or Van der Waals force [13]. Thus, proper surface engineering of radionanomaterials can be crucial to tune the interactions (e.g. reduce undesired ones) between them and those biological molecules. For instance, by adjusting the surface properties (e.g. charges), radionanomaterials can have higher escape rate from phagocyte system, lower adsorption onto plasma proteins, or more specific accumulation into given cell populations [14]. Additionally, surface coating agents such as PEG can be very useful to regulate the residence time of radionanomaterials in vivo [10, 15]. Thus, surface properties of radionanomaterials contribute directly to their in vivo toxicity [16].

Various biomolecules, e.g. peptides, antibodies, proteins etc., can be attached to the surface of radionanomaterials relying on the proper surface modification [17, 18]. The incorporation of these molecules (termed "targeting ligands") can facilitate the trafficking of radionanomaterials more efficiently into the target tissue. Despite the fact that nanomaterials can possess the well-known enhanced permeability and retention (EPR) effect and accumulate in tissues with disrupted/irregular vasculature structures (e.g. passive targeting in tumor) [19], tissue permeability can vary significantly even within the same individual. Thus, these biomolecules enable radionanomaterials to undergo ligand-directed cell targeting and tissue microenvironment targeting. An important consideration during the targeting ligand conjunction is that the targeting moieties should be avoided to bury in the protein 'corona' when administered in vivo. Also, the ligand molecule numbers on nanomaterial surface should be carefully investigated since previous studies have revealed that high-density surface ligands can accelerate the clearance of nanomaterials and compromise their targeting efficiency [20]. Thus, optimizing the ligand number on radionanomaterials does not indicate just increasing the ligand number per nanomaterial. On the other hand, biomolecules like cell-penetrating peptides (CPPs) can enhance the general cell permeability of nanomaterials [21]. CPPs can facilitate nanoparticle internalization to various types of cells and are especially useful to deliver nanomaterials otherwise impermeable for given cell types [22].

Surface modification is sometimes important to bring radioisotopes into nanomaterials. In those scenarios, radioisotopes were actually incorporated into the surface coating molecules (or extra surface modification layer) [23]. This strategy is particularly suitable when the isotopes loaded on nanomaterials have a relatively short physical half-life (e.g. ^{18}F (118 min), ^{99m}Tc (6 h), etc.). One obvious limitation of this method is that the stability of surface coating becomes the limiting factor for the overall efficacy of radionanomedicines. However, compared with

embedding isotopes into structure of nanomaterials, this method is fast, cost-effective, and with the lowest technical difficulties.

Another important goal for surface modification is to incorporate new functions into radionanomaterials, e.g. stimuli-responsiveness. To date, selective coating of nanomaterials with proper polymer molecules can bring tunable degradability [24], and selective cargo release (e.g. loaded drugs or therapeutic isotopes) triggered by a variety of stimuli including pH, heat, redox status, or enzymes [25–29]. These properties can assist more accurate control of radionanomaterials to be used as radionanomedicines.

Judging from these facts, how to choose the right surface modification method/molecules for the right nanomaterials is very important and we predict that it will continue to be a hot research area. The ideal molecules for surface modification of radionanomaterials should preferably be biocompatible and biodegradable. Also, these molecules should possess good affinity for the chosen radionanomaterials and cause minimal response by the immune system [30, 31]. The decay half-life of isotopes in radionanomaterials is usually not very long, thus the surface modification procedure should be adequately fast to prevent the isotopes from significant decay loss. In the following section, we will discuss various strategies already used for radionanomaterial surface modification.

10.2 Strategies for Radionanomedicine Surface Modification

Generally there are two categories of methods for surface modification—chemical reaction (covalent coupling) and physical interactions (Fig. 10.2). It is usually hard to use only single strategy during the radionanomaterial surface modification, thus in this section we will only provide a brief discussion on the basic rules in each strategy. In Sect. 10.3, we will give representative examples for radionanomaterial surface modification.

10.2.1 Chemical Reaction (Covalent Coupling)

There are four popular chemical groups on material surface which can be used to attach surface-coating molecules: amine (e.g. reactable with e.g. from polyacrylic acid (PAA), carboxymethylcellulose, PEG with –COOH terminal etc.), carboxylic (e.g. reacting with polyethylenimine (PEI), poly(L-lysine), PEG with $–NH_2$ terminal etc.), thiol (e.g. reacting with maleimide-bearing macromolecules etc.), and hydroxyl groups [32]. Among those surface groups, hydroxyl group is quite unique since it can react with carboxyl group on decorating molecules or cargo molecules (e.g. anti-cancer drug) to form ester bond, which can be used for either controlled

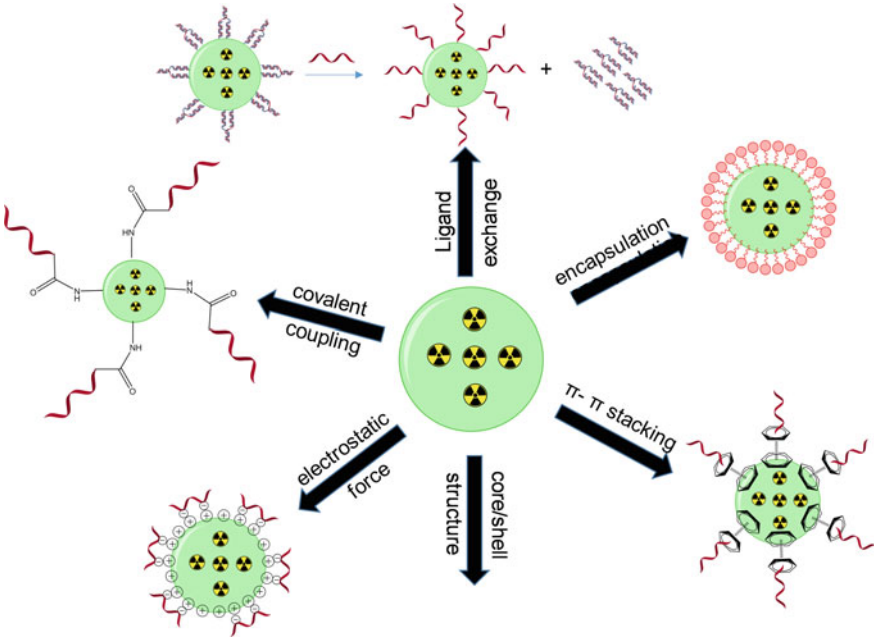

Fig. 10.2 Representative surface modification strategies for radionanomaterials

cargo release or pH-controllable surface property/size change [33]. The carboxylic-amine reaction (resultant amide bond) or thiol-involved reaction (e.g. with maleimide) can usually result in chemical bonds with satisfactory in vivo stability, thus they are commonly adopted in surface modification of various inorganic/organic nanomaterials [32, 34]. Post the initial surface coating, click chemistry is another dominant approach for further surface modification [35]. The most popular reactions include azide-alkyne cycloaddition (copper catalyzed or strain promoted), the inverse electron demand Diels-Alder cycloaddition [e.g. between tetrazine (Tz) and trans-cyclooctene (TCO)], or more rarely, the Staudinger ligation. These chemical modification methods are usually fast, in very high chemical yields, and the product separation is relatively simple.

Another unique surface reaction is based on coverage of original nanomaterials in silica. Afterwards, silane coupling agents can be used for surface modification [8] since the silica shell usually has abundant silanol groups on the surface [36]. These agents usually have bifunctional structures with one end attached to the silica shell (via reaction with silanol groups) while the other end can provide reaction sites for conjugation of other molecules. For example, metalloporphyrins were successfully immobilized onto the surface of silica-coated iron oxide particles using this method and click chemistry [37].

An underexplored area for surface modification is to use enzyme-mediated reaction. Especially when sensitive peptide or protein ligands were attempted to

attach onto the surface of radionanomaterials. For example, sortase A was used to functionalize the surface of different protein-derived nanomaterials for catalysis, sensing, or imaging applications [38]. More recently, this method was used to produce a nano-vaccine platform by effective antigen coupling onto virus nanoparticles [39]. To date, there is only very limited report using this surface modification strategy for radionanomaterials. One example is that furin was used to control the condensation and self-assembly of a benzothiazole-derived nanoparticle and facilitate the incorporation of ^{18}F onto the surface of this nanoparticle [40].

When we use chemical reaction to modify radionanomaterial surface, the choice of agents and reaction condition should be very careful. The basic rules should include: (1) the structural integrity of radionanomaterials should be mostly maintained post reaction (including the property and quantity of loaded isotopes inside), (2) the reaction should be fast, efficient, and environment friendly, (3) separation of the resultant modified radionanomaterials from the reactants should be relatively simple, and (4) the obtained surface-modified radionanomaterial should be sufficiently biocompatible.

10.2.2 Physical Interaction

Surface modification from physical interactions between nanomaterials and decorating molecules has several advantages. First, these methods usually can maintain the physiochemical and structural properties of original nanomaterials to a better extent compared with chemical reaction methods. Also, the overall stability of modified nanomaterials from these methods is adequate for most biomedical applications. In addition, some biomolecules (e.g. nucleic acids) can be loaded effectively onto nanomaterial surface without tedious chemical reaction/purification and can also be unloaded at the desired location afterwards [41].

10.2.2.1 Ligand Exchange/Replacement

Utilization of molecules which can replace the initial surface coating during the synthesis has been a well-accepted approach for surface modification of inorganic radionanomaterials [42]. Usually small hydrodynamic size can be maintained using this strategy. For example, up-conversional nanoparticles (UCNPs) are usually obtained with oleic acid (OA) as the 'capping' agent, while OA can be further exchanged by a diversity of hydrophilic molecules [43]. These replacement ligand molecules are composed by two portions—anchoring part which has strong affinity for nanomaterial surface [e.g. thiols/disulfides/amines/phosphines for noble metal nanoparticles or quantum dots (QD)], and stability/functional part which can bestow the nanomaterial with satisfactory colloidal stability as well as provide functionalization site for attachment of other molecules [44]. The stability/functional part can also determine the molecular adsorption in vivo.

10.2.2.2 Encapsulation

More frequently for inorganic nanomaterials, lipid or surfactants can coat their surface to form bilayers or micelles to encapsulate those materials. The hydrophobic tails of these molecules can form relatively stable interaction with hydrophobic nanomaterial surface (e.g. pristine carbon nanotubes) or initial surface coatings. The surface of nanomaterials can be further modified based on the terminal active groups from lipid/surfactant coating. For effective incorporation of lipid/surfactant, two leading strategies, i.e. lipid film hydration and microemulsion methods [45, 46], were actively adopted. The film hydration method usually involves the mixture of nanomaterial and lipid/surfactant in an organic solvent, while the solvent is subsequently evaporated with the addition of aqueous solution (e.g. water) [47, 48]. On the other hand, the microemulsion method is to add aqueous surfactant solution into nanomaterial-containing organic solvent (with vigorous stirring) and form an oil-in-water microemulsion. Later, organic solvent will be evaporated to facilitate both the interaction of lipid/surfactant-nanomaterial and the transfer of nanomaterial into the aqueous phase [49]. Nanomaterials post encapsulation usually possess improved stability and functionality, which makes it easier for further modification. More recently, to further increase nanomaterial biocompatibility, natural cell membrane was also used as a vesicle to encapsulate/functionalize various nanomaterials [50].

10.2.2.3 π–π Interaction/Stacking

Utilization of π–π interaction/stacking is one of the most efficient method for nanomaterials with electron-rich aromatic components inside the structure (e.g. graphene, carbon nanotubes etc.) [51]. For example, pyrene-derived PEG molecules can be used for surface engineering of carbon nanotubes [52], and more recently, nano-sized metal organic framework (MOF) containing 1,4-benzenedicarboxylate (BDC) as the bridging molecules inside the structure [53]. The in vivo pharmacokinetics of modified nanomaterials are satisfactory from these studies.

10.2.2.4 Electrostatic Interaction

Electrostatic interaction (complexation) stands as an alternative to chemical conjugation for nanomaterials bearing strong surface charges [54]. For example, in one study, bovine serum albumin (BSA), which bears negative charges on surface, was used to form strong interaction with cetyltrimethylammonium bromide (CTAB) on gold nanoparticle surface to neutralize the toxicity from CTAB [55]. Another example is that sodium thioglycolate was covered onto the surface of gold nanoparticles to increase their interaction with neutral red [56].

10.2.2.5 Core/Shell Structure Formation

As discussed previously, an extra layer of 'nano-shell' can be formed onto radionanomaterials to facilitate further surface engineering, especially when the stability of initial radionanomaterials is not very ideal. In a very interesting recent study, a protective gold shell was grown on ^{124}I-labeled gold nanoparticles and the core/shell structured nanoplatform was used for in vivo tracking of dendritic cells [9]. Similar strategy was adopted by the same research group in another study for visualization of macrophage recruitment in an inflammation model [57]. The whole radiolabeling and shell growth cost less than 30 min.

Compared with covalent conjugation method, the most dominant limitation of physical interaction-based surface modification methods is that the overall stability is lower. Also, other physical interaction forces, such as hydrogen bond [58], or coordination bond [59], can also be readily useful for material surface engineering.

10.3 Examples for Radionanomedicine Surface Modification

10.3.1 Inorganic Nanomaterials

In this section, we listed several representative categories of inorganic nanomaterials, which include silica nanomaterials, carbon nanomaterials (graphene as examples), and metal (oxide) nanomaterials [17, 32]. From these examples, we can have a better understanding about how the methods discussed in Sect. 10.2 can be properly used in the previous research reports.

10.3.1.1 Silica-Based Nanomaterials

Silica nanomaterials, especially mesoporous silica nanoparticles (MSNs), were considered as important drug delivery vectors owing to their ultrahigh surface area and good biocompatibility [60]. As stated previously, the most frequently adopted method for surface modification is the usage of silane coupling agents [8]. The pristine silica nanomaterials usually have abundant silanol groups on the surface, which can cause the irregular agglomeration of silica nanomaterials via the hydrogen bonding [36]. These agents usually have bifunctional structures with one end attached to the silica nanomaterials (via reaction with silanol groups) while the other end can provide reaction sites for biomolecule conjugation.

In an early study, MSNs were functionalized with 3-aminopropyltriethoxysilane (APTES) for incorporation of amine groups on the surface, after which DOTA-NHS was reacted with surface NH_2 for subsequent ^{64}Cu labeling [61]. As expected, the MSNs still tend to aggregate in vivo (judging by potent accumulation

in the spleen). Further studies incorporated PEG (react with surface amine) to modify MSNs or hollow MSNs (Fig. 10.3a), which eventually achieved very good in vivo stability, where the radioisotopes were incorporated either on the surface (^{64}Cu) or doped inside (^{45}Ti, ^{89}Zr) the silica structure [62–67]. Although silica nanomaterials were usually used as the 'shell' to hold other nano-cores (e.g. gold, CuS, quantum dots (QD) etc.), one recent study revealed that formation of lipid bilayer 'shell' on MSNs can result in prolonged cargo retention and lower premature cargo leakage [68], and this strategy may be readily useful for silica-based radionanomaterials in the future, despite that further validation is still needed.

10.3.1.2 Nano-graphene Derivatives

Although there are various types of carbon nanomaterials [69], here we chose nano-graphene derivatives as the example since their surface modification method

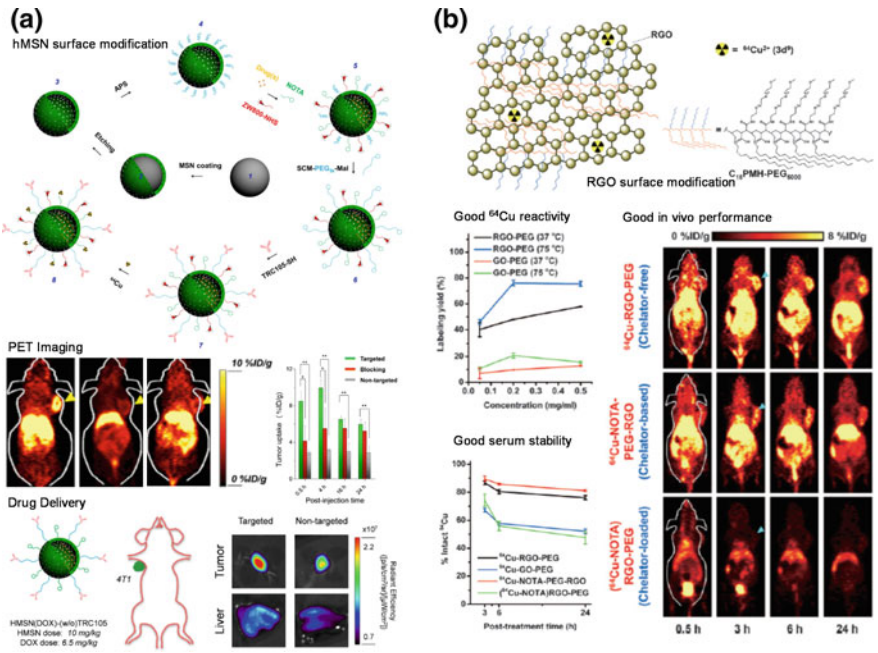

Fig. 10.3 Covalent and noncovalent surface modification of inorganic radionanomaterials. **a** Surface modification of hMSN via covalent PEGylation. Post covalent PEGylation the antibody ligand against tumor neovasculature was also attached, demonstrating good in vivo tumor targeting efficacy, also the surface-engineered hMSN can serve as a good in vivo drug delivery vector. Adapted with permission from [66]. **b** Surface modification of RGO via noncovalent C_{18}PMH-PEGylation. Satisfactory radiolabeling yield, serum stability, and in vivo performance were all observed. hMSN: hollow mesoporous silica nanoparticle, RGO: reduced graphene oxide. Adapted with permission from [77]

is very representative, which can be readily applicable in other carbon nanomaterials. Functionalized nano-graphene derivatives have attracted continuous attention in biomedical applications [70]. Generally, graphene derivatives have two primary chemical components—graphene oxide (GO) and reduced graphene oxide (rGO). To conduct surface modification with more biocompatible polymers (mostly PEG), GO can react with amine-containing molecules due to the abundant oxygen-containing groups (e.g. carboxyl, hydroxyl, or ketone moieties) on surface [70]. In a recent study, the investigators indicated that PAA functionalization of graphene oxide may be superior to PEGylation in terms of biocompatibility in vivo [71]. On the other hand, rGO derivatives possess much scarce oxygen-containing groups, the surface engineering is usually achieved via π–π interactions with their aromatic structure.

Surface modification of graphene-based nanomaterials has been thoroughly discussed in a recent review article [72]. Amine-containing branched PEG molecules can be a frequent option for GO surface decoration. Post this modification, various radiometals (e.g. ^{64}Cu or ^{66}Ga)—labeled nano-GO was used for targeting of both primary and metastatic breast tumors in murine models [73–75]. In an early study, trastuzumab (against HER2 receptor) was directly conjugated onto nano-GO via amide bonding without PEGylation, and benzyl- diethylenetriaminepentaacetic acid (BnDTPA) was loaded onto GO via π–π stacking for further labeling with ^{111}In [76]. A surprisingly high uptake was achieved in HER-2 positive tumor (~15% injection dose per gram, %ID/g at 72 h post-injection with a tumor-to-muscle of 7:1) from this study, and despite that the liver uptake was high, the accumulation of ^{111}In-GO-trastuzumab in spleen was not high, proving that direct surface engineering of GO with biomolecules like antibodies was also acceptable for their in vivo applications. On the other hand, C_{18}PMH-PEG is one of the star molecules for rGO surface functionalization. Very recently, rGO was proved to possess strong interaction with ^{64}Cu via metal-π electron interactions, and this chelator-free labeled ^{64}Cu-rGO-PEG was confirmed to have good stability in vivo along with tumor-homing properties (Fig. 10.3b) [77], while ^{64}Cu was previously labeled onto NOTA molecules attached on C_{18}PMH-PEG [78]. In some situation, when rGO was complexed with other nanomaterials, e.g. iron oxide nanoparticles, covalent PEGylation could be achieved onto the surface of 'loaded' nanomaterials [79].

10.3.1.3 Metal-Based Nanomaterials

Metal-based or metal-containing nanomaterials represents one of the largest family within the inorganic nanomaterials, and representative examples include (but not limited to) noble metal-based (e.g. gold) nanomaterials [80], quantum dots [81], upconversion nanoparticles (UCNPs) [82], zinc oxide (ZnO) nanomaterials [83], among many others. Judging from their metal contents, the initial step for metal nanomaterial surface engineering is to use metal-coordinating molecules for interactions. One good example is that thiol-containing molecules (e.g. glutathione) are

versatile tools for surface engineering of those nanomaterials and prepared them for further imaging/therapy applications [84, 85]. Also, as discussed previously, ligand exchange (e.g. OA is replaced by PAA [86] or polyphosphoric acid capping [87]) was frequently adopted for further incorporation of stabilizing/functionalizing molecules. Surface-decorating molecules (e.g. mPEG-grafted poly(L-lysine) [88]) can also be added during the synthetic route to save the extra ligand exchange procedures, and interestingly, it was shown that this method did not bestow advantageous properties to the radionanomaterial, while the overall synthesis yield was considerably lower than the ligand exchange method [88]. Similar to what we have discussed for graphene materials, sometimes disease-targeting molecules (e.g. folate) can be simultaneously used as surface functionalization agent for metal nanomaterials [89]. Proteins like BSA can cover the metal nanomaterial surface via electrostatic interactions (Fig. 10.4a) [90, 91], while silica/gold shell can also be a good starting material for further functionalization of metal nanomaterials (Fig. 10.4b) [57, 92].

Among all the metal-based nanomaterials, supermagnetic iron oxide nanomaterials (SPIONs) process many unique properties and can be exploited in various biomedical applications (e.g. imaging, cargo delivery, biological separation etc.) [93], post appropriate surface engineering. Radioactive SPION was usually modified via the ligand exchange method. In two sequential studies, PAA was used to replace the original oleate coating on SPION surface (incorporated with ^{69}Ge and ^{72}As) and served as a template for further conjugation with PEG [94, 95]. With the

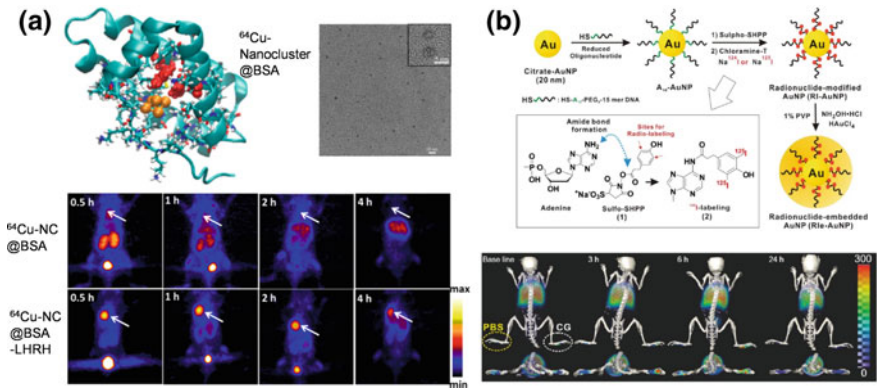

Fig. 10.4 Representative surface modification examples for metal-based radionanomaterials. **a** The structure and size of ^{64}Cu-nanocluster (NC)@BSA. Here BSA was used as the reaction template for synthesis of NC, and it stabilizes NC by both electrostatic interactions and forming a binding pocket for NC. With conjugation of LHRH (tumor targeting) peptide onto BSA, PET findings demonstrated that good accumulation of ^{64}Cu-NC@BSA-LHRH in A549 lung tumors. Adapted with permission from [90]. **b** Extra gold nano-shell was formed onto the ^{124}I-labeled gold nanoparticles and used for macrophage tracking. Significant macrophage migration onto inflammation site was observed from PET imaging starting from 3 h post-injection of carrageenan. PET: positron emission tomography. Adapted with permission from [57]

similar strategy, distearoylphosphotidylethanolamine-PEG (DSPE-PEG) was used to substitute OA to stabilize SPION while simultaneous replacement of OA with dimyristoylphosphatidylethanolamine-DTPA (DMPE-DTPA) enabled the radiolabeling of ^{111}In onto SPION [48]. Porous silica shell was also added onto SPION to attach chelators for ^{64}Cu, potentially useful for PET/MR imaging [23]. Another rare strategy for SPION functionalization is that it can be incorporated between the layers of poly(vinyl alcohol) (PVA) microbubbles via both encapsulation and electrostatic interactions [96], and the resulting SPION-MB was radiolabeled with ^{99m}Tc and successfully used for SPECT/CT and MR imaging.

10.3.2 Organic Nanomaterials

Compared with inorganic nanomaterials, the structural integrity of organic nanomaterials is more susceptible to chemical/physical modifications. Surface engineering for nanomaterials of this type requires more careful consideration. Here we discussed three categories of organic nanomaterials—protein-based (e.g. albumin) nanomaterials, liposomes, and polymeric nanomaterials.

10.3.2.1 Protein Nanoparticles

Despite the fact that the chemical conjugation is time-consuming and requires tedious purification and quality control, and the structure of protein nanoparticles might be disrupted post modification, the majority surface modification strategy for protein nanoparticle is based on chemical conjugation [97, 98], although physical interaction techniques (encapsulation and electrostatic interaction) are sometimes adopted as well [99]. Protein nanoparticles usually bear many residual functional groups (e.g. carboxylic and amine), thus it facilitates the surface modification of albumin nanoparticles via all kinds of chemical conjugation. Covalent bonds are more robust than physical interaction, which avoids the dissociation of the post-modification ligands from protein nanoparticles in vivo [100–102].

For example, high-density lipoprotein (HDL) nanoparticles were chemically conjugated with deferoxamine (DFO) for ^{89}Zr labeling and successfully imaged tumor-associated macrophages (Fig. 10.5a) [103]. The nano-sized capsid protein of bacteriophage MS2 was chemically linked to ^{18}F-fluorobenzaldehyde via tyrosine side chains or 1,4,7,10-tetraazacyclododecane-1,4,7,10-tetraacetic acid (DOTA) for ^{64}Cu labeling [104] and eventually proven useful for tumor imaging by PET. Another unique protein nanomaterial is called protein polymers, usually composed from repetitive amino acid sequences, which can assemble into monodisperse nanoparticles [105]. With site-specific conjugation of sarcophagine chelator AmBaSar, elastin-like polypeptides (ELP)-based protein polymers were radiolabeled with ^{64}Cu for in vivo administration, and several hours of circulation time was observed for these protein polymers [105].

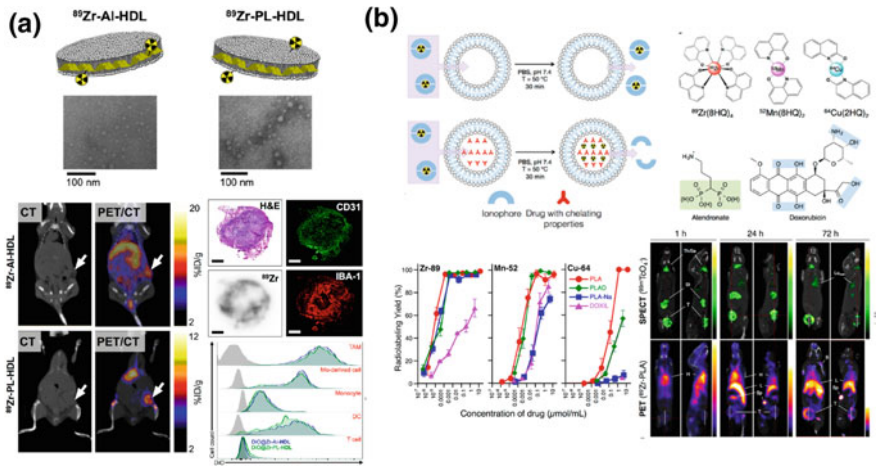

Fig. 10.5 Surface engineering of protein-based nanoparticles and liposomes. **a** HDL-based nanoparticles were radiolabeled with ^{89}Zr covalently. PET imaging, histology analysis, and flow cytometry all confirmed these functionalized HDL nanoparticles can accumulate specifically in tumor-associated macrophages (TAM). Adapted with permission from [103]. **b** The interactions between liposome and radiometals can be adjusted by proper drug cargo loading. With the loading of suitable drug cargo, liposome can be labeled by these radiometals (^{64}Cu/^{52}Mn/^{89}Zr) easily, ready for in vivo cancer imaging. HDL: high-density lipoprotein, PET: positron emission tomography. Adapted with permission from [122]

Albumin-based nanoparticle is another most investigated protein-based nanoparticles that hold many advantages as drug delivery system, such as good biodegradability, excellent biocompatibility, non-immunogenicity [106–108]. Albumins have been widely reported as nanocarriers for the delivery of quite a few of drugs or imaging contrasted agents [109]. Zhou et al. reported size-tunable Gd_2O_3@albumin nanoparticle conjugating chlorin e6 (Ce6) for MRI-guided phototherapy [110]. Hollow albumin was employed as the nanoreactor to control the growth of Gd_2O_3 crystals, whose sizes were well regulated with the reaction time. Next, the protein corona of Gd_2O_3@BSA was functionalized with chlorin e6 through conjugating the carboxylic group on Ce6 with free amine groups in BSA. The obtained Gd_2O_3@albumin nanoparticle conjugating Ce6 nanoparticles demonstrated high photostability, excellent T1 contrast ability and remarkable photothermal and photodynamic property.

The surface modification of protein nanoparticles can introduce functional groups that endow the nanoparticles with targeting property or helps the nanoparticles to cross physiological barriers in vivo. For example, Lin and colleagues reported an albumin-based drug delivery system for the treatment of glioma [111]. The albumin nanoparticle could cross the blood-brain-barrier (BBB) via the mechanism of albumin-binding proteins (SPAC and gp60) pathway. The BBB penetration efficiency was further enhanced by conjugating a cell-penetrating peptide, LMWP, to the surface.

10.3.2.2 Liposomes

Liposome is a spherical vesicle which is composed of one or multiple bilayers [112]. The size of liposome can range from tens of nanometers to several micrometers. Compared with other nanocarriers, liposomes possess many advantages, such as excellent biocompatibility and biodegradability, low toxicity and immunogenicity [113]. Thus, liposomes have been widely investigated as vehicle for chemo drugs and genes since its first description in 1961 [114]. However, one of the most disadvantages is the poor stability. In order to improve their stability and endow liposomes with some new functionality, different strategies have been adopted to modify the surface of liposomes [115, 116]. Unlike protein nanoparticles whose modification is predominantly achieved by chemical reaction, both physical and chemical modification are widely adopted for liposome preparation [117, 118].

Physical functionalization strategies include adsorption with surfactants, coating with polymers and layer-by-layer electrostatic deposition [119]. Huang et al. reported that the formation of elastic liposomes with Tween 80 could greatly improve their stability [120]. The as-prepared liposomes were employed as drug carriers, which could not only protect the encapsulated drug from enzymatic degradation in gastrointestinal fluids, but also successfully deliver the drug to the blood and brain in a sustained manner. As the presence of dipalmitoylphosphatidylcholine (DPPC) and stearyl amine, the liposomes were positively charged and they were easily coated with negatively charged polymeric molecules with high stability. Jain et al. developed polyelectrolyte-coated liposome via layer-by-layer electrostatic deposition for the oral delivery of doxorubicin (DOX) [121]. Stearyl amine containing liposomes were firstly coated with anionic PAA and then the cationic polyallyl amine hydrochloride (PAH) was introduced by a layer-by-layer electrostatic deposition strategy. The obtained liposomes possessed a robust structure after formulation optimization and were used for delivery of DOX. Occasionally, the loaded cargo (e.g. doxorubicin or bisphosphonates) in liposomes can serve as a 'physical attractor and stabilizer' for radioisotopes (e.g. ^{64}Cu/^{52}Mn/^{89}Zr) loading via metal-π electron interactions (Fig. 10.5b) [122, 123]. Another study used liposome to encapsulate folate-conjugated DFO for radiolabeling of ^{89}Zr via ligand exchange [124].

The chemical modification strategies of liposomes could be categorized into pre-modification and post-modification methods. In pre-modification methods, the ingredients were firstly modified with functional molecules (PEG, targeting ligands, or stimuli-responsive linkers) before their self-assembly into liposomes [125, 126] while in post-modification techniques, liposomes were incubated with micelles formed from functional molecules to form functionalized liposomes. Although the pre-modification methods are tedious and difficult for quality control compared with the latter ones, they were more widely adopted to synthesize functional liposomes as this method can maintain the integrity of liposomes to a better extent while the latter method is only applicable in some specific liposome. For example, during the

assembly of liposome, DOTA could be modified onto DSPC while a fluorescence dye was attached onto DSPE along with a PD-1 antibody [127], which makes liposome not only tumor-targeting, but also applicable for both PET and fluorescence imaging. Other metal chelators like NODAGA or DTPA can also be incorporated into DSPE for liposome formation and subsequent labeling with other radiometals (e.g. ^{68}Ga or ^{111}In) [128, 129].

10.3.2.3 Polymeric Nanoparticles

Polymeric nanoparticles, including block copolymer micelles and branched polymeric structures, are widely used as versatile nanomedicine platforms [34, 130]. Their building blocks (dendrimer and block copolymer) are used to form polymeric nanoparticles via either covalent assembly or supramolecular interactions [131]. The modification of polymeric nanoparticles plays important roles in their physiochemical properties, including their sizes, morphologies, stabilities, biocompatibilities, targeting properties and responsive ability to stimuli [45, 132]. Unlike liposomes, the modification of polymeric nanoparticles can take place before (modification on the building blocks) and after (modification on polymeric nanoparticles themselves) the formation of polymeric nanoparticles [133]. Still, the modification on the building blocks is more popular in the synthesis of polymeric nanoparticles.

The building blocks of polymeric micelles are usually amphiphilic and they can form nanoparticles through self-assembly by hydrophobic-hydrophobic interaction in aqueous solution. The hydrophobic core can provide accommodation for lipophilic drugs and the hydrophilic shell impart the nanoparticles with high stability [134]. By simple incorporation of functional groups to the outer shell, the modified polymeric micelle can possess some advantages [15, 135]. For example, Hu and coworkers synthesized core-crosslinked poly (thiolether ester) micelles that could respond to multiple stimuli (reactive oxygen species (ROS), acidic and reductant environment) for smart drug delivery [136]. To increase the stability of micelles, one of the previous studies proposed a concept of unimolecular micelles, in which targeting ligand (RGD), radiometal chelator (NOTA for ^{64}Cu) and PEG were all bound into Boltorn H40 hyperbranched copolymer, for in vivo PET imaging of breast tumors [137].

Dendrimers- or polyester- (e.g. PLGA) based nanomaterials are another important polymeric nanoparticles for biomedical applications [138–140]. The chemical surface engineering of these nanomaterials have been summarized elsewhere [141–143]. Those surface-engineered radionanomaterials can be used for detection of atherosclerotic plaque [144], tumor-targeted gene therapy [145], and detection of ischemia in the living subjects [146].

10.4 Concluding Remarks

Over the past two decades, radionanomaterials have attracted a lot of attentions thus the concept of 'radionanomedicines' is also rapidly formed. Surface engineering is very critical for the quality of radionanomaterials for biomedical applications. There is certainly no single perfect method for successful surface modification of radionanomaterials, but here in this chapter our goal is to categorize these surface modification strategies and illustrate how to prepare these radionanomaterials into multifunctional nanoplatform for theranostic (diagnostic/therapy) applications. A lot of further optimization will still be needed before radionanomaterials can serve as radionanomedicines clinically. We hope that this chapter can provide some insights into future development of new radionanomedicines and possible further optimization of current existing ones.

References

1. S. Hajiw, J. Schmitt, M. Imperor-Clerc, B. Pansu, Solvent-driven interactions between hydrophobically-coated nanoparticles. Soft Matter **11**(19), 3920–3926 (2015)
2. M. Muthiah, I.K. Park, C.S. Cho, Surface modification of iron oxide nanoparticles by biocompatible polymers for tissue imaging and targeting. Biotechnol. Adv. **31**(8), 1224–1236 (2013)
3. A.A. D'Souza, R. Shegokar, Polyethylene glycol (PEG): a versatile polymer for pharmaceutical applications. Expert Opin. Drug Deliv. **13**(9), 1257–1275 (2016)
4. Y. Chen, Y. Xianyu, X. Jiang, Surface modification of gold nanoparticles with small molecules for biochemical analysis. Acc. Chem. Res. **50**(2), 310–319 (2017)
5. X.S. Zheng, P. Hu, Y. Cui, C. Zong, J.M. Feng, X. Wang et al., BSA-coated nanoparticles for improved SERS-based intracellular pH sensing. Anal. Chem. **86**(24), 12250–12257 (2014)
6. L. Liu, X. Li, L. Chen, X. Zhang, Nanoscale functional biomaterials for cancer theranostics. Curr. Med. Chem. (2017) (Epub)
7. A.M. Dias, A. Hussain, A.S. Marcos, A.C. Roque, A biotechnological perspective on the application of iron oxide magnetic colloids modified with polysaccharides. Biotechnol. Adv. **29**(1), 142–155 (2011)
8. S. Shi, F. Chen, W. Cai, Biomedical applications of functionalized hollow mesoporous silica nanoparticles: focusing on molecular imaging. Nanomedicine **8**(12), 2027–2039 (2013)
9. S.B. Lee, S.W. Lee, S.Y. Jeong, G. Yoon, S.J. Cho, S.K. Kim et al., Engineering of radioiodine-labeled gold core-shell nanoparticles as efficient nuclear medicine imaging agents for trafficking of dendritic cells. ACS Appl. Mater. Interfaces **9**(10), 8480–8489 (2017)
10. N. Feliu, D. Docter, M. Heine, P. Del Pino, S. Ashraf, J. Kolosnjaj-Tabi et al., In vivo degeneration and the fate of inorganic nanoparticles. Chem. Soc. Rev. **45**(9), 2440–2457 (2016)
11. T. Cedervall, I. Lynch, S. Lindman, T. Berggard, E. Thulin, H. Nilsson et al., Understanding the nanoparticle-protein corona using methods to quantify exchange rates and affinities of proteins for nanoparticles. Proc. Nat. Acad. Sci. U S A **104**(7), 2050–2055 (2007)

12. M. Neagu, Z. Piperigkou, K. Karamanou, A.B. Engin, A.O. Docea, C. Constantin et al., Protein bio-corona: critical issue in immune nanotoxicology. Arch. Toxicol. **91**(3), 1031–1048 (2017)
13. P. Rivera-Gil, D. Jimenez de Aberasturi, V. Wulf, B. Pelaz, P. del Pino, Y. Zhao et al., The challenge to relate the physicochemical properties of colloidal nanoparticles to their cytotoxicity. Acc. Chem. Res. **46**(3), 743–749 (2013)
14. S. Salatin, S. Maleki Dizaj, A. Yari Khosroushahi, Effect of the surface modification, size, and shape on cellular uptake of nanoparticles. Cell Biol. Int. **39**(8), 881–890 (2015)
15. A. Wicki, D. Witzigmann, V. Balasubramanian, J. Huwyler, Nanomedicine in cancer therapy: challenges, opportunities, and clinical applications. J. Control Release. **200**, 138–157 (2015)
16. P.N. Navya, H.K. Daima, Rational engineering of physicochemical properties of nanomaterials for biomedical applications with nanotoxicological perspectives. Nano Convergence **3**(1), 1 (2016)
17. X. Sun, W. Cai, X. Chen, Positron emission tomography imaging using radiolabeled inorganic nanomaterials. Acc. Chem. Res. **48**(2), 286–294 (2015)
18. D.C. Julien, S. Behnke, G. Wang, G.K. Murdoch, R.A. Hill, Utilization of monoclonal antibody-targeted nanomaterials in the treatment of cancer. MAbs **3**(5), 467–478 (2011)
19. Y. Bi, F. Hao, G. Yan, L. Teng, R.J. Lee, J. Xie, Actively targeted nanoparticles for drug delivery to tumor. Curr. Drug Metab. **17**(8), 763–782 (2016)
20. A. Salvati, A.S. Pitek, M.P. Monopoli, K. Prapainop, F.B. Bombelli, D.R. Hristov et al., Transferrin-functionalized nanoparticles lose their targeting capabilities when a biomolecule corona adsorbs on the surface. Nat. Nanotechnol. **8**(2), 137–143 (2013)
21. T. Tashima, Intelligent substance delivery into cells using cell-penetrating peptides. Bioorg. Med. Chem. Lett. **27**(2), 121–130 (2017)
22. M.L. Amin, J.Y. Joo, D.K. Yi, S.S. An, Surface modification and local orientations of surface molecules in nanotherapeutics. J. Control Release **207**, 131–142 (2015)
23. D. Patel, A. Kell, B. Simard, J. Deng, B. Xiang, H.Y. Lin et al., Cu^{2+} -labeled, SPION loaded porous silica nanoparticles for cell labeling and multifunctional imaging probes. Biomaterials **31**(10), 2866–2873 (2010)
24. D. Hong, H. Lee, B.J. Kim, T. Park, J.Y. Choi, M. Park et al., A degradable polydopamine coating based on disulfide-exchange reaction. Nanoscale **7**(47), 20149–20154 (2015)
25. Y. Zhang, C.Y. Ang, M. Li, S.Y. Tan, Q. Qu, Z. Luo et al., Polymer-coated hollow mesoporous silica nanoparticles for triple-responsive drug delivery. ACS Appl. Mater. Interfaces **7**(32), 18179–18187 (2015)
26. H. Kakwere, M.P. Leal, M.E. Materia, A. Curcio, P. Guardia, D. Niculaes et al., Functionalization of strongly interacting magnetic nanocubes with (thermo)responsive coating and their application in hyperthermia and heat-triggered drug delivery. ACS Appl. Mater. Interfaces **7**(19), 10132–10145 (2015)
27. J. Zhuang, R. Chacko, D.F. Amado Torres, H. Wang, S. Thayumanavan, Dual stimuli—dual response nanoassemblies prepared from a simple homopolymer. ACS Macro Lett. **3**(1), 1–5 (2014)
28. J. Fu, T. Chen, M. Wang, N. Yang, S. Li, Y. Wang et al., Acid and alkaline dual stimuli-responsive mechanized hollow mesoporous silica nanoparticles as smart nanocontainers for intelligent anticorrosion coatings. ACS Nano **7**(12), 11397–11408 (2013)
29. X. Chen, J. Gao, B. Song, M. Smet, X. Zhang, Stimuli-responsive wettability of nonplanar substrates: pH-controlled floatation and supporting force. Langmuir **26**(1), 104–108 (2010)
30. E. Frohlich, Action of nanoparticles on platelet activation and plasmatic coagulation. Curr. Med. Chem. **23**(5), 408–430 (2016)
31. J.P. Almeida, A.L. Chen, A. Foster, R. Drezek, In vivo biodistribution of nanoparticles. Nanomedicine **6**(5), 815–835 (2011) (London, England)
32. J. Nam, N. Won, J. Bang, H. Jin, J. Park, S. Jung et al., Surface engineering of inorganic nanoparticles for imaging and therapy. Adv. Drug Deliv. Rev. **65**(5), 622–648 (2013)

33. F. Farjadian, S. Ghasemi, S. Mohammadi-Samani, Hydroxyl-modified magnetite nanoparticles as novel carrier for delivery of methotrexate. Int. J. Pharm. **504**(1–2), 110–116 (2016)
34. N.R. Boase, I. Blakey, K.J. Thurecht, Molecular imaging with polymers. Polym. Chem. **3** (6), 1384–1389 (2012)
35. J.P. Meyer, P. Adumeau, J.S. Lewis, B.M. Zeglis, Click chemistry and radiochemistry: the first 10 years. Bioconjug. Chem. **27**(12), 2791–2807 (2016)
36. R.P. Bagwe, L.R. Hilliard, W. Tan, Surface modification of silica nanoparticles to reduce aggregation and nonspecific binding. Langmuir **22**(9), 4357–4362 (2006)
37. J.V. Hollingsworth, N.V. Bhupathiraju, J. Sun, E. Lochner, M.G. Vicente, P.S. Russo, Preparation of metalloporphyrin-bound superparamagnetic silica particles via "click" reaction. ACS Appl. Mater. Interfaces **8**(1), 792–801 (2016)
38. Q. Chen, Q. Sun, N.M. Molino, S.W. Wang, E.T. Boder, W. Chen, Sortase A-mediated multi-functionalization of protein nanoparticles. Chem. Commun. **51**(60), 12107–12110 (2015)
39. A. Therien, M. Bedard, D. Carignan, G. Rioux, L. Gauthier-Landry, M.E. Laliberte-Gagne et al., A versatile papaya mosaic virus (PapMV) vaccine platform based on sortase-mediated antigen coupling. J. Nanobiotechnol. **15**(1), 54 (2017)
40. Y. Liu, Q. Miao, P. Zou, L. Liu, X. Wang, L. An et al., Enzyme-controlled intracellular self-assembly of ^{18}F nanoparticles for enhanced microPET imaging of tumor. Theranostics **5** (10), 1058–1067 (2015)
41. L. Tang, Y. Wang, J. Li, The graphene/nucleic acid nanobiointerface. Chem. Soc. Rev. **44**(19), 6954–6980 (2015)
42. X. Mao, J. Xu, H. Cui, Functional nanoparticles for magnetic resonance imaging. Wiley Interdiscip. Rev. Nanomed. Nanobiotechnol. **8**(6), 814–841 (2016)
43. W. Kong, T. Sun, B. Chen, X. Chen, F. Ai, X. Zhu et al., A general strategy for ligand exchange on upconversion nanoparticles. Inorg. Chem. **56**(2), 872–877 (2017)
44. S. Bhattacharyya, R.A. Kudgus, R. Bhattacharya, P. Mukherjee, Inorganic nanoparticles in cancer therapy. Pharm. Res. **28**(2), 237–259 (2011)
45. J. Nicolas, S. Mura, D. Brambilla, N. Mackiewicz, P. Couvreur, Design, functionalization strategies and biomedical applications of targeted biodegradable/biocompatible polymer-based nanocarriers for drug delivery. Chem. Soc. Rev. **42**(3), 1147–1235 (2013)
46. F. Canfarotta, S.A. Piletsky, Engineered magnetic nanoparticles for biomedical applications. Adv. Health Mater. **3**(2), 160–175 (2014)
47. O. Carion, B. Mahler, T. Pons, B. Dubertret, Synthesis, encapsulation, purification and coupling of single quantum dots in phospholipid micelles for their use in cellular and in vivo imaging. Nat. Protoc. **2**(10), 2383–2390 (2007)
48. H. Wang, R. Kumar, D. Nagesha, R.I. Duclos Jr., S. Sridhar, S.J. Gatley, Integrity of ^{111}In-radiolabeled superparamagnetic iron oxide nanoparticles in the mouse. Nucl. Med. Biol. **42**(1), 65–70 (2015)
49. H. Fan, E.W. Leve, C. Scullin, J. Gabaldon, D. Tallant, S. Bunge et al., Surfactant-assisted synthesis of water-soluble and biocompatible semiconductor quantum dot micelles. Nano Lett. **5**(4), 645–648 (2005)
50. R.J. Bose, S.H. Lee, H. Park, Biofunctionalized nanoparticles: an emerging drug delivery platform for various disease treatments. Drug Discov. Today **21**(8), 1303–1312 (2016)
51. G. Shim, M.G. Kim, J.Y. Park, Y.K. Oh, Graphene-based nanosheets for delivery of chemotherapeutics and biological drugs. Adv. Drug Deliv. Rev. **105**(Pt B), 205–227 (2016)
52. G. Prencipe, S.M. Tabakman, K. Welsher, Z. Liu, A.P. Goodwin, L. Zhang et al., PEG branched polymer for functionalization of nanomaterials with ultralong blood circulation. J. Am. Chem. Soc. **131**(13), 4783–4787 (2009)
53. D. Chen, D. Yang, C.A. Dougherty, W. Lu, H. Wu, X. He et al., In vivo targeting and positron emission tomography imaging of tumor with intrinsically radioactive metal-organic frameworks nanomaterials. ACS Nano **11**(4), 4315–4327 (2017)

54. A.O. Elzoghby, M.M. Elgohary, N.M. Kamel, Implications of protein- and peptide-based nanoparticles as potential vehicles for anticancer drugs. Adv. Protein Chem. Struct. Biol. **98**, 169–221 (2015)
55. E. Yasun, C. Li, I. Barut, D. Janvier, L. Qiu, C. Cui et al., BSA modification to reduce CTAB induced nonspecificity and cytotoxicity of aptamer-conjugated gold nanorods. Nanoscale **7**(22), 10240–10248 (2015)
56. T.V. Verissimo, N.T. Santos, J.R. Silva, R.B. Azevedo, A.J. Gomes, C.N. Lunardi, In vitro cytotoxicity and phototoxicity of surface-modified gold nanoparticles associated with neutral red as a potential drug delivery system in phototherapy. Mater. Sci. Eng. C Mater. Biol. Appl. **65**, 199–204 (2016)
57. S.B. Lee, H.W. Lee, T.D. Singh, Y. Li, S.K. Kim, S.J. Cho et al., Visualization of macrophage recruitment to inflammation lesions using highly sensitive and stable radionuclide-embedded gold nanoparticles as a nuclear bio-imaging platform. Theranostics **7**(4), 926–934 (2017)
58. H. Heinz, H. Ramezani-Dakhel, Simulations of inorganic-bioorganic interfaces to discover new materials: insights, comparisons to experiment, challenges, and opportunities. Chem. Soc. Rev. **45**(2), 412–448 (2016)
59. Y. Kapilov-Buchman, E. Lellouche, S. Michaeli, J.P. Lellouche, Unique surface modification of silica nanoparticles with polyethylenimine (PEI) for siRNA delivery using cerium cation coordination chemistry. Bioconjug. Chem. **26**(5), 880–889 (2015)
60. S. Shi, F. Chen, W. Cai, Biomedical applications of functionalized hollow mesoporous silica nanoparticles: focusing on molecular imaging. Nanomed. (Lond.) **8**(12), 2027–2039 (2013)
61. X. Huang, F. Zhang, S. Lee, M. Swierczewska, D.O. Kiesewetter, L. Lang et al., Long-term multimodal imaging of tumor draining sentinel lymph nodes using mesoporous silica-based nanoprobes. Biomaterials **33**(17), 4370–4378 (2012)
62. F. Chen, H.F. Valdovinos, R. Hernandez, S. Goel, T.E. Barnhart, W. Cai, Intrinsic radiolabeling of Titanium-45 using mesoporous silica nanoparticles. Acta Pharmacol. Sin. **38**(6), 907–913 (2017)
63. P.A. Ellison, F. Chen, S. Goel, T.E. Barnhart, R.J. Nickles, O.T. DeJesus et al., Intrinsic and stable conjugation of thiolated mesoporous silica nanoparticles with radioarsenic. ACS Appl. Mater. Interfaces **9**(8), 6772–6781 (2017)
64. S. Goel, F. Chen, S. Luan, H.F. Valdovinos, S. Shi, S.A. Graves et al., Engineering intrinsically zirconium-89 radiolabeled self-destructing mesoporous silica nanostructures for in vivo biodistribution and tumor targeting studies. Adv. Sci. **3**(11), 1600122 (2016)
65. F. Chen, S. Goel, H.F. Valdovinos, H. Luo, R. Hernandez, T.E. Barnhart et al., In vivo integrity and biological fate of chelator-free zirconium-89-labeled mesoporous silica nanoparticles. ACS Nano **9**(8), 7950–7959 (2015)
66. F. Chen, H. Hong, S. Shi, S. Goel, H.F. Valdovinos, R. Hernandez et al., Engineering of hollow mesoporous silica nanoparticles for remarkably enhanced tumor active targeting efficacy. Sci. Rep. **4**, 5080 (2014)
67. F. Chen, H. Hong, Y. Zhang, H.F. Valdovinos, S. Shi, G.S. Kwon et al., In vivo tumor targeting and image-guided drug delivery with antibody-conjugated, radiolabeled mesoporous silica nanoparticles. ACS Nano **7**(10), 9027–9039 (2013)
68. D. Desai, J. Zhang, J. Sandholm, J. Lehtimaki, T. Gronroos, J. Tuomela et al., Lipid bilayer-gated mesoporous silica nanocarriers for tumor-targeted delivery of zoledronic acid in Vivo. Mol. Pharm. **14**(9), 3218–3227 (2017)
69. D. Chen, C.A. Dougherty, K. Zhu, H. Hong, Theranostic applications of carbon nanomaterials in cancer: focus on imaging and cargo delivery. J. Control Release **210**, 230–245 (2015)
70. K. Yang, L. Feng, H. Hong, W. Cai, Z. Liu, Preparation and functionalization of graphene nanocomposites for biomedical applications. Nat. Protoc. **8**(12), 2392–2403 (2013)
71. M. Xu, J. Zhu, F. Wang, Y. Xiong, Y. Wu, Q. Wang et al., Improved in vitro and in vivo biocompatibility of graphene oxide through surface modification: poly (acrylic acid)-functionalization is superior to PEGylation. ACS Nano **10**(3), 3267–3281 (2016)

72. S. Shi, F. Chen, E.B. Ehlerding, W. Cai, Surface engineering of graphene-based nanomaterials for biomedical applications. Bioconjug. Chem. **25**(9), 1609–1619 (2014)
73. H. Hong, Y. Zhang, J.W. Engle, T.R. Nayak, C.P. Theuer, R.J. Nickles et al., In vivo targeting and positron emission tomography imaging of tumor vasculature with ^{66}Ga-labeled nano-graphene. Biomaterials **33**(16), 4147–4156 (2012)
74. H. Hong, K. Yang, Y. Zhang, J.W. Engle, L. Feng, Y. Yang et al., In vivo targeting and imaging of tumor vasculature with radiolabeled, antibody-conjugated nanographene. ACS Nano **6**(3), 2361–2370 (2012)
75. D. Yang, L. Feng, C.A. Dougherty, K.E. Luker, D. Chen, M.A. Cauble et al., In vivo targeting of metastatic breast cancer via tumor vasculature-specific nano-graphene oxide. Biomaterials **104**, 361–371 (2016)
76. B. Cornelissen, S. Able, V. Kersemans, P.A. Waghorn, S. Myhra, K. Jurkshat et al., Nanographene oxide-based radioimmunoconstructs for in vivo targeting and SPECT imaging of HER2-positive tumors. Biomaterials **34**(4), 1146–1154 (2013)
77. S. Shi, C. Xu, K. Yang, S. Goel, H.F. Valdovinos, H. Luo et al., Chelator-free radiolabeling of nanographene: breaking the stereotype of chelation. Angew. Chem. Int. Ed. Engl. **56**(11), 2889–2892 (2017)
78. S. Shi, K. Yang, H. Hong, H.F. Valdovinos, T.R. Nayak, Y. Zhang et al., Tumor vasculature targeting and imaging in living mice with reduced graphene oxide. Biomaterials **34**(12), 3002–3009 (2013)
79. C. Xu, S. Shi, L. Feng, F. Chen, S.A. Graves, E.B. Ehlerding et al., Long circulating reduced graphene oxide-iron oxide nanoparticles for efficient tumor targeting and multimodality imaging. Nanoscale **8**(25), 12683–12692 (2016)
80. S. Same, A. Aghanejad, S. Akbari Nakhjavani, J. Barar, Y. Omidi, Radiolabeled theranostics: magnetic and gold nanoparticles. BioImpacts **6**(3), 169–181 (2016)
81. H. Hong, F. Chen, W. Cai, Pharmacokinetic issues of imaging with nanoparticles: focusing on carbon nanotubes and quantum dots. Mol. Imaging Biol. **15**(5), 507–520 (2013)
82. Y.I. Park, K.T. Lee, Y.D. Suh, T. Hyeon, Upconverting nanoparticles: a versatile platform for wide-field two-photon microscopy and multi-modal in vivo imaging. Chem. Soc. Rev. **44**(6), 1302–1317 (2015)
83. Y. Zhang, T.R. Nayak, H. Hong, W. Cai, Biomedical applications of zinc oxide nanomaterials. Cur Mol Med. **13**(10), 1633–1645 (2013)
84. F. Chen, S. Goel, R. Hernandez, S.A. Graves, S. Shi, R.J. Nickles et al., Dynamic positron emission tomography imaging of renal clearable gold nanoparticles. Small **12**(20), 2775–2782 (2016)
85. M. Felber, M. Bauwens, J.M. Mateos, S. Imstepf, F.M. Mottaghy, R. Alberto, ^{99m}Tc radiolabeling and biological evaluation of nanoparticles functionalized with a versatile coating ligand. Chemistry **21**(16), 6090–6099 (2015)
86. J. Lee, T.S. Lee, J. Ryu, S. Hong, M. Kang, K. Im et al., RGD peptide-conjugated multimodal $NaGdF_4$:Yb^{3+}/Er^{3+} nanophosphors for upconversion luminescence, MR, and PET imaging of tumor angiogenesis. J. Nucl. Med. **54**(1), 96–103 (2013)
87. J. Peng, Y. Sun, L. Zhao, Y. Wu, W. Feng, Y. Gao et al., Polyphosphoric acid capping radioactive/upconverting NaLuF4: Yb, Tm, 153Sm nanoparticles for blood pool imaging in vivo. Biomaterials **34**(37), 9535–9544 (2013)
88. A.A. Bogdanov Jr., S. Gupta, N. Koshkina, S.J. Corr, S. Zhang, S.A. Curley et al., Gold nanoparticles stabilized with MPEG-grafted poly(l-lysine): in vitro and in vivo evaluation of a potential theranostic agent. Bioconjug. Chem. **26**(1), 39–50 (2015)
89. M. Zhou, S. Song, J. Zhao, M. Tian, C. Li, Theranostic CuS nanoparticles targeting folate receptors for PET image-guided photothermal therapy. J Mater. Chem B **3**(46), 8939–8948 (2015)
90. F. Gao, P. Cai, W. Yang, J. Xue, L. Gao, R. Liu et al., Ultrasmall [^{64}Cu] Cu nanoclusters for targeting orthotopic lung tumors using accurate positron emission tomography imaging. ACS Nano **9**(5), 4976–4986 (2015)

91. S. Shi, B.C. Fliss, Z. Gu, Y. Zhu, H. Hong, H.F. Valdovinos et al., Chelator-free labeling of layered double hydroxide nanoparticles for in vivo PET imaging. Sci. Rep. **5**, 16930 (2015)
92. F. Chen, H. Hong, S. Goel, S.A. Graves, H. Orbay, E.B. Ehlerding et al., In vivo tumor vasculature targeting of CuS@ MSN based theranostic nanomedicine. ACS Nano **9**(4), 3926–3934 (2015)
93. M. Mahdavi, M.B. Ahmad, M.J. Haron, F. Namvar, B. Nadi, M.Z.A. Rahman et al., Synthesis, surface modification and characterisation of biocompatible magnetic iron oxide nanoparticles for biomedical applications. Molecules **18**(7), 7533–7548 (2013)
94. R. Chakravarty, H.F. Valdovinos, F. Chen, C.M. Lewis, P.A. Ellison, H. Luo et al., Intrinsically germanium-69-labeled iron oxide nanoparticles: synthesis and in-vivo dual-modality PET/MR imaging. Adv. Mater. **26**(30), 5119–5123 (2014)
95. F. Chen, P.A. Ellison, C.M. Lewis, H. Hong, Y. Zhang, S. Shi et al., Chelator-free synthesis of a dual-modality PET/MRI agent. Angew. Chem. Int. Ed. Engl. **52**(50), 13319–13323 (2013)
96. A.A. Barrefelt, T.B. Brismar, G. Egri, P. Aspelin, A. Olsson, L. Oddo et al., Multimodality imaging using SPECT/CT and MRI and ligand functionalized ^{99m}Tc-labeled magnetic microbubbles. EJNMMI Res. **3**(1), 12 (2013)
97. J.-S. Choi, N. Meghani, Impact of surface modification in BSA nanoparticles for uptake in cancer cells. Colloid Surf. B **145**, 653–661 (2016)
98. J. Zhang, L. Lang, Z. Zhu, F. Li, G. Niu, X. Chen, Clinical translation of an albumin-binding PET radiotracer ^{68}Ga-NEB. J. Nucl. Med. **56**(10), 1609–1614 (2015)
99. G. Niu, L. Lang, D.O. Kiesewetter, Y. Ma, Z. Sun, N. Guo et al., In vivo labeling of serum albumin for PET. J. Nucl. Med. **55**(7), 1150–1156 (2014)
100. A. Todica, S. Brunner, G. Böning, S. Lehner, S.G. Nekolla, M. Wildgruber et al., [^{68}Ga]-albumin-PET in the monitoring of left ventricular function in murine models of ischemic and dilated cardiomyopathy: comparison with cardiac MRI. Mol. Imaging Biol. **15**(4), 441 (2013)
101. D.A. Heuveling, A. van Schie, D.J. Vugts, N.H. Hendrikse, M. Yaqub, O.S. Hoekstra et al., Pilot study on the feasibility of PET/CT lymphoscintigraphy with ^{89}Zr-nanocolloidal albumin for sentinel node identification in oral cancer patients. J. Nucl. Med. **54**(4), 585–589 (2013)
102. D.A. Heuveling, G.W. Visser, M. Baclayon, W.H. Roos, G.J. Wuite, O.S. Hoekstra et al., ^{89}Zr-nanocolloidal albumin-based PET/CT lymphoscintigraphy for sentinel node detection in head and neck cancer: preclinical results. J. Nucl. Med. **52**(10), 1580–1584 (2011)
103. C. Perez-Medina, J. Tang, D. Abdel-Atti, B. Hogstad, M. Merad, E.A. Fisher et al., PET imaging of tumor-associated macrophages with ^{89}Zr-labeled high-density lipoprotein nanoparticles. J. Nucl. Med. **56**(8), 1272–1277 (2015)
104. S. Shukla, N.F. Steinmetz, Virus-based nanomaterials as positron emission tomography and magnetic resonance contrast agents: from technology development to translational medicine. Wiley Interdiscip. Rev. Nanomed. Nanobiotechnol. **7**(5), 708–721 (2015)
105. S.M. Janib, S. Liu, R. Park, M.K. Pastuszka, P. Shi, A.S. Moses et al., Kinetic quantification of protein polymer nanoparticles using non-invasive imaging. Integr. Biol. **5**(1), 183–194 (2013)
106. D. Sleep, Albumin and its application in drug delivery. Expert Opin. Drug Deliv. **12**(5), 793–812 (2015)
107. D. Sleep, J. Cameron, L.R. Evans, Albumin as a versatile platform for drug half-life extension. Biochim. Biophys. Acta **1830**(12), 5526–5534 (2013)
108. E. Frei, Albumin binding ligands and albumin conjugate uptake by cancer cells. Diabetol. Metab. Syndr. **3**(1), 11 (2011)
109. N.N. Davanzo, D.S. Pellosi, L.P. Franchi, A.C. Tedesco, Light source is critical to induce glioblastoma cell death by photodynamic therapy using chloro-aluminiumphtalocyanine albumin-based nanoparticles. Photodiagn. Photodyn. Ther. **19**, 181–183 (2017)

110. L. Zhou, T. Yang, J. Wang, Q. Wang, X. Lv, H. Ke et al., Size-tunable Gd_2O_3@ albumin nanoparticles conjugating chlorin e6 for magnetic resonance imaging-guided photo-induced therapy. Theranostics **7**(3), 764 (2017)
111. T. Lin, P. Zhao, Y. Jiang, Y. Tang, H. Jin, Z. Pan et al., Blood–brain-barrier-penetrating albumin nanoparticles for biomimetic drug delivery via albumin-binding protein pathways for antiglioma therapy. ACS Nano **10**(11), 9999–10012 (2016)
112. A. Akbarzadeh, R. Rezaei-Sadabady, S. Davaran, S.W. Joo, N. Zarghami, Y. Hanifehpour et al., Liposome: classification, preparation, and applications. Nanoscale Res. Lett. **8**(1), 102 (2013)
113. T.M. Allen, P.R. Cullis, Liposomal drug delivery systems: from concept to clinical applications. Adv. Drug Deliv. Rev. **65**(1), 36–48 (2013)
114. Y. Xia, J. Tian, X. Chen, Effect of surface properties on liposomal siRNA delivery. Biomaterials **79**, 56–68 (2016)
115. S. Hu, M. Niu, F. Hu, Y. Lu, J. Qi, Z. Yin et al., Integrity and stability of oral liposomes containing bile salts studied in simulated and ex vivo gastrointestinal media. Int. J. Pharm. **441**(1), 693–700 (2013)
116. Y.-Y. Lin, J.-J. Li, C.-H. Chang, Y.-C. Lu, J.-J. Hwang, Y.-L. Tseng et al., Evaluation of pharmacokinetics of ^{111}In-labeled VNB-PEGylated liposomes after intraperitoneal and intravenous administration in a tumor/ascites mouse model. Cancer Biother. Radiopharm. **24**(4), 453–460 (2009)
117. J.W. Seo, H. Zhang, D.L. Kukis, C.F. Meares, K.W. Ferrara, A novel method to label preformed liposomes with ^{64}Cu for positron emission tomography (PET) imaging. Bioconjug. Chem. **19**(12), 2577–2584 (2008)
118. J. Kim, D.N. Pandya, W. Lee, J.W. Park, Y.J. Kim, W. Kwak et al., Vivid tumor imaging utilizing liposome-carried bimodal radiotracer. ACS Med. Chem. Lett. **5**(4), 390–394 (2014)
119. T.X. Nguyen, L. Huang, M. Gauthier, G. Yang, Q. Wang, Recent advances in liposome surface modification for oral drug delivery. Nanomedicine **11**(9), 1169–1185 (2016)
120. Y.-B. Huang, M.-J. Tsai, P.-C. Wu, Y.-H. Tsai, Y.-H. Wu, J.-Y. Fang, Elastic liposomes as carriers for oral delivery and the brain distribution of (+)-catechin. J. Drug Target **19**(8), 709–718 (2011)
121. S. Jain, S.R. Patil, N.K. Swarnakar, A.K. Agrawal, Oral delivery of doxorubicin using novel polyelectrolyte-stabilized liposomes (layersomes). Mol. Pharm. **9**(9), 2626–2635 (2012)
122. S. Edmonds, A. Volpe, H. Shmeeda, A.C. Parente-Pereira, R. Radia, J. Baguna-Torres et al., Exploiting the metal-chelating properties of the drug cargo for in vivo positron emission tomography imaging of liposomal nanomedicines. ACS Nano **10**(11), 10294–10307 (2016)
123. L. Feng, L. Cheng, Z. Dong, D. Tao, T.E. Barnhart, W. Cai et al., Theranostic liposomes with hypoxia-activated prodrug to effectively destruct hypoxic tumors post-photodynamic therapy. ACS Nano **11**(1), 927–937 (2017)
124. N. Li, Z. Yu, T.T. Pham, P.J. Blower, R. Yan, A generic ^{89}Zr labeling method to quantify the in vivo pharmacokinetics of liposomal nanoparticles with positron emission tomography. Int. J. Nanomed. **12**, 3281–3294 (2017)
125. H. Xing, C.L. Zhang, G. Ruan, J. Zhang, K. Hwang, Y. Lu, Multimodal detection of a small molecule target using stimuli-responsive liposome triggered by aptamer-enzyme conjugate. Anal. Chem. **88**(3), 1506–1510 (2016)
126. A.L. Petersen, T. Binderup, P. Rasmussen, J.R. Henriksen, D.R. Elema, A. Kjær et al., ^{64}Cu loaded liposomes as positron emission tomography imaging agents. Biomaterials **32**(9), 2334–2341 (2011)
127. Y. Du, X. Liang, Y. Li, T. Sun, Z. Jin, H. Xue et al., Nuclear and fluorescent labeled PD-1-liposome-DOX-^{64}Cu/IRDye800CW allows improved breast tumor targeted imaging and therapy. Mol. Pharm. (2017) (Epub)
128. C. Rangger, A. Helbok, J. Sosabowski, C. Kremser, G. Koehler, R. Prassl et al., Tumor targeting and imaging with dual-peptide conjugated multifunctional liposomal nanoparticles. Int. J. Nanomed. **8**, 4659–4671 (2013)

129. J. Malinge, B. Geraudie, P. Savel, V. Nataf, A. Prignon, C. Provost et al., Liposomes for PET and MR imaging and for dual targeting (magnetic field/glucose moiety): synthesis, properties, and in vivo studies. Mol. Pharm. **14**(2), 406–414 (2017)
130. H. Cabral, K. Kataoka, Progress of drug-loaded polymeric micelles into clinical studies. J. Control Release **190**, 465–476 (2014)
131. M. Elsabahy, K.L. Wooley, Design of polymeric nanoparticles for biomedical delivery applications. Chem. Soc. Rev. **41**(7), 2545–2561 (2012)
132. D.E. Owens, N.A. Peppas, Opsonization, biodistribution, and pharmacokinetics of polymeric nanoparticles. Int. J. Pharm. **307**(1), 93–102 (2006)
133. L.H. Feng, C.L. Zhu, H.X. Yuan, L.B. Liu, F.T. Lv, S. Wang, Conjugated polymer nanoparticles: preparation, properties, functionalization and biological applications. Chem. Soc. Rev. **42**(16), 6620–6633 (2013)
134. N.J. Warren, S.P. Armes, Polymerization-induced self-assembly of block copolymer nano-objects via RAFT aqueous dispersion polymerization. J. Am. Chem. Soc. **136**(29), 10174–10185 (2014)
135. M. Huo, J. Yuan, L. Tao, Y. Wei, Redox-responsive polymers for drug delivery: from molecular design to applications. Polym. Chem. **5**(5), 1519–1528 (2014)
136. Y. Hu, M. Deng, H. Yang, L. Chen, C. Xiao, X. Zhuang et al., Multi-responsive core-crosslinked poly (thiolether ester) micelles for smart drug delivery. Polymer **110**, 235–241 (2017)
137. Y. Xiao, H. Hong, A. Javadi, J.W. Engle, W. Xu, Y. Yang et al., Multifunctional unimolecular micelles for cancer-targeted drug delivery and positron emission tomography imaging. Biomaterials **33**(11), 3071–3082 (2012)
138. K. Tanaka, E.R. Siwu, K. Minami, K. Hasegawa, S. Nozaki, Y. Kanayama et al., Noninvasive imaging of dendrimer-type N-glycan clusters: in vivo dynamics dependence on oligosaccharide structure. Angew. Chem. Int. Ed. Engl. **49**(44), 8195–8200 (2010)
139. S. Kannan, H. Dai, R.S. Navath, B. Balakrishnan, A. Jyoti, J. Janisse et al., Dendrimer-based postnatal therapy for neuroinflammation and cerebral palsy in a rabbit model. Sci. Transl. Med. **4**(130), 130ra46-ra46 (2012)
140. R. Kannan, E. Nance, S. Kannan, D. Tomalia, Emerging concepts in dendrimer-based nanomedicine: from design principles to clinical applications. J. Intern. Med. **276**(6), 579–617 (2014)
141. L. Zhao, M. Zhu, Y. Li, Y. Xing, J. Zhao, Radiolabeled dendrimers for nuclear medicine applications. Molecules **22**(9), E1350 (2017)
142. B. Nottelet, V. Darcos, J. Coudane, Aliphatic polyesters for medical imaging and theranostic applications. Eur. J. Pharm. Biopharm. **97**(Pt B), 350–370 (2015)
143. J.H. Myung, H.J. Hsu, J. Bugno, K.A. Tam, S. Hong, Chemical structure and surface modification of dendritic nanomaterials tailored for therapeutic and diagnostic applications. Curr. Top. Med. Chem. **17**(13), 1542–1554 (2017)
144. J.W. Seo, H. Baek, L.M. Mahakian, J. Kusunose, J. Hamzah, E. Ruoslahti et al., ^{64}Cu-labeled LyP-1-dendrimer for PET-CT imaging of atherosclerotic plaque. Bioconjug. Chem. **25**(2), 231–239 (2014)
145. G.K. Grunwald, A. Vetter, K. Klutz, M.J. Willhauck, N. Schwenk, R. Senekowitsch-Schmidtke et al., EGFR-targeted adenovirus dendrimer coating for improved systemic delivery of the theranostic NIS gene. Mol. Ther. Nucl. Acids **2**, e131 (2013)
146. A. Hagooly, A. Almutairi, R. Rossin, M. Shokeen, A. Ananth, C. Anderson et al., Evaluation of a RGD-dendrimer labeled with ^{76}Br in hindlimb ischemia mouse model. J. Nucl. Med. **49**(supplement 1), 184P (2008)

Chapter 11
Radiolabeling Method: Core/Surface Labeling, Chemical and Physical Labeling

Dong Soo Lee, Minseok Suh and Yun-Sang Lee

Abstract Radiolabeled nanomaterials can be used for diagnosis, therapy and theranostics of certain diseases. The core concept of radionanomedicine relies on efficient and reliable radiolabeling methods, to bind appropriate isotope with well-functionalized nanoparticles (NPs), and the use of tracer amounts of radiolabeled NPs. In this chapter, we focused on the three issues of producing radiolabeled NPs: choosing appropriate radionuclides for labeling, construction of well-functionalized NPs with surface modification and different labeling methods of NPs with radionuclides. Firstly, choosing ideal isotope starts from understanding the characteristics of each isotopes, such as half-life, decay energy and availability, and understanding of purpose of the study. Secondly, to increase the specific delivery of NPs to the target tissues while decreasing the nonspecific binding to normal tissues well functionalized NPs are necessary, which can be achieved by surface modification. Especially, micelle encapsulation method is an efficient method for producing multifunctional NPs. Finally, ideal labeling method should be adopted, which should not only be quick, easy, and highly efficient but also should not change the biological properties of target molecules. Both intrinsic and extrinsic radiolabeling methods should be chosen in the base of thorough understanding of pros and cons of each labeling methods. In conclusion, the development of the methods to enable surface labeling with ligands and chelators should be solved first. The development of the imaging methods to track the in vivo administered

D. S. Lee (✉) · M. Suh · Y.-S. Lee
Department of Nuclear Medicine, Seoul National University College of Medicine, Seoul 03080, Republic of Korea
e-mail: dsl@snu.ac.kr

M. Suh
e-mail: mandu0902@hotmail.com

Y.-S. Lee
e-mail: wonza43@snu.ac.kr

D. S. Lee · M. Suh · Y.-S. Lee
Department of Molecular Medicine and Biopharmaceutical Sciences, Graduate School of Convergence Science and Technology, Seoul National University, Seoul 03080, Republic of Korea

D. S. Lee (ed.), *Radionanomedicine*, Biological and Medical Physics, Biomedical Engineering, https://doi.org/10.1007/978-3-319-67720-0_11

radiolabeled NPs is the next issue to be addressed. With the improvement of above-mentioned issues, radiolabeled NPs can be successfully translated to clinical use.

11.1 Radiolabeling of Nanomaterials

Radiolabeled nanomaterials can be used for diagnosis, therapy and theranostics of certain diseases. The radionanomedicine relies on efficient and reliable radiolabeling methods, to bind appropriate isotope with well-functionalized nanoparticles (NPs), and the use of tracer amounts of radiolabeled NPs for in vivo theranostics. An ideal radiolabeling method should be quick, easy, and highly efficient and should not change the biological properties of target molecules [1]. The labeling of NPs with radionuclides can be done in two ways [2, 3], extrinsically using chelators bound to the surface of NPs [4] and intrinsically in the core (Fig. 11.1) [5, 6]. Representative examples of intrinsically and extrinsically labeled NPs are summarized in Table 11.1.

In this chapter, we will focus on the three issues of producing radiolabeled NPs: choosing appropriate radionuclides for labeling, construction of well-functionalized NPs with surface modification and different labeling methods of NPs with radionuclides. With the intention of recapitulating the methods parts of radionanomedicine, that is radiolabeling methods, we adopted parts of the review we wrote in review articles [2, 3] with the permission by the journal publishers and of course ourselves and coauthors.

11.2 Choice of Ideal Radioisotopes

Characteristics of isotopes such as, decay half-life, decay energy, and availability of isotope should be considered to choose the ideal radioisotope for radionanomedicine. Commonly used radioisotopes range from generator-produced ^{68}Ga [50], cyclotron-produced ^{64}Cu [51, 52] or ^{89}Zr [53], reactor-produced ^{177}Lu [54, 55],

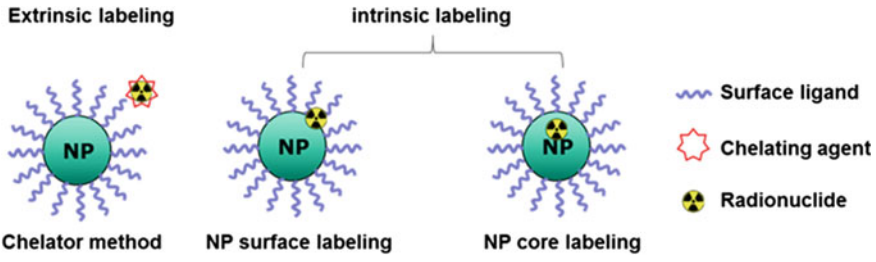

Fig. 11.1 Core or surface labeling of NPs with radionuclides

Table 11.1 Radiolabeling of NPs (modified from [1])

Radiolabeling	Radioisotope (half-life)	Nanoparticles	Chelator	References
Intrinsic	^{64}Cu (12.7 h)	CuS		[7]
		IO		[8]
		Gold		[9]
		Ferritin nanocage		[10]
		Porphysomes		[11]
	^{198}Au(2.69 d)	Gold		[12–16]
		Gold nanocages		[17]
	^{153}Sm (46.3 h)	Ln doped NP		[18, 19]
	^{109}Cd (461.4 d)	QD		[4]
	^{111}In (2.8 d)	IO		[20]
	^{18}F (109.8 min)	Ln doped NP		[21, 22]
	^{72}As (12.6 h)	IO		[23]
	^{69}Ge (39.05 h)	IO		[24]
Extrinsic	^{99m}Tc (6 h)	Gold	Hynic	[25–27]
			DTPA	[28]
		IO	DTPA	[29]
	^{64}Cu (12.7 h)	QD	DOTA	[30, 31]
		Gold nanoshell	DOTA	[32]
		IO	DOTA	[33–35]
		Carbon nanotube	DOTA	[36]
		Liposome	DOTA	[37]
	^{111}In (2.8 d)	Carbon nanotube	DTPA	[38, 39]
			DOTA	[40]
		Micelle	DTPA	[41]
	^{124}I (4.18 d)	IO	Iodo-bead	[42]
		Ln doped NP	Iodo-bead	[43]
	^{188}Re (16.9 h)	IO	$[M(CO)_3(OH_2)_3]^+$	[44, 45]
		Liposome	BMEDA	[46]
	^{177}Lu (6.73 d)	Gold	DOTA	[47]
	^{68}Ga (67.7 min)	QD	DOTA	[48]
	^{67}Ga (78.3 h)	Cobalt-ferrite	NOTA	[7, 49]

QD quantum dot, *IO* iron oxide, *Ln* lanthanide, BMEDA = *N*,*N*-bis(2-mercaptoethyl)-*N*′,*N*′-diethylethylenediamine

generator or reactor-produced ^{90}Y [56], and generator-produced ^{188}Re [57, 58]. The former three radioisotopes are used for diagnostic and the latter three for therapeutic purposes.

11.2.1 Diagnostic Radioisotopes

For the diagnostic purpose, usually radioisotope which emits gamma rays is used. In the early days, gamma camera was used to detect these single photons of gamma rays, however after the development of positron emission tomography (PET), positron-emitting radioisotopes are now widely used. Low positron energy and high branching ratio of β+ decay are the desired decay characteristics of positron emitting radioisotopes for PET imaging. The physical half-life of radioisotopes is also of great concern. Adequate radioisotopes are to be chosen among those with short half-lives such as ^{13}N ($t_{1/2}$ = 9.97 min), ^{68}Ga ($t_{1/2}$ = 67.7 min), ^{18}F ($t_{1/2}$ = 109.8 min), and ^{99m}Tc ($t_{1/2}$ = 6 h), or those with longer half-lives such as ^{64}Cu ($t_{1/2}$ = 12.7 h), ^{72}As ($t_{1/2}$ = 26 h), ^{111}In ($t_{1/2}$ = 67 h), and ^{89}Zr ($t_{1/2}$ = 78.4 h) according to the imaging purposes. The physical half-lives of the isotopes should match the biological half-lives of the vectors being labeled with these isotopes to allow them to reach the targets of interest. It is also important that the decay time would be as short as possible in order to avoid unnecessary radiation exposure. In case of tracking NPs, relatively long-lived isotopes such as ^{89}Zr are preferred for monitoring the clearance profiles [53].

11.2.2 Therapeutic Radionuclides

Radioisotopes which decay by emission of beta particles, alpha particles, or Auger electron are potential therapeutic isotopes. The ^{131}I is a key example of radioisotope used for therapeutic purpose in the medical field, and this isotope continues to be used in many technologies focused on treatment including the field of radionanomedicine [59]. In 2004, Cao et al. had labeled ^{188}Re on the surface of silica-coated magnetite NP immobilized with histidine with labeling yield of 91% [44]. Liang et al. in 2007 reported ^{188}Re labeled superparamagnetic iron oxide NPs (SPIONs) with a greater than 90% labeling efficiency and a good in vitro stability. The NPs demonstrated the dose-dependent therapeutic effect in hepatocellular carcinoma cells in vitro [45]. Interestingly, therapeutic radioisotopes, ^{131}I, ^{177}Lu and ^{188}Re can be used for diagnostic imaging as well. This is because they emit both beta and gamma rays and thus these radioisotopes are inherently theranostic.

NPs with proper type of intrinsic radioactivity can also be used for both imaging and therapy. ^{198}Au/^{199}Au is one prime example of this strategy. The radioactive properties of ^{198}Au (beta ray = 0.96 meV, gamma ray = 411 keV) and ^{199}Au (beta ray = 0.46 meV, gamma ray = 158 keV) make them ideal candidates for use in

theranostic applications [13]. Khan et al. reported the therapeutic efficacy of ^{198}Au composite nano-devices in mouse melanoma tumor model by intratumoral injection of the NPs [14]. Chanda et al. reported that gum arabic glycoprotein (GA)-functionalized ^{198}Au showed therapeutic effect in mouse prostate cancer model after intratumoral injection of the NPs. They also showed the biocompatibility of their approach by showing no or minimal leakage of the NPs and no pathologic change in blood cells after the treatment [12]. In 2012, Shukla et al. developed prostate tumor specific epigallocatechin-gallate (EGCg) functionalized ^{198}Au (^{198}Au NP-EGCg). In this study, ^{198}Au NP-EGCg was injected in prostate cancer mouse model. Approximately 72% NPs were retained in the tumor after 24 h and 80% of the tumor volume was reduced after 28 days [15].

11.3 Functionalization of Nanoparticles

In radionanomedicine trace amounts of radiolabeled NPs can be used for in vivo theragnosis. This requires increasing the specific delivery of NPs to the target tissues while decreasing the nonspecific binding to normal tissues, which was proven to be difficult to achieve in practice. The biological properties of NPs depend on the ligands attached to their surfaces, and targeting ligands as well as polyethylene glycol (PEG) molecules are used to reduce the nonspecific normal-tissue uptake [60]. Surface modification of NPs to produce the well-functionalized NPs should focus on the ligand selection and PEG. However, the conventional method, which adopts multistep and step-by-step approach for surface modification of NPs, has many difficulties necessitating a novel method and recently several methods came to be available to overcome these difficulties.

11.3.1 PEGylation

The majority of the NPs have hydrophobic surfaces after the core synthesis. So the use of PEG or natural and synthetic polymers including dextran is necessary for making the surface hydrophilic and retaining the material's stability in a biological environment [61]. The addition of PEG to the NPs' surface reduce reticuloendothelial system uptake of NPs, NPs' interaction with small molecules, and their aggregation, and thus increase circulation time, solubility in serum, and enhanced permeability and retention (EPR) effect [62–64]. Using the PEGylation technique Doxil® (liposomal delivery vehicle for doxorubicin) and Oncospar® (PEG-L-asparaginase) became the first FDA-approved NP therapeutics [65]. PEGylation yielded the drug half-life of 72 h with the circulation half-life of 36 h.

11.3.2 Ligand Selection

In addition, ligands and chelators needed to be added to the termini of PEGs or the surface of dextran [66]. Ligands should have been chosen from the molecules already known to chase the targets, which included small molecules or biomacromolecules. The well-known biomacromolecules are either mouse (momab), chimeric (ximab), humanized (zumab), or human (mumab) monoclonal antibodies. Their recently introduced competitors are affibodies [67], aptamers [68]—either peptide aptamers or nucleic acid aptamers—and the even more recently aptides [69] and avibodies [70, 71]. Radiolabeled antibodies have been used for imaging and/or therapy. Both ^{90}Y-labeled ibritumomab tiuxetan (Zevalin®, Biogen Inc., Cam-bridge, MA, USA), an anti-CD20 monoclonal antibody, and ^{131}I-labeled tositumomab (Bexxar, GlaxoSmithKline, UK), which is a murine anti-CD20 mono-clonal antibody were approved by the FDA for the treatment of non-Hodgkin lymphoma [72, 73]. However, ^{131}I-tositumomab was discontinued in February 2014 because of low sales. The effort to develop clinically applicable radiolabeled antibodies continued and in an example report, Hong et al. reported a dual labeling method of an anti-CD105 monoclonal antibody with ^{89}Zr and near-infrared fluorescent dye [74].

Small molecular ligands are recognized by their target infrequently, while they sometimes are recognized as opsonins by their target cells or tissues. In that they are recognized more effectively if they are bound to the surface of the NPs, the aptamers or affibodies can be advantageous as ligands. The advantage of these newly introduced aptamers and the likes is derived from the fact that they are produced based on combinatorics, which selects the most desirable macromolecules with optimal affinity and avidity for the target from a large pool of candidates.

Surface modification of NPs with monoclonal antibodies needs the correct combination of the best antibody with the correct direction of conjugation. If the binding motif itself is bound to the surface of NPs and hidden from the open space, the modified NPs will not bind their target. The most commonly used conjugation method is the coupling of the primary amine-group present on the Fab fragment of the active site of the antibody molecule with the carbodiimide and/or N-hydroxysuccinimide derivatives of the acid-group on the surface of the NPs. Using this method, the antibody-NP conjugate has a limited number of active groups for efficient targeting [75, 76]. To overcome this limitation, site directional conjugation methods have been developed to target the Fc fragment of the antibody through its hydroxyl or disulfide-groups [75, 77]. Recently, Jeong et al. reported a new method for site-specific and orientation controlled antibody conjugation on the NP surface using copper-free click chemistry [78].

Some investigators have even attempted to label protein A, which has high affinity for the Fc region of IgG, onto the entire surface of the NPs [79]. Then they further labeled the epitope of protein A with monoclonal antibodies [80–82]. This approach was successful for in vitro diagnostics but was not employed for in vivo use because of the increased size of the NPs and the fact that the two-step

modification process makes the production procedure cumbersome and delivers a low final yield. Hence, a breakthrough in this particular field was necessary.

11.3.3 Micelle Encapsulation

The conventional method for functionalizing the NPs, which is a multistep and step-by-step approach for surface modification of NPs, has many difficulties. First of all, the multistep chemical reactions can cause decreasing total yield of modified NPs. In addition, in each reaction step, we have to consider the reaction time, temperature, pH, impurities, solvents, reagent concentrations, etc. Sometimes, a complicated situation can be induced by the conjugation of two or more ligands. Such difficulties necessitated a novel method, which we think is micelle encapsulation method.

Hydrophilization of NPs using the micelle encapsulation method was first pro-posed by Dubertret et al. [83]. This method evolved from the use of a two-tailed phospholipid to the use of a one-tailed C-12 alkanethiol [84]. Fan and colleagues introduced microencapsulation and the solvent evaporation method, which was optimized to a quick and simple method [85] (Fig. 11.2a). The Dubertret's group, again using a two-tailed phospholipid, successfully introduced recently functional biomolecules [86]. Wu and colleagues produced micelles by adopting PEG sorbitan fatty acid esters [87] (Fig. 11.2b). Recently, Jeong's group integrated these developments to make a quick and straightforward method of mixing, sonicating, and size exclusion chromatography for producing functionally active multi-specific NPs [48] (Fig. 11.2c). This should be the ultimate solution to the challenge posed in radiolabeling of functional NPs. Jeong ingeniously proposed this one-step method under mild conditions to preserve ligand integrity, which is now called the micelle-encapsulation method [48, 78]. This method was inspired by the hydrophilization method used for quantum dots (QD) [83, 86], surface-enhanced Raman scattering (SERS) dots [88], QD-embedded silica NPs [89], gold or iron oxide NPs [84, 90], or other hydrophobic NPs, which were also found to be the appropriate core for encapsulation.

Jeong's contribution relies on the use of combined multiplex amphiphiles with different functional groups simultaneously to achieve surface multifunctionality and hydrophilicity of NPs (Fig. 11.3). In the micelle-encapsulation method, the ligands and the chelator as well as the PEGs are specifically prepared to form a micelle. The micelle in the aqueous phase is then mixed with the NPs in the lipid phase and sonicated to yield the encapsulated NPs. The final multiplexed NPs were purified by size exclusion chromatography. If the small molecules such as mannose, lactose, or cRGD (cyclic Arginine-Glycine-Aspartate) were to be used as ligands, these ligands were covalently bound to the tip of an alkyl chain of optimal length. Using this method, Lee et al. labeled QD544T with ^{68}Ga and added functional group of RGD and showed specific targeted imaging of ^{68}Ga-NOTA-QD655T-RGD in glioma tumor mouse model [48]. Figure 11.4 depicts the dimension of the modifier

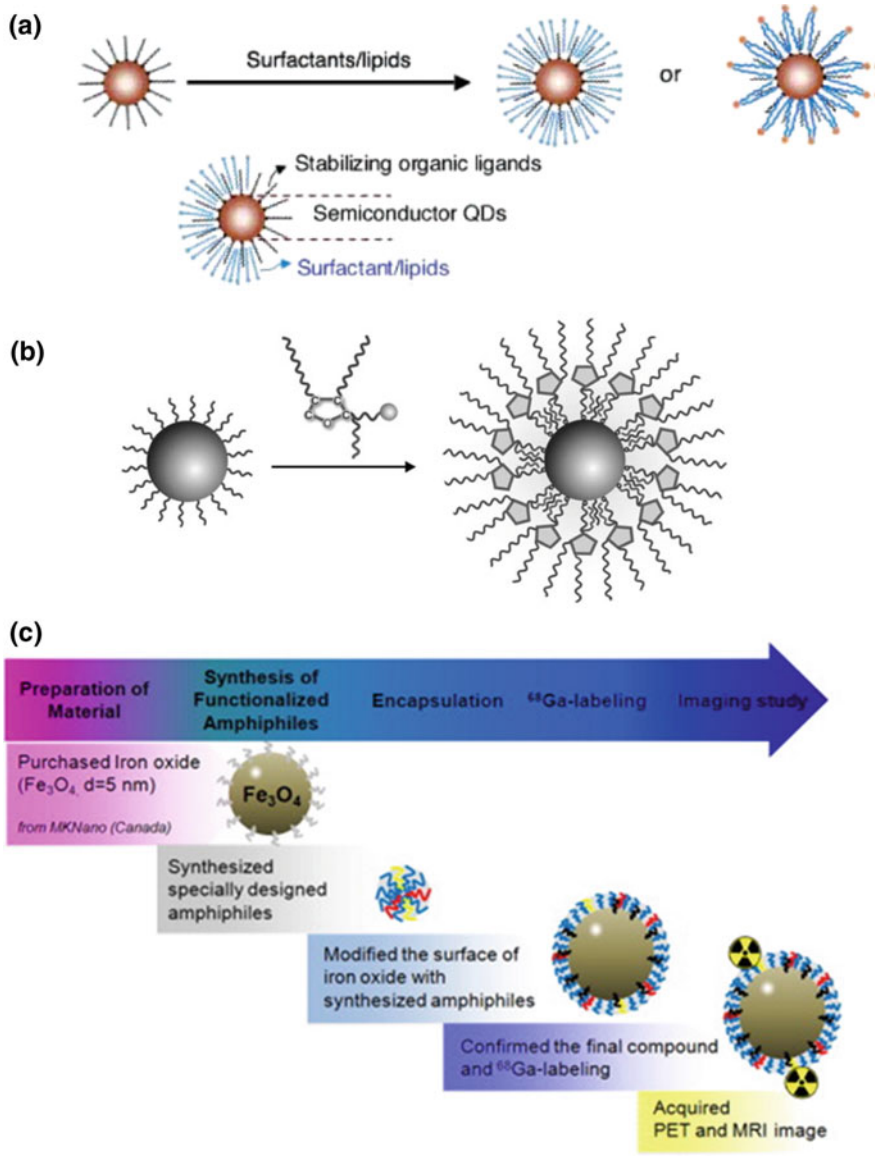

Fig. 11.2 Encapsulation method of nanomaterials using micelles. **a** Quantum dots (QDs) were encapsulated using one-tailed or two-tailed lipids (reprinted with permission from [85]. **b** Gold, quantum dots, and iron oxide were encapsulated using polyethylene-glycol (PEG) sorbitan fatty acid esters (reprinted with permission from [86]). **c** Iron oxide particles were mixed with multifunctional amphiphiles, vortexed, and separated using size exclusion chromatography. ^{68}Ga was used as radiolabel (reprinted with permission from [90]

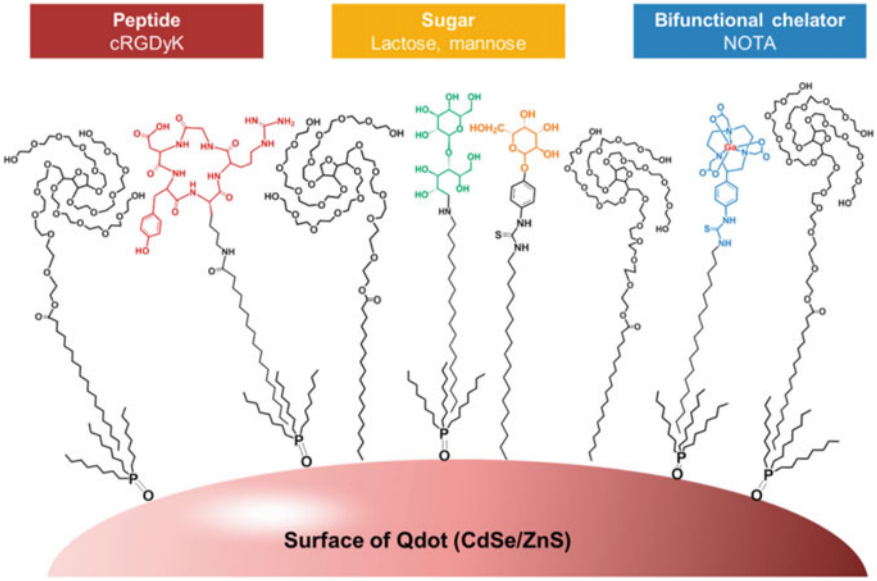

Fig. 11.3 Scheme of the surface modification of nanomaterials (for example, quantum dots) with functional multispecific and multimodal chelator/ligand/Tween60-complex micelles (reprinted with permission from [48])

ligands and the surface of the NPs if antibodies, aptamer ligands, PEG-chelators, and PEGs were used. Micelle-encapsulation method was employed for iron oxide particles with a diameter of 5 nm [90, 91], upconverting NPs with a diameter of 50 nm, and other compounds [92]. SERS dots [88, 93] or QD-dot-embedded silica NPs [89] are other examples of successful encapsulation. If a specific antibody or related peptide/nucleic acid affinity tool is chosen as ligand, chelators and ligands can be used in parallel to surface-label NPs.

This method also could be the solution to the challenge for the preparation or radiolabeling of multifunctional NPs. In a previous study, a multifunctional NPs that has two or more different types of targeting ligands enabled specific and effective agent delivery [94]. Jeong's micelle-encapsulation method proposed a quick and easy method to prepare multifunctional NP in one-step under mild conditions, which could preserve ligand integrity. The multifunctional NP can be used for multi-radioisotope labeling or a multitargeting strategy. Here, we can suggest the use of this multifunctional NP for theragnosis (^{68}Ga/^{64}Cu and ^{177}Lu) or dual-energy combined internal therapy using (^{177}Lu and ^{90}Y) dual radioisotope tagging (Fig. 11.5a, b). Further suggestion of multifunctional NPs for clinical application can be expected by multiple ligands for efficient tumor targeting {e.g., prostate-specific membrane antigen (PSMA) [95], Arg-Gly-Asp (RGD) [96], etc.}, and ^{64}Cu for biologic effective dose prediction and validation, and ^{177}Lu for radionuclide therapy (Fig. 11.5c).

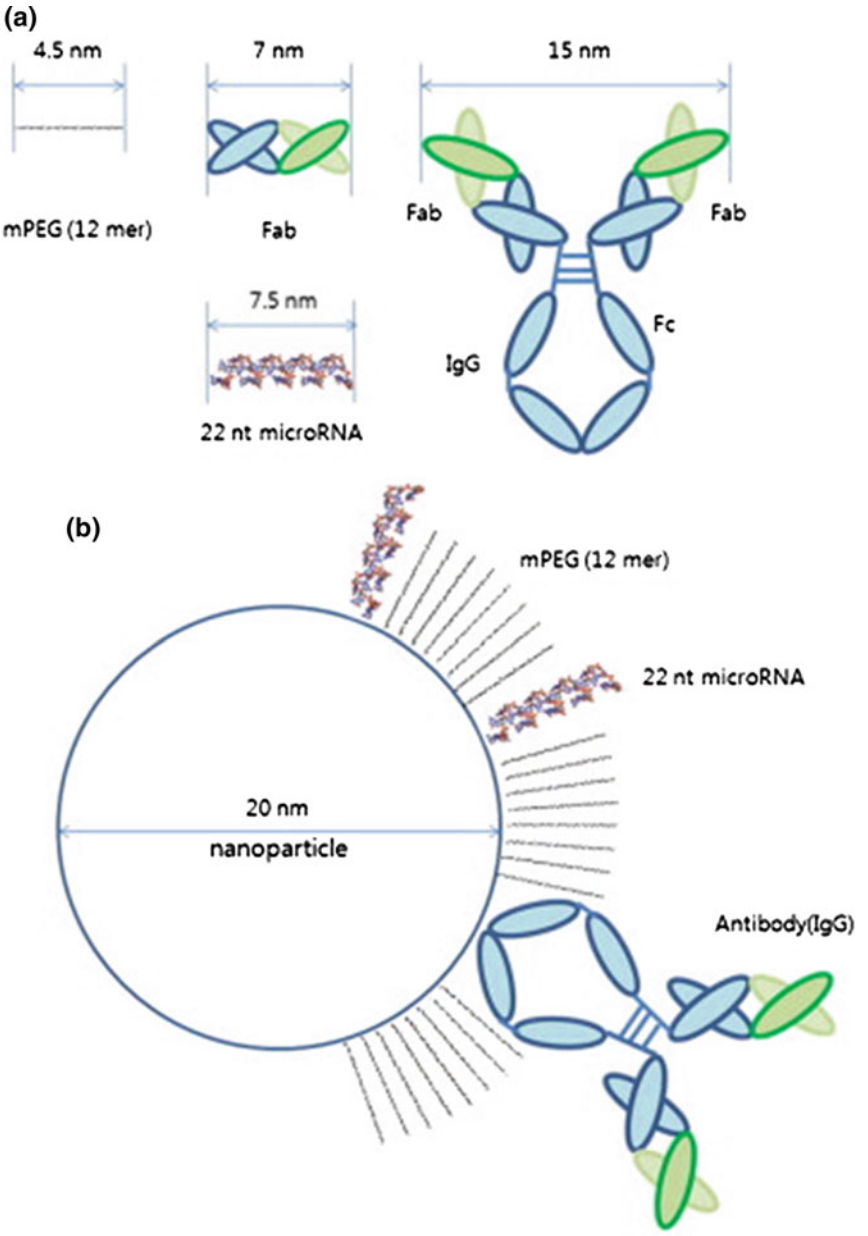

Fig. 11.4 Dimension of an example of a nanoparticle and its surface modifiers such as an antibody, the antibody's Fab fragment, microRNA, or any analogous aptamer or PEG of shorter (12mer) or longer length

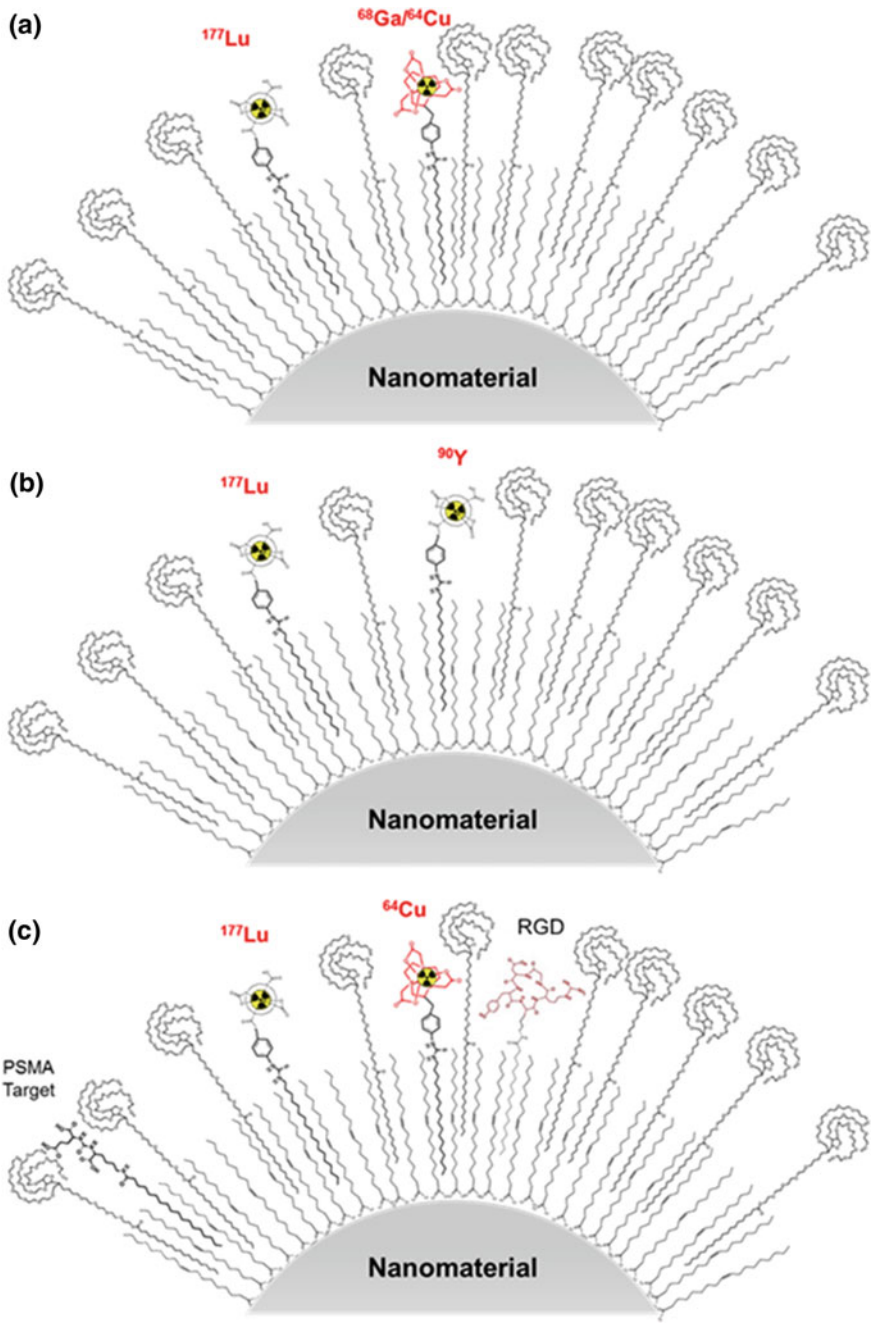

Fig. 11.5 Expected usage of multifunctional nanoparticles using dual radiotracers, **a** using ^{68}Ga/^{64}Cu for imaging and ^{177}Lu for therapy, **b** using ^{177}Lu and ^{90}Y for combined therapy with dual energy and **c** using PSMA target and RGD target with ^{177}Lu/^{64}Cu for theranostic (reprinted with permission from [3])

Another important issue of radionanomedicine is quality control of the NPs. This concern can also be solved by Jeong's method, which can provide monodisperse NPs even after the multifunctional surface modification [90]. Although Jeong's method has great feasibility and a future in radionanomedicine, we have to thoroughly evaluate the unexpected toxicity from lipid contents used for encapsulation and also develop the quantification method of functional groups encapsulated on their nanoplatforms.

11.4 Different Radiolabeling Methods

11.4.1 Extrinsic Radiolabeling

The most widely used radio-labeling method involves the use of chelators which could coordinate with certain isotopes to form stable complexes [97]. Extrinsically labeled NPs using chelators according to labeling methods and materials are well summarized in the review articles by Xing et al. [98] and Enrique Morales-Avila et al. [99]. Chelators used for this purpose include DTPA (diethylene triamine pentaacetic acid), DOTA (1,4,7,10-tetraazacyclododecane-1,4,7,10-tetraacetic acid), NOTA (1,4,7-triazacyclononane-1,4,7-triacetic acid), and others [100, 101] (Fig. 11.6). In 2007, Cai et al. labeled QD with ^{64}Cu (^{64}Cu-DOTA-QD-RGD) with conjugation of DOTA and RGD peptides. ^{64}Cu-DOTA-QD-RGD showed better integrin positive tumor targeting than ^{64}Cu-DOTA-QD [30]. Despite the wide use of extrinsically radiolabeled NPs, selection of the right chelator, radiolabeling condition, alteration of pharmacokinetics and in vivo stability should always be considered [102, 103]. Hence, in-depth knowledge of the labeling chemistry is required for the successful extrinsic radiolabeling.

11.4.2 Intrinsic Radiolabeling

Studies regarding four different methods of intrinsically radiolabeled NPs are well summarized in a recent review article by Goel et al. [104]. Briefly speaking these four methods are as below. The first method is 'Hot-plus-cold precursors'. As its name implies, this method is performed by adding trace amount of radioactive precursors to the non-radioactive precursors. As an example, Zhou et al. developed intrinsically ^{64}Cu-labeled copper sulfide (CuS) and the NPs showed passive targeting in mouse tumor model [7]. The second method is 'Specific trapping', which is a specific absorption of certain isotopes into appropriate NPs. Intrinsically radioactive upconverting NPs were made by trapping ^{18}F to rare-earth NPs, [^{18}F] NaYF4:Gd,Yb,Er [22]. The third strategy is 'Cation exchange', which have been utilized largely in ionic and semiconductor nanocrystals. This method is not yet

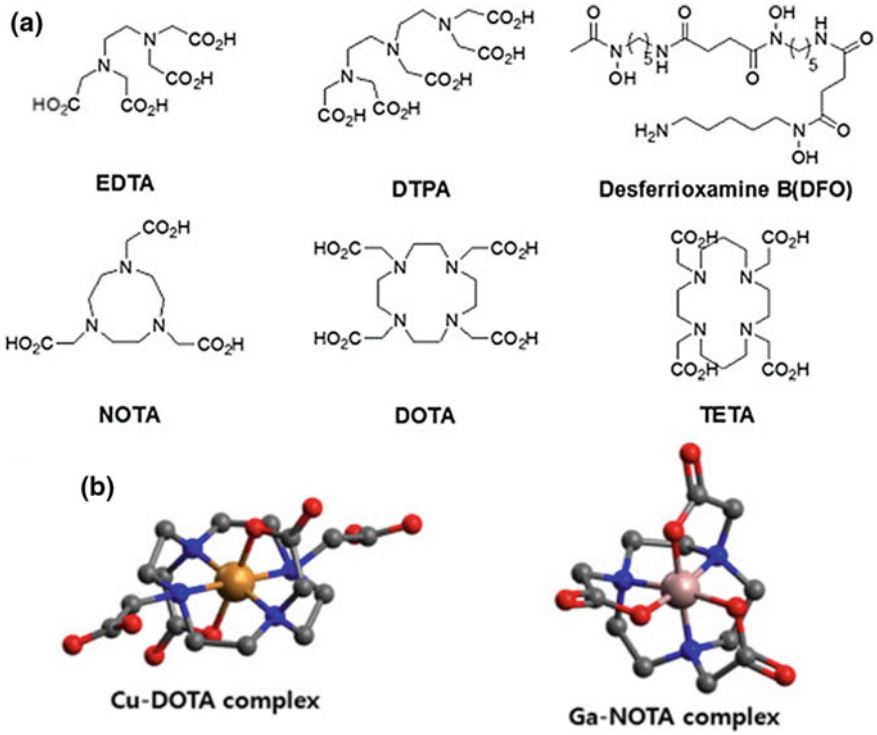

Fig. 11.6 Structures of the chelators for PET radioisotopes such as ^{68}Ga, ^{64}Cu, and ^{89}Zr. **a** The structures of EDTA, DTPA, DOTA, NOTA, TETA and DFO. **b** ^{64}Cu is shown to be positioned with the chelator DOTA and ^{68}Ga with NOTA (reprinted with permission from [52]. DTPA: diethylene triamine pentaacetic acid, DOTA: 1,4,7,10-tetraazacyclododecane-1,4,7,10-tetraacetic acid, NOTA: 1,4,7-triazacyclononane-1,4,7-triacetic acid, DFO: deferoxamine or desferrioxamine B

fully explored. Finally 'Proton beam activation' method involves direct irradiation of certain NPs with protons. The application of this method was limited due to the difficulty in accessing the proton beams. All the methods have in common that they do not use any chelator. This chelator-free method is attractive in that it offers an easier, faster, more stable and specific radiolabeling for radionanomedicine and further studies are warranted.

11.5 Conclusion

In conclusion, the development of the methods to enable surface labeling with ligands and chelators should be solved first. The development of the imaging methods to track the in vivo administered radiolabeled NPs is the next issue to be

addressed. With the improvement of above-mentioned issues, radiolabeled NPs can be successfully translated to clinical use.

The advantage of multifunctional radionanomedicines for in vivo application is that the amount of NPs can be decreased as low as possible even to trace amount. And multifunctional radionanomedicines can eliminate the concerns about the possible hazards of administering pharmacologic amount of NPs, and be used in a versatile way for a multiradioisotope or multitargeting approach. Finally, the tracer principle of this technology behind radionanomedicine using multifunctional radionanomaterials will help imaging and quantification so as to stimulate the progress of the translation of nanomedicine.

References

1. X. Sun, W. Cai, X. Chen, Positron emission tomography imaging using radiolabeled inorganic nanomaterials. Acc. Chem. Res. **48**(2), 286–294 (2015)
2. D.S. Lee, H.J. Im, Y.S. Lee, Radionanomedicine: widened perspectives of molecular theragnosis. Nanomedicine **11**(4), 795–810 (2015)
3. Y.-S. Lee, Y. Kim, D.S. Lee, Future perspectives of radionanomedicine using the novel micelle-encapsulation method for surface modification. Nucl. Med. Mol. Imaging **49**(3), 170–173 (2015)
4. M. Sun, D. Hoffman, G. Sundaresan, L. Yang, N. Lamichhane, J. Zweit, Synthesis and characterization of intrinsically radiolabeled quantum dots for bimodal detection. Am. J. Nucl. Med. Mol. Imaging **2**(2), 122–135 (2012)
5. G. Sun, J. Xu, A. Hagooly, R. Rossin, Z. Li, D.A. Moore et al., Strategies for optimized radiolabeling of nanoparticles for in vivo pet imaging. Adv. Mater. **19**(20), 3157–3162 (2007)
6. L. Yang, G. Sundaresan, M. Sun, P. Jose, D. Hoffman, P.R. McDonagh et al., Intrinsically radiolabeled multifunctional cerium oxide nanoparticles for in vivo studies. J. Mater. Chem. B Mater. Biol. Med. **1**(10), 1421–1431 (2013)
7. M. Zhou, R. Zhang, M. Huang, W. Lu, S. Song, M.P. Melancon et al., A chelator-free multifunctional [^{64}Cu]CuS nanoparticle platform for simultaneous micro-PET/CT imaging and photothermal ablation therapy. J. Am. Chem. Soc. **132**(43), 15351–15358 (2010)
8. R.M. Wong, D.A. Gilbert, K. Liu, A.Y. Louie, Rapid size-controlled synthesis of dextran-coated, 64Cu-doped iron oxide nanoparticles. ACS Nano **6**(4), 3461–3467 (2012)
9. Y. Zhao, D. Sultan, L. Detering, S. Cho, G. Sun, R. Pierce et al., Copper-64-alloyed gold nanoparticles for cancer imaging: improved radiolabel stability and diagnostic accuracy. Angew. Chem. Int. Ed. Engl. **53**(1), 156–159 (2014)
10. X. Lin, J. Xie, G. Niu, F. Zhang, H. Gao, M. Yang et al., Chimeric ferritin nanocages for multiple function loading and multimodal imaging. Nano Lett. **11**(2), 814–819 (2011)
11. T.W. Liu, T.D. MacDonald, J. Shi, B.C. Wilson, G. Zheng, Intrinsically copper-64-labeled organic nanoparticles as radiotracers. Angew. Chem. Int. Ed. Engl. **51**(52), 13128–13131 (2012)
12. N. Chanda, P. Kan, L.D. Watkinson, R. Shukla, A. Zambre, T.L. Carmack et al., Radioactive gold nanoparticles in cancer therapy: therapeutic efficacy studies of GA-^{198}AuNP nanoconstruct in prostate tumor-bearing mice. Nanomed. (Lond.) **6**(2), 201–209 (2010)
13. K.V. Katti, R. Kannan, K. Katti, V. Kattumori, R. Pandrapraganda, V. Rahing et al., Hybrid gold nanoparticles in molecular imaging and radiotherapy. Czech J. Phys. **56**(1), D23–D34 (2006)

14. M.K. Khan, L.D. Minc, S.S. Nigavekar, M.S. Kariapper, B.M. Nair, M. Schipper et al., Fabrication of ^{198}Au radioactive composite nanodevices and their use for nanobrachytherapy. Nanomed. (Lond.) **4**(1), 57–69 (2008)
15. R. Shukla, N. Chanda, A. Zambre, A. Upendran, K. Katti, R.R. Kulkarni et al., Laminin receptor specific therapeutic gold nanoparticles (^{198}AuNP-EGCg) show efficacy in treating prostate cancer. Proc. Natl. Acad. Sci. U S A **109**(31), 12426–12431 (2012)
16. C. Zhou, G. Hao, P. Thomas, J. Liu, M. Yu, S. Sun et al., Near-infrared emitting radioactive gold nanoparticles with molecular pharmacokinetics. Angew. Chem. Int. Ed. Engl. **51**(40), 10118–10122 (2012)
17. Y. Wang, Y. Liu, H. Luehmann, X. Xia, D. Wan, C. Cutler et al., Radioluminescent gold nanocages with controlled radioactivity for real-time in vivo imaging. Nano Lett. **13**(2), 581–585 (2013)
18. Y. Sun, X. Zhu, J. Peng, F. Li, Core-shell lanthanide upconversion nanophosphors as four-modal probes for tumor angiogenesis imaging. ACS Nano **7**(12), 11290–11300 (2013)
19. Y. Yang, Y. Sun, T. Cao, J. Peng, Y. Liu, Y. Wu et al., Hydrothermal synthesis of NaLuF4:153Sm, Yb, Tm nanoparticles and their application in dual-modality upconversion luminescence and SPECT bioimaging. Biomaterials **34**(3), 774–783 (2013)
20. J. Zeng, B. Jia, R. Qiao, C. Wang, L. Jing, F. Wang et al., In situ 111In-doping for achieving biocompatible and non-leachable ^{111}In-labeled Fe3O4 nanoparticles. Chem. Commun. (Camb.) **50**(17), 2170–2172 (2014)
21. Q. Liu, Y. Sun, C. Li, J. Zhou, T. Yang, X. Zhang et al., ^{18}F-Labeled magnetic-upconversion nanophosphors via rare-Earth cation-assisted ligand assembly. ACS Nano **5**(4), 3146–3157 (2011)
22. Y. Sun, M. Yu, S. Liang, Y. Zhang, C. Li, T. Mou et al., Fluorine-18 labeled rare-earth nanoparticles for positron emission tomography (PET) imaging of sentinel lymph node. Biomaterials **32**(11), 2999–3007 (2011)
23. F. Chen, P.A. Ellison, C.M. Lewis, H. Hong, Y. Zhang, S. Shi et al., Chelator-free synthesis of a dual-modality PET/MRI agent. Angew. Chem. Int. Ed. Engl. **52**(50), 13319–13323 (2013)
24. R. Chakravarty, H.F. Valdovinos, F. Chen, C.M. Lewis, P.A. Ellison, H. Luo et al., Intrinsically germanium-69-labeled iron oxide nanoparticles: synthesis and in-vivo dual-modality PET/MR imaging. Adv. Mater. **26**(30), 5119–5123 (2014)
25. A.N. Mendoza-Sanchez, G. Ferro-Flores, B.E. Ocampo-Garcia, E. Morales-Avila, F. de M Ramírez, L.M. De Leon-Rodriguez et al., Lys3-bombesin conjugated to ^{99m}Tc-labeled gold nanoparticles for in vivo gastrin releasing peptide-receptor imaging. J. Biomed. Nanotechnol. **6**(4), 375–384 (2010)
26. E. Morales-Avila, G. Ferro-Flores, B.E. Ocampo-Garcia, L.M. De Leon-Rodriguez, C.L. Santos-Cuevas, R. Garcia-Becerra et al., Multimeric system of ^{99m}Tc-labeled gold nanoparticles conjugated to c[RGDfK(C)] for molecular imaging of tumor alpha(v)beta(3) expression. Bioconjug. Chem. **22**(5), 913–922 (2011)
27. B.E. Ocampo-Garcia, M. Ramirez Fde, G. Ferro-Flores, L.M. De Leon-Rodriguez, C.L. Santos-Cuevas, E. Morales-Avila et al., ^{99m}Tc-labeled gold nanoparticles capped with HYNIC-peptide/mannose for sentinel lymph node detection. Nucl. Med. Biol. **38**(1), 1–11 (2011)
28. G. Zhang, Z. Yang, W. Lu, R. Zhang, Q. Huang, M. Tian et al., Influence of anchoring ligands and particle size on the colloidal stability and in vivo biodistribution of polyethylene glycol-coated gold nanoparticles in tumor-xenografted mice. Biomaterials **30**(10), 1928–1936 (2009)
29. R. Torres Martin de Rosales R, R. Tavare, A. Glaria, G. Varma, A. Protti, P.J. Blower, ^{99m}Tc-bisphosphonate-iron oxide nanoparticle conjugates for dual-modality biomedical imaging. Bioconjug. Chem. **22**(3), 455–465 (2011)
30. W. Cai, K. Chen, Z.B. Li, S.S. Gambhir, X. Chen, Dual-function probe for PET and near-infrared fluorescence imaging of tumor vasculature. J. Nucl. Med. **48**(11), 1862–1870 (2007)

31. K. Chen, P.S. Conti, Target-specific delivery of peptide-based probes for PET imaging. Adv. Drug Deliv. Rev. **62**(11), 1005–1022 (2010)
32. H. Xie, P. Diagaradjane, A.A. Deorukhkar, B. Goins, A. Bao, W.T. Phillips et al., Integrin alphavbeta3-targeted gold nanoshells augment tumor vasculature-specific imaging and therapy. Int. J. Nanomed. **6**, 259–269 (2011)
33. C. Glaus, R. Rossin, M.J. Welch, G. Bao, In vivo evaluation of ^{64}Cu-labeled magnetic nanoparticles as a dual-modality PET/MR imaging agent. Bioconjug. Chem. **21**(4), 715–722 (2010)
34. B.R. Jarrett, B. Gustafsson, D.L. Kukis, A.Y. Louie, Synthesis of ^{64}Cu-labeled magnetic nanoparticles for multimodal imaging. Bioconjug. Chem. **19**(7), 1496–1504 (2008)
35. H.Y. Lee, Z. Li, K. Chen, A.R. Hsu, C. Xu, J. Xie et al., PET/MRI dual-modality tumor imaging using arginine-glycine-aspartic (RGD)-conjugated radiolabeled iron oxide nanoparticles. J. Nucl. Med. **49**(8), 1371–1379 (2008)
36. Z. Liu, W. Cai, L. He, N. Nakayama, K. Chen, X. Sun et al., In vivo biodistribution and highly efficient tumour targeting of carbon nanotubes in mice. Nat. Nanotechnol. **2**(1), 47–52 (2007)
37. A.L. Petersen, T. Binderup, P. Rasmussen, J.R. Henriksen, D.R. Elema, A. Kjaer et al., ^{64}Cu loaded liposomes as positron emission tomography imaging agents. Biomaterials **32**(9), 2334–2341 (2011)
38. J. Guo, X. Zhang, Q. Li, W. Li, Biodistribution of functionalized multiwall carbon nanotubes in mice. Nucl. Med. Biol. **34**(5), 579–583 (2007)
39. R. Singh, D. Pantarotto, L. Lacerda, G. Pastorin, C. Klumpp, M. Prato et al., Tissue biodistribution and blood clearance rates of intravenously administered carbon nanotube radiotracers. Proc. Natl. Acad. Sci. U S A **103**(9), 3357–3362 (2006)
40. M.R. McDevitt, D. Chattopadhyay, B.J. Kappel, J.S. Jaggi, S.R. Schiffman, C. Antczak et al., Tumor targeting with antibody-functionalized, radiolabeled carbon nanotubes. J. Nucl. Med. **48**(7), 1180–1189 (2007)
41. R. Zhang, W. Lu, X. Wen, M. Huang, M. Zhou, D. Liang et al., Annexin A5-conjugated polymeric micelles for dual SPECT and optical detection of apoptosis. J. Nucl. Med. **52**(6), 958–964 (2011)
42. J.C. Park, M.K. Yu, G.I. An, S.I. Park, J. Oh, H.J. Kim et al., Facile preparation of a hybrid nanoprobe for triple-modality optical/PET/MR imaging. Small **6**(24), 2863–2868 (2010)
43. J. Lee, T.S. Lee, J. Ryu, S. Hong, M. Kang, K. Im et al., RGD peptide-conjugated multimodal $NaGdF_4$:Yb^{3+}/Er^{3+} nanophosphors for upconversion luminescence, MR, and PET imaging of tumor angiogenesis. J. Nucl. Med. **54**(1), 96–103 (2013)
44. J. Cao, Y. Wang, J. Yu, J. Xia, C. Zhang, D. Yin et al., Preparation and radiolabeling of surface-modified magnetic nanoparticles with rhenium-188 for magnetic targeted radiotherapy. J. Magn. Magn. Mater. **277**(1–2), 165–174 (2004)
45. S. Liang, Y. Wang, J. Yu, C. Zhang, J. Xia, D. Yin, Surface modified superparamagnetic iron oxide nanoparticles: as a new carrier for bio-magnetically targeted therapy. J. Mater. Sci. Mater. Med. **18**(12), 2297–2302 (2007)
46. Y.J. Chang, C.H. Chang, T.J. Chang, C.Y. Yu, L.C. Chen, M.L. Jan et al., Biodistribution, pharmacokinetics and microSPECT/CT imaging of ^{188}Re-bMEDA-liposome in a C26 murine colon carcinoma solid tumor animal model. Anticancer Res. **27**(4B), 2217–2225 (2007)
47. M. Luna-Gutiérrez, G. Ferro-Flores, B.E. Ocampo-García, C.L. Santos-Cuevas, N. Jiménez-Mancilla, L.M. De León-Rodríguez et al., A therapeutic system of ^{177}Lu-labeled gold nanoparticles-RGD internalized in breast cancer cells. J. Mex. Chem. Soc. **57**, 212–219 (2013)
48. Y.K. Lee, J.M. Jeong, L. Hoigebazar, B.Y. Yang, Y.-S. Lee, B.C. Lee et al., Nanoparticles modified by encapsulation of ligands with a long alkyl chain to affect multispecific and multimodal imaging. J. Nucl. Med. **53**(9), 1462–1470 (2012)

49. W. do Hwang, H.Y. Ko, J.H. Lee, H. Kang, S.H. Ryu, I.C. Song et al., A nucleolin-targeted multimodal nanoparticle imaging probe for tracking cancer cells using an aptamer. J. Nucl. Med. **51**(1), 98–105 (2010)
50. I. Velikyan, Prospective of ^{68}Ga-radiopharmaceutical development. Theranostics **4**(1), 47–80 (2013)
51. C.J. Anderson, R. Ferdani, Copper-64 radiopharmaceuticals for PET imaging of cancer: advances in preclinical and clinical research. Cancer Biother. Radiopharm. **24**(4), 379–393 (2009)
52. A. Niccoli Asabella, G.L. Cascini, C. Altini, D. Paparella, A. Notaristefano, G. Rubini, The copper radioisotopes: a systematic review with special interest to ^{64}Cu. Biomed. Res. Int. 786463 (2014)
53. G. Fischer, U. Seibold, R. Schirrmacher, B. Wangler, C. Wangler, ^{89}Zr, a radiometal nuclide with high potential for molecular imaging with PET: chemistry, applications and remaining challenges. Molecules **18**(6), 6469–6490 (2013)
54. B.L.R. Kam, J.J.M. Teunissen, E.P. Krenning, W.W. de Herder, S. Khan, E.I. van Vliet et al., Lutetium-labeled peptides for therapy of neuroendocrine tumours. Eur. J. Nucl. Med. Mol. Imaging **39**(1), 103–112 (2012)
55. A. Sainz-Esteban, V. Prasad, C. Schuchardt, C. Zachert, J.M. Carril, R.P. Baum, Comparison of sequential planar ^{177}Lu-DOTA-TATE dosimetry scans with ^{68}Ga-DOTA-TATE PET/CT images in patients with metastasized neuroendocrine tumours undergoing peptide receptor radionuclide therapy. Eur. J. Nucl. Med. Mol. Imaging **39**(3), 501–511 (2012)
56. V. Goffredo, A. Paradiso, G. Ranieri, C.D. Gadaleta, Yttrium-90 (^{90}Y) in the principal radionuclide therapies: an efficacy correlation between peptide receptor radionuclide therapy, radioimmunotherapy and transarterial radioembolization therapy. Ten years of experience (1999–2009). Crit. Rev. Oncol. Hematol. **80**(3), 393–410 (2011)
57. H. Hong, Y. Zhang, J. Sun, W. Cai, Molecular imaging and therapy of cancer with radiolabeled nanoparticles. Nano Today. **4**(5), 399–413 (2009)
58. J.M. Jeong, J.K. Chung, Therapy with ^{188}Re-labeled radiopharmaceuticals: an overview of promising results from initial clinical trials. Cancer Biother. Radiopharm. **18**(5), 707–717 (2003)
59. L. Tian, Q. Chen, X. Yi, G. Wang, J. Chen, P. Ning et al., Radionuclide I-131 labeled albumin-paclitaxel nanoparticles for synergistic combined chemo-radioisotope therapy of cancer. Theranostics **7**(3), 614–623 (2017)
60. M.E. Akerman, W.C. Chan, P. Laakkonen, S.N. Bhatia, E. Ruoslahti, Nanocrystal targeting in vivo. Proc. Natl. Acad. Sci. U S A **99**(20), 12617–12621 (2002)
61. J.V. Jokerst, T. Lobovkina, R.N. Zare, S.S. Gambhir, Nanoparticle PEGylation for imaging and therapy. Nanomed. (Lond.) **6**(4), 715–728 (2011)
62. L.E. van Vlerken, T.K. Vyas, M.M. Amiji, Poly(ethylene glycol)-modified nanocarriers for tumor-targeted and intracellular delivery. Pharm. Res. **24**(8), 1405–1414 (2007)
63. H. Maeda, J. Wu, T. Sawa, Y. Matsumura, K. Hori, Tumor vascular permeability and the EPR effect in macromolecular therapeutics: a review. J. Control Release **65**(1–2), 271–284 (2000)
64. G.S. Kwon, Polymeric micelles for delivery of poorly water-soluble compounds. Crit. Rev. Ther. Drug Carr. Syst. **20**(5), 357–403 (2003)
65. Y. Barenholz, Doxil(R)–the first FDA-approved nano-drug: lessons learned. J. Control Release **160**(2), 117–134 (2012)
66. J. Nam, N. Won, J. Bang, H. Jin, J. Park, S. Jung et al., Surface engineering of inorganic nanoparticles for imaging and therapy. Adv. Drug Deliv. Rev. **65**(5), 622–648 (2013)
67. R.P. Baum, V. Prasad, D. Müller, C. Schuchardt, A. Orlova, A. Wennborg et al., Molecular imaging of HER2-expressing malignant tumors in breast cancer patients using synthetic ^{111}In- or ^{68}Ga-labeled affibody molecules. J. Nucl. Med. **51**(6), 892–897 (2010)

68. O.C. Farokhzad, S. Jon, A. Khademhosseini, TNT Tran, DA LaVan, R. Langer, Nanoparticle-aptamer bioconjugates: a new approach for targeting prostate cancer cells. Cancer Res. **64**(21), 7668–7672 (2004)
69. P.E. Saw, S. Kim, Lee I-h, J. Park, M. Yu, J. Lee et al., Aptide-conjugated liposome targeting tumor-associated fibronectin for glioma therapy. J. Mater. Chem. B Mater. Biol. Med. **1**(37), 4723–4726 (2013)
70. V.J. Ruigrok, M. Levisson, M.H. Eppink, H. Smidt, J. van der Oost, Alternative affinity tools: more attractive than antibodies? Biochem. J. **436**(1), 1–13 (2011)
71. A.M. Scott, J.D. Wolchok, L.J. Old, Antibody therapy of cancer. Nat. Rev. Cancer **12**(4), 278–287 (2012)
72. T.E. Witzig, L.I. Gordon, F. Cabanillas, M.S. Czuczman, C. Emmanouilides, R. Joyce et al., Randomized controlled trial of yttrium-90–labeled ibritumomab tiuxetan radioimmunotherapy versus rituximab immunotherapy for patients with relapsed or refractory low-grade, follicular, or transformed b-cell non-hodgkin's lymphoma. J. Clin. Oncol. **20**(10), 2453–2463 (2002)
73. R.L. Wahl, Tositumomab and (131)I therapy in non-Hodgkin's lymphoma. J. Nucl. Med. **46** (Suppl 1), 128S–140S (2005)
74. H. Hong, Y. Zhang, G.W. Severin, Y. Yang, J.W. Engle, G. Niu et al., Multimodality imaging of breast cancer experimental lung metastasis with bioluminescence and a monoclonal antibody dual-labeled with ^{89}Zr and IRdye 800cw. Mol. Pharm. **9**(8), 2339–2349 (2012)
75. R. Rezaeipoor, R. John, S.G. Adie, E.J. Chaney, M. Marjanovic, A.L. Oldenburg et al., Fc-directed antibody conjugation of magnetic nanoparticles for enhanced molecular targeting. J. Innov. Opt. Health Sci. **2**(4), 387–396 (2009)
76. S. Kumar, J. Aaron, K. Sokolov, Directional conjugation of antibodies to nanoparticles for synthesis of multiplexed optical contrast agents with both delivery and targeting moieties. Nat. Protoc. **3**(2), 314–320 (2008)
77. M.M. Cardoso, I.N. Peca, A.C. Roque, Antibody-conjugated nanoparticles for therapeutic applications. Curr. Med. Chem. **19**(19), 3103–3127 (2012)
78. S. Jeong, J.Y. Park, M.G. Cha, H. Chang, Y.I. Kim, H.M. Kim et al., Highly robust and optimized conjugation of antibodies to nanoparticles using quantitatively validated protocols. Nanoscale **9**(7), 2548–2555 (2017)
79. H. Wang, Y.L. Liu, Y.H. Yang, T. Deng, G.L. Shen, R.Q. Yu, A protein A-based orientation-controlled immobilization strategy for antibodies using nanometer-sized gold particles and plasma-polymerized film. Anal. Biochem. **324**(2), 219–226 (2004)
80. S. Mazzucchelli, M. Colombo, C. De Palma, A. Salvade, P. Verderio, M.D. Coghi et al., Single-domain protein a-engineered magnetic nanoparticles: toward a universal strategy to site-specific labeling of antibodies for targeted detection of tumor cells. ACS Nano **4**(10), 5693–5702 (2010)
81. A. Makaraviciute, A. Ramanaviciene, Site-directed antibody immobilization techniques for immunosensors. Biosens. Bioelectron. **50**, 460–471 (2013)
82. M. Salehi, L. Schneider, P. Strobel, A. Marx, J. Packeisen, S. Schlucker, Two-color SERS microscopy for protein co-localization in prostate tissue with primary antibody-protein A/G-gold nanocluster conjugates. Nanoscale **6**(4), 2361–2367 (2014)
83. B. Dubertret, P. Skourides, D.J. Norris, V. Noireaux, A.H. Brivanlou, A. Libchaber, In vivo imaging of quantum dots encapsulated in phospholipid micelles. Science **298**(5599), 1759–1762 (2002)
84. H. Fan, K. Yang, D.M. Boye, T. Sigmon, K.J. Malloy, H. Xu et al., Self-assembly of ordered, robust, three-dimensional gold nanocrystal/silica arrays. Science **304**(5670), 567–571 (2004)
85. H. Fan, E.W. Leve, C. Scullin, J. Gabaldon, D. Tallant, S. Bunge et al., Surfactant-assisted synthesis of water-soluble and biocompatible semiconductor quantum dot micelles. Nano Lett. **5**(4), 645–648 (2005)

86. O. Carion, B. Mahler, T. Pons, B. Dubertret, Synthesis, encapsulation, purification and coupling of single quantum dots in phospholipid micelles for their use in cellular and in vivo imaging. Nat. Protoc. **2**(10), 2383–2390 (2007)
87. H. Wu, H. Zhu, J. Zhuang, S. Yang, C. Liu, Y.C. Cao, Water-soluble nanocrystals through dual-interaction ligands. Angew. Chem. Int. Ed. Engl. **47**(20), 3730–3734 (2008)
88. A. Samanta, K.K. Maiti, K.S. Soh, X. Liao, M. Vendrell, U.S. Dinish et al., Ultrasensitive near-infrared Raman reporters for SERS-based in vivo cancer detection. Angew. Chem. Int. Ed. Engl. **50**(27), 6089–6092 (2011)
89. B.-H. Jun, D.W. Hwang, H.S. Jung, J. Jang, H. Kim, H. Kang et al., Ultrasensitive, biocompatible, quantum-dot-embedded silica nanoparticles for bioimaging. Adv. Funct. Mater. **22**(9), 1843–1849 (2012)
90. B.Y. Yang, S.H. Moon, S.R. Seelam, M.J. Jeon, Y.S. Lee, D.S. Lee et al., Development of a multimodal imaging probe by encapsulating iron oxide nanoparticles with functionalized amphiphiles for lymph node imaging. Nanomed. (Lond.) **10**(12), 1899–1910 (2015)
91. D.S. Lee, Preparation of multifunctional multimodal nanoparticles using specific amphiphiles: click chemistry for nanoparticles. Annu. Congress Clinam (Abstr.) (2013)
92. D.S. Lee, In vivo application of Cu-64 labeled upconversion nanoparticles. Annu. Congress Clinam (Abstr.) (2014)
93. H. Kang, S. Jeong, Y. Park, J. Yim, B.-H. Jun, S. Kyeong et al., Near-infrared SERS nanoprobes with plasmonic Au/Ag hollow-shell assemblies for in vivo multiplex detection. Adv. Funct. Mater. **23**(30), 3719–3727 (2013)
94. K. Susumu, H.T. Uyeda, I.L. Medintz, T. Pons, J.B. Delehanty, H. Mattoussi, Enhancing the stability and biological functionalities of quantum dots via compact multifunctional ligands. J. Am. Chem. Soc. **129**(45), 13987–13996 (2007)
95. J. Hrkach, D. Von Hoff, M. Mukkaram Ali, E. Andrianova, J. Auer, T. Campbell et al., Preclinical development and clinical translation of a PSMA-targeted docetaxel nanoparticle with a differentiated pharmacological profile. Sci. Transl. Med. **4**(128), 128ra39 (2012)
96. F. Danhier, B. Vroman, N. Lecouturier, N. Crokart, V. Pourcelle, H. Freichels et al., Targeting of tumor endothelium by RGD-grafted PLGA-nanoparticles loaded with paclitaxel. J. Control Release **140**(2), 166–173 (2009)
97. D. Sarko, M. Eisenhut, U. Haberkorn, W. Mier, Bifunctional chelators in the design and application of radiopharmaceuticals for oncological diseases. Curr. Med. Chem. **19**(17), 2667–2688 (2012)
98. Y. Xing, J. Zhao, P.S. Conti, K. Chen, Radiolabeled nanoparticles for multimodality tumor imaging. Theranostics **4**(3), 290–306 (2014)
99. G.F.F. Enrique Morales-Avila, B.E. Ocampo-García, F. de María Ramírez, *Radiolabeled Nanoparticles for Molecular Imaging*, ed. by B. Schaller. (InTech) (2012)
100. T.J. Wadas, E.H. Wong, G.R. Weisman, C.J. Anderson, Coordinating radiometals of copper, gallium, indium, yttrium, and zirconium for PET and SPECT imaging of disease. Chem. Rev. **110**(5), 2858–2902 (2010)
101. Y.-S. Lee, in *Radiopharmaceutical Chemistry*, ed. by E.E. Kim, U. Tateishi, R. Baum. Handbook of Nuclear Medicine and Molecular Imaging (World Scientific Publishing Co. Pte. Ltd, NJ, 2012) pp. 21–51
102. W.T. Phillips, B.A. Goins, A. Bao, Radioactive liposomes. Wiley Interdiscip. Rev. Nanomed. Nanobiotechnol. **1**(1), 69–83 (2009)
103. S. Jeger, K. Zimmermann, A. Blanc, J. Grunberg, M. Honer, P. Hunziker et al., Site-specific and stoichiometric modification of antibodies by bacterial transglutaminase. Angew. Chem. Int. Ed. Engl. **49**(51), 9995–9997 (2010)
104. S. Goel, F. Chen, E.B. Ehlerding, W. Cai, Intrinsically radiolabeled nanoparticles: an emerging paradigm. Small **10**(19), 3825–3830 (2014)

Part IV
Targeted Delivery with Click Chemistry

Chapter 12: Click Chemistry for Radionanomedicine Platform
Chapter 13: Preservation of Ligand Functionality by Click Chemistry
Chapter 14: Bioorthogonal Reaction for Fluorine-18 Labeling

Surface-modified and radiolabeled nanomaterials are now to be delivered to the targets, i.e., tumors in destructive therapy and injured/degenerative tissues in regenerative therapy. Targeted delivery is the goal of administering the radionanomaterials or radionanomedicines, in another word, the radiolabeled nanomaterials as pharmaceuticals, to the body. Preserving the functional integrity of the targeting ligand is now essential for the desired success of targeted delivery, which will be the bottleneck of the entire endeavor of developing, introducing and translating the radionanomedicines to humans and clinics. There have been and are controversy that nanomaterials reach targets by passive delivery or active targeting. One needs to prove the effectiveness of active targeting over the passive delivery and this is also the case with radiolabeled nanomaterials. Click chemistry especially copper-free reaction is now well established so that the remaining works are finding wider application and optimization for each nanomaterial of interest. Copper-catalyzed click chemistry should have been avoided because surplus coppers are going to interact with bodily peptides and macromolecules and prevent the use of Cu-64 or other radiometals competing with the chelation. This meant that click chemistry should have been aloof from intrinsic biomacromolecules which is later expressed as "bioorthogonal". Bioorthogonal reaction among cycloaddition click chemistry even allowed two-step approach for targeted delivery and their imaging. Using bioorthogonal reaction and click chemistry, one could follow the biodistribution of pretargeted biomolecules and nanomaterials by injecting later the radiolabeled tracer. This could overcome the difference of long half-time of clearance or accumulation of nanomaterials and the short half-life of tracer.

In this part, the readers will find the multifaceted interpretation, the first of which in Chap. 12 emphasized the incorporation of proper kinds of click chemistry to

make radionanomaterials based on nanoplatform concept. This will make (1) manufacturing part making precursor chelator or click donor-conjugated nanomaterials and (2) compounding part labeling radionuclide to the chelators on the nanomaterials or mixing click recipient-chelator prelabeled with radionuclides, respectively. In Chap. 13, the authors will emphasize the advantage of click chemistry which allows very rapid reaction in vitro under ambient condition and underline the functional integrities of the product and even enabling pretargeted imaging strategy. The readers will find the core concept of click chemistry overcoming the delicate problem of maintaining integrity of surface-modifying materials bound in various ways. In Chap. 14, the author emphasized bioorthogonal reaction and finally focused on the F-18 labeling of biomacromolecules and nanomaterials. Successful report of pretargeting imaging strategy with F-18 was detailed and the beauty of this approach is that its expandability can be found in this chapter. Now, we need more practical examples of this reaction.

Chapter 12
Click Chemistry for Radionanomedicine Platform

Yun-Sang Lee, Lingyi Sun and Dexing Zeng

Abstract The emerging radionanomedicine has multifunctional and theranostic purposes. To fulfill these purposes, the radionanomedicine should achieve efficient and specific delivery of therapeutic agents by their multifunctionality with very low amount of nanomaterials used in vivo. Recent researches on radiolabeled micelle-encapsulated nanomaterials are promising for their efficacy and safety as one-step surface modification method. This one-step multifunctional approach to the nanoparticles is important to meet the challenges of manufacturing and is the basis for making the effective nano-platforms for disease-targeted imaging and therapy. Based on 'click chemistry' concept, great progress have been achieved in the field of radiochemistry and nanomedicine. Click chemistry can be used for the surface modification of nanomedicines, such as hydrophilization, target molecule ligation, therapeutic drug conjugation, and labeling sensor molecules including fluorescence dyes or radioisotopes. By the conventional step-by-step chemical modification method of nanomaterials, two or more combination of those modifications can hardly achieve practicability, because of the low yield of each step of

Y.-S. Lee (✉)
Department of Nuclear Medicine, Seoul National University College of Medicine, Seoul 03080, Republic of Korea
e-mail: wonza43@snu.ac.kr

Y.-S. Lee
Department of Molecular Medicine and Biopharmaceutical Sciences, Graduate School of Convergence Science and Technology, Seoul National University, Seoul 08826, Republic of Korea

L. Sun · D. Zeng (✉)
Department of Medicine, University of Pittsburgh School of Medicine, Pittsburgh, PA 15260, USA
e-mail: zengd@upmc.edu

L. Sun
e-mail: lis85@pitt.edu

D. Zeng
Department of Radiology, University of Pittsburgh School of Medicine, Pittsburgh, PA 15213, USA

D. S. Lee (ed.), *Radionanomedicine*, Biological and Medical Physics, Biomedical Engineering, https://doi.org/10.1007/978-3-319-67720-0_12

the purification and modification. Another beauty of click chemistry for nanomedicine is the avoidance of harsh reaction condition, such as high/low pH, temperature, or reducing/oxidizing conditions, which result in the aggregation of nanomaterials or degradation of biomolecules. Numerous nanomedicine platforms have been proposed and used in in vitro assay, in vivo imaging, drug delivery, or theranostics. However, in considering manufacturing or commercialization of radionanomedicine platform, still there are much rooms to be improved. In this chapter, we focus on the current status for the 'clickable' nanomedicine platforms and how we can or will be able to reach the goal of clinical translation using this technology.

The key concept of "click chemistry", which was firstly coined by K. Barry Sharpless group in 2001, is the any kind of chemical reaction that can be easily and rapidly achieved [1]. Following this concept, great progress have been achieved in the field of radiochemistry and nanomedicine [2–4]. Click chemistry can be used for the surface modification of nanomedicine, such as hydrophilization, target molecule ligation, therapeutic drug conjugation, labeling sensor molecules, such as fluorescence dye or radioisotope. By the conventional step-by-step chemical modification method of nanomaterials, two or more combination of those modifications can by hardly achieved, because of the low yield of the purification after each modification step. Another beauty of click chemistry for nanomedicine is the avoidance of harsh reaction condition, such as high/low pH, temperature, or reductant/oxidant, which can result in the aggregation of nanomaterials or degradation of biomolecules.

Numerous nanomedicine platforms have been proposed and used in in vitro assay, in vivo imaging, drug delivery, or theragnosis. However, in considering manufacturing or commercialization of nanomedicine platform, still there are so many things to be improved. In this chapter, we focus on the current status for the "clickable" radionanomedicine platform and how we can or will be able to reach the goal of clinical translation.

12.1 Click Chemistry Overview

Cu(I)-catalyzed azide-alkyne cycloaddtion (CuAAC) [5], strain-promoted azide-alkyne cycloaddition (SPAAC) [6], and inverse electron demand Diels-Alder cycloaddition (iEDDA) using tetrazine and *trans*-cyclooctene (TCO) [7] are most widely used click reaction in radiochemistry and nanomedicine application (Fig. 12.1). Relatively aged-reaction in organic chemistry, CuAAC reaction has been more frequently used in radiolabeling. However, Cu(I/II) cations accidentally formed Cu-peptide complexes in ^{18}F labeling using CuAAC [8]. This problem is more complicated in radiolabeling with radiometals and chelating agent, because the labeled radiometal-chelate complex could be trans-chelated by cold Cu in click

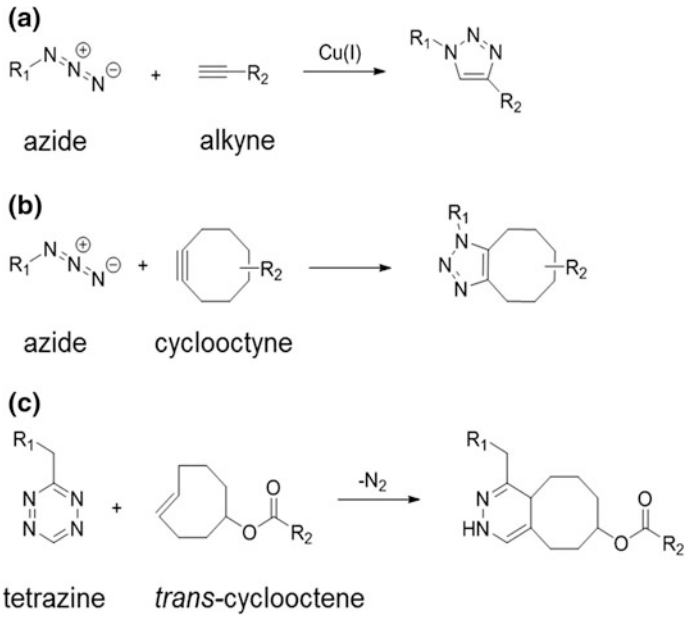

Fig. 12.1 Frequently used click chemistry for nanomaterial application. **a** Azide-alkyne reaction with Cu(I) catalyst. **b** Cupper-free azide-cyclooctyne reaction. **c** Cupper-free tetrazine-*trans*-cyclooctene (TCO) reaction

reaction step [9]. SPAAC and iEDDA reaction have an advantage with the bioorthogonal and Cu-free reaction over CuAAC. In the concern of reaction time, iEDDA reaction (10^2–10^5 M^{-1} s^{-1}) is faster than SPAAC reaction (0.0012–0.96 M^{-1} s^{-1}) [10]. From this comparison, SPAAC or iEDDA will be the better choice for chemical modification of nanomaterials.

12.2 Hydrophilization

Normally, hard core nanomaterials has hydrophobic tails on their surface after the core synthesis, therefore, we need to hydrophilize the nanomaterials using polyethylene glycol (PEG) or natural and synthetic polymers including dextran for in vivo application. Other soft nanomaterials, such as liposome, exosome, micelle, protein nanoparticles or synthetic polymer, do not need further hydrophilization, because they have the hydrophilic moiety on their surface.

The inspiration from the success of hydrophilization of nanomaterials using the micelle encapsulation method by Dubertret and colleagues [11], Jeong's group integrated these developments to make a quick and straightforward method of mixing, sonicating, and size exclusion chromatography for producing

multifunctional nanoparticles [12]. This method has been successfully applied other hard core nanomaterials, such as iron oxide particles with a diameter of 5 nm [13, 14], upconverting NPs (UCNPs) with a diameter of 35 nm [15]. After the micelle encapsulation, total size of nanoparticle is increased for 5–6 nm, and this increase is matched with the length of PEGs from Tween 60®. The size distribution of encapsulated nanoparticles is quite narrow (poly dispersity index: PDI < 0.2) by dynamic light scattering (DLS) measurement [13, 14]. Because the size of nanomaterials affect the in vivo distribution of nanomaterials, nanomaterials should maintain the narrow size distribution after core synthesis and any chemical modification including hydrophilization and radiolabeling.

For construction of clickable radionanomedicine platform, we can simply mix the alkyl-chained click moiety, such as azide- or diarylcyclooctyne (DBCO)-C_{18}, with Tween 60® (Fig. 12.1). This nano-platform can be used for further modification for target molecule ligation, therapeutic drug conjugation or radio/fluorescent-labeling.

12.3 Conjugation of Targeting Molecules

Enhanced permeability and retention (EPR) effect has been believed to constitute a major mechanism for the passive delivery and accumulation of nanomaterials in the tumor tissue for several decades [16]. Despite the success of nanomedicines without targeting molecules, in early approval from US Food and Drug Administration (FDA), such as Doxil®, doxorubicin containing liposomal system, or Abraxane®, paclitaxel-albumin nanoparticles, which suggested EPR was sufficient for drug efficacy, this EPR effect is still under controversy because of its poor treatment score in clinical setting probably due to the heterogeneity of tumor and microenvironment [17, 18]. To overcome this problem, active or disease-specific targeting strategy would be another option for nanomedicines, which can be accomplished by attaching targeting molecules on the surface of nanomaterials. Considering that the click chemistry has the great advantage over conventional conjugation method, there are so far the limited numbers of application of this click chemistry on nanomaterials. Therefore, here we summarize all the possible targeting molecules that the investigators can use click chemistry for modification but not. However, all these targeting molecules, which were well summarized in Theranostics [19], as will be discussed below can be modified with click chemical and applied for click chemistry.

12.3.1 Small Molecules

There are huge varieties of target disease and disease-specific targeting molecules, and these molecules are categorized by size from small molecules to

macromolecules. Nowadays, by the help of the great contribution of scientists on drug development, for selection of target disease and disease-targeting molecules, one can simply search on the internet or database to find enough candidate molecules to choose a proper disease-targeting molecule for each disease. Small molecules including low molecular-weight chemicals, carbohydrates, nucleic acids, or small peptides have good potential as a disease targeting molecule on nanomaterials.

Arginine-glycine-aspartate (RGD) peptide targets the integrin $\alpha_v\beta_3$, which is an ideal vascular target protein considering its high expression on endothelial cells of newly formed vessels in correlation with disease progression [20]. The RGD peptide has been the most widely used as modification or the surface of nanomaterials, either for therapy or drug delivery. This is because integrin $\alpha_v\beta_3$ expression was high on U87MG cells, and it was easy to get this cell line and to establish animal model for the proof-of concept study. Lee et al. showed the typical example of tumor targeting strategy using RGD peptide [12]. In this study, ^{68}Ga labeled quantum dots (QDs) decorated with RGD peptide accumulated at integrin $\alpha_v\beta_3$ positive tumor (U87MG), not at the negative tumor (A431) and showed the specificity on the blocking study using excess cold RGD (Fig. 12.2). There were also other reports using RGD conjugated nanomaterials for targeting or delivery of

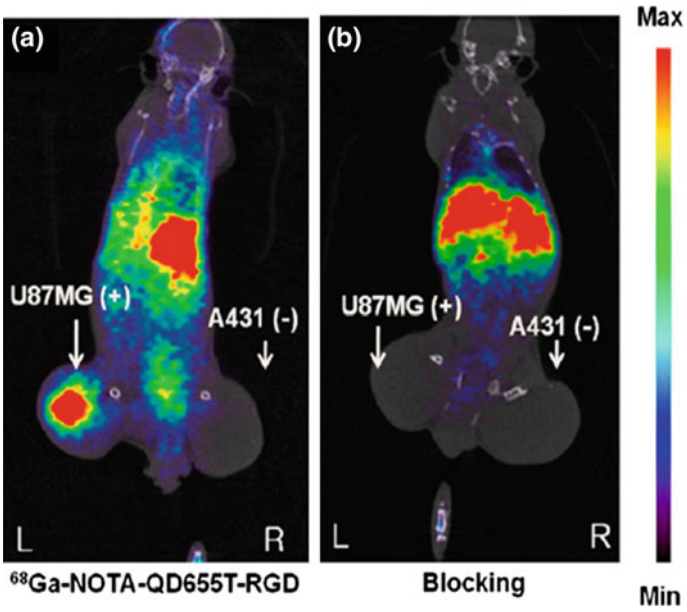

Fig. 12.2 PET images of U87MG and A431 tumor–bearing nude mice ac-quired at 60 min after intravenous injection. **a** ^{68}Ga-NOTA-QD655TRGD shows high uptake in U87MG tumor but not in A431 tumor. **b** ^{68}Ga-NOTA-QD655T-RGD can be completely blocked by co-injection of free c(RGDyK), representing specific uptake (copyright permission from [12])

therapeutic drugs to the tumors, using liposome [21, 22], iron oxide nanoparticles [23], or gold nanoparticles [24], etc.

Carbohydrates are another class of small molecules requiring targeting ligands that selectively recognize cell surface receptors, such as mannose receptor (cluster of differentiation or classification determinant 206, CD 206) or asialoglycoprotein receptor (ASGP-R). Lymphoseek (^{99m}Tc-tilmanocept) is the ^{99m}Tc labeled nanocomposite using dextran polymer decorated mannose molecules on it, which can target the mannose receptor of monocytes/macrophages homing to lymph nodes and has the clinical indication for lymphatic mapping with a hand-held gamma counter to assist in the localization of lymph nodes draining the primary tumor in patients with breast cancer or melanoma [25]. Jeong et al. reported the ^{99m}Tc labeled mannosylated albumin nanoparticles for sentinel node detection with targeting mannose receptor of monocytes on lymph node [26]. In this study, they could find the specific targeting ability of ^{99m}Tc-mannosylated human serum albumin (MSA) to the lymphatic system (14.0%ID/organ at 1 h post-injection), on the other hand, ^{99m}Tc-human serum albumin (HSA) showed low uptake (2.4%ID/organ at 1 h post-injection). Recently, they developed the ^{68}Ga version of MSA nanoparticles for targeting mannose receptors on monocytes/macrophages in the myocardium after the induction of myocardial inflammation using myocarditis model in animals [27]. Another examples of mannose-tagged iron oxide nanoparticles for lymph node imaging using multimodal positron emission tomography (PET) and magnetic resonance imaging (MRI) has been also addressed [13]. Galactose is the potential ligand for the target of ASGP-R, which is highly expressed on hepatocyte [28, 29], and Lee et al. clearly showed the targeting ability of galactose-conjugated superparamagnetic iron oxide nanoparticles (SPION) to the hepatocyte in the liver using in vivo animal model [30].

Folic acid (folate) receptors, a glycosylphosphatidylinositol-anchored cell surface receptor, is overexpressed on the vast majority of cancer tissues, while its expression is limited in healthy tissues and organs, therefore, folate can be used as a target molecule for targeted delivery of imaging and therapeutic agents to tumors [31]. Lu et al. demonstrated the targeting and therapeutic efficacy of folate-tagged mesoporous silica nanoparticles [32].

The extracellular domain of prostate-specific mem-brane antigen (PSMA, also known as folate hydrolase 1 or glutamate carboxypeptidase II) has gained increasing interest for imaging and therapeutic target of prostate cancer [33]. From the great success of ^{68}Ga labeled PSMA inhibitor, ^{68}Ga-glutamate-urea-lysine (EuK) derivatives [34], numerous nanoparticles conjugated with EuK have been developed for imaging and therapy of prostate cancer. Sachin et al. have established the docetaxel encapsulated into poly(lactide-β-ethylene glycol-β-lactide) (PLA-PEG-PLA) nanoparticles with the decoration of EuK as a PSMA targeting molecules, and showed the specific uptake in PSMA positive, LNCaP cell-lines [35]. Moon et al. also showed the specific uptake of EuK-tagged iron oxide nanoparticles (IONP) in the tumor bearing mouse model using PET/MR dual modality [14]. Another approach of EuK-tagged docetaxel-containing nanoparticle, BIND-014 is now under Phase 1 clinical study [36].

12.3.2 Macromolecules

Also, there are huge varieties of macromolecules which can target the specific disease or diseased site. Any kinds of macromolecules with 3D structures that can interact with target proteins, including antibody or its fragments, protein, affibody®, nucleic acid, nucleic acid aptamer, and peptide aptamer, can be used or developed as a targeting ligand molecule for nanomedicine.

First famous targeting molecules are the antibodies and their fragments. The antibody has two epitope binding sites in a single molecule and offers an exceedingly high selectivity and binding affinity for the target proteins of interest. Several antibodies are used in clinic by approval of FDA. Hadjipanayis et al. [37] employed an antibody against epidermal growth factor receptor (EGFR) deletion mutant to fabricate iron oxide nanoparticles for targeted imaging and therapeutic treatment of glioblastoma. Selective binding to this mutant EGFR was achieved by creating a polyclonal rabbit antibody toward the chemically synthesized 14-amino-acid fusion junction sequence (EGFRvIIIAb). Covalent conjugation of the purified rabbit polyclonal EGFRvIIIAb to the amphiphilic triblock copolymer-coated iron oxide nanoparticles showed glioblastoma-targeting ability as a potential theranostic agent. Even though the well-established targeting ability and selectivity of antibody itself, antibody fragment is used frequently as a targeting molecules for nanomaterials, because of the relatively large size of antibody with 10–15 nm (150 kDa) compared to nanomaterials. Ling et al. reported iron oxide nanoparticles with the single chain anti-prostate stem cell antigen (PSCA) antibody fragment (scAbP-SCA) as a specific targeting molecule for prostate cancer targeted imaging and therapy [38]. In a similar way, Chen et al. constructed iron oxide and non-viral polymeric vector nanocomposite using a CD3 single chain antibody (scAbCD3) as a targeting molecules for gene delivery to T cells [39]. Antibody-conjugated liposomes, so called immunoliposomes, are common pharmaceutical carriers for targeted drug delivery because of their unique ability to encapsulate both hydrophilic and hydrophobic therapeutic agents. Lu et al. developed in vivo lung cancer targeting immunoliposomes using an anti-c-Met single chain variable fragment (scFv) antibody [40].

Aptamers are small nucleic acid ligands (15–40 bases) and used as targeting molecules that bind to targets with high specificity due to the ability of the molecules to fold into unique conformations with three-dimensional structures [41]. Aptamers have potential advantage over antibodies, such as the small size (15 kDa), low immunogenicity, and easy scale-up preparation without batch-to-batch variations. Lupold et al. identified 2′-fluoro-pyridine-RNA aptamers generated against the extracellular domain of prostate-specific membrane antigen (PSMA) [42] and attached on self-assembled polymeric nanoparticles [43] or QDs [44] to investigate targeted imaging and delivery.

Hyaluronic acid (HA), a copolymer of *N*-acetyl-D-glucosamine and D-glucuronic acid, is a widely used targeting macromolecule that can bind to CD44, which is overexpressed in various tumors [45]. Wu et al. used HA as a targeting ligand to develop a thermo-responsive hybrid nanogel for simultaneous temperature sensing, cancer cell targeting, fluorescence imaging, and combined chemo-photothermal treatment [46]. Recently, Hwang et al. constructed a fluorescence-switchable theranostic nano-platform using HA-conjugated graphene oxide (GO), which is capable of both sensing oncogenic miR-21 and inhibiting its tumorigenicity simultaneously [47].

12.3.3 Conjugation Methods

The possible conjugation method can be categorized as conventional method, click chemistry, and physicochemical interaction. Because there are several merits or demerits on each method, we should thoroughly review and select the conjugation method for each nano-system.

The major portion of conventional method is the peptide bond formation between nanoparticle and targeting molecule. Amine and acid functionalized moieties are linked as a peptide bond and in most cases the acid-group is activated with active ester derivatives, such as *N*-hydroxysuccinimide (NHS) ester, to improve the conjugation efficiency. Amino-group also can react with aldehyde or isothiocyanate (–SCN) to form imine or thiourea bond. Thiol-group can react with maleimide derivatives to form thio-ether bond. Several types of chemical linker between nanoparticles and targeting molecules can be used for the conjugation. Sulfosuccinimidyl-4-(*N*-maleimidomethyl)cyclohexane-1-carboxylate (SMCC) can be used between amino-group and thiol-group.

Click chemistry can be done on click chemical combinations, such as azide and diarylcyclooctyne (DBCO) or tetrazine and *trans*-cyclooctene (TCO) combinations.

Physicochemical interactions, which is non-covalent bond formation, come from electrostatic, hydrophobic, and affinity interactions between nanoparticles and targeting molecules. Physicochemical conjugation strategies are particularly useful for the assembly of therapeutic agents onto nanoparticles. Typical example of physicochemical interactions is the positively charged nanomaterials and negatively charged siRNA can form a very stable nanocomposite even in in vivo condition.

Each chemical reaction should need chemicals such as base/acid or reducing/oxidation agent, therefore, we should consider and check the chemical instability of each nanomaterials or targeting molecules for each reaction condition, and finally we can select the optimal conjugation method for each conjugation.

12.3.4 Consideration of Targeting Molecules Geometry on Nanomaterials

For ligation of targeting molecules to the surface of nanoparticle, there are several factors we have to concern. Despite the targeting molecules play the critical role in targeting of nanomaterials to disease site, relatively few studies have been reported to maximize in vivo targeting efficiency through systematic variation of the geometry or number of targeting molecules on nanomaterials.

The number of targeting molecules on nanomaterials has to be concerned because that affects the affinity or avidity of nanoparticles for the target proteins, the rate of nanoparticle-target interaction, and of course, the shape or surface charge of nanomaterials. There are several reports on number of targeting molecule issue. Garg et al. and Gindy et al. reported higher concentrations of the targeting molecules on the nanoparticles often increase cellular uptake [48, 49]. Olivier et al. reported that targeting molecules must be present on the nanoparticle surfaces at concentrations that exceed a minimum threshold for binding [50]. Gao et al. synthesize 0, 5, or 16% RGD ligand-immobilized Dox-loaded polymeric micelles to compare their in vitro targeting and therapeutic properties, and the 16% RGD ligand-bearing nanoparticles displayed the highest cellular uptake and cytotoxicity in $\alpha_v\beta_3$ integrin-overexpressing SLK cells. However, several studies also insisted that high targeting molecule densities did not improve binding to the target cancer cells and could even promote nonspecific interactions with endothelial and other non-cancerous cells, which increases immunogenicity, thereby causing opsonization-mediated clearance of the nanoparticles [51]. Gu et al. prepared with different compositions of the self-assembled block-copolymers and aptamers, and the optimal aptamer density on the nanoparticle surface was initially determined in vitro [52]. Increasing the density of targeting ligand molecule to 5% significantly increased the nanoparticles uptake by the target cells (LNCaP), whereas further increase in aptamer density did not increase the uptake. These results indicated that the optimal density of targeting molecules for PSMA-specific endocytosis in vitro was 10–80 nmol aptamer per μmol nanoparticle. They injected the targeting nanoparticles to LNCaP xenograft mouse models and showed that increasing the aptamer density from 0 to 5% significantly increased nanoparticle retention in tumors, but the retention decreased for aptamer densities beyond 10%. The authors suggested that higher aptamer densities may have reduced the nanoparticle stealth properties, resulting in rapid clearance by the liver. Another report from Shmeeda et al. optimized the ligand density in the Her2-targeted PEGylated liposomal Dox system (HT-PLD) in vivo for the ligand ratios of 7.5, 15, or 30 per liposome [53]. The best in vivo performance resulted from 15 ligands per liposome in the HT-PLD formulation. A 30 ligands per liposome showed the accelerated plasma clearance in the tumor-bearing mice, and the 7.5 ligand per liposome reduced cytotoxicity after in vivo passage.

The geometry of targeting molecules on nanomaterials is also important for the binding affinity of nanomaterials to target proteins. There are few reports on this issue. Park et al. prepared two types of tumor-targeting nanoparticles for varying PEG lengths. For a given number of peptides bound to nanoparticles, the presence of a PEG linker facilitated peptide targeting by reducing conformational restriction as well as increasing the residence time of the nanostructures in the blood stream [54]. The short length of sulfosuccinimidyl-4-(*N*-maleimidomethyl)cyclohexane-1-carboxylate (SMCC) linker restricted the targeting peptide conformation. Recently, Jeong et al. reported that antibody orientation on nanoparticles could significantly affect the maintenance of full bio-functionality [55]. They prepared the site-specific and orientation-controlled antibody conjugation on nanoparticles and showed the 8-times higher target-binding ability than those prepared by the conventional non-site-specific and random amine-acid coupling using 1-ethyl-3-(3-dimethylaminopropyl)carbodiimide (EDC) (Fig. 12.3).

Finally, all these results suggest that there should be the optimal number or geometry on nanomaterials for each disease targeting strategy, and we should carefully consider and investigate to find the optimal structure for the development of targeted multifunctional nanoparticle systems for imaging and therapy.

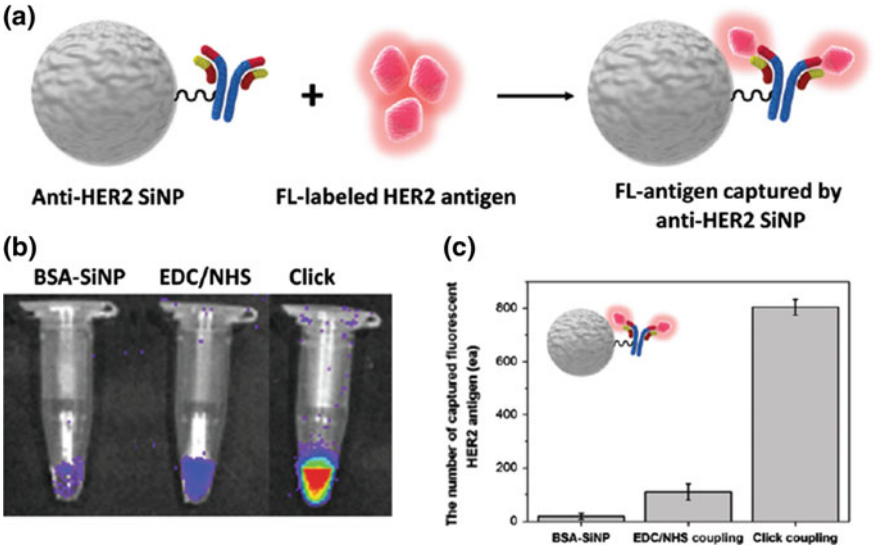

Fig. 12.3 Quantitative evaluation of the antigen-binding capability of anti-bodies conjugated to SiNPs. **a** Schematic of the quantitative bio-assay using a fluorescent HER2 antigen. **b** Fluorescence images of the fluorescent HER2 antigen bound BSA treated SiNPs and anti-HER2 antibody conjugated SiNPs prepared using the EDC/NHS coupling or click coupling method, respectively. **c** Quantitative analysis of the number of antigens bound to a single SiNP us-ing the fluorescence signal. The fluorescence images were obtained by IVIS with 2 s acquisition time. SiNP: silica nanoparticle (copyright permission from [55])

12.4 Radiolabeling

Radionanomedicine can be used for diagnosis or therapy or theranosis of certain disease. For in vivo or clinical application, the radiolabeling of nanomaterials should be done by easy- and fast-way and this step should be located in just before in vivo administration. Radiolabeled nanomaterials should be stable for certain time in vitro and in vivo after the radiolabeling because the in vitro and in vivo metabolite can affect the imaging or therapeutic efficacy of radiolabeled nanomaterials.

There are two types of radiolabeling method, extrinsic and intrinsic method. Extrinsic method is the most widely used method for radiolabeling of nanomaterials, and the chelator modified nanomaterials can be labeled with radioisotopes. The click radiolabeling is also categorized as extrinsic method. Intrinsic method is the radiolabeling of the nanoparticle core or nanoparticle surface. Extrinsic method can be divided into two ways, pre- and post-labeling. Like click chemistry, pre-labeling can be used for the nanomaterials containing the conjugation motifs, such as click chemicals, on the surface and post-labeling method for the chelators on the surface.

Click chemistry has advantages over conventional chelate labeling method. First, using click chemistry, the nanomaterials may not meet the radiolabeling condition directly, such as low or high pH, high temperature, in the pre-labeling method, therefore this method will be the better choice for the acid/base or high temperature-labile nanomaterials. Zeng et al. has reported an approach to label shell-cross-linked nanoparticles with ^{64}Cu via metal free click chemistry [56]. Specifically, ^{64}Cu was complexed with DOTA functionalized with a DBCO group, which was subsequently conjugated with nanoparticles bearing azide group to generate the desired ^{64}Cu labeled nanoparticles. Second, labeling via the click chemistry offers the flexibility to select radioisotopes according to the requirement of the study by conjugating nanoparticles bearing click chemistry motifs with different chelators functionalized with corresponding complimentary click chemistry motifs, unlike the traditional approach in which a specific chelator has been attached to nanoparticles thus restricting the selection of radio isotopes (e.g. DFO conjugated nanoparticles can only be labeled by ^{89}Zr). Third, click chemistry provides the possibility to conduct the labeling of nanoparticles in vivo via pre-targeting strategies. In particular, nanoparticles functionalized with a click reaction moeity could be administrated in advance to allow sufficient accumulation at the tumor site and enough clearance from blood, and then the radioisotope-chelator complex bearing the corresponding other click reaction moiety could be injected, which could significantly reduce the uptake in normal organs and consequently improving tumor/non-tumor ratios substantially [57].

As we discussed above, in vivo integrity of radiolabeled nanomaterials is very important because that can affect the imaging or therapeutic efficacy. Recently, there are exactly opposite results that the extrinsically labeled radioisotope can or cannot be detached from nanomaterials published in same year. Kreyling et al.

prepared the nanoparticle core was labeled with ^{198}Au and the attached chelator on the surface of nanoparticle labeled with ^{111}In, and they thoroughly traced the ^{198}Au and ^{111}In radioactivity and concluded that in vivo degradation of the chelator on the surface of nanoparticle due to proteolytic digestion [58]. On the other hand, Seo et al. confirmed that extrinsically labeled radioisotope was not detached from upconverting nanoparticle core even after the long-term journey through the hepato-biliary tract [15]. Still, we cannot fully understand of this kind of controversy and there is far way to go to evaluate the exact fate of radiolabeled nanomaterials. However, from this point, we should keep in mind and confirm the in vivo integrity after the radiolabeling of nanomaterials.

12.5 Applications of Radionanomedicine Prepared by Click Chemistry

Nanomaterials labeled with different radioisotopes via either extrinsic or intrinsic methods described above have been applied in diagnosis [59, 60], image guided therapy [61] or radiotherapy [62–65].

12.5.1 Applied in Diagnosis

Nanoparticles could accumulate in tumor tissues either passively by EPR effects or actively by the targeting molecules conjugated on nanoparticle surface, and thus radiolabeled nanoparticles have been extensively investigated as diagnosis tools for tumor detection.

In particular, nanoparticles labeled with positron emitter have been applied in the PET imaging. Among many different positron emitted radionuclides, ^{18}F is the most widely used one due to its good availability and ideal imaging characteristics. Although the half-life time of ^{18}F is relatively short (110 min) compared to the slow EPR process, application of a pretargeting strategy has demonstrated the great potential to overcome this problem. Lee et al. [57] have recently reported an ^{18}F-based pretargeting strategy via SPAAC for nanoparticle-based PET imaging. In particular, DBCO functionalized nanoparticles were administrated 24 h in advance to allow sufficient accumulation of nanoparticles in tumor tissues before the subsequent administration of [^{18}F]fluoropentaethylene glycolic azide, and the sequentially injected [^{18}F]fluoropentaethylene glycolic azide could ligate with previously administrated DBCO functionalized nanoparticles, which resulted in the significantly improved signal to background ratios.

Another widely used radioisotope in nanoparticles based PET imaging is ^{64}Cu, and its half-life time is relatively longer (12.7 h) and closer to the physical half life time of small nanoparticles. Therefore, nanoparticles had been directly labeled with

^{64}Cu via pre or post-labeling for PET imaging of tumor tissues. One representative example is provided by Lee et al. [59], in which azide functionalized glycol chitosan nanoparticles (CNPs) were conjugated with ^{64}Cu labeled DBCO via the copper free click chemistry to yield the ^{64}Cu labeled CNPs. Labeled CNPs were subsequently administrated to mice bearing the SCC tumor, and the PET imaging results demonstrate the clear visualization of tumor tissues with this type of ^{64}Cu labeled CNPs, rendering their potential clinical applications for the tumor detection.

Besides ^{18}F and ^{64}Cu, ^{89}Zr has also been considered as a promising radionuclide for radiolabeling of nanoparticles for PET imaging. The major advantage of ^{89}Zr includes its preferred imaging characteristics as well as its relatively long half-life time (3.3 days), which well matches the time frame of the EPR process. Ruggiero et al. [60] reported the ^{89}Zr labeling of single walled nanotubes (SWNT) for PET imaging. In their study, SWNT conjugated with an antiVE-cad (vascular endothelial cadherin) antibody was labeled with ^{89}Zr, which was subsequently applied in the imaging of human colon adenocarcinoma on a mouse model via targeting angiogenesis. High uptakes in targeted tissues were identified with a fast blood clearance, demonstrating the great potential for detecting malignant tissues.

In addition to PET imaging, applications of nanoparticles in SPECT imaging for tumor diagnosis have also been reported. Harrington et al. reported their successful evaluation of seventeen patients with different types of cancer using ^{111}In-DTPA-labeled liposomes [61]. Another example was the application of ^{188}Re labeled liposomes in imaging C26-colon tumor on a mice model. Results indicated high tumor uptakes at all time points, indicating this type of nanodevice could be an ideal diagnostic tool for tumor detection [62].

12.5.2 Applied in Image Guided Therapy

Besides diagnosis, another major application of radioisotope labeled nanoparticles is image-guided therapy.

Feng et al. reported the construction of ^{64}Cu labeled mesoporous silica ($mSiO_2$) nanoparticles as well as the subsequent evaluation of its in vivo performance for tumor-targeting drug delivery [63]. The TRC105 antibody-attached nanoparticles exhibited excellent tumor accumulation due to the combinatory effects of passive EPR and active TRC105 mediated tumor targeting. Further tumor targeted delivery of Doxorubicin using this designed nanoplatform successfully improved the efficiency of drug delivery, rendering the developed $mSiO_2$ nanoparticles could serve as a promising vehicle for tumor targeted drug delivery.

Another representative example could be ^{64}Cu labeled melanin nanoparticles (MNPs) that has been used to investigate their efficiency on delivering sorafenib to the tumor site [64]. PET imaging results revealed a peak tumor uptake at 4 h post injection, which was consistent with the results obtained from in vitro cumulative release study, where less than 20% of loaded sorafenib was released from MNPs in the first 4 h. Those study results indicated that the designed MNPs could efficiently

load sorafenib which were delivered to the tumor site. Furthermore, long term retention of MNPs in the tumor tissues was also observed by comparing the tumor uptake value at 4 h post injection with that at 24 h post injection, ensuring the gradual release of sorafenib from its carrier at the tumor site.

Sun et al. has recently made use of ^{64}Cu and ^{89}Zr labeled POVF micelles to monitor their in vivo bio-distribution as well as predict corresponding therapeutic outcomes (unpublished data). Specifically, via SPAAC based click chemistry approach, paclitaxel (PTX) loaded POVF micelles, which contained free azide groups on their surface, were labeled with either ^{64}Cu or ^{89}Zr for monitoring their tumor uptakes at early time points (1, 4, and 8 h) and late time points (24, 48, 72, 96 h), respectively. Results indicated that the accumulation of the designed drug delivery system in tumor tissues started as early as 4 h and maintained at a high level (around 10%ID/g) for up to 72 h. Based on the in vitro PTX release curve, most of PTX would still be kept in the designed micelles at 4 h time points, indicating that an efficient drug delivery to tumor could be anticipated with this system. Subsequent in vivo therapeutic study showed significant reduction of tumor size in mice treated with this PTX loaded POVF compared with the vehicle control group, demonstrating its potential clinical value for the cancer treatment.

12.5.3 Applied in Internal Radiotherapy

Targeted internal radiotherapy has been considered as a promising radiotherapy strategy due to significantly reduced radio exposure to normal organs as compared with traditional radiotherapy using external radio beams. Nanoparticles, which can not only target the tumor tissues via EPR effects but also provide prominent loading capacity for delivery of therapeutic radionuclides, could serve as an ideal device for targeted internal radiotherapy. Pioneering clinical imaging studies revealed an effective targeting of solid tumors in patients via nanoparticles, indicating the potential of using radiolabeled nanoparticles to deliver therapeutic radioisotopes for internal radiotherapy [61].

Initial trial of internal radiotherapy using nanoparticles employed ^{188}Re as the β source. Excellent suppression of tumor growth was observed while side effects were minimized in the head and neck squamous cell carcinoma xenograft model [65]. Co-labeling of ^{111}In and ^{188}Re for nanotargeted radio-therapeutics was also reported in which ^{111}In provided the Auger electron for killing single tumor cells or small tumor cluster while ^{188}Re provided the high-energy beta ray for killing large tumor clusters [62, 66, 67].

However, ^{188}Re has a half-life time of 17 h, which is a little bit shorter compared with the time frame of the EPR process. Therefore, other beta emitter with more compatible half-life time have also been investigated. One ideal alternative choice is ^{90}Y with a half-life time of 64 h. In particular, lipid nanoparticles conjugated with anti VEGFR-2 antibody has been labeled with ^{90}Y and evaluated in vivo for their internal radio therapeutic efficacy [68]. Growth of tumor was obviously inhibited as

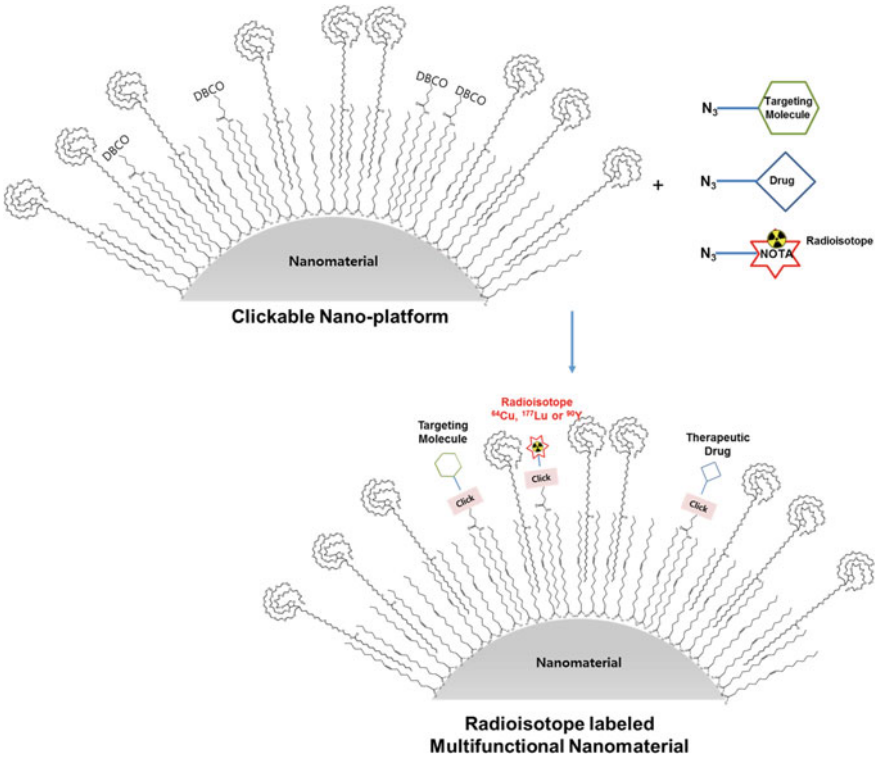

Fig. 12.4 Scheme of clickable nano-platform for multifunctional radionanomedicine

compared with the control group, demonstrating the potential of applying this nanodevice in internal radiotherapy.

Another preferred radionuclide for internal radiotherapy is ^{177}Lu with a half-life time of 161 h. Yook et al. [69] reported that administration of 4.5 MBq ^{177}Lu labeled gold nanoparticles, which exhibited an excellent tumor uptake (as high as 300–400%ID/g) via intratumorally injection, could successfully arrest the growth of breast cancer tumor in CD-1 athymic mice for over 90 days, indicating the feasibility of developing ^{177}Lu labeled nanoparticles into therapeutic reagents for cancer treatment.

It has been proved by several studies that immune system activation is crucial for the success of the traditional radiotherapy [70, 71]. Therefore, nanoparticles had been engineered into immune response modifiers (IRM) as the vehicle for delivering radiation dose, and such strategy could further enhance the therapeutic effect of the nanoparticle based internal radiation therapy. Vanpouille-Box et al. [72] reported the application of ^{188}Re carried nanoparticles in the cancer treatment, which possessed the strong capability of stimulating the immune response.

12.6 Clickable Radionanomedicine Platform

Radionanomedicine platform can be devised by combining amphiphile encapsulation method and click chemistry. Hydrophilic monodispersed nanomaterials can be prepared by using an amphiphile encapsulation method. And terminal click moiety on the nanomaterial surface can be used for conjugation of targeting molecules, radioisotopes, optical probes, and/or therapeutic drugs by click chemistry (Fig. 12.4). For this radionanomedicine platform, the FDA approval process can be done for each separate vials, such as nano platform, targeting molecule, radioisotope-chelator, optical probe, and therapeutic drug, independently. And the final use of radionanomedicine platform by the simple compounding process at the clinical practice sites.

Here we propose the final goal of the versatile radionanomedicine platform that looks to multi-purpose uses for diagnosis, therapy, or even theragnosis by using one nano-platform in the clinic. For example, a patient can be diagnosed specifically by the image or in vitro assay using the adequate diagnostic nano-platform containing proper targeting molecule and radioisotope combination. Thus, we can select proper therapeutic drug or radionuclide for therapy of this disease (Fig. 12.5).

In conclusion, the multi-purpose versatile radionanomedicine platform, can be established by the combination of amphiphile encapsulation and the click chemistry, show another possibility of radionanomedicine and would contribute the successful translation journey to the clinical application of nanomedicine.

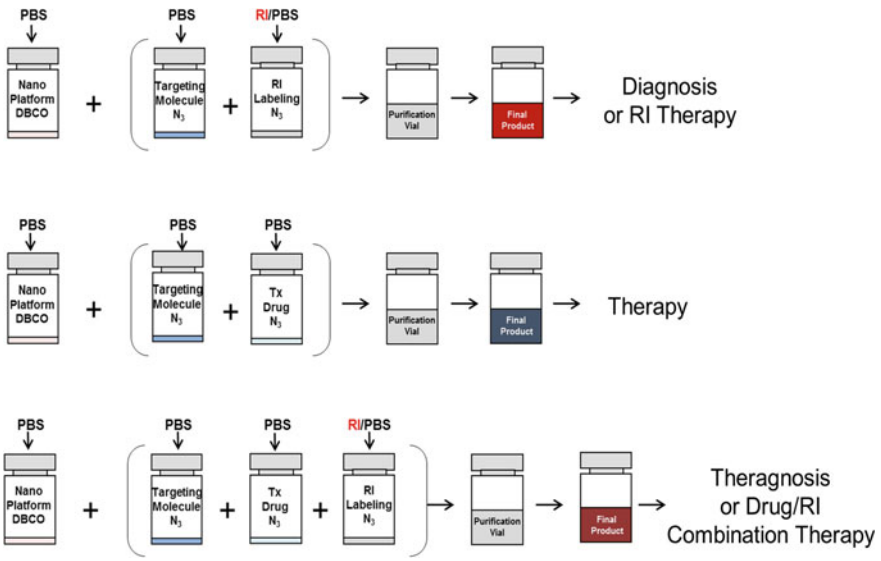

Fig. 12.5 Possible clinical application of radionanomedicine using nano-platform

References

1. H.C. Kolb, M.G. Finn, K.B. Sharpless, Click chemistry: diverse chemical function from a few good reactions. Angew. Chem. Int. Ed. Engl. **40**(11), 2004–2021 (2001)
2. H.K. He, C. Gao, Click chemistry on nano-surfaces. Curr. Org. Chem. **15**(21), 3667–3691 (2011)
3. J.P. Meyer, P. Adumeau, J.S. Lewis, B.M. Zeglis, Click chemistry and radiochemistry: the first 10 years. Bioconjuga. Chem. **27**(12), 2791–2807 (2016)
4. E.Y. Sun, L. Josephson, R. Weissleder, "Clickable" nanoparticles for targeted imaging. Mol. Imaging **5**(2), 122–128 (2006)
5. J.E. Hein, V.V. Fokin, Copper-catalyzed azide-alkyne cycloaddition (CuAAC) and beyond: new reactivity of copper(I) acetylides. Chem. Soc. Rev. **39**(4), 1302–1315 (2010)
6. N.J. Agard, J.A. Prescher, C.R. Bertozzi, A strain-promoted [3+2] azide-alkyne cycloaddition for covalent modification of blomolecules in living systems. J. Am. Chem. Soc. **126**(46), 15046–15047 (2004)
7. M.L. Blackman, M. Royzen, J.M. Fox, Tetrazine ligation: fast bioconjugation based on inverse-electron-demand Diels-Alder reactivity. J. Am. Chem. Soc. **130**(41), 13518–13519 (2008)
8. M. Pretze, M. Kuchar, R. Bergmann, J. Steinbach, J. Pietzsch, C. Mamat, An efficient bioorthogonal strategy using CuAAC click chemistry for radiofluorinations of SNEW peptides and the role of copper depletion. Chem. Med. Chem. **8**(6), 935–945 (2013)
9. H.L. Evans, L. Carroll, E.O. Aboagye, A.C. Spivey, Bioorthogonal chemistry for Ga-68 radiolabelling of DOTA-containing compounds. J. Label. Compd. Radiopharm. **57**(4), 291–297 (2014)
10. K. Kang, J. Park, E. Kim, Tetrazine ligation for chemical proteomics. Proteome. Sci. **15**, 15 (2017)
11. B. Dubertret, P. Skourides, D.J. Norris, V. Noireaux, A.H. Brivanlou, A. Libchaber, In vivo imaging of quantum dots encapsulated in phospholipid micelles. Science **298**(5599), 1759–1762 (2002)
12. Y.K. Lee, J.M. Jeong, L. Hoigebazar, B.Y. Yang, Y.S. Lee, B.C. Lee et al., Nanoparticles modified by encapsulation of ligands with a long alkyl chain to affect multispecific and multimodal imaging. J. Nucl. Med. **53**(9), 1462–1470 (2012)
13. B.Y. Yang, S.H. Moon, S.R. Seelam, M.J. Jeon, Y.S. Lee, D.S. Lee et al., Development of a multimodal imaging probe by encapsulating iron oxide nanoparticles with functionalized amphiphiles for lymph node imaging. Nanomed. (Lond.) **10**(12), 1899–1910 (2015)
14. S.H. Moon, B.Y. Yang, Y.J. Kim, M.K. Hong, Y.S. Lee, D.S. Lee et al., Development of a complementary PET/MR dual-modal imaging probe for targeting prostate-specific membrane antigen (PSMA). Nanomedicine **12**(4), 871–879 (2016)
15. H.J. Seo, S.H. Nam, H.J. Im, J.Y. Park, J.Y. Lee, B. Yoo et al., Rapid hepatobiliary excretion of micelle-encapsulated/radiolabeled upconverting nanoparticles as an integrated form. Sci. Rep. **5**, 15685 (2015)
16. Y. Matsumura, H. Maeda, A new concept for macromolecular therapeutics in cancer-chemotherapy—mechanism of tumoritropic accumulation of proteins and the antitumor agent Smancs. Cancer Res. **46**(12), 6387–6392 (1986)
17. F. Danhier, To exploit the tumor microenvironment: since the EPR effect fails in the clinic, what is the future of nanomedicine? J. Control Release **244**, 108–121 (2016)
18. H. Maeda, Toward a full understanding of the EPR effect in primary and metastatic tumors as well as issues related to its heterogeneity. Adv. Drug Deliver. Rev. **91**, 3–6 (2015)
19. M.K. Yu, J. Park, S. Jon, Targeting strategies for multifunctional nanoparticles in cancer imaging and therapy. Theranostics **2**(1), 3–44 (2012)
20. G. Gasparini, P.C. Brooks, E. Biganzoli, P.B. Vermeulen, E. Bonoldi, L.Y. Dirix et al., Vascular integrin alpha(v)beta(3): a new prognostic indicator in breast cancer. Clin. Cancer Res. **4**(11), 2625–2634 (1998)

21. X.F. He, M.H. Na, J.S. Kim, G.Y. Lee, J.Y. Park, A.S. Hoffman et al., A novel peptide probe for imaging and targeted delivery of liposomal doxorubicin to lung tumor. Mol. Pharmaceut. **8**(2), 430–438 (2011)
22. E.A. Murphy, B.K. Majeti, L.A. Barnes, M. Makale, S.M. Weis, K. Lutu-Fuga et al., Nanoparticle-mediated drug delivery to tumor vasculature suppresses metastasis. Proc. Natl. Acad. Sci. U.S.A. **105**(27), 9343–9348 (2008)
23. H.Y. Lee, Z. Li, K. Chen, A.R. Hsu, C.J. Xu, J. Xie et al., PET/MRI dual-modality tumor imaging using arginine-glycine-aspartic (RGD)—conjugated radiolabeled iron oxide nanoparticles. J. Nucl. Med. **49**(8), 1371–1379 (2008)
24. D. Arosio, L. Manzoni, E.M.V. Araldi, C. Scolastico, Cyclic RGD functionalized gold nanoparticles for tumor targeting. Bioconjug. Chem. **22**(4), 664–672 (2011)
25. D.R. Vera, A.M. Wallace, C.K. Hoh, R.F. Mattrey, A synthetic macromolecule for sentinel node detection: Tc-99 m-DTPA-mannosyl-dextran. J. Nucl. Med. **42**(6), 951–959 (2001)
26. J.M. Jeong, M.K. Hong, Y.J. Kim, J. Lee, J.H. Kang, D.S. Lee et al., Development of Tc-99 m-neomannosyl human serum albumin (Tc-99 m-MSA) as a novel receptor binding agent for sentinel lymph node imaging. Nucl. Med. Commun. **25**(12), 1211–1217 (2004)
27. S.P. Lee, H.J. Im, S. Kang, S.J. Chung, Y.S. Cho, H. Kang et al., Noninvasive imaging of myocardial inflammation in myocarditis using Ga-68-tagged mannosylated human serum albumin positron emission tomography. Theranostics **7**(2), 413–424 (2017)
28. Z.Y. Shen, W. Wei, H. Tanaka, K. Kohama, G.H. Ma, T. Dobashi et al., A galactosamine-mediated drug delivery carrier for targeted liver cancer therapy. Pharmacol. Res. **64**(4), 410–419 (2011)
29. E.M. Kim, H.J. Jeong, I.K. Park, C.S. Cho, H.B. Moon, D.Y. Yu et al., Asialoglycoprotein receptor targeted gene delivery using galactosylated polyethylenimine-graft-poly(ethylene glycol): in vitro and in vivo studies. J. Control Release **108**(2–3), 557–567 (2005)
30. C.M. Lee, H.J. Jeong, E.M. Kim, D.W. Kim, S.T. Lim, H.T. Kim et al., Superparamagnetic iron oxide nanoparticles as a dual imaging probe for targeting hepatocytes in vivo. Magn. Reson. Med. **62**(6), 1440–1446 (2009)
31. H.S. Yoo, T.G. Park, Folate-receptor-targeted delivery of doxorubicin nano-aggregates stabilized by doxorubicin-PEG-folate conjugate. J. Control Release **100**(2), 247–256 (2004)
32. J. Lu, M. Liong, Z.X. Li, J.I. Zink, F. Tamanoi, Biocompatibility, biodistribution, and drug-delivery efficiency of mesoporous silica nanoparticles for cancer therapy in animals. Small **6**(16), 1794–1805 (2010)
33. T. Maurer, M. Eiber, M. Schwaiger, J.E. Gschwend, Current use of PSMA—PET in prostate cancer management. Nat. Rev. Urol. **13**(4), 226–235 (2016)
34. M. Eder, M. Schafer, U. Bauder-Wust, W.E. Hull, C. Wangler, W. Mier et al., Ga-68-complex lipophilicity and the targeting property of a urea-based PSMA inhibitor for PET imaging. Bioconjug. Chem. **23**(4), 688–697 (2012)
35. S.S. Chandran, S.R. Banerjee, R.C. Mease, M.G. Pomper, S.R. Denmeade, Characterization of a targeted nanoparticle functionalized with a urea-based inhibitor of prostate-specific membrane antigen (PSMA). Cancer Biol. Ther. **7**(6), 978–986 (2008)
36. D.D. Von Hoff, M.M. Mita, R.K. Ramanathan, G.J. Weiss, A.C. Mita, P.M. LoRusso et al., Phase I study of PSMA-targeted docetaxel-containing nanoparticle BIND-014 in patients with advanced solid tumors. Clin. Cancer Res. **22**(13), 3157–3163 (2016)
37. C.G. Hadjipanayis, R. Machaidze, M. Kaluzova, L. Wang, A.J. Schuette, H. Chen et al., EGFRvIII antibody-conjugated iron oxide nanoparticles for magnetic resonance imaging-guided convection-enhanced delivery and targeted therapy of glioblastoma. Cancer Res. **70**(15), 6303–6312 (2010)
38. Y. Ling, K. Wei, Y. Luo, X. Gao, S.Z. Zhong, Dual docetaxel/superparamagnetic iron oxide loaded nanoparticles for both targeting magnetic resonance imaging and cancer therapy. Biomaterials **32**(29), 7139–7150 (2011)
39. G.H. Chen, W.J. Chen, Z. Wu, R.X. Yuan, H. Li, J.M. Gao et al., MRI-visible polymeric vector bearing CD3 single chain antibody for gene delivery to T cells for immunosuppression. Biomaterials **30**(10), 1962–1970 (2009)

40. R.M. Lu, Y.L. Chang, M.S. Chen, H.C. Wu, Single chain anti-c-Met antibody conjugated nanoparticles for in vivo tumor-targeted imaging and drug delivery. Biomaterials **32**(12), 3265–3274 (2011)
41. D.S. Wilson, J.W. Szostak, In vitro selection of functional nucleic acids. Annu. Rev. Biochem. **68**, 611–647 (1999)
42. S.E. Lupold, B.J. Hicke, Y. Lin, D.S. Coffey, Identification and characterization of nuclease-stabilized RNA molecules that bind human prostate cancer cells via the prostate-specific membrane antigen. Cancer Res. **62**(14), 4029–4033 (2002)
43. O.C. Farokhzad, S.Y. Jon, A. Khademhosseini, T.N.T. Tran, D.A. LaVan, R. Langer, Nanopartide-aptamer bioconjugates: a new approach for targeting prostate cancer cells. Cancer Res. **64**(21), 7668–7672 (2004)
44. V. Bagalkot, L. Zhang, E. Levy-Nissenbaum, S. Jon, P.W. Kantoff, R. Langer et al., Quantum dot—aptamer conjugates for synchronous cancer imaging, therapy, and sensing of drug delivery based on Bi-fluorescence resonance energy transfer. Nano Lett. **7**(10), 3065–3070 (2007)
45. U. Gunthert, M. Hofmann, W. Rudy, S. Reber, M. Zoller, I. Haussmann et al., A new variant of glycoprotein CD44 confers metastatic potential to rat carcinoma-cells. Cell **65**(1), 13–24 (1991)
46. W.T. Wu, J. Shen, P. Banerjee, S.Q. Zhou, Core-shell hybrid nanogels for integration of optical temperature-sensing, targeted tumor cell imaging, and combined chemo-photothermal treatment. Biomaterials **31**(29), 7555–7566 (2010)
47. D.W. Hwang, H.Y. Kim, F.Y. Li, J.Y. Park, D. Kim, J.H. Park et al., In vivo visualization of endogenous miR-21 using hyaluronic acid-coated graphene oxide for targeted cancer therapy. Biomaterials **121**, 144–154 (2017)
48. A. Garg, A.W. Tisdale, E. Haidari, E. Kokkoli, Targeting colon cancer cells using PEGylated liposomes modified with a fibronectin-mimetic peptide. Int. J. Pharm. **366**(1–2), 201–210 (2009)
49. M.E. Gindy, S.X. Ji, T.R. Hoye, A.Z. Panagiotopoulos, R.K. Prud'homme, Preparation of poly(ethylene glycol) protected nanoparticles with variable bioconjugate ligand density. Biomacromol **9**(10), 2705–2711 (2008)
50. V. Olivier, I. Meisen, B. Meckelein, T.R. Hirst, J. Peter-Katalinic, M.A. Schmidt et al., Influence of targeting ligand flexibility on receptor binding of particulate drug delivery systems. Bioconjug. Chem. **14**(6), 1203–1208 (2003)
51. M. Ferrari, Beyond drug delivery. Nat. Nanotechnol. **3**(3), 131–132 (2008)
52. F. Gu, L. Zhang, B.A. Teply, N. Mann, A. Wang, A.F. Radovic-Moreno et al., Precise engineering of targeted nanoparticles by using self-assembled biointegrated block copolymers. Proc. Natl. Acad. Sci. U.S.A. **105**(7), 2586–2591 (2008)
53. H. Shmeeda, D. Tzernach, L. Mak, A. Gabizon, Her2-targeted pegylated liposomal doxorubicin: retention of target-specific binding and cytotoxicity after in vivo passage. J. Control Release **136**(2), 155–160 (2009)
54. J.H. Park, G. von Maltzahn, L.L. Zhang, A.M. Derfus, D. Simberg, T.J. Harris et al., Systematic surface engineering of magnetic nanoworms for in vivo tumor targeting. Small **5**(6), 694–700 (2009)
55. S. Jeong, J.Y. Park, M.G. Cha, H. Chang, Y.I. Kim, H.M. Kim et al., Highly robust and optimized conjugation of antibodies to nanoparticles using quantitatively validated protocols. Nanoscale **9**(7), 2548–2555 (2017)
56. D. Zeng, N.S. Lee, Y. Liu, D. Zhou, C.S. Dence, K.L. Wooley et al., ^{64}Cu core-labeled nanoparticles with high specific activity via metal-free click chemistry. ACS Nano **6**(6), 5209–5219 (2012)
57. S.B. Lee, H.L. Kim, H.J. Jeong, S.T. Lim, M.H. Sohn, D.W. Kim, Mesoporous silica nanoparticle pretargeting for PET imaging based on a rapid bioorthogonal reaction in a living body. Angew. Chem. Int. Ed. Engl. **52**(40), 10549–10552 (2013)
58. W.G. Kreyling, A.M. Abdelmonem, Z. Ali, F. Alves, M. Geiser, N. Haberl et al., In vivo integrity of polymer-coated gold nanoparticles. Nat. Nanotechnol. **10**(7), 619–623 (2015)

59. D.E. Lee, J.H. Na, S. Lee, C.M. Kang, H.N. Kim, S.J. Han et al., Facile method to radiolabel glycol chitosan nanoparticles with ^{64}Cu via copper-free click chemistry for microPET imaging. Mol. Pharm. **10**(6), 2190–2198 (2013)
60. A. Ruggiero, C.H. Villa, J.P. Holland, S.R. Sprinkle, C. May, J.S. Lewis et al., Imaging and treating tumor vasculature with targeted radiolabeled carbon nanotubes. Int. J. Nanomed. **5**, 783–802 (2010)
61. K.J. Harrington, S. Mohammadtaghi, P.S. Uster, D. Glass, A.M. Peters, R.G. Vile et al., Effective targeting of solid tumors in patients with locally advanced cancers by radiolabeled pegylated liposomes. Clin. Cancer Res. **7**(2), 243–254 (2001)
62. Y.J. Chang, C.H. Chang, T.J. Chang, C.Y. Yu, L.C. Chen, M.L. Jan et al., Biodistribution, pharmacokinetics and microSPECT/CT imaging of ^{188}Re-bMEDA-liposome in a C26 murine colon carcinoma solid tumor animal model. Anticancer Res. **27**(4b), 2217–2225 (2007)
63. F. Chen, H. Hong, Y. Zhang, H.F. Valdovinos, S. Shi, G.S. Kwon et al., In vivo tumor targeting and image-guided drug delivery with antibody-conjugated, radiolabeled mesoporous silica nanoparticles. ACS Nano **7**(10), 9027–9039 (2013)
64. R. Zhang, Q. Fan, M. Yang, K. Cheng, X. Lu, L. Zhang et al., Engineering melanin nanoparticles as an efficient drug-delivery system for imaging-guided chemotherapy. Adv. Mater. **27**(34), 5063–5069 (2015)
65. S.X. Wang, A. Bao, S.J. Herrera, W.T. Phillips, B. Goins, C. Santoyo et al., Intraoperative ^{186}Re-liposome radionuclide therapy in a head and neck squamous cell carcinoma xenograft positive surgical margin model. Clin. Cancer Res. **14**(12), 3975–3983 (2008)
66. H.-E. Wang, H.-M. Yu, Y.-C. Lu, N.-N. Heish, Y.-L. Tseng, K.-L. Huang et al., Internal radiotherapy and dosimetric study for ^{111}In/^{177}Lu-pegylated liposomes conjugates in tumor-bearing mice. Nucl. Instrum. Methods Phys. Res. A. **569**(2), 533–537 (2006)
67. L.C. Chen, C.H. Chang, C.Y. Yu, Y.J. Chang, W.C. Hsu, C.L. Ho et al., Biodistribution, pharmacokinetics and imaging of ^{188}Re-BMEDA-labeled pegylated liposomes after intraperitoneal injection in a C26 colon carcinoma ascites mouse model. Nucl. Med. Biol. **34**(4), 415–423 (2007)
68. L. Li, C.A. Wartchow, S.N. Danthi, Z. Shen, N. Dechene, J. Pease et al., A novel antiangiogenesis therapy using an integrin antagonist or anti-Flk-1 antibody coated ^{90}Y-labeled nanoparticles. Int. J. Radiat. Oncol. Biol. Phys. **58**(4), 1215–1227 (2004)
69. S. Yook, Z. Cai, Y. Lu, M.A. Winnik, J.P. Pignol, R.M. Reilly, Intratumorally injected ^{177}Lu-labeled gold nanoparticles: Gold nanoseed brachytherapy with application for neoadjuvant treatment of locally advanced breast cancer. J. Nucl. Med. **57**(6), 936–942 (2016)
70. L. Apetoh, F. Ghiringhelli, A. Tesniere, M. Obeid, C. Ortiz, A. Criollo et al., Toll-like receptor 4-dependent contribution of the immune system to anticancer chemotherapy and radiotherapy. Nat. Med. **13**(9), 1050–1059 (2007)
71. M. Obeid, T. Panaretakis, N. Joza, R. Tufi, A. Tesniere, P. van Endert et al., Calreticulin exposure is required for the immunogenicity of gamma-irradiation and UVC light-induced apoptosis. Cell Death Differ. **14**(10), 1848–1850 (2007)
72. C. Vanpouille-Box, F. Lacoeuille, C. Belloche, N. Lepareur, L. Lemaire, J.-J. LeJeune et al., Tumor eradication in rat glioma and bypass of immunosuppressive barriers using internal radiation with ^{188}Re-lipid nanocapsules. Biomaterials **32**(28), 6781–6790 (2011)

Chapter 13
Preservation of Ligand Functionality by Click Chemistry

James C. Knight and Bart Cornelissen

Abstract Click chemistry reactions have had a considerable impact in the effort to develop efficient synthetic strategies towards new radiopharmaceutical agents. This is largely due to the ability of these reactions to proceed rapidly under ambient conditions, resulting in an easily isolated product. These reaction properties are particularly desirable in the synthesis of positron emission tomography (PET) imaging agents containing short-lived radioisotopes, such as carbon-11 and fluorine-18. Striving to further improve on the suitability of these reactions, chemists have succeeded in developing new, streamlined click chemistry reactions with additional advantages. These versatile reactions have now been used extensively in the preparation of radiolabeled small molecules, peptides, proteins, and nanomaterials for nuclear imaging applications. A small number of these click chemistry reactions are also bioorthogonal as they have the ability to proceed efficiently and selectively within the complex biological medley of a living system. This rare and valuable attribute has led to their utilisation in pretargeted imaging strategies which have the potential to provide superior image quality and reduced radiation burden compared with conventional imaging approaches. In this chapter, we aim to introduce the click chemistry reactions which have had the greatest impact in the preparation of radiolabeled ligands for nuclear imaging applications, with special focus on the application of nanoparticles. In addition, we also describe the use of these reactions in combination with nanoparticle vectors to facilitate a pretargeted imaging strategy.

J. C. Knight (✉) · B. Cornelissen (✉)
Department of Oncology, CR-UK/MRC Oxford Institute for Radiation Oncology, University of Oxford, Oxford, UK
e-mail: james.knight@oncology.ox.ac.uk

B. Cornelissen
e-mail: bart.cornelissen@oncology.ox.ac.uk

D. S. Lee (ed.), *Radionanomedicine*, Biological and Medical Physics, Biomedical Engineering, https://doi.org/10.1007/978-3-319-67720-0_13

13.1 Click Chemistry

The concept of 'click chemistry' was introduced in 2001 by Kolb et al. who identified a variety of chemical reactions which have a specific set of advantageous properties in common [1]. Specifically, the reactions which fall under this umbrella term must be: (i) modular, (ii) wide in scope, (iii) very high yielding, (iv) incapable of generating offensive by-products, and (v) stereospecific. From a practical perspective, click chemistry reactions must be capable of proceeding efficiently in ambient reaction conditions (e.g. not requiring precautions against oxygen) and involve easily accessible chemical precursors. In addition, these reactions must be able to take place either in the absence of solvent or in a solvent which is benign and/or easily removed. Lastly, it is also important that the desired product is easily isolated from the reaction mixture.

13.1.1 The Huisgen 1,3-Dipolar Cycloaddition

While several reaction types abide by these highly specific criteria, one reaction in particular has gained prominence across many sub-disciplines of chemistry (including the field of radiochemistry), namely the Huisgen 1,3-dipolar cycloaddition [2]. This reaction between azide and alkyne functional groups yielding a triazole species was originally reported by Rolf Huisgen in 1963 (Fig. 13.1a) [3, 4]. While this reaction requires high temperatures and/or pressures (and frequently yields an undesirable mixture of 1,4- and 1,5-substituted triazole regioisomers), it was later discovered that the introduction of a copper(I) catalyst allows this reaction to proceed efficiently at room temperature and in a much more regiospecific manner (exclusively generating the 1,4-substituted triazole; Fig. 13.1b) [5, 6]. In addition, the copper(I) catalyst also greatly increases the rate of the reaction ($\sim 10^6$-fold).

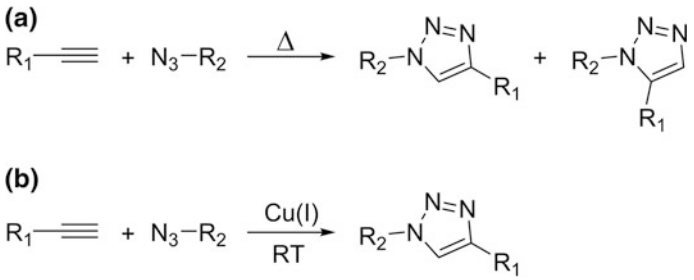

Fig. 13.1 **a** The archetypal Huisgen 1,3-dipolar cycloaddition requires heat and leads to a mixture of regioisomers. **b** The addition of a Cu(I) catalyst allows the reaction to proceed efficiently at room temperature and only generates the 1,4-substituted triazole

13.1.2 The Use of Conventional Click Chemistry Reactions in Radiochemistry

The refined version of the original Huisgen 1,3-dipolar cycloaddition reaction was quickly recognised by radiochemists as a valuable tool for the production of positron emission tomography (PET) and single-photon emission computed tomography (SPECT) imaging agents [7, 8]. The radiosynthesis and isolation of these imaging agents is often rendered challenging by the short radioactive half-lives of many important radioisotopes (such as carbon-11 [$t_{1/2}$ = 20.3 min] and fluorine-18 [$t_{1/2}$ = 109.8 min]) and therefore the rapid, facile, and clean nature of click chemistry reactions make them well-suited to these applications.

The attractiveness of the Huisgen 1,3-dipolar cycloaddition reaction in radiochemistry is also attributable to the ease with which azide and alkyne substituents can be incorporated into a range of chemical scaffolds. These functional groups also exhibit kinetic stability and inertness towards a range of other chemical species and reaction conditions. As such, azide and alkyne groups can frequently be incorporated early on during a multi-step synthesis often without risk of degradation or transformation, thereby offering flexibility in terms of chemical synthetic strategies.

There are several examples in which the Huisgen 1,3-dipolar cycloaddition reaction has been utilised in the preparation of radiolabeled small molecules [9, 10], peptides [11–15], proteins [16, 17], and nanomaterials [18, 19]. In 2009, Devaraj et al. reported the synthesis and preclinical in vivo evaluation of an [^{18}F]-labeled trimodal nanoparticle ([^{18}F]-CLIO) constructed around a core of superparamagnetic iron oxide that was cross-linked with dextran molecules [18]. During the preparation of these nanoparticles, surface modifications were made with both the near-infrared fluorochrome VT680 and azide groups, the latter of which facilitated a copper-catalysed click chemistry reaction with the radiofluorinated alkyne compound [^{18}F]-PEG_3. This nanoparticle radiolabelling strategy was shown to be moderately efficient as an average decay-corrected radiochemical yield of 57% was obtained under relatively mild reaction conditions (40 °C) and although DMSO was used as a partial solvent in this reaction, the resulting [^{18}F]-CLIO nanoparticles were isolated very simply via microcentrifuge filtration and resuspension. The average specific activity was 11 mCi mg^{-1} of nanoparticles. While no disease-targeting ligands were attached to the nanoparticles in this study, the remaining azide groups present on the exterior represent an attractive opportunity for further functionalisation.

In another example, copper-catalysed click chemistry has also been applied in the preparation of [^{18}F]-labeled nanoparticles of zinc oxide (ZnO) with the objective of understanding the effects of exposure to nanoparticles of this type upon the body [19]. In this case, ZnO nanoparticles of two different sizes (20 or 100 nm) were coated with alkyne residues and were then subjected to reaction with the radiofluorinated compound, [^{18}F]-ethoxy azide. In a similar fashion to the previous example, the radiolabeled nanoparticles were purified via filtration and obtained in

high purity (>95%) with specific activities of 0.0197 and 0.0192 mCi mg^{-1} for 20 and 100 nm particle sizes, respectively.

In the effort to develop the most optimal synthetic strategies for the preparation of radiopharmaceuticals, the requirement of a copper catalyst in these reactions is problematic. Excessive intake of this metal is known to exert in vivo toxicity [20–22] and therefore it requires complete removal in a fast and facile manner. Another important consideration is that radiotracers based on peptides and proteins may often be—given their abundance of electron donating groups—naturally primed for coordinating metals such as copper in a manner which is often non-specific and difficult to predict. This may of course have a detrimental impact on important binding properties such as target affinity and specificity towards the epitope of interest. Lastly, the necessity of a catalyst represents an additional reaction parameter which requires thorough optimisation and, therefore, is another hurdle in the research and development process. The simplification of these reactions by removal of the catalyst is therefore highly desirable.

13.2 The Evolution of Copper-Free Click Chemistry Reactions

A notable advancement in the effort to circumvent the requirement of a metal catalyst in click chemistry reactions was pioneered by Bertozzi et al. in 2004 [23]. Inspired by early literature on this topic [24], it was recognised that 'activating' alkynes via their insertion into a ring-strained structure offered an attractive method for tagging azide-modified structures despite the lack of a copper(I) catalyst. Reactions of this type are now referred to as strain-promoted [3+2] azide-alkyne cycloadditions (SPAAC; Fig. 13.2a) [25–31].

While early SPAAC reactions exhibited lower rates of reaction in comparison to analogous copper-catalysed cycloaddition reactions, this obstacle was overcome with the recognition that electron-withdrawing substituents (such as fluorine atoms) in positions adjacent to the strained alkyne group [32] or dibenzoannulation [33] effectively enhance the rate of these reactions. For example, in reactions with benzyl azide (or a similar aliphatic azide), a 'first generation' cyclooctyne species (OCT) yielded a rate constant of 2.4×10^{-3} M^{-1} s^{-1}, while the more highly-strained alkyne dibenzoazacyclooctyne (DBCO; Fig. 13.2b) revealed a greatly enhanced rate constant of 310×10^{-3} M^{-1} s^{-1} [33–35]. SPAAC reactions have now been used widely for the synthesis of radiolabeled imaging agents for PET and SPECT applications. Notably, in 2011, Bouvet et al. reported an [^{18}F]-labeled prosthetic group based on DBCO ([^{18}F]-FB-DBCO; Fig. 13.2b) which was used successfully for radiolabelling a variety of azide-containing precursors including the complex natural product geldanamycin and obtained excellent radiochemical yields under mild reaction conditions [36].

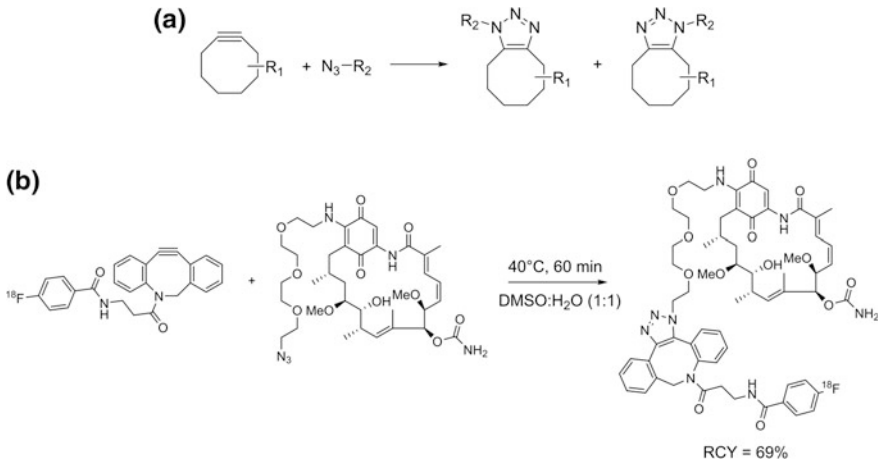

Fig. 13.2 **a** The strain-promoted [3+2] azide-alkyne cycloaddition (SPAAC) reaction is an excellent example of a copper-free click chemistry reaction. **b** The radiofluorinated dibenzocyclooctyne, [^{18}F]-FB-DBCO, developed by Bouvet et al. (adapted from [36] with permission) has been used successfully as a prosthetic group for radiolabelling a variety of azide-containing compounds, including the complex natural product geldanamycin

SPAAC reactions have now also been utilised in the construction of nanomaterials for several applications, including nuclear imaging. In 2012, SPAAC chemistry was applied in the preparation of shell-cross-linked nanoparticles (SCK-NPs) labeled with the PET radiometal copper-64 [^{64}Cu] [37]. This class of nanomaterial has a micellar structure composed of a hydrophobic (typically polystyrene) interior and an exterior shell containing hydrophilic groups, such as poly (acrylic acid-*co*-acrylamide). SCK-NPs have previously been explored as potential drug delivery vehicles and in this example were utilised as the basis of a PET imaging agent. In an initial attempt to radiolabel these nanoparticles with [^{64}Cu], the authors utilised traditional Cu(I)-catalysed click chemistry in a reaction between azide-functionalised SCK-NPs and [^{64}Cu]-DOTA-acetylene. Ultimately, this approach led to poor radiolabelling yields ($\sim$10%) and was deemed unsuccessful, largely due to exchange between the non-radioactive Cu(I) catalyst and the DOTA-bound [^{64}Cu], and the inability of the water soluble Cu(I) catalyst to access the hydrophobic interior of the nanoparticles. To circumvent these issues, an alternative [^{64}Cu]-containing precursor based on the ring-strained DBCO species was utilised in a Cu-free SPAAC reaction. This innovative approach was more successful and enabled the efficient preparation of [^{64}Cu]-SCK-NPs with improved radiolabelling yields ($\sim$64%) and high specific activity (975 Ci/μmol). Here, the adoption of SPAAC had additional advantages as the absence of copper also prevented undesirable click reactions between azide and acetylene residues within the interior of each nanoparticle.

Later, in 2014, Reiner and colleagues prepared liposomal nanoparticles modified with DBCO moieties and then utilised an azide-derivative of desferrioxamine

(DFO) complexed with the PET radiometal zirconium-89 for the preparation of [^{89}Zr]-labeled liposomes (Fig. 13.3) [38]. Notably, this method was less efficient in comparison to an alternative 'surface chelation' method which involved incubating DFO-modified liposomes with [^{89}Zr]-oxalate. These two approaches resulted in radiolabelling yields of 14 ± 4 and 80 ± 10%, respectively.

While SPAAC reactions have undoubtedly had a positive impact in radiochemistry, the ring-strained cycloalkyne groups are often highly hydrophobic which can pose challenges during synthesis and also have detrimental effects on the biodistribution of the resulting imaging agents (e.g. promoting hepatobiliary excretion).

The inverse electron-demand Diels-Alder (IEDDA) reaction between tetrazine (Tz) and *trans*-cyclooctene (TCO) species has also drawn considerable attention in recent years as it represents another excellent example of a catalyst-free reaction with extremely fast reaction kinetics (up to k = 380,000 M^{-1} s^{-1} [39–43]) and high chemoselectivity (Fig. 13.4a) [44, 45]. Consequently, IEDDA reactions have found great utility in the preparation of a variety of radiopharmaceutical agents [46–51]. For example, [^{18}F]-TCO has been used as a prosthetic group in reactions with Tz-appended peptides, including Exendin-4 [52] and RGD (Fig. 13.4b) [49]. This versatile compound has also been used in the preparation of a PET radiotracer based on a small molecule PARP1 inhibitor, AZD2281 (Fig. 13.4b) [47]. Here, the reaction between [^{18}F]-TCO and a Tz-modified derivative of AZD2281 was shown to be highly efficient as decay-corrected radiochemical yields of 59.6 ± 5.0% were obtained following a mere 3 min reaction time at room temperature. In this case, it was shown that modifying AZD2281 in this manner only had a slight negative impact on this ligands functional ability to bind to PARP1 compared with the parent compound AZD2281 (IC_{50} values of 17.9 ± 1.1 and 5 nM, respectively) despite the addition of a rather bulky chemical attachment.

Due to the ability of the IEDDA reaction between Tz and TCO species to proceed efficiently and largely unimpeded in vivo, it has also been used successfully in pretargeting studies in vivo in which typically a TCO-modified antibody is first administered intravenously and then followed at a later time point by a

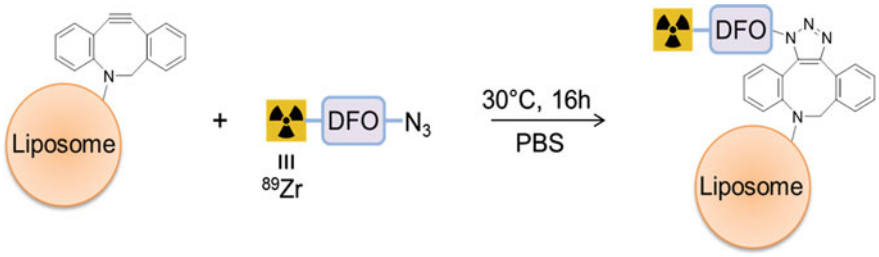

Fig. 13.3 SPAAC chemistry has been applied in the construction of radiolabeled nanomaterials for nuclear imaging applications. In one example, Reiner et al. (adapted from [38] with permission) developed liposomes modified with DBCO and performed a successful copper-free click reaction with a [^{89}Zr]-containing azide precursor

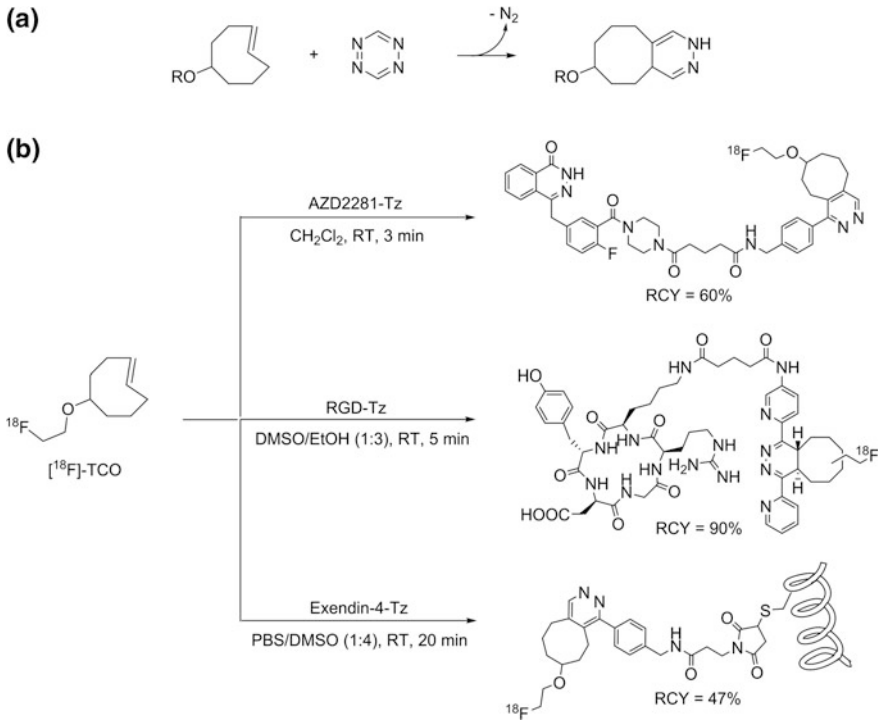

Fig. 13.4 **a** The inverse electron-demand Diels-Alder (IEDDA) reaction between *trans*-cyclooctene (TCO) and tetrazine (Tz) species is an extremely rapid copper-free click chemistry reaction with high chemoselectivity. **b** The prosthetic group [^{18}F]-TCO is a highly versatile compound which has been used effectively for the production of a wide variety of PET imaging agents, including those based on the small molecule PARP inhibitor, AZD2281 [47], the cyclic peptide RGD [49], and Exendin-4 [52]

radiolabeled Tz species (Fig. 13.5) [53–56]. The alternative scenario (i.e. involving a Tz-modified antibody/nanomaterial and a radiolabeled TCO secondary agent) has not been so extensively studied, most likely because TCO has a tendency to undergo rapid isomerisation to its comparatively unreactive *cis* isomer in the presence of copper-containing proteins within the plasma. Such pretargeting strategies based on IEDDA reactions have demonstrated a promising ability in preclinical studies to improve upon some of the limitations of directly radiolabeled antibodies (e.g. slow blood clearance) leading to enhanced image quality and a lower radiation burden to the body [56]. Recently, the scope of this approach has also been significantly expanded as primary agents based on nanomaterials have been evaluated within the context of IEDDA-based pretargeting strategies.

In a highly innovate study, Hou et al. developed supramolecular nanoparticles (SNPs) comprised of a cyclodextrin-polyethylenimine polymer (CD-PEI), adamantine-grafted polyamidoamine, and adamantine-grafted polyethylene glycol [57]. In this case, TCO was grafted on to the CD-PEI polymer and was

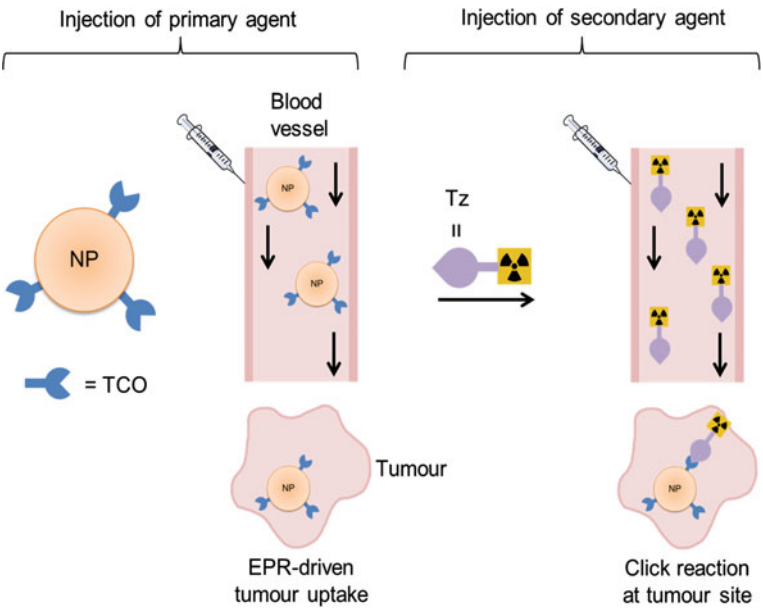

Fig. 13.5 Nanoparticles (NPs) functionalised with click chemistry groups have been studied as primary agents in pretargeted imaging strategies. The high loading potential, versatility, diverse functionality, and potential multi-modal imaging offered by many nanoparticle frameworks are attractive qualities for this application

consequently encapsulated within the nanoparticle framework. Following intravenous administration, these SNPs were found to accumulate within xenograft tumours in mice as a result of the enhanced permeability and retention (EPR) effect which is often the case for large macromolecular species [58–60]. Notably, these particles then disassembled at the tumour site thereby affording access to the TCO groups by a [^{64}Cu]-radiolabeled Tz secondary agent. Promisingly, this pretargeting approach resulted in the acquisition of PET images in which tumours were strongly contrasted against surrounding tissues and organs.

In another notable example, Keinänen et al. have recently developed a pretargeting strategy based upon TCO-modified mesoporous silica nanoparticles and an [^{18}F]-labeled Tz secondary agent [61]. Mesoporous silica nanoparticles are an attractive nanoplatform for this application due to their high loading potential, low toxicity, and biodegradability. In this example, no tumour model was employed, however the authors found evidence of IEDDA reaction products within the spleen. While this particular approach did not involve targeting of any specific disease biomarker, the promising ability of this reaction to proceed efficiently in vivo is a good indicator of the potential that nanoparticle frameworks have to offer pretargeting applications in imaging and therapy.

In summary, click chemistry reactions have found great utility in the production of a wide variety of radiopharmaceutical agents, particularly for PET radiotracers.

The continual refinement of these reactions using innovative chemistry is offering highly versatile synthetic methods which are becoming faster, simpler, and higher yielding. In many cases, these reactions have offered a convenient and efficient means of obtaining radiolabeled derivatives of ligands without compromising the ligands' functional ability to bind to its target epitope. The application of click chemistry methods for the production of a wide variety of radiolabeled nanomaterials is also showing much promise. Lastly, bioorthogonal IEDDA chemistry has now become established as the basis of a novel pretargeting strategy for both nuclear imaging and therapeutic applications. Pretargeting methods based on nanoparticle primary agents have demonstrated some efficacy despite in most cases relying on passive tumour targeting via the EPR effect. Given the high ligand loading capacity offered by most nanoparticles, it will be of interest to expand this approach to include targeting of specific disease biomarkers.

References

1. H.C. Kolb, M.G. Finn, K.B. Sharpless, Click chemistry: diverse chemical function from a few good reactions. Angew. Chem. Int. Ed. Engl. **40**(11), 2004–2021 (2001)
2. M. Meldal, C.W. Tornøe, Cu-catalyzed azide–alkyne cycloaddition. Chem. Rev. **108**(8), 2952–3015 (2008)
3. R. Huisgen, 1,3-dipolar cycloadditions. Past and future. Angew. Chem. Int. Ed. Engl. **2**(10), 565–598 (1963)
4. R. Huisgen, Kinetics and mechanism of 1,3-dipolar cycloadditions. Angew. Chem. Int. Ed. Engl. **2**(11), 633–645 (1963)
5. V.V. Rostovtsev, L.G. Green, V.V. Fokin, K.B. Sharpless, A stepwise Huisgen cycloaddition process: copper(I)-catalyzed regioselective "ligation" of azides and terminal alkynes. Angew. Chem. Int. Ed. Engl. **41**(14), 2596–2599 (2002)
6. C.W. Tornøe, C. Christensen, M. Meldal, Peptidotriazoles on solid phase: [1,2,3]-triazoles by regiospecific copper(I)-catalyzed 1,3-dipolar cycloadditions of terminal alkynes to azides. J. Org. Chem. **67**(9), 3057–3064 (2002)
7. K. Nwe, M.W. Brechbiel, Growing applications of "click chemistry" for bioconjugation in contemporary biomedical research. Cancer Biother Radiopharm. **24**(3), 289–302 (2009)
8. C. Wängler, R. Schirrmacher, P. Bartenstein, B. Wängler, Click-chemistry reactions in radiopharmaceutical chemistry: fast & easy introduction of radiolabels into biomolecules for in vivo imaging. Curr. Med. Chem. **17**(11), 1092–1116 (2010)
9. T.L. Ross, M. Honer, P.Y.H. Lam, T.L. Mindt, V. Groehn, R. Schibli et al., Fluorine-18 click radiosynthesis and preclinical evaluation of a new ^{18}F-labeled folic acid derivative. Bioconjug Chem. **19**(12), 2462–2470 (2008)
10. E. Galante, W.B. Schoultz, M. Koepp, E. Årstad, Chelator-accelerated one-pot 'Click' labeling of small molecule tracers with 2-[^{18}F] fluoroethyl azide. Molecules **18**(5) (2013)
11. J. Marik, J.L. Sutcliffe, Click for PET: rapid preparation of [^{18}F] fluoropeptides using CuI catalyzed 1,3-dipolar cycloaddition. Tetrahedron Lett. **47**(37), 6681–6684 (2006)
12. S.H. Hausner, J. Marik, M.K.J. Gagnon, J.L. Sutcliffe, In vivo positron emission tomography (PET) imaging with an αvβ6 specific peptide radiolabeled using ^{18}F-"click" chemistry: evaluation and comparison with the corresponding 4-[^{18}F] fluorobenzoyl- and 2-[^{18}F] fluoropropionyl-peptides. J. Med. Chem. **51**(19), 5901–5904 (2008)

13. Z.-B. Li, Z. Wu, K. Chen, F.T. Chin, X. Chen, Click chemistry for 18F-labeling of RGD peptides and microPET imaging of tumor integrin αvβ3 expression. Bioconjug. Chem. **18**(6), 1987–1994 (2007)
14. T. Ramenda, R. Bergmann, F. Wuest, Synthesis of ^{18}F-labeled neurotensin(8-13) via copper-mediated 1,3-dipolar [3+2] cycloaddition reaction. Lett. Drug Des. Discov. **4**(4), 279–285 (2007)
15. M. Glaser, E. Årstad, "Click labeling" with 2-[^{18}F] fluoroethylazide for positron emission tomography. Bioconjug Chem. **18**(3), 989–993 (2007)
16. T. Ramenda, T. Kniess, R. Bergmann, J. Steinbach, F. Wuest, Radiolabeling of proteins with fluorine-18 via click chemistry. Chem. Commun (Camb) **48**, 7521–7523 (2009)
17. T. Ramenda, J. Steinbach, F. Wuest, 4-[18F] Fluoro-N-methyl-N-(propyl-2-yn-1-yl) benzenesulfonamide ([^{18}F] F-SA): a versatile building block for labeling of peptides, proteins and oligonucleotides with fluorine-18 via Cu(I)-mediated click chemistry. Amino Acids **44** (4), 1167–1180 (2013)
18. N.K. Devaraj, E.J. Keliher, G.M. Thurber, M. Nahrendorf, R. Weissleder, ^{18}F labeled nanoparticles for in vivo PET-CT imaging. Bioconjug. Chem. **20**(2), 397–401 (2009)
19. C.M. Lee, H.J. Jeong, D.W. Kim, M.H. Sohn, S.T. Lim, The effect of fluorination of zinc oxide nanoparticles on evaluation of their biodistribution after oral administration. Nanotechnology **23**(20), 205102 (2012)
20. C.D. Hein, X.-M. Liu, D. Wang, Click chemistry, a powerful tool for pharmaceutical sciences. Pharm. Res. **25**(10), 2216–2230 (2008)
21. T. Wang, Z. Guo. Copper in Medicine: Homeostasis, chelation therapy and antitumor drug design. Curr. Med. Chem. **13**(5), 525–537 (2006)
22. K.D. Held, F.C. Sylvester, K.L. Hopcia, J.E. Biaglow, Role of fenton chemistry in thiol-induced toxicity and apoptosis. Radiat. Res. **145**(5), 542–553 (1996)
23. N.J. Agard, J.A. Prescher, C.R. Bertozzi, A strain-promoted [3+2] azide–alkyne cycloaddition for covalent modification of biomolecules in living systems. J. Am. Chem. Soc. **126**(46), 15046–15047 (2004)
24. G. Wittig, A. Krebs, Zur existenz niedergliedriger cycloalkine I. Chem. Ber. **94**(12), 3260–3275 (1961)
25. M.F. Debets, S.S. van Berkel, J. Dommerholt, A.J. Dirks, F.P.J.T. Rutjes, F.L. van Delft, Bioconjugation with strained alkenes and alkynes. Acc. Chem. Res. **44**(9), 805–815 (2011)
26. E.M. Sletten, C.R. Bertozzi, From mechanism to mouse: a tale of two bioorthogonal reactions. Acc. Chem. Res. **44**(9), 666–676 (2011)
27. C.R. Becer, R. Hoogenboom, U.S. Schubert, Click chemistry beyond metal-catalyzed cycloaddition. Angew. Chem. Int. Ed. Engl. **48**(27), 4900–4908 (2009)
28. J.C. Jewett, C.R. Bertozzi, Cu-free click cycloaddition reactions in chemical biology. Chem. Soc. Rev. **39**(4), 1272–1279 (2010)
29. J.M. Baskin, C.R. Bertozzi, Bioorthogonal click chemistry: covalent labeling in living systems. QSAR Comb. Sci. **26**(11–12), 1211–1219 (2007)
30. E.M. Sletten, C.R. Bertozzi, Bioorthogonal chemistry: fishing for selectivity in a sea of functionality. Angew. Chem. Int. Ed. Engl. **48**(38), 6974–6998 (2009)
31. J.M. Baskin, C.R. Bertozzi, Copper-free click chemistry: bioorthogonal reagents for tagging azides. Aldrichimica Acta **43**(1), 15–23 (2010)
32. J.A. Codelli, J.M. Baskin, N.J. Agard, C.R. Bertozzi, Second-generation difluorinated cyclooctynes for copper-free click chemistry. J. Am. Chem. Soc. **130**(34), 11486–11493 (2008)
33. C.G. Gordon, J.L. Mackey, J.C. Jewett, E.M. Sletten, K.N. Houk, C.R. Bertozzi, Reactivity of biarylazacyclooctynones in copper-free click chemistry. J. Am. Chem. Soc. **134**(22), 9199–9208 (2012)
34. J. Dommerholt, O. Van Rooijen, A. Borrmann, C.F. Guerra, F.M. Bickelhaupt, F.L. Van Delft, Highly accelerated inverse electron-demand cycloaddition of electron-deficient azides with aliphatic cyclooctynes. Nat. Commun. **5**, 5378 (2014)

35. J. Dommerholt, F.P.J.T. Rutjes, F.L. van Delft, Strain-promoted 1,3-dipolar cycloaddition of cycloalkynes and organic azides. Top. Curr. Chem. **374**(2), 16 (2016)
36. V. Bouvet, M. Wuest, F. Wuest, Copper-free click chemistry with the short-lived positron emitter fluorine-18. Org. Biomol. Chem. **9**(21), 7393–7399 (2011)
37. D. Zeng, N.S. Lee, Y. Liu, D. Zhou, C.S. Dence, K.L. Wooley et al., ^{64}Cu core-labeled nanoparticles with high specific activity via metal-free click chemistry. ACS Nano **6**(6), 5209–5219 (2012)
38. C. Pérez-Medina, D. Abdel-Atti, Y. Zhang, V.A. Longo, C.P. Irwin, T. Binderup et al., A modular labeling strategy for in vivo PET and near-infrared fluorescence imaging of nanoparticle tumor targeting. J. Nucl. Med. **55**(10), 1706–1711 (2014)
39. J. Schoch, M. Staudt, A. Samanta, M. Wiessler, A. Jäschke, Site-specific one-pot dual labeling of DNA by orthogonal cycloaddition chemistry. Bioconjug. Chem. **23**(7), 1382–1386 (2012)
40. M.R. Karver, R. Weissleder, S.A. Hilderbrand, Synthesis and evaluation of a series of 1,2,4,5-tetrazines for bioorthogonal conjugation. Bioconjug. Chem. **22**(11), 2263–2270 (2011)
41. K. Lang, L. Davis, S. Wallace, M. Mahesh, D.J. Cox, M.L. Blackman et al., Genetic encoding of bicyclononynes and trans-cyclooctenes for site-specific protein labeling in vitro and in live mammalian cells via rapid fluorogenic Diels-Alder reactions. J. Am. Chem. Soc. **134**(25), 10317–10320 (2012)
42. M.L. Blackman, M. Royzen, J.M. Fox, Tetrazine ligation: fast bioconjugation based on inverse-electron-demand Diels–Alder reactivity. J. Am. Chem. Soc. **130**(41), 13518–13519 (2008)
43. M.T. Taylor, M.L. Blackman, O. Dmitrenko, J.M. Fox, Design and synthesis of highly reactive dienophiles for the tetrazine-trans-cyclooctene ligation. J. Am. Chem. Soc. **133**(25), 9646–9649 (2011)
44. A.-C. Knall, C. Slugovc, Inverse electron demand Diels-Alder (iEDDA)-initiated conjugation: a (high) potential click chemistry scheme. Chem. Soc. Rev. **42**(12), 5131–5142 (2013)
45. J. Sauer, D.K. Heldmann, J. Hetzenegger, J. Krauthan, H. Sichert, J. Schuster, 1,2,4,5-Tetrazine: synthesis and reactivity in [4+2] cycloadditions. Euro. J. Org. Chem. **1998**(12), 2885–2896 (1998)
46. Z. Li, H. Cai, M. Hassink, M.L. Blackman, R.C.D. Brown, P.S. Conti et al., Tetrazine-trans-cyclooctene ligation for the rapid construction of ^{18}F labeled probes. Chem. Commun. **46**(42), 8043–8045 (2010)
47. E.J. Keliher, T. Reiner, A. Turetsky, S.A. Hilderbrand, R. Weissleder, High-yielding, two-step ^{18}F labeling strategy for ^{18}F-PARP1 inhibitors. Chem. Med. Chem. **6**(3), 424–427 (2011)
48. T. Reiner, J. Lacy, E.J. Keliher, K.S. Yang, A. Ullal, R.H. Kohler et al., Imaging therapeutic PARP inhibition in vivo through bioorthogonally developed companion imaging agents. Neoplasia **14**, 169–177 (2012)
49. R. Selvaraj, S. Liu, M. Hassink, C. Huang, L. Yap, R. Park et al., Tetrazine-trans-cyclooctene ligation for the rapid construction of integrin $\alpha v\beta 3$ targeted PET tracer based on a cyclic RGD peptide. Bioorg. Med. Chem. Lett. **21**(17), 5011–5014 (2011)
50. S. Liu, M. Hassink, R. Selvaraj, L.-P. Yap, R. Park, H. Wang et al., Efficient ^{18}F labeling of cysteine-containing peptides and proteins using tetrazine–trans-cyclooctene ligation. Mol. Imaging **12**, 121–128 (2013)
51. Z. Wu, S. Liu, M. Hassink, I. Nair, R. Park, L. Li et al., Development and evaluation of ^{18}F-TTCO-Cys40-Exendin-4: a PET probe for imaging transplanted islets. J. Nucl. Med. **54**(2), 244–251 (2013)
52. E.J. Keliher, T. Reiner, G.M. Thurber, R. Upadhyay, R. Weissleder, Efficient ^{18}F-labeling of synthetic exendin-4 analogues for imaging beta cells. ChemistryOpen. **1**(4), 177–183 (2012)
53. J.C. Knight, B. Cornelissen, Bioorthogonal chemistry: implications for pretargeted nuclear (PET/SPECT) imaging and therapy. Am. J. Nucl. Med. Mol. Imaging **4**(2), 96–113 (2014)

54. R. Rossin, M.S. Robillard, Pretargeted imaging using bioorthogonal chemistry in mice. Curr. Opin. Chem. Biol. **21**, 161–169 (2014)
55. R. Rossin, P. Renart Verkerk, S.M. van den Bosch, R.C.M. Vulders, I. Verel, J. Lub et al., In vivo chemistry for pretargeted tumor imaging in live mice. Angew. Chem. Int. Ed. Engl. **122** (19), 3447–3450 (2010)
56. B.M. Zeglis, K.K. Sevak, T. Reiner, P. Mohindra, S.D. Carlin, P. Zanzonico et al., A pretargeted PET imaging strategy based on bioorthogonal Diels–Alder click chemistry. J. Nucl. Med. **54**(8), 1389–1396 (2013)
57. S. Hou, J. Choi, M.A. Garcia, Y. Xing, K.-J. Chen, Y.-M. Chen et al., Pretargeted positron emission tomography imaging that employs supramolecular nanoparticles with in vivo bioorthogonal chemistry. ACS Nano **10**(1), 1417–1424 (2016)
58. H. Maeda, The enhanced permeability and retention (EPR) effect in tumor vasculature: the key role of tumor-selective macromolecular drug targeting. Adv. Enzyme Regul. **41**(1), 189–207 (2001)
59. H. Maeda, H. Nakamura, J. Fang, The EPR effect for macromolecular drug delivery to solid tumors: improvement of tumor uptake, lowering of systemic toxicity, and distinct tumor imaging in vivo. Adv. Drug Deliv. Rev. **65**(1), 71–79 (2013)
60. C. Heneweer, J.P. Holland, V. Divilov, S. Carlin, J.S. Lewis, Magnitude of enhanced permeability and retention effect in tumors with different phenotypes: ^{89}Zr-albumin as a model system. J. Nucl. Med. **52**(4), 625–633 (2011)
61. O. Keinänen, E.M. Mäkilä, R. Lindgren, H. Virtanen, H. Liljenbäck, V. Oikonen et al., Pretargeted PET imaging of trans-cyclooctene-modified porous silicon nanoparticles. ACS Omega **2**(1), 62–69 (2017)

Chapter 14
Bioorthogonal Reaction for Fluorine-18 Labeling

Dong Wook Kim

Abstract Specific molecular imaging probes including radiopharmaceuticals labeled with positron-emitters, such as fluorine-18 (^{18}F, $t_{1/2}$ = 109.8 min), need to expand their applications of positron emission tomography (PET) molecular imaging study. In recent years, bioorthogonal chemistry such as inverse electron-demand Diels-Alder cycloaddition reactions and strain-promoted alkyne azide cycloaddition (SPAAC) has been regarded as alternative bioorthogonal ligation reactions of bioactive molecules with radiolabeled building blocks. In this chapter, I will introduce an overview of this emerging synthetic strategies based on the catalyst-free SPAAC conjugation reaction and Diels-Alder cycloaddition reactions using tetrazine/*trans*-cyclooctene (TCO) derivatives under physiologically-friendly reaction conditions. I will also introduce that the pretargeting method by the SPAAC reaction for tracking mesoporous silica nanoparticles (MSNs) in in vivo system. This bioorthogonal SPAAC-based pretargeting protocol allow ^{18}F with a short half-life to be used for labeling of the MSNs to obtain their tracking PET images.

14.1 Cu-Catalyzed Click Reaction

Copper (I) catalyzed azide alkyne [3+2] cycloaddition (CuAAC), which referred to as "click chemistry", has received much attention in biomedical area because this click chemistry provided the facile conjugation protocol of biomolecules with a range of functional groups as well as radiolabeling method for the synthesis of molecular imaging probes [1–5]. On the other hand, this CuAAC reaction-based click bioconjugation reaction had limitations in synthetic operation as follows; the frequent undesired interaction of Cu(I) catalyst with biomolecules, such as peptide and antibody, that make this CuAAC reaction blocked or reduce the reaction rate.

D. W. Kim (✉)
Department of Chemistry, Inha University, 100 Inha-ro, Nam-gu, Incheon 402-751, Korea
e-mail: kimdw@inha.ac.kr

D. S. Lee (ed.), *Radionanomedicine*, Biological and Medical Physics, Biomedical Engineering, https://doi.org/10.1007/978-3-319-67720-0_14

This unexpected interaction can cause the denaturation of biomolecules and the cytotoxicity by residual copper in the bioactive products during this bioconjugation process [6–8].

14.2 Bioorthogonal Reaction

In recent advances in molecular imaging, bioorthogonal ligation reactions played an important role for synthesis of radiolabeled probes [9]. These bioorthogonal reaction s are useful tools to conjugate bioactive compounds with radiolabeled synthon, highly chemoselectively without need for metal catalyst under physiologically friendly condition i.e., in water, aqueous media or even cell media, tolerance of a broad range of functionality [9, 10]. Among various bioorthogonal reactions, the strain promoted alkyne azide cycloaddition (SPAAC) and the inverse Diels-Alder tetrazine click reaction have been widely used for this purpose.

Firstly, the SPAAC reaction, which is referred to as copper-free click chemistry, has acted as a straightforward and fast ligation method for biological applications, as well as an alternative bioorthogonal conjugation reaction of biomolecules with radiolabeled building blocks for the preparation of radiopharmaceuticals [9]. In this regard, many researchers have developed a variety of cyclooctyne building blocks for a variety of applications in molecular imaging [11–20]. Among various cyclooctyne derivatives, aza-dibenzocyclooctyne (ADIBO) or dibenzocyclooctyne (DIBO) compounds have been used widely with azide building blocks to rapidly produce the corresponding triazole derivatives for efficient SPAAC reaction (Fig. 14.1a) [21–23]. The strain promoted inverse electron-demand Diels-Alder cycloaddition reactions of 1,2,4,5-tetrazines are known to be another popular bioconjugation method for molecular imaging applications (Fig. 14.1b). The cycloaddition of a tetrazine with *trans*-cyclooctene (TCO) derivatives to the corresponding cycloocta[*d*]pyridazines can also provide the unusually fast reaction rates in the absence of any catalyst under physiologically friendly condition [24].

It is well known that positron emission tomography (PET) is one of excellent biomedical imaging modality. This PET system has been able to help early detection, characterization, and real time monitoring of disease pathologies. Nowadays, it is also useful for characterizing fundamental biological processes and helping new drug developments [25, 26]. In order to obtain high-quality PET images for this purpose, it is necessary to synthesize specific radiolabeled molecular imaging probes using positron-emitters, such as carbon-11 (^{11}C, $t_{1/2}$ = 20.4 min), nitrogen-13 (^{13}N, $t_{1/2}$ = 10 min), oxygen-15 (^{15}O, $t_{1/2}$ = 2.05 min), copper-64 (^{64}Cu, $t_{1/2}$ = 12.7 h), fluorine-18 (^{18}F, $t_{1/2}$ = 109.8 min) [27, 28]. In particular, ^{18}F is known to be the most prominent positron emitter for PET molecular imaging due to its favorable properties as follow; (i) its minimal steric interference can allow ^{18}F labeled biologically active molecules to maintain favorable interactions with the target proteins or receptors for tracing biological processes; (ii) ^{18}F can be generated easily from a cyclotron through the ^{18}O(p, n)^{18}F nuclear reaction using [^{18}O] water

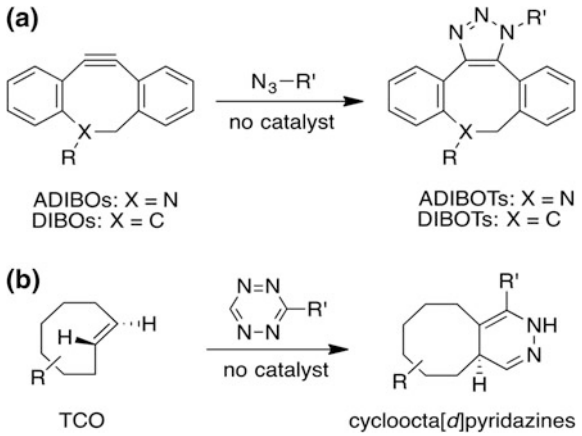

Fig. 14.1 Bioorthogonal reactions without need of catalyst under physiologically friendly condition. **a** Strain promoted alkyne azide cycloaddition (SPAAC) reaction. ADIBO = aza-dibenzocyclooctynes; DIBOs = dibenzocyclooctynes; ADIBOT = aza-dibenzocycloocta-triazoles. **b** Strain promoted inverse electron-demand Diels-Alder cycloaddition reactions. TCO = *trans*-cyclooctenes

targets with proton beams; (iii) a fluorine can form a stable covalent bond with carbon, which can increase its metabolic stability; (iv) fluorine in fluorine-containing compounds can form an unexpected hydrogen bonding with the desired biological target; (v) the half-life of ^{18}F allow ^{18}F labeled molecular imaging probes to be shipped regionally to nearby research sites or hospitals which are not equipped with cyclotron as radionuclide production facility [27–31].

14.3 SPAAC Reaction Based In Vivo ^{18}F-Labeling of Mesoporous Silica Nanoparticles

Since biocompatible nanoparticles which have an optimal size can accumulate in the tumor by passive targeting such as the enhanced permeability and retention (EPR) effects [32–34], they have attracted much interest in therapy and early diagnosis of cancer in broad nanomedicine research field [25–37]. Therefore, the pharmacokinetic studies of the nanoparticles became a crucial topic for investigating the safety of these nanoparticles and their in vivo behavior via real-time tracking using a PET system in the living body. In general, MSNs can show good performance in the biomedical field as the vehicles for drug-delivery [38]. However, because these nanoparticles generally require a long circulation time for homing at the tumor region [37, 38], ^{18}F may be not a suitable radioisotope for the labeling of nanoparticles for PET imaging considering its short half-life ($t_{1/2}$ = 109.8 min) [27–29].

In 2013, Kim et al. firstly reported the pretargeting concept for in vivo covalent ^{18}F labeling reaction of nanoparticles using a bioorthogonal chemistry [39]. In this report, highly efficient MSN pretargeting and PET imaging was successfully done with this short half-life ^{18}F using a rapid and bioorthogonal SPAAC reaction of ADIBO-substituted MSNs with ^{18}F-labeled azide in tumor-bearing mice [39]. Using the strategy of bioorthogonal chemistry, an ADIBO group-tethered PEGylated MSNs (ADIBO–PEG–MSNs) were prepared with such a size of 100–150 nm that MSNs accumulate in the tumor by the EPR effect [40]. To investigate the expected reaction rate in an in vivo system, the model SPAAC reaction was carried out under physiologically similar conditions (pH 7.4 and 36.5 °C) in vitro as shown in Fig. 14.2. The model SPAAC reaction of ADIBO–PEG–MSNs (0.48 mmol of ADIBO portion, 4 mg) with ^{18}F-labeled azide was completed within 15–20 min, and the desired ^{18}F-labeled ADIBOT–PEG–MSNs was produced in almost quantitative radiochemical yield (RCY).

As results of the tumor targeting ability of MSNs by the EPR effect and the fast rate of SPAAC reaction under physiologically similar conditions, a further MSNs-based pretargeting and later covalent ^{18}F labeling via SPAAC was performed in the living body (Fig. 14.3a). As shown in PET-CT images in Fig. 14.3c, ^{18}F-labeled azide, even though it has no targeting capability to the tumor tissue, exhibited high tumor uptake in the mice pretreated with ADIBO–PEG–MSNs 24 h earlier via in situ synthesis of ^{18}F-labeled ADIBO–PEG–MSNs by in vivo SPAAC reaction within 2 h after injection of the ^{18}F-labeled azide. In contrast, the PET-CT images of the non-pretargeted mice, to which only the ^{18}F-labeled azide was administered, showed transient initial ^{18}F uptake with lower signal intensity, washing out soon via kidneys (Fig. 14.3b). This bioorthogonal SPAAC reaction-based pretargeting protocol could provide a feasibility that the nanoparticles were given first and wait until they are localized in the target region and with later administration of the tracer ^{18}F-azide to track them using PET. Later injected ^{18}F-azide is bound to the nanoparticles via an in situ ^{18}F labeling reaction on site in the tumor in a living body. More recently, this SPAAC reaction-based pretargeting protocol was applied in tracking in vivo other macrobiomolecules such as peptides or antibodies while using PET with short half-life radioisotope.

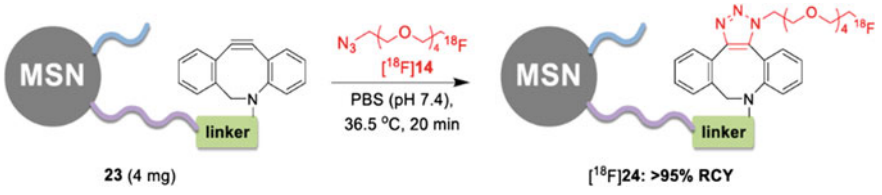

Fig. 14.2 Formation of ^{18}F-labeled ADIBOT-PEG-MSNs under physiologically similar conditions (pH 7.4, 36.5 °C) in PBS by SPAAC reaction of ADIBO-PEG-MSNs with ^{18}F-labeled azide. Adapted from [39] with permission

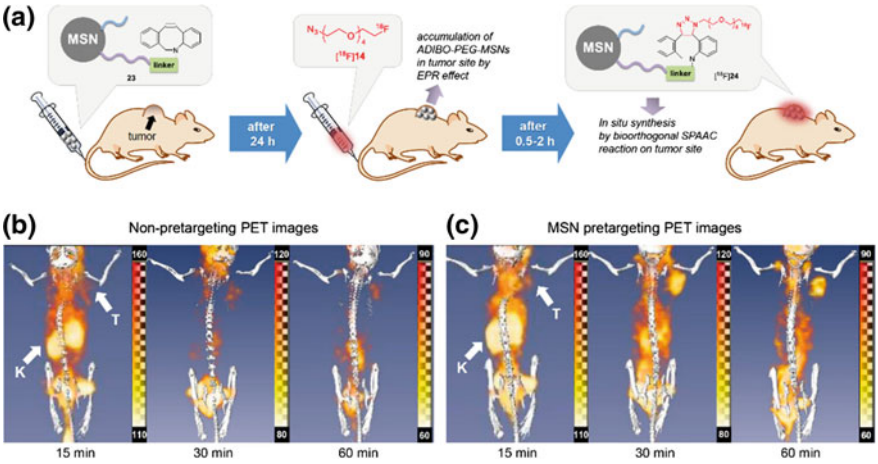

Fig. 14.3 **a** Bioorthogonal SPAAC reaction for the in situ synthesis of ^{18}F-labeled MSNs in a living specimen for the MSNs pretargeting PET-imaging in tumor mice model. **b** PET-CT images of ^{18}F-labeled azide in a U87MG tumor-xenograft mouse administrated only ^{18}F-labeled azide alone (non-pretargeted). **c** PET-CT images in a U87MG tumor-xenograft mouse pre-treated ADIBO-PEG-MSNs 24 h earlier (pretargeted procedure) at 15, 30, and 60 min after injection of ^{18}F-labeled azide. T = tumor, K = kidneys. Adapted from [40] with permission

14.4 General Radiolabeling Procedure with ^{18}F for Peptides

Over the past few decades, the development of the combinatorial chemistry and phage display technology allowed to discover novel bioactive peptide sequences In particular, the phage display has provided about 160 sequences of tumor targeting peptides [41]. Based on high expectation to use these new peptide sequences as the molecular imaging probe or new drug candidates, development of peptide radiolabeling reactions with various radioisotopes came to be an important research topic for nuclear molecular imaging, diagnosis, and therapy [42].

^{18}F labeled peptides can be prepared through two synthetic pathways as shown in Fig. 14.4. Firstly, the direct ^{18}F labeling procedure can be applied to produce ^{18}F labeled peptides by radiofluorination with no-carrier-added (n.c.a.) ^{18}F. This direct labeling reaction requires the harsh strong basic reaction conditions in organic solvent, which is known to be not suitable for maintain the integrity of these peptides molecules. As a result, the direct radiofluorination reaction was hardly used to incorporate ^{18}F atom into the peptides, as the bioactive peptides are sure to be denatured or decomposed under this direct ^{18}F labeling scheme (Fig. 14.4a) [43, 44]. Secondly, the other ^{18}F labeling of peptides is an indirect labeling method with stable ^{18}F labeled building blocks (referred to prosthetic groups or synthons) by a conjugation reaction. This indirect synthetic pathway is generally suitable to synthesize ^{18}F-labeled peptides via the conjugation reactions between the peptides and

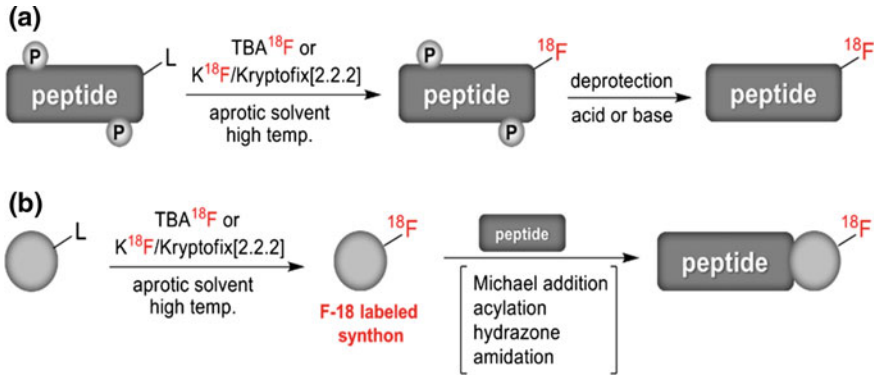

Fig. 14.4 Synthetic pathway for the synthesis of ^{18}F labeled peptides. **a** Direct ^{18}F labeling procedure by the radiofluorination with n.c.a. fluoride-18. **b** Indirect ^{18}F labeling procedure by a conjugation reaction using ^{18}F labeled synthon

^{18}F labeled prosthetic groups, such as amidation, acylation, alkylation, or hydrazone formation reaction with reactive amino- or thiol groups (Fig. 14.4b) [43, 44].

However, the reactive reagents or organic solvents for the preparation of ^{18}F labeled peptides by these indirect radiolabeling methods still lead to the denaturation of peptides. In addition, the half-life of ^{18}F is occasionally too short to complete these two step indirect radiolabeling processes. To accomplish the labeling or conjugation reaction with the ^{18}F labeled building blocks within a reasonable reaction time and with sufficient RCY, excess amounts of peptide precursor should have been used. As a result, trace quantities of ^{18}F labeled peptides should be separated and isolated from the remaining excess precursors, other non-labeled molecules and chemical reagents after the reaction. High molar specific activity is needed to ascertain imaging quality of PET and reduce the toxicity or side-effects of the collateral administration of unlabeled peptides (Fig. 14.5a). High performance liquid chromatography (HPLC) is the most popular purification process and is well-known to take long time [27, 28]. This time-consuming purification process using HPLC as well as the complicated synthetic procedures cannot frequently provide the satisfactory product to be used for imaging in preparation of the peptide radiotracer with reasonable RCY or/and molar activity [43–45].

14.5 Chemically Orthogonal Scavenger-Assisted ^{18}F Labelling Method

It is well-known that bioorthogonal click conjugation reactions such as the SPAAC reaction and the inverse electron-demand Diels-Alder cycloaddition reactions can work well in aqueous media without chemical reagents or any catalysts [11, 24]. This fact can allow the ^{18}F labeled peptides or other bioactive molecules to be

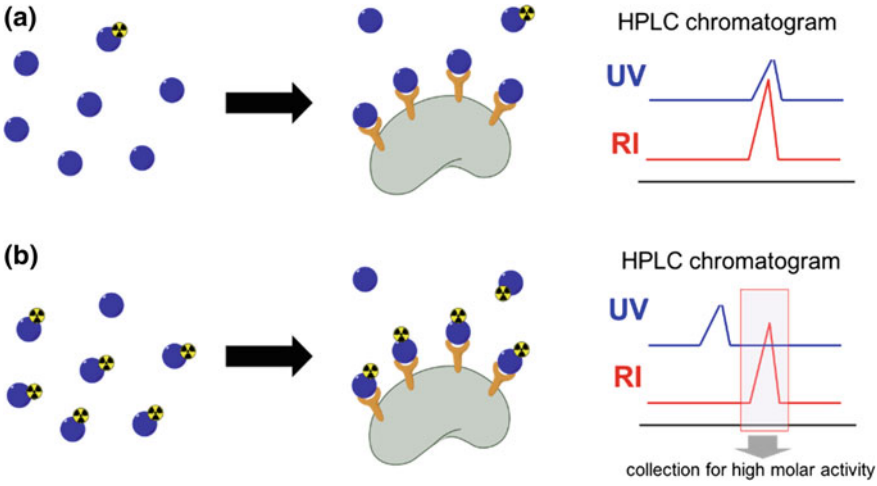

Fig. 14.5 Concept of the molar activity of radiolabeled molecular imaging probes for targeting. **a** Low molar activity of radiotracer: bad image quality with high toxicity. **b** High molar activity of radiotracer: good image quality with low toxicity

obtained by these bioorthogonal click conjugation reactions under physiologically friendly reaction conditions (such as room temperature, pH 7 and water solvent) to avoid the decomposition and denaturation of these bio-molecules. In addition, the ^{18}F labeling procedure became simple for easy handling. In 2011, Weissleder et al. firstly reported a chemically orthogonal scavenger-assisted high-performance ^{18}F labeling protocol using the inverse electron-demand Diels-Alder cycloaddition reactions to synthesize ^{18}F labeled PARP1 inhibitor derivative (Fig. 14.6a) [46]. Using this protocol, ^{18}F labeled PARP1 inhibitor was prepared from the tetrazine-tethered precursor in 59.6% RCY within 3 min, by the bioorthogonal tetrazine-*trans*-cyclooctene ligation reaction with an ^{18}F labeled TCO synthon. Moreover, the excess non-labeled tetrazine-tethered precursor could be removed using a magnetic TCO scavenger resin and they could increase its molar activity. In 2012, it was reported that the bioorthogonal SPAAC based ^{18}F peptide labeling reaction could provide various ^{18}F labeled peptide tracers under physiologically-friendly reaction conditions without HPLC purification process. According to this protocol, the SPAAC reaction of ADIBO-tethered cRGD peptide was reacted with the ^{18}F labeled azide synthon in aqueous media and reaction completed within 15 min to afford an ^{18}F-labeled cRGD peptide quantitatively [47]. Based on chemically orthogonal scavenger-assisted purification-concept above mentioned, a subsequent treatment of the mixture solution with the polystyrene-supported azide scavenger resin for 20 min could allow remove the excess cold ADIBO–cRGD precursors (Fig. 14.6b). Just after filtration and washing using a PBS, the ^{18}F labeled cRGD peptide could be synthesized in a 92% RCY within the total reaction time of 35 min. What is more appealing was that this RGD radiotracer was obtained

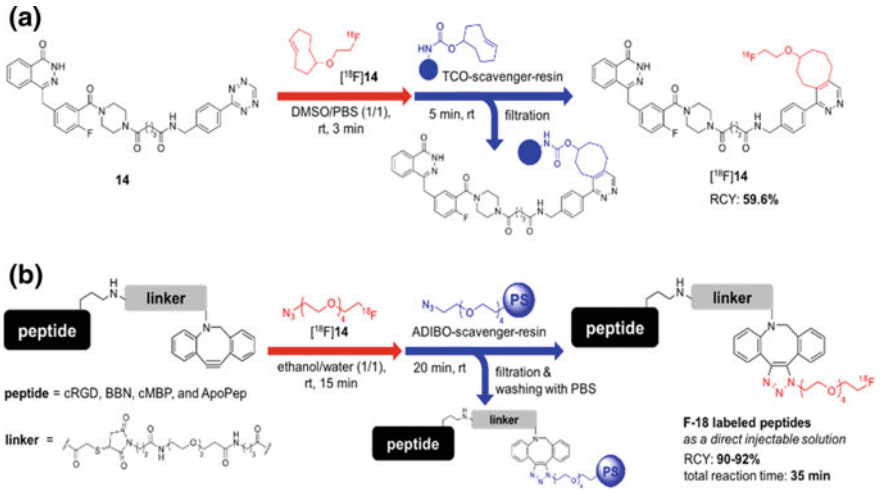

Fig. 14.6 Overview of chemically orthogonal scavenger-assisted ^{18}F labelling protocol platform. **a** The bioorthogonal tetrazine-TCO ligation based ^{18}F labeling and purification procedure for synthesis of ^{18}F labeled PARP1 inhibitor derivative. **b** The SPAAC based synthesis of various ^{18}F labeled peptides with ^{18}F labeled azide synthons and subsequent chemo-orthogonal purification using a polystyrene-supported azide resin. Adapted from [46] with permission

as a directly injectable solution for PET molecular imaging study without HPLC purification and formulation process. More recently, Kim et al. reported that ^{18}F labeled di-cRGD peptide, which was prepared by this ^{18}F peptide labeling protocol, could visualize successfully the tumor in vivo on PET imaging study [48].

In particular, the high throughput synthesis of various ^{18}F labeled peptide tracers can be achieved efficiently by this ^{18}F labeling protocol platform [47]. With only once production of ^{18}F labeled azide synthon, three different peptides such as bombesin (BBN), c-Met binding peptide (cMBP), and apoptosis targeting peptide (ApoPep) could be radiolabeled simultaneously from the corresponding ADIBO-substituted peptide precursors via this SPAAC based ligation reaction and subsequent scavenger-assisted separation process in 90–92% of RCYs (molar activities of 55–45 GBq/μmol).

14.6 Bioorthogonal Chemistry for ^{18}F Peptide Labeling

The catalyst-free bioorthogonal chemistry have been applied to peptide labeling with ^{18}F as a chemo-orthogonal conjugation of bioactive peptides with the ^{18}F-labeled building blocks. For this purpose, two synthetic approaches were generally used such as the SPAAC and the tetrazine-TCO Diels-Alder cycloaddition. The ^{18}F peptide labeling based on SPAAC approach focused on the

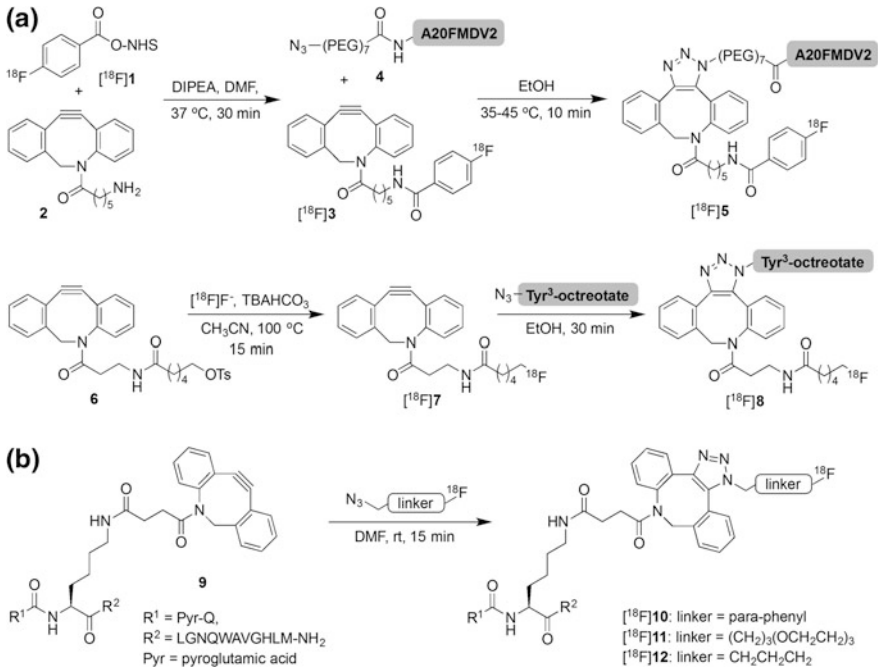

Fig. 14.7 ^{18}F peptides labeling. **a** SPAAC reaction of ^{18}F labeled ADIBO-synthon with azide-tagged peptides. **b** SPAAC reaction of ^{18}F-labeled azides building blocks with the ADIBO-functionalized peptide

development of the conjugation between ^{18}F labeled cyclooctyne building blocks and azido-tagged peptides [9]. For example, ^{18}F labeled A20FMDV2, which is an integrin $\alpha_v\beta_6$-specific peptide, was prepared using this SPAAC based protocol by Sutcliffe et al. [49]. In this report, the acylation of an ADIBO derivative **2** using *N*-succinimidyl-4-[^{18}F]fluorobenzoate proceeded at 37 °C for 30 min in DMF, giving an ^{18}F labeled ADIBO synthon. Then, its SPAAC reaction with azide-tagged A20FMDV2 peptide provided the desired ^{18}F labeled peptide in 11.9% RCY with a molar activity of 68 ± 25 GBq/μmol after HPLC purification process (Fig. 14.7a, up) [50]. An ^{18}F labeled ADIBO building block could be obtained directly in 65% RCY using the nucleophilic displacement reaction of the corresponding tosylate **6** with ^{18}F at 100 °C for 15 min in CH_3CN [49]. Then, ^{18}F labeled Tyr^3-octreotate peptide was produced in 95% RCY by treatment of the corresponding azide-substituted precursor for 30 min in ethanol (Fig. 14.7a, down) [51].

The other SPAAC based labeling approach was reported by Campbell-Verduyn et al. In this approach, an ^{18}F labeled azides were used as radiolabeled building blocks for the SPAAC conjugation reaction with ADIBO functionalized peptide. An ADIBO substituted lys[3] -bombesin peptide was synthesized for this purpose. Then, the ^{18}F labeled bombesin peptide derivatives were produced in 19–37% RCY by the SPAAC conjugation of a bombesin peptide with three different ^{18}F-labeled

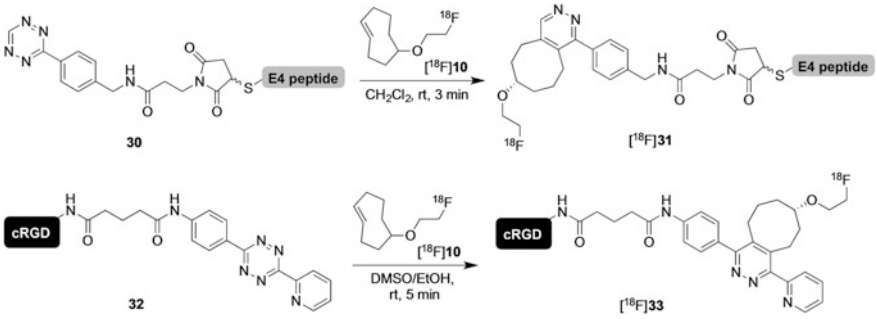

Fig. 14.8 Bioorthogonal tetrazine-TCO Diels-Alder cycloaddition for ^{18}F labeling of peptides

azide synthons at ambient temperature within 15 min (Fig. 14.7b). In the aspect of RCY and reaction step, this protocol employing using the ^{18}F labeled azide synthons is generally known to be more efficient than those using ^{18}F labeled cyclooctyne synthons for the ^{18}F labeling [52].

The bioorthogonal tetrazine-TCO Diels-Alder cycloaddition is also extremely efficient conjugation reaction for ^{18}F labeling of peptides. It have been reported that ^{18}F labeled cRGD [^{18}F]**x** and exendin-4-affine peptide radiotracer could be prepared in excellent RCYs by this cycloaddition reaction of a ^{18}F labeled TCO synthon with the corresponding tetrazine-substituted peptides as shown in Fig. 14.8 [53, 54].

References

1. H.C. Kolb, M.G. Finn, K.B. Sharpless, Click chemistry: diverse chemical function from a few good reactions. Angew. Chem. Int. Ed. Engl. **40**(11), 2004–2021 (2001)
2. C. Mamat, T. Ramenda, F.R. Wuest, Recent applications of click chemistry for the synthesis of radiotracers for molecular imaging. Mini Rev. Org. Chem. **6**(1), 21–34 (2009)
3. T.L. Mindt, H. Struthers, L. Brans, T. Anguelov, C. Schweinsberg, V. Maes et al., "Click to chelate": synthesis and installation of metal chelates into biomolecules in a single step. J. Am. Chem. Soc. **128**(47), 15096–15097 (2006)
4. D. Thonon, C. Kech, J. Paris, C. Lemaire, A. Luxen, New strategy for the preparation of clickable peptides and labeling with 1-(azidomethyl)-4-[^{18}F]-fluorobenzene for PET. Bioconjug. Chem. **20**(4), 817–823 (2009)
5. S. Maschauer, J. Einsiedel, R. Haubner, C. Hocke, M. Ocker, H. Hübner et al., Labeling and glycosylation of peptides using click chemistry: a general approach to ^{18}F-glycopeptides as effective imaging probes for positron emission tomography. Angew. Chem. Int. Ed. Engl. **49**(5), 976–979 (2010)
6. J.M. Baskin, J.A. Prescher, S.T. Laughlin, N.J. Agard, P.V. Chang, I.A. Miller et al., Copper-free click chemistry for dynamic in vivo imaging. Proc. Natl. Acad. Sci. U.S.A. **104**(43), 16793–16797 (2007)
7. E. Lallana, E. Fernandez-Megia, R. Riguera, Surpassing the use of copper in the click functionalization of polymeric nanostructures: a strain-promoted approach. J. Am. Chem. Soc. **131**(16), 5748–5750 (2009)

8. D.C. Kennedy, C.S. McKay, M.C. Legault, D.C. Danielson, J.A. Blake, A.F. Pegoraro et al., Cellular consequences of copper complexes used to catalyze bioorthogonal click reactions. J. Am. Chem. Soc. **133**(44), 17993–18001 (2011)
9. M. Pretze, D. Pietzsch, C. Mamat, Recent trends in bioorthogonal click-radiolabeling reactions using fluorine-18. Molecules **18**(7), 8618–8665 (2013)
10. J.C. Jewett, C.R. Bertozzi, Cu-free click cycloaddition reactions in chemical biology. Chem. Soc. Rev. **39**(4), 1272–1279 (2010)
11. E.M. Sletten, C.R. Bertozzi, From mechanism to mouse: a tale of two bioorthogonal reactions. Acc. Chem. Res. **44**(9), 666–676 (2011)
12. M.F. Debets, S.S. van Berkel, J. Dommerholt, A.T. Dirks, F.P. Rutjes, F.L. van Delft, Bioconjugation with strained alkenes and alkynes. Acc. Chem. Res. **44**(9), 805–815 (2011)
13. E.M. Sletten, C.R. Bertozzi, Bioorthogonal chemistry: fishing for selectivity in a sea of functionality. Angew. Chem. Int. Ed. Engl. **48**(38), 6974–6998 (2009)
14. S.T. Laughlin, J.M. Baskin, S.L. Amacher, C.R. Bertozzi, In vivo imaging of membrane-associated glycans in developing zebrafish. Science **320**(5876), 664–667 (2008)
15. J.C. Jewett, E.M. Sletten, C.R. Bertozzi, Rapid Cu-free click chemistry with readily synthesized biarylazacyclooctynones. J. Am. Chem. Soc. **132**(11), 3688–3690 (2010)
16. Y. Jiang, J. Chen, C. Deng, E.J. Suuronen, Z. Zhong, Click hydrogels, microgels and nanogels: emerging platforms for drug delivery and tissue engineering. Biomaterials **35**(18), 4969–4985 (2014)
17. L. Carroll, H.L. Evans, E.O. Aboagye, A.C. Spivey, Bioorthogonal chemistry for pre-targeted molecular imaging–progress and prospects. Org. Biomol. Chem. **11**(35), 5772–5781 (2013)
18. V. Bouvet, M. Wuest, F. Wuest, Copper-free click chemistry with the short-lived positron emitter fluorine-18. Org. Biomol. Chem. **9**(21), 7393–7399 (2011)
19. P. Ostrovskis, C.M.R. Volla, M. Turks, D. Markovic, Application of metal free click chemistry in biological studies. Curr. Org. Chem. **17**, 610–640 (2013)
20. J.M. Baskin, C.R. Bertozzi, Copper-free click chemistry: Bioorthogonal reagents for tagging azides. Aldrichimica Acta. **43**, 15–23 (2010)
21. X. Ning, J. Guo, M.A. Wolfert, G.J. Boons, Visualizing metabolically labeled glycoconjugates of living cells by copper-free and fast Huisgen cycloadditions. Angew. Chem. Int. Ed. Engl. **47**(12), 2253–2255 (2008)
22. A.A. Poloukhtine, N.E. Mbua, M.A. Wolfert, G.J. Boons, V.V. Popik, Selective labeling of living cells by a photo-triggered click reaction. J. Am. Chem. Soc. **131**(43), 15769–15776 (2009)
23. M.F. Debets, S.S. van Berkel, S. Schoffelen, F.P. Rutjes, J.C. van Hest, F.L. van Delft, Aza-dibenzocyclooctynes for fast and efficient enzyme PEGylation via copper-free (3 + 2) cycloaddition. Chem. Commun. (Camb.) **46**(1), 97–99 (2010)
24. N.K. Devaraj, R. Weissleder, Biomedical applications of tetrazine cycloadditions. Acc. Chem. Res. **44**(9), 816–827 (2011)
25. M.E. Phelps, Positron emission tomography provides molecular imaging of biological processes. Proc. Natl. Acad. Sci. U.S.A. **97**, 9226–9233 (2000)
26. T.F. Massoud, S.S. Gambhir, Molecular imaging in living subjects: seeing fundamental biological processes in a new light. Genes Dev. **17**(5), 545–580 (2003)
27. S. Vallabhajosula, *Molecular Imaging: Radiopharmaceuticals for PET and SPECT*, 1st edn. (Springer, New York, 2009), pp. 133–193
28. S.M. Ametamey, M. Honer, P.A. Schubiger, Molecular imaging with PET. Chem. Rev. **108**, 1501–1516 (2008)
29. S.S. Gambhir, Molecular imaging of cancer with positron emission tomography. Nat. Rev. Cancer **2**, 683–693 (2002)
30. R. Schirrmacher, C. Wängler, E. Schirrmacher, Recent developments and trends in 18F-radiochemistry: syntheses and applications. Mini Rev. Org. Chem. **4**, 317–329 (2007)
31. D.W. Kim, D.S. Ahn, Y.H. Oh, S. Lee, H.S. Kil, S.J. Oh et al., A new class of SN2 reactions catalyzed by protic solvents: Facile fluorination for isotopic labeling of diagnostic molecules. J. Am. Chem. Soc. **128**(50), 16394–16397 (2006)

32. L.Y.T. Chou, K. Ming, W.C.W. Chan, Strategies for the intracellular delivery of nanoparticles. Chem. Soc. Rev. **40**, 233–245 (2011)
33. E. Ruoslahti, S.N. Bhatia, M.J. Sailor, Targeting of drugs and nanoparticles to tumors. J. Cell Biol. **188**(6), 759–768 (2010)
34. Z. Cheng, A. Al Zaki, J.Z. Hui, V.R. Muzykantov, A. Tsourkas, Multifunctional nanoparticles: cost versus benefit of adding targeting and imaging capabilities. Science **338** (6109), 903–910 (2012)
35. M.W. Ambrogio, C.R. Thomas, Y.L. Zhao, J.I. Zink, J.F. Stoddart, Mechanized silica nanoparticles: a new frontier in theranostic nanomedicine. Acc. Chem. Res. **44**(10), 903–913 (2011)
36. Z. Li, J.C. Barnes, A. Bosoy, J.F. Stoddart, J.I. Zink, Mesoporous silica nanoparticles in biomedical applications. Chem. Soc. Rev. **41**(7), 2590–2605 (2012)
37. A. De la Zerda, C. Zavaleta, S. Keren, S. Vaithilingam, S. Bodapati, Z. Liu et al., Carbon nanotubes as photoacoustic molecular imaging agents in living mice. Nat. Nanotechnol. **3**(9), 557–562 (2008)
38. J.M. Rosenholm, V. Mamaeva, C. Sahlgren, M. Lindén, Nanoparticles in targeted cancer therapy: mesoporous silica nanoparticles entering preclinical development stage. Nanomedicine (London) **7**(1), 111–120 (2012)
39. S.B. Lee, H.L. Kim, H.J. Jeong, S.T. Lim, M.H. Sohn, D.W. Kim, Mesoporous silica nanoparticle pretargeting for PET imaging based on a rapid bioorthogonal reaction in a living body. Angew. Chem. Int. Ed. Engl. **52**, 10549–10552 (2013)
40. J. Lu, M. Liong, Z. Li, J.I. Zink, F. Tamanoi, Biocompatibility, biodistribution, and drug-delivery efficiency of mesoporous silica nanoparticles for cancer therapy in animals. Small **6**(16), 1794–1805 (2010)
41. S.L. Deutscher, Phage display in molecular imaging and diagnosis of cancer. Chem. Rev. **110** (5), 3196–3211 (2010)
42. K. Chen, P.S. Conti, Target-specific delivery of peptide-based probes for PET imaging. Adv. Drug Deliv. Rev. **62**(11), 1005–1022 (2010)
43. S.M. Okarvi, Recent progress in fluorine-18 labelled peptide radiopharmaceuticals. Eur. J. Nucl. Med. **28**(7), 929–938 (2001)
44. S. Gester, F. Wuest, B. Pawelke, R. Bergmann, J. Pietzsch, Synthesis and biodistribution of an ^{18}F-labelled resveratrol derivative for small animal positron emission tomography. Amino Acids **29**(4), 415–428 (2005)
45. S. Lee, J. Xie, Chen X. Peptides and peptide hormones for molecular imaging and disease diagnosis. Chem. Rev. **110**(5), 3087–3111 (2010)
46. T. Reiner, E.J. Keliher, S. Earley, B. Marinelli, R. Weissleder, Synthesis and in vivo imaging of a ^{18}F-labeled PARP1 inhibitor using a chemically orthogonal scavenger-assisted high-performance method. Angew. Chem. Int. Ed. Engl. **50**(8), 1922–1925 (2011)
47. K. Sachin, V.H. Jadhav, E.M. Kim, H.L. Kim, S.B. Lee, H.J. Jeong et al., F-18 labeling protocol of peptides based on chemically orthogonal strain-promoted cycloaddition under physiologically friendly reaction conditions. Bioconjug. Chem. **23**(8), 1680–1686 (2012)
48. H.L. Kim, K. Sachin, H.J. Jeong, W. Choi, H.S. Lee, D.W. Kim, F-18 Labeled RGD probes based on bioorthogonal strain-promoted click reaction for PET imaging. ACS Med. Chem. Lett. **6**(4), 402–407 (2015)
49. R.D. Carpenter, S.H. Hausner, J.L. Sutcliffe, Copper-free click for PET: rapid 1,3-dipolar cycloadditions with a fluorine-18 cyclooctyne. ACS Med. Chem. Lett. **2**(12), 885–889 (2011)
50. S.H. Hausner, R.D. Carpenter, N. Bauer, J.L. Sutcliffe, Evaluation of an integrin $\alpha_v\beta_6$-specific peptide labeled with [^{18}F]fluorine by copper-free, strain-promoted click chemistry. Nucl. Med. Biol. **40**(2), 233–239 (2013)
51. S. Arumugam, J. Chin, R. Schirrmacher, V.V. Popik, A.P. Kostikov, [^{18}F] Azadibenzocyclooctyne ([^{18}F]ADIBO): A biocompatible radioactive labeling synthon for peptides using catalyst free [3 + 2] cycloaddition. Bioorg. Med. Chem. Lett. **21**(23), 6987–6991 (2011)

52. L.S. Campbell-Verduyn, L. Mirfeizi, A.K. Schoonen, R.A. Dierckx, P.H. Elsinga, B.L. Feringa, Strain-promoted copper-free "click" chemistry for 18F radiolabeling of bombesin. Angew. Chem. Int. Ed. Engl. **50**(47), 11117–11120 (2011)
53. S. Liu, M. Hassink, R. Selvaraj, L.P. Yap, R. Park, H. Wang et al., Efficient ^{18}F labeling of cysteine-containing peptides and proteins using tetrazine-trans-cyclooctene ligation. Mol. Imaging **12**(2), 121–128 (2013)
54. E.J. Keliher, T. Reiner, G.M. Thurber, R. Upadhyay, R. Weissleder, Efficient ^{18}F-labeling of synthetic exendin-4 analogues for imaging beta cells. ChemistryOpen **1**(4), 177–183 (2012)

Part V
In Vivo Biodistribution Using PET and SPECT

Chapter 15: Preclinical PET and SPECT for Radionanomedicine
Chapter 16: Tracer Kinetic in Radionanomedicine

In this part, readers will find the very concise summary of what tracer technology can give the in vivo behavior of administered radionanomedicines, in other words, pharmacokinetics of radionanomaterials. The advantages of tracing radionanomaterials using PET and SPECT are 1) seeing their whereabouts serially, 2) visualization in a tomographic way, with attenuation correction in humans and 3) even quantification. In Chap. 15, the readers can find the basic facts about PET and SPECT associated with CT or MRI (PET/CT or PET/MRI) especially expecting human clinical applications of radionanomedicines. To understand the quantifiability of PET and SPECT, one needs to know the acquisition and reconstruction of serial images with quantifiable accuracy and precision in Chap. 15. With the acquired images, we do tracer kinetic modeling and find the rate constants or representative parameters to explain the biodistribution or uptake/excretion of radiolabeled nanomaterials in exact fashion, and this is called quantification. This quantification is detailed in such a great abstraction not losing the comprehensiveness in this chapter. After browsing the first part of summary of well-established knowledge of tracer kinetics acquired from radiolabeled small molecule PET, the readers are going to learn how the tracer kinetic studies helped understand the factors contributing the uptake and excretion. Once pharmacokinetic understanding is completed using PET or SPECT tracer kinetic studies, one can now turn to the exact understanding of pharmacodynamics to explain biological effect of tumor regression or regenerative success.

Chapter 15
Preclinical PET and SPECT for Radionanomedicine

Hyung-Jun Im and Gi Jeong Cheon

Abstract Quantitative evaluation of in vivo biodistribution is a prerequisite for the development of new targeted theranostic probes in nanomedicine. Here in this chapter the principles of positron emission tomography (PET) and single-photon emission computed tomography (SPECT) were explained. These two modalities are now popularly used for small animal studies and yield valuable information of the biodistribution, pharmacokinetics and final fates of radionanomedicines injected systemically. Great penetration depth, no background signal and the high sensitivity of PET and SPECT are the advantages for accurate quantification of in vivo biodistribution. MRI as well as CT was added to these modalities and clarifies the anatomical details. Simultaneous or sequential acquisition of PET/CT or PET/MRI allow the understanding of the accurate anatomical distribution of the administered radiolabeled nanomaterials. In this chapter, basic technical aspects and the application to radionanomedicine of PET and SPECT are detailed.

15.1 Introduction

Quantitative evaluation of in vivo biodistribution is a prerequisite for the development of new targeted theranostic probes in nanomedicine. Radionanomedicine can provide the real time, quantitative information regarding in vivo biodistribution including targeting efficiency of nanoparticles (NPs). The positron emission tomography (PET) and single-photon emission computed tomography (SPECT) are

H.-J. Im (✉)
Department of Transdisciplinary Studies, Graduate School of Convergence Science and Technology, Seoul National University, Seoul, Korea
e-mail: iiihjjj@gmail.com

G. J. Cheon
Department of Nuclear Medicine, Seoul National University College of Medicine, Seoul, Korea
e-mail: larrycheon@gmail.com

D. S. Lee (ed.), *Radionanomedicine*, Biological and Medical Physics, Biomedical Engineering, https://doi.org/10.1007/978-3-319-67720-0_15

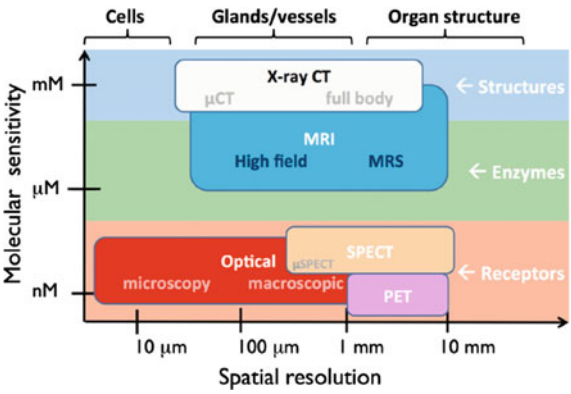

Fig. 15.1 Comparison of in vivo imaging modalities regarding molecular sensitivity and spatial resolution Reproduced with permission [1]

the two tomographic imaging techniques which are used in radionanomedicine. PET and SPECT have a clear benefit over other small animal imaging modalities. Most of all, there is no background signal in the body system, which enables accurate quantification of tissue uptake of tracers. Also, the sensitivity of PET and SPECT is many orders of magnitude higher than that of computed tomography (CT) or magnetic resonance imaging (MRI). Furthermore, the greater penetration depth is an advantage over optical imaging or photoacoustic imaging (Fig. 15.1) [1]. However, lack of anatomical information is the limitation of the PET or SPECT. Thus, hybrid imaging techniques have been developed including PET/CT and SPECT/CT which has been successfully incorporated into clinical practice. Recently PET/MR and SPECT/MR have been developed by the advancement of MR compatible photodiodes. PET/MR has several potential advantages over PET/CT. Firstly, MR has the higher soft tissue resolution than CT and no radiation exposure. High soft tissue resolution is beneficial in the field of small animal imaging. Furthermore, there is a difference in PET images between the two devices. PET/MR can achieve simultaneous acquisition, unlike PET/CT. The conventional PET/CT cannot be obtained simultaneously because the simultaneous acquisition of PET and CT can cause signal disturbance each other. The attenuation correction is a limitation for clinical PET/MR, however it is not necessary for mouse imaging. In this chapter, basic technical aspects and the application to radionanomedicine of hybrid imaging techniques using PET and SPECT will be described.

15.2 Preclinical SPECT/CT and SPECT/MR

15.2.1 SPECT System

SPECT imaging is produced by the detection of gamma photons that are emitted from the single photon-emitting radioisotopes accumulated in target areas. A gamma camera is used for SPECT imaging and consists of a collimator, a light

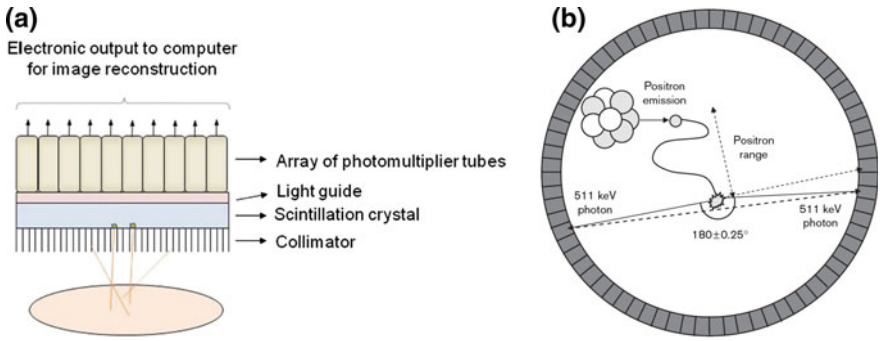

Fig. 15.2 **a** Basic structures of a gamma camera: among single photons from a subject, only straight ones can hit the scintillation crystal due to the collimation. The photons are converted to visible light which strike photomultiplier tubes to be converted to electrons. Reproduced with permission from [2]. **b** Physical basis of PET and the limitation. Positron range indicates the length from the radioisotope to the place that positron is annihilated. Non-collinearity refers to the difference of the angle of antiparallel photons emitted from positron annihilation. Reproduced with permission [36]

guide, a scintillator crystal, photomultiplier tubes (PMTs), pulse height analyzer and position logic circuit (Fig. 15.2a) [2, 3]. Lead or tungsten collimator is used to accept the photons arriving with only appropriate angles. The selection of the photons by the collimator enables gamma camera to localize the source of the photons. A scintillator converts each accepted photon with energy between 70 and 300 keV to the optical photons with lower energy [4]. The scintillator is coupled to a PMT. The photoelectrons are emitted in the PMT by the strike of optical photons on the photocathode of the PMT. The signal is amplified by applying a high voltage, and the amplified electrons hit the PMT's anode. The pulse height analyzer is used to select particular energy signal using energy spectrum information of gamma photons emitted from radioisotopes (Table 15.1). For tomographic image (SPECT), the gamma camera obtains multiple 2D projection images while the camera is rotating around the object to be imaged. This sinogram from the multiple projection images is used to reconstruct tomographic SPECT images [5]. SPECT has a relatively low spatial resolution because of the intrinsic limitation from scintillation crystal and PMT system. In particular, the intrinsic spatial resolution of a conventional gamma camera using NaI(Tl) scintillator is around 3.8 mm full-width-at-half-maximum (FWHM) [4]. In late 1990, position sensitive photomultiplier tubes (PSPMTs) were developed to improve the spatial resolution of SPECT by maintaining position information during electrons multiplication [4, 5]. The spatial resolution of SPECT was further enhanced by the magnification of the geometry using the pinhole collimators [6, 7]. Another way to improve the resolution was to utilize pixelated detectors using discrete NaI(Tl) or CsI(Tl) crystals [8–11] or cadmium telluride (CdTe) or cadmium zinc telluride (CZT) semiconductor detectors [12–15]. This pixelated detectors enhanced the spatial resolution at the sacrifice of the detection sensitivity. Recently, a superior resolution-sensitivity

Table 15.1 Radionuclides for PET and SPECT

Radionuclide	Decay	Photon energy (keV)	Half-life
^{11}C	β+	511	20.3 min
^{13}N	β+	511	10.0 min
^{15}O	β+	511	2.07 min
^{18}F	β+	511	110 min
^{68}Ga	β+	511	68 min
^{82}Rb	β+	511	1.25 min
^{64}Cu	β+	511	12.7 h
^{89}Zr	β+	511	3.3 day
^{99m}Tc	IT	140	6.03 h
^{111}In	EC	172, 247	2.81 day
^{123}I	EC	159	13.0 h
^{125}I	EC	27–35	59.4 day
^{201}Tc	EC	68–80	3.05 day

IT Isomeric transition; *EC* electron capture. Reproduced with permission [34]

collimator called slithole has been developed which needs further testing in animal models [16]. The CZT system provides higher energy resolution [17] which is beneficial for using multiple radiotracers with a different energy in a single scan [18]. Also, silicon photomultipliers (SiPMs) coupled with pixelated crystal showed higher spatial resolution and emerged as a prominent alternative to PMTs in SPECT. SiPMs have a significant advantage that it can be used in SPECT/MR system as well [19, 20].

15.2.2 SPECT/CT and SPECT/MR in Radionanomedicine

In the field of radionanomedicine, SPECT is used primarily for evaluation of in vivo biodistribution of injected theranostic NPs. In one study, vascular endothelial growth factor (VEGF) loaded ^{99m}Tc labeled chitosan hydrogel NPs were injected into a rat model of myocardial ischemia and showed alleviation of ischemia. In the meantime, SPECT imaging was used to monitor the whereabouts of the radionanomedicines which may be used for dose adjustment in the following experiment or clinical trial [21]. In another study, ^{111}In labeled mesoporous silica NPs (MSNs) was used to tracking neural stem cells in the orthotopic glioblastoma model of mouse. For the monitoring of injected neural stem cells (NSCs), ^{111}In labeled MSN was taken up by NSCs before the injection to the mouse. NSC was injected to the brain of the mouse model and the migration of the NSC to the cancer lesion was observed by SPECT/CT imaging (Fig. 15.3) [22]. Parrott et al. reported the renal clearance of ^{99m}Tc labeled polyester dendrimers using SPECT/CT imaging [23]. In another study, silver NPs were radiolabeled with ^{125}I for SPECT

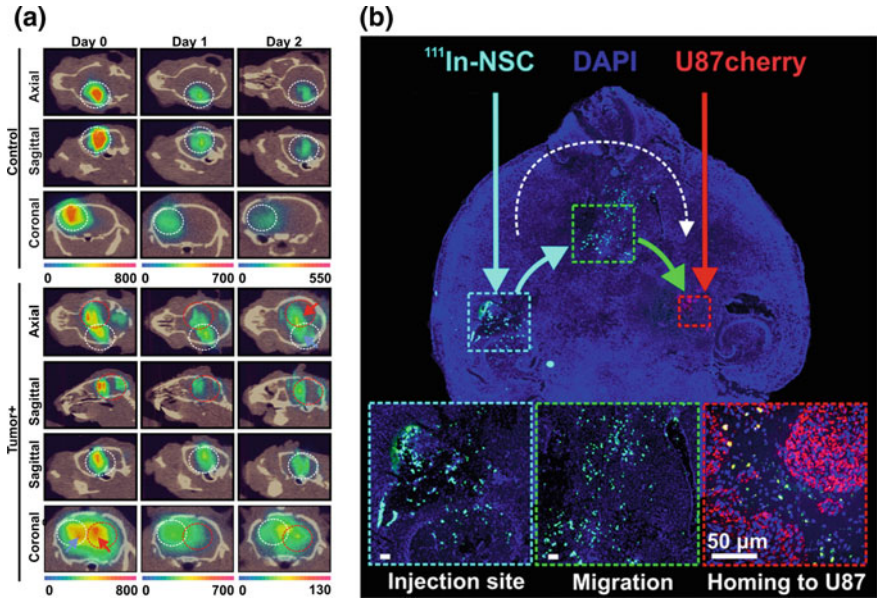

Fig. 15.3 **a** SPECT/CT imaging of mouse brain after intracerebral injection of neural stem cells (NSCs) containing ^{111}In-MSNs (mesoporous silica nanoparticles). In SPECT/CT image, radiolabeled NSCs can be seen at the injection site. In brain tumor model, radiolabeled NSCs migrate from injection site (white circle) toward brain tumor lesion (red circle). **b** Fluorescent microscopy revealed that NSCs loaded with ^{111}In-MSN (green cells) was migrated to tumor lesion site (glioma xenograft, cherry cell). Reproduced with permission from [22]

imaging. The NPs had 12 nm size and showed predominant splenic uptake (41.5% ID/g) [24]. In vivo tracking of DNA NPs also have been reported using SPECT/CT imaging. Patil et al. reported the time courses of ^{111}In labeled DNA micelle deposition, and the distribution was compared between the different administration routes, which are intrabiliary, hydrodynamic and intravenous infusion [25]. In another study, SPECT/CT revealed the tumor targeting efficiency of ^{99m}Tc labeled tetrahedral DNA nanostructures [26].

There have been radionanoprobes for SPECT with the dual imaging ability. ^{99m}Tc labeled superparamagnetic iron oxide (SPION) was developed and showed dual imaging property for SPECT/MR for sentinel lymph node mapping [27]. Wang et al. developed a SPECT/MR probe, ^{125}I-c(RGDyK) peptide PEGylated Fe@Fe_3O_4 NPs (^{125}I–RGD–PEG–MNPs). The probe was able to target glioblastoma xenograft tumor in the mouse model with the uptake of 6.75%ID/g, and the uptake can be seen in both SPECT and MR images (Fig. 15.4) [28]. Black et al. reported the development of dual radiolabeled (^{125}I and ^{111}In) gold NPs. The single SPECT scan can be separated into two SPECT images according to the energy levels which showed distinct characteristics (Fig. 15.5) [29].

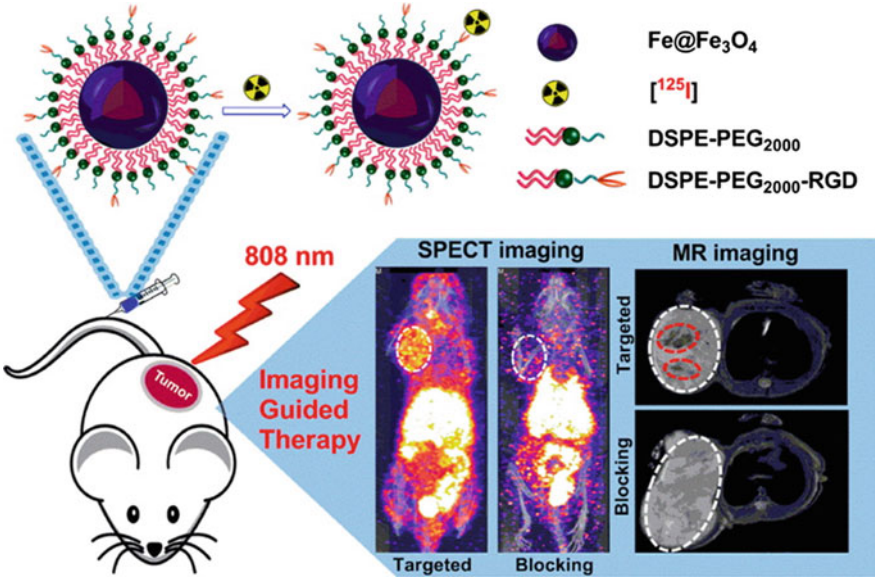

Fig. 15.4 The ^{125}I-c(RGDyK) peptide PEGylated Fe@Fe_3O_4 nanoparticles (^{125}I–RGD–PEG–MNPs) was able to target tumor site confirmed by SPECT/MR imaging. The NPs can be used for photothermal therapy Reproduced with permission [28]

With the advances of small animal SPECT, SPECT has a higher resolution than that of PET unlikely with the clinical systems. Cheng et al. compared dedicated small animal PET and SPECT systems [^{99m}Tc on a Nano-SPECT/CT camera (Bioscan Inc., Washington D.C., USA) vs. ^{18}F on a Mosaic HP PET (Philips Medical Systems, Inc., Cleveland, Ohio, USA)]. The phantom images and mouse images using radiolabeled anti-HER2 NPs showed superior spatial resolution of SPECT system (Fig. 15.6) [30].

Theranostic radioisotope including ^{177}Lu, ^{131}I can be utilized for both SPECT imaging and radionuclide therapy. ^{177}Lu labeled lipid calcium phosphate (LCP) NPs were used for tumor SPECT imaging and therapy. In a subcutaneous xenograft tumor mouse model, ^{177}Lu–LCP showed the higher tumor uptake than free ^{177}Lu. Also, ^{177}Lu–LCP demonstrated the superior ability to inhibit the tumor growth than free ^{177}Lu [31]. SPECT/CT imaging was used to monitor the intratumorally injected ^{177}Lu labeled gold NPs in the subcutaneous breast cancer mouse model. Regional distribution of radiation dose of a tumor can be calculated using SPECT image. Finally, the NPs were able to inhibit the tumor growth and prolong the survival (Fig. 15.7) [32]. Also, Ming et al. reported the development of theranostic ^{131}I labeled arginine-glycine-aspartate (RGD) bovine serum albumin polycaprolactone for imaging and treatment of murine lung cancer models [33].

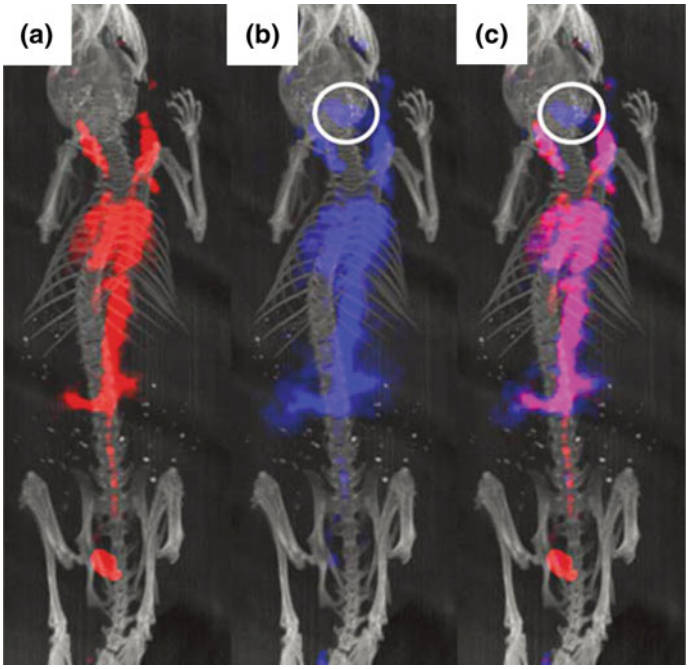

Fig. 15.5 In vivo SPECT/CT imaging of dual-radiolabeled nanoparticles. **a** 200 ± 60 keV energy channel for detection of ^{111}In, **b** 28 ± 3 keV energy channel for detection of ^{125}I, and **c** for both energy channels. Thyroid accumulation can be only seen in the ^{125}I channel (circle) Reproduced with permission [29]

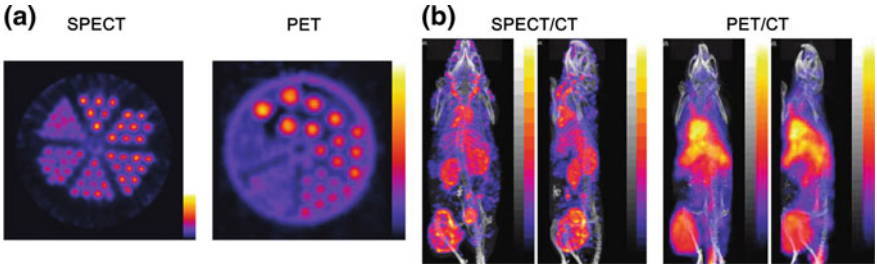

Fig. 15.6 **a** SPECT image of ^{99m}Tc phantom (1.2–1.7 mm rods) (left), and PET image of ^{18}F phantom (1.2–4.8 mm rods) (right). **b** SPECT/CT (left) and PET/CT (right) image of mouse tumor model Reproduced with permission [30]

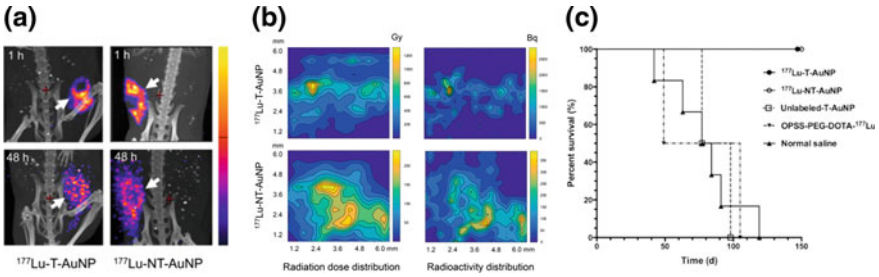

Fig. 15.7 **a** SPECT/CT images of mouse breast cancer xenograft model (white arrows) at 1 or 48 h after intratumoral injection of ^{177}Lu–T–AuNP (with targeting moiety) or ^{177}Lu–NT–AuNP (without targeting moiety). **b** Visualization of radiation-absorbed dose distribution (left) and radioactivity distribution (right) of xenograft tumor after intratumoral injection of ^{177}Lu-T-AuNP (top) or ^{177}Lu–NT–AuNP (bottom). **c** Kaplan Meyer survival curve of breast cancer xenograft model treated with ^{177}Lu–T–AuNP, ^{177}Lu–NT–AuNP, unlabeled T–AuNP or OPSS–PEG–DOTA–^{177}Lu (not conjugated to AuNP) or normal saline for control groups Reproduced with permission [32]

15.3 Preclinical PET/CT and PET/MR

15.3.1 PET System

Unlike SPECT tracers, PET tracers emit positrons instead of photons (Table 15.1) [34]. The emitted positron travels a few millimeters (positron range) before it hits an electron. When the positron hits the electron, they are annihilated and produce two anti-parallel photons with the energy of 511 keV. This annihilation and consequent production of two antiparallel photons occur in the same manner for all PET tracer thus PET does not allow simultaneous imaging of multiple tracers. The antiparallel photons are detected by a full ring shaped PET detector [35]. Since the antiparallel photons provide the direction from the source, thus PET scanner does not require a collimator, which is the most notable hardware difference between PET and SPECT scanners.

A line between the two points on the PET detector that are hit by two antiparallel photons within 4–20 ns is called line-of-response (LOR). PET scanner does not need a collimator thus has a significantly higher sensitivity (two or three orders of magnitude) than SPECT scanner. However, PET has more intrinsic, physics-related, limitation regarding spatial resolution than SPECT, which are positron range and photon non-collinearity (Fig. 15.2b) [36]. The spatial resolution of PET scanner is around 4 mm in clinical systems and 1 mm in dedicated pre-clinical scanners.

15.3.2 PET/CT, PET/MR Imaging in Radionanomedicine

PET has also been utilized in radionanomedicine for quantitative evaluation of in vivo biodistribution including targeting efficiency. Majority of the studies were about cancer imaging [37–45] or theranostics [46–53]. Liang et al. reported photodynamic therapy using polyethylene glycol (PEG)-coated nanomicelles conjugated with chlorin e6 (PEG-Ce6 nanomicelles). Tumor targeting efficiency of the PEG-Ce6 nanomicelles was evaluated by PET/CT imaging after radiolabeling of ^{64}Cu (Fig. 15.8) [52]. ^{64}Cu labeled copper sulfide NPs were used for targeted imaging and photothermal therapy (PTT) in an orthotopic ovarian cancer model. PET image showed moderate uptake of 6.4%ID/g by the passive targeting, and subsequent PTT using near infrared laser (980 nm, 2 min) was able to destroy over 90% of the tumor [53].

Also, PET has been utilized in cardiovascular diseases including peripheral arterial disease [54, 55], and ischemic heart disease [56–58]. Keliher et al. reported PET imaging of ^{18}F labeled Macroflor which is a modified polyglucose NP with the ability to target macrophages [56]. In the study, ^{18}F Macroflor was able to detect macrophage infiltration in the atherosclerotic aorta in mice and rabbits using PET/CT and PET/MR. Furthermore, PET/MR revealed the macrophage infiltration in myocardial infarction model of mice (Fig. 15.9). England and Im et al. reported that ^{64}Cu labeled reduced graphene oxide–iron oxide NPs were able to target ischemic tissue ($\sim$ 15%ID/g) in a mouse model of peripheral arterial disease by enhanced permeability and retention effect [55]. Also, they found that the NPs exhibit accelerated blood clearance phenomenon upon re-injection of the NPs in the same animal, which effectively reduced the efficiency of the passive targeting [54].

Radionanomedicine has rarely been applied to brain diseases because of the presence of blood brain barrier (BBB) which can effectively inhibit the entrance of NPs to the brain parenchyma. In one study, the neuropeptide functionalization of ultra-small gold NP could improve the penetration of BBB. Even with the

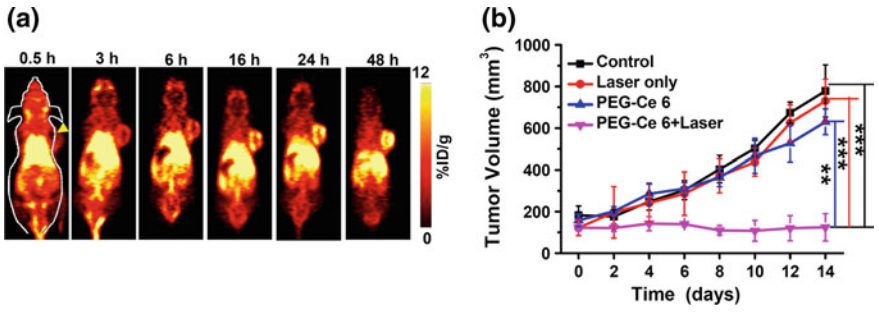

Fig. 15.8 **a** In vivo PET imaging of ^{64}Cu-labeled PEG-Ce 6 nanomicelles in a mouse xenograft model (yellow arrowhead indicates the tumor). **b** Tumor growth curves of treatment and control groups show the efficient growth inhibition by the photodynamic therapy Reproduced with permission [52]

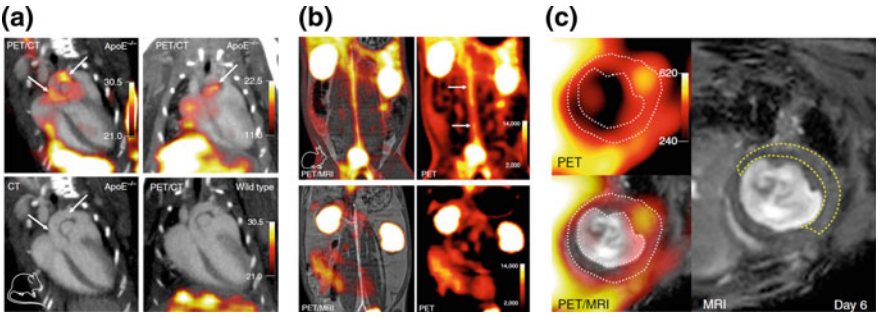

Fig. 15.9 **a** Macroflor PET/CT in mice with atherosclerosis. PET/CT images in ApoE-/- and wild-type control mice after IV Macroflor injection. **b** Macroflor PET imaging reveals atherosclerotic aortic plaques in rabbits (upper). Control rabbits (lower). **c** PET/MRI on day six post-MI in wild-type mice (white dotted line: myocardium, yellow dashed line: infarct) Reproduced with permission [56]

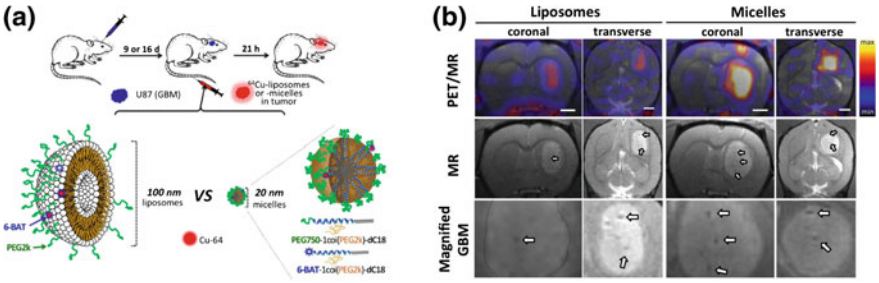

Fig. 15.10 **a** Schematic representation of the accumulation of liposomes and micelles in orthotopic glioblastoma model of rat. PEG: polyethylene glycol. **b** PET/MR images (upper) and contrast enhanced MR images (bottom and lower) of the rat brain after injection of ^{64}Cu-liposomes and ^{64}Cu-micelles Reproduced with permission [60]

improvement, minimal amount of the NPs (0.02%ID/g) was able to enter inside of the brain [59]. BBB is destroyed in the brain cancer, thus targeting NPs to brain cancer is more feasible than normal brain tissue. Seo et al. reported that ^{64}Cu labeled liposome and micelle can be targeted to brain cancer lesion in orthotopic glioblastoma model of mouse. They also found that 20 nm sized micelles showed the higher uptake than 110 nm sized liposome (0.77 vs. 0.45%ID/g) (Fig. 15.10) [60].

15.4 Conclusion

Small animal imaging using PET or SPECT has unique advantages over other in vivo imaging modalities in its sensitivity and depth penetration and quantifiability. Furthermore, anatomical information can be added to PET or SPECT by the hybrid scanner with CT or MR. Evaluation of in vivo biodistribution including targeting efficiency using PET and SPECT imaging of radiolabeled NPs is beneficial to facilitate the development of the novel theranostic NPs. Furthermore, the radiolabeled NPs themselves can be utilized as novel theranostic radionanomedicines.

References

1. K.M. Tichauer, Y. Wang, B.W. Pogue, J.T. Liu, Quantitative in vivo cell-surface receptor imaging in oncology: kinetic modeling and paired-agent principles from nuclear medicine and optical imaging. Phys. Med. Biol. **60**(14), R239–R269 (2015)
2. H.O. Anger, M.R. Powell, D.C. van Dyke, L.R. Schaer, R. Fawwaz, Y. Yano, Recent applications of the scintillation camera. Strahlentherapie Sonderb. **65**, 70–93 (1967)
3. E. Wolfs, C.M. Verfaillie, K. Van Laere, C.M. Deroose, Radiolabeling strategies for radionuclide imaging of stem cells. Stem Cell Rev. **11**(2), 254–274 (2015)
4. M.T. Madsen, Recent advances in SPECT imaging. J. Nucl. Med. **48**(4), 661–673 (2007)
5. M.K. O'Connor, B.J. Kemp, Single-photon emission computed tomography/computed tomography: basic instrumentation and innovations. Semin. Nucl. Med. **36**(4), 258–266 (2006)
6. M.C. Wu, B.H. Hasegawa, M.W. Dae, Performance evaluation of a pinhole SPECT system for myocardial perfusion imaging of mice. Med. Phys. **29**(12), 2830–2839 (2002)
7. F.J. Beekman, F. van der Have, B. Vastenhouw, A.J. van der Linden, P.P. van Rijk, J. P. Burbach et al., U-SPECT-I: a novel system for submillimeter-resolution tomography with radiolabeled molecules in mice. J. Nucl. Med. **46**(7), 1194–1200 (2005)
8. A.G. Weisenberger, R. Wojcik, E.L. Bradley, P. Brewer, S. Majewski, J. Qian et al., SPECT-CT system for small animal imaging. IEEE Trans. Nucl. Sci. **50**(1), 74–79 (2003)
9. E. Lage, J.J. Vaquero, J. Villena, A. Carlos, G. Tapias, A. Sisniega et al. (ed.), Performance evaluation of a new gamma imager for small animal SPECT applications, in *2007 IEEE Nuclear Science Symposium Conference Record* (2007)
10. S. Xishan, W. Shi, M. Tianyu, Z. Rong, L. Xin, Z. Zhang et al. (ed.), A high resolution and high sensitivity small animal SPECT system based on H8500, in *2007 IEEE Nuclear Science Symposium Conference Record* (2007)
11. J.B. Freek, V. Brendan, Design and simulation of a high-resolution stationary SPECT system for small animals. Phys. Med. Biol. **49**(19), 4579 (2004)
12. G.A. Kastis, H.B. Barber, H.H. Barrett, S.J. Balzer, D. Lu, D.G. Marks et al., Gamma-ray imaging using a CdZnTe pixel array and a high-resolution, parallel-hole collimator. IEEE Trans. Nucl. Sci. **47**(6), 1923–1927 (2000)
13. G.A. Kastis, M.C. Wu, S.J. Balzer, D.W. Wilson, L.R. Furenlid, G. Stevenson et al. (ed.) Tomographic small-animal imaging using a high-resolution semiconductor camera, in *2000 IEEE Nuclear Science Symposium. Conference Record (Cat. No.00CH37149)* (2000)
14. B. Mueller, M.K. O'Connor, I. Blevis, D.J. Rhodes, R. Smith, D.A. Collins et al., Evaluation of a small cadmium zinc telluride detector for scintimammography. J. Nucl. Med. **44**(4), 602–609 (2003)

15. H. Kim, L.R. Furenlid, M.J. Crawford, D.W. Wilson, H.B. Barber, T.E. Peterson et al., SemiSPECT: A small-animal single-photon emission computed tomography (SPECT) imager based on eight cadmium zinc telluride (CZT) detector arrays. Med. Phys. **33**(2), 465–474 (2006)
16. H. Mahani, G. Raisali, A. Kamali-Asl, M.R. Ay, Spinning slithole collimation for high-sensitivity small animal SPECT: Design and assessment using GATE simulation. Phys. Med. **40**, 42–50 (2017)
17. K. Ogawa, N. Ohmura, H. Iida, K. Nakamura, T. Nakahara, A. Kubo, Development of an ultra-high resolution SPECT system with a CdTe semiconductor detector. Ann. Nucl. Med. **23** (8), 763–770 (2009)
18. S. Ben-Haim, K. Kacperski, S. Hain, D. Van Gramberg, B.F. Hutton, W.A. Waddington et al., Simultaneous dual-radionuclide myocardial perfusion imaging with a solid-state dedicated cardiac camera. Eur. J. Nucl. Med. Mol. Med. **37**(9), 1710–1721 (2010)
19. B. Carmen, V. Stefaan, Van H. Roel, Evaluation of a compact, high-resolution SPECT detector based on digital silicon photomultipliers. Phys. Med. Biol. **59**(23), 7521 (2014)
20. P. Busca, M. Occhipinti, P. Trigilio, G. Cozzi, C. Fiorini, C. Piemonte et al., Experimental Evaluation of a SiPM-Based Scintillation Detector for MR-Compatible SPECT Systems. IEEE Trans. Nucl. Sci. **62**(5), 2122–2128 (2015)
21. H. Hwang, J. Kwon, P.S. Oh, T.K. Lee, K.S. Na, C.M. Lee et al., Peptide-loaded nanoparticles and radionuclide imaging for individualized treatment of myocardial ischemia. Radiology **273**(1), 160–167 (2014)
22. S.H. Cheng, D. Yu, H.M. Tsai, R.A. Morshed, D. Kanojia, L.W. Lo et al., Dynamic in vivo SPECT imaging of neural stem cells functionalized with radiolabeled nanoparticles for tracking of glioblastoma. J. Nucl. Med. **57**(2), 279–284 (2016)
23. M.C. Parrott, S.R. Benhabbour, C. Saab, J.A. Lemon, S. Parker, J.F. Valliant et al., Synthesis, radiolabeling, and bio-imaging of high-generation polyester dendrimers. J. Am. Chem. Soc. **131**(8), 2906–2916 (2009)
24. A. Chrastina, J.E. Schnitzer, Iodine-125 radiolabeling of silver nanoparticles for in vivo SPECT imaging. Int. J. Nanomed. **5**, 653–659 (2010)
25. R.R. Patil, J. Yu, S.R. Banerjee, Y. Ren, D. Leong, X. Jiang et al., Probing in vivo trafficking of polymer/DNA micellar nanoparticles using SPECT/CT imaging. Mol. Ther. **19**(9), 1626–1635 (2011)
26. D. Jiang, Y. Sun, J. Li, Q. Li, M. Lv, B. Zhu et al., Multiple-armed tetrahedral DNA nanostructures for tumor-targeting, dual-modality in vivo imaging. ACS Appl. Mater. Inter. **8** (7), 4378–4384 (2016)
27. R. Madru, P. Kjellman, F. Olsson, K. Wingardh, C. Ingvar, F. Stahlberg et al., ^{99m}Tc-labeled superparamagnetic iron oxide nanoparticles for multimodality SPECT/MRI of sentinel lymph nodes. J. Nucl. Med. **53**(3), 459–463 (2012)
28. J. Wang, H. Zhao, Z. Zhou, P. Zhou, Y. Yan, M. Wang et al., MR/SPECT imaging guided photothermal therapy of tumor-targeting Fe@Fe_3O_4 nanoparticles in vivo with low mononuclear phagocyte uptake. ACS Appl. Mater. Inter. **8**(31), 19872–19882 (2016)
29. K.C.L. Black, W.J. Akers, G. Sudlow, B. Xu, R. Laforest, S. Achilefu, Dual-radiolabeled nanoparticle SPECT probes for bioimaging. Nanoscale **7**(2), 440–444 (2015)
30. D. Cheng, Y. Wang, X. Liu, P.H. Pretorius, M. Liang, M. Rusckowski et al., Comparison of ^{18}F PET and ^{99m}Tc SPECT imaging in phantoms and in tumored mice. Bioconjug. Chem. **21** (8), 1565–1570 (2010)
31. A.B. Satterlee, H. Yuan, L. Huang, A radio-theranostic nanoparticle with high specific drug loading for cancer therapy and imaging. J. Control Release **217**, 170–182 (2015)
32. S. Yook, Z. Cai, Y. Lu, M.A. Winnik, J.P. Pignol, R.M. Reilly, Intratumorally injected ^{177}Lu-labeled gold nanoparticles: Gold nanoseed brachytherapy with application for neoadjuvant treatment of locally advanced breast cancer. J. Nucl. Med. **57**(6), 936–942 (2016)
33. H. Ming, L. Fang, J. Gao, C. Li, Y. Ji, Y. Shen et al., Antitumor effect of nanoparticle ^{131}I-labeled arginine-glycine-aspartate–bovine serum albumin–polycaprolactone in lung cancer. AJR Am. J. Roentgenol. **208**(5), 1116–1126 (2017)

34. C. Decristoforo, U. Haberkorn, R. Haubner, W. Mier, S.I. Ziegler, PET and SPECT, in *Small animal imaging: basics and practical guide*, ed. by F. Kiessling, B.J. Pichler, P. Hauff (Springer, Cham, 2017), pp. 361–402
35. S. Kalman, Introduction to PET instrumentation. J. Nucl. Med. Technol. **30**(2), 63 (2002)
36. A. Rahmim, H. Zaidi, PET versus SPECT: strengths, limitations and challenges. Nucl. Med. Commun. **29**, 193–207 (2008)
37. N. Oku, M. Yamashita, Y. Katayama, T. Urakami, K. Hatanaka, K. Shimizu et al., PET imaging of brain cancer with positron emitter-labeled liposomes. Int. J. Pharm. **403**(1–2), 170–177 (2011)
38. S. Goel, F. Chen, H. Hong, H.F. Valdovinos, R. Hernandez, S. Shi et al., $VEGF_{121}$-conjugated mesoporous silica nanoparticle: a tumor targeted drug delivery system. ACS Appl. Mater. Inter. **6**(23), 21677–21685 (2014)
39. R. Chakravarty, S. Goel, H. Hong, F. Chen, H.F. Valdovinos, R. Hernandez et al., Hollow mesoporous silica nanoparticles for tumor vasculature targeting and PET image-guided drug delivery. Nanomedicine (London) **10**(8), 1233–1246 (2015)
40. F. Gao, P. Cai, W. Yang, J. Xue, L. Gao, R. Liu et al., Ultrasmall [^{64}Cu]Cu nanoclusters for targeting orthotopic lung tumors using accurate positron emission tomography imaging. ACS Nano **9**(5), 4976–4986 (2015)
41. H. Hong, F. Wang, Y. Zhang, S.A. Graves, S.B. Eddine, Y. Yang et al., Red fluorescent zinc oxide nanoparticle: a novel platform for cancer targeting. ACS Appl. Mater. Inter. **7**(5), 3373–3381 (2015)
42. K. Hu, H. Wang, G. Tang, T. Huang, X. Tang, X. Liang et al., In vivo cancer dual-targeting and dual-modality imaging with functionalized quantum dots. J. Nucl. Med. **56**(8), 1278–1284 (2015)
43. P. Huda, T. Binderup, M.C. Pedersen, S.R. Midtgaard, D.R. Elema, A. Kjaer et al., PET/CT based in vivo evaluation of ^{64}Cu labeled nanodiscs in tumor bearing mice. PLoS ONE **10**(7), e0129310 (2015)
44. J. Key, A.L. Palange, F. Gentile, S. Aryal, C. Stigliano, D. Di Mascolo et al., Soft discoidal polymeric nanoconstructs resist macrophage uptake and enhance vascular targeting in tumors. ACS Nano **9**(12), 11628–11641 (2015)
45. Z. Yang, R. Tian, J. Wu, Q. Fan, B.C. Yung, G. Niu et al., Impact of semiconducting perylene diimide nanoparticle size on lymph node mapping and cancer imaging. ACS Nano **11**(4), 4247–4255 (2017)
46. J. Key, Y.S. Kim, F. Tatulli, A.L. Palange, B. O'Neill, S. Aryal et al., Opportunities for nano theranosis in lung cancer and pulmonary metastasis. Clin. Transl. Imaging **2**(5), 427–437 (2014)
47. D. Chen, C.A. Dougherty, K. Zhu, H. Hong, Theranostic applications of carbon nanomaterials in cancer: Focus on imaging and cargo delivery. J. Control Release **210**, 230–245 (2015)
48. F. Chen, H. Hong, S. Goel, S.A. Graves, H. Orbay, E.B. Ehlerding et al., In vivo tumor vasculature targeting of CuS@MSN based theranostic nanomedicine. ACS Nano **9**(4), 3926–3934 (2015)
49. L. Cui, Q. Lin, C.S. Jin, W. Jiang, H. Huang, L. Ding et al., A PEGylation-free biomimetic porphyrin nanoplatform for personalized cancer theranostics. ACS Nano **9**(4), 4484–4495 (2015)
50. Y. Yu, S. Xu, H. You, Y. Zhang, B. Yang, X. Sun et al., In vivo synergistic anti-tumor effect of paclitaxel nanoparticles combined with radiotherapy on human cervical carcinoma. Drug Deliv. **24**(1), 75–82 (2017)
51. K. Pant, O. Sedlacek, R.A. Nadar, M. Hruby, H. Stephan, Radiolabeled polymeric materials for imaging and treatment of cancer: Quo vadis? Adv. Healthcare Mater. **6**(6) (2017)
52. L. Cheng, A. Kamkaew, H. Sun, D. Jiang, H.F. Valdovinos, H. Gong et al., Dual-modality positron emission tomography/optical image-guided photodynamic cancer therapy with chlorin e6-containing nanomicelles. ACS Nano **10**(8), 7721–7730 (2016)

53. M. Zhou, M. Melancon, R.J. Stafford, J. Li, A.M. Nick, M. Tian et al., Precision nanomedicine using dual PET and MR temperature imaging-guided photothermal therapy. J. Nucl. Med. **57**(11), 1778–1783 (2016)
54. H.J. Im, C.G. England, L. Feng, S.A. Graves, R. Hernandez, R.J. Nickles et al., Accelerated blood clearance phenomenon reduces the passive targeting of PEGylated nanoparticles in peripheral arterial disease. ACS Appl. Mater. Inter. **8**(28), 17955–17963 (2016)
55. C.G. England, H.J. Im, L. Feng, F. Chen, S.A. Graves, R. Hernandez et al., Re-assessing the enhanced permeability and retention effect in peripheral arterial disease using radiolabeled long circulating nanoparticles. Biomaterials **100**, 101–109 (2016)
56. E.J. Keliher, Y.X. Ye, G.R. Wojtkiewicz, A.D. Aguirre, B. Tricot, M.L. Senders et al., Polyglucose nanoparticles with renal elimination and macrophage avidity facilitate PET imaging in ischaemic heart disease. Nat. Commun. **8**, 14064 (2017)
57. D.B. Cowan, R. Yao, V. Akurathi, E.R. Snay, J.K. Thedsanamoorthy, D. Zurakowski et al., Intracoronary delivery of mitochondria to the ischemic heart for cardioprotection. PLoS ONE **11**(8), e0160889 (2016)
58. A. Ahmadi, S.L. Thorn, E.I. Alarcon, M. Kordos, D.T. Padavan, T. Hadizad et al., PET imaging of a collagen matrix reveals its effective injection and targeted retention in a mouse model of myocardial infarction. Biomaterials **49**, 18–26 (2015)
59. J. Frigell, I. Garcia, V. Gomez-Vallejo, J. Llop, S. Penades, ^{68}Ga-labeled gold glyconanoparticles for exploring blood-brain barrier permeability: preparation, biodistribution studies, and improved brain uptake via neuropeptide conjugation. J. Am. Chem. Soc. **136**(1), 449–457 (2014)
60. J.W. Seo, J. Ang, L.M. Mahakian, S. Tam, B. Fite, E.S. Ingham et al., Self-assembled 20-nm ^{64}Cu-micelles enhance accumulation in rat glioblastoma. J. Control Release **220**(Pt A), 51–60 (2015)

Chapter 16
Tracer Kinetics in Radionanomedicine

Jae Sung Lee, Seongho Seo and Dong Soo Lee

Abstract Quantification of the amount of radiolabeled nanomaterials distributed in the animal and human body is important for understanding their in vivo properties (e.g., target delivery, radiolabeling stability, and excretion pathway) and determining future applications. Tracer kinetic analyses could play a vital role in the success of radionanomedicine as it facilitates the development of clinically relevant nanomaterials by providing the pharmacokinetic information. In this chapter, we describe the methodology used in the tracer kinetic analysis of dynamic positron emission tomography (PET) and single photon emission computed tomography (SPECT), starting from how to record the time profiles of tracer concentration in the blood and tissues, two sources of data required for a tracer kinetic model. Compartment models commonly used in PET and SPECT tracer kinetic analysis and their operational equations for fitting the tissue time-activity curves will be introduced. Then, several robust parameter estimation methods will be described. Finally, we will introduce a few examples of the tracer kinetic analysis in radio-nanomaterial studies.

J. S. Lee (✉) · D. S. Lee
Department of Nuclear Medicine, Seoul National University
College of Medicine, Seoul, Republic of Korea
e-mail: jaes@snu.ac.kr

D. S. Lee
e-mail: dsl@snu.ac.kr

J. S. Lee
Department of Biomedical Sciences, Seoul National University
College of Medicine, Seoul, Republic of Korea

S. Seo
Department of Neuroscience, College of Medicine, Gachon University,
Incheon, Republic of Korea
e-mail: dansoc@snu.ac.kr

D. S. Lee
Department of Molecular Medicine and Biopharmaceutical Sciences,
Graduate School of Convergence Science and Technology,
Seoul National University, Seoul, Republic of Korea

D. S. Lee (ed.), *Radionanomedicine*, Biological and Medical Physics,
Biomedical Engineering, https://doi.org/10.1007/978-3-319-67720-0_16

16.1 Introduction

Radionanomedicine is anticipated to expedite the clinical translation of nanomedicines, because it has the potential to address critical issues, such as possible toxicity and lesser-known pharmacokinetic characteristics of nanomaterials (or nanoparticles) by leveraging very low doses of radiolabeled nanomaterials (radionanomaterials) instead. Radiolabeling of a nanomaterial enables the visualization of its distribution in living bodies up to great depths using nuclear medicine imaging modalities, such as the positron emission tomography (PET) and single photon emission computed tomography (SPECT). Even if a very small amount of radiolabeled material (known as a radiotracer) is administered, its in vivo spatiotemporal biodistribution can be quantitatively measured by the above-mentioned modalities owing to their high molecular sensitivity. Consequently, through tracer kinetic analyses, one can obtain quantitative information regarding the underlying physiological and biochemical processes associated with radiotracers by making use of such spatiotemporal data [1, 2]. As such, radionanomedicine practices based on the use of these techniques can not only avoid the use of high pharmacological amounts of nanomaterials but can also provide relevant preliminary information regarding the fate of nanomaterials, such as a rapid clearance from the body.

Tracer kinetic analyses could play a vital role in the success of radionanomedicines as it facilitates the development of clinically applicable nanomaterials by providing quantitative pharmacokinetic information. In fact, tracer kinetic analysis is now attracting considerable interest from several emerging disciplines, such as PET microdosing and precision medicine, because of the increased importance of obtaining quantitative information for new drug development.

Tracer kinetic analysis of radiotracers based on their spatiotemporal distribution enables quantitative measurement of the rate constants associated with various physiological and biochemical processes. A tracer-kinetic model is a mathematical description of the movement of radiotracers within a living biological system. In most cases, the radiotracer movement is tracked from the arterial plasma to target tissues. The rate of radiotracer movement (or a change in radiotracer concentration) often provides direct information on the rate of a biological process. Therefore, one can trace and understand dynamic physiological and biological processes through tracer kinetic analysis [3–5].

The following describes a typical procedure followed in tracer kinetic analysis providing quantitative measurement.

- Define the physiological and biochemical parameters to be determined.
- Introduce a tracer that follows the physiology of the mother substance without disturbing the system.
- Record the time profiles of tracer concentrations in the blood and tissues.
- Apply a suitable mathematical model.
- Estimate the parameters of interest.

The following sections describe the methodology used in the tracer kinetic analysis of dynamic PET and SPECT. A few examples of their application in radionanomaterial studies have also been discussed.

16.2 Tissue Time–Activity Curves and Input Functions

In general, there exist two sources of data required for a tracer kinetic model: the time course of the measured concentration of the radiotracer disposed in the tissue (the tissue response) and that of the injected radiotracer in the blood or plasma (the input function) [6].

Tissue time–activity curves are usually obtained by drawing a region of interest (ROI) or volume of interest (VOI) on PET or SPECT images. Template- or atlas-based ROIs (and VOIs) could be used as an alternative to them being drawn manually, which is a laborious and time-consuming process [7–9]. Parametric images can also be generated by applying the kinetic analysis to time–activity curves of every image voxel. Each voxel of a parametric image then represents a value of some physiological parameter [10–14].

The standard method to obtain a plasma input function consists of manual or automated continuous arterial blood sampling. Plasma is extracted from arterial blood samples using a centrifuge, and the radioactivity concentration in these plasma samples is measured using a gamma counter and corrected for radioactive decay. If the radioactive metabolite of the injected radiotracer in the plasma does not reach the target (ROI), the metabolite fraction should be measured to obtain a metabolite corrected input function. In brain studies, metabolite correction is necessary, since radioactive metabolites usually cannot cross the blood–brain barrier due to their decreased lipophilicity. Dispersion and time delay corrections may be done if necessary [15, 16].

For radiotracers that do not require metabolite correction (or if applying the population-based metabolite fraction is a feasible option), one can use an image-derived input function (IDIF) obtained by applying the ROIs to heart cavities or large arteries. The IDIF approach is commonly used in myocardial perfusion PET studies using [^{13}N]NH_3 (ammonia) and ^{82}Rb. IDIF is also important in small animal imaging studies, wherein frequent blood sampling is not possible [17–19]. However, in human brain PET studies, there still exist many methodological challenges facing the routine use of the IDIF approach. Some of these challenges include accurate segmentation of carotid arteries and the partial volume effect [20]. Multivariate analysis techniques, such as factor and independent component analyses, may, at times, prove useful for separating the IDIF approach from the tissue time–activity curves [21–23].

Another less-invasive alternative to arterial sampling is the population-based input function (PBIF), which has been validated mostly for [^{18}F]FDG PET studies [24, 25]. The arterial plasma input functions obtained from the subject population are averaged after normalization. PBIF is then scaled using few blood samples to

obtain individual input functions. Unlike IDIF, the accuracy of PBIF does not depend upon partial volume effects, scanner characteristics, or reconstruction algorithms, and neither does it require post-processing of images. Because of the interindividual variability in the tracer metabolite fraction and peak estimation error, PBIF has limited accuracy in case of radiotracers with low parent concentration at the end of the scan [20].

Reference tissue approaches are widely used for radio ligands that bind to some molecular target but possess a reliable reference region devoid of specific binding. One can derive a relationship between reference regions and ROIs with specific binding under the assumption that they share the input function and that the non-displaceable volume of distribution (V_{ND}) is constant throughout the regions [11, 26, 27]. The simplified reference tissue model (SRTM) is also popular because it has fewer parameters to be estimated than the full model, and multiple linear models for SRTM are also available [13, 14, 26, 28]. Details of these approaches have been described in the following sections.

16.3 Compartment Modeling

Biological systems can be modelled as a combination of compartments linked by kinetic processes (i.e., the exchange of materials among compartments). Compartment modeling is commonly used in tracer kinetic analyses. In the compartment model, each compartment represents an effective radiotracer amount occupying a distinct physical space and having different chemical forms or pharmacological states. The radiotracer in the compartment should be well-mixed, kinetically homogeneous, and distinct. Compartment models frequently used for in vivo nuclear imaging studies are shown in Fig. 16.1. In this Fig., the arrows indicate the paths followed by the radiotracer [5, 29, 30]. Radiotracers within a tissue can be modeled with more than one compartment depending on the kinetic properties of the tissue.

In one-tissue compartment models (or two-compartment models) shown in Fig. 16.1a, a change in radiotracer concentration in the tissue compartment can be described by the following equation.

$$\frac{dC_T(t)}{dt} = K_1 C_p(t) - k_2 C_T(t), \tag{16.1}$$

where t represents time; $C_p(t)$ and $C_T(t)$ are, respectively, the arterial plasma and tissue concentrations of the radiotracer; K_1 (mL/min/g) and k_2 (min^{-1}) respectively are the rate constants defined for describing the delivery and washout of the radiotracer.

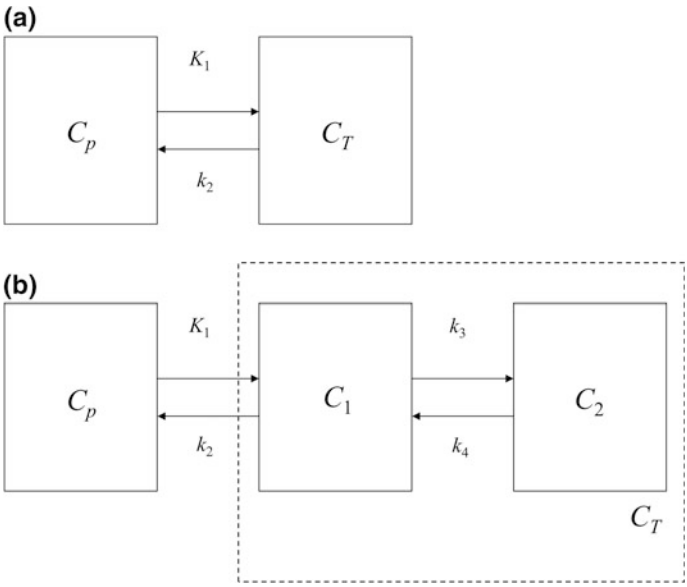

Fig. 16.1 Compartment models. **a** One-tissue. **b** Two-tissue (in the kinetic modeling of receptor–ligand interaction, C_1 and C_2, respectively, represent the free or non-specifically bound radio ligand and the radio ligand specifically bound by receptors)

Solving the above equation for $C_T(t)$ gives

$$C_T(t) = K_1 \int_0^t C_p(\tau) e^{-k_2(t-\tau)} d\tau = K_1 C_p(t) \otimes e^{-k_2 t}, \tag{16.2}$$

where $\otimes$ denotes a convolution integral.

The two-tissue compartment model (or three-compartment model) shown in Fig. 16.1b can be described by the following set of equations.

$$\frac{dC_1(t)}{dt} = K_1 C_p(t) - k_2 C_1(t) - k_3 C_1(t) + k_4 C_2(t) \tag{16.3}$$

$$\frac{dC_2(t)}{dt} = k_3 C_1(t) - k_4 C_2(t) \tag{16.4}$$

where the additional parameters k_3 (min^{-1}) and k_4 (min^{-1}) describe the exchange of materials (e.g., phosphorylation and dephosphorylation in [^{18}F]FDG, association and dissociation of radio ligands and receptors) between tissue compartments $C_1(t)$ and $C_2(t)$.

In this model, the tissue time–activity curves, fitted using measurements performed by the imaging devices, amount to the sum of $C_1(t)$ and $C_2(t)$ (Fig. 16.1b).

$$C_T(t) = C_1(t) + C_2(t)$$
$$= K_1 C_p(t) \otimes \left[\left(\frac{k_3 + k_4 - q_1}{q_2 - q_1} \right) e^{-q_1 t} - \left(\frac{k_3 + k_4 - q_2}{q_2 - q_1} \right) e^{-q_2 t} \right] \quad (16.5)$$

$$q_1, q_2 = \frac{(k_2 + k_3 + k_4) \mp \sqrt{(k_2 + k_3 + k_4)^2 - 4k_2 k_4}}{2} \quad (16.6)$$

The combination of rate constants employed in the two-tissue compartment model can be related to the commonly used parameters for in vivo imaging of reversibly binding radio ligands ($C_1(t)$ and $C_2(t)$ correspond to non-displaceable and specific binding compartments, respectively), as listed in Table 16.1.

Radiotracer kinetics with irreversible binding or uptake can be described by assigning a value equal to zero to k_4 thereby leading to the following simpler solution.

$$C_T(t) = \frac{K_1}{k_2 + k_3} C_p(t) \otimes \left[k_3 + k_2 e^{-(k_2 + k_3)t} \right] \quad (16.7)$$

The net transport rate of the radiotracer (K_{in} or K_i) into the irreversibly bound second tissue compartment ($C_2(t)$) is defined as the product of K_1 and $k_3/(k_2 + k_3)$.

As previously mentioned, the reference tissue model is a widely-used approach that does not require arterial sampling. The relationship between the time–activity curves of ROI and the reference region is derived with the assumption of constant non-displaceable volume of distribution. The SRTM equation applicable to radio ligands with relatively rapid exchange between non-displaceable and specific binding compartments ($C_1(t)$ and $C_2(t)$) is given by

$$C_T(t) = R_1 C_R(t) + \left\{ k_2 - \frac{R_1 k_2}{(1 + BP_{ND})} \right\} C_R(t) \otimes e^{\frac{-k_2 t}{(1 + BP_{ND})}} \quad (16.8)$$

where $C_R(t)$ is the concentration of radio ligands in the reference region, R_1 is the ratio of K_1 for ROI to that for the reference region, k_2 is the wash out from ROI, and BP_{ND} is the binding potential relative to the non-displaceable compartment.

Table 16.1 Parameter nomenclature commonly used for in vivo imaging of reversibly binding radio ligands and their relationship with the rate constants employed in the two-tissue compartment model

Parameter	Description	Equation
V_{ND}	Distribution volume of non-displaceable (free or nonspecifically bound) compartment	$\frac{K_1}{k_2}$
V_T	Total distribution volume	$\frac{K_1}{k_2}\left(1 + \frac{k_3}{k_4}\right)$
DVR	Distribution volume ratio	$\frac{V_T}{V_{ND}} = 1 + \frac{k_3}{k_4}$
BP_{ND}	Binding potential relative to the non-displaceable compartment	$\frac{V_T - V_{ND}}{V_{ND}} = \frac{k_3}{k_4}$

Sometimes, correction factors for mitigating the partial volume and spillover effects on the tissue time–activity curves are incorporated into model equations. The correction factors may or may not be coupled with each other, as shown in (16.9) and (16.10), as the case may be.

$$\tilde{C}_T(t) = (1 - V_a)C_T(t) + V_a C_p(t) \tag{16.9}$$

$$\tilde{C}_T(t) = \alpha C_T(t) + V_a C_p(t) \tag{16.10}$$

Here, V_a is a correction factor for the spillover effect and $(1 - V_a)$ or α is the correction factor for the partial volume effect.

If the specific activity of a radio ligand or receptor density is not high enough in the receptor–ligand binding, the rate constant describing the forward receptor–ligand reaction (k_3) in the two-tissue compartment model (Fig. 16.1b) is not constant anymore. k_3 is then time-varying and dependent on the activity concentration of the specifically binding compartment (C_2) and the specific activity. Also, the analytical solution of $C_T(t)$, shown in (16.5), does not work anymore, requiring the following numerical generation.

$$\begin{aligned} k_3(t) &= k_{on}\left(B_{\max} - \frac{C_2(t)}{A_s}\right) \\ C_1(t+\Delta t) &= C_1(t) + \Delta t\left[K_1 C_p(t) - (k_2 + k_3(t))C_1(t) + k_4 C_2(t)\right] \\ C_2(t+\Delta t) &= C_2(t) + \Delta t[k_3(t)C_1(t) - k_4 C_2(t)] \\ C_T(t+\Delta t) &= C_1(t+\Delta t) + C_2(t+\Delta t) \end{aligned} \tag{16.11}$$

Here, k_{on} is the bimolecular association rate constant (g/pmol/min), $B_{\max}$ is the density of receptor sites available for radio ligand binding (apparent $B_{\max}$, pmol/g), and A_s is the specific activity (radioactivity per mole of a labeled compound, μCi/pmol) [31, 32]. Figure 16.2 shows examples of the simulated time–activity curves at different specific activities. Noiseless total tissue time–activity curves ($C_1 + C_2 + V_0 \cdot C_p$) were generated using the above equations and a metabolite-corrected plasma input function was obtained from a human [^{11}C]raclopride PET study involving intermittent arterial blood sampling for 90 min. The input function was interpolated every second, and the tissue time–activity curves were calculated. K_1, k_2, k_{on}, k_{off} (=k_4), $B_{\max}$, and V_0 were fixed at 0.17 min^{-1}, 0.42 min^{-1}, 0.014 ml/pmol/min, 0.10 min^{-1}, 22 pmol/ml, and 5%, respectively [33]. Specific activities varied within the range 0.02–5 μCi/pmol (20–5000 mCi/μmol).

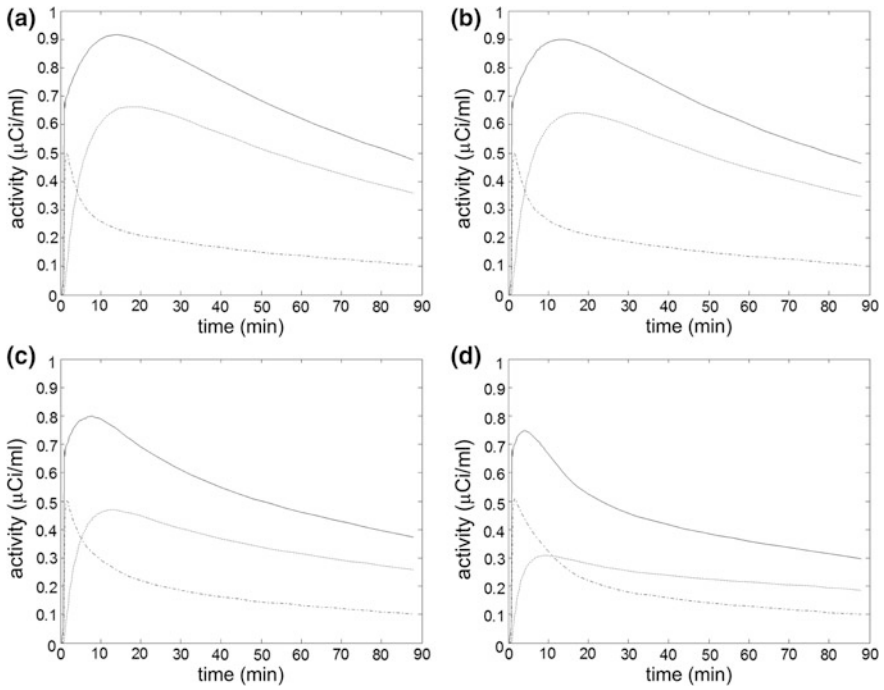

Fig. 16.2 Tissue time–activity curves with different specific activities. Solid line: total tissue time–activity curve (C_T). Dotted line: specifically bound time–activity curve (C_2). Dashed and dotted line: nonspecifically bound time–activity curve (C_1). **a** specific activity = 5000 mCi/μmol. **b** 500 mCi/μmol. **c** 50 mCi/μmol. **d** 20 mCi/μmol

16.4 Parameter Estimation

Noise in the tissue time–activity curve and input function leads to bias and a variation in the estimated kinetic parameters. Usually, this bias and variation increase as the noise level becomes higher (Fig. 16.3). Nonlinear parameter estimation based on an iterative search of the final solution is vulnerable to noise, as noise generates a local minima in the parameter search space. As such, one needs to assign proper initial values relatively close to the final solution to avoid convergence to the local minima. Constraints in the bounds of estimates and some regularizations based on prior knowledge regarding the properties of radiotracers are sometimes helpful in finding the best solution.

The parameter estimation procedure can be simplified by transforming the differential equations of the kinetic model into a linearized form. Several different graphical analysis (GA) methods based on simple linear regression models are available. Two most popular GA methods comprise the Gjedde–Patlak plot for an irreversible system [34–36] and the Logan plot for a reversible one [37, 38]. Additionally, methods like the relative equilibrium-based graphical method for

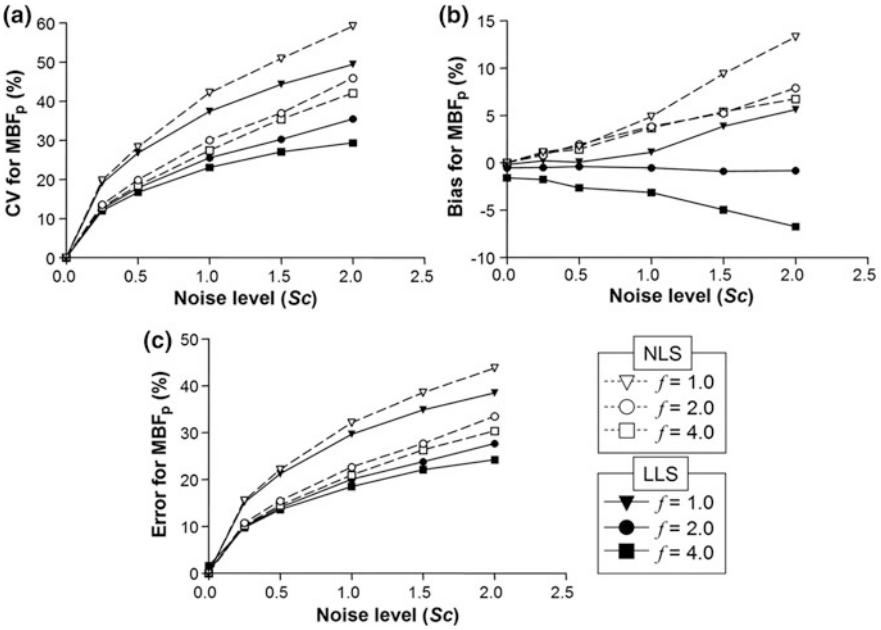

Fig. 16.3 Example of the relationship between noise level and variation (**a**), bias (**b**), and error (**c**) in kinetic parameter estimation based on the parameter estimation method (comparison between nonlinear and linear least squares (NLS and LLS); MBF: myocardial blood flow. Reprint with permission from [12])

addressing the bias issue in the Logan plot [39] and bi-graphical analysis methods for the quantification of slowly reversible radiotracers are also sometimes used [40, 41]. Each of the GA methods depend on different assumptions to simplify the model equation, and only the latter portion of the measured data usually satisfies these assumptions [42]. Because the violation of these assumptions and improper selection of the linear fitting range leads to bias in the kinetic parameter estimation, a proper understanding of the uptake mechanism in radiotracers and a careful observation of the time course of measured data is necessary. The characteristics of each GA method is summarized in Table 16.2, which is modified based on the authors' review of advances in graphical analysis [42].

Multiple linear regression models with more than one independent variable are more complex but represent an accurate approach than the simple GA. For example, by integrating (16.1), the following linear equation with two independent variables (K_1 and k_2) can be obtained.

$$C_T(t) = K_1 \int_0^t C_p(\tau)d\tau - k_2 \int_0^t C_T(\tau)d\tau \tag{16.12}$$

Table 16.2 Characteristics of graphical analysis methods

	Logan plot	RE plot	GP plot	Non-invasive Logan	Non-invasive RE	Non-invasive GP
Binding type	Reversible	Reversible	Irreversible	Reversible	Reversible	Irreversible
Input function	C_P	C_P	C_P	C_R	C_R	C_R
Major parameters of interest	V_T	V_T	K_{in}	$V_T/V_T^{'}$	$V_T/V_T^{'}$	$K_{in}/V_T^{'}$ (or $K_{in}/K_{in}^{'}$)
Linearity condition	$\frac{C_S(t)}{C_T(t)} \rightarrow const$ (1TCM after t^*)	$\frac{C_T(t)}{C_P(t)} \rightarrow const$	$\frac{C_{ND}(t)}{C_P(t)} \rightarrow const$	Logan condition for tissue and reference	RE condition for tissue and reference	Logan for reversible and GP for irreversible
Reference	[38]	[39]	[34, 36]	[37]	[39]	[35, 56]

Modified from Table 1 in [42] with permission

1TCM one-tissue compartment model; V_T and V_T' total distribution volumes in ROI and reference region

Rearranging the above equation in the matrix form and applying matrix inversion yields solutions for the independent variables [43]. The following are examples of linearized equations that can be formulated for reversible ($k_4 > 0$) and irreversible ($k_4 = 0$) two-tissue compartment models [19, 44, 45].

$$\begin{aligned} C_T(t) &= P_1 \int_0^t C_T(\tau)d\tau + P_2 \int_0^t \int_0^\tau C_T(s)dsd\tau + P_3 \int_0^t C_p(\tau)d\tau + P_4 \int_0^t \int_0^\tau C_p(s)dsd\tau \\ P_1 &= -(k_2 + k_3 + k_4) \\ P_2 &= -k_2k_4 \\ P_3 &= K_1 \\ P_4 &= K_1(k_3 + k_4) \end{aligned} \tag{16.13}$$

$$\begin{aligned} \int_0^t C_T(\tau)d\tau &= P_1 \int_0^t \int_0^\tau C_p(s)dsd\tau + P_2 \int_0^t C_p(\tau)d\tau + P_3C_p(t) + P_4C_T(t) \\ P_1 &= \frac{K_1k_3}{k_2 + k_3} = K_{in} \\ P_2 &= \frac{K_1}{k_2 + k_3} \\ P_3 &= \frac{V_a}{k_2 + k_3} \\ P_4 &= -\frac{1}{k_2 + k_3} \end{aligned} \tag{16.14}$$

Linearized SRTM augmented by applying spatial constrains into parameter estimation has also been suggested for computationally efficient and robust parametric image generation [13, 14].

$$\int_0^t C_T(\tau)d\tau = DVR \int_0^t C_R(\tau)d\tau + \frac{DVR}{k_2/R_1}C_R(t) - \frac{DVR}{k_2}C_T(t) \tag{16.15}$$

Another approach towards obtaining a robust kinetic parameter estimation is the basis function method [11, 46, 47] based on linearization of the convolution ($\otimes$) terms in the solution of tissue time–activity curves. For example, the SRTM (16.8) can be transformed into a linear equation as follows.

$$C_T(t) = \theta_1 C_R(t) + \theta_2 C_R(t) \otimes e^{-\theta_3 t} = \theta_1 C_R(t) + \theta_2 B_i(t) \tag{16.16}$$

Here, $\theta_1 = R_1$, $\theta_2 = k_2 - R_1 k_2(1 + BP)$, and $\theta_3 = k_2/(1 + BP)$. Each $B_i(t) = C_R(t) \otimes \exp(-\theta_{3i} t)$ is a basis function formed by choosing a discrete spectrum of parameter values for θ_3. The above equation is solved using the linear least squares for each basis function and (θ_1, θ_2, θ_3) and (BP, R_1, k_2) solutions are determined using the basis function that yields the smallest residual sum of squares between the measured and estimated values of $C_T(t)$ [11].

16.5 Application in Radionanomedicine

There exist a limited number of studies on the kinetics of nanoparticle transportation within living organisms. The complicated kinetics of nanoparticle transport and the preclinical stage of radiolabeled nanoparticles (mostly involving mice as subjects) are the main obstacles in the widespread acceptance of the application of tracer kinetic techniques in nanoparticle investigations for imaging and therapy. The following three examples provide an insight into how tracer kinetic modeling can facilitate nanoparticle investigations.

Tylcz et al. studied the kinetics of antiangiogenic ATWLPPR peptide-targeted silica-based nanoparticle-encapsulated gadolinium oxide as an MRI contrast agent and chlorin as a photosensitizer (NP-PEP) [48]. The kinetics of this hybrid non-biodegradable nanoparticle in orthotopic U87 brain tumors in nude rats was compared to that of nanoparticles without photosensitizers or surface targeting peptides synthesized as a control (NP-CONT). A one-tissue compartment model with three rate constants associated with the elimination, uptake, and release of nanoparticles and an additional parameter to estimate the amount of captured nanoparticles by the biological host was used in this MRI-based kinetic modeling study. MR images were acquired using dynamic T1-weighted FLASH sequences in a 7-Tesla MRI machine. The normalized MRI signal with respect to the signal value prior to nanoparticle injection was assumed to be proportional to the amount of nanoparticles. The results of this pilot study involving a small number of animals suggest that the proposed one-tissue compartment model is suitable for describing the observed responses of these gadolinium-oxide-based contrast agents. Although larger values for the rate constants describing the uptake and elimination characteristics were observed in NP-PEP studies, the small sample size undermined the validity of this observation.

Compartment modeling in radionanomedicine enables an investigation of the impact of the attachment of cell-specific targeting ligands to nanoparticle surfaces. The nanoparticles accumulate non-specifically in tumors due to the enhanced permeability and retention (EPR) effect along with a passive but selective delivery mechanism for tumors with a leaky vasculature [49, 50]. However, not all tumors are amendable by EPR-dependent deliveries [2]. For tumors with weak EPRs, an

active targeting of the tumor by attaching tumor-specific ligands to nanoparticles enhances the nanoparticle potency [1, 51–53]. Barlett et al. comparatively evaluated the in vivo biodistribution and functional activity of siRNA targeting (silencing) luciferase mRNA delivered by transferrin-targeted or non-targeted DOTA-conjugated nanoparticles labeled with ^{64}Cu [54]. The results of the PET/CT study demonstrate the negligible impact of transferrin targeting on the accumulation of nanoparticles in the luciferase-expressing Neuro2A s.c. tumors in mice. However, the active targeting altered the functional activity of the tumors (approximately 50% lower relative increase of tumor luciferase activity measured by bioluminescent imaging in mice treated with transferrin targeted nanoparticles compared to those treated with non-targeted nanoparticles). In the compartment model analysis performed to explicate the discrepancy between biodistribution and functional activity of tumor-specific targeting nanoparticles, the tumor tissue time–activity curves were reasonably fitted with zero k_2. Also, one-tissue and two-tissue compartment models yielded equivalent curve-fitting qualities. In this situation, where the radiotracers do not return to the bloodstream and C_1 (tumor interstitial space in this specific model) and C_2 (specific tumor targeting) quickly attain the equilibrium state (Fig. 16.1b), temporal changes in the total tissue activity measurable by PET is not influenced by changes in k_3 associated with the tumor-specific binding. In addition, mathematical solutions of C_1 and C_2 composed with different k_3 values and other fixed parameters enable us to comprehend how tumor-specific targeting enhances intracellular uptake in tumor cells. Figure 16.4 shows relationship between the relative tumor accumulation 1d after injection and the ratio of kinetic parameters [54].

Kinetic analysis in radionanomedicine also facilitates an understanding of the in vivo biological mechanisms of nanoparticles, such as disassembly and clearance. In vivo distribution and excretion of nanoparticles are dependent on several properties of nanoparticles, such as size, aspect ratio, charge, stiffness, and surface

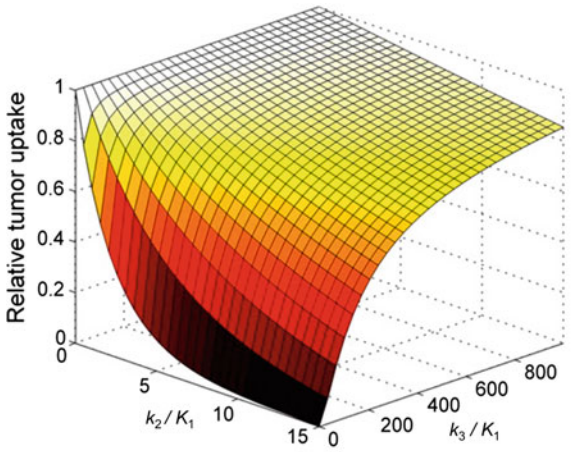

Fig. 16.4 The effect of tumor clearance (k_2) and tumor-specific binding (k_3) on tumor accumulation. Modified with permission from [54]

chemistry [2]. Zuckerman et al. investigated the mechanism of the unexpected rapid renal clearance of cationic cyclodextrin-containing polymer (CDP)-based siRNA nanoparticles. This mechanism prevents nanoparticles from prolonging the siRNA delivery to the tumor thereby enhancing the anticancer efficacy. These siRNA nanoparticles were designed to have a much bigger size (D ≈ 100 nm) than the effective cut-off size of the renal filtration barrier (D ≈ 10 nm) [55]. Microscopic imaging studies conducted on mice have demonstrated that CDP-based siRNA nanoparticles transiently accumulate and can be dissembled by the glomerular basement membrane (GBM) of the kidneys, prior to being fragmented into sufficiently small components that enter the urinary tract. Also, dynamic PET studies have demonstrated the delayed and augmented peaks in the kidney and the delayed transit from the kidney to the bladder in the time–activity curves of ^{64}Cu-labeled siRNA nanoparticles in comparison to the free ^{64}Cu-labeled siRNA thereby supporting the validity of the microscopic findings. Finally, the in vivo kinetics of ^{64}Cu-labeled free siRNA and siRNA nanoparticles, measured by PET, were further

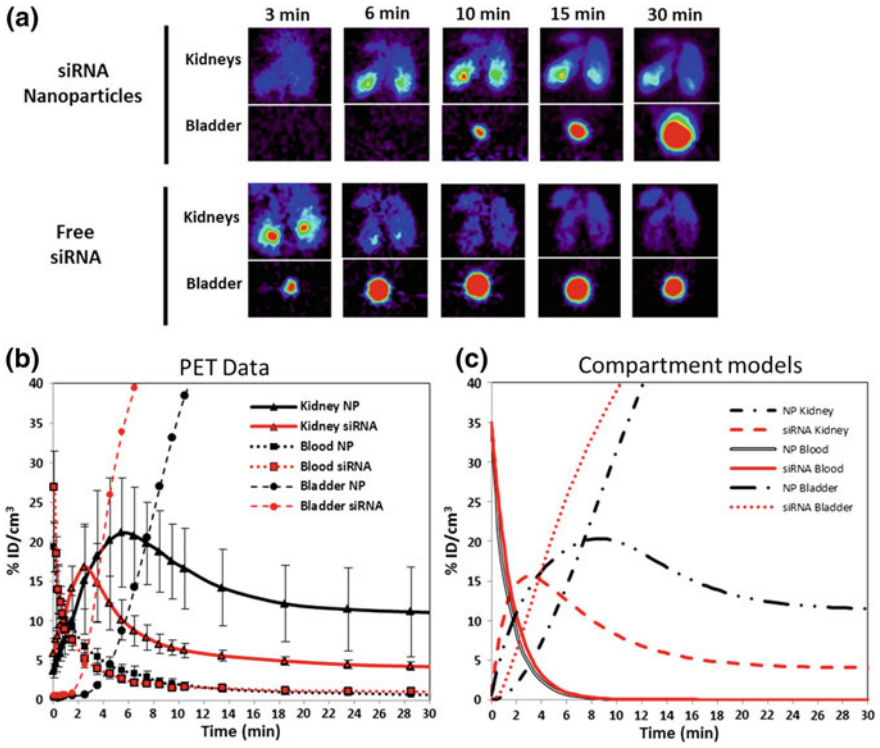

Fig. 16.5 PET image data and compartment modeling results showing the transient accumulation and disassembly of SiRNA nanoparticles in the glomerular basement membrane of the kidney. **a** PET images of mice receiving ^{64}Cu-labeled siRNA nanoparticle (NP) and free siRNA. **b** Measured PET time–activity curves. **c** Simulated PET time–activity curves using compartment model data. Reprint with permission from [55]

quantified and analyzed using compartment models to better understand the kidney transit of free siRNA and siRNA nanoparticles. The parameters for modeling the kinetics of free siRNA was derived from anatomical properties of the kidney and by fitting the PET time-activity curves. The siRNA nanoparticle models were then constructed by adding the parameters describing the GBM accumulation and disassembly and the peri-tubule endothelial uptake into the model for free siRNA. The two models well describe the kinetics of both ^{64}Cu-labeled free siRNA and siRNA nanoparticles thereby conforming the suggested underlying mechanism of rapid renal excretion of CDP-based nanoparticles (Fig. 16.5) [55]. This improved understanding of the clearance mechanism of CDP-based nanoparticles provides invaluable insights to guide the design of more effective nanoparticles for siRNA delivery.

References

1. D.S. Lee, H.-J. Im, Y.-S. Lee, Radionanomedicine: widened perspectives of molecular theragnosis. Nanomedicine **11**(4), 795–810 (2015)
2. E.C. Pratt, T.M. Shaffer, J. Grimm, Nanoparticles and radiotracers: advances toward radionanomedicine. Wiley Interdiscip. Rev. Nanomed. Nanobiotechnol. **8**(6), 872–890 (2016)
3. R.E. Carson, Tracer kinetic modeling in PET, in *Positron Emission Tomography* (Springer, Berlin, 2005), pp. 127–159
4. A. Gjedde, W.R. Bauer, D. Wong, *Neurokinetics: The Dynamics of Neurobiology In Vivo* (Springer Science & Business Media, Berlin. 2010)
5. J.S. Lee, D.S. Lee, Tracer kinetic analysis for PET and SPECT. Med. Imaging Technol. Appl. **201**(3) (2013)
6. S.R. Cherry, J. Sorenson, M.E. Phelps, B.M. Methé, Physics in nuclear medicine. Med. Phys. **31**(8), 2370–2371 (2004)
7. E. Kim, O.D. Howes, B.-H. Kim, M.-W. Chon, S. Seo, F.E. Turkheimer et al., Regional differences in serotonin transporter occupancy by escitalopram: an [^{11}C] DASB PK-PD study. Clin. Pharmacokinet. **56**(4), 371–381 (2017)
8. J.S. Lee, D.S. Lee, Analysis of functional brain images using population-based probabilistic atlas. Curr. Med. Imaging Rev. **1**(1), 81–87 (2005)
9. J.-Y. Lee, S.H. Seo, Y.K. Kim, H.B. Yoo, Y.E. Kim, I.C. Song et al., Extrastriatal dopaminergic changes in Parkinson's disease patients with impulse control disorders. J. Neurol. Neurosurg. Psychiatry (2013)
10. Y. Choi, R.A. Hawkins, S.-C. Huang, S.S. Gambhir, R.C. Brunken, M.E. Phelps et al., Parametric images of myocardial metabolic rate of glucose generated from dynamic cardiac PET and 2-[^{18}F] fluoro-2-deoxy-d-glucose studies. J. Nucl. Med. **32**(4), 733–738 (1991)
11. R.N. Gunn, A.A. Lammertsma, S.P. Hume, V.J. Cunningham, Parametric imaging of ligand-receptor binding in PET using a simplified reference region model. Neuroimage **6**(4), 279–287 (1997)
12. J.S. Lee, D.S. Lee, J.Y. Ahn, J.S. Yeo, G.J. Cheon, S.-K. Kim et al., Generation of parametric image of regional myocardial blood flow using $H_2^{15}O$ dynamic PET and a linear least-squares method. J. Nucl. Med. **46**(10), 1687–1695 (2005)
13. S. Seo, S.J. Kim, Y.K. Kim, J.-Y. Lee, J.M. Jeong, D.S. Lee et al., Comparative assessment of parametric neuroreceptor mapping approaches based on the simplified reference tissue model using [^{11}C] ABP688 PET. J. Cereb. Blood Flow Metab. **35**(12), 2098–2108 (2015)

14. Y. Zhou, C.J. Endres, J.R. Brašić, S.-C. Huang, D.F. Wong, Linear regression with spatial constraint to generate parametric images of ligand-receptor dynamic PET studies with a simplified reference tissue model. Neuroimage. **18**(4), 975–989 (2003)
15. H. Iida, T. Jones, S. Miura, Modeling approach to eliminate the need to separate arterial plasma in oxygen-15 inhalation positron emission tomography. J. Nucl. Med. **34**(1333–1340), 18 (1993)
16. E. Meyer, Simultaneous correction for tracer arrival delay and dispersion in CBF measurements by the $H_2^{15}O$ autoradiographic method and dynamic PET. J. Nucl. Med. **30** (6), 1069–1078 (1989)
17. J.H. Kim, Y.H. Kim, Y.J. Kim, B.Y. Yang, J.M. Jeong, H. Youn et al., Quantitative positron emission tomography imaging of angiogenesis in rats with forelimb ischemia using ^{68}Ga-NOTA-c(RGDyK). Angiogenesis **16**(4), 837–846 (2013)
18. J.W. Kim, S. Seo, H.S. Kim, D.-Y. Kim, H.-Y. Lee, K.W. Kang et al., Comparative evaluation of the algorithms for parametric mapping of the novel myocardial PET imaging agent ^{18}F-FPTP. Ann. Nucl. Med. 1–11 (2017)
19. S.J. Kim, J.S. Lee, Y.K. Kim, J. Frost, G. Wand, M.E. McCaul et al., Multiple linear analysis methods for the quantification of irreversibly binding radiotracers. J. Cereb. Blood Flow Metab. **28**(12), 1965–1977 (2008)
20. P. Zanotti-Fregonara, K. Chen, J.S. Liow, M. Fujita, R.B. Innis, Image-derived input function for brain PET studies: many challenges and few opportunities. J. Cereb. Blood Flow Metab. **31**(10), 1986–1998 (2011)
21. J.Y. Ahn, D.S. Lee, J.S. Lee, S.K. Kim, G.J. Cheon, J.S. Yeo et al., Quantification of regional myocardial blood flow using dynamic $H_2^{15}O$ PET and factor analysis. J. Nucl. Med. **42**(5), 782–787 (2001)
22. J.S. Lee, D.S. Lee, J.Y. Ahn, G.J. Cheon, S.K. Kim, J.S. Yeo et al., Blind separation of cardiac components and extraction of input function from $H_2^{15}O$ dynamic myocardial PET using independent component analysis. J. Nucl. Med. **42**(6), 938–943 (2001)
23. M. Naganawa, Y. Kimura, K. Ishii, K. Oda, K. Ishiwata, A. Matani, Extraction of a plasma time-activity curve from dynamic brain PET images based on independent component analysis. IEEE Trans. Biomed. Eng. **52**(2), 201–210 (2005)
24. S. Eberl, A.R. Anayat, R.R. Fulton, P.K. Hooper, M.J. Fulham, Evaluation of two population-based input functions for quantitative neurological FDG PET studies. Eur. J. Nucl. Med. **24**(3), 299–304 (1997)
25. S. Takikawa, V. Dhawan, P. Spetsieris, W. Robeson, T. Chaly, R. Dahl et al., Noninvasive quantitative fluorodeoxyglucose PET studies with an estimated input function derived from a population-based arterial blood curve. Radiology **188**(1), 131–136 (1993)
26. A.A. Lammertsma, S.P. Hume, Simplified reference tissue model for PET receptor studies. Neuroimage **4**(3), 153–158 (1996)
27. Y. Wu, R.E. Carson, Noise reduction in the simplified reference tissue model for neuroreceptor functional imaging. J. Cereb. Blood Flow Metab. **22**(12), 1440–1452 (2002)
28. M. Ichise, J.-S. Liow, J.-Q. Lu, A. Takano, K. Model, H. Toyama et al., Linearized reference tissue parametric imaging methods: application to [^{11}C] DASB positron emission tomography studies of the serotonin transporter in human brain. J. Cereb. Blood Flow Metab. **23**(9), 1096–1112 (2003)
29. C. Cobelli, D. Foster, G. Toffolo, *Tracer Kinetics in Biomedical Research: From Data to Model* (Springer Science & Business Media, Berlin, 2007)
30. A.J. Fischman, N.M. Alpert, R.H. Rubin, Pharmacokinetic imaging. Clin. Pharmacokinet. **41** (8), 581–602 (2002)
31. S.-C. Huang, J.R. Barrio, M.E. Phelps, *Neuroreceptor Assay with Positron Emission Tomography: Equilibrium Versus Dynamic Approaches* (SAGE Publications, Sage, 1986)
32. D.F. Wong, A. Gjedde, H.N. Wagner Jr., Quantification of neuroreceptors in the living human brain. I. Irreversible binding of ligands. J. Cereb. Blood Flow Metab. **6**(2), 137–146 (1986)

33. L. Farde, L. Eriksson, G. Blomquist, C. Halldin, Kinetic analysis of central [11C] raclopride binding to D2-dopamine receptors studied by PET—a comparison to the equilibrium analysis. J. Cereb. Blood Flow Metab. **9**(5), 696–708 (1989)
34. A. Gjedde, High-and low-affinity transport of D-glucose from blood to brain. J. Neurochem. **36**(4), 1463–1471 (1981)
35. C.S. Patlak, R.G. Blasberg, Graphical evaluation of blood-to-brain transfer constants from multiple-time uptake data. Generalizations. J. Cereb. Blood Flow Metab. **5**(4), 584–590 (1985)
36. C.S. Patlak, R.G. Blasberg, J.D. Fenstermacher, Graphical evaluation of blood-to-brain transfer constants from multiple-time uptake data. J. Cereb. Blood Flow Metab. **3**(1), 1–7 (1983)
37. J. Logan, J.S. Fowler, N.D. Volkow, G.-J. Wang, Y.-S. Ding, D.L. Alexoff, Distribution volume ratios without blood sampling from graphical analysis of PET data. J. Cereb. Blood Flow Metab. **16**(5), 834–840 (1996)
38. J. Logan, J.S. Fowler, N.D. Volkow, A.P. Wolf, S.L. Dewey, D.J. Schlyer et al., Graphical analysis of reversible radioligand binding from time—activity measurements applied to [N-^{11}C-methyl]-(−)-cocaine PET studies in human subjects. J. Cereb. Blood Flow Metab. **10**(5), 740–747 (1990)
39. Y. Zhou, W. Ye, J.R. Brašić, A.H. Crabb, J. Hilton, D.F. Wong, A consistent and efficient graphical analysis method to improve the quantification of reversible tracer binding in radioligand receptor dynamic PET studies. Neuroimage **44**(3), 661–670 (2009)
40. S. Seo, S.J. Kim, H.B. Yoo, J.-Y. Lee, Y.K. Kim, D.S. Lee et al., Noninvasive bi-graphical analysis for the quantification of slowly reversible radioligand binding. Phys. Med. Biol. **61**(18), 6770 (2016)
41. Y. Zhou, W. Ye, J.R. Brašić, D.F. Wong, Multi-graphical analysis of dynamic PET. Neuroimage **49**(4), 2947–2957 (2010)
42. S. Seo, S.J. Kim, D.S. Lee, J.S. Lee, Recent advances in parametric neuroreceptor mapping with dynamic PET: basic concepts and graphical analyses. Neurosci. Bull. **30**(5), 733–754 (2014)
43. D. Feng, Z. Wang, S.-C. Huang, A study on statistically reliable and computationally efficient algorithms for generating local cerebral blood flow parametric images with positron emission tomography. IEEE Trans. Med. Imaging **12**(2), 182–188 (1993)
44. D. Feng, S.-C. Huang, Z. Wang, D. Ho, An unbiased parametric imaging algorithm for nonuniformly sampled biomedical system parameter estimation. IEEE Trans. Med. Imaging **15**(4), 512–518 (1996)
45. M. Ichise, H. Toyama, R.B. Innis, R.E. Carson, Strategies to improve neuroreceptor parameter estimation by linear regression analysis. J. Cereb. Blood Flow Metab. **22**(10), 1271–1281 (2002)
46. R.N. Gunn, P.A. Sargent, C.J. Bench, E.A. Rabiner, S. Osman, V.W. Pike et al., Tracer kinetic modeling of the 5-HT 1A receptor ligand [carbonyl-^{11} C] WAY-100635 for PET. Neuroimage **8**(4), 426–440 (1998)
47. H. Watabe, H. Jino, N. Kawachi, N. Teramoto, T. Hayashi, Y. Ohta et al., Parametric imaging of myocardial blood flow with ^{15}O-water and PET using the basis function method. J. Nucl. Med. **46**(7), 1219–1224 (2005)
48. J.-B. Tylcz, T. Bastogne, H. Benachour, D. Bechet, E. Bullinger, H. Garnier et al., A model-based pharmacokinetics characterization method of engineered nanoparticles for pilot studies. IEEE Trans. Nanobiosci. **14**(4), 368–377 (2015)
49. H. Maeda, J. Wu, T. Sawa, Y. Matsumura, K. Hori, Tumor vascular permeability and the EPR effect in macromolecular therapeutics: a review. J. Control Release **65**(1), 271–284 (2000)
50. Y. Matsumura, H. Maeda, A new concept for macromolecular therapeutics in cancer chemotherapy: mechanism of tumoritropic accumulation of proteins and the antitumor agent smancs. Cancer Res. 46(12 Part 1), 6387–6392 (1986)
51. J.D. Byrne, T. Betancourt, L. Brannon-Peppas, Active targeting schemes for nanoparticle systems in cancer therapeutics. Adv. Drug Deliv. Rev. **60**(15), 1615–1626 (2008)

52. W. Cai, K. Chen, Z.-B. Li, S.S. Gambhir, X. Chen, Dual-function probe for PET and near-infrared fluorescence imaging of tumor vasculature. J. Nucl. Med. **48**(11), 1862–1870 (2007)
53. R. Lehner, X. Wang, S. Marsch, P. Hunziker, Intelligent nanomaterials for medicine: carrier platforms and targeting strategies in the context of clinical application. Nanomedicine **9**(6), 742–757 (2013)
54. D.W. Bartlett, H. Su, I.J. Hildebrandt, W.A. Weber, M.E. Davis, Impact of tumor-specific targeting on the biodistribution and efficacy of siRNA nanoparticles measured by multimodality in vivo imaging. Proc. Natl. Acad. Sci. U.S.A. **104**(39), 15549–15554 (2007)
55. J.E. Zuckerman, C.H.J. Choi, H. Han, M.E. Davis, Polycation-siRNA nanoparticles can disassemble at the kidney glomerular basement membrane. Proc. Natl. Acad. Sci. U.S.A. **109**(8), 3137–3142 (2012)
56. Y.-G. Wu, Noninvasive quantification of local cerebral metabolic rate of glucose for clinical application using positron emission tomography and ^{18}F-fluoro-2-deoxy-D-glucose. J. Cereb. Blood Flow Metab. **28**(2), 242–250 (2008)

Part VI
Factors Affecting Biodistribution and Their Consequences

Chapter 17: Size-, Shape- and Charge-dependent Pharmacokinetics of Radiolabeled Nanoparticles
Chapter 18: PEGylation and the Similar
Chapter 19: Excretion and Clearance

In this part, radiolabeled nanoparticles are at most the radionuclide labeled nanomaterials with various sizes, shapes, charges, and hydrophilicity and affinity for hard or soft corona proteins in the plasma. If the readers understand the effects of the factors affecting the in vivo fates of the nanomaterials, then the biodistribution and final disposal of radionanomaterials are easily predicted. What really matters are the lack of knowledge of the effects of each factor affecting the biodistribution of nanomaterials. If the procedures of surface modification and radiolabeling are standardized and production of size-varied, shape-characterized, charge-measured and variously hydrophilized with PEGs or zwitterions are to be realized, then the consequences of these factors and further corona modification of these radionanomaterials are to be examined. The easy and standardized surface modification and acquisition of homogenous final products of radionanomaterials will enable us to understand the effects of the factors just like making multidimensional periodic tables to explain the in vivo behavior of radionanomaterials.

Fortunately, the traceability of radionanomaterials in vivo in animals first and then in humans later will greatly increase the chances of reaching the goal of the most desired combination of factors to yield the best product as reasonably fabricable. Chapter 17 explained the effect of factors in common for any nanomaterials such as size, shape, and charge. Chapter 18 explained the effect of hydrophilization using PEGs and zwitterions. Further subtle effect of corona wrapping of PEGylated size, shape, and charge-controlled nanomaterials in vivo was touched upon in every chapter, if systemically injected, upon the biodistribution of nanomaterials. Corona wrapping of radionanomaterials is to be examined in a similar setting of experiments. Chapter 19 finally summarized the clearance and excretion of nanomaterials

in the literature and emphasized that the previously accepted bias that some nanomaterials would stay somewhere in the body permanently is very often incorrect. The readers are recommended to refer to Chap. 4 about the recently observed finding that graphene oxides are metabolized and excreted. Renal excretion is well elucidated, and hepatobiliary excretion is being recently begun to be understood but the contribution of immune responses to the nanomedicines or radionanomedicines is yet beyond our explicit comprehension. After reading Chap. 19, the readers cannot but move forward to the next part of "immune response to nanomaterials".

Chapter 17
Size-, Shape- and Charge-Dependent Pharmacokinetics of Radiolabeled Nanoparticles

Feng Chen

Abstract The pharmacokinetics (PK) of nanoparticles is believed to be controlled by a complex array of interrelated physicochemical and biological factors, and an in-depth knowledge of the nanoparticle-organ interaction is critical for not only the nanoplatform design but also its potential clinical translation. Since, it largely defines their in vivo performance and potential toxicity. It is generally accepted that the biodistribution of nanoparticle is determined by the hydrodynamic size, shape, surface chemistry, in vivo stability and the administration route of the injected nanoparticles. The optimal characteristics for the nanoparticle, to be used in the clinical field, is being investigated and not yet clearly known. So far, highly sensitive and quantitative nuclear imaging is perhaps the best tool for assessing the PK profile of radiolabeled nanoparticles in vivo. However, since nuclear imaging technique detects the radioisotopes but not the nanoparticles themselves, the radiolabeling technique and the in vivo stability of the radiolabeled nanoparticles are critical and needs to be well addressed to achieve a reliable evaluation of nanoparticle fate in vivo.

17.1 Introduction

The last three decades have witnessed rapid advances in not only controlling the synthesis and surface modification of nanoparticles with varied size, shape and surface charge [1–6], but also better understanding of nanoparticle-cell interactions [7–14]. However, due to the complexity of the in vivo system and lack of reliable non-invasive, highly sensitive and quantitative imaging tools, challenges still exist when investigating the nanoparticle-organ interaction and visualizing the impact of differences in nanoparticle size, shape and surface charge on nanoparticle's pharmacokinetics (PK). The PK of nanoparticles is believed to be controlled by a

F. Chen (✉)
Department of Radiology, Sloan Kettering Institute for Cancer Research, New York, NY 10065, USA
e-mail: chenf@mskcc.org

D. S. Lee (ed.), *Radionanomedicine*, Biological and Medical Physics, Biomedical Engineering, https://doi.org/10.1007/978-3-319-67720-0_17

complex array of interrelated physicochemical and biological factors, and an in-depth knowledge of the nanoparticle-organ interaction is critical for not only the nanoplatform design but also its potential clinical translation.

Semi-quantitative optical imaging technique has been the primary tool for accessing the PK of the nanoparticles in small animals. However, due to the limitation in tissue penetration depth, the influence of autofluorescence and light scattering, and the potential detachment of free organic dyes in vivo, achieving an accurate nanoparticle biodistribution over time can be quite challenging. For example, based on the ex vivo optical imaging of tissue slides, an early study showed liver, spleen and renal excretion of over 80 nm sized dye-conjugated spherical mesoporous silica nanoparticles (MSNs) after intravenous injection (i.v.) injection in ICR mice [15]. The study might require additional validation to rule out the possible leakage of the conjugated dyes since renal cut-off was generally believed to be around 5.5 nm (or less than 10 nm) [16]. Over-estimated tumor-to-organ ratios is another concern when using an optical imaging technique, since some organs, like liver, might absorb the emission light more than the tumor tissue even when performing the optical imaging ex vivo. Although other imaging modalities, such as Computed Tomography (CT) and Magnetic Resonance Imaging (MRI), are also available for whole body non-invasive imaging, they are not capable of providing a quantitative PK assessment.

So far, highly sensitive and quantitative nuclear imaging is perhaps the best tool for assessing the PK profile of radiolabeled nanoparticles in vivo [17–21]. Non-invasive nuclear imaging (such as positron emission tomography, or PET) of small animals could also allow for a serial imaging of live subjects, which obviates the need to sacrifice animals and minimizes inter-individual variations. Although previous review articles have summarized the effect of nanoparticle size, shape and surface chemistry on the biological system (in vivo) [2, 3, 22, 23], most of them have focused on PK of nanoparticles based on semi-quantitative optical imaging technique. Here in this chapter, we will provide an overview of size-, shape- and charge-dependent PK of the widely studied radiolabeled nanoparticles (such as silica nanoparticles, quantum dots, gold nanoparticles, etc.) accessed by using nuclear imaging technique.

17.2 Impact of Particle Size

It is generally accepted that the biodistribution of nanoparticle is determined by the hydrodynamic (HD) size, shape, surface chemistry, in vivo stability and the administration route of the injected nanoparticles [21]. It is worthy to mention that protein adsorption on nanoparticle surface after i.v. injection could dramatically increase the HD size, change the surface charge, cause aggregation, leading to dramatic alterations in their fate in vivo. Studies also suggested that the extent of non-specific binding (or adsorption) of proteins in the bloodstream is highly dependent on the nanoparticle size, curvature, hydrophobicity, surface charge, etc.

[24, 25]. Although numerous pre-clinical research papers on the PK of nanoparticles with varied sizes have been published during the last 30 years, conclusions drawn by a specific nanoplatform (or in a specific animal model) might not be easily applied to the others. Researchers still rely on extensive experiments to select the best size or size range for their given project. Considering that most of the previous review articles only covered the general PK of nanoparticles with an HD size greater than 10 nm [22], and multi-functional renal clearable nanoparticles have attracted increasing interests recently [26, 27], PK of radiolabeled nanoparticles with a less than 10 nm HD size will be our main focus in the following sections.

17.2.1 Radiolabeled Silica Nanoparticles

Silica (or silicon dioxide) is "generally recognized as safe" by the US Food and Drug Administration (FDA) (ID Code: 14808-60-7) [28]. For more than 30 years, scientists all over the world have been focusing on the engineering pre-clinical applications of silica-based nanoparticles in cancer detection and treatment [29–32]. However, it was not until year 2014 that the nanomedicine community started to celebrate the first-in-human clinical trial of ultrasmall fluorescent dye-encapsulated silica PET-optical hybrid nanoparticles (also known as Cornell dots, or C dots) [33]. The clinical translation history of C dot involved great efforts in optimizing the particle size, surface functionalities, surface charge, particle manufacturing and stability (shelf-life), radiolabeling techniques, PK (especially minimizing the liver/spleen uptake and maintaining bulk renal clearance) study, toxicity, in vitro/in vivo (small and large animal) tumor targeting efficacy studies, etc. [33–36], and should serve a great example when explaining how the size, surface chemistry could affect the PK of silica nanoparticles and their clinical translation.

Developed by Wiesner and co-workers in 2005, the first dye-encapsulated silica nanoparticles were created by using a modified Stöber method, and had a physical size of 20–30 nm [37]. Although no in vivo PK study was mentioned in that early work, high liver, spleen uptake and no renal clearance were expected due to the >10 nm particle size. Great efforts were later devoted in engineering of dye-encapsulated silica nanoparticle with efficient urinary excretion by introducing two major upgrades [34] (Fig. 17.1a). Firstly, the hydrodynamic (HD) size was tuned down to <10 nm. Secondly, nanoparticles were covalently coated with methoxy-terminated poly(ethylene glycol) chains (PEG, ~0.5 kDa) to prevent aggregation and opsonization in vivo. Dramatic difference in nanoparticle biodistribution after i.v. injection was observed for particle with and without PEGylation (Fig. 17.1b). Results showed a dominant liver and spleen uptake for silica nanoparticles with no PEGylation (highly negatively charged surface), while bulk renal clearance and significant bladder uptake was observed for the same particle with a PEGylation (neutral surface charge) (Fig. 17.1b). The study further compared the whole body biodistribution pattern and clearance rate of silica nanoparticles with two different HD sizes. As expected, smaller sized silica particle showed

a fast, greater renal excretion, and shorter blood circulation half-life. No radioactive tag was conjugated to these particles, and all of estimations were purely based on optical imaging and quantification in this research.

To better quantify the PK profile of silica nanoparticles and ensure a specific tumor active targeting in vivo, two years later, the same group reported the systematic pre-clinical study in both small and large animals by further upgrading their platform with cRGDY (small peptides that target integrin $\alpha_v\beta_3$ from human melanoma) and radioiodine (^{124}I, $t_{1/2}$ = 4.2 days), forming the first generation of tumor-targeting C dots [35]. The final HD size was well-controlled to be around 7 nm with about 6–7 cRGDY ligands in each C dot. Systematic in vitro receptor-binding studies showed high and specific binding affinity of ^{124}I–cRGDY–PEG–C dots. In vivo tumor targeting, biodistribution and clearance studies were then performed in M21 tumor xenograft models. When compared with small peptides, which usually have less than 10 min blood circulation half-life, ^{124}I–cRGDY–PEG–C dots showed a nearly 6 h half-life in vivo. Efficient renal excretion was found in both targeted and non-targeted groups, with nearly 50%ID excreted within 24 h and over 70%ID by 96 h. Whole body PET imaging revealed a 3-fold higher nanoparticle uptake in M21 tumors in the targeted group than the

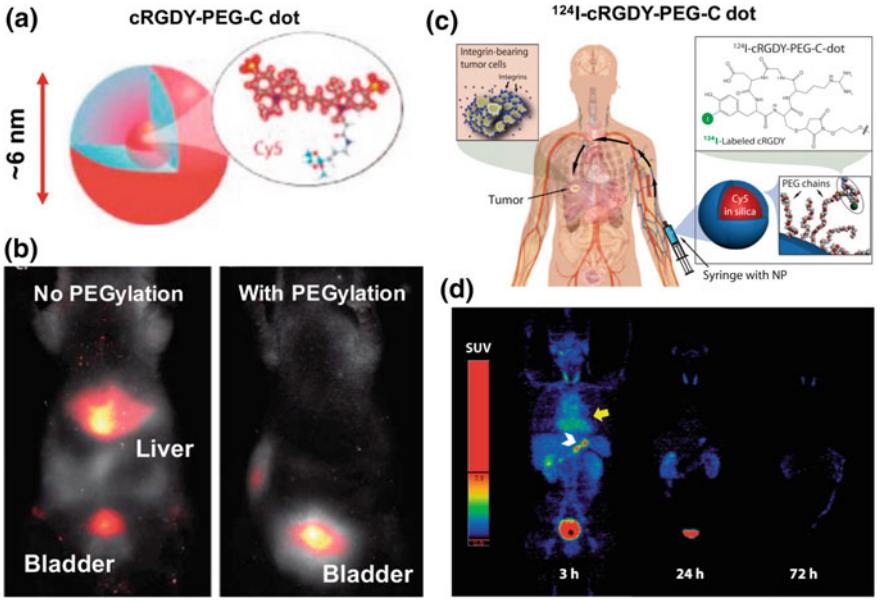

Fig. 17.1 **a** A schematic illustration of C dots. **b** In vivo optical imaging showing the differences in the biodistribution of non-PEGylated (left) and PEGylated (right) C dots. **c** A schematic illustration of using ^{124}I–cRGDY–PEG–C dots as hybrid (PET-optical) imaging probes in a human patient. **d** Maximum intensity projection PET images at 3, 24, and 72 h after i.v. injection of ^{124}I–cRGDY–PEG–C dots in a human patient. Reproduced with permission from [33, 34]

non-targeted group (in M21L tumor mice). In vivo optical imaging was also performed to show their potential in local and regional lymph node mapping.

In 2010, FDA approved C dots as the Investigational New Drug (IND) for first-in-human clinical trial studies (Fig. 17.1c). The Phase 1 safety study of ^{124}I–cRGDY–PEG–C dots in five human patients with metastatic melanoma was led by Dr. Michelle Bradbury of Memorial Sloan Kettering Cancer Center [33]. Systematic investigation showed relatively low tissue activities in most of the patients. Whole body tracer clearance half-life was estimated to range from 13 to 21 h with no notable accumulation observed in the Reticuloendothelial system (RES) (Fig. 17.1d). Radiation dosimetry study further showed an average effective dose of 0.183 ± 0.065 mSv/MBq, which was comparable to the estimated values from their previous preclinical data (∼0.157 mSv/MBq) [35]. Although the tracer was not yet optimized for active tumor targeting, lesion uptake and localization were seen in several patients. Specific tracer localization in liver metastasis was also observed in one of the patients. Multimodality (PET/MRI) imaging also showed the accumulation of ^{124}I–cRGDY–PEG–C dots in a pituitary lesion in one patient. The same tracer also showed high and retained uptake in both renal cortices over several days in one patient. Renal function assessment study showed no substantially change of average blood urea nitrogen and creatinine concentrations over the 2-week study interval, indicating that renal function was unaffected by the C dot tracer. No changes in liver function were found either. These first-in-human results clearly suggest safe use and great potential of ^{124}I–cRGDY–PEG–C dots in human cancer diagnostics. Besides optimizing the clearance profiles and the in vivo targeting efficacy, great efforts have also been devoted to the manufacturing of a newer generation Cornell prime dots, or C′ dots, with better reproducibility in a water-based environment [38, 39]. Both the pre-clinical and clinical translation of the newer generation C′ dots are actively ongoing.

For radiolabeled silica nanoparticles with a HD size greater than 10 nm, they usually share a quite similar biodistribution pattern with a rapid, high and non-specific particle accumulation in mouse RES organs (e.g., liver and spleen). For example, in 2013, Cai and his group reported the first example of in vivo tumor vasculature-targeting TRC105-conjugated and ^{64}Cu-labeled MSN (HD: >150 nm, surface charge: about-3 mV) in a murine breast cancer model (4T1) [40]. MSN was surface modified step-by-step with PEG, radio-chelator ((S)-2-(4-isothiocyanatobenzyl)-1,4,7-triazacyclononane-1,4,7-triacetic acid, or p-SCN–Bn–NOTA), and vasculature targeting full antibody (i.e., TRC105) before radiolabeled with copper-64 (^{64}Cu, $t_{1/2}$ = 12.6 h). Systematic in vivo tumor targeting studies demonstrated the specific accumulation of ^{64}Cu–NOTA–MSN–PEG–TRC105 at 4T1 tumor site (∼5%ID/g) with the liver uptake estimated to be the highest of 16%ID/g (Fig. 17.2a). In a follow-up study, water-soluble photothermally sensitive copper sulfide nanoparticles were encapsulated in biocompatible mesoporous silica shells, followed by multi-step surface engineering to form theranostic nanoparticles named ^{64}Cu–NOTA–CuS@MSN–PEG–TRC105 [41]. The newly designed multi-functional nanoplatform showed a slightly improved active 4T1 tumor targeting efficacy and two times higher liver uptake than the pure MSN structure [40], possibly

due to the complexity of the core@shell structure and the reduced stability in vivo (Fig. 17.2b). By creating a big cavity inside each MSN, and functionalizing the particle with organic dyes, targeting antibody and radioisotopes, Cai and his group later developed a hollow MSN (or HMSN) based nanoconjugate, and demonstrated a significantly enhanced tumor active targeting and drug delivery efficacy (Fig. 17.2c) [42]. Quantitative PET imaging study showed an over 3-fold higher tumor uptake in the target area when compared with the non-targeted group, making ^{64}Cu–NOTA–HMSN–ZW800–TRC105 one of the few vasculature targeting nanoparticles with ~10%ID/g tumor uptake. With the presence of hollow space inside each HMSN, doxorubicin-loading capacity was 3–5 times higher when compared with pure MSN. The liver and spleen uptake was as high as the previously reported MSN counterparts [40, 43]. Instead of using a traditional chelator-based radiolabeling technique, the same group also developed a chelator-free method to stably label porous silica nanoparticles with zirconium-89 (^{89}Zr, $t_{1/2}$ = 78 h) [44]. Using such technique, the authors demonstrated the feasibility of creating a self-destructible and biodegradable mesoporous silica (bMSN) drug carrier which was intrinsically labeled with ^{89}Zr and conjugated with antibody for targeting the tumor vasculature (Fig. 17.2d) [45]. Chelator-free ^{89}Zr labeling demonstrated excellent yield and in vivo stability with marginal ^{89}Zr detachment and bone uptake. Careful tailoring of the synthesis of [^{89}Zr]bMSN–PEG–TRC105 also resulted in excellent CD105 specificity, which was confirmed by extensive in vivo and ex vivo testing. Vascular targeting exhibited greater than threefold enhancement in absolute tumor uptake and normal tissue contrast, when compared with enhanced permeability and retention (EPR) dependent uptake of the nanoconjugates. Dominant liver and spleen uptake was observed as well. Similar PK (relatively short blood circulation half-life, no renal clearance, dominant liver and spleen uptake, low tumor accumulation rate) was repeatedly found with MSNs labeled with other radioisotopes, such as radioarsenic [46] and titanium-45 [47]. MSNs were conjugated with different targeting ligands [43, 48], and other radiolabeled nanoparticles, such as nanographene [49–51], iron oxide nanoparticles [52, 53], Gd_2O_2S:Eu [54, 55], reduced graphene oxide-iron oxide nanoparticles [56], and many others [57–61]. All these radiolabeled nanoparticles had a greater than 10 nm HD size. In the next section, we will review the size-dependent PK of radiolabeled quantum dots.

17.2.2 Radiolabeled Quantum Dots

Fluorescent semiconductor quantum dots (QDs) have attracted tremendous attention in the field of biomedical imaging over the last 3 decades due to their superior optical properties over conventional organic dyes [62–69]. As mentioned above, successful surface protection (i.e., PEGylation) could neutralize the surface negative charge and improve in vivo stability of radiolabeled silica nanoparticles, leading to a prolonged blood circulation half-life and reduced RES uptake. This was

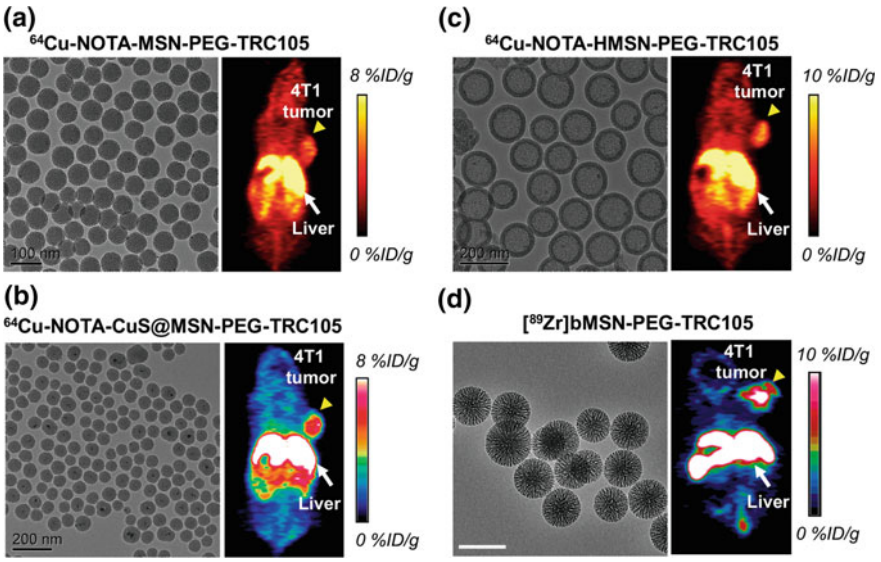

Fig. 17.2 In vivo PET imaging studies of larger sized radiolabeled silica or core@shell silica nanoparticles. **a** ^{64}Cu–NOTA–MSN–PEG–TRC105. **b** ^{64}Cu–NOTA–CuS@MSN–PEG–TRC105. **c** ^{64}Cu–NOTA–HMSN–PEG–TRC105. **d** [^{89}Zr]bMSN–PEG–TRC105. The 4T1 tumors were marked with yellow arrow headsman: mesoporous silica nanoparticle. Reproduced with permission from [40–42, 45]

confirmed by many other studies on the in vivo fate of QDs [67, 70–73]. For example, Choi et al. reported the ability to control circulation half-life, organ- and even tissue-selective biodistribution, and elimination route of dihydrolipoic acid (DHLA)/PEG modified QDs (i.e., QD@DHLA–PEG$_n$, n = 2–22) by altering the length of PEG chains [74]. Results showed that QD@DHLA–PEG$_2$ (HD = 5.1 nm) accumulated primarily in the liver (Fig. 17.3a), while the majority of QD@DHLA–PEG$_3$ (HD = 5.3 nm) ended up in the kidney and bladder (Fig. 17.3b). QDs with DHLA–PEG$_4$ coating (HD = 5.6 nm) had accelerated body excretion via the liver and kidneys (Fig. 17.3c). In addition, uptake of QDs in the pancreas was only observed when QDs were coated with DHLA–PEG$_8$ (HD = 6.5 nm) and DHLA–PEG$_{14}$ (HD = 8.7 nm) (Fig. 17.3d, e). QD@DHLA–PEG$_{22}$ (HD = 16 nm) exhibited poor clearance and were primarily detected in the vasculature at 4 h post-injection, with delayed excretion through renal and hepatic routes (Fig. 17.3f). Although distribution of QDs in different organs can be visualized based on whole body or ex vivo fluorescence imaging [74], accurate quantification of individual organ uptake over time might be challenging due to the prominent and variable background autofluorescence and absorbance/scattering in blood and tissues.

In 2007, using serial non-invasive small animal PET imaging for a more accurate assessment of the PK of QDs, Gambhir et al. reported for the first time the quantitative biodistribution of commercially available CdSe QDs (>10 nm) labeled with

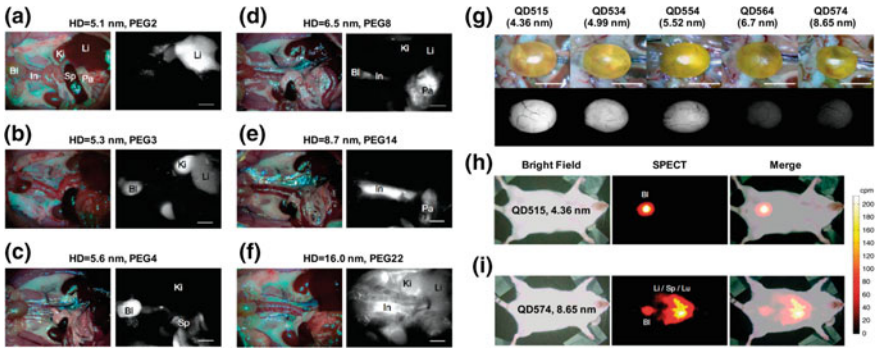

Fig. 17.3 Optical imaging based biodistribution study of QDs with varied PEG chain length and hydrodynamic (HD) size. **a** HD: 5.1 nm, PEG2. **b** HD: 5.3 nm, PEG3. **c** HD: 5.6 nm, PEG4. **d** HD: 6.5 nm, PEG8. **e** HD: 8.7 nm, PEG14. **f** HD: 16.0 nm, PEG22. **g** Renal clearable cutoff study of QDs. Top: color photos of bladders. Bottom: fluorescence images at 4 h post injection of QDs with varied HD sizes (4–8 nm). SPECT imaging of ^{99m}Tc-labled. **h** QD515 (HD: 4.36 nm) and **i** QD574 (HD: 8.65 nm). Reproduced with permission from [16, 74]

^{64}Cu [75]. It was found that radiolabeled QDs with a larger HD size had a faster accumulation in both the liver and spleen, while PEGylated QDs exhibited slightly slower rate of accumulation in these organs. The liver (27.4–38.9%ID/g) and spleen (8.0–12.4%ID/g) uptake of ^{64}Cu-labeled QD800 ($\sim$21 nm) and QD525 ($\sim$12 nm) were found to be quite close. A much higher liver ($\sim$50%ID/g) uptake was later reported in RGD-functionalized, ^{64}Cu labeled QD705 in U87MG tumor-bearing mice, possibly due to the larger particle size and relatively shorter blood circulation half-life [76]. No evidence of QDs renal clearance was reported in either of these early studies [75, 76].

A few months after this report, Choi et al. reported the first extensive size-dependent renal clearance study of ultrasmall (HD size range: 4–8 nm) radiolabeled QDs, and concluded that renal cut-off for spherically shaped QDs coated with cysteine should be about 5.5 nm (Fig. 17.3g, f) [16]. Since then, many studies have confirmed that QDs with HD sizes larger than this renal clearance cutoff usually ended up in the liver and spleen, with only very limited renal clearance over the study period [77, 78]. However, the exact renal cut-off for a specific ultrasmall nanoparticle might be different considering the differences in surface chemistry, shape, blood circulation half-life of the testing nanoparticle. For example, with a larger than 5.5 nm HD size, C dots (HD: 6–7 nm) still showed a dominant renal clearance both in small animals and human patients [33–35]. A general renal cut-off of solid nanoparticle is believed to be less than 10 nm.

It is worthwhile to note that physical size of nanoparticle is not the only parameter that determines the shifting of biodistribution from dominant RES uptake to bulk renal excretion. The key prerequisite is preventing the aggregation of nanoparticles after i.v. injection by introducing a robust surface protection. For example, despite its HD size smaller than 5.5 nm, aqueous QD705 still showed a

rapid accumulation in the liver (up to 30%ID/g) [79], clearly indicating a concerning aggregation in vivo.

17.2.3 Radiolabeled Gold and Copper Sulfide Nanoparticles

Ultra-small gold nanoparticles (AuNPs) have also been developed as radiological and luminescence imaging contrast agents [27, 80–82] Gold-198 (^{198}Au) intrinsically labeled, glutathione-coated 2–3 nm sized AuNPs (or GS–[^{198}Au]AuNP) were found to allow over 50% of the particles to be excreted in the urine within 24 h post injection (Fig. 17.4a) [83]. A dynamic PET imaging of ^{64}Cu–NOTA–Au–GS with a similar HD size showed a rapid renal clearance with an over 75%ID within the first day post-injection [84] (Fig. 17.4b). Interestingly, based on dynamic PET imaging the elimination half-life of ^{64}Cu–NOTA–Au–GS was estimated to be extremely short of <6 min, which was over 130 times shorter than previously reported similar nanoparticles based on quantification using optical imaging [83, 85]. PEGylation was found to be a useful surface modification method for ultrasmall Au nanoparticles. In one study, PEGylated AuNPs (PEG molecular weight: 1 kDa) were shown to have three times higher passive targeting efficacy when compared with non-PEGylated GS-AuNPs [81]. Although more nuclear imaging-based quantitative validations are warranted to confirm the above findings, a recent study showed that renal clearance depended on the density found by comparing heavier ultrasmall GS-coated gold with lighter silver nanoparticles [86]. Results showed that the renal clearance decreased exponentially in the early elimination phase with an increase in particle density and that tumor targeting is linearly dependent on the particle density. The authors further suggested that such density dependence of the in vivo behavior might very likely originate from density-dependent margination.

Similarly to the intrinsic labeling of ^{198}Au with ultrasmall Au nanoparticles, researchers also developed renal clearable (HD <6 nm) ^{64}Cu-labeled CuS nanoparticles (i.e., [^{64}Cu]CuS). These nanoparticles efficiently absorbed near-infrared light for photothermal ablation therapy, and were visible on PET imaging [87]. About 95%ID of i.v. injected [^{64}Cu]CuS was found to be excreted intact through the kidneys within 24 h, while the RES organs showed only minimal retention of the radioactivity. These findings were dramatically different from the older version of [^{64}Cu]CuS, which had a physical size of 11 nm, and showed dominant liver and spleen uptake after i.v. injection [88]. Although the passive tumor uptake of [^{64}Cu]CuS in 4T1 tumors was still quite low, the authors showed definitely a proof-of-concept study of photothermal therapy using such theranostic nanoparticles.

Renal clearable functional nanoparticles showed greater potential for future cancer imaging and therapy, however, great challenges still remain to find methods to further functionalize the surface with tumor-targeting ligands and better balance

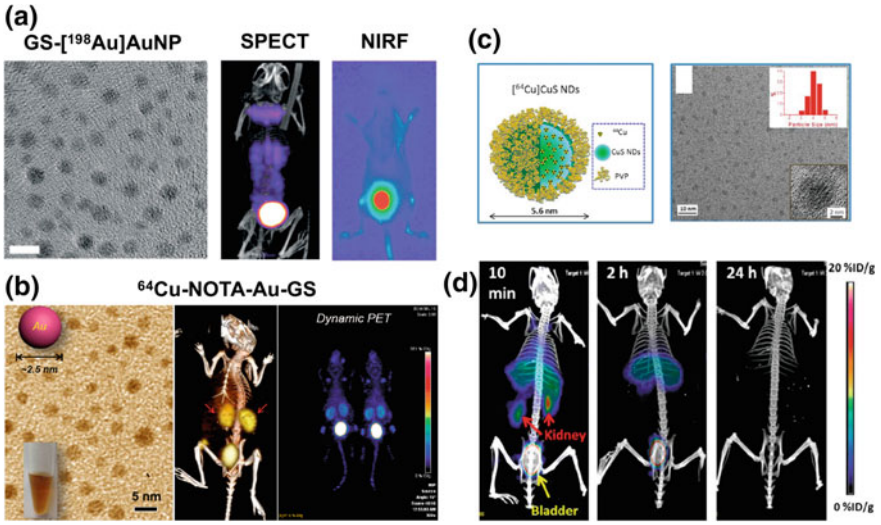

Fig. 17.4 **a** From left to right: a TEM image of ultrasmall glutathione-coated GS-[^{198}Au]AuNP, a SPECT and near-infrared fluorescence imaging (NIRF) of GS-[^{198}Au]Au nanoparticle (NP) at 1 h post-injection. **b** From left to right: a TEM image of ultrasmall Au–GS, a PET/CT and dynamic PET imaging of ^{64}Cu–NOTA–Au–GS. **c** (Left) A schematic illustration of polyvinylpyrrolidone (PVP) coated ultrasmall [^{64}Cu]CuS nanodots. (Right) A TEM image of [^{64}Cu]CuS nanodots. **d** A PET imaging of [^{64}Cu]CuS nanodots in mice at 10 min, 2 and 24 h post-injection. TEM: transmission electron microscopy. Reproduced with permission from [84, 85, 87]

between renal clearance and blood circulation time. Only by addressing these problems we can further enhance the in vivo tumor targeting efficacy of renal clearable nanoparticles. For PK investigations of other radiolabeled nanoparticles, such as iron oxide nanoparticle, upconversion nanoparticle, readers are advised to refer to reviews or articles [89, 90].

17.3 Impact of Particle Shape and Surface Charge

Early work on polymer-based nanoparticles have shown the effect of nanoparticle's shape on the circulation time, efficacy of drug delivery as well as targeting efficacy to the lungs and brain [91–93]. Although general conclusions about how to select the optimal shape for certain applications could be drawn from previous review articles [22, 94], it is still not clear how these could be applied to other nanoplatforms or in other animal models. So far, very few systematic studies were reported on shape-dependent PK (or tumor-targeting) using radiolabeled nanoparticles. Using intravital microscopy and QDs (HD size: 20–25 nm) and single-walled carbon nanotubes (SWNTs) ($\sim$200 nm in length) with similar charge, surface coating, and density as the model nanoparticles, researchers have shown a highly

complex dynamics of shape-dependent tumor extravasation [95]. For example, significantly more extravasation was detected for QDs in the LS174T when compared with U87MG, where the opposite result was observed for the SWNTs (Fig. 17.5). Although in vitro simulated diffusion experiments were carried out to provide a rationale for such findings, the exact reason behind such surprising geometrical dependence of nanoparticles in tumor extravasation remained to be elucidated in future studies, and none of these studies used radiolabeled nanoparticles to confirm the main findings.

The charge of nanoparticle surface coating could have a profound effect on nanoparticles' PK due to the adsorption of serum proteins and the change of HD size in vivo. For example, studies showed that net anionic or cationic charges are usually associated with an increase in the HD size [96, 97], leading to rapid RES uptake in vivo. By coating QDs with a zwitterionic surface, Choi et al. demonstrated that undesirable serum protein adsorption could be prevented to obtain a series of QDs with extremely small HD size [16]. Similar results were reported

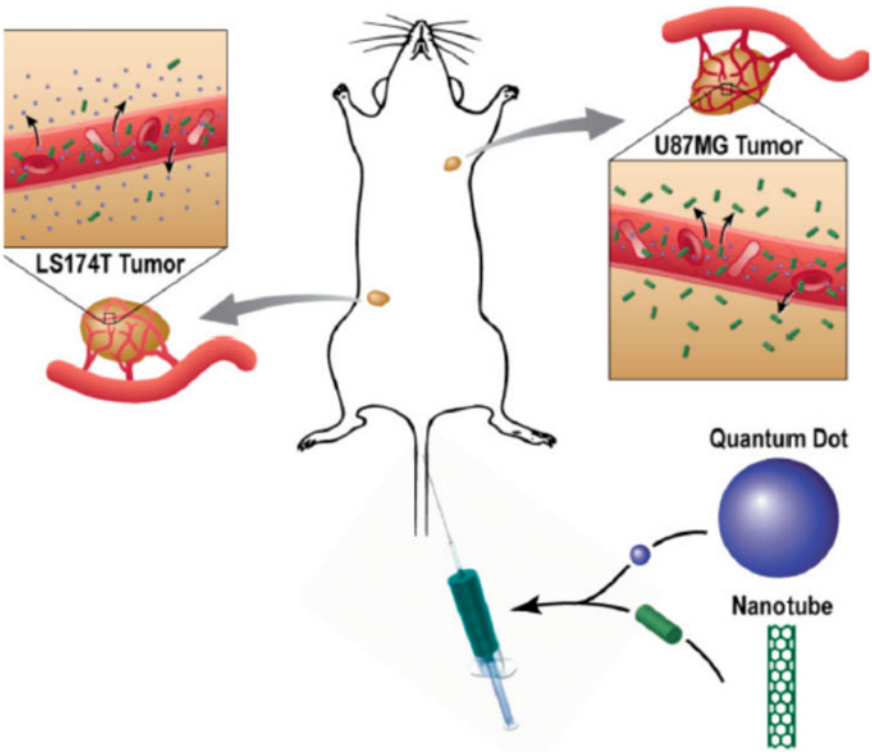

Fig. 17.5 A schematic illustration showing that QDs extravasate from the LS174T tumor but not the U87MG tumor, whereas SWNTs extravasate from the U87MG tumor but only minimally from the LS174T tumor. QD: quantum dot, T: single walled carbon nanotube. Reproduced with permission from [95]

when developing renal clearable gold nanoparticles [83, 85]. PEGylation has been demonstrated to be another great strategy to prevent the aggregation of ultrasmall C dots or >100 nm sized MSN in vivo [34, 45].

17.4 Conclusion

The PK of nanoparticles largely define their in vivo performance and potential toxicity, and needs to be elucidated before clinical translation. In this chapter, we summarized the size-, shape- and surface charge-dependent PK of radiolabeled nanoparticles with our special focus on renal clearable radiolabeled silica, quantum dots, gold and copper sulfide nanoparticles. Since nuclear imaging technique detects the radioisotopes but not the nanoparticles themselves, the radiolabeling technique and the in vivo stability of the radiolabeled nanoparticles are critical and needs to be well addressed to achieve a reliable evaluation of nanoparticle fate in vivo. With many desirable properties, we believe actively tumor-targeting nanoparticles with predictable and controllable clearance pathway hold tremendous promises for non-invasive cancer detection, treatment management and response monitoring in the near future.

References

1. B.H. Kim, M.J. Hackett, J. Park, T. Hyeon, Synthesis, characterization, and application of ultrasmall nanoparticles. Chem. Mater. **26**(1), 59–71 (2014)
2. Y. Chen, H. Chen, J. Shi, In vivo bio-safety evaluations and diagnostic/therapeutic applications of chemically designed mesoporous silica nanoparticles. Adv. Mater. **25**(23), 3144–3176 (2013)
3. F. Tang, L. Li, D. Chen, Mesoporous silica nanoparticles: synthesis, biocompatibility and drug delivery. Adv. Mater. **24**(12), 1504–1534 (2012)
4. B. Zhou, B. Shi, D. Jin, X. Liu, Controlling upconversion nanocrystals for emerging applications. Nat. Nanotechnol. **10**(11), 924–936 (2015)
5. C. Walkey, E.A. Sykes, W.C. Chan, Application of semiconductor and metal nanostructures in biology and medicine. Hematology **2009**, 701–707 (2009)
6. A. Burns, H. Ow, U. Wiesner, Fluorescent core-shell silica nanoparticles: towards "lab on a particle" architectures for nanobiotechnology. Chem. Soc. Rev. **35**(11), 1028–1042 (2006)
7. B.D. Chithrani, W.C.W. Chan, Elucidating the mechanism of cellular uptake and removal of protein-coated gold nanoparticles of different sizes and shapes. Nano Lett. **7**(6), 1542–1550 (2007)
8. W. Jiang, B.Y.S. Kim, J.T. Rutka, W.C.W. Chan, Nanoparticle-mediated cellular response is size-dependent. Nat. Nanotechnol. **3**(3), 145–150 (2008)
9. H. Jin, D.A. Heller, R. Sharma, M.S. Strano, Size-dependent cellular uptake and expulsion of single-walled carbon nanotubes: single particle tracking and a generic uptake model for nanoparticles. ACS Nano. **3**(1), 149–158 (2009)
10. C.D. Walkey, J.B. Olsen, H. Guo, A. Emili, W.C.W. Chan, Nanoparticle size and surface chemistry determine serum protein adsorption and macrophage uptake. J. Am. Chem. Soc. **134**(4), 2139–2147 (2012)

11. L. Shang, K. Nienhaus, G.U. Nienhaus, Engineered nanoparticles interacting with cells: size matters. J. Nanobiotechnology **12**, 5 (2014)
12. Y. Jiang, S.D. Huo, T. Mizuhara, R. Das, Y.W. Lee, S. Hou et al., The interplay of size and surface functionality on the cellular uptake of sub-10 nm gold nanoparticles. ACS Nano. **9** (10), 9986–9993 (2015)
13. J. Jiang, G. Oberdoerster, A. Elder, R. Gelein, P. Mercer, P. Biswas, Does nanoparticle activity depend upon size and crystal phase? Nanotoxicology **2**(1), 33–42 (2008)
14. S. Zhang, J. Li, G. Lykotrafitis, G. Bao, S. Suresh, Size-dependent endocytosis of nanoparticles. Adv. Mater. **21**(4), 419–424 (2009)
15. Q. He, Z. Zhang, F. Gao, Y. Li, J. Shi, In vivo biodistribution and urinary excretion of mesoporous silica nanoparticles: effects of particle size and PEGylation. Small **7**(2), 271–280 (2011)
16. H.S. Choi, W. Liu, P. Misra, E. Tanaka, J.P. Zimmer, B. Itty Ipe et al., Renal clearance of quantum dots. Nat. Biotech. **25**(10), 1165–1170 (2007)
17. H. Hong, Y. Zhang, J. Sun, W. Cai, Molecular imaging and therapy of cancer with radiolabeled nanoparticles. Nano Today **4**(5), 399–413 (2009)
18. S. Goel, F. Chen, E.B. Ehlerding, W. Cai, Intrinsically radiolabeled nanoparticles: an emerging paradigm. Small **10**(19), 3825–3830 (2014)
19. X. Sun, W. Cai, X. Chen, Positron emission tomography imaging using radiolabeled inorganic nanomaterials. Acc. Chem. Res. **48**(2), 286–294 (2015)
20. S. Goel, C.G. England, F. Chen, W. Cai, Positron emission tomography and nanotechnology: a dynamic duo for cancer theranostics. Adv. Drug. Deliv. Rev. **113**, 157–176 (2017)
21. H. Hong, F. Chen, W. Cai, Pharmacokinetic issues of imaging with nanoparticles: focusing on carbon nanotubes and quantum dots. Mol. Imaging Biol. **15**(5), 507–520 (2013)
22. A. Albanese, P.S. Tang, W.C. Chan, The effect of nanoparticle size, shape, and surface chemistry on biological systems. Annu. Rev. Biomed. Eng. **14**, 1–16 (2012)
23. D. Ling, N. Lee, T. Hyeon, Chemical synthesis and assembly of uniformly sized iron oxide nanoparticles for medical applications. Acc. Chem. Res. **48**(5), 1276–1285 (2015)
24. S.H. Lacerda, J.J. Park, C. Meuse, D. Pristinski, M.L. Becker, A. Karim et al., Interaction of gold nanoparticles with common human blood proteins. ACS Nano. **4**(1), 365–379 (2010)
25. H.S. Choi, S.L. Gibbs, J.H. Lee, S.H. Kim, Y. Ashitate, F. Liu et al., Targeted zwitterionic near-infrared fluorophores for improved optical imaging. Nat. Biotechnol. **31**(2), 148–153 (2013)
26. E.B. Ehlerding, F. Chen, W. Cai, Biodegradable and renal clearable inorganic nanoparticles. Adv. Sci. (Weinh). **3**(2), 1500223–1500231 (2016)
27. M. Yu, J. Zheng, Clearance pathways and tumor targeting of imaging nanoparticles. ACS Nano. **9**(7), 6655–6674 (2015)
28. http://www.fda.gov/Food/IngredientsPackagingLabeling/GRAS/SCOGS/ucm261095.htm
29. X. Ma, Y. Zhao, X.-J. Liang, Theranostic nanoparticles engineered for clinic and pharmaceutics. Acc. Chem. Res. **44**(10), 1114–1122 (2011)
30. D. Tarn, C.E. Ashley, M. Xue, E.C. Carnes, J.I. Zink, C.J. Brinker, Mesoporous silica nanoparticle nanocarriers: biofunctionality and biocompatibility. Acc. Chem. Res. **46**(3), 792–801 (2013)
31. K. Wang, X. He, X. Yang, H. Shi, Functionalized silica nanoparticles: a platform for fluorescence imaging at the cell and small animal levels. Acc. Chem. Res. **46**(7), 1367–1376 (2013)
32. S. Shi, F. Chen, W. Cai, Biomedical applications of functionalized hollow mesoporous silica nanoparticles: focusing on molecular imaging. Nanomedicine (Lond.) **8**(12), 2027–2039 (2013)
33. E. Phillips, O. Penate-Medina, P.B. Zanzonico, R.D. Carvajal, P. Mohan, Y. Ye et al., Clinical translation of an ultrasmall inorganic optical-PET imaging nanoparticle probe. Sci. Transl. Med. **6**(260), 260ra149 (2014)

34. A.A. Burns, J. Vider, H. Ow, E. Herz, O. Penate-Medina, M. Baumgart et al., Fluorescent silica nanoparticles with efficient urinary excretion for nanomedicine. Nano Lett. **9**(1), 442–448 (2009)
35. M. Benezra, O. Penate-Medina, P.B. Zanzonico, D. Schaer, H. Ow, A. Burns et al., Multimodal silica nanoparticles are effective cancer-targeted probes in a model of human melanoma. J. Clin. Invest. **121**(7), 2768–2780 (2011)
36. M. Benezra, E. Phillips, M. Overholtzer, P.B. Zanzonico, E. Tuominen, U. Wiesner et al., Ultrasmall integrin-targeted silica nanoparticles modulate signaling events and cellular processes in a concentration-dependent manner. Small **11**(14), 1721–1732 (2015)
37. H. Ow, D.R. Larson, M. Srivastava, B.A. Baird, W.W. Webb, U. Wiesner, Bright and stable core-shell fluorescent silica nanoparticles. Nano Lett. **5**(1), 113–117 (2005)
38. K. Ma, C. Mendoza, M. Hanson, U. Werner-Zwanziger, J. Zwanziger, U. Wiesner, Control of ultrasmall sub-10 nm ligand-functionalized fluorescent core–shell silica nanoparticle growth in water. Chem. Mater. **27**(11), 4119–4133 (2015)
39. K. Ma, D.H. Zhang, Y. Cong, U. Wiesner, Elucidating the mechanism of silica nanoparticle PEGylation processes using fluorescence correlation spectroscopies. Chem. Mater. **28**(5), 1537–1545 (2016)
40. F. Chen, H. Hong, Y. Zhang, H.F. Valdovinos, S. Shi, G.S. Kwon et al., In vivo tumor targeting and image-guided drug delivery with antibody-conjugated, radiolabeled mesoporous silica nanoparticles. ACS Nano. **7**(10), 9027–9039 (2013)
41. F. Chen, H. Hong, S. Goel, S.A. Graves, H. Orbay, E.B. Ehlerding et al., In vivo tumor vasculature targeting of CuS@MSN based theranostic nanomedicine. ACS Nano. **9**(4), 3926–3934 (2015)
42. F. Chen, H. Hong, S. Shi, S. Goel, H.F. Valdovinos, R. Hernandez et al., Engineering of hollow mesoporous silica nanoparticles for remarkably enhanced tumor active targeting efficacy. Sci. Rep. **4**, 5080 (2014)
43. F. Chen, T.R. Nayak, S. Goel, H.F. Valdovinos, H. Hong, C.P. Theuer et al., In vivo tumor vasculature targeted PET/NIRF imaging with TRC105(Fab)-conjugated, dual-labeled mesoporous silica nanoparticles. Mol. Pharm. **11**(11), 4007–4014 (2014)
44. F. Chen, S. Goel, H.F. Valdovinos, H. Luo, R. Hernandez, T.E. Barnhart et al., In vivo integrity and biological fate of chelator-free zirconium-89-labeled mesoporous silica nanoparticles. ACS Nano. **9**(8), 7950–7959 (2015)
45. S. Goel, F. Chen, S. Luan, H.F. Valdovinos, S. Shi, S.A. Graves et al., Engineering intrinsically zirconium-89 radiolabeled self-destructing mesoporous silica nanostructures for in vivo biodistribution and tumor targeting studies. Adv. Sci. (Weinh.) **3**(11), 1600122 (2016)
46. P.A. Ellison, F. Chen, S. Goel, T.E. Barnhart, R.J. Nickles, O.T. DeJesus et al., Intrinsic and stable conjugation of thiolated mesoporous silica nanoparticles with radioarsenic. ACS Appl. Mater. Interfaces **9**(8), 6772–6781 (2017)
47. F. Chen, H.F. Valdovinos, R. Hernandez, S. Goel, T.E. Barnhart, W. Cai, Intrinsic radiolabeling of Titanium-45 using mesoporous silica nanoparticles. Acta Pharmacol. Sin. **38**(6), 907–913 (2017)
48. S. Goel, F. Chen, H. Hong, H.F. Valdovinos, R. Hernandez, S. Shi et al., $VEGF_{121}$-conjugated mesoporous silica nanoparticle: a tumor targeted drug delivery system. ACS Appl. Mater. Interfaces **6**(23), 21677–21685 (2014)
49. S. Shi, C. Xu, K. Yang, S. Goel, H.F. Valdovinos, H. Luo et al., Chelator-free radiolabeling of nanographene: breaking the stereotype of chelation. Angew. Chem. Int. Ed. Engl. **56**(11), 2889–2892 (2017)
50. S. Shi, K. Yang, H. Hong, F. Chen, H.F. Valdovinos, S. Goel et al., VEGFR targeting leads to significantly enhanced tumor uptake of nanographene oxide in vivo. Biomaterials **39**, 39–46 (2015)
51. H. Hong, K. Yang, Y. Zhang, J.W. Engle, L. Feng, Y. Yang et al., In vivo targeting and imaging of tumor vasculature with radiolabeled, antibody-conjugated nanographene. ACS Nano. **6**(3), 2361–2370 (2012)

52. R. Chakravarty, H.F. Valdovinos, F. Chen, C.M. Lewis, P.A. Ellison, H. Luo et al., Intrinsically germanium-69-labeled iron oxide nanoparticles: synthesis and in-vivo dual-modality PET/MR imaging. Adv. Mater. **26**(30), 5119–5123 (2014)
53. F. Chen, P.A. Ellison, C.M. Lewis, H. Hong, Y. Zhang, S. Shi et al., Chelator-free synthesis of a dual-modality PET/MRI agent. Angew. Chem. Int. Ed. Engl. **52**(50), 13319–13323 (2013)
54. Y. Zhan, F. Ai, F. Chen, H.F. Valdovinos, H. Orbay, H. Sun et al., Intrinsically zirconium-89 labeled Gd2O2S: Eu nanoprobes for in vivo positron emission tomography and gamma-ray-induced radioluminescence imaging. Small **12**(21), 2872–2876 (2016)
55. F. Ai, S. Goel, Y. Zhan, H.F. Valdovinos, F. Chen, T.E. Barnhart et al., Intrinsically 89Zr-labeled Gd2O2S: Eu nanophosphors with high in vivo stability for dual-modality imaging. Am. J. Transl Res. **8**(12), 5591–5600 (2016)
56. C. Xu, S. Shi, L. Feng, F. Chen, S.A. Graves, E.B. Ehlerding et al., Long circulating reduced graphene oxide-iron oxide nanoparticles for efficient tumor targeting and multimodality imaging. Nanoscale **8**(25), 12683–12692 (2016)
57. L. Cheng, A. Kamkaew, H. Sun, D. Jiang, H.F. Valdovinos, H. Gong et al., Dual-modality positron emission tomography/optical image-guided photodynamic cancer therapy with chlorin e6-containing nanomicelles. ACS Nano. **10**(8), 7721–7730 (2016)
58. L. Cheng, A. Kamkaew, S. Shen, H.F. Valdovinos, H. Sun, R. Hernandez et al., Facile preparation of multifunctional WS2/WOx nanodots for chelator-free ^{89}Zr-labeling and in vivo PET imaging. Small **12**(41), 5750–5758 (2016)
59. S. Shi, B.C. Fliss, Z. Gu, Y. Zhu, H. Hong, H.F. Valdovinos et al., Chelator-free labeling of layered double hydroxide nanoparticles for in vivo PET imaging. Sci. Rep. **5**, 16930 (2015)
60. T. Liu, S. Shi, C. Liang, S. Shen, L. Cheng, C. Wang et al., Iron oxide decorated MoS_2 nanosheets with double PEGylation for chelator-free radiolabeling and multimodal imaging guided photothermal therapy. ACS Nano. **9**(1), 950–960 (2015)
61. H. Hong, J. Shi, Y. Yang, Y. Zhang, J.W. Engle, R.J. Nickles et al., Cancer-targeted optical imaging with fluorescent zinc oxide nanowires. Nano Lett. **11**(9), 3744–3750 (2011)
62. X. Michalet, F.F. Pinaud, L.A. Bentolila, J.M. Tsay, S. Doose, J.J. Li et al., Quantum dots for live cells, in vivo imaging, and diagnostics. Science **307**(5709), 538–544 (2005)
63. W.C. Chan, S. Nie, Quantum dot bioconjugates for ultrasensitive nonisotopic detection. Science **281**(5385), 2016–2018 (1998)
64. W. Cai, A.R. Hsu, Z.B. Li, X. Chen, Are quantum dots ready for in vivo imaging in human subjects? Nanoscale Res. Lett. **2**, 265–281 (2007)
65. X.G. Peng, L. Manna, W.D. Yang, J. Wickham, E. Scher, A. Kadavanich et al., Shape control of CdSe nanocrystals. Nature **404**(6773), 59–61 (2000)
66. J.K. Jaiswal, H. Mattoussi, J.M. Mauro, S.M. Simon, Long-term multiple color imaging of live cells using quantum dot bioconjugates. Nat. Biotechnol. **21**(1), 47–51 (2003)
67. X. Gao, Y. Cui, R.M. Levenson, L.W. Chung, S. Nie, In vivo cancer targeting and imaging with semiconductor quantum dots. Nat. Biotechnol. **22**(8), 969–976 (2004)
68. J.K. Jaiswal, E.R. Goldman, H. Mattoussi, S.M. Simon, Use of quantum dots for live cell imaging. Nat. Methods **1**(1), 73–78 (2004)
69. S. Kim, Y.T. Lim, E.G. Soltesz, A.M. De Grand, J. Lee, A. Nakayama et al., Near-infrared fluorescent type II quantum dots for sentinel lymph node mapping. Nat. Biotechnol. **22**(1), 93–97 (2004)
70. I.L. Medintz, H.T. Uyeda, E.R. Goldman, H. Mattoussi, Quantum dot bioconjugates for imaging, labelling and sensing. Nat. Mater. **4**(6), 435–446 (2005)
71. H.S. Choi, W. Liu, F. Liu, K. Nasr, P. Misra, M.G. Bawendi et al., Design considerations for tumour-targeted nanoparticles. Nat. Nanotechnol. **5**(1), 42–47 (2010)
72. W. Cai, D.W. Shin, K. Chen, O. Gheysens, Q. Cao, S.X. Wang et al., Peptide-labeled near-infrared quantum dots for imaging tumor vasculature in living subjects. Nano Lett. **6**(4), 669–676 (2006)
73. B. Ballou, B.C. Lagerholm, L.A. Ernst, M.P. Bruchez, A.S. Waggoner, Noninvasive imaging of quantum dots in mice. Bioconjug. Chem. **15**(1), 79–86 (2004)

74. H.S. Choi, B.I. Ipe, P. Misra, J.H. Lee, M.G. Bawendi, J.V. Frangioni, Tissue- and organ-selective biodistribution of NIR fluorescent quantum dots. Nano Lett. **9**(6), 2354–2359 (2009)
75. M.L. Schipper, Z. Cheng, S.W. Lee, L.A. Bentolila, G. Iyer, J. Rao et al., microPET-based biodistribution of quantum dots in living mice. J. Nucl. Med. **48**(9), 1511–1518 (2007)
76. W. Cai, K. Chen, Z.B. Li, S.S. Gambhir, X. Chen, Dual-function probe for PET and near-infrared fluorescence imaging of tumor vasculature. J. Nucl. Med. **48**(11), 1862–1870 (2007)
77. J.A. Fitzpatrick, S.K. Andreko, L.A. Ernst, A.S. Waggoner, B. Ballou, M.P. Bruchez, Long-term persistence and spectral blue shifting of quantum dots in vivo. Nano Lett. **9**(7), 2736–2741 (2009)
78. K.-T. Yong, I. Roy, H. Ding, E.J. Bergey, P.N. Prasad, Biocompatible near-infrared quantum dots as ultrasensitive probes for long-term in vivo imaging applications. Small **5**(17), 1997–2004 (2009)
79. R.S. Yang, L.W. Chang, J.P. Wu, M.H. Tsai, H.J. Wang, Y.C. Kuo et al., Persistent tissue kinetics and redistribution of nanoparticles, quantum dot 705, in mice: ICP-MS quantitative assessment. Environ. Health Perspect. **115**(9), 1339–1343 (2007)
80. C. Zhou, M. Long, Y. Qin, X. Sun, J. Zheng, Luminescent gold nanoparticles with efficient renal clearance. Angew. Chem. **123**(14), 3226–3230 (2011)
81. J. Liu, M. Yu, X. Ning, C. Zhou, S. Yang, J. Zheng, PEGylation and zwitterionization: pros and cons in the renal clearance and tumor targeting of near-IR-emitting gold nanoparticles. Angew. Chem. Int. Ed. Engl. **52**(48), 12572–12576 (2013)
82. J. Liu, M. Yu, C. Zhou, S. Yang, X. Ning, J. Zheng, Passive tumor targeting of renal-clearable luminescent gold nanoparticles: long tumor retention and fast normal tissue clearance. J. Am. Chem. Soc. **135**(13), 4978–4981 (2013)
83. C. Zhou, M. Long, Y. Qin, X. Sun, J. Zheng, Luminescent gold nanoparticles with efficient renal clearance. Angew. Chem. Int. Ed. Engl. **50**(14), 3168–3172 (2011)
84. F. Chen, S. Goel, R. Hernandez, S.A. Graves, S. Shi, R.J. Nickles et al., Dynamic positron emission tomography imaging of renal clearable gold nanoparticles. Small **12**(20), 2775–2782 (2016)
85. C. Zhou, G. Hao, P. Thomas, J. Liu, M. Yu, S. Sun et al., Near-infrared emitting radioactive gold nanoparticles with molecular pharmacokinetics. Angew. Chem. Int. Ed. Engl. **51**(40), 10118–10122 (2012)
86. Tang S, Peng C, Xu J, Du B, Wang Q, Vinluan RD 3rd et al., Tailoring renal clearance and tumor targeting of ultrasmall metal nanoparticles with particle density. Angew. Chem. Int. Ed. Engl. (2016)
87. M. Zhou, J. Li, S. Liang, A.K. Sood, D. Liang, C. Li, CuS Nanodots with ultrahigh efficient renal clearance for positron emission tomography imaging and image-guided photothermal therapy. ACS Nano. **9**(7), 7085–7096 (2015)
88. M. Zhou, R. Zhang, M. Huang, W. Lu, S. Song, M.P. Melancon et al., A chelator-free multifunctional [^{64}Cu]CuS nanoparticle platform for simultaneous micro-PET/CT imaging and photothermal ablation therapy. J. Am. Chem. Soc. **132**(43), 15351–15358 (2010)
89. F. Ai, C.A. Ferreira, F. Chen, W. Cai, Engineering of radiolabeled iron oxide nanoparticles for dual-modality imaging. Wiley Interdiscip. Rev. Nanomed. Nanobiotechnol. **8**(4), 619–630 (2016)
90. T. Cao, Y. Yang, Y. Sun, Y. Wu, Y. Gao, W. Feng et al., Biodistribution of sub-10 nm PEG-modified radioactive/upconversion nanoparticles. Biomaterials **34**(29), 7127–7134 (2013)
91. Y. Geng, P. Dalhaimer, S. Cai, R. Tsai, M. Tewari, T. Minko et al., Shape effects of filaments versus spherical particles in flow and drug delivery. Nat. Nanotechnol. **2**(4), 249–255 (2007)
92. P. Kolhar, A.C. Anselmo, V. Gupta, K. Pant, B. Prabhakarpandian, E. Ruoslahti et al., Using shape effects to target antibody-coated nanoparticles to lung and brain endothelium. Proc. Natl. Acad. Sci. U.S.A. **110**(26), 10753–10758 (2013)
93. A. Banerjee, J. Qi, R. Gogoi, J. Wong, S. Mitragotri, Role of nanoparticle size, shape and surface chemistry in oral drug delivery. J. Control Release **238**, 176–185 (2016)

94. E. Blanco, H. Shen, M. Ferrari, Principles of nanoparticle design for overcoming biological barriers to drug delivery. Nat. Biotechnol. **33**(9), 941–951 (2015)
95. B.R. Smith, P. Kempen, D. Bouley, A. Xu, Z. Liu, N. Melosh et al., Shape matters: intravital microscopy reveals surprising geometrical dependence for nanoparticles in tumor models of extravasation. Nano Lett. **12**(7), 3369–3377 (2012)
96. S. Hirn, M. Semmler-Behnke, C. Schleh, A. Wenk, J. Lipka, M. Schaffler et al., Particle size-dependent and surface charge-dependent biodistribution of gold nanoparticles after intravenous administration. Eur. J. Pharm. Biopharm. **77**(3), 407–416 (2011)
97. H.C. Fischer, L.C. Liu, K.S. Pang, W.C.W. Chan, Pharmacokinetics of nanoscale quantum dots: In vivo distribution, sequestration, and clearance in the rat. Adv. Funct. Mater. **16**(10), 1299–1305 (2006)

Chapter 18
Polyethylene Glycolation (PEGylation) and the Similar

Dong Soo Lee and Yun-Sang Lee

Abstract To overcome the adverse effect of hydrophobicity of nanomaterials, polyethylene glycolation (PEGylation) is popularly used, which were already in clinical use of peptide or monoclonal antibodies. The same PEGylation is tried to hydrophilize nanomaterials but the results of this PEGylation differs according to the size, shape, terminal residues and others. The bodily response to the nanomaterials depend upon immune recognition of the PEG by IgM or innate immune cells. Mechanism of innate immune response to PEGylated nanomaterials are poorly understood. Zwitterions such as polybetaines were proposed to replace PEGs for hydrophilization. The mechanism is being investigated and not yet clearly known. The method to modify the surface of nanomaterials with PEGs and zwitterions can also influence final bodily response and thus simple and easy method of encapsulation was developed. The effect of diverse modification of nanomaterials with PEGs or zwitterions shall be understood with nanomaterials modified with this encapsulation method.

18.1 Introduction

Hydrophobicity of nanomaterials cause problems in vivo when injected systemically. The problems are associated with aggregation-proneness of hydrophobic materials in aqueous plasma and also the addition of corona proteins. Once aggregated,

D. S. Lee (✉) · Y.-S. Lee
Department of Nuclear Medicine, Seoul National University
College of Medicine, Seoul 03080, Republic of Korea
e-mail: dsl@snu.ac.kr

Y.-S. Lee
e-mail: wonza43@snu.ac.kr

D. S. Lee · Y.-S. Lee
Department of Molecular Medicine and Biopharmaceutical Sciences,
Graduate School of Convergence Science and Technology,
Seoul National University, Seoul 08826, Republic of Korea

D. S. Lee (ed.), *Radionanomedicine*, Biological and Medical Physics,
Biomedical Engineering, https://doi.org/10.1007/978-3-319-67720-0_18

these nanomaterials cannot pass through alveolar capillaries of the lungs if the size is over the capillary lumen size [1] or draw attention of the innate immune cells [2]. Innate immune cells recognize pathogen-associated molecular pattern (PAMP) or damage-associated molecular pattern (DAMP) [3]. Hydrophobicity was found to be the major factor in these responses (Fig. 18.1) [4, 5].

Polyethylene glycols (PEGs) of various length and branches were proposed. The modification with PEGs, so called, PEGylation was the first to be approved by regulatory bodies of each country's government and had been widely used to make nanomaterials hydrophilic. PEGylated nanomaterials are hydrophilic and according to the density and the length the PEGs show the brush or mushroom shape to cover up the surfaces (Figs. 18.2 and 18.3) [6, 7]. Zwitterionic molecules such as poly-betaines of polysaccharides were proposed as alternatives to PEGs (Fig. 18.4) [8–10]. After PEGylation, ligands for targeted delivery or chelators to bind metals or radionuclides were also attached to the surface of the nanomaterials or these ligands or chelators were bound to the free end of PEGs. Thus, PEGs might have terminals having carboxylic acid (–COOH), amine ($–NH_2$), alcohol (–OH), thiol

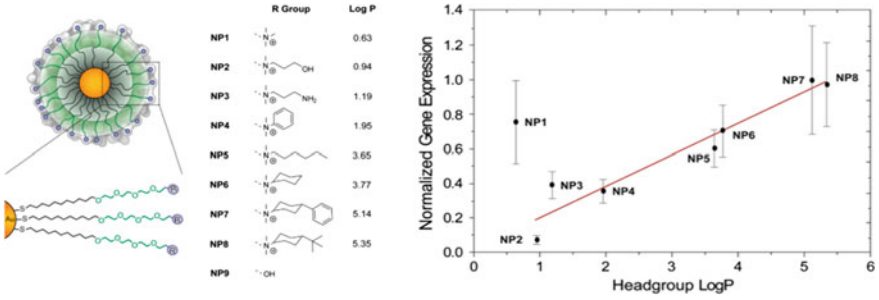

Fig. 18.1 Hydrophobicity of head group of PEG and TNF-α gene expression. Adapted from [4] with permission

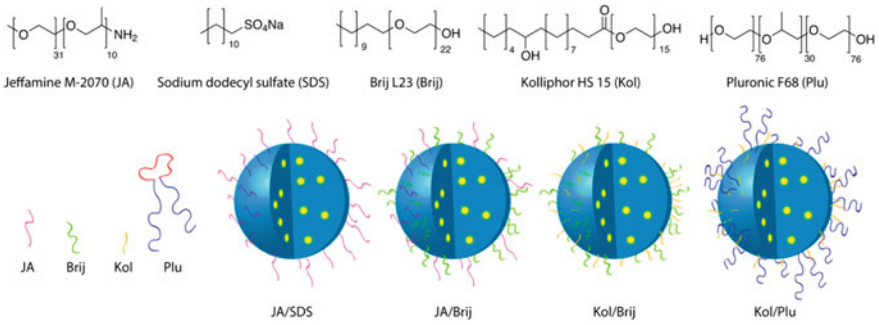

Fig. 18.2 Different types of polyethylene glycol and its density and half-life of clearance. Adapted from [6] with permission

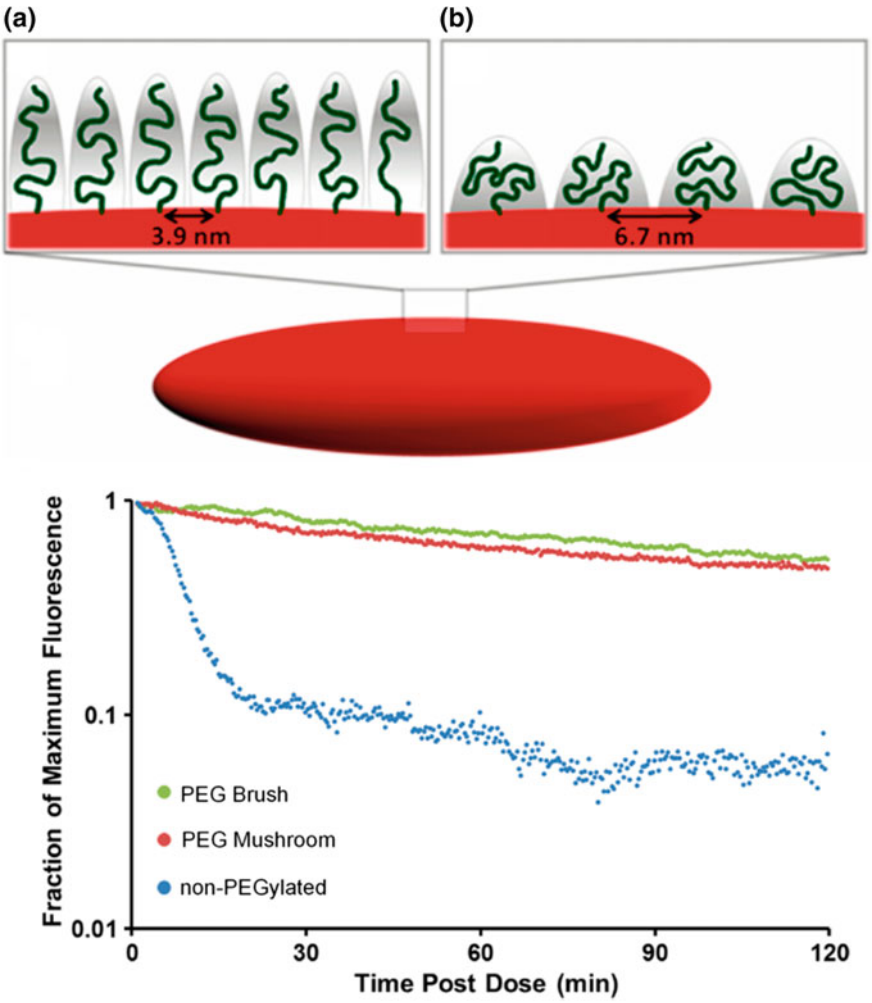

Fig. 18.3 Brush and mushroom types of PEG configuration and blood clearance. Adapted from [9] with permission

(–SH), azide ($–N_3$), or maleimide ends which might interact with plasma proteins and moreover with innate immune cells or endothelial cells.

PEGylation had been more popularly used for decorating peptide drugs and other macromolecules including monoclonal antibodies (Fig. 18.5) [11–13]. Investigators assumed and confirmed that the circulation time is increased and thus injected molecules had more time to reach the target or to be taken up by the target cells. The problem to solve was which PEGs to choose and how to bind them with peptides or monoclonal antibodies while not decreasing biological activity of the peptides or macromolecules. There have been a lot of progresses which were

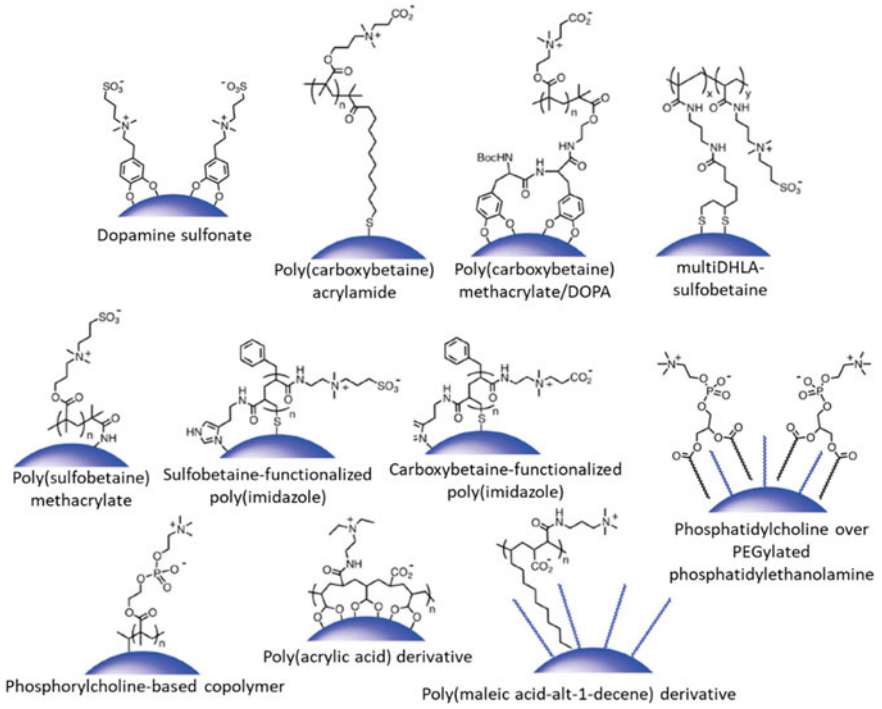

Fig. 18.4 Polymeric zwitterionic coating materials. Adapted modified from [9] with permission

patented and commercialized (Table 18.1) [11]. Similarity (or uniqueness) of PEGylated nanomaterials to PEGylated peptides/macromolecules should be unraveled very soon so that the product can be approved, marketed and clinically used. Especially development of the simultaneous binding of ligands and PEGs over the surface of the nanomaterials shall facilitate the clinical translation of nanomaterials owing to their advantage over sequential labeling of ligands and PEGs.

Recent introduction of corona proteins and their consequences made our understanding explicit in terms of elucidation of the effect or impact of corona modification of the surface of the PEGylated nanomaterials injected into the body systemically via intravenous routes [14–18]. Corona proteins were previously supposed to change over the surface of surface-modified nanomaterials along the time lapse after administration, that is to say, the components are changing over the hours until being taken up by the cells or excretion [14–18]. However, based on the laborious characterization of hard and soft corona proteins, investigators conclude that the changes are more quantitative than not changing dramatically the component proteins over the surface of nanomaterials [19–21]. Living organisms have evolved to cope with the invading live infectious materials immediately and in a consistent way and thus they seem to use the same strategy to handle extraneous

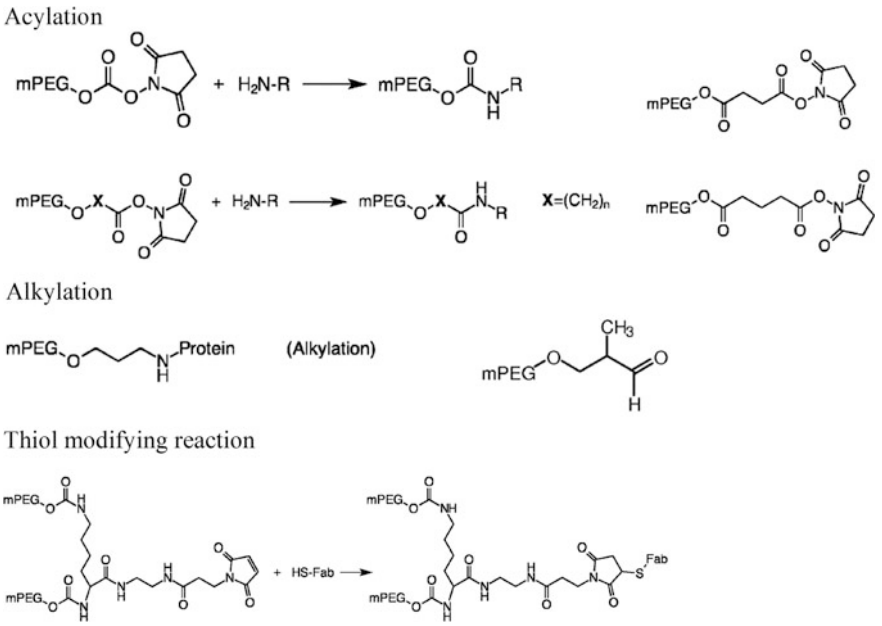

Fig. 18.5 Three types of PEGylation used for clinical biopharmaceuticals made of peptides and proteins in Table 18.1. Adapted modified from [11] with permission

Table 18.1 PEGylated biopharmaceuticalalready in clinical use and their PEGylation methods (modified from Table 1 [11])

PEGylation with	Brand name	Drug (M.W.)	PEG size (M.W.) [PEG number/drug]
Acylating reagent i.e. succinimidyl succinate or succinimidyl glutarate	Adagen	Adenosine deaminase (96k–126k)	5k [11–17/molecule]
	Oncapar	L-asparaginase (483k–548k)	5k [69–82/molecule]
	Krystexxa	Uricase (540k)	10k [9/homotetramer]
	PEGIntron	INF-α2b (31k)	12k [1/molecule]
	Pegasys	INF- α2a (60k)	40k [1 branched/molecule]
	Mircera	Epoietin β (60k)	30k [1/molecule]
	Macugen	28 nucleotide aptamer (50k)	40k [1 branched/molecule]
Alkylating agent	Neulasta	rhGCSF (39k)	20k [1/molecule]
	Plegridy	INF β1 (44k)	20k [1/molecule]
Thiol-modifying agent	Cimzia	Certolizumab (91k)	40k [1 branched/molecule]

nanomaterials. Thus PEGylation or the surface modification with the same goal of hydrophilization and stealth effect shall be understood for their efficacy or mechanism regarding whether to achieve this goal.

Corona proteins consist of hard and soft ones, the difference of which lay only in the binding affinity determining the kinetic fate in the blood or the plasma [14, 15]. Many reports showed that corona-modified nanomaterials act rather differently from the bare nanomaterials [15–17, 19]. This difference ranged from interaction with innate immune cells [16], the binding to the target cells [17, 22–25], circulation time [24–28], endocytosis into the cells [29–31] and final fate of the nanomaterials inside the cells [19, 22, 26, 27, 31, 32]. This would seem obvious in vivo [23, 24], however, such was also the case in the investigation done in vitro upon cultured cells [16, 17, 23, 28, 29, 31]. Serum or plasma-incubated nanomaterials began to be included in the investigation to simulate the status of systemically-injected nanomaterials in vitro. Consequences of PEGylated nanomaterials are now understood considering these factors.

Stealth effect was once proposed that PEGylated materials are not recognized by mononuclear phagocytic system (MPS) and thus increase circulation time almost indefinitely and have advantageous freedom to find and reach targets. Even passive targeting strategy was proposed to be enough to deliver sufficient amount of PEGylated peptides/macromolecules or PEGylated nanomaterials. Stealth effect is being also recapitulated by further experiments with or without corona wrapping of the PEGylation of the nanomaterials [27, 28, 33]. As the terminal residues of PEGs can influence binding of corona proteins and their consequential effect upon the assumed stealth effect should now be investigated. Different forms of PEGs [11, 12] and the density of the PEGs over the surface [5–7, 32], in combination with surface zeta potential as well as the size and even the core contents [5, 6] increase hugely the combination of the constitution of surface-modified PEGylated ligand-attached nanomaterials finally decorated with hard/soft corona [23, 25, 30]. PEGylation might be changed by PPE (polyphosphoester)-coating [28, 34] or zwitterion coating [35, 36]. The same understanding regarding the biodistribution, targeting and immune response should be elucidated for these improved coatings just like PEGylation. Host immune response to certain PEGs were reported and was associated with shortened blood clearance time [37, 38]. Inherent antiPEG antibodies were reported and speculated to be due to prior unrecognized exposure to PEGs administered to the skin as cosmetics or to the gastrointestinal tracts as food additives [39, 40]. PEGylated treatment regimens (Table 18.1) might be also the source of immunization. PEGylated radioisotope-labeled nanomaterials will meet the same challenge to achieve the optimal biodistribution and target disposal and least immune responses. Diagnostic PEGylated radionanomaterials was reported to reveal easily the improved pharmacokinetic [41] but therapeutic and theranostic radionanomaterials are meticulously produced considering all the know-hows acquired when the previous investigators overcame the unpredictability or combining PEGs and peptides/antibodies for successful clinical translation. Finding out the best PEGylated nanomaterials fit for in vivo theranostic use is a really big problem desired to be solved.

18.2 Variety of Hydrophilization of the Surface of Nanoparticles

Polyethylene glycol (H–(O–CH_2–CH_2)$_n$–OH) (synonym; polyethylene oxide or polyoxyethylene) was the most popular substrate to hydrophilize the surface of hydrophobic nanomaterials. Linear or branched PEGs of variable length can be coated on the surface of the nanoparticles. Or there were reported an easy way of PEGylation of hydrophobic nanoparticles by making micelle capsule and encapsulation, which were applied to various nanoparticles including quantum dots [42, 43], iron oxide [44, 45], upconversion nanoparticles [46], surface-enhanced Raman scattering (SERS) dots [47, 48]. Methods of PEGylation of peptides or proteins was classified as (1) acylation, (2) alkylation and (3) thioether formation [11] (Fig. 18.5). These methods were used to manufacture the biopharmaceuticals of peptide, aptamer, protein and antibody. Mostly linear PEGs and rarely branched PEG were used with the molecular weights of 5–40 kD. 1–82 molecules of PEGs were attached per molecules (Table 18.1).

The eloquent goal of PEGylation of nanoparticles is hydrophilization as hydrophobicity cause two problems for nanoparticles; (1) aggregation and making huge cluster which will block alveolar capillaries of the lungs and (2) stimulation of hostile innate immune response. Aggregation is immediately noticed and though detergents are mixed, immune response cannot be avoided. When the gold nanoparticles were decorated with PEGs having tuned functionalities at the terminal having different log P (0.63–5.35) representing hydrophobic values of these functional head-groups. While IL-10 gene expression did not differ between tuned PEGylated gold nanoparticles, TNFα gene expression was correlated with the hydrophobicity [4]. Next parameter was the length of PEG along with the composition or the shape [5, 6]. There is a tendency that longer and more dense (not sparse) and brush type (not mushroom type) of PEGs' configuration are the key to increase circulation time and to decrease macrophage uptake. The exact effect of configuration, shape, and constitution are being elucidated ever and ever.

Though the details are mostly not known regarding the effect of zwitterion coating and the determining parameters thereof, PEGs are being challenged to be replaced by zwitterions as PEGs are eliciting IgM response and in certain cases even preexisting IgG responses, and consequently PEGs do not achieve sufficient circulation time. In several reports proposing low immunogenicity and longer circulation time, we don't have enough data by which we can sort out the effects of the polymer length, zwitterion density, characteristics of head-group on circulation time, innate immune response, targeting capability and cellular uptake [35, 36]. What we know currently are mainly based on molecular dynamics modeling [36], using sulfobetaine or carboxybetaine materials (Fig. 18.6). Jiang and coworkers explain principles of sulfobetaines and carboxybetaines which will endow the zwitterions the characteristics of plenty of hydration, less self-association and resistance to the protein adsorption [49]. The most important of these characteristics is the resistance to the protein adsorption, which should be validated by in vitro

experiment of mixing the zwitterion coated nanoparticle with serum and at last by in vivo experiment of proteomics analysis of systemically injected zwitterion coated nanoparticles.

Zwitterion-modification of nanoparticles were recently reported by several groups for small iron oxide, silica or gold nanoparticles [35, 50–54]. Sulfobetaine small molecule [35, 52, 54], carboxybetaine small molecule [53] or polymeric carboxybetaine or sulfobetaine were used to coat the nanoparticles. Interestingly,

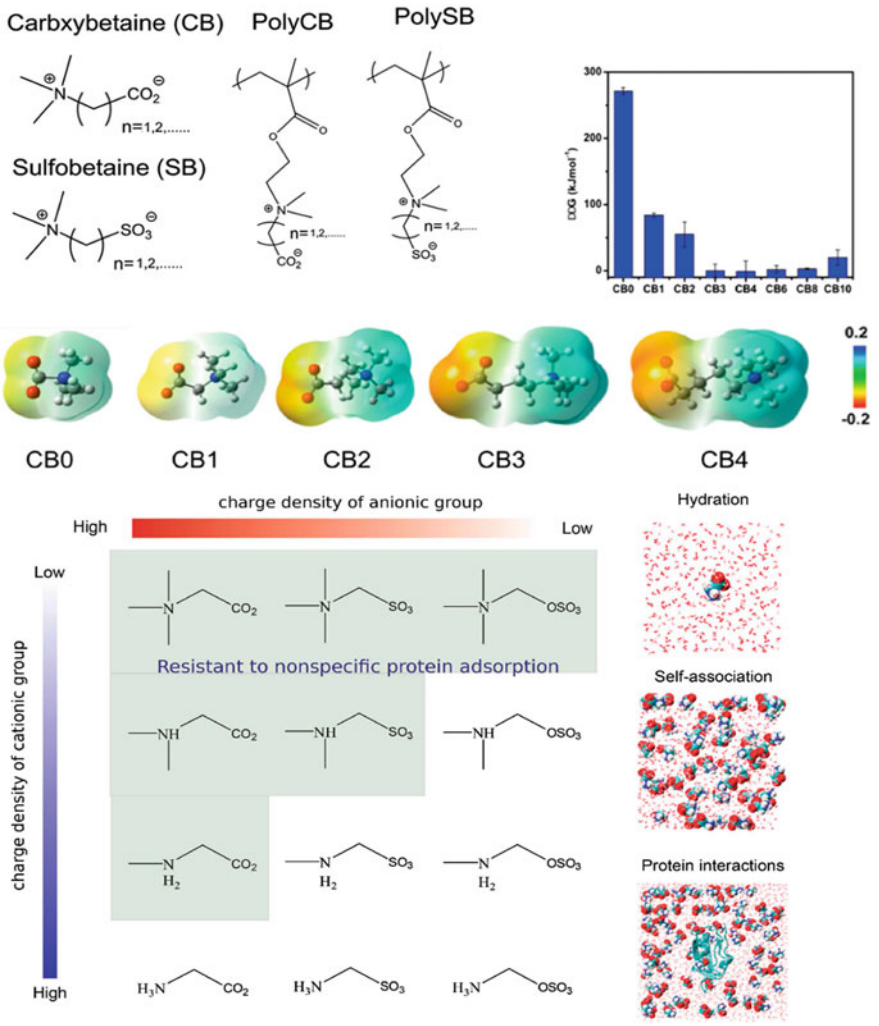

Fig. 18.6 Zwitterionic polymeric materials made of sulfobetaines and carboxybetaines and their molecular dynamics showing hydration, abhorrence of self-aggregation, and resistance to nonspecific protein adsorption. Adapted modified from [36] with permission

self-assembled monolayer [50] or hydrophobic/van der Waals interaction over oleic acid-modified nanoparticles [51] was used to make facile preparation. The latter has adopted the same encapsulation methods as was in the report by Jeong's group [42]. Multiple steps of binding the surface-modifiers had become the essential point of concern. In every case, protein adsorption could be avoided [9, 10, 53] and also the non-specific uptake by tumor [35] or macrophage cells [9]. Functional residues at the end of sulfobetaine or carboxybetaine were also proposed for further modification to let the nanoparticles to have targeting capability in vivo after systemic administration.

18.3 PEGylation/Zwitterion-Coating Countering Protein Corona Formation

Hydrophobic nanoparticles mimics invading infective microorganism and cause aggregation once they meet plasma, whose water solution expels nanoparticles to make bigger particles and then whose many proteins wrap up the nanoparticles. Beside hydrophobic nanoparticles, hydrophilic nanoparticles also are wrapped up by plasma proteins in a non-random way so that their identity is now determined after the corona protein surrounded the nanoparticles. It was easy to divide the proteins into hard (having higher affinity) and soft (competitively bound and reversible or exchangeable). And soft corona proteins are easily changed with other soft corona proteins, however, this concept was challenged by recent findings by Tenzer and colleagues [20], where the characteristic corona was established within 1 min after mixing or injection, the constituent corona proteins did not change much and at most change only in quantitative terms. Though we don't know that this is universally applied to nanoparticles and plasma of healthy or diseased humans, if true, it came to be easy to characterize the systemically administered nanoparticles [21] and to predict the behavior of these nanoparticles in vivo. The behavior here means biodistribution in general and target disposition which will be affected by the determinants of physiology and immune response.

Now if we try to understand the characteristics of a kind of nanoparticles, we need to determine size, surface charge, density and shape of the surface modifier and also adsorbed proteins, i.e. corona. Adding corona to the model to predict nanoparticles' interaction with target cells or non-target scavenger cells improved the prediction up to 50% [21]. By the way, these reports about corona modification of nanoparticles were sometimes investigated in in vitro conditions, or in other times, in in vivo but without optimized hydrophilization. Few reports [23, 28] dealt with the effect of concomitant PEGylation and corona of the nanoparticles on their targeted cellular uptake [23] and stealth effects [28]. In the former report, the investigators observed the reduced receptor binding due to corona proteins wrapping anti-MUC1-targeted PEGylated liposome. Or in the latter report corona proteins rather helped nanoparticles enjoy stealth effect. PEG or other PPE-coated

nanoparticles, once exposed to plasma or clusterin (apolipoprotein J), decreased non-specific cellular uptake. However, this was again an in vitro study. And the delicate, but sometimes definitively different, in vivo condition should be investigated for their effect upon non-specific cellular uptake, targeted receptor mediated uptake to the target cells or uptake by immune cells especially macrophages. Zwitterion capsulation was also reported using phosphatidylinositol as zwitterion and capsulation methods using liposome as capsules [55]. Similarly to but unlike Jeong's method of using micelle [42], they used liposome (lipid bilayer) to wrap the gold nanoparticles. They called the final product as the artificial viral nanoparticles as they mimicked membraned viruses. The effect of corona adsorption was modestly considered for in vitro and subcutaneous injection in vivo experiments.

18.4 Radiolabeling with PEGylation or Zwitterion Coating of Nanoparticles

There are two methods of PEGylation, one of which is the functionalization of the surface and then the consequent conjugation of PEGs or small zwitterions at the later step. The density and shape of the PEGs on the surface of the nanoparticles are well known factors to influence the physiological behavior of the PEG or zwitterion-coated nanoparticles. The other method is simultaneous encapsulation using Jeong's method. This has become more and more popular because if we adopt the sequential method, this PEGylation and binding of other ligands and chelators needed further repeated steps of binding and purification. Simultaneity of PEGylation and ligand/chelator binding was enabled by micelle encapsulation which evolved from the first report by Dubertret and optimized by Jeong [42].

Hydrophilization of nanomaterials using the micelle encapsulation method was first proposed by Dubertret et al. [56]. Via several evolutions of methods [57, 58] functional biomolecules were introduced successfully [59]. Jeong's group integrated these proposed methods to devise the simplest method of mixing, vortexing, and size exclusion chromatography yielding active multi-specific nanoparticles [42]. By exploiting this one-step method under mild conditions to preserve ligand integrity, feasibility of multiplexing is now being investigated to embrace both therapeutic and diagnostic radionuclides simultaneously (Fig. 18.7) [43, 60]. The key step of manufacturing here is how we make micelles containing mixtures of linear or branched PEGs, ligands and chelators optimally for the further use in the next step of capsulation.

There are two approaches, pre- and post-labeling methods, for radiolabeling of these surface modified nanomaterials (Fig. 18.8) [61]. Pre-labeling method can be used for the nanomaterials containing the conjugation motifs on the surface and post-labeling method for the chelators on the surface. Very often, the nanomaterials

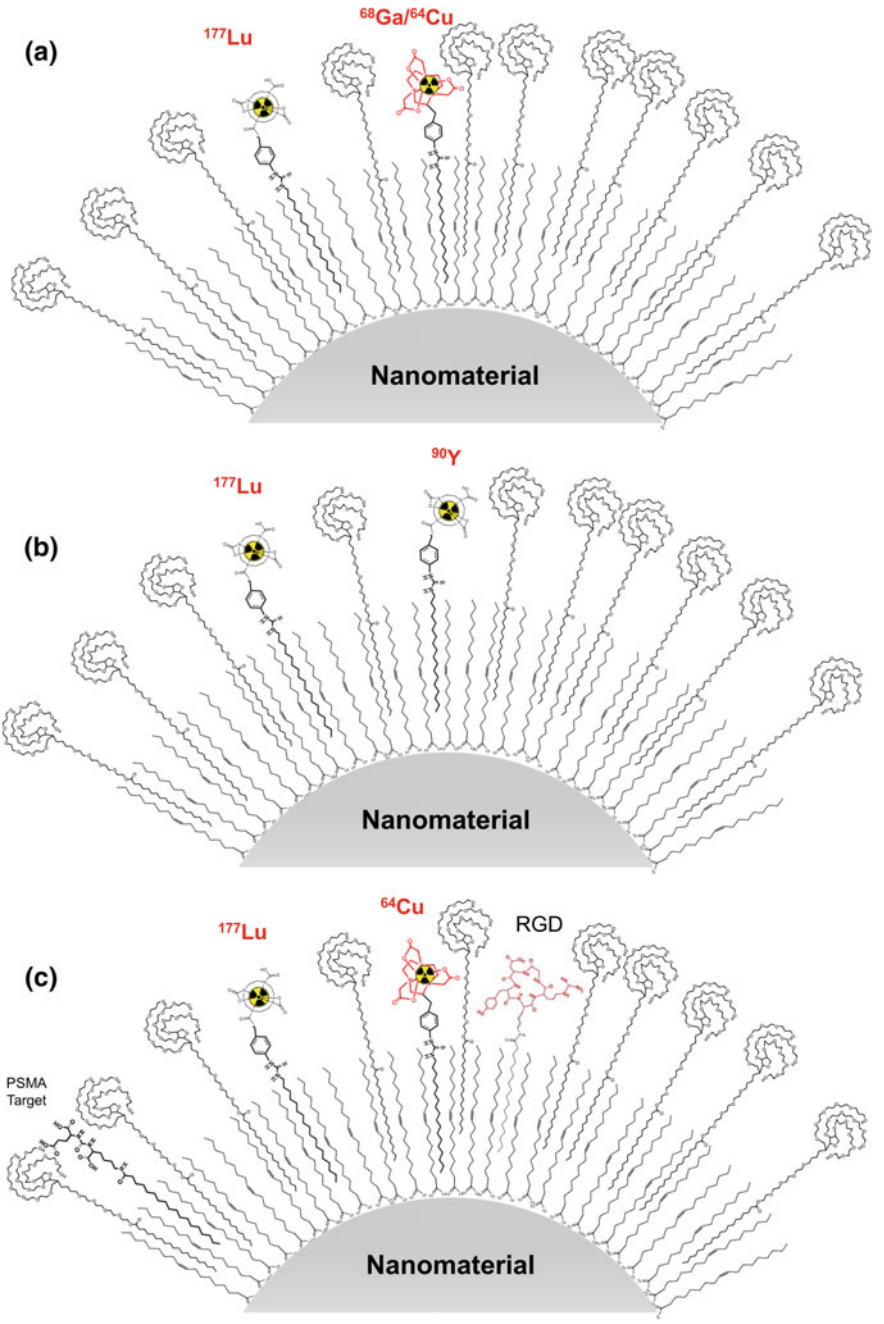

Fig. 18.7 Multifunctional nano-platform for radionanomedicine. **a** Combination of diagnostic and therapeutic radionuclides. **b** Combination of two different therapeutic radionuclides with different particle energy and physical half-life. **c** Combination of two different targeting molecules and diagnostic and therapeutic radionuclides

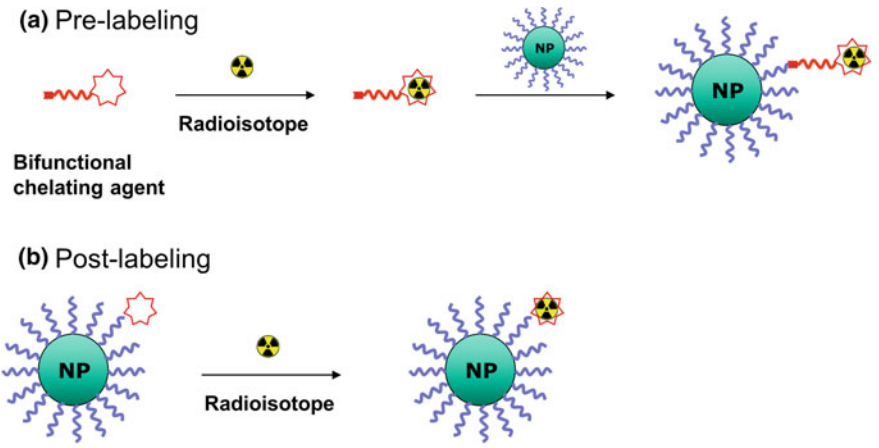

Fig. 18.8 Conventional radiolabeling methods for radionanomedicine. **a** Pre-labeling method: radiolabeling first, then mixed with nanomaterials. **b** Post-labeling method: radiolabeling using chelator on nanomaterials

cannot endure the conditions of radiolabeling, such as low or high pH, high temperature, and if so, the pre-labeling method would be better for the keeping the integrity of labile nanomaterials.

References

1. M.C. Lee, J.-K. Chung, D.S. Lee, *Koh Chang-Soon Nuclear Medicine* (Korea Medical Books, Seoul, 2008)
2. S.Y. Seong, P. Matzinger, Hydrophobicity: an ancient damage-associated molecular pattern that initiates innate immune responses. Nat. Rev. Immunol. **4**(6), 469–478 (2004)
3. X. Cao, Self-regulation and cross-regulation of pattern-recognition receptor signalling in health and disease. Nat. Rev. Immunol. **16**(1), 35–50 (2016)
4. D.F. Moyano, M. Goldsmith, D.J. Solfiell, D. Landesman-Milo, O.R. Miranda, D. Peer et al., Nanoparticle hydrophobicity dictates immune response. J. Am. Chem. Soc. **134**(9), 3965–3967 (2012)
5. D.F. Moyano, Y. Liu, D. Peer, V.M. Rotello, Modulation of immune response using engineered nanoparticle surfaces. Small **12**(1), 76–82 (2016)
6. A.K. Åslund, E. Sulheim, S. Snipstad, E. von Haartman, H. Baghirov, N. Starr et al., Quantification and qualitative effects of different PEGylations on poly (butyl cyanoacrylate) nanoparticles. Mol. Pharm. **14**, 2560–2569 (2017)
7. J.L. Perry, K.G. Reuter, M.P. Kai, K.P. Herlihy, S.W. Jones, J.C. Luft et al., PEGylated PRINT nanoparticles: the impact of PEG density on protein binding, macrophage association, biodistribution, and pharmacokinetics. Nano Lett. **12**(10), 5304–5310 (2012)
8. Z.G. Estephan, P.S. Schlenoff, J.B. Schlenoff, Zwitteration as an alternative to PEGylation. Langmuir **27**(11), 6794–6800 (2011)
9. K. Pombo García, K. Zarschler, L. Barbaro, J.A. Barreto, W. O'Malley, L. Spiccia et al., Zwitterionic-coated "stealth" nanoparticles for biomedical applications: recent advances in

countering biomolecular corona formation and uptake by the mononuclear phagocyte system. Small **10**(13), 2516–2529 (2014)
10. P. Zhang, F. Sun, C. Tsao, S. Liu, P. Jain, A. Sinclair et al., Zwitterionic gel encapsulation promotes protein stability, enhances pharmacokinetics, and reduces immunogenicity. Proc. Natl. Acad. Sci. U S A **112**(39), 12046–12051 (2015)
11. P.L. Turecek, M.J. Bossard, F. Schoetens, I.A. Ivens, PEGylation of biopharmaceuticals: a review of chemistry and nonclinical safety information of approved drugs. J. Pharm. Sci. **105** (2), 460–475 (2016)
12. M.J. Roberts, M.D. Bentley, J.M. Harris, Chemistry for peptide and protein PEGylation. Adv. Drug Deliv. Rev. **54**(4), 459–476 (2002)
13. L. Wu, J. Chen, Y. Wu, B. Zhang, X. Cai, Z. Zhang et al., Precise and combinatorial PEGylation generates a low-immunogenic and stable form of human growth hormone. J. Control Release **249**, 84–93 (2017)
14. S. Milani, F.B. Bombelli, A.S. Pitek, K.A. Dawson, J. Rädler, Reversible versus irreversible binding of transferrin to polystyrene nanoparticles: soft and hard corona. ACS Nano **6**(3), 2532–2541 (2012)
15. M.P. Monopoli, C. Aberg, A. Salvati, K.A. Dawson, Biomolecular coronas provide the biological identity of nanosized materials. Nat. Nanotechnol. **7**(12), 779–786 (2012)
16. A. Salvati, A.S. Pitek, M.P. Monopoli, K. Prapainop, F.B. Bombelli, D.R. Hristov et al., Transferrin-functionalized nanoparticles lose their targeting capabilities when a biomolecule corona adsorbs on the surface. Nat. Nanotechnol. **8**(2), 137–143 (2013)
17. Y. Yan, K.T. Gause, M.M. Kamphuis, C.S. Ang, N.M. O'Brien-Simpson, J.C. Lenzo et al., Differential roles of the protein corona in the cellular uptake of nanoporous polymer particles by monocyte and macrophage cell lines. ACS Nano **7**(12), 10960–10970 (2013)
18. P.M. Kelly, C. Åberg, E. Polo, A. O'Connell, J. Cookman, J. Fallon et al., Mapping protein binding sites on the biomolecular corona of nanoparticles. Nat. Nanotechnol. **10**(5), 472–479 (2015)
19. D. Docter, D. Westmeier, M. Markiewicz, S. Stolte, S.K. Knauer, R.H. Stauber, The nanoparticle biomolecule corona: lessons learned—challenge accepted? Chem. Soc. Rev. **44** (17), 6094–6121 (2015)
20. S. Tenzer, D. Docter, J. Kuharev, A. Musyanovych, V. Fetz, R. Hecht et al., Rapid formation of plasma protein corona critically affects nanoparticle pathophysiology. Nat. Nanotechnol. **8** (10), 772–781 (2013)
21. C.D. Walkey, J.B. Olsen, F. Song, R. Liu, H. Guo, D.W. Olsen et al., Protein corona fingerprinting predicts the cellular interaction of gold and silver nanoparticles. ACS Nano **8** (3), 2439–2455 (2014)
22. C. Corbo, R. Molinaro, A. Parodi, N.E. Toledano Furman, F. Salvatore et al., The impact of nanoparticle protein corona on cytotoxicity, immunotoxicity and target drug delivery. Nanomed. (Lond). **11**(1), 81–100 (2016)
23. M. Hadjidemetriou, Z. Al-Ahmady, M. Mazza, R.F. Collins, K. Dawson, K. Kostarelos, In vivo biomolecule corona around blood-circulating, clinically used and antibody-targeted lipid bilayer nanoscale vesicles. ACS Nano **9**(8), 8142–8156 (2015)
24. S. Huo, S. Chen, N. Gong, J. Liu, X. Li, Y. Zhao et al., Ultrasmall gold nanoparticles behavior in vivo modulated by surface polyethylene glycol (PEG) grafting. Bioconjug. Chem. **28**(1), 239–243 (2017)
25. B. Kang, P. Okwieka, S. Schöttler, S. Winzen, J. Langhanki, K. Mohr et al., Carbohydrate-based nanocarriers exhibiting specific cell targeting with minimum influence from the protein corona. Angew. Chem. Int. Ed. Engl. **54**(25), 7436–7440 (2015)
26. Z. Amoozgar, Y. Yeo, Recent advances in stealth coating of nanoparticle drug delivery systems. Wiley Interdiscip. Rev. Nanomed. Nanobiotechnol. **4**(2), 219–233 (2012)
27. S. Schöttler, K. Landfester, V. Mailänder, Controlling the stealth effect of nanocarriers through understanding the protein corona. Angew. Chem. Int. Ed. Engl. **55**(31), 8806–8815 (2016)

28. S. Schöttler, G. Becker, S. Winzen, T. Steinbach, K. Mohr, K. Landfester et al., Protein adsorption is required for stealth effect of poly(ethylene glycol)- and poly(phosphoester)-coated nanocarriers. Nat. Nanotechnol. **11**(4), 372–377 (2016)
29. S. Ritz, S. Schöttler, N. Kotman, G. Baier, A. Musyanovych, J. Kuharev et al., Protein corona of nanoparticles: distinct proteins regulate the cellular uptake. Biomacromolecules **16**(4), 1311–1321 (2015)
30. E. Harrison, J.R. Nicol, M. Macias-Montero, G.A. Burke, J.A. Coulter, B.J. Meenan et al., A comparison of gold nanoparticle surface co-functionalization approaches using Polyethylene Glycol (PEG) and the effect on stability, non-specific protein adsorption and internalization. Mater Sci. Eng. C Mater Biol. Appl. **62**, 710–718 (2016)
31. K. Peynshaert, S.J. Soenen, B.B. Manshian, S.H. Doak, K. Braeckmans, S.C. De Smedt et al., Coating of quantum dots strongly defines their effect on lysosomal health and autophagy. Acta Biomater. **48**, 195–205 (2017)
32. J. Wolfram, Y. Yang, J. Shen, A. Moten, C. Chen, H. Shen et al., The nano-plasma interface: implications of the protein corona. Coll. Surf. B Biointerfaces **124**, 17–24 (2014)
33. L. Sanchez, Y. Yi, Y. Yu, Effect of partial PEGylation on particle uptake by macrophages. Nanoscale **9**(1), 288–297 (2017)
34. G. Settanni, J. Zhou, T. Suo, S. Schöttler, K. Landfester, F. Schmid et al., Protein corona composition of poly(ethylene glycol)- and poly(phosphoester)-coated nanoparticles correlates strongly with the amino acid composition of the protein surface. Nanoscale **9**(6), 2138–2144 (2017)
35. S. Mondini, M. Leonzino, C. Drago, A.M. Ferretti, S. Usseglio, D. Maggioni et al., Zwitterion-coated iron oxide nanoparticles: surface chemistry and intracellular uptake by hepatocarcinoma (HepG2) cells. Langmuir **31**(26), 7381–7390 (2015)
36. Q. Shao, S. Jiang, Molecular understanding and design of zwitterionic materials. Adv. Mater. **27**(1), 15–26 (2015)
37. A.S. Abu Lila, H. Kiwada, T. Ishida, The accelerated blood clearance (ABC) phenomenon: clinical challenge and approaches to manage. J. Control Release **172**(1), 38–47 (2013)
38. T. Shimizu, T. Ishida, H. Kiwada, Transport of PEGylated liposomes from the splenic marginal zone to the follicle in the induction phase of the accelerated blood clearance phenomenon. Immunobiology **218**(5), 725–732 (2013)
39. N.J. Ganson, T.J. Povsic, B.A. Sullenger, J.H. Alexander, S.L. Zelenkofske, J.M. Sailstad et al., Pre-existing anti-polyethylene glycol antibody linked to first-exposure allergic reactions to pegnivacogin, a PEGylated RNA aptamer. J. Allergy Clin. Immunol. **137**(5):1610–1613.e7 (2016)
40. P. Zhang, F. Sun, S. Liu, S. Jiang, Anti-PEG antibodies in the clinic: current issues and beyond PEGylation. J. Control Release **244**(Pt B):184–193 (2016)
41. J.W. Lee, Y.J. Lee, U.C. Shin, S.W. Kim, B.I. Kim, K.C. Lee et al., Improved pharmacokinetics following PEGylation and dimerization of a c(RGD-ACH-K) conjugate used for tumor positron emission tomography imaging. Cancer Biother. Radiopharm. **31**(8), 295–301 (2016)
42. Y.K. Lee, J.M. Jeong, L. Hoigebazar, B.Y. Yang, Y.S. Lee, B.C. Lee et al., Nanoparticles modified by encapsulation of ligands with a long alkyl chain to affect multispecific and multimodal imaging. J. Nucl. Med. **53**(9), 1462–1470 (2012)
43. Y.S. Lee, Y.I. Kim, D.S. Lee, Future perspectives of radionanomedicine using the novel micelle-encapsulation method for surface modification. Nucl. Med. Mol. Imaging **49**(3), 170–173 (2015)
44. B.Y. Yang, S.H. Moon, S.R. Seelam, M.J. Jeon, Y.S. Lee, D.S. Lee et al., Development of a multimodal imaging probe by encapsulating iron oxide nanoparticles with functionalized amphiphiles for lymph node imaging. Nanomed. (Lond). **10**(12), 1899–1910 (2015)
45. S.H. Moon, B.Y. Yang, Y.J. Kim, M.K. Hong, Y.S. Lee, D.S. Lee et al., Development of a complementary PET/MR dual-modal imaging probe for targeting prostate-specific membrane antigen (PSMA). Nanomedicine **12**(4), 871–879 (2016)

46. H.J. Seo, S.H. Nam, H.J. Im, J.Y. Park, J.Y. Lee, B. Yoo et al., Rapid hepatobiliary excretion of micelle-encapsulated/radiolabeled upconverting nanoparticles as an integrated form. Sci. Rep. **5**, 15685 (2015)
47. S. Jeong, Y.I. Kim, H. Kang, G. Kim, M.G. Cha, H. Chang et al., Fluorescence-Raman dual modal endoscopic system for multiplexed molecular diagnostics. Sci. Rep. **5**, 9455 (2015)
48. Y.I. Kim, S. Jeong, K.O. Jung, M.G. Song, C.H. Lee, S.J. Chung et al., Simultaneous detection of EGFR and VEGF in colorectal cancer using fluorescence-Raman endoscopy. Sci. Rep. **7**(1), 1035 (2017)
49. L. Zhang, Z. Cao, T. Bai, L. Carr, J.R. Ella-Menye, C. Irvin, B.D. Ratner, S. Jiang, Zwitterionic hydrogels implanted in mice resist the foreign-body reaction. Nat. Biotechnol. **31** (6), 553–556 (2013)
50. W. Yang, J.R. Ella-Menye, S. Liu, T. Bai, D. Wang, Q. Yu, Y. Li, S. Jiang, Cross-linked carboxybetaine SAMs enable nanoparticles with remarkable stability in complex media. Langmuir **30**(9), 2522–2529 (2014)
51. D. Kim, M.K. Chae, H.J. Joo, I.H. Jeong, J.H. Cho, C. Lee, Facile preparation of zwitterion-stabilized superparamagnetic iron oxide nanoparticles (ZSPIONs) as an MR contrast agent for in vivo applications. Langmuir **28**(25), 9634–9639 (2012)
52. Z. Zhou, L. Wang, X. Chi, J. Bao, L. Yang, W. Zhao et al., Engineered iron-oxide-based nanoparticles as enhanced T1 contrast agents for efficient tumor imaging. ACS Nano **7**(4), 3287–3296 (2013)
53. F. Hu, K. Chen, H. Xu, H. Gu, Functional short-chain zwitterion coated silica nanoparticles with antifouling property in protein solutions. Coll. Surf. B Biointerfaces **126**, 251–256 (2015)
54. H. Wei, O.T. Bruns, M.G. Kaul, E.C. Hansen, M. Barch, A. Wiśniowska et al., Exceedingly small iron oxide nanoparticles as positive MRI contrast agents. Proc. Natl. Acad. Sci. U S A. **114**(9), 2325–2330 (2017)
55. F. Xu, M. Reiser, X. Yu, S. Gummuluru, L. Wetzler, B.M. Reinhard, Lipid-mediated targeting with membrane-wrapped nanoparticles in the presence of corona formation. ACS Nano **10**(1), 1189–1200 (2016)
56. B. Dubertret, P. Skourides, D.J. Norris, V. Noireaux, A.H. Brivanlou, A. Libchaber, In vivo imaging of quantum dots encapsulated in phospholipid micelles. Science **298**(5599), 1759–1762 (2002)
57. H. Fan, K. Yang, D.M. Boye, T. Sigmon, K.J. Malloy, H. Xu et al., Self-assembly of ordered, robust, three-dimensional gold nanocrystal/silica arrays. Science **304**(5670), 567–571 (2004)
58. H. Fan, E.W. Leve, C. Scullin, J. Gabaldon, D. Tallant, S. Bunge et al., Surfactant-assisted synthesis of water-soluble and biocompatible semiconductor quantum dot micelles. Nano Lett. **5**(4), 645–648 (2005)
59. O. Carion, B. Mahler, T. Pons, B. Dubertret, Synthesis, encapsulation, purification and coupling of single quantum dots in phospholipid micelles for their use in cellular and in vivo imaging. Nat. Protoc. **2**(10), 2383–2390 (2007)
60. D.S. Lee, H.J. Im, Y.S. Lee, Radionanomedicine: widened perspectives of molecular theragnosis. Nanomedicine **11**(4), 795–810 (2015)
61. K. Stockhofe, J.M. Postema, H. Schieferstein, T.L. Ross, Radiolabeling of nanoparticles and polymers for PET imaging. Pharmaceuticals **7**(4), 392–418 (2014)

Chapter 19
Excretion and Clearance

Hyung-Jun Im

Abstract The nanomaterials administered to the body systems are cleared, degraded and finally excreted from the body. After the initial interaction of administered nanomaterials with the body systems, clearance/excretion process of the nanomaterials is started. Mononuclear phagocytic system clears nanomaterials from the circulation by sequestering them and hepatobiliary and renal excretion works thereafter. Considering the possible toxicity of nanomaterials, controlling the clearance and excretion of injected nanomaterials are mandatory. All the factors affecting clearance and excretion have veen investigated systematically and partially established. In this chapter, we describe the physiology of clearance and excretion, and factors affecting them. Designing better nanomaterials should be based on the thorough knowledge about this physiology of nanomaterials and radionanomaterials.

19.1 Introduction

The nanomaterials can be administered to an organism for targeted imaging, targeted drug delivery, and tissue engineering. From the moment of the administration, nanomaterials interact with the body systems, and clearance/excretion process begins. The term clearance generally indicates the elimination of the nanomaterials from circulating blood while excretion refers to the removal of nanomaterials from the organism. The nanomaterials can be cleared from the blood circulation through the mononuclear phagocytic system (MPS) (also called the reticuloendothelial system) and renal system (Fig. 19.1) [1]. Meanwhile, there are two major excretory pathways which are hepatobiliary and renal routes. Since almost all nanomaterials can exert toxicity in vivo, the knowledge of clearance/excretion characteristics of nanomaterials is a prerequisite for clinical translation of the nanomaterials. Multiple

H.-J. Im (✉)
Department of Transdisciplinary Studies, Graduate School of Convergence Science and Technology, Seoul National University, Seoul, Korea
e-mail: iiihjjj@gmail.com

D. S. Lee (ed.), *Radionanomedicine*, Biological and Medical Physics, Biomedical Engineering, https://doi.org/10.1007/978-3-319-67720-0_19

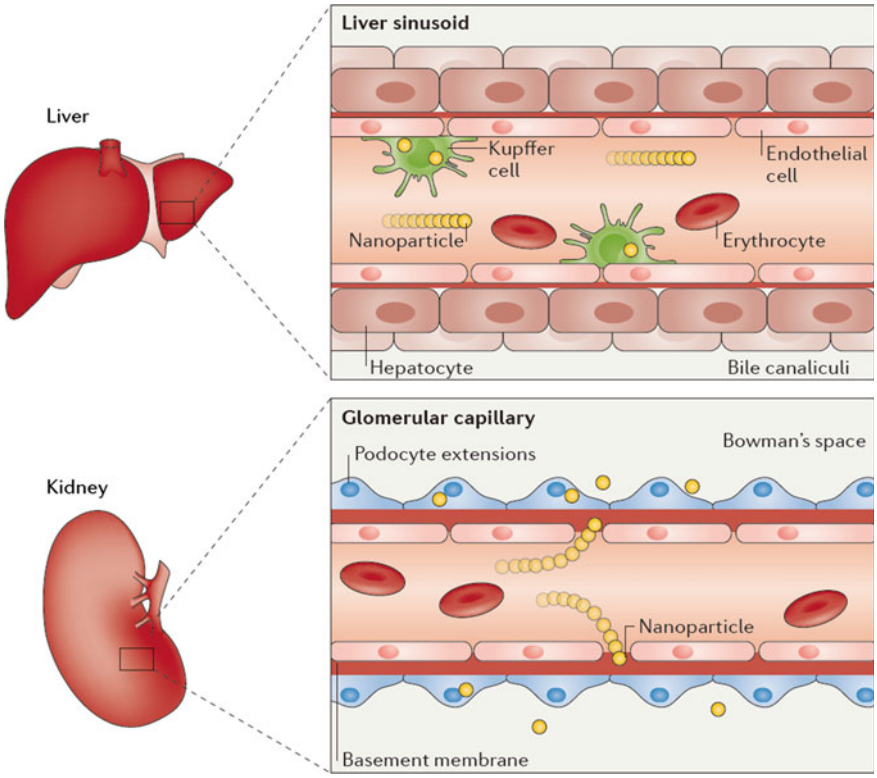

Fig. 19.1 Two major pathways for clearance of intravenously injected nanomaterials: reticuloendothelial system (RES, also called the mononuclear phagocytic system; MPS) and renal system. Reproduced with permission [1]

factors can affect the route and efficiency of clearance/excretion of nanomaterials, which includes size, charge, shape, component, and functional moiety of the nanomaterials. In this chapter, we will describe the physiology of clearance and excretion, and factors affecting the clearance/excretion, also, perspectives to design the nanomaterials with favorable clearance/excretion characteristics.

19.2 Renal Excretion of Nanoparticles

19.2.1 Physiology of Renal Excretion

The kidney is the major organ for the drug excretion. The nephron is the functional unit of the kidney and consists of a renal corpuscle and renal tubules. Renal corpuscle is composed of a glomerulus and Bowman's capsule. The glomerulus is a

capillary cluster which receives its blood flow from an afferent arteriole. Unlike other capillary beds, glomerulus drains into an efferent arteriole rather than a venule. The high resistance of an efferent arteriole results in a high pressure within the glomerulus. The high blood pressure inside the glomerulus is the driving force for water and solute to be filtered out of blood and into the space of Bowman's capsule. Bowman's capsule surrounds the glomerulus and collects filtered fluid and solutes from blood in the glomerulus. Glomerulus consists of three layers, which are endothelium, basement membrane and epithelium (podocyte). Endothelial cells have numerous, relatively large pores (fenestrae) with a diameter of 70–90 nm. While basement membrane prevents filtration of plasma proteins with 2–8 nm-sized holes and consists of laminins, type IV collagen, agrin and nidogen. Epithelium consists of podocytes which are attached to the basement membrane by their foot processes with 4–11 nm-sized slits. This layer is the final filtration barrier of plasma proteins before the fluid enters the Bowman's capsule. Additionally, negatively charged foot processes limit the filtration of negatively charged substances, such as albumin. As a result, only low molecular weight molecules (<30,000 Dalton) are filtered out of blood in the glomerulus (Fig. 19.2) [2].

Bowman's capsule is the starting point of the renal tubules. Filtered fluid runs through renal tubule and enters into collecting duct system. In the proximal tubule, weak electrolyte drugs are actively secreted, and water is reabsorbed. In the loop of Henle, water reabsorption occurs. Also, passive reabsorption of water and lipophilic drugs takes place in the distal tubules. In the collecting duct system, the concentration of the urine can be adjusted by action of antidiuretic hormone. Urine depart the medullary collecting ducts and go through the renal papilla, calyces, pelvis, and finally into the bladder via the ureter.

19.2.2 Renal Excretion of Nanomaterials

Nanomaterials with hydrodynamic diameters (HD) <6 nm are filtered in the glomerulus and thus can be excreted in urine. Generally, nanoparticles (NP) with HD >8 nm are not filtered with some exceptions which will be discussed in the last part of this section. In case of NPs with the intermediate size of 6–8 nm, the charge of the NPs determine the filtration and positively charged NPs are prone to be filtered more because of negatively charged foot process. Once NPs cleared out from blood at renal corpuscle, the majority of the NPs are excreted via urine because nanomaterials are generally not reabsorbed at proximal/distal tubules.

Rapid renal excretion of NPs is a huge advantage in their biocompatibility, and thus renal clearable nanoprobes were developed using multiple types of NP platforms including quantum dots (QD), C dots (or Cornell dots), and ultrasmall gold NPs [3] (Table 19.1). In 2007, renal clearable QDs were developed (Fig. 19.3a) [4], and other inorganic NPs followed including ultrasmall fluorescent silica NPs such as C dots [11, 12, 17], glutathione-coated gold NPs [6, 18] and carbon nanotubes [15]. Ultra-small dye encapsulated fluorescence silica NPs, also known as C dots

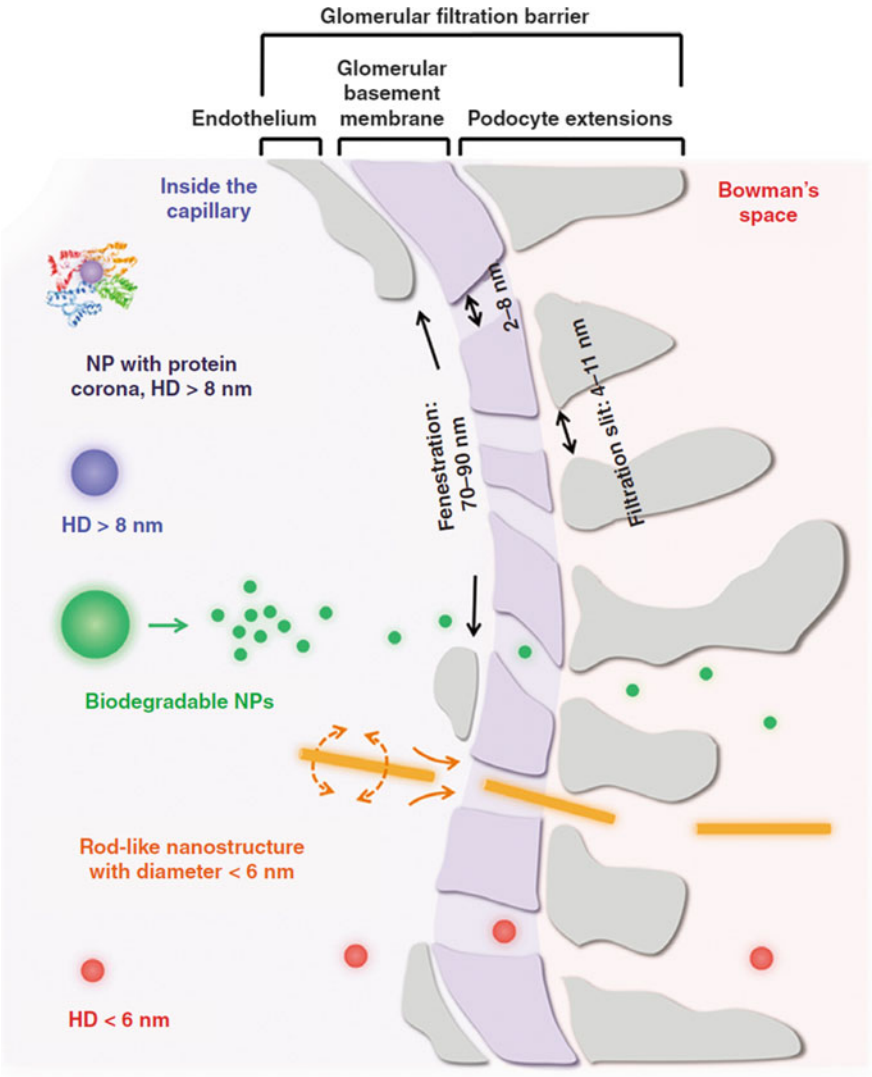

Fig. 19.2 The structure of the filtration barriers in the glomerulus. Reproduced with permission [2]

already entered into clinical trials in 2011 (NCT01266096, NCT02106598). These NPs are functionalized with near infrared (NIR) dye, cyclic RGD, and radioisotopes for multimodal targeted imaging of cancer.

With HD of 6–8 nm and neutral charge, the NPs can be cleared through kidneys effectively with sufficiently long blood circulation time (half-life = 190 min). In a melanoma xenograft mouse model, the NPs showed the tumor uptake of only 2.0% ID/g, but tumor to muscle ratio was as high as five [12]. In the first report of the human clinical trial of C dots, the NPs were cleared out by the kidneys, and there

Table 19.1 Renal excretable nanoparticles

Nanoparticle core	Surface coating	Core size/ HD	Strategy	Animal model	Imaging	Quantification	Renal clearance	References
Quantum dot	Cystein	2.9/4.4	Ultrasmall core + Zwitterionic surface	SD rats	Fluorescence	Gamma counting	75%ID in 4 h	[4]
	cRGD-cystein	3.4/5.5	Ultrasmall core + Zwitterionic surface	Tumor bearing CD-1 mice	Fluorescence	Gamma counting	>65%ID in 4 h	[5]
	GPI-cystein	3.4/5.5	Ultrasmall core + Zwitterionic surface	Tumor bearing CD-1 mice	Fluorescence	Gamma counting	>65%ID in 4 h	[5]
AuNP	GSH	1.7/2.1	Ultrasmall core + Zwitterionic surface	BALB/c	Fluorescence/ CT	ICP–MS	>50%ID in 24 h	[6]
	^{198}Au doped/GSH	2.6/3.0	Ultrasmall core + Zwitterionic surface	BALB/c	Fluorescence/ SPECT	Gamma counting	>50%ID in 48 h	[7]
	^{111}In–DTPA	2.4/6.6	Ultrasmall core + Zwitterionic surface	FISHER rats	Fluorescence/ SPECT	Gamma counting	64%ID in 24 h	[8]
	^{64}Cu–NOTA, GSH	2–3/2.6	Ultrasmall core + Zwitterionic surface	BALB/c mice	PET	Gamma counting	>75%ID in 24 h	[9]
	FA–PEG1000-GSH	2.0, 6.1	Ultrasmall core + PEGylation	Tumor-bearing BALB/c mice	Fluorescence	None	NR	[10]
Silica nanoparticles (Cornell dots)	PEG500	NR/3.3	Ultrasmall core + PEGylation	Nude mice	Fluorescence	Fluorescence	73%ID in 48 h	[11]

(continued)

Table 19.1 (continued)

Nanoparticle core	Surface coating	Core size/ HD	Strategy	Animal model	Imaging	Quantification	Renal clearance	References
	^{124}I–cRGD–PEG500	NR/6.8	Ultrasmall core + PEGylation	Athymic nude mice	PET	Gamma counting	72%ID in 72 h	[12]
Gd-Carbon dots	ZW800-PET1500 and ^{64}Cu–DOTA–PEG	NR/12	Unknown	Nude mice	MRI	None	NR	[13]
Porous silica nanoparticle	NR	NR/126	Biodegradable NP	BALB/c	Fluorescence	NR	NR	[14]
Carbon nanotube	^{86}Y–DOTA(AF488) (AF680)	200–300	High aspect ratio	Nude mouse	PET	PET	$T_{1/2}$: 6 min	[15]
		500–2000	High aspect ratio	BALB/c	TEM	None	NR	[16]

NP nanoparticle, *HD* hydrodynamic diameter, *SD* Sprague Dawley, *ID* injected dose, *RGD* Arginylglycylaspartic acid. *GPI* (2-[((3-amino-3-carboxypropyl)(hydroxy)phosphinyl)-methyl]pentane-1,5-dioic acid, *GSH* glutathione, *CT* computed tomography, *ICP–MS* Inductively coupled plasma mass spectrometry, *SPECT* single photon emission computed tomography, *DTDTPA* dithiolated diethylenetriamine pentaacetic acid, *NR* not reported, *NOTA* 1,4,7-triazacyclononane-triacetic acid, *DOTA* 1,4,7,10-tetraazacyclododecane-tetraacetic acid, *FA* folic acid, *PET* positron emission tomography, *TEM* transmission electron microscopy. Modified and reproduced with permission [60]

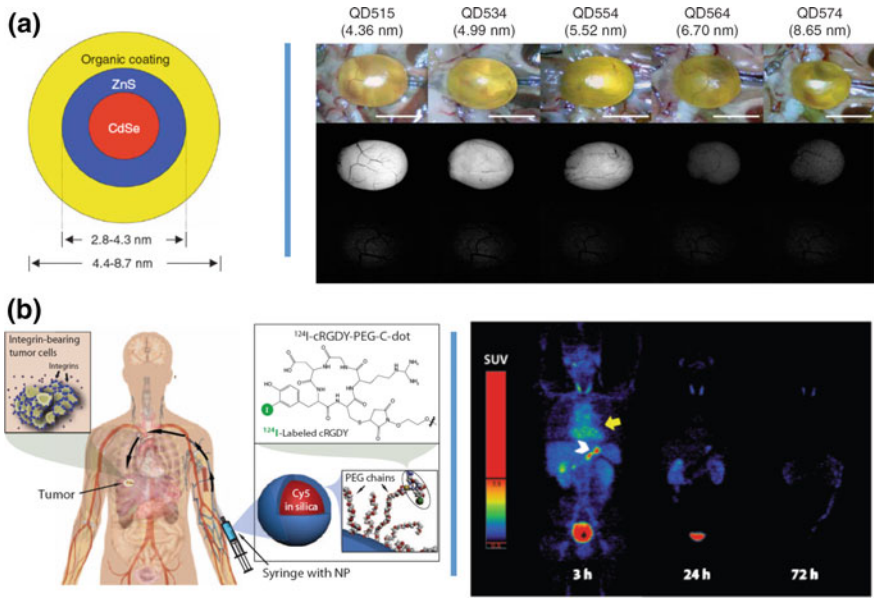

Fig. 19.3 **a** The structure of ultrasmall quantum dot (QD) on the left. Surgically exposed mouse bladders 4 h after intravenous injection of QD515, QD534, QD554, QD564 or QD574 of defined hydrodynamic diameters (shown in parenthesis) on the right. Color photo (top), fluorescence images (middle), uninjected control bladder (bottom). Reproduced with permission [4]. **b** Schematic illustration of the use of cRGDY peptide functionalized, ^{124}I-labeled C dot NPs in a human patient (left). Maximum intensity projection PET images after intravenous injection of ^{124}I–cRGDY–PEG–C dots showed tracer uptake at urinary bladder (*), blood pool (yellow arrow), and intestine (white arrowhead) (right). Reproduced with permission [17]

was no adverse reaction and C dots was proposed to be safe in human cancer diagnostics (Fig. 19.3b) [17]. Ultrasmall gold NPs (AuNPs) which are coated with glutathione (GSH) and have sizes of 2–3 nm also showed efficient renal clearance. These NPs had very short blood circulation time and thus had a shortcoming in tumor targeting which needed high enhanced permeability and retention (EPR) effect, and rather highly suitable for noninvasive renal functional imaging. GSH–AuNP showed the ability of noninvasive assessment of kidney clearance which was enabled by intrinsic NIR luminescence in mice. In a unilateral ureteral obstruction mouse model, the NPs were able to detect the decreased renal function of obstructed kidney and further stratify the severity of the renal dysfunction [19]. Nevertheless, this approach is hardly going to be used in the clinic because of the limitation of penetration depth of the luminescence and existing clinically successful radiopharmaceuticals such as ^{99m}Tc–MAG3 (mercaptoacetyltriglycine) or ^{99m}Tc–DTPA (diethylenetriaminepentaacetic acid). Luminescence imaging using GSH–AuNP may be useful for renal function evaluation in mice where radioisotope imaging is not available since there is no need for radioisotope.

As in the case of GSH–AuNP, short circulation time of renal clearable NPs reduces the chance of delivering NPs to a target lesion. Thus balancing the efficient renal excretion and sufficient circulation time is an important issue. Enhancing EPR without sacrificing renal clearance is quite challenging but can be achieved. Switching surface ligand of AuNPs from GSH to PEGylated ligand can significantly increase the blood retention time of AuNPs, which can further enhance tumor targeting efficiency of renal clearable AuNPs [20]. Renal clearable PEG–AuNPs exhibited the higher targeting efficiency than GSH–AuNPs (8.3 vs. 2.3%ID/g). Pharmacokinetics analysis indicated that enhanced circulation half-life resulted in high EPR effect and thus high tumor targeting of PEG–AuNPs. Liang et al. reported the efficient renal excretion and passive targeting of tetra (4-carboxyphenyl)porphyrin (TCPP) NPs with variable PEGylation (Fig. 19.4a) [21]. They compared TCPP NPs conjugated with 2, 5, 10, and 30 K PEG and found that TCPP NPs with 10 K PEG showed enough circulation time for passive targeting and acceptable range of renal excretion as well (Fig. 19.4b).

Although, 6 or 8 nm is the well-known limit of renal clearable NPs, there are outliers for this rule. Ruggiero et al. [22] and Lacerda et al. [23] reported the unexpected glomerular filtration and urinary excretion of carbon nanotubes (CNTs) with the length of 200–300 nm. It seems that the glomerular filtration of this long CNTs is caused by its high aspect ratio (1:100–500), however, the exact mechanism has not yet been proved. Parts of the CNTs were reabsorbed to proximal tubules after glomerular filtration, which is also an unusual phenomenon for NPs (Fig. 19.5).

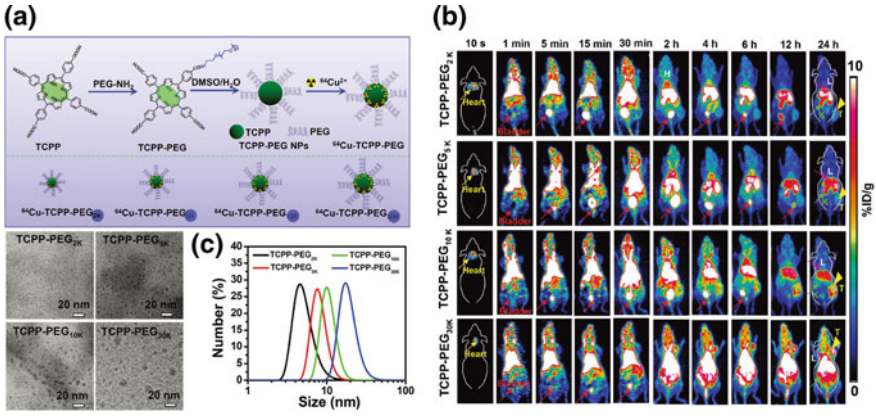

Fig. 19.4 **a** Synthesis and characterization of tetra(4-carboxyphenyl)porphyrin (TCPP) PEG NPs. (Upper) TCPP molecule conjugated with different molecular weight PEG molecules and ^{64}Cu labeling. (bottom left) TEM images of TCPP–PEG2 K, TCPP–PEG5 K, TCPP–PEG10 K, and TCPP–PEG30 K NPs. (bottom right) The hydrodynamic diameters (HDs) of TCPP–PEG NPs with various PEG (4.6 nm for TCPP–PEG2 K, 7.5 nm for TCPP–PEG5 K, 10.1 nm for TCPP–PEG10 K, and 17.3 nm for TCPP–PEG30 K). **b** In vivo PET images of 4T1 tumor-bearing mice using ^{64}Cu–TCPP–PEG2 K, ^{64}Cu–TCPP–PEG5 K, ^{64}Cu–TCPP–PEG10 K, and ^{64}Cu–TCPP–PEG30 K NPs. Liver (L), kidneys (K, yellow arrowhead), heart, and bladder are indicated. Reproduced with permission [21]

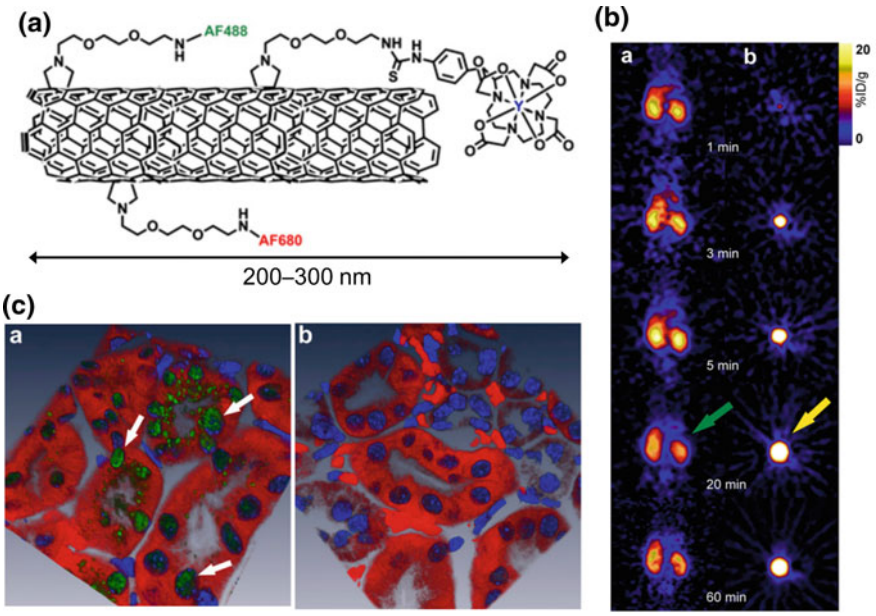

Fig. 19.5 **a** (Upper) Schematic representation of single walled carbon nanotubes (SWCNT) functionalized with DOTA, AF488, and AF680, (SWCNT–[([^{86}Y]DOTA)(AF488)(AF680)]). **b** In vivo PET images after injection of SWCNT–[([^{86}Y]DOTA)(AF488)(AF680)] showing rapid renal clearance (green arrow: kidney, yellow arrow: urinary bladder) **c** Confocal microscopic immunofluorescence image of the renal cortex at 1 h post injection of SWCNT–[(DOTA)(AF488)(AF680)], showing both cytoplasmic and nuclear accumulation (left, green), and control (not-injected) mice (right). Blue: nucleus, Red: cytoplasm. Reproduced with permission [15]

19.3 Opsonization and Mononuclear Phagocytic System (MPS) Clearance

19.3.1 Opsonization

Opsonization is the molecular event that NPs, microbes, or apoptotic cells are chemically modified in the blood to have stronger interactions with phagocytes (monocytes, macrophages, neutrophils and dendritic cells) and natural killer cells. An opsonin (from a Greek word meaning "to prepare for eating") is any molecule that enhances phagocytosis by marking on the NPs or microbes to be more recognizable to phagocytes. After opsonization, NPs binding to phagocytes is greatly increased. Opsonin molecules include an antibody, complement proteins and other circulating proteins such as pentraxins, collectins and ficolins [24–26]. There are over 1000 kinds of proteins in the blood circulation, and the proteins interact with intravenously injected NPs and form a shell like coverage surrounding the NPs which is called collectively corona proteins [27]. Opsonization could be regarded as

a part of the protein corona formation process. However, not all the circulating proteins can facilitate phagocytosis of the NPs.

The efficiency of opsonization can differ according to their surface properties including charge and hydrophobicity. The characteristics and consequences of the protein corona formation have been well described in several review articles and another chapter "Corona and its Consequences". This protein adsorption significantly affect the biodistribution of the NPs, speedy recognition and clearance by MPS (also called the reticuloendothelial system; RES) in particular [28]. The hydrophobic and electrostatic interactions are the main forces for protein adsorption on NPs [29, 30]. Higher charge and higher hydrophobicity of NPs are the major factors to make NPs prone to be opsonized [31, 32]. Without the opsonization, phagocytes are generally not able to capture the foreign materials. After opsonization, bound opsonins such as complement may undergo a conformational change to have an activated protein structure that can be well recognized by the receptors of the phagocytes [33].

19.3.2 Interaction Between MPS and Nanoparticles

Circulating nanomaterials are recognized after opsonization by tissue macrophage system, MPS also known as RES [34]. MPS is a part of the innate immune system which can be found in kidneys, lungs, bone marrow, liver, spleen and lymph nodes etc. MPS eliminates foreign invaders non-specifically via direct interactions with the phagocytic cells. Kupffer cells in the liver sinusoid are a major portion of MPS which makes up 80–90% total body macrophage population. Further detailed information regarding innate immune response to NPs is found in the chapter "Innate Immunity". NPs cleared by MPS are not excreted from body system shortly, because NPs are not well dissolved by a chemical reaction in lysosomes of the phagocytes (Fig. 19.6) [35–38]. This can be problematic since persistence in the phagocytic system can induce cell/tissue toxicity [39, 40]. Also, fast clearance to MPS results in a short blood circulation time. Short blood circulation time effectively limits the targeting efficiency of the NPs, especially when NPs are targeted by passive targeting. Lower or slower MPS clearance of NPs is challenging in most cases but mandatory for effective targeted imaging/therapy using NPs. Thus, MPS recognition of NPs is the major hurdle for development and clinical translation of the targeted delivery of NPs [28, 34, 41, 42].

Lowering MPS recognition of the NPs, i.e. the stealth effect of NPs, can be primarily achieved by reducing the opsonization and there are several strategies (Fig. 19.7). Polysaccharides (dextrans) and polyethylene glycols (PEGs) are the two popular methods to reduce opsonization [43]. Flexibility and high hydrophilicity of these polymers interfere the hydrophobic interaction between NPs and blood proteins. However, when the same PEGylated NPs are injected into the same animal second time, MPS recognition of the NPs become faster resulting in faster blood clearance. This phenomenon is known as Accelerated Blood Clearance

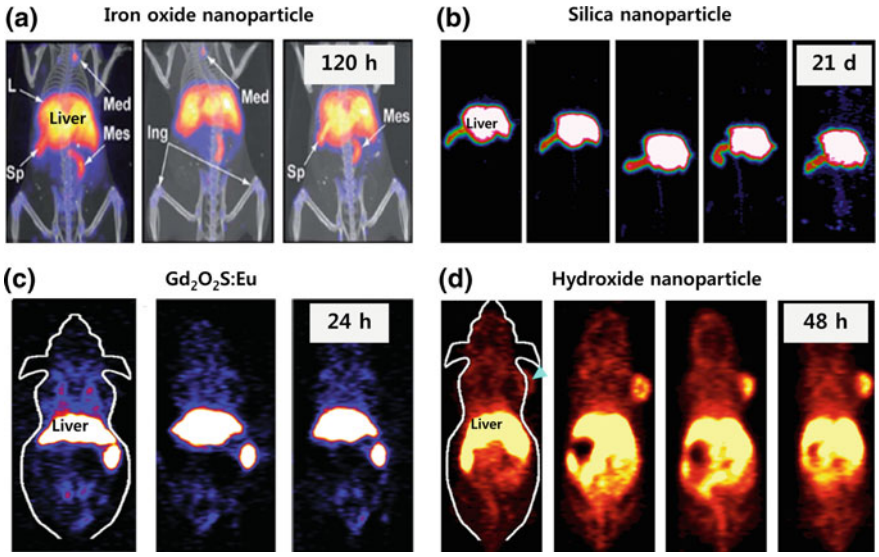

Fig. 19.6 Sustained liver uptake of NPs **a** PET/CT maximum intensity projection (MIP) images recorded between 0–120 h post-i.v. injection of ^{89}Zr-ferumoxytol in mice. Reproduced with permission [35] **b** In vivo PET MIP images of mice at different time points up to 21 days after i.v. injection of ^{89}Zr-mesoporous silica NPs (MSN). Reproduced with permission [36]. **c** Serial in vivo PET images of [^{89}Zr]Gd2O2S:Eu@PEG in mice at different post-injection time points Reproduced with permission [37]. **d** Serial coronal PET images at different time points post-injection of ^{64}Cu-Layered double hydroxide(LDH)-bovine serum albumin(BSA) acquired in 4T1 tumor-bearing mice. Reproduced with permission [38]

(ABC). This is caused by the formation of anti-PEG IgM antibody after the first injection of the PEGylated NPs. When the same PEGylated NPs are injected, the preformed anti-PEG IgM recognizes the PEGylated NPs. Consequently, opsonization and complement activation take place which can facilitate RES recognition of the NPs [44]. Another way to reduce opsonization is called "active stealth" approach. Rodriguez et al. attached CD47 'self' peptides on the NPs, and the NPs showed longer blood half-life by delaying splenic phagocytic clearance [45]. Biomimetic particle coating can also reduce the opsonization and consequent phagocytic clearance. Parodi et al. reported that NP coated using cell membranes from leukocytes showed a reduction of serum protein attachment and lower MPS uptake [46].

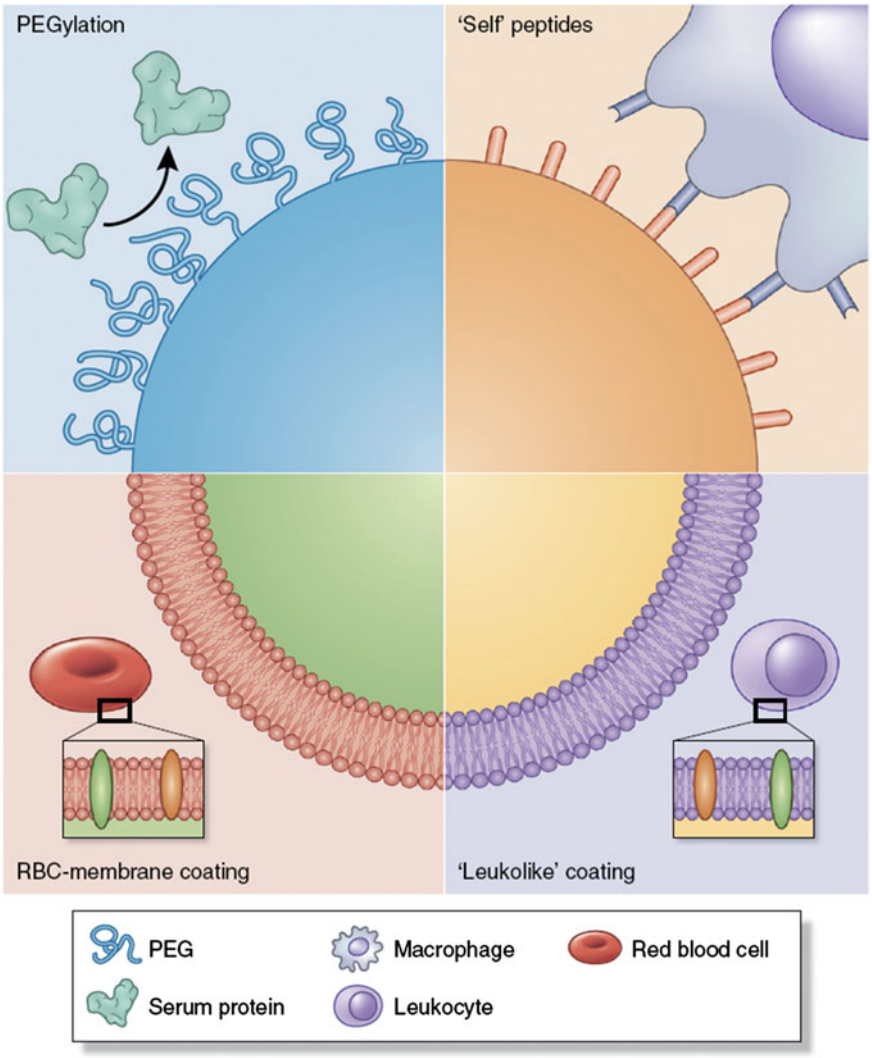

Fig. 19.7 Strategies for NPs to avoid MPS (or RES) recognition and prolong blood circulation. PEGylation is a classic strategy. The attachment of PEG to the surface makes a hydrating layer to inhibit protein corona formation. An active stealth strategy includes attachment of a self CD47 peptides, which makes macrophages consider the NPs as 'self' so that the NPs escape phagocytosis. Coating of NPs with biological cell membranes obtained from autologous leukocytes and red blood cells (RBC) provides a biomimetic surface shown to prolong in vivo circulation substantially. Reproduced with permission [34]

19.4 Hepatobiliary Excretion of Nanoparticles

19.4.1 Anatomy and Physiology of the Liver

The liver is the biggest solid organ weighing 1.5–2.0 kg on average in the human adult. The liver can be found just below the right side diaphragm and partially covered by rib cage [47]. The liver consists of the larger right and the smaller left lobes which are separated by the hepatic vein in the middle. The primary functions of the liver include: (1) regulation of the glucose and fat metabolism, (2) production and secretion of bile, (3) metabolism of drugs, chemicals, and alcohol (4) production of essential body proteins including albumin, coagulation factors (5) regulation of hormone balances including sex, thyroid hormones, and cortisone. The liver consists of functional groups of hepatic lobules. The lobules are composed of plates of hepatocytes radiating from a central vein and form roughly hexagonal shapes. The central vein drains into hepatic vein. At the each corner of the lobule, porta triads run vertically. The porta triads was named because there are branches of the hepatic artery, hepatic portal vein, bile duct, but currently, it has been revealed that there is two more components in the porta triads, which are a lymphatic vessel and the vagus nerve.

Inside the hepatic lobules, there are multiple radial arrays of hepatocytes and sinusoids. The sinusoid is a type of capillary system which has fenestrated endothelium. The sinusoid receives blood from both oxygen-rich hepatic artery and nutrient-rich portal vein. The blood is mixed in the sinusoids and drains into hepatic vein. Hepatocytes are located beside the sinusoids with gaps named space of Disse while Kupffer cell resides inside of the sinusoid. However, hepatocytes can interact with materials in the sinusoid though fenestration in the sinusoids. Between the hepatocytes, biliary canaliculus can be found which consists of biliary epithelial cells. Bile in the biliary canaliculi drains into larger bile ducts in the porta triad and further collected through the biliary tree (Fig. 19.8) [48]. Bile can be directly secreted into the duodenum via extrahepatic bile duct or accumulated in the gall bladder and secreted into duodenum when the gall bladder squeezes. Sixty to eighty percent of the cells in the liver are hepatocytes and the other twenty to forty percent of the cells include Kupffer cells, sinusoidal endothelial cells, stellate cells, biliary epithelial cells, lymphocytes and circulating blood cells [49].

19.4.2 Hepatobiliary Excretion

Not all NPs in the liver are captured in the MPS. Although the hepatocytes are separated from the sinusoid, the capillary system in the liver, some NPs can make their way to the hepatocytes. To be excreted via the hepatobiliary pathway, size of NPs should be smaller than 120–150 nm which is the size of hepatic sinusoidal fenestration. In 1989, Renaud et al. reported that low-density lipoprotein

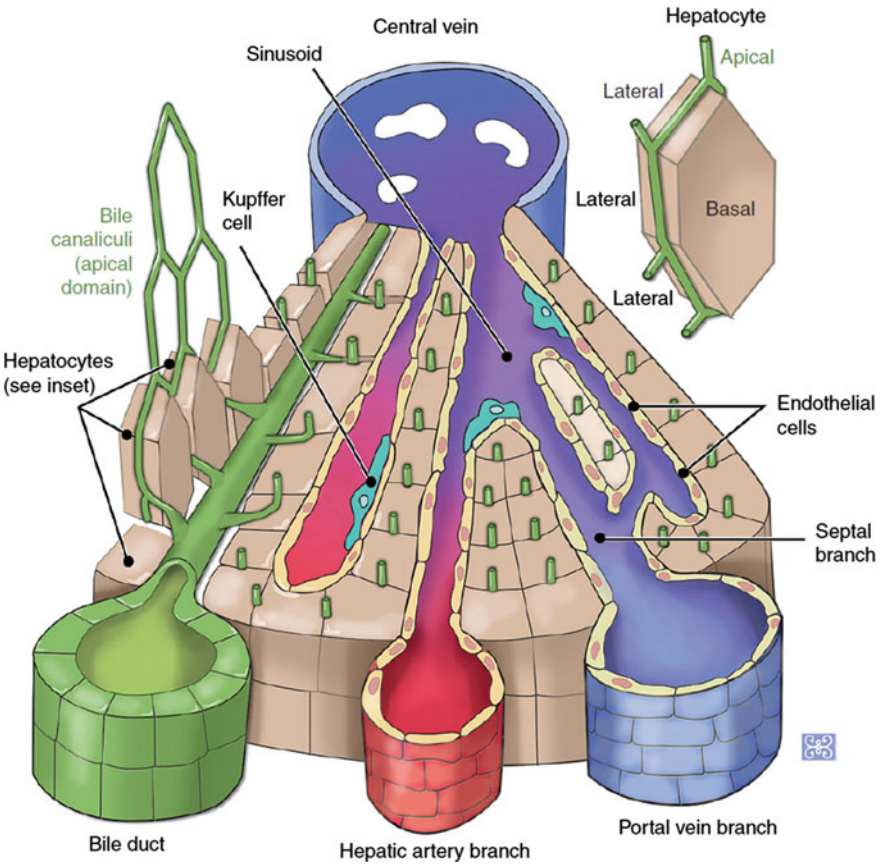

Fig. 19.8 Microanatomy of the hepatic lobule. Hepatocytes, Kupffer cells, bile ducts, and sinusoids are represented. The shape of a hepatocyte is shown with its apical, basal, and lateral sides. In the sinusoid, blood from a hepatic artery and portal vein is mixed and drains to central vein. Bile canaliculi are shown between the hepatocytes merge into larger biliary ducts. Kupffer cells attach to endothelial cells, the inner side of sinusoids. Reproduced with permission [48]

(LDL) gold complex could enter into the hepatocytes after MPS depletion using gadolinium chloride [50]. Recently, several in vivo imaging studies accompanied by transmission electron microscopy (TEM) experiments revealed that the NPs reached the hepatocytes and could be excreted via hepatobiliary excretion [40, 51, 52]. Several in vivo imaging studies including fluorescence [53, 54], magnetic resonance imaging (MRI) [55–57], positron emission tomography (PET) [40] showed the efficient hepatobiliary excretion of NPs after initial hepatic uptake of the NPs (Fig. 19.9; Table 19.2). Also, several studies among them were able to show that the NPs were taken up by hepatocytes and moved to bile canaliculi by TEM imaging which proved the hepatobiliary excretion of the NPs [40, 52]. The process of hepatobiliary excretion of NPs is schematically explained in Fig. 19.10 [64].

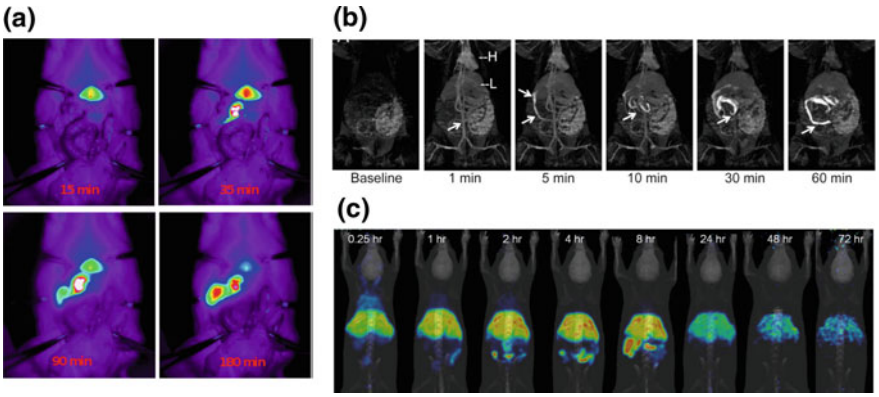

Fig. 19.9 **a** Fluorescence imaging of hepatobiliary transport of mesoporous silica NPs–amine–indocyanine green (MSN–NH2–ICG) into the intestine in the rat after i.v. injection. At 15 min after injection, most of the MSN–NH2–ICG has been taken up by the liver. A substantial amount of the NPs is progressively excreted to the intestine until 180 min after the injection. Reproduced with permission [53]. **b** Magnetic resonance (MR) cholangiogram in a rat after the intravenous injection of gadolinium functionalized NP. Baseline image shows no enhanced signal at bile duct. 1 min after the injection, heart, aorta (arrow), and peripheral vasculature show strong T1-weighted positive contrast, which indicates that NPs are still in the blood circulation. H = heart, L = liver. At 5 min, the NP is excreted through the common bile duct (arrows). Passage through the small intestines and large intestines can be seen at 10 and 30 min after the injection. Reproduced with permission [56]. **c** In vivo PET images at different time points after intravenous injection of micelle encapsulated ^{64}Cu–NOTA–UCNPs. NPs were sequestered in the liver up to two hours after the injection. Intestinal uptake was found one hour after the injection followed by the increased intestinal uptake until 8 h. The intestinal uptake was minimal at 24 h after injection, indicating the hepatobiliary excretion of the NPs. Reproduced with permission [40]

If the NPs are not recognized by MPS and have a smaller size than 120 nm (size of sinusoidal fenestration), there is a high chance for NPs to be taken up by hepatocytes and excreted via a hepatobiliary pathway. Thus, the strategy to enhance the hepatobiliary excretion of the NPs is similar to that of lowering MPS recognition. Surface modification such as higher charge or micelle encapsulation can improve the efficiency of hepatobiliary excretion. Souris et al. reported that mesoporous silica NPs with higher positive surface charge (+34.4 mV) showed faster hepatobiliary excretion than those with negative surface charge (−17.6 mV) [53]. In vivo biodistribution analysis, substantial excretion to intestine was observed after initial uptake to the liver [40, 53]. Seo et al. reported the micelle encapsulated upconverting NP (UCNP) can be cleared via hepatobiliary excretion in their integral forms [40]. We observed the substantial amount of NPs were excreted from liver after initial liver accumulation. It is speculated that micelle encapsulation of the NPs may lower the protein corona formation and thus lower MPS recognition.

Table 19.2 Hepatobiliary excretable nanoparticles

	Type of Nanoparticle	Size (nm)	Strategy	Animal model	Imaging	Quantification	Hepatobiliary excretion	References
Silica NP	MSN	80	High surface charge	Nude mice/SD rat	Fluorescence	ICP–AES	Clearance onset from 30 min	[53]
	MSN	110	None	ICR mice	TEM	ICP–AES	Elimination within 24 h	[51]
	ORMOSIL	20	High surface charge	Athymic nude mice	Fluorescence	Gammacounting	100% after 15 days	[54]
	MSN–FITC	100–130	None	Xenograft tumor-bearing BALB/c nude mice	None	ICP–AES	21% in 96 h	[58]
	Aminoclay	36–65	None	ICR mice	Fluorescence	HPLC	41% in 72 h	[59]
Gadolinium NP	Gd-diethylenetriamine-pentaacetate-bis-oleate	220	None	Rat	MR cholangiography	None	Entry into biliary tree within 5 min	[56]
	Gd-cholesterol-HDL nanoparticle	20–25	Cholesterol and HDL	SD rats	MRI	None	Enters duodenum in 5 min	[55]
Gold NP	^{195}Au–LDL	20	Gadolinium chloride (RES saturation), LDL	SD rats	TEM	Gamma counting	50%ID in 22 days after RES saturation	[50]
	BSA–Au nanorods	55.6 × 13.3	None	SD rats	None	ICP–MS	1.5%ID in 14 days	[60]

(continued)

Table 19.2 (continued)

	Type of Nanoparticle	Size (nm)	Strategy	Animal model	Imaging	Quantification	Hepatobiliary excretion	References
Manganese oxide NP	MnO	6.3	Phosphor-dendron ligands	BALB/c mice	MRI	Neutron activation analysis	>70%ID in 48 h	[57]
	Mn_3O_4	9	None	Kunming white mice	MRI	ICP–MS	50% in 1.5 weeks	[61]
Iron oxide NP	FeO–HDL	7–13	HDL	ApoE KO and WT mice	TEM	None	NR	[52]
	Ferumoxtran-10	30	None	SD rats	None	Gamma counting (^{59}Fe)	16–21%ID in 84 days	[62]
UCNP	Micelle encapsulated UCNP	34	Micelle encapsulation	BALB/c mice	PET	Gamma counting	84% of initial hepatic uptake in 72 h	[40]
	UCNP	5.1, 18.5	None	LS180 tumor bearing BALB/c nude mice	None	ICP–AES	5.1 nm: 53% ID in 14 days 18.5 nm: 78% ID in 14 days	[63]

NP nanoparticle, *MSN* mesoporous silica nanoparticle, *SD* Sprague Dawley, *ID* injected dose, *ICP–AES* Inductively coupled plasma atomic emission spectroscopy, *ORMOSIL* Organically modified silica, *HPLC* High-performance liquid chromatography, *Gd* gadolinium, *HDL* High-density lipoprotein, *LDL* low-density lipoprotein, *MRI* magnetic resonance imaging, *RES* reticuloendothelial system, *UCNP* upconverting nanoparticle, *ICP–MS* Inductively coupled plasma mass spectrometry, *NR* not reported, *PET* positron emission tomography, *TEM* transmission electron microscopy. Modified and reproduced with permission [51]

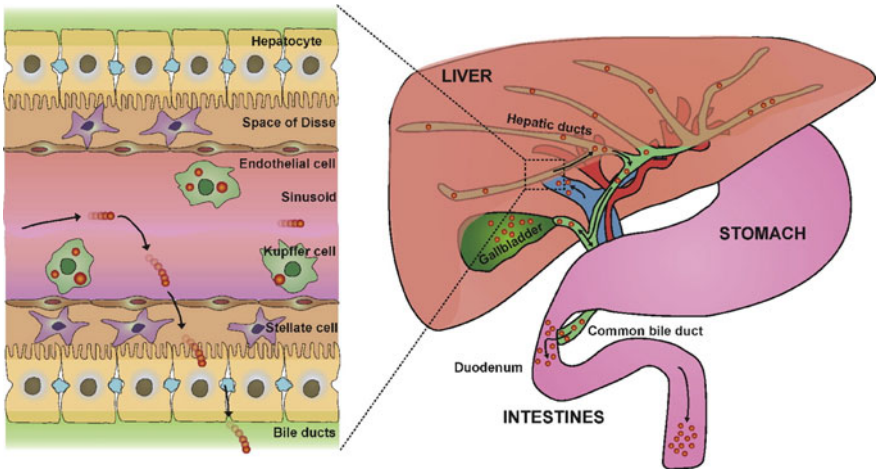

Fig. 19.10 Schematic representation of the hepatobiliary excretion process of the NPs. NPs enter the liver via the portal vein or hepatic artery. While NPs pass through the sinusoid, NPs may be phagocytosed and sequestered in MPS (or RES) in the liver, the Kupffer cells. Otherwise, NPs can be filtered out from sinusoid into the space of Disse and be endocytosed by hepatocytes. Inside the hepatocytes, NPs can be transcytosed and excreted to the bile duct via bile canaliculi. NPs may first be collected inside the gallbladder or directly secreted into the common bile duct. NPs are excreted into the duodenum under the control of the sphincter of Oddi. NPs in the duodenum travel the entire small and large intestine and finally excreted in the feces. Reproduced with permission [64]

19.5 Perspectives

Understanding the mechanism of clearance and excretion of the NPs is the key to open the wide gate to the clinical translation of nanomedicines. Renal clearance can be achieved more easily by utilizing the NPs with ultrasmall core than hepatobiliary clearance. However short circulation time may be the fundamental shortcoming for the renal clearable NPs. While the strategies to enhance the hepatobiliary excretion and circulation time are similar, strategy to enhance hepatobiliary excretion has not been well established, and not all NPs with extended circulation time can be excreted via hepatobiliary pathway. There is a strong need for a better understanding of the interaction between the NPs and the liver structures especially hepatocytes. Further investigation should be done to reveal the way to develop NPs with sufficient blood circulation and good hepatobiliary excretion property.

References

1. S. Wilhelm, A.J. Tavares, Q. Dai, S. Ohta, J. Audet, H.F. Dvorak et al., Analysis of nanoparticle delivery to tumours. Nat. Rev. Mater. **1**, 16014 (2016)
2. J. Xu, C. Peng, M. Yu, J. Zheng, Renal clearable noble metal nanoparticles: photoluminescence, elimination, and biomedical applications. Wiley Interdiscip. Rev. Nanomed. Nanobiotechnol. **9**, 5 (2017)
3. E.B. Ehlerding, F. Chen, W. Cai, Biodegradable and renal clearable inorganic nanoparticles. Adv. Sci. (Weinh.) **3**(2), 1500223 (2016)
4. H.S. Choi, W. Liu, P. Misra, E. Tanaka, J.P. Zimmer, B. Itty Ipe et al., Renal clearance of quantum dots. Nat. Biotechnol. **25**(10), 1165–1170 (2007)
5. H.S. Choi, W. Liu, F. Liu, K. Nasr, P. Misra, M.G. Bawendi et al., Design considerations for tumour-targeted nanoparticles. Nat Nano. **5**(1), 42–47 (2010)
6. C. Zhou, M. Long, Y. Qin, X. Sun, J. Zheng, Luminescent gold nanoparticles with efficient renal clearance. Angew. Chem. Int. Ed. Engl. **50**(14), 3168–3172 (2011)
7. C. Zhou, G. Hao, P. Thomas, J. Liu, M. Yu, S. Sun et al., Near-infrared emitting radioactive gold nanoparticles with molecular pharmacokinetics. Angew. Chem. Int. Ed. Engl. **51**(40), 10118–10122 (2012)
8. C. Alric, I. Miladi, D. Kryza, J. Taleb, F. Lux, R. Bazzi et al., The biodistribution of gold nanoparticles designed for renal clearance. Nanoscale **5**(13), 5930–5939 (2013)
9. F. Chen, S. Goel, R. Hernandez, S.A. Graves, S. Shi, R.J. Nickles et al., Dynamic positron emission tomography imaging of renal clearable gold nanoparticles. Small **12**(20), 2775–2782 (2016)
10. C. Zhang, C. Li, Y. Liu, J. Zhang, C. Bao, S. Liang et al., Gold nanoclusters-based nanoprobes for simultaneous fluorescence imaging and targeted photodynamic therapy with superior penetration and retention behavior in tumors. Adv. Funct. Mater. **25**(8), 1314–1325 (2015)
11. A.A. Burns, J. Vider, H. Ow, E. Herz, O. Penate-Medina, M. Baumgart et al., Fluorescent silica nanoparticles with efficient urinary excretion for nanomedicine. Nano Lett. **9**(1), 442–448 (2009)
12. M. Benezra, O. Penate-Medina, P.B. Zanzonico, D. Schaer, H. Ow, A. Burns et al., Multimodal silica nanoparticles are effective cancer-targeted probes in a model of human melanoma. J. Clin. Invest. **121**(7), 2768–2780 (2011)
13. H. Chen, G.D. Wang, W. Tang, T. Todd, Z. Zhen, C. Tsang et al., Gd-encapsulated carbonaceous dots with efficient renal clearance for magnetic resonance imaging. Adv. Mater. **26**(39), 6761–6766 (2014)
14. J.-H. Park, L. Gu, G. von Maltzahn, E. Ruoslahti, S.N. Bhatia, M.J. Sailor, Biodegradable luminescent porous silicon nanoparticles for in vivo applications. Nat. Mater. **8**(4), 331–336 (2009)
15. A. Ruggiero, C.H. Villa, E. Bander, D.A. Rey, M. Bergkvist, C.A. Batt et al., Paradoxical glomerular filtration of carbon nanotubes. Proc. Natl. Acad. Sci. U.S.A. **107**(27), 12369–12374 (2010)
16. L. Lacerda, M.A. Herrero, K. Venner, A. Bianco, M. Prato, K. Kostarelos, Carbon-nanotube shape and individualization critical for renal excretion. Small **4**(8), 1130–1132 (2008)
17. E. Phillips, O. Penate-Medina, P.B. Zanzonico, R.D. Carvajal, P. Mohan, Y. Ye et al., Clinical translation of an ultrasmall inorganic optical-PET imaging nanoparticle probe. Sci. Transl Med. **6**(260), 260ra149 (2014)
18. J. Liu, M. Yu, C. Zhou, S. Yang, X. Ning, J. Zheng, Passive tumor targeting of renal-clearable luminescent gold nanoparticles: long tumor retention and fast normal tissue clearance. J. Am. Chem. Soc. **135**(13), 4978–4981 (2013)
19. M. Yu, J. Liu, X. Ning, J. Zheng, High-contrast noninvasive imaging of kidney clearance kinetics enabled by renal clearable nanofluorophores. Angew. Chem. Int. Ed. Engl. **54**(51), 15434–15438 (2015)

20. J. Liu, M. Yu, X. Ning, C. Zhou, S. Yang, J. Zheng, PEGylation and Zwitterionization: pros and cons in the renal clearance and tumor targeting of near-IR-emitting gold nanoparticles. Angew. Chem. Int. Ed. Engl. **52**(48), 12572–12576 (2013)
21. L. Cheng, D. Jiang, A. Kamkaew, H.F. Valdovinos, H.-J. Im, L. Feng et al., Renal-clearable PEGylated porphyrin nanoparticles for image-guided photodynamic cancer therapy. Adv. Funct. Mater. **27**, 34 (2017)
22. A. Ruggiero, C.H. Villa, E. Bander, D.A. Rey, M. Bergkvist, C.A. Batt et al., Paradoxical glomerular filtration of carbon nanotubes. Proc. Natl. Acad. Sci. U.S.A. **107**(27), 12369–12374 (2010)
23. L. Lacerda, A. Soundararajan, R. Singh, G. Pastorin, K.T. Al-Jamal, J. Turton et al., Dynamic Imaging of functionalized multi-walled carbon nanotube systemic circulation and urinary excretion. Adv. Mater. **20**(2), 225 (2008)
24. M.F. Tosi, Innate immune responses to infection. J. Allergy Clin. Immunol. **116**(2), 241–249 (2005); quiz 50
25. J.V. Sarma, P.A. Ward, The complement system. Cell Tissue Res. **343**(1), 227–235 (2011)
26. M.L. Litvack, N. Palaniyar, Review: Soluble innate immune pattern-recognition proteins for clearing dying cells and cellular components: implications on exacerbating or resolving inflammation. Innate Immun. **16**(3), 191–200 (2010)
27. M. Lundqvist, J. Stigler, G. Elia, I. Lynch, T. Cedervall, K.A. Dawson, Nanoparticle size and surface properties determine the protein corona with possible implications for biological impacts. Proc. Natl. Acad. Sci. U.S.A. **105**(38), 14265–14270 (2008)
28. S. Nie, Understanding and overcoming major barriers in cancer nanomedicine. Nanomedicine (Lond.) **5**(4), 523–528 (2010)
29. A. Gessner, A. Lieske, B. Paulke, R. Muller, Influence of surface charge density on protein adsorption on polymeric nanoparticles: analysis by two-dimensional electrophoresis. Eur. J. Pharm. Biopharm. **54**(2), 165–170 (2002)
30. A. Vonarbourg, C. Passirani, P. Saulnier, J.P. Benoit, Parameters influencing the stealthiness of colloidal drug delivery systems. Biomaterials **27**(24), 4356–4373 (2006)
31. P. Aggarwal, J.B. Hall, C.B. McLeland, M.A. Dobrovolskaia, S.E. McNeil, Nanoparticle interaction with plasma proteins as it relates to particle biodistribution, biocompatibility and therapeutic efficacy. Adv. Drug Deliv. Rev. **61**(6), 428–437 (2009)
32. C.D. Walkey, W.C. Chan, Understanding and controlling the interaction of nanomaterials with proteins in a physiological environment. Chem. Soc. Rev. **41**(7), 2780–2799 (2012)
33. M.M. Frank, L.F. Fries, The role of complement in inflammation and phagocytosis. Immunol. Today **12**(9), 322–326 (1991)
34. E. Blanco, H. Shen, M. Ferrari, Principles of nanoparticle design for overcoming biological barriers to drug delivery. Nat. Biotechnol. **33**(9), 941–951 (2015)
35. E. Boros, A.M. Bowen, L. Josephson, N. Vasdev, J.P. Holland, Chelate-free metal ion binding and heat-induced radiolabeling of iron oxide nanoparticles. Chem. Sci. **6**(1), 225–236 (2015)
36. F. Chen, S. Goel, H.F. Valdovinos, H. Luo, R. Hernandez, T.E. Barnhart et al., In vivo integrity and biological fate of chelator-free zirconium-89-labeled mesoporous silica nanoparticles. ACS Nano **9**(8), 7950–7959 (2015)
37. Y. Zhan, F. Ai, F. Chen, H.F. Valdovinos, H. Orbay, H. Sun et al., Intrinsically zirconium-89 labeled Gd2O2S: Eu nanoprobes for in vivo positron emission tomography and gamma-ray-induced radioluminescence imaging. Small **12**(21), 2872–2876 (2016)
38. S. Shi, B.C. Fliss, Z. Gu, Y. Zhu, H. Hong, H.F. Valdovinos et al., Chelator-free labeling of layered double hydroxide nanoparticles for in vivo PET imaging. Sci. Rep. **5**, 16930 (2015)
39. M.A. Abdelhalim, B.M. Jarrar, Histological alterations in the liver of rats induced by different gold nanoparticle sizes, doses and exposure duration. J. Nanobioechnol. **10**, 5 (2012)
40. H.J. Seo, S.H. Nam, H.J. Im, J.Y. Park, J.Y. Lee, B. Yoo et al., Rapid hepatobiliary excretion of micelle-encapsulated/radiolabeled upconverting nanoparticles as an integrated form. Sci. Rep. **5**, 15685 (2015)

41. D.S. Lee, H.J. Im, Y.S. Lee, Radionanomedicine: widened perspectives of molecular theragnosis. Nanomedicine **11**(4), 795–810 (2015)
42. J. Shi, P.W. Kantoff, R. Wooster, O.C. Farokhzad, Cancer nanomedicine: progress, challenges and opportunities. Nat. Rev. Cancer **17**(1), 20–37 (2017)
43. C.G. England, H.J. Im, L. Feng, F. Chen, S.A. Graves, R. Hernandez et al., Re-assessing the enhanced permeability and retention effect in peripheral arterial disease using radiolabeled long circulating nanoparticles. Biomaterials **100**, 101–109 (2016)
44. H.J. Im, C.G. England, L. Feng, S.A. Graves, R. Hernandez, R.J. Nickles et al., Accelerated blood clearance phenomenon reduces the passive targeting of PEGylated nanoparticles in peripheral arterial disease. ACS Appl. Mater. Interfaces. **8**(28), 17955–17963 (2016)
45. P.L. Rodriguez, T. Harada, D.A. Christian, D.A. Pantano, R.K. Tsai, D.E. Discher, Minimal "self" peptides that inhibit phagocytic clearance and enhance delivery of nanoparticles. Science **339**(6122), 971–975 (2013)
46. A. Parodi, N. Quattrocchi, A.L. van de Ven, C. Chiappini, M. Evangelopoulos, J.O. Martinez et al., Synthetic nanoparticles functionalized with biomimetic leukocyte membranes possess cell-like functions. Nat. Nanotechnol. **8**(1), 61–68 (2013)
47. S.R.Z. Abdel-Misih, M. Bloomston, Liver anatomy. Surg. Clin. North Am. **90**(4), 643–653 (2010)
48. X. Chu, K. Korzekwa, R. Elsby, K. Fenner, A. Galetin, Y. Lai et al., Intracellular drug concentrations and transporters: measurement, modeling, and implications for the liver. Clin. Pharmacol. Ther. **94**(1), 126–141 (2013)
49. V. Racanelli, B. Rehermann, The liver as an immunological organ. Hepatology **43**(2 Suppl 1), S54–S62 (2006)
50. G. Renaud, R.L. Hamilton, R.J. Havel, Hepatic metabolism of colloidal gold-low-density lipoprotein complexes in the rat: evidence for bulk excretion of lysosomal contents into bile. Hepatology **9**(3), 380–392 (1989)
51. C. Fu, T. Liu, L. Li, H. Liu, D. Chen, F. Tang, The absorption, distribution, excretion and toxicity of mesoporous silica nanoparticles in mice following different exposure routes. Biomaterials **34**(10), 2565–2575 (2013)
52. T. Skajaa, D.P. Cormode, P.A. Jarzyna, A. Delshad, C. Blachford, A. Barazza et al., The biological properties of iron oxide core high-density lipoprotein in experimental atherosclerosis. Biomaterials **32**(1), 206–213 (2011)
53. J.S. Souris, C.H. Lee, S.H. Cheng, C.T. Chen, C.S. Yang, J.A. Ho et al., Surface charge-mediated rapid hepatobiliary excretion of mesoporous silica nanoparticles. Biomaterials **31**(21), 5564–5574 (2010)
54. R. Kumar, I. Roy, T.Y. Ohulchanskky, L.A. Vathy, E.J. Bergey, M. Sajjad et al., In vivo biodistribution and clearance studies using multimodal organically modified silica nanoparticles. ACS Nano **4**(2), 699–708 (2010)
55. M. Rui, W. Guo, Q. Ding, X. Wei, J. Xu, Y. Xu, Recombinant high-density lipoprotein nanoparticles containing gadolinium-labeled cholesterol for morphologic and functional magnetic resonance imaging of the liver. Int. J. Nanomed. **7**, 3751–3768 (2012)
56. J.W. Bulte, A.H. Schmieder, J. Keupp, S.D. Caruthers, S.A. Wickline, G.M. Lanza, MR cholangiography demonstrates unsuspected rapid biliary clearance of nanoparticles in rodents: implications for clinical translation. Nanomedicine **10**(7), 1385–1388 (2014)
57. P. Chevallier, A. Walter, A. Garofalo, I. Veksler, J. Lagueux, S. Begin-Colin et al., Tailored biological retention and efficient clearance of pegylated ultra-small MnO nanoparticles as positive MRI contrast agents for molecular imaging. J. Mater. Chem. B Mater. Biol. Med. **2** (13), 1779–1790 (2014)
58. J. Lu, M. Liong, Z. Li, J.I. Zink, F. Tamanoi, Biocompatibility, biodistribution, and drug-delivery efficiency of mesoporous silica nanoparticles for cancer therapy in animals. Small **6**(16), 1794–1805 (2010)
59. L. Yang, Y.-C. Lee, M.I. Kim, H.G. Park, Y.S. Huh, Y. Shao et al., Biodistribution and clearance of aminoclay nanoparticles: implication for in vivo applicability as a tailor-made drug delivery carrier. J. Mater. Chem. B Mater. Biol. Med. **2**(43), 7567–7574 (2014)

60. L. Wang, Y.F. Li, L. Zhou, Y. Liu, L. Meng, K. Zhang et al., Characterization of gold nanorods in vivo by integrated analytical techniques: their uptake, retention, and chemical forms. Anal. Bioanal. Chem. **396**(3), 1105–1114 (2010)
61. J. Xiao, X.M. Tian, C. Yang, P. Liu, N.Q. Luo, Y. Liang et al., Ultrahigh relaxivity and safe probes of manganese oxide nanoparticles for in vivo imaging. Sci. Rep. **3**, 3424 (2013)
62. P. Bourrinet, H.H. Bengele, B. Bonnemain, A. Dencausse, J.-M. Idee, P.M. Jacobs et al., Preclinical safety and pharmacokinetic profile of ferumoxtran-10, an ultrasmall superparamagnetic iron oxide magnetic resonance contrast agent. Invest. Radiol. **41**(3), 313–324 (2006)
63. C. Liu, Z. Gao, J. Zeng, Y. Hou, F. Fang, Y. Li et al., Magnetic/upconversion fluorescent NaGdF4:Yb, Er nanoparticle-based dual-modal molecular probes for imaging tiny tumors in vivo. ACS Nano **7**(8), 7227–7240 (2013)
64. Y.N. Zhang, W. Poon, A.J. Tavares, I.D. McGilvray, W.C. Chan, Nanoparticle-liver interactions: Cellular uptake and hepatobiliary elimination. J. Control Release **240**, 332–348 (2016)

Part VII
Immune Responses to Nanomaterials

Chapter 20: Immune Response to PEGylated Nanomedicines: Impact of IgM Response
Chapter 21: Innate Immunity to Nanomaterials

In this part, the readers can get to the facts and principles of immune responses to the administered nanomaterials or the radionanomaterials elucidated so far in animals and in humans. There has been a hope that radionanomedicines when they are used in trace amount, will avoid any adverse reaction from its pharmacological effects. Increasing specific activity of radiolabeling will decrease the amount or nanomaterials to eliminate the concerns of pharmacologic effect. However, we also know that very small amount of exogenous infectious or noninfectious materials can elicit any amount of adverse immune responses. As was commented at the end of the introductory editorial to the previous Part VI, and also as I don't think that there should be much difference between nanomaterials and radionanomaterials, this chapter is entitled with immune response to nanomaterials but not to radionanomaterials. And this is also the case with any use or trace amount of radiolabeled nanomaterials. The prediction of immune responses to the injected pharmaceuticals and even nanomaterials is extremely difficult, however, nuclear medicine physicians all know well that the trace amount of radiopharmaceuticals has shown far less risk of eliciting immune responses. To be conservative, and as we don't know that the size of nanomaterials might or might not make difference in eliciting pseudoallergy, innate immune response, or IgM or other possible cellular responses from biomacromolecules or even small molecules.

In Chap. 20, the readers will gain the well-summarized information regarding the IgM responses to nanomaterials mostly against liposomes. Recent addition of the IgM responses to other nanomaterials or even graphene oxides was touched upon. In Chap. 21, the readers will enjoy the summary of the recent radical changes in the role of innate immunity and tissue-resident macrophages, as the progress of understanding these areas was remarkable and thus thought experiment was

included about what the nanomaterials would meet, after being injected, the immune response charged cells and molecules in the body. Above all these details, the body just responds to the invading nanomaterials with all their armamentarium and we are interpreting the mechanism with limited knowledge of immune responses. Much more are to be understood with careful observation when the radionanomaterials are being used in humans in clinical settings.

Chapter 20
Immune Response to PEGylated Nanomedicines: Impact of IgM Response

Amr S. Abu Lila and Tatsuhiro Ishida

Abstract PEGylation is one of the most commonly applied approaches to realize the stealthiness of the conjugated nanomaterials in the systemic circulation. Nevertheless, despite the fact that Polyethylene glycol (PEG) is biologically inert, a mounting body of evidences has confirmed the presence of anti-PEG antibodies (anti-PEG Abs) that trigger an immunogenic response against PEG conjugates in a manner wherein PEG acts as a hapten. Since anti-PEG Abs are correlated with the accelerated clearance of subsequently administered doses of PEGylated nanocarriers, via a phenomenon known as "accelerated blood clearance" phenomenon, the existence of anti-PEG Abs has been claimed for the reduced efficiency of PEGylated therapeutics and/or development of severe adverse effects. Accordingly, careful monitoring for anti-PEG Abs is necessary prior to and throughout a course of treatment with PEGylated therapeutics. Furthermore, strategies to avert the challenges of PEG-specific immunity are needed with a deeper understanding of the mechanism of anti-PEG immunity.

20.1 Introduction

PEGylation, covalent coupling of the hydrophilic polymer polyethylene glycol (PEG) to nanocarriers-based and/or protein therapeutics, is one of the commonly applied approaches to realize the stealthiness of the conjugated nanomaterials in the

A. S. Abu Lila · T. Ishida (✉)
Department of Pharmacokinetics and Biopharmaceutics, Institute of Medical Biosciences, Tokushima University, 1-78-1, Sho-Machi, Tokushima 770-8505, Japan
e-mail: ishida@tokushima-u.ac.jp

A. S. Abu Lila
Department of Pharmaceutics and Industrial Pharmacy, Faculty of Pharmacy, Zagazig University, Zagazig 44519, Egypt

A. S. Abu Lila
Department of Pharmaceutics, College of Pharmacy, Hail University, Hail 81442, Saudi Arabia

D. S. Lee (ed.), *Radionanomedicine*, Biological and Medical Physics, Biomedical Engineering, https://doi.org/10.1007/978-3-319-67720-0_20

systemic circulation [1, 2]. The hydrophilic nature of PEG is reported to favor the formation of a hydration layer on the surface of nanocarriers-based and/or protein therapeutics, resulting in decreased adsorption of opsonins and serum proteins and, thus, less recognition and uptake by the cells of the mononuclear phagocyte system (MPS), which would lead to extended blood circulation [3, 4]. In addition, PEG has been reported to silence both humoral and cellular immunogenicity [5].

Nonetheless, in contrast to the typical assertion that PEG is non-immunogenic, a mounting body of literature has emerged claiming PEG to be immunogenic [6, 7]. Many reports have demonstrated that an intravenous administration of PEGylated substances in rats, rabbits, dogs and Rhesus monkeys could elicit antibody responses against PEG (anti-PEG antibodies) limiting the therapeutic efficiency and/or reducing the tolerance of PEGylated therapeutics [8, 9]. In addition, an emerging body of literature has demonstrated that anti-PEG antibodies produced in response to the first dose may harmfully trigger the rapid systemic clearance of subsequently injected doses of PEGylated nanocarriers- the so-called "accelerated blood clearance (ABC)" phenomenon [10–15]. Such phenomenon is of concern for clinical translation of nanocarriers systems as it limits their passive accumulation in many disease sites.

Of interest, the existence of naturally occurring anti-PEG antibodies in normal individuals who have never received PEGylated therapeutics have been recently emphasized [5, 16, 17]. Armstrong et al. [17] revealed that these naturally occurring anti-PEG antibodies could prime the host immune system against administered PEGylated therapeutics, and thereby, compromise their therapeutic efficacies. Consequently, the US Food and Drug Administration (FDA) has recently emphasized the need for assessing the immunogenicity of PEGylated therapeutics, to assure their safety, prior their approval for clinical use [18].

20.2 Anti-PEG IgM Response to PEGylated Proteins

Biomedicines, such as protein drugs, have received much attention because of their high biological activity and specificity against target molecules. Nevertheless, limitations regarding to their ability to generate neutralizing antibodies, in tandem with, rapid systemic clearance have potentially compromised their clinical applications [19–21]. As described earlier, covalent conjugation of PEG to biologically active molecules is considered one of the promising strategies to circumvent such limitations. PEG is generally believed to be a biologically inert, non-immunogenic polymer that is commonly used in the production of cosmetics and many pharmaceuticals, and is approved by FDA as a constituent of various medicines and medical procedures [22, 23]. Therefore, the immunogenicity of PEGylated substances was formerly and directly tested against a primary substance, rather than against covalently coupled PEG. However, a strong anti-PEG immunological response, exemplified by the extensive production of anti-PEG antibodies, was reported upon conjugating this hydrophilic polymer to some proteins, particularly

ovalbumin (OVA) [24–26]. These findings potentially contradict the basic assumption that PEG is a bio-inert and non-immunogenic substance. In 1983, Richter and Akerblom [26] firstly reported the elicitation of PEG-specific antibodies following either subcutaneous or intramuscular injections of different PEG-modified proteins in complete Freund's adjuvant. By contrary, under similar experimental conditions, free PEG showed little or no immunogenicity. Similarly, we have confirmed the induction of an anti-PEG antibody response (mainly anti-PEG IgM) following a single intravenous injection of either PEGylated OVA or PEGylated bovine serum albumin (BSA), despite the fact that a single injection does not induce specific neutralizing antibodies to either OVA or BSA [27]. These results support the scenario that the elicitation of anti-PEG immune response only occurs against PEG conjugates in a manner wherein PEG acts as a hapten. A hapten is a non-immunogenic small molecule that triggers antibody response only when attached to an immunogenic protein that can provide $CD4^+$ T cell epitopes, which are required to initiate the antibody response. This haptenic characteristic of PEG has been revealed to be dependent on the molecular weight and the immunogenicity of the carrier protein and/or the presence of adjuvants [21, 28, 29]. This explains why PEGylated proteins such as uricase, asparaginase and OVA could harmfully elicit anti-PEG antibody response, whereas others are relatively safer [30–33].

20.3 Anti-PEG Response to PEGylated Nanocarriers

Nanocarriers are currently explored extensively as a vehicle of various medicinal agents in biomedical fields including targeted drug delivery systems, medical imaging and diagnosis [34–36]. Surface decoration of nanocarrier systems with PEG is reported to prevent the uptake of nanocarriers by the cells of MPS and improve their in vivo fate following intravenous administration [37, 38]. Nonetheless, in spite of the usefulness and importance of PEGylation, surface decoration of nanocarriers with PEG has been reported to elicit an immunogenic response against PEGylated nanocarriers [10, 14, 39, 40].

While single dose of PEGylated nanocarriers often demonstrates in vivo extended blood circulation time, some PEGylated nanocarriers exhibit rapid systemic clearance upon repeated administration. In 1997, Moghimi and Gray [41] demonstrated that a single intravenous dose of particles coated with the amphiphilic polymer poloxamine 908 (a PEG-containing surfactant) triggered enhanced clearance of subsequently administered doses in rats. Similarly, we and other research groups have demonstrated that empty PEGylated liposomes could also trigger a strong immune response that significantly compromise circulation time in the blood of the subsequent dose via enhancing its hepatic clearance [10, 11, 14, 42, 43]. Such unexpected pharmacokinetic alteration of PEGylated nanocarriers upon repeated administration is now well recognized as the "accelerated blood clearance (ABC)"

phenomenon. Currently, the ABC phenomenon is of clinical concern because it compromises the therapeutic efficiency of PEGylated therapeutics upon repeated administration, in tandem with, eliciting the development of adverse effects.

20.4 Mechanism of the ABC Phenomenon

Since the first report concerning the pharmacokinetic irregularities upon repeated injections of PEGylated liposomes (the ABC phenomenon) by Dams el al. [10], research efforts have focused on elucidating the underlying mechanism of the ABC phenomenon. Laverman et al. [11] identified 2 phases of the ABC phenomenon: the induction phase, in which the host immune system is "primed" by the first injection of PEGylated liposome, and, the effectuation phase, in which a subsequent dose of PEGylated liposomes is rapidly opsonized and cleared from systemic circulation by the cells of MPS. Later on, in a series of our studies [14, 40, 43–45], we emphasized the crucial role of anti-PEG antibodies, mainly anti-PEG IgM, elicited in response to the first dose, in the induction of the ABC phenomenon. In addition, we emphasized the vital role of the spleen in the induction of anti-PEG IgM immune response [46]. Where, splenectomy was found to significantly alleviate the production of anti-PEG IgM and consequently attenuate the induction of the ABC phenomenon following the administration of PEGylated liposomes, suggesting that splenic cells serve as the primary site of anti-PEG IgM induction [27, 47]. Furthermore, it has been reported that the ABC phenomenon was only observed in T-cell-deficient BALB/c nude mice but not in BALB/c SCID mice (T and B cells-deficient mice) [47, 48]. Consequently, the ABC phenomenon seems to involve B cells functioning through T-cell independent (TI) mechanism. Collectively, based on the aforementioned data, we postulated the following mechanism to explain the ABC phenomenon (Fig. 20.1): anti-PEG IgM, produced in the spleen in response to the first dose, selectively bind to the PEG upon the second dose of PEGylated liposome injected several days later and subsequently activates the complementary system, and, as a consequence, the liposomes are taken up by the Kupffer cells via complement receptor-mediated endocytosis.

20.5 Correlation Between Complement Activation and the ABC Phenomenon

Many reports have highlighted the role of the complement system in the accelerated blood clearance of PEGylated nanocarriers from blood circulation upon repeated injection [49–51]. It is well recognized that IgM antibodies per se are unable to directly induce phagocytosis via specific receptor on phagocytic cells such as macrophages because IgM is not an opsonizing antibody due to the absence of

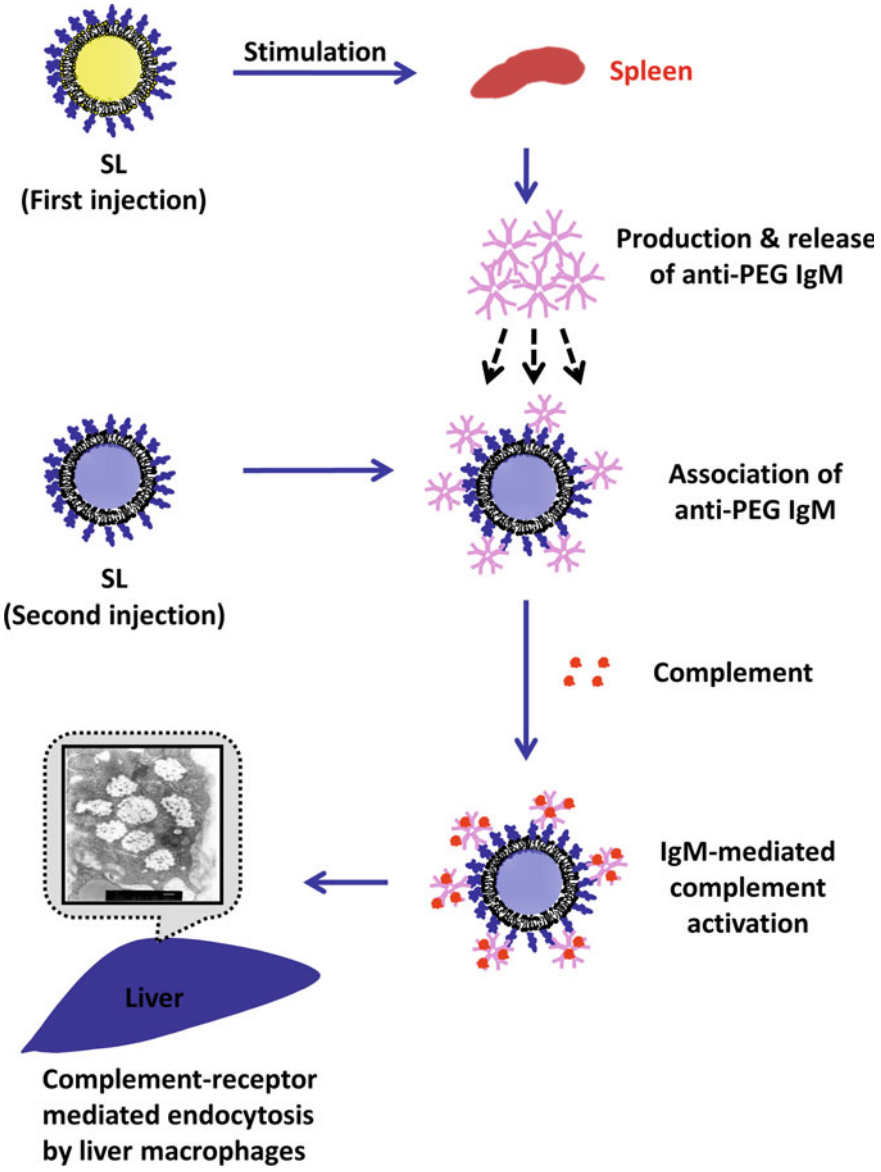

Fig. 20.1 Cartoon depicting the sequence of events leading from anti-PEG IgM induction to accelerated blood clearance of PEGylated liposomes. Modified from [15]

specific receptors for IgM such as Fc receptor on the surface of macrophages [52]. IgM-mediated complement activation has been anticipated to be the rate-limiting step of the ABC phenomenon of PEGylated products.

In earlier, Dams et al. [10] demonstrated that rats transfused with serum from rats pretreated with PEGylated liposomes rapidly cleared the dose when they were treated with PEGylated liposomes for the first time. Moreover, this accelerated clearance of the PEGylated liposomes was not observed upon pre-heating the serum at 56 °C for 30 min prior to transfusion. Later on, in a series of our studies [49, 50, 53], we have demonstrated that, following incubation with PEGylated liposomes, extensive IgM binding with subsequent complement consumption was remarkably detected only in sera from rats exhibiting an enhanced clearance of the second dose. In the same context, Yang et al. [51] also emphasized the consumption of a massive amount of complement in the serum obtained from rats pretreated with PEGylated liposomes upon incubation with PEGylated liposome. These results suggest that complement activation plays a crucial role in the induction of the accelerated blood clearance of subsequent dose of PEGylated liposome. Nevertheless, the influence of other serum factor(s) rather than complement in the elicitation of the ABC phenomenon should not be excluded.

20.6 Properties of Anti-PEG Antibody Epitope

Many reports have highlighted the contribution of anti-PEG antibodies to the accelerated blood clearance of PEGylated therapeutics. However, the antigenic determinant of the PEG polymer still remains a mystery. Based on its highly repetitive structure, PEG is acceptably classified as TI-2 antigen. TI-2 antigens are composed of identical repeating epitopes that act by cross-linking the cell-surface immunoglobulins of specific B cells leading to a significant and prolonged activation of B cells without co-stimulation by T cells [54]. In an earlier study, Richter and Akerblom [26] observed the inhibition of anti-PEG antibody precipitation with PEG_{300}, suggesting that the antigenic determinant of PEG may be a sequence of 6–7 $–CH_2$-CH_2-O- units. Cheng et al. [55] found that the monoclonal anti-PEG antibody (IgM) generated by immunization with PEGylated β-glucuronide recognizes the repeating sequence $–(O–CH_2–CH_2)_n–$ subunit (16 units) of PEG. Saifer et al. [56] later reported that triethylene glycol (MW 150–160) was bound by anti-PEG antibodies in direct and competitive ELISAs. These data suggest that the minimum epitope recognition by anti-PEG antibodies could range from 3 to 4 repeated oxyethylene units.

Nevertheless, several studies showed that PEG polymer per se does not elicit an anti-PEG response. On the other hand, PEG conjugated to proteins and/or nanocarriers would induce an anti-PEG immune response. Accordingly, the antigenic determinant for anti-PEG antibodies is supposed to ensue at the linkage between PEG and other materials. Shiraishi et al. [57] observed cross-reactivity between anti-PEG IgMs elicited by hydrophobic PEGylated micelles and liposomes, but hydrophilic PEGylated micelles did not induce either an anti-PEG IgM response or the ABC phenomenon. Accordingly, they suggested that the anti-PEG antibody epitope lies at the interphase between a hydrophobic core and conjugated

PEG groups. Furthermore, due to the difference in the immune responses between free PEG and PEGylated conjugates, PEG is projected to function as a hapten, which is a non-immunogenic small molecule that can elucidate an immune response only when conjugated to a larger carrier [7, 58, 59].

20.7 Anti-PEG Immunity in Humans

Despite the fact that PEGylation has been acknowledged for the success of numerous PEGylated products currently on the market, an emerging body of literature has emphasized the existence of anti-PEG antibodies in the sera of normal donors and/or sera of PEGylated therapeutics-treated patients that specifically recognize and bind to PEG [7, 17, 30]. The presence of anti-PEG antibodies, consequently, might represent potential challenges against the clinical deployment of PEGylated therapeutics since such antibodies could compromise the therapeutic efficiency and increase the risk of treatment-related adverse effects [7, 17, 30, 31, 60].

20.7.1 Pre-existing Anti-PEG Antibodies in Normal Donors

In contrast to the basic perception that anti-PEG immunity arises predominantly by previous exposure to PEGylated therapeutics, a growing body of literature has emphasized the elicitation of immunogenic responses against PEGylated substances in normal subjects upon first exposure to PEGylated therapeutics [17, 25, 28, 31, 33, 60–63]. Richter and Akerlom [28] first noticed that 0.2 and 3.3% of normal subjects and untreated allergy patients, respectively, exhibits remarkably higher titers of anti-PEG IgM. Later on, Armstrong et al. [17] declared significantly higher incidence rates of anti-PEG IgM ($\sim$27%) in healthy blood donors. More recently, Yang and Lai [25] reported an even higher anti-PEG antibody (up to 42%) in healthy adult individuals. Such variations reflect a significant increment in the prevalence of pre-existing anti-PEG antibodies in normal subjects over time. The underlying mechanism of anti-PEG antibodies production in healthy individuals has not been fully elucidated yet. However, since PEG has been classified by the FDA under the category of products that are Generally Recognized As Safe (GRAS), it has become commonly used in processed foods, cosmetics and pharmaceuticals. Accordingly, frequent exposure to PEG in daily use products is supposed to induce the production of anti-PEG antibodies. Based on the aforementioned data, Yang and Lai [25] have recently postulated the following tentative mechanism elucidating the existence of anti-PEG antibodies in normal subjects: as the human body is vulnerable to certain conditions such as ulcerations, abrasions and skin tears that might cause local inflammatory responses and/or recruitment of immune cells.

Upon exposure to PEG in the daily use of common products, PEG is likely introduced to sites of inflammation and to come into close vicinity to highly active immune cells, which in turn may trigger the induction of anti-PEG antibodies.

20.7.2 Clinical Implications of Anti-PEG Antibodies on the Efficacy of PEGylated Therapeutics

To date, with an increasing number of PEGylated products entering the clinic, many reports have emphasized the immunogenicity of PEGylated therapeutics and have claimed the reconsideration of the safety profile of PEGylated products [28, 62]. Nonetheless, the issue of the clinical implications of anti-PEG antibodies on the efficiency of PEGylated therapeutics is controversial. In 1984, Richter and Akerblom [28] have revealed that pre-existing anti-PEG antibodies did not ruin hypersensitization treatment of allergic patients with PEG-modified honeybee venom or ragweed extract. In the same context, Tillmann et al. [62] have demonstrated that, despite the high prevalence of pre-existing anti-PEG antibodies in 44% of patients with hepatitis C, the presence of pre-existing anti-PEG antibodies was found not to compromise the therapeutic efficacy of PEG-INF-α. However, the impact of impaired immunity and hepatic damage induced by hepatitis C virus on the therapeutic efficacy of PEG-INF-α has not been justified. Furthermore, unlike most reports demonstrate that the presence of anti-PEG response in a subset of patients, anti-PEG antibodies were detected in all phenylketonurea patients treated with PEGylated phenylalanine ammonia lyase (PEG-PAL). Nonetheless, neither pre-existing nor induced anti-PEG antibodies adversely affected the therapeutic efficiency of a single dose of PEG-PAL [60]. Collectively, these findings played an integral role in creating the perception that anti-PEG antibody response has no clinical implications for the therapeutic efficacy of PEGylated therapeutics in humans.

By contrary, recent reports have highlighted the detrimental effect of anti-PEG antibodies on the therapeutic efficiency of PEGylated therapeutic [17, 31, 64, 65]. In pediatric patients treated with PEG-Asparaginase (PEG-ASNase) for acute lymphoblastic leukemia, anti-PEG IgM antibodies were detected in about half of the patients and the presence of such anti-PEG antibodies was reported to correlate closely to the enhanced clearance of PEG-ASNase and loss of therapeutic efficiency. Notably, anti-PEG antibodies present in the sera of patients treated with unmodified ASNase affected neither the systemic clearance nor the therapeutic efficiency of the therapeutic protein (ASNase). In the same context, the clinical use of Pegloticase, a PEGylated uric acid-specific enzyme, in patients with chronic gout has been hampered by the occurrence of PEG antibodies; anti-PEG antibodies was detected in 89% of patients treated with Pegloticase, resulting in enhanced Pegloticase clearance, loss of activity and increased risk of treatment-induced infusion reactions [66]. These findings highlight the potential impact of anti-PEG

immunity on the growing clinical development of PEGylated therapeutics and underscore the rationale for testing for anti-PEG antibodies in clinical trials of PEGylated therapeutics. It is worth noting that anti-PEG immunity not only contributes to the compromised therapeutic efficacy of PEGylated therapeutics, but also participates to the development of severe side effects as well [60, 61]. In the case of PEGylated phenylalanine ammonia lyase (PEG-PAL), despite the fact that neither pre-existing nor induced anti-PEG antibodies affected the therapeutic efficacy of the injected drug, severe adverse reactions were observed in two patients who had further treated with an intramuscular injections of medroxyprogestrone acetate, a drug containing free PEG and polysorbate as excipients [60]. Ganson et al. [61] also revealed the contribution of pre-existing anti-PEG antibodies to the safety profile of a PEGylated RNA aptamer used in the treatment of acute coronary syndrome (ACS); pegnivacogin. They demonstrated that treatment with pegnivacogin could elicit the development of severe life-threatening allergic reactions in three ACS patients upon their first exposure to pegnivacogin leading to early termination of the trial.

20.8 Non-antibody Mediated Hypersensitivity Reactions

Besides the slow specific immunogenic response manifested in antibody formation against PEGylated nanocarriers [11, 40, 42], a mounting body of evidences has also revealed that intravenous administration of nanocarriers could provoke acute hypersensitivity reactions (HSR) that are classified as complement activation-related pseudoallergy (CARPA) since they are not initiated/mediated by pre-existing IgE antibodies but rather arise as a consequence of activation of complement system [39, 67–69]. Such "hypersensitivity reactions" or "anaphylactoid reactions" typically occur directly at first exposure to the nanocarriers without prior sensitization, and the symptoms usually lessen and/or disappear on later treatment, that is why these reactions have recently been called "pseudoallergic" [70]. The symptoms of HSR are mostly minor and transient and include cardiopulmonary distress such as tachypnea, dyspnea, tachycardia, hypertension/hypotension, chest pain and back pain. However, life-threatening or even deadly reactions can occur occasionally in hypersensitive individuals [71].

Drugs and agents causing CARPA include radio-contrast media, liposomal drugs (Ambisome®, Doxil® and DaunoXome®), micellar solvents (e.g. Cremophore EL; the vehicle of Taxol), PEGylated proteins and monoclonal antibodies [70–76]. The first direct evidence for the causal relationship between complement activation and hypersensitivity reactions (CARPA) to PEGylated liposomes was provided by Brouwers et al. [77], who reported that three out of nine patients receiving ^{99m}Tc-labeled PEGylated liposomes for scintigraphic detection of bowel inflammation have developed severe hypersensitivity reactions. Later on, Szebeni and his colleges, in a series of their studies [39, 68, 73, 78], have emphasized the potential contribution of complement activation to infusion reactions encountered in one

fourth the patients treated with Doxil® (PEGylated liposomal doxorubicin). Chanan-Khan et al. [79] also reported that Doxil® therapy activated complement in the majority of patients and elicited moderate to severe hypersensitivity reactions in about 50% of cancer patients infused with Doxil® for the first time. Furthermore, CARPA reactions have been elicited with other liposomal formulations regardless their structure or the presence/absence of PEG surface modification [70, 75, 80]. Currently, CARPA phenomenon is considered one of the safety issues for nanomedicines, including radionanomedicines, that to be evaluated prior the clinical approval of generic intravenous liposomal formulations.

20.9 Alternative Approaches to PEGylation

An emerging body of literature has been proposed to avert the immunogenicity of PEGylated therapeutics [81–84]. Among them, the application of alternative polymers to PEG has gained increased attention. Zhang et al. [83] have emphasized the utility of liposome surface coating with hyaluronic acid (HA), instead of PEG, to improve pharmacokinetics and to reduce immune response of administered liposomes while preserving their long circulating characteristics. They demonstrated that HA-liposomes showed good stealth properties without inducing neither anti-polymer antibodies nor the ABC phenomenon. Moreover, HA-liposomes did not trigger complement activation neither in human serum in vitro nor in rat blood in vivo. On the other hand, PEGylated liposomes could elicit complement activation and consequent ABC phenomenon accompanied by an enhanced accumulation of PEGylated liposomes in the liver. In the same context, we have employed a polyglycerol (PG)-derived lipid, as an alternative to PEG, to mitigate the immune response against injected liposomes [81, 82]. We demonstrated that surface decoration with PG potentially attenuated the anti-polymer immune response. The hydroxymethyl side group in the repeating $–(O–CH_2–CH(CH_2OH))_n–$ subunit of PG was reported to sterically hinder the interaction and effective binding to surface immunoglobulins on reactive splenic B-cells, and thus, prevents the direct stimulation of splenic B cells and the production of anti-polymer IgM (Fig. 20.2). In a subsequent study, surface modification of pDNA-lipoplex with PG, instead of PEG, was also confirmed to efficiently attenuate the immunogenicity of PEGylated lipoplex, and thereby, enhanced the accumulation of the PG-modified lipoplexes in the tumor tissue upon repeated administration (Fig. 20.3) [81]. More recently, we examined the potential of incorporating porcine ganglioside into the membrane of PEGylated liposome in alleviating/abrogating the anti-PEG IgM response against PEGylated liposomes (PL). Insertion of ganglioside into PEGylated liposomes significantly mitigated the anti-PEG IgM immune response and alleviated the incidence of the accelerated clearance of subsequently injected PEGylated liposomes, presumably via inducing B cell tolerance. These findings emphasize the feasibility of liposomal surface decoration with ganglioside in attenuating the immunogenicity of PEGylated nanocarriers upon repeated administration [84].

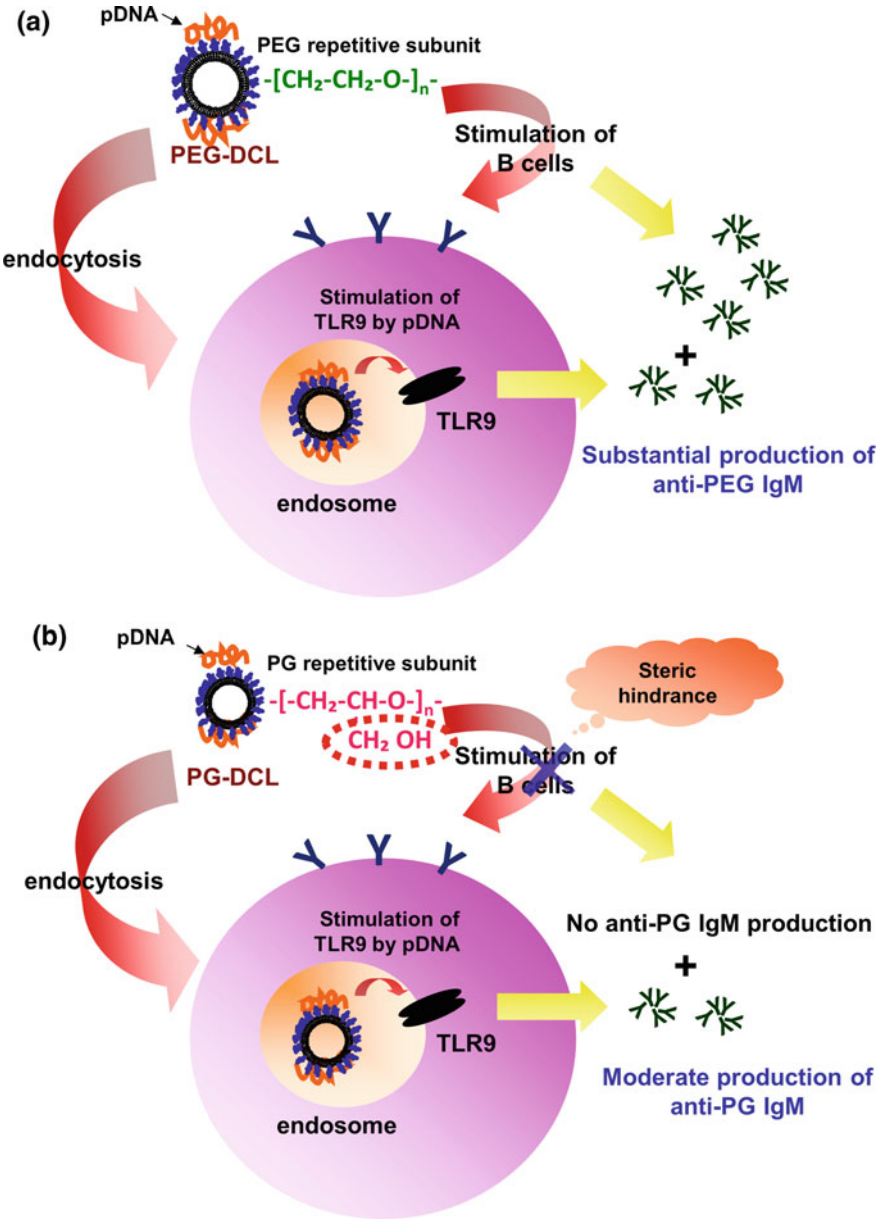

Fig. 20.2 Cartoon depicting the possible mechanism underlying the differences in anti-polymer IgM production in response to **a** PEG-coated pDNA-lipoplex (PEG-DCL) or **b** PG-coated pDNA-lipoplex (PG-DCL). Modified from [81]

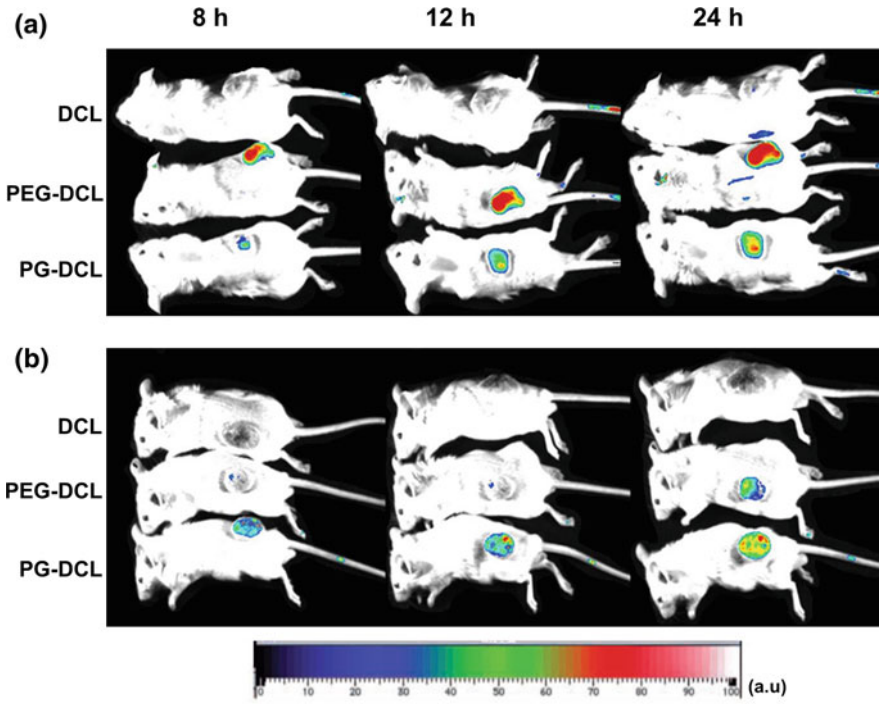

Fig. 20.3 Effect of a prior dose on the tumor accumulation of a fluorescence-labeled test dose of either PEG-coated pDNA-lipoplex (PEG-DCL) or PG-coated pDNA-lipoplex (PG-DCL). C26-tumor bearing mice received a single administration (**a**) or two administrations within a 5-day interval (**b**) of either pDNA-lipoplex (DCL), PEG-coated pDNA-lipoplex (PEG-DCL) or PG-coated pDNA-lipoplex (PG-DCL) (0.4 μmol PL/mouse and 10 μg pDNA/mouse). The first dose was given on day 7 after tumor inoculation. To visualize the tumor accumulation, the dose was labeled with fluorescence (DiD). At 8, 12 and 24 h after the last injection, in vivo optical images were recorded. All fluorescence images were acquired using a 1/8 exposure time. A typical image from three independent experiments is expressed. Modified from [81]

Zwitterionic materials, keeping electric neutrality with equivalent positive and negative charged groups, have been recently challenged for their stealth-inducing ability [85, 86]. Surface modification of nanocarriers and/or proteins with the zwitterionic material, poly(carboxybetaine) (PCB), has been acknowledged for extending the blood circulating characteristics of conjugated material [87]. In addition, immunological studies on rat proteins conjugated with either PEG or PCB polymers have emphasized the lack of immunogenicity of PCB-conjugated proteins, as manifested by the absence of anti-PCB IgM and IgG, while, the corresponding anti-PEG immunity were clearly identified [83].

XTEN technology, the conjugation of polypeptide to a protein, has been verified to extend the circulation half-life of the conjugated product [88]. The polypeptide used is composed of threonine, serine, proline, glycine, glutamic acid and alanine.

XTEN sequences have been reported to be well-tolerated and being weakly immunogenic in many animal studies [89]. Currently, an exenatide-XTEN fusion construct (VRS-859) for the treatment of type II diabetes and a growth hormone-XTEN fusion construct (VRS 317) for growth hormone deficiency are undergoing Phase I clinical trials [89–91].

20.10 Conclusion

In contrast to the general perception that PEG is biologically inert, many reports have clearly underscored the detrimental effect of anti-PEG immunity, elicited by either pre-existing or treatment-induced antibodies, on the therapeutic efficiency and/or safety of PEGylated therapeutics. Accordingly, in light of the large arsenal of PEGylated therapeutics that are FDA-approved or under clinical investigation, patients should be pre-screened and monitored for anti-PEG antibodies prior to and throughout a course of treatment with PEGylated therapeutics. Furthermore, a deep understanding of the mechanism of anti-PEG immunity along with strategies to avert the challenges of PEG-specific immunity is urgently needed.

Acknowledgements We thank Dr. J. L. McDonald for his helpful advice in writing the manuscript. This study was supported, in part, by a Grant-in-Aid for Scientific Research (B) 15H04639, the Ministry of Education, Culture, Sports, Science and Technology, Japan.

Disclosures and Conflicts of Interest
The authors declare that they have no conflicts of interest. The authors have received no payment for the preparation of this chapter.

References

1. D.D. Lasic, F.J. Martin, A. Gabizon, S.K. Huang, D. Papahadjopoulos, Sterically stabilized liposomes: a hypothesis on the molecular origin of the extended circulation times. Biochim. Biophys. Acta **1070**(1), 187–192 (1991)
2. T.M. Allen, C. Hansen, Pharmacokinetics of stealth versus conventional liposomes: effect of dose. Biochim. Biophys. Acta **1068**(2), 133–141 (1991)
3. V.P. Torchilin, Recent advances with liposomes as pharmaceutical carriers. Nat. Rev. Drug Discov. **4**(2), 145–160 (2005)
4. J.M. Harris, R.B. Chess, Effect of pegylation on pharmaceuticals. Nat. Rev. Drug Discov. **2** (3), 214–221 (2003)
5. B. Gorovits, A. Clements-Egan, M. Birchler, M. Liang, H. Myler, K. Peng et al., Pre-existing antibody: biotherapeutic modality-based review. AAPS J. **18**(2), 311–320 (2016)
6. H. Schellekens, W.E. Hennink, V. Brinks, The immunogenicity of polyethylene glycol: facts and fiction. Pharm. Res. **30**(7), 1729–1734 (2013)

7. R.P. Garay, R. El-Gewely, J.K. Armstrong, G. Garratty, P. Richette, Antibodies against polyethylene glycol in healthy subjects and in patients treated with PEG-conjugated agents. Expert Opin. Drug Deliv. **9**(11), 1319–1323 (2012)
8. C. Li, J. Cao, Y. Wang, X. Zhao, C. Deng, N. Wei et al., Accelerated blood clearance of pegylated liposomal topotecan: influence of polyethylene glycol grafting density and animal species. J. Pharm. Sci. **101**(10), 3864–3876 (2012)
9. T. Suzuki, M. Ichihara, K. Hyodo, E. Yamamoto, T. Ishida, H. Kiwada et al., Influence of dose and animal species on accelerated blood clearance of PEGylated liposomal doxorubicin. Int. J. Pharm. **476**(1–2), 205–212 (2014)
10. E.T. Dams, P. Laverman, W.J. Oyen, G. Storm, G.L. Scherphof, J.W. van Der Meer et al., Accelerated blood clearance and altered biodistribution of repeated injections of sterically stabilized liposomes. J. Pharmacol. Exp. Ther. **292**(3), 1071–1079 (2000)
11. P. Laverman, M.G. Carstens, O.C. Boerman, E.T. Dams, W.J. Oyen, N. van Rooijen et al., Factors affecting the accelerated blood clearance of polyethylene glycol-liposomes upon repeated injection. J. Pharmacol. Exp. Ther. **298**(2), 607–612 (2001)
12. R. Saadati, S. Dadashzadeh, Z. Abbasian, H. Soleimanjahi, Accelerated blood clearance of PEGylated PLGA nanoparticles following repeated injections: effects of polymer dose, PEG coating, and encapsulated anticancer drug. Pharm. Res. **30**(4), 985–995 (2013)
13. H.J. Im, C.G. England, L. Feng, S.A. Graves, R. Hernandez, R.J. Nickles et al., Accelerated blood clearance phenomenon reduces the passive targeting of PEGylated nanoparticles in peripheral arterial disease. ACS Appl. Mater. Interfaces. **8**(28), 17955–17963 (2016)
14. T. Ishida, R. Maeda, M. Ichihara, Y. Mukai, Y. Motoki, Y. Manabe et al., The accelerated clearance on repeated injection of pegylated liposomes in rats: laboratory and histopathological study. Cell. Mol. Biol. Lett. **7**(2), 286 (2002)
15. A.S. Abu Lila, H. Kiwada, T. Ishida, The accelerated blood clearance (ABC) phenomenon: clinical challenge and approaches to manage. J. Control Release **172**(1), 38–47 (2013)
16. T.J. Povsic, M.G. Lawrence, A.M. Lincoff, R. Mehran, C.P. Rusconi, S.L. Zelenkofske et al., Pre-existing anti-PEG antibodies are associated with severe immediate allergic reactions to pegnivacogin, a PEGylated aptamer. J. Allergy Clin. Immunol. **138**(6), 1712–1715 (2016)
17. J.K. Armstrong, G. Hempel, S. Koling, L.S. Chan, T. Fisher, H.J. Meiselman et al., Antibody against poly(ethylene glycol) adversely affects PEG-asparaginase therapy in acute lymphoblastic leukemia patients. Cancer **110**(1), 103–111 (2007)
18. http://www.fda.gov/downloads/drugs/guidancecomplianceregulatoryinformation/guidances/
19. I. Wala, S.J. Swanson, S. Jing, A non-radioactive method for detecting neutralizing antibodies against therapeutic proteins in serum. J. Pharm. Biomed. Anal. **45**(4), 583–589 (2007)
20. P.S. Sorensen, Neutralizing antibodies against interferon-Beta. Ther. Adv. Neurol. Disord. **1**(2), 125–141 (2008)
21. T. Ishida, H. Kiwada, Anti-polyethyleneglycol antibody response to PEGylated substances. Biol. Pharm. Bull. **36**(6), 889–891 (2013)
22. E.A. Bell, G.C. Wall, Pediatric constipation therapy using guidelines and polyethylene glycol 3350. Ann. Pharmacother. **38**(4), 686–693 (2004)
23. R. Webster, E. Didier, P. Harris, N. Siegel, J. Stadler, L. Tilbury et al., PEGylated proteins: evaluation of their safety in the absence of definitive metabolism studies. Drug Metab. Dispos. **35**(1), 9–16 (2007)
24. Y. Mima, Y. Hashimoto, T. Shimizu, H. Kiwada, T. Ishida, Anti-PEG IgM is a major contributor to the accelerated blood clearance of polyethylene glycol-conjugated protein. Mol. Pharm. **12**(7), 2429–2435 (2015)
25. Q. Yang, S.K. Lai, Anti-PEG immunity: emergence, characteristics, and unaddressed questions. Wiley Interdiscip. Rev. Nanomed. Nanobiotechnol. **7**(5), 655–677 (2015)
26. A.W. Richter, E. Akerblom, Antibodies against polyethylene glycol produced in animals by immunization with monomethoxy polyethylene glycol modified proteins. Int. Arch. Allergy Appl. Immunol. **70**(2), 124–131 (1983)

27. T. Shimizu, M. Ichihara, Y. Yoshioka, T. Ishida, S. Nakagawa, H. Kiwada, Intravenous administration of polyethylene glycol-coated (PEGylated) proteins and PEGylated adenovirus elicits an anti-PEG immunoglobulin M response. Biol. Pharm. Bull. **35**(8), 1336–1342 (2012)
28. A.W. Richter, E. Akerblom, Polyethylene glycol reactive antibodies in man: titer distribution in allergic patients treated with monomethoxy polyethylene glycol modified allergens or placebo, and in healthy blood donors. Int. Arch. Allergy Appl. Immunol. **74**(1), 36–39 (1984)
29. P. Caliceti, O. Schiavon, F.M. Veronese, Immunological properties of uricase conjugated to neutral soluble polymers. Bioconjug. Chem. **12**(4), 515–522 (2001)
30. P.E. Lipsky, L.H. Calabrese, A. Kavanaugh, J.S. Sundy, D. Wright, M. Wolfson et al., Pegloticase immunogenicity: the relationship between efficacy and antibody development in patients treated for refractory chronic gout. Arthritis Res. Ther. **16**(2), R60 (2014)
31. M.S. Hershfield, N.J. Ganson, S.J. Kelly, E.L. Scarlett, D.A. Jaggers, J.S. Sundy, Induced and pre-existing anti-polyethylene glycol antibody in a trial of every 3-week dosing of pegloticase for refractory gout, including in organ transplant recipients. Arthritis Res. Ther. **16**(2), R63 (2014)
32. J.T. White, S.D. Newsome, B.C. Kieseier, R.A. Bermel, Y. Cui, A. Seddighzadeh et al., Incidence, characterization, and clinical impact analysis of peginterferon beta1a immunogenicity in patients with multiple sclerosis in the ADVANCE trial. Ther. Adv. Neurol. Disord. **9**(4), 239–249 (2016)
33. A. Tocoian, P. Buchan, H. Kirby, J. Soranson, M. Zamacona, R. Walley et al., First-in-human trial of the safety, pharmacokinetics and immunogenicity of a PEGylated anti-CD40L antibody fragment (CDP7657) in healthy individuals and patients with systemic lupus erythematosus. Lupus **24**(10), 1045–1056 (2015)
34. S.K. Nune, P. Gunda, P.K. Thallapally, Y.Y. Lin, M.L. Forrest, C.J. Berkland, Nanoparticles for biomedical imaging. Expert Opin. Drug Deliv. **6**(11), 1175–1194 (2009)
35. A. Makino, S. Kimura, Solid tumor-targeting theranostic polymer nanoparticle in nuclear medicinal fields. Sci. World J. **2014**, 424513 (2014)
36. L. Yildirimer, N.T. Thanh, M. Loizidou, A.M. Seifalian, Toxicology and clinical potential of nanoparticles. Nano Today **6**(6), 585–607 (2011)
37. Y. Barenholz, Doxil(R)–the first FDA-approved nano-drug: lessons learned. J. Control Release **160**(2), 117–134 (2012)
38. T.M. Allen, P.R. Cullis, Liposomal drug delivery systems: from concept to clinical applications. Adv. Drug Deliv. Rev. **65**(1), 36–48 (2013)
39. J. Szebeni, Complement activation-related pseudoallergy: a stress reaction in blood triggered by nanomedicines and biologicals. Mol. Immunol. **61**(2), 163–173 (2014)
40. T. Ishida, M. Harada, X.Y. Wang, M. Ichihara, K. Irimura, H. Kiwada, Accelerated blood clearance of PEGylated liposomes following preceding liposome injection: effects of lipid dose and PEG surface-density and chain length of the first-dose liposomes. J. Control Release **105**(3), 305–317 (2005)
41. S.M. Moghimi, T. Gray, A single dose of intravenously injected poloxamine-coated long-circulating particles triggers macrophage clearance of subsequent doses in rats. Clin. Sci. (Lond.) **93**(4), 371–379 (1997)
42. T. Ishida, X. Wang, T. Shimizu, K. Nawata, H. Kiwada, PEGylated liposomes elicit an anti-PEG IgM response in a T cell-independent manner. J. Control Release **122**(3), 349–355 (2007)
43. M. Ichihara, T. Shimizu, A. Imoto, Y. Hashiguchi, Y. Uehara Y, T. Ishida et al., Anti-PEG IgM Response against PEGylated liposomes in mice and rats. Pharmaceutics **3**(1), 1–11 (2010)
44. T. Ishida, K. Masuda, T. Ichikawa, M. Ichihara, K. Irimura, H. Kiwada, Accelerated clearance of a second injection of PEGylated liposomes in mice. Int. J. Pharm. **255**(1–2), 167–174 (2003)
45. T. Ishida, R. Maeda, M. Ichihara, K. Irimura, H. Kiwada, Accelerated clearance of PEGylated liposomes in rats after repeated injections. J. Control Release **88**(1), 35–42 (2003)

46. T. Ishida, M. Ichihara, X. Wang, H. Kiwada, Spleen plays an important role in the induction of accelerated blood clearance of PEGylated liposomes. J. Control Release **115**(3), 243–250 (2006)
47. S.C. Semple, T.O. Harasym, K.A. Clow, S.M. Ansell, S.K. Klimuk, M.J. Hope, Immunogenicity and rapid blood clearance of liposomes containing polyethylene glycol-lipid conjugates and nucleic Acid. J. Pharmacol. Exp. Ther. **312**(3), 1020–1026 (2005)
48. H. Koide, T. Asai, K. Hatanaka, S. Akai, T. Ishii, E. Kenjo et al., T cell-independent B cell response is responsible for ABC phenomenon induced by repeated injection of PEGylated liposomes. Int. J. Pharm. **392**(1–2), 218–223 (2010)
49. X. Wang, T. Ishida, H. Kiwada, Anti-PEG IgM elicited by injection of liposomes is involved in the enhanced blood clearance of a subsequent dose of PEGylated liposomes. J. Control Release **119**(2), 236–244 (2007)
50. T. Ishida, K. Atobe, X. Wang, H. Kiwada, Accelerated blood clearance of PEGylated liposomes upon repeated injections: effect of doxorubicin-encapsulation and high-dose first injection. J. Control Release **115**(3), 251–258 (2006)
51. Q. Yang, Y. Ma, Y. Zhao, Z. She, L. Wang, J. Li et al., Accelerated drug release and clearance of PEGylated epirubicin liposomes following repeated injections: a new challenge for sequential low-dose chemotherapy. Int. J. Nanomed. **8**, 1257–1268 (2013)
52. C.A. Janeway Jr., How the immune system works to protect the host from infection: a personal view. Proc. Natl. Acad. Sci. U.S.A. **98**(13), 7461–7468 (2001)
53. Y. Hashimoto, T. Shimizu, A.S. Abu Lila, T. Ishida, H. Kiwada, Relationship between the concentration of anti-polyethylene glycol (PEG) immunoglobulin M (IgM) and the intensity of the accelerated blood clearance (ABC) phenomenon against PEGylated liposomes in mice. Biol. Pharm. Bull. **38**(3), 417–424 (2015)
54. A. Cerutti, M. Cols, I. Puga, Marginal zone B cells: virtues of innate-like antibody-producing lymphocytes. Nat. Rev. Immunol. **13**(2), 118–132 (2013)
55. T.L. Cheng, P.Y. Wu, M.F. Wu, J.W. Chern, S.R. Roffler, Accelerated clearance of polyethylene glycol-modified proteins by anti-polyethylene glycol IgM. Bioconjug. Chem. **10** (3), 520–528 (1999)
56. M.G. Saifer, L.D. Williams, M.A. Sobczyk, S.J. Michaels, M.R. Sherman, Selectivity of binding of PEGs and PEG-like oligomers to anti-PEG antibodies induced by methoxyPEG-proteins. Mol. Immunol. **57**(2), 236–246 (2014)
57. K. Shiraishi, M. Hamano, H. Ma, K. Kawano, Y. Maitani, T. Aoshi et al., Hydrophobic blocks of PEG-conjugates play a significant role in the accelerated blood clearance (ABC) phenomenon. J. Control Release **165**(3), 183–190 (2013)
58. J.J. Verhoef, J.F. Carpenter, T.J. Anchordoquy, H. Schellekens, Potential induction of anti-PEG antibodies and complement activation toward PEGylated therapeutics. Drug Discov. Today **19**(12), 1945–1952 (2014)
59. L.M. Kaminskas, V.M. McLeod, C.J. Porter, B.J. Boyd, Differences in colloidal structure of PEGylated nanomaterials dictate the likelihood of accelerated blood clearance. J. Pharm. Sci. **100**(11), 5069–5077 (2011)
60. N. Longo, C.O. Harding, B.K. Burton, D.K. Grange, J. Vockley, M. Wasserstein et al., Single-dose, subcutaneous recombinant phenylalanine ammonia lyase conjugated with polyethylene glycol in adult patients with phenylketonuria: an open-label, multicentre, phase 1 dose-escalation trial. Lancet **384**(9937), 37–44 (2014)
61. N.J. Ganson, T.J. Povsic, B.A. Sullenger, J.H. Alexander, S.L. Zelenkofske, J.M. Sailstad et al., Pre-existing anti-polyethylene glycol antibody linked to first-exposure allergic reactions to pegnivacogin, a PEGylated RNA aptamer. J. Allergy Clin. Immunol. **137**(5), 1610–1613 (2016)
62. H.L. Tillmann, A,J. Thompson, K. Patel, M. Wiese, H. Tenckhoff, H.D. Nischalke et al., A polymorphism near IL28B is associated with spontaneous clearance of acute hepatitis C virus and jaundice. Gastroenterology **139**(5), 1586–1592 (2010)
63. P. Dewachter, C. Mouton-Faivre, Anaphylaxis to macrogol 4000 after a parenteral corticoid injection. Allergy **60**(5), 705–706 (2005)

64. N.J. Ganson, S.J. Kelly, E. Scarlett, J.S. Sundy, M.S. Hershfield, Control of hyperuricemia in subjects with refractory gout, and induction of antibody against poly(ethylene glycol) (PEG), in a phase I trial of subcutaneous PEGylated urate oxidase. Arthritis Res. Ther. **8**(1), R12 (2006)
65. I.A. Ivens, W. Achanzar, A. Baumann, A. Brandli-Baiocco, J. Cavagnaro, M. Dempster et al., PEGylated biopharmaceuticals: current experience and considerations for nonclinical development. Toxicol. Pathol. **43**(7), 959–983 (2015)
66. S. Sharma, R.W. Johnson, T.A. Desai, XPS and AFM analysis of antifouling PEG interfaces for microfabricated silicon biosensors. Biosens. Bioelectron. **20**(2), 227–239 (2004)
67. P. Bedocs, J. Capacchione, L. Potts, R. Chugani, Z. Weiszhar, J. Szebeni et al., Hypersensitivity reactions to intravenous lipid emulsion in swine: relevance for lipid resuscitation studies. Anesth. Analg. **119**(5), 1094–1101 (2014)
68. J. Szebeni, Complement activation-related pseudoallergy: a new class of drug-induced acute immune toxicity. Toxicology **216**(2–3), 106–121 (2005)
69. J. Szebeni, G. Storm, Complement activation as a bioequivalence issue relevant to the development of generic liposomes and other nanoparticulate drugs. Biochem. Biophys. Res. Commun. **468**(3), 490–497 (2015)
70. D.S. Alberts, D.J. Garcia, Safety aspects of pegylated liposomal doxorubicin in patients with cancer. Drugs **54**(Suppl 4), 30–35 (1997)
71. A.J. Andersen, S.H. Hashemi, T.L. Andresen, A.C. Hunter, S.M. Moghimi, Complement: alive and kicking nanomedicines. J. Biomed. Nanotechnol. **5**(4), 364–372 (2009)
72. J. Szebeni, Complement activation-related pseudoallergy caused by liposomes, micellar carriers of intravenous drugs, and radiocontrast agents. Crit. Rev. Ther. Drug Carrier Syst. **18**(6), 567–606 (2001)
73. B. Uziely, S. Jeffers, R. Isacson, K. Kutsch, D. Wei-Tsao, Z. Yehoshua et al., Liposomal doxorubicin: antitumor activity and unique toxicities during two complementary phase I studies. J. Clin. Oncol. **13**(7), 1777–1785 (1995)
74. O. Ringden, E. Andstrom, M. Remberger, B.M. Svahn, J. Tollemar, Allergic reactions and other rare side-effects of liposomal amphotericin. Lancet **344**(8930), 1156–1157 (1994)
75. J.P. Sculier, A. Coune, C. Brassinne, C. Laduron, G. Atassi, J.M. Ruysschaert et al., Intravenous infusion of high doses of liposomes containing NSC 251635, a water-insoluble cytostatic agent. A pilot study with pharmacokinetic data. J. Clin. Oncol. **4**(5), 789–797 (1986)
76. S.J. Levine, T.J. Walsh, A. Martinez, P.Q. Eichacker, G. Lopez-Berestein, C. Natanson, Cardiopulmonary toxicity after liposomal amphotericin B infusion. Ann. Intern. Med. **114**(8), 664–666 (1991)
77. A.H. Brouwers, D.J. De Jong, E.T. Dams, W.J. Oyen, O.C. Boerman, P. Laverman et al., Tc-99m-PEG-Liposomes for the evaluation of colitis in Crohn's disease. J. Drug Target. **8**(4), 225–233 (2000)
78. J. Szebeni, P. Bedocs, Z. Rozsnyay, Z. Weiszhár, R. Urbanics, L. Rosivall et al., Liposome-induced complement activation and related cardiopulmonary distress in pigs: factors promoting reactogenicity of Doxil and Am Bisome. Nanomedicine **8**(2), 176–184 (2012)
79. A. Chanan-Khan, J. Szebeni, S. Savay, L. Liebes, N.M. Rafique, C.R. Alving et al., Complement activation following first exposure to pegylated liposomal doxorubicin (Doxil): possible role in hypersensitivity reactions. Ann. Oncol. **14**(9), 1430–1437 (2003)
80. R.B. Laing, L.J. Milne, C.L. Leen, G.P. Malcolm, A.J. Steers, Anaphylactic reactions to liposomal amphotericin. Lancet **344**(8923), 682 (1994)
81. A.S. Abu Lila, Y. Uehara, T. Ishida, H. Kiwada, Application of polyglycerol coating to plasmid DNA lipoplex for the evasion of the accelerated blood clearance phenomenon in nucleic acid delivery. J. Pharm. Sci. **103**(2), 557–566 (2014)
82. A.S. Abu Lila, K. Nawata, T. Shimizu, T. Ishida, H. Kiwada, Use of polyglycerol (PG), instead of polyethylene glycol (PEG), prevents induction of the accelerated blood clearance

phenomenon against long-circulating liposomes upon repeated administration. Int. J. Pharm. **456**(1), 235–242 (2013)
83. P. Zhang, F. Sun, S. Liu, S. Jiang, Anti-PEG antibodies in the clinic: current issues and beyond PEGylation. J. Control Release **244**, 184–193 (2016)
84. Y. Mima, A.S. Abu Lila, T. Shimizu, M. Ukawa, H. Ando, Y. Kurata et al., Ganglioside inserted into PEGylated liposome attenuates anti-PEG immunity. J. Control Release **250**, 20–26 (2017)
85. T. Moro, Y. Takatori, K. Ishihara, T. Konno, Y. Takigawa, T. Matsushita et al., Surface grafting of artificial joints with a biocompatible polymer for preventing periprosthetic osteolysis. Nat. Mater. **3**(11), 829–836 (2004)
86. S. Jiang, Z. Cao, Ultralow-fouling, functionalizable, and hydrolyzable zwitterionic materials and their derivatives for biological applications. Adv. Mater. **22**(9), 920–932 (2010)
87. P. Zhang, F. Sun, C. Tsao et al., Zwitterionic gel encapsulation promotes protein stability, enhances pharmacokinetics, and reduces immunogenicity. Proc. Natl. Acad. Sci. U.S.A. **112** (39), 12046–12051 (2015)
88. V. Schellenberger, C.W. Wang, N.C. Geething, B.J. Spink, A. Campbell, W. To et al., A recombinant polypeptide extends the in vivo half-life of peptides and proteins in a tunable manner. Nat. Biotechnol. **27**(12), 1186–1190 (2009)
89. N.C. Geething, W. To, B.J. Spink, M.D. Scholle, C.W. Wang, Y. Yin et al., Gcg-XTEN: an improved glucagon capable of preventing hypoglycemia without increasing baseline blood glucose. PLoS ONE **5**(4), e10175 (2010)
90. J.L. Cleland, N.C. Geething, J.A. Moore, B.C. Rogers, B.J. Spink, C.W. Wang et al., A novel long-acting human growth hormone fusion protein (VRS-317): enhanced in vivo potency and half-life. J. Pharm. Sci. **101**(8), 2744–2754 (2012)
91. S.E. Alters, B. McLaughlin, B. Spink, T. Lachinyan, C.W. Wang, V. Podust et al., GLP2-2G-XTEN: a pharmaceutical protein with improved serum half-life and efficacy in a rat Crohn's disease model. PLoS ONE **7**(11), e50630 (2012)

Chapter 21
Innate Immunity to Nanomaterials

Dong Soo Lee and Young Kee Shin

Abstract Nanomaterials, if injected to the body systemically, will meet circulating innate immune mediators first and then tissue-resident macrophages. In this chapter, the recent development of the understanding of the innate immunity, mostly the origin and contribution of tissue-resident macrophages was explained. Interestingly, recently tissue-resident macrophages, major player of innate immunity are not derived from circulating monocyte, especially in liver. Tissue resident-macrophages, which are in non-activated state and will act as first-hand gate-keeper to respond to the injected nanomaterials. This innate immunity has the capability of memory and trainability, which means on the second injection, the degree of response will be higher. This trained innate immunity is now known to be meditated by epigenetic modification. Accelerated blood clearance is the minor and benign aftereffect of the action of innate immune response and the activation of pentraxin and complement system or provocation of humoral or cellular adaptive immune response is the consequential aftereffect of immune responses to the nanomaterials. The differentiation between innate and adaptive immunity lies in the presence or absence of involvement of major histocompatibility (MHC) molecules and of V(D)J recombination in effector cells and molecules (Immunoglobulins or T

D. S. Lee (✉)
Department of Nuclear Medicine, Seoul National University
College of Medicine, Seoul, Republic of Korea
e-mail: dsl@snu.ac.kr

D. S. Lee · Y. K. Shin
Department of Molecular Medicine and Biopharmaceutical Sciences,
Graduate School of Convergence Science and Technology,
Seoul National University, Seoul 03080, Republic of Korea
e-mail: ykeeshin@snu.ac.kr

Y. K. Shin
The Center for Anti-Cancer Companion Diagnostics, Bio-MAX/N-Bio,
Seoul National University, Seoul 08826, Republic of Korea

Y. K. Shin
Laboratory of Molecular Pathology and Cancer Genomics, College of Pharmacy,
Seoul National University, Seoul 08826, Republic of Korea

D. S. Lee (ed.), *Radionanomedicine*, Biological and Medical Physics,
Biomedical Engineering, https://doi.org/10.1007/978-3-319-67720-0_21

cell receptors). As is expected, circulation physiology predates immune response and thus one can refer to the anatomy of liver and spleen detailed in the chapter to predict the fate and final disposal of injected nanomaterials.

21.1 Immune Responses to Foreign Materials

Immunity works for the defense of the body to extraneous materials, either living or non-living things. Immune response to the living things are well understood and even controlled for therapeutic or diagnostic purposes. Investigators tried to understand how the human body recognize the patterns of invasive living things to defend individuals. Understanding immune response has progressed a lot to reach the re-interpretation of the entire feature by systems immunology and/or single cell immunology. The most striking is that the discrimination between innate and adaptive immune responses has been being obliterated [1–3].

Immune response to the invading foreign materials is classified to innate and adaptive immunity (Table 21.1). Cells in charge for innate immunity are monocyte/macrophage, neutrophil and innate lymphoid cells including natural killer (NK) cells, and cells for adaptive immunity are dendritic cells and T and B cells, and natural killer T (NKT) cells. Humoral mediators for innate immunity have been known as acute phase proteins and are currently non-specific protein mediators of pentraxin family of which short-chain subtype are C-reactive protein (CRP) and serum-amyloid P (SAP) component and long-chain subtype is PTX3 [4]. Humoral mediators for adaptive immunity are antibodies with various subtypes.

Cells for innate immunity do not discriminate the antigen pattern and thus is known to be non-specific, however, they were found to respond to specific molecular patterns, which came to be known and named as pattern recognition receptor (PRR) including pathogen-associated molecular pattern (PAMP) and damage-associated molecular pattern (DAMP) [5, 6]. PAMP is associated with invading microbes and DAMP with altered self-molecules. Surface or intracellular recognition molecules such as toll-like receptors (TLRs) [7, 8] and nucleotide-binding and oligomerization domain (NOD)-like receptors [9] were discovered two decades ago and we now know that monocytes/macrophages, neutrophils recognize pathogens or the hosts' own damaged molecules based on

Table 21.1 Cellular and humoral components of innate and adaptive immunity

	Innate immunity	Adaptive immunity
Cellular	Monocyte/Macrophage Neutrophil Innate lymphoid cell (NK cell)	Dendritic cells T cells NKT cells
Humoral	Nonspecific proteins: Pentraxins (short (CRP, SAP) and long (PTX3))	IgM, IgG, IgA, IgD, IgE B cells/Plasma Cells Dendritic cells

molecular pattern of hydrophobicity. Each PAMP has the corresponding TLR which makes homo- or heterodimer to elicit downward signal transduction. For example, lipopolysaccharide (LPS) of Gram-negative bacteria is bound to TLR4 to make homodimer of TLR4-TLR4 to cause inflammation [7] (Table 21.2).

Cells for adaptive immunity recognize antigens by antigen-antibody interaction specifically. Antigen candidates are processed to become antigen by antigen-presenting cells such as macrophage, dendritic cells or virtually all form of the cells. The processed antigens on the surface of antigen presenting cells (APCs) are presented to T cells in association with major histocompatibility complex (MHC) molecules in the secondary lymphoid organ such as lymph nodes. T cell receptor (TCR) of the CD8+ or CD4+ T cells recognize non-self antigens associated with MHC I or MHC II molecules on the surface of APC, respectively, and with these recognition, the naïve CD8+ or CD4+ T cells come to mature to cytotoxic T cells (Tc cells) or helper T cells (Th1, Th2 cells). Th1 cells are now devoted to cellular adaptive immunity to help macrophages or Tc cells and Th2 cells to humoral immunity to help B cells [10, 11]. Tc cells recognize the antigens with much lower affinity but cells proliferate, and owing to the tight binding of TCR of Tc cells with antigen-bound MHC I complex of APC with the help of associated CD8-MHC I binding, they kill the target cells.

Humoral mediators for innate immunity reside mainly in the plasma and do not discriminate the targets but rather they recognize His-x-Cys-x-Ser/Thr-Trp-x-Ser sequence of the target molecules [4]. Short-chain pentraxin CRP and SAP bind the peptides of the foreign materials and act as opsonins which facilitate phagocytosis to the macrophages or act to enhance further binding by C1q, complement component. Long-chain pentraxins PTX3 act similarly [4].

Table 21.2 Ligands and their pattern recognition receptors and the receptor location of innate immunity

Ligands	Pattern recognition receptor	Location
Bacterial lipopeptide	TLR 1/2	Cell membrane
Gram − bacterial lipopolysaccharide (LPS)	TLR 4	Cell membrane
Bacterial flagellin	TLR5	Endosomal membrane
Gram + bacterial lipoteichoic acid	TLR3	Endosomal membrane
Double-stranded RNA (dsRNA)	TLR3	Endosomal membrane
Single-stranded DNA	TLR9	Endosomal membrane
Single-stranded RNA	TLR7/8 or RIG-I	Endosomal membrane

TLR toll-like receptor; *RIG-I* retinoic acid inducible gene-I

Humoral mediators for adaptive immunity are the famous immunoglobulins whose subtypes are IgM, IgG, IgA and IgE. Once stimulated by the intruding foreign materials (or organisms), APC process and present antigens with MHC II to immature CD4+ T helper cells to let these cells become effector Th1 or Th2 cells to help B cells to differentiate into plasma cells. At initial phase of antigen exposure, low affinity plasma cells produce multivalent IgM, which bind antigens with high avidity. Some plasma cells produce high-affinity IgG after class switch recombination, and somatic hypermutation and affinity maturation in germinal center. IgM and IgG make immune complexes that will be cleared by complement system in the blood or by tissue-resident macrophages. Th1 pathway is considered to be mainly in charge of defending intracellular bacteria or protozoa, and Th2 pathway in charge of defending extracellular parasites including helminth. IgA is just the secretary type and working mainly in mucosal surfaces such as intestinal mucus layers.

21.2 Recent Updates of Innate and Adaptive Immunity

Innate and adaptive immune responses have been considered to have characteristic discernable features from each other in terms of specificity of response, trainability of response strength [3], source of the cells involved, and memory capability [1]. However, the recent development of molecular mechanistic scrutiny revealed that the differences are not clear-cut and there is a spectrum of the responses [1]. This is also the case with the characterization of the cells involved in both types of immune responses. The cells of interest are monocyte/macrophages of innate immunity and T cells of adaptive immunity.

Firstly, specificity of response is prominent in T helper/B cells (and associated Ig's) and moderate in cytotoxic T cells (and associated TCRs) and very low in monocytes and macrophages (almost nonspecific). Dendritic cells are involved to present antigens to both T helper cells and cytotoxic T cells and there is an overlap in their function with macrophages and monocytes [12]. Specificity should be considered not in terms of dichotomous characteristics of innate or adaptive immunity but as a spectrum from specific, cross-reactive, not-so-selective, changing along time, or persistently non-specific.

Secondly, trainability of response strength was once thought to be the characteristic feature of adaptive immunity, however, recent discovery of trained innate immunity cast a challenge that trainability should not be the criteria to discern adaptive immunity from innate immunity [3]. Response strength of innate immunity came to be higher at the second challenge of invading organism. Epigenetic modification of the cells in charge of innate immunity is now considered to cause this phenomenon [3]. Obviously, cellular and humoral adaptive immunity shows brisk and higher immune response to the second challenge of invading foreign materials. This trained response is associated with the memory of effector T cells consisting of helper T cells in humoral response and cytotoxic T cells in cellular response.

Thirdly, sources of the cells involved in innate and adaptive immunity used to be considered different between both types of immunity. Myeloid or myelogenous meant monocyte/macrophages and neutrophils and these cells alone were assumed to arise from bone marrow. Myeloid cells were considered to be in charge of innate immunity and lymphoid cells in adaptive immunity. However, lymphoid T cells or B cells also originate from bone marrow (myelogenous) but need to mature in the thymus or in the gut-associated mucosal tissue (GALT), respectively. NK cells belonging to innate lymphoid cells are lymphoid and involved in innate immunity in that they do not need the co-presentation of MHC I molecules for killing infected or damaged cells without self-signal (missing-self). As was stated above, cytotoxic response by NK cells to the second challenge of foreign materials are higher than the first, meaning trainability [3]. NK cells do not have antigen specificity or TCR and also lack recombination activation gene (RAG) obviating the re-arrangement of V(D)J TCR gene. They are myelogenous and lymphoid, associated with innate immunity, and trainable. Source does not help discriminate innate and adaptive immunity. Unlike NK cells, NKT cells have TCR, TCR recombination, and are myelogenous and lymphoid, and should have been trained in the thymus and belong to adaptive immunity.

Fourthly, memory capability resides in central memory T cells or effector memory T cells (helper T or cytotoxic T cells) or memory B cells. The exact molecular mechanism of memory is still under active investigation using genomics, epigenomics and single cell immunology. Memory, if we call trained innate immunity as memory, is via epigenetic modification in innate immune cells. NK cells belonging to innate lymphoid cell subgroup 1 (ILC1) remember the previous challenges with the help of innate lymphoid cell subgroup 2 (ILC2). ILC2 cells mimic helper T cells to help ILC1 such as NK cells [13–15].

In summary, key difference between adaptive immunity and innate immunity might reside in whether they use V(D)J recombination to produce specific immune response in Ig or TCR family genes or whether they use preset limited selectivity of using molecules such as pentraxins (humoral) or TLR isotypes (TLR4 for LPS). If one assumes that myeloid cells alone are responsible for innate immunity, one can immediately find innate lymphoid cells as an exception. If one assumes that adaptive immunity is associated with MHC I (cytotoxic) or MHC II (helper) restriction, there is an easy exception that NKT cells sometimes use CD1 restriction instead to MHC I restriction [16]. Sources, trainability or memory are not appropriate to characterize or discern innate and adaptive immunity. Due to this ambiguity of discriminating innate and adaptive immunity, understanding of bodily immune responses to exogenous nanomaterials should not be prejudiced owing to the past or even current dogma of differential characteristics of innate and adaptive immunity. The immune response to the exogenous nanomaterials will be explained further below keeping this confusion and progress of understanding in mind.

21.3 Innate Immunity and the Relevant Cells

Monocyte/macrophage system is called as a system, as mononuclear phagocytic system (MPS). Mononuclear phagocytic system was previously called as reticuloendothelial system (RES). Monocytes and macrophages had been categorized as the same lineage as myeloid (pertaining to bone marrow) or myelogenous (derived from bone-marrow) and macrophages were assumed to be the committed tissue-localized monocytes having circulated once in the blood. As expected, monocytes and macrophages shared the same surface marker of CD14. The difference looked like the subtypes and related surface markers. While monocytes have subtypes according to the expression level of CD14 and CD16 [12, 17], macrophages showed greater diversity of cell surface markers [18]. And, recent ingenious studies changed the entire understanding of tissue macrophages, especially their embryological and developmental origins and thus the functional significance [18–22] (Table 21.3).

According to the revised understanding of the origins of tissue macrophages, we now know that tissue macrophages are derived from circulating monocytes in certain tissues but in other tissues they are the resident tissue-dedicated ones [19]. Of course, in embryonic period monocytes and tissue macrophages share common originality but the difference arises in terms of when the common ancestral monocytes populated the organ and began to reside as an entity in the tissues [20] (Fig. 21.1). In the myocardium and the lamina propria of the intestinal mucosa, tissue macrophages were found to be populated from the differentiating circulating monocytes in adult period, but in the brain, kidneys, liver and the alveoli of the lung, tissue macrophages were already residing in each organ and self-renew in situ since the birth. Adult bone marrow monocytes were not the sources to populate the MPS of these organs in the physiological status [21]. Interestingly, skin has tissue macrophages consisting of epidermal Langerhans cells, originated from yolk sac

Table 21.3 Subtypes and origin of monocytes and macrophages in the adult at the steady state

	Subtypes (organ)	Origin
Monocytes	Classical CD14++ CD16−	Myeloid
	Intermediate CD14++ CD16+	
	Nonclassical CS14+ CD16++	
Macrophages	Microglia (brain)	Yolk sac macrophages
	Langerhans cell (epidermis, skin)	Yolk sac macrophages/Fetal liver monocytes
	Dermal macrophage (skin)	Adult bone marrow monocytes
	Kidney macrophage	Fetal liver monocytes
	Kupffer cell (liver)	Fetal liver monocytes
	Alveolar macrophage (lungs)	Fetal liver monocytes
	Intestine	Adult bone marrow monocytes
	Heart macrophage	Adult bone marrow monocytes

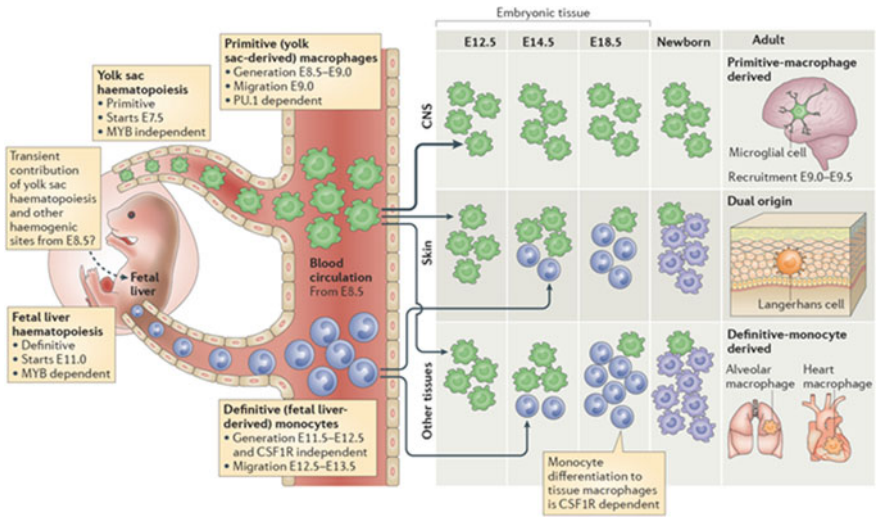

Fig. 21.1 Macrophages according to their origin in mice. Yolk sac or fetal liver are the embryonic origin of tissue-resident macrophages. In the brain, kidneys, and liver, microglia, renal macrophage and Kupffer cells become tissue-resident macrophages since the birth. Bone marrow monocyte-derived macrophages are resident at low levels in physiologic conditions in these organs. In contrast, alveolar or cardiac macrophages are mostly derived from circulating monocytes. Skin has both tissue-resident macrophages and circulating monocytes derived from fetal liver or bone marrow. Modified from [21] with permission

macrophages and fetal monocytes, and dermal macrophages derived from adult bone marrow monocytes [21, 22] (Fig. 21.1 and Table 21.3).

This clarification of the difference between tissue macrophages already resident in the tissues and monocyte-derived tissue macrophages stimulated the understanding of the roles of the former tissue-resident macrophages in physiology and inflammation. Specifically in liver, Kupffer cells are the main cells in MPS and occupies almost more than 80% of entire MPS of the body [23]. Kupffer cells are not derived from circulating monocytes and they are in the state of M2 and tissue-resident macrophages. Only after activation of TLRs, PRRs such as PAMP or DAMP and inflammatory cytokine receptors, M2 Kupffer cells came to be M1 [24–26]. Kupffer cells are considered to be derived from liver-resident self-renewing cells seeded during embryogenesis and stationary throughout the adult life in non-pathologic conditions [8, 27, 28].

Several decades ago, physiologic and pathologic status of MPS were frequently evaluated by colloid liver-spleen scan. Tc-99m labeled tin or sulfur colloid was mostly taken up by MPS system (85% in liver, 10% in spleen and 5% in bone marrow). The size of colloids ranged sub-micron or around 1 μm. As is known, when colloids were clumped to make 10 μm or larger aggregates, they were trapped immediately by alveolar capillaries of the lungs. Cumulated experience acquired from the routine practice of clinical nuclear medicine revealed how consistent these

findings were in normal individuals. These colloids were redistributed to the spleen and the bone marrow in chronic liver diseases, especially in liver cirrhosis [29].

Kupffer cells and hepatocytes in the liver competes for the clearing of the extraneous molecules such as biomacromolecules or larger particulate materials as well as small molecules from the circulation. These extraneous molecules, if they are trapped in colloids and escaped the size filter of pulmonary capillary flow, meet circulating humoral mediators of antibodies or pentraxins [4] or circulating innate immune cells [17]. They can act as hapten, make opsonin, activate complement system, make circulating immune complex and further again phagocytosed by macrophages or trapped by neutrophil extracellular trap (NET) in the localized inflammation sites by neutrophils by neutrophil extracellular trap, and presented again to adaptive immune cells to elicit further production of antibodies or retaliation by cytotoxic T cells [10, 11]. This continues repetitiously until resolution. Among these complicated purposeful surveillance system, Kupffer cells take important roles to remove most of the injected foreign materials [8, 23, 25]. Considering their high proportion among MPS and easy accessibility from both the intestines via portal vein and the systemic circulation via hepatic artery, Kupffer cells do the role of gatekeeping [8]. Any infective living or injected non-living materials should pass this toll. In this line of reasoning, systemically injected therapeutic monoclonal antibodies were considered to be mostly processed in the liver especially by Kupffer cells.

By the way, the roles of hepatocytes to metabolize and excrete the extraneous small molecules have been very well-known as detoxification. The fate of nanomaterials, if injected systemically via intravenous routes, are up to the disposal of differential participation of hepatocytes and Kupffer cells. While hepatocytes are mainly using hepatobiliary excretion system sometimes using the help of bile acids, Kupffer cells act as tissue-resident macrophages [27, 28], stationary to maintain the removal process interacting closely with innate or adaptive immune system. How these two cells collaborate with each other or these two cells collaborate with endothelial cells or other minor liver cells are recently reported [30]. Macrophages can redirect non-professional phagocytes such as endothelial cells to phagocytes. Among the 20% of non-parenchymal cells of the liver, endothelial cells occupying 50% of these non-parenchymal cells do phagocytize invading or injected materials, animate or inanimate, under the direction of Kupffer cells occupying the other 20% of non-parenchymal cells of the liver.

Tissue macrophages of the spleen are also the major player to eradicate the foreign infectious and injected materials. As capillary size is 5–10 μm, materials less than this size reach spleen as well as liver, and spleen weighs 150 g just 1/10 of the liver and taking up the same equivalent of Tc-99m colloid in colloid liver-spleen scan. In the sinusoid of the spleen, the infective and injected materials meet immune cells of innate immunity and adaptive immunity. They need to evade immune response to circulate further in systemic circulation and also they might modulate innate immune response as well as activate naïve T cells. Pretending-self strategy of infective or injected materials was reported. While infectious agents have developed this strategy by evolutionary processes, recent investigation has tried to use

self-recognition mechanism of spleen cells to use CD47 as another component for surface modification of nanomaterials [31]. CD47 is thought to represent self-signal for the spleen-resident macrophages.

21.4 Innate Immunity to Nanomaterials

Immune response to the nanomaterials should be understood in the context of how body is accustomed to respond to invading organisms such as viruses, bacteria, protozoas and helminths. Most of them are extracellular organisms but can be engulfed by macrophages or trapped by NET. Platelets also are involved to cooperate with neutrophils or macrophages and trapped organisms are lysed by extracellular enzymes released by platelets. Extracellular organisms per se can elicit immune response, and if this response belongs to adaptive immunity, they elicit Th2 activation and following stimulation of B cells or Tc cells [32]. Sometimes, Treg cells previously known to be suppressor T cells are activated and the tolerance is induced.

21.4.1 How Nanomaterials Meet Bodily Immune System

Investigators do not make hydrophobic nanomaterials to be injected systemically as they already know very well that hydrophobic materials do aggregate in aqueous milieu and make no feature of nanomaterials any more. Thus, they hydrophilize first the surface of the nanomaterials using many known substances. And the most popular one is polyethylene glycol (PEG) and the recently proposed ones are polybetaines or other zwitterion polymers [33–35]. PEGylated nanomaterials do not aggregate and can pass through alveolar capillaries to reach any peripheral tissues except for brain, testis and cornea, which are sanctuaries having barriers or no vascularity.

Now investigators would now imagine what will meet injected PEGylated nanomaterials. PEGylated nanomaterials enter the blood circulation in concentrates and meet plasma components, mainly proteins consisting of albumins and globulins. Some plasma proteins wrap the nanomaterials with high affinity and are called hard corona proteins and others bind loosely and transiently and called soft corona proteins [36–39]. Recent progress of proteomics revealed the heterogeneous constitution of these corona proteins [40]. Corona proteins are believed to influence the bodily response to the injected nanomaterials and because of this, the response of the cells cultured in vitro to the nanomaterials mixed in the culture fluid will rarely simulate the cellular response in vivo [41–43]. In addition, the flow of the nanomaterials along the surface of endothelial cells will affect much the chance of nanomaterials to encounter the tissue cells. In brief, peripheral endothelial cells see the circulating nanomaterials very infrequently and might almost ignore the

corona-protein wrapped PEGylated nanomaterials circulating in a very dilute concentration which would occur very soon after systemic injection [44].

Immune system would have evolved to handle this naughty situation to enforce surveillance over the injected circulating nanomaterials as well as invading organisms. MPS is the expert clearance system and used to make a very slow flow in the liver, spleen or bone marrow than the usual venous capillaries of every corner of the periphery of the entire body. Passage of nanomaterials through peripheral capillaries of these organs are much slow and endow nanomaterials more chance to interact with endothelial cells, however, these endothelial cells are non-professional phagocytes [30]. Professional phagocytes are called tissue-resident macrophages [27, 28], the best-known of which is hepatic macrophages, i.e. Kupffer cells [24, 26]. Kupffer cells reside alongside hepatic sinusoid in association with sinusoidal endothelial cells in the hepatic column and they comprise about 80% of total bodily tissue-resident macrophages. Using this location advantage, Kupffer cells are very prone to check nanomaterials and process and degrade and/or present them to the immune cells. Roles of hepatic macrophages as phagocytic cells or APCs are now begun to be understood in detail [26] (Fig. 21.2). Spleen is another organ majoring in orchestrating immune response, innate and adaptive ones, and their follicles and germinal centers are performing pivotal role to compartmentalize immune cells involved in establishing naïve and memorized immune responses to the injected PEGylated nanomaterials to reach the specific compartment [45]. Spleen's resident macrophages will interact with T cells to make helper T cells later to help B cells or Tc cells. This further paths of responses belong to adaptive immune responses.

Once nanomaterials are engulfed by tissue-resident macrophages, macrophages process the nanomaterials. The fate of dis-encapsulated, fragmented, degraded nanomaterials, their cores and coats, or their surface binders and constituents should have been understood much better, however, dissecting the outcomes of degradation is very difficult and by any chance if ever done, the endeavor to elucidate the fate would have been laborious. This job reminds the metabolomics, which produces a huge galaxy of data based on the analysis of small molecule drug's metabolism.

21.4.2 Kupffer Cells Examine Nanomaterials as Gatekeeper

In normal healthy subjects, liver has heterogeneous macrophages consisting mostly of embryonal yolk-sac-derived or fetal liver-derived tissue-resident macrophages and in minor amount of bone marrow monocyte-converted myeloid dendritic cells [26] (Fig. 21.2). Of course injured liver can have further the monocyte-derived macrophages, either inflammatory or restorative, and monocytic myeloid-derived suppressor cells [26]. Alongside the hepatocytes, conventional dendritic cells (cDC) or plasmacytoid dendritic cells (pDC) reside and have their own

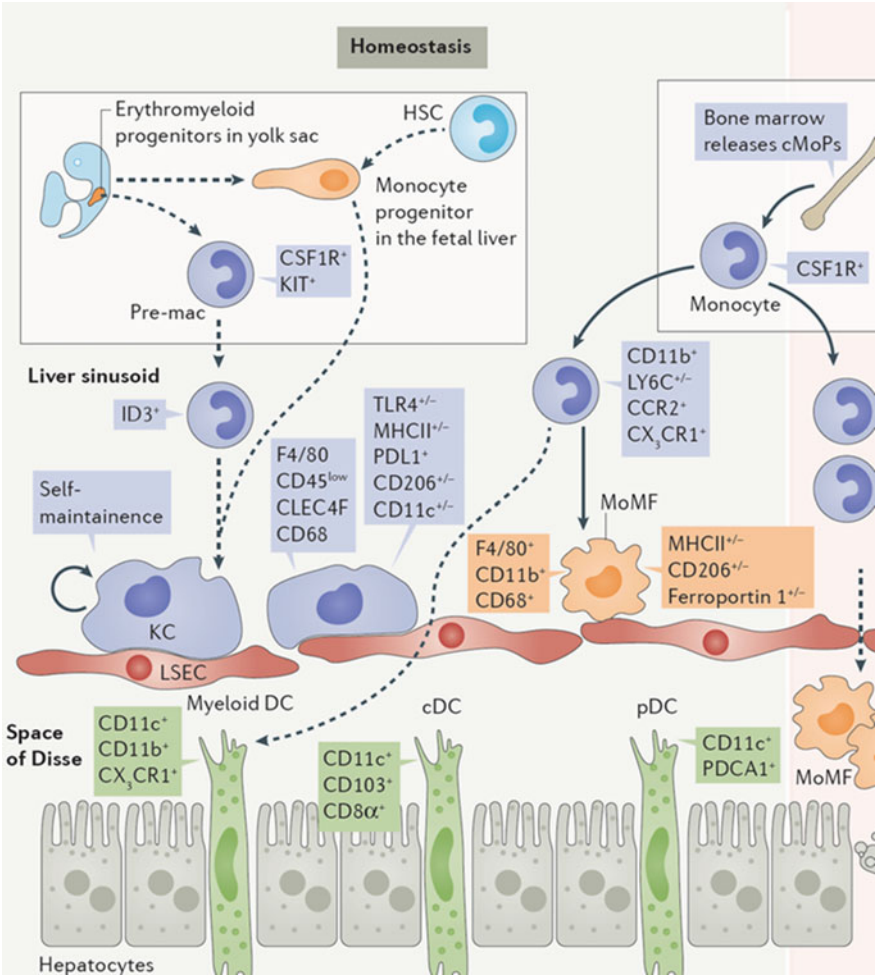

Fig. 21.2 Tissue-resident macrophages as Kupffer cells (KC). Nanomaterials reach the sinusoid to meet Kupffer cells or endothelial cells (LSEC: liver sinusoidal endothelial cells), or pass through fenestrae to arrive at space of Disse. Here nanomaterials will meet myeloid dendritic cells (DC), conventional DC (cDC) or plasmacytoid DC (pDC). Hepatocytes are also watching the nanoparticles. Monocyte-derived macrophage (MoMF) is usually in the sinusoid and enters the space of Disse in injury. cMoP: common monocyte progenitor, HSC: hematopoietic stem cell. Modified from [26] with permission

characteristic phenotypes (Fig. 21.2). Dendritic cells are sampling the pattern of non-self invaders using PRRs such as TLR and contribute as APCs to evoke adaptive immunity and harbor MHC molecules on their surfaces.

Kupffer cells engulf most of the circulating pathogens and the similar objects by recognizing their repetitive patterns of invasive ones such as protozoa, bacteria and viruses. They also have FcγR which recognize immunoglobulins and immune

complexes [46]. If the antigens were exogenous antibodies (immunoglobulins), those antibodies are also recognized by Kupffer cells using this receptor FcγR too. In contrast, FcRn (neonatal Fc receptor) resides in hepatocytes, most of the epithelial and endothelial cells as well as macrophages, which act to protect IgG from degradation, by recycling the endocytosed IgG to the circulation [46, 47].

Once nanomaterials reach liver via systemic circulation, they will be contacted by macrophages or non-professional phagocytic cells or dendritic cells (in liver, mDC, pDC) and these cells examine whether these nanomaterials have the patterns of pathogens or damaged cells. Nanomaterials would be taken up by Kupffer cells, escape via fenestrae to space of Disse to reach hepatocytes and/or pDC, or circulate back to the systemic veins (hepatic vein and inferior vena cava) via the heart to come back again to the sinusoids [26]. It is known that the surface characteristics of nanomaterials influence their fates in biodistribution and the innate immune responses to systemic-injected nanomaterials had better be understood according to the composition of the modified surfaces of these nanomaterials.

Nanomaterials are usually PEGylated and have the ligands such as antibodies on their surface. PEGylated nanomaterials circulate longer and have been stealthy in that they hide from immune responses [44]. PEGylated surface, either brush or mushroom [48], should not have induced immune responses either innate or adaptive. Interestingly, it caused IgM responses on the second injection, which raised concern [49]. Kupffer cells would have either engulfed PEGylated nanomaterials removing completely them from the circulation very rapidly, not presenting them to the lymphocytes of adaptive immunity, or would have digested and presented them to the cells in charge of adaptive immunity. Or the cells in charge of this latter endeavor of antigen presenting would have been rather mDC cells or other myeloid cells than Kupffer cells [50].

Elimination of biologics or specifically of therapeutic monoclonal antibodies have come to be understood in very much detail during the last two decades [51–53]. As we can decorate the surfaces of nanomaterials with human, humanized, chimeric or murine monoclonal antibodies or their engineered fragments, our knowledge of the disposal of biomacromolecules are now be cited to predict the fate of engineered antibody-bound nanomaterials. When the therapeutic monoclonal antibodies were to be approved from regulatory agencies, humoral immune responses were routinely examined and we know that ‘immunogenicity’ of these antibodies range from 0 to 99% [54, 55]. Murine antibodies tended to elicit higher anti-antibody responses, however, human antibodies were not without antibody responses and this antibody was supposed to be against complementarity-determining region (CDR) among variable domains of the light and heavy chains [55]. Investigators have tried to avoid this antibody response to the therapeutic antibodies by removing such problematic non-human glycosylation as galactose-α1,3-galactose, N-glycolylneuraminic acid, β1,2-xylose and α1,3 fucose during their manufacturing or by adding carbohydrate residues to improve biodistribution [55].

Summarizing the current understanding, IgG types of therapeutic antibodies are supposed to be cleared via FcγR after uptake by expert phagocytic cells such as Kupffer cells or recycled via FcRn after endocytosis by non-professional phagocytic

endothelial and epithelial cells and even hepatocytes as well as professional phagocytic cells. The difference between immunoglobulins and immunoglobulin-bound nanomaterials lies possibly in their presentation pattern. Immune complex are formed with immunoglobulins against therapeutic antibodies and presented to tissue-resident macrophages including Kupffer cells, while immunoglobulins on the nanomaterials' surface may be hidden and thus may not be detected by anti-Ig immunoglobulins or anti-Ig TCR.

21.4.3 Macrophages Respond to the Exogenous Nanomaterials in Spleen

Spleen is the organ in charge of adaptive immunity and innate immunity [45]. Red pulp sinusoidal macrophages (RpMΦ) may be tissue-resident macrophages specialized in aged or damaged erythrocyte disposal. However, during infection, circulating monocyte-derived macrophages join the pool of RpMΦ [56]. Marginal zone macrophages (MZMΦ) phagocytize blood-borne pathogens and clear them from the circulation. Marginal metalophillic macrophages (MMMΦ) also phagocytize and process the pathogens to present them, in collaboration with DCs, to the T lymphocyte. MZMΦs work for innate immunity and MMMΦ for adaptive immunity [56].

PEGylated nanomaterials, if they are administered via intravenous routes, will arrive at spleen crossing white pulp to reach marginal zones and red pulp. They will meet either MZMΦs or MMMΦs (Fig. 21.3). If they mimic LPS and meet TLR4, or have glycosylphosphatidylinositol (GPI) and meet TLR2/TLR4 or have CpG motif and meet TLR9, they will be endocytosed by MZMΦs as final destiny or by MMMΦs to be presented to immune cells [56]. Extracellular matrix protein, fibronectin or intracellular DNA binding protein or oxidized low-density lipoprotein (LDL) were found to be taken up by these splenic macrophages and thus, surface-mimicry of nanomaterials will make these nanomaterials be treated like invading pathogens. The possibility of PEGylated nanomaterials to stimulate innate or adaptive immunity reside in their similarity in structure to invading pathogens.

21.4.4 Prediction of Immune Responses of Therapeutic-Radioisotope-Labeled Nanomaterials

Therapeutic radioisotopes such as lutetium-177 (^{177}Lu) or yttrium-90 (^{90}Y) were shown to be labeled easily with chelators surface-bound to the nanomaterials. In recent reports, Jeong and others [57] presented their approach of simply modifying the surface of alkylated nanomaterials simultaneously with PEG, chelator-alkyl linker, ligand-alkyl linkers or antibodies. This was called encapsulation and the

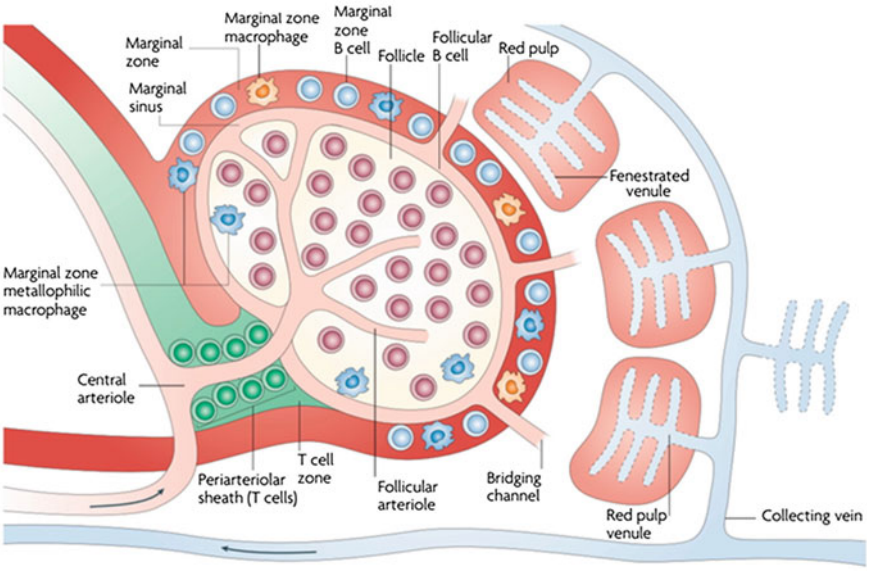

Fig. 21.3 Microstructure of spleen emphasizing microcirculation. Nanomaterials will arrive at spleen via central arteriole and follicular arteriole crossing follicles to reach marginal zone. In and near marginal zone, nanomaterials shall meet marginal zone macrophages (MZMΦ) and marginal metalophillic macrophages (MMMΦ). Modified from [45] with permission

production of capsule was the most elaborate step and further procedure was just as simple as mixing, vortexing and separation, which takes advantage of van der Waals' force interaction. This physical labeling interestingly stabilized the labeling even after being administered to the systemic circulation and elimination was via hepatobiliary tract without detachment of capsules, i.e., as an integral entity [58].

Investigators have tried to understand the immune responses to biologics especially liposomes and found that the liposome-drug-conjugates could eliminate IgM-mediated accelerated blood clearance. Oxaloplatin within the liposome delivered to the spleen, if taken up by the MZMΦs or MMMΦs, it could abrogate the antibody-production responses [59]. We expect that therapeutic radioisotope-labeled nanomaterials would mimic this phenomenon because ^{177}Lu or ^{90}Y reach and kill macrophages and might abrogate further generation of innate or adaptive immunity.

Investigators have tried to predict the biodistribution of biologics especially therapeutic antibodies using the murine experimental data of pharmacokinetics for therapeutic antibodies [60, 61]. They first developed allometry-based conversion equations and found that they worked well in gross terms [60]. However, the problems of the species differences between mouse and human ranged from differences in mouse/human target receptors, mouse/human antibody affinity for the target, mouse/human FcRn to yield differences in half-lives of administered therapeutic antibodies [46]. Pharmacokinetics of newly-developed therapeutic

antibodies was measured in mouse models, and recently even in humanized FcRn mouse models [62]. Findings in mouse models were extrapolated to humans taking the inter-species differences into account with further modification than simple allometry. Once physiologically-based pharmacokinetic model (PBPK) was established [51, 60], predictive projection to human pharmacokinetics using mouse data and PBPK has been highly recommended [46].

Radiolabeled PEGylated nanomaterials will enhance the predictability of human pharmacokinetics while they allow single-photon emission computed tomography (SPECT) or positron emission tomography (PET) acquisition which enable to elucidate the exact biodistribution and its temporal changes. Target-mediated drug disposition (TMDD) model which was originally developed and used for small-molecule drugs such as tyrosine kinase inhibitors, was further used for understanding target disposition of biologics (therapeutic monoclonal antibodies) in small animals [51, 60]. Recently again, like PBPK, TMDD model was also used for projection to predict human target disposition of therapeutic monoclonal antibodies such as rituximab [60].

If we bind rituximab upon the surface of PEGylated nanomaterials, we are going to measure the biodistribution and thus understand pharmacokinetics of new therapeutic nanomaterials, and then the projection to human pharmacokinetics will be tried using inter-species scaling methods, allometry, PBPK and TMDD models [46, 60]. Though physiological differences between mouse and human are considered with these models, immunogenicity and its difference between species will still cast a great ambiguity in this projection. We think that we need to know the confounding variables for the determination of in vivo fates of radionanomaterials and devise how to remove the effect of these variables to grossly-correct prediction of the estimated amount of antibody-bound PEGylated nanomaterials in humans.

Of course, the exact amount of nanomaterials in the target tissues can only be obtained from the human imaging studies using PET or SPECT [63, 64]. Cupper-64 (^{64}Cu) or zirconium-89 (^{89}Zr) are for PET and indium-111 (^{111}In) is for SPECT studies with appropriate physical half-lives. The amount of nanomaterials is not important for therapeutic radioisotopes as the beta radiation is usually used for the treatment. When we are able to increase the specific activity (Bq/g for radionuclides, Bq/mole for radiopharmaceutical or nanomaterials), the radioactivity really counts but not the antibody or ligand on the nanomaterials' surfaces, which originally was used for targeting. Nanomaterials would be less than 30 nmole/injection for microdosing study in humans according to the rules announced by the each country's agency for nanomaterials as well as biomacromolecules. If 1 mCi is going to be injected to human, 3.7×10^7 Bq/$30 \times 10^{-9} \times 6 \times 10^{23}$ is allowed and thus theoretically 10^{16} particles can be given.

In summary, in case of therapeutic radioisotope-labeled nanomaterials, we need to examine the biodistribution of radioactivity using PET or SPECT in small animals or monkeys and project the preclinical findings the human pharmacokinetics [46, 60]. The target disposition is also to be projected. To keep in mind, the therapeutic effect is not from the biological action of target-cumulated biologics, but instead, from the radioactivity of nanomaterials' surface-bound chelator labeled

beta-ray-emitting radioisotopes. Beside therapeutic responses, immune responses to these therapeutic radioisotope-labeled nanomaterials might be modified by the radioactivity. This radioactivity might destroy tissue macrophages such as Kupffer cells and/or change the response of immune cells of innate immunity (Kupffer cells of hepatic sinusoid or MZMΦs of the spleen) or even immune cells of adaptive immunity (mDC of space of Disse of the liver or MMMΦs of the spleen) [26, 45]. Though anti-PEG IgM antibody was developed against PEG coating the nanomaterials at second injection of the PEGylated nanomaterials, and blood clearance was accelerated concordantly [49], we are not sure that IgM response of adaptive immunity is the unique aspect of this trained memory response. We need to remind that innate immune responses can also be trained and thus be enhanced at second injection [3], and the cells involved in innate and adaptive responses are often overlapped implying the concomitant activation of the downstream immune activation [2]. Considering all these phenomena of bodily immune responses to therapeutic radioisotope-labeled PEGylated nanomaterials, what we need to get is how much of the injected materials are reaching the targets while other innate or adaptive immune organs are responding to the collateral accumulation of the same therapeutic materials. Further to this, how much amount of radioactivity should be given to the patients should also be elucidated using the preclinical PET/SPECT imaging and individualized dosimetry. Understanding the fate of radionanomedicines made of radiolabeled nanomaterials in human will be feasible referring all the facts and principles of innate immunity as well as adaptive immunity and physiology unique to the human being.

References

1. L.L. Lanier, Shades of grey–the blurring view of innate and adaptive immunity. Nat. Rev. Immunol. **13**(2), 73–74 (2013)
2. E. Vivier, D.H. Raulet, A. Moretta, M.A. Caligiuri, L. Zitvogel, L.L. Lanier et al., Innate or adaptive immunity? The example of natural killer cells. Science **331**(6013), 44–49 (2011)
3. M.G. Netea, L.A. Joosten, E. Latz, K.H. Mills, G. Natoli, H.G. Stunnenberg et al., Trained immunity: a program of innate immune memory in health and disease. Science **352**(6284), aaf1098 (2016)
4. A. Doni, C. Garlanda, A. Mantovani, Innate immunity, hemostasis and matrix remodeling: PTX3 as a link. Semin. Immunol. **28**(6), 570–577 (2016)
5. X. Cao, Self-regulation and cross-regulation of pattern-recognition receptor signalling in health and disease. Nat. Rev. Immunol. **16**(1), 35–50 (2016)
6. S.Y. Seong, P. Matzinger, Hydrophobicity: an ancient damage-associated molecular pattern that initiates innate immune responses. Nat. Rev. Immunol. **4**(6), 469–478 (2004)
7. D. Gao, W. Li, Structures and recognition modes of toll-like receptors. Proteins **85**(1), 3–9 (2017)
8. N. Nakamoto, T. Kanai, Role of toll-like receptors in immune activation and tolerance in the liver. Front. Immunol. **5**, 221 (2014)
9. J.D. Jones, R.E. Vance, J.L. Dangl, Intracellular innate immune surveillance devices in plants and animals. Science **354**(6316), 1117 (2016)
10. J. Zhu, W.E. Paul, CD4 T cells: fates, functions, and faults. Blood **112**(5), 1557–1569 (2008)

11. S. Nakayamada, H. Takahashi, Y. Kanno, J.J. O'Shea, Helper T cell diversity and plasticity. Curr. Opin. Immunol. **24**(3), 297–302 (2012)
12. M. Guilliams, F. Ginhoux, C. Jakubzick, S.H. Naik, N. Onai, B.U. Schraml et al., Dendritic cells, monocytes and macrophages: a unified nomenclature based on ontogeny. Nat. Rev. Immunol. **14**(8), 571–578 (2014)
13. H. Spits, D. Artis, M. Colonna, A. Diefenbach, J.P. Di Santo, G. Eberl et al., Innate lymphoid cells—a proposal for uniform nomenclature. Nat. Rev. Immunol. **13**(2), 145–149 (2013)
14. K. Juelke, C. Romagnani, Differentiation of human innate lymphoid cells (ILCs). Curr. Opin. Immunol. **38**, 75–85 (2016)
15. Y. Jiao, N.D. Huntington, G.T. Belz, C. Seillet, Type 1 innate lymphoid cell biology: lessons learnt from natural killer cells. Front. Immunol. **7**, 426 (2016)
16. D.I. Godfrey, S. Stankovic, A.G. Baxter, Raising the NKT cell family. Nat. Immunol. **11**(3), 197–206 (2010)
17. L. Ziegler-Heitbrock, P. Ancuta, S. Crowe, M. Dalod, V. Grau, D.N. Hart, P.J. Leenen et al., Nomenclature of monocytes and dendritic cells in blood. Blood **116**(16), e74–e80 (2010)
18. S. Yona, K.W. Kim, Y. Wolf, A. Mildner, D. Varol, M. Breker et al., Fate mapping reveals origins and dynamics of monocytes and tissue macrophages under homeostasis. Immunity **38** (1), 79–91 (2013)
19. E. Gomez Perdiguero, K. Klapproth, C. Schulz, K. Busch, E. Azzoni, L. Crozet et al., Tissue-resident macrophages originate from yolk-sac-derived erythro-myeloid progenitors. Nature **518**(7540), 547–551 (2015)
20. F. Ginhoux, J.L. Schultze, P.J. Murray, J. Ochando, S.K. Biswas, New insights into the multidimensional concept of macrophage ontogeny, activation and function. Nat. Immunol. **17**(1), 34–40 (2016)
21. F. Ginhoux, S. Jung, Monocytes and macrophages: developmental pathways and tissue homeostasis. Nat. Rev. Immunol. **14**(6), 392–404 (2014)
22. E. Mass, I. Ballesteros, M. Farlik, F. Halbritter, P. Günther, L. Crozet et al., Specification of tissue-resident macrophages during organogenesis. Science **353**(6304), aaf4238 (2016)
23. C. Ju, F. Tacke, Hepatic macrophages in homeostasis and liver diseases: from pathogenesis to novel therapeutic strategies. Cell. Mol. Immunol. **13**(3), 316–327 (2016)
24. L.J. Dixon, M. Barnes, H. Tang, M.T. Pritchard, L.E. Nagy, Kupffer cells in the liver. Compr. Physiol. **3**(2), 785–797 (2013)
25. J. Jager, M. Aparicio-Vergara, M. Aouadi, Liver innate immune cells and insulin resistance: the multiple facets of Kupffer cells. J. Intern. Med. **280**(2), 209–220 (2016)
26. O. Krenkel, F. Tacke, Liver macrophages in tissue homeostasis and disease. Nat. Rev. Immunol. **17**(5), 306–321 (2017)
27. L.C. Davies, S.J. Jenkins, J.E. Allen, P.R. Taylor, Tissue-resident macrophages. Nat. Immunol. **14**(10), 986–995 (2013)
28. D. Hashimoto, A. Chow, C. Noizat, P. Teo, M.B. Beasley, M. Leboeuf et al., Tissue-resident macrophages self-maintain locally throughout adult life with minimal contribution from circulating monocytes. Immunity **38**(4), 792–804 (2013)
29. M.C. Lee, J.-K. Chung, D.S. Lee, *Koh Chang-Soon Nuclear Medicine* (Korea Medical Books, Seoul Korea, 2008)
30. C.Z. Han, I.J. Juncadella, J.M. Kinchen, M.W. Buckley, A.L. Klibanov, K. Dryden et al., Macrophages redirect phagocytosis by non-professional phagocytes and influence inflammation. Nature **539**(7630), 570–574 (2016)
31. P.L. Rodriguez, T. Harada, D.A. Christian, D.A. Pantano, R.K. Tsai, D.E. Discher, Minimal "Self" peptides that inhibit phagocytic clearance and enhance delivery of nanoparticles. Science **339**(6122), 971–975 (2013)
32. S.W. Jones, R.A. Roberts, G.R. Robbins, J.L. Perry, M.P. Kai, K. Chen et al., Nanoparticle clearance is governed by Th1/Th2 immunity and strain background. J. Clin. Invest. **123**(7), 3061–3073 (2013)
33. Z.G. Estephan, P.S. Schlenoff, J.B. Schlenoff, Zwitteration as an alternative to PEGylation. Langmuir **27**(11), 6794–6800 (2011)

34. Z. Amoozgar, Y. Yeo, Recent advances in stealth coating of nanoparticle drug delivery systems. Wiley Interdiscip. Rev. Nanomed. Nanobiotechnol. **4**(2), 219–233 (2012)
35. S. Mondini, M. Leonzino, C. Drago, A.M. Ferretti, S. Usseglio, D. Maggioni et al., Zwitterion-coated iron oxide nanoparticles: surface chemistry and intracellular uptake by hepatocarcinoma (HepG2) cells. Langmuir **31**(26), 7381–7390 (2015)
36. T. Cedervall, I. Lynch, S. Lindman, T. Berggård, E. Thulin, H. Nilsson et al., Understanding the nanoparticle-protein corona using methods to quantify exchange rates and affinities of proteins for nanoparticles. Proc. Natl. Acad. Sci. USA **104**(7), 2050–2055 (2007)
37. M. Lundqvist, J. Stigler, G. Elia, I. Lynch, T. Cedervall, K.A. Dawson, Nanoparticle size and surface properties determine the protein corona with possible implications for biological impacts. Proc. Natl. Acad. Sci. USA **105**(38), 14265–14270 (2008)
38. P. Aggarwal, J.B. Hall, C.B. McLeland, M.A. Dobrovolskaia, S.E. McNeil, Nanoparticle interaction with plasma proteins as it relates to particle biodistribution, biocompatibility and therapeutic efficacy. Adv. Drug Deliv. Rev. **61**(6), 428–437 (2009)
39. S. Milani, F.B. Bombelli, A.S. Pitek, K.A. Dawson, J. Rädler, Reversible versus irreversible binding of transferrin to polystyrene nanoparticles: soft and hard corona. ACS Nano. **6**(3), 2532–2541 (2012)
40. P.M. Kelly, C. Åberg, E. Polo, A. O'Connell, J. Cookman, J. Fallon et al., Mapping protein binding sites on the biomolecular corona of nanoparticles. Nat. Nanotechnol. **10**(5), 472–479 (2015)
41. A. Lesniak, F. Fenaroli, M.P. Monopoli, C. Åberg, K.A. Dawson, A. Salvati, Effects of the presence or absence of a protein corona on silica nanoparticle uptake and impact on cells. ACS Nano. **6**(7), 5845–5857 (2012)
42. A. Salvati, A.S. Pitek, M.P. Monopoli, K. Prapainop, F.B. Bombelli, D.R. Hristov et al., Transferrin-functionalized nanoparticles lose their targeting capabilities when a biomolecule corona adsorbs on the surface. Nat. Nanotechnol. **8**(2), 137–143 (2013)
43. M.P. Monopoli, C. Aberg, A. Salvati, K.A. Dawson, Biomolecular coronas provide the biological identity of nanosized materials. Nat. Nanotechnol. **7**(12), 779–786 (2012)
44. S. Schöttler, K. Landfester, V. Mailänder, Controlling the stealth effect of nanocarriers through understanding the protein corona. Angew. Chem. Int. Ed. Engl. **55**(31), 8806–8815 (2016)
45. M. Cataldi, C. Vigliotti, T. Mosca, M. Cammarota, D. Capone, Emerging role of the spleen in the pharmacokinetics of monoclonal antibodies, nanoparticles and exosomes. Int. J. Mol. Sci. **18**(6), E1249 (2017)
46. W. Wang, E.Q. Wang, J.P. Balthasar, Monoclonal antibody pharmacokinetics and pharmacodynamics. Clin. Pharmacol. Ther. **84**(5), 548–558 (2008)
47. D.C. Roopenian, S. Akilesh, FcRn: the neonatal Fc receptor comes of age. Nat. Rev. Immunol. **7**(9), 715–725 (2007)
48. J.L. Perry, K.G. Reuter, M.P. Kai, K.P. Herlihy, S.W. Jones, J.C. Luft et al., PEGylated PRINT nanoparticles: the impact of PEG density on protein binding, macrophage association, biodistribution, and pharmacokinetics. Nano Lett. **12**(10), 5304–5310 (2012)
49. A.S. Abu Lila, H. Kiwada, T. Ishida, The accelerated blood clearance (ABC) phenomenon: clinical challenge and approaches to manage. J. Control Release **172**(1), 38–47 (2013)
50. T. Shimizu, T. Ishida, H. Kiwada, Transport of PEGylated liposomes from the splenic marginal zone to the follicle in the induction phase of the accelerated blood clearance phenomenon. Immunobiology **218**(5), 725–732 (2013)
51. S. Shi, Biologics: an update and challenge of their pharmacokinetics. Curr. Drug Metab. **15**(3), 271–290 (2014)
52. J.W. Lee, ADME of monoclonal antibody biotherapeutics: knowledge gaps and emerging tools. Bioanalysis **5**(16), 2003–2014 (2013)
53. P. Chames, M. Van Regenmortel, E. Weiss, D. Baty, Therapeutic antibodies: successes, limitations and hopes for the future. Br. J. Pharmacol. **157**(2), 220–233 (2009)

54. J.D. Gómez-Mantilla, I.F. Trocóniz, Z. Parra-Guillén, M.J. Garrido, Review on modeling anti-antibody responses to monoclonal antibodies. J. Pharmacokinet Pharmacodyn. **41**(5), 523–536 (2014)
55. A. Kuriakose, N. Chirmule, P. Nair, Immunogenicity of biotherapeutics: causes and association with posttranslational modifications. J. Immunol. Res. **2016**, 1298473 (2016)
56. H.B. da Silva, R. Fonseca, R.M. Pereira, A. Cassado Ados, J.M. Álvarez, M.R. D'Império Lima, Splenic macrophage subsets and their function during blood-borne infections. Front Immunol. **6**, 480 (2015)
57. Y.K. Lee, J.M. Jeong, L. Hoigebazar, B.Y. Yang, Y.S. Lee, B.C. Lee et al., Nanoparticles modified by encapsulation of ligands with a long alkyl chain to affect multispecific and multimodal imaging. J. Nucl. Med. **53**(9), 1462–1470 (2012)
58. H.J. Seo, S.H. Nam, H.J. Im, J.Y. Park, J.Y. Lee, B. Yoo et al., Rapid hepatobiliary excretion of micelle-encapsulated/radiolabeled upconverting nanoparticles as an integrated form. Sci. Rep. **5**, 15685 (2015)
59. A. Nagao, A.S. Abu Lila, T. Ishida, H. Kiwada, Abrogation of the accelerated blood clearance phenomenon by SOXL regimen: promise for clinical application. Int. J. Pharm. **441**(1–2), 395–401 (2013)
60. J. Wang, S. Iyer, P.J. Fielder, J.D. Davis, R. Deng, Projecting human pharmacokinetics of monoclonal antibodies from nonclinical data: comparative evaluation of prediction approaches in early drug development. Biopharm. Drug Dispos. **37**(2), 51–65 (2016)
61. A.V. Kamath, Translational pharmacokinetics and pharmacodynamics of monoclonal antibodies. Drug Discov. Today Technol. **21–22**, 75–83 (2016)
62. G. Proetzel, D.C. Roopenian, Humanized FcRn mouse models for evaluating pharmacokinetics of human IgG antibodies. Methods **65**(1), 148–153 (2014)
63. A.M. Wu, Engineered antibodies for molecular imaging of cancer. Methods **65**(1), 139–147 (2014)
64. L.E. Lamberts, S.P. Williams, A.G. Terwisscha van Scheltinga, M.N. Lub-de Hooge, C. P. Schröder et al., Antibody positron emission tomography imaging in anticancer drug development. J. Clin. Oncol. **33**(13), 1491–1504 (2015)

Part VIII
Prospects

Chapter 22: Molecular Imaging Using Radionanomedicine
Chapter 23: Therapeutic/Theranostic Use of Radionanomedicine

In this part, the eternal goal of radionanomedicine is explained. I, as editor of this book, coauthored these two chapters. I can assure you that the readers will feel the direction of radionanomedicine, one is for molecular imaging and the other is for therapeutic application which should be translated to the clinics for human use to classify the diseases and to predict the prognosis which are the premises of nuclear medicine as well as radiology/ diagnostic imaging. The credit of nuclear medicine goes into its pioneering activities of personalizing the therapeutic options based on diagnostic or theranostic imaging with personalized dosimetry. Development of instruments even for the small animals and refinement of tracer kinetic analysis was the bases of this capability of nuclear medicine and nuclear medicine is now adopting the outputs of nanotechnology researches and products thereof, as radionanomedicines, once radiolabeled, the products are going to be the substances to be able to be used for clinical tomographic quantitative imaging and therapy. These two chapters were coauthored by my youngest nuclear medicine physician colleagues and the readers can feel the hue of the future direction of radionanomedicine from the perspectives of the next generation. I am sure that the next generation nuclear medicine physicians and nanomedicine experts, scientists, and engineers will bring the field to the clinical ones, eventually.

I wish the direction should be in developing personalized theranostics, which means that therapeutics are going to be imaged for their in vivo behaviors elucidating the molecular impact of the radionanomedicine therapeutics. Radionanomedicines as theranostics and therapeutics are now to be tested for their

translatability to the clinical application. No more hype with the profuse possibilities of application of new materials and the principle of evidence-based medicine will prove or disprove the applicability of the new radionanomedicines. Radionanomedicine as combined nuclear and nanomedicine will succeed in moving forward to clinics just as clinical nuclear medicine had been successful for the last six decades since its birth.

Chapter 22
Molecular Imaging Using Radionanomedicine

Yong-il Kim and Dong Soo Lee

Abstract Nanoparticles (NPs) have recently attracted great attention as biomedical imaging agents. Many types of NPs have been investigated with combinations of various molecular targeting groups. In addition, multiplex imaging has been studied with NPs, including surface-enhanced Raman scattering (SERS) NPs. Single-photon emission computed tomography (SPECT) or positron emission tomography (PET) by molecularly targeted, radiolabeled NPs provides several benefits over usual imaging probes in the aspect of sensitivity and quantitation. In addition, multimodal imaging probes that are combinations of both radionuclide-based and non-radionuclide-based imaging approaches, such as optical imaging or magnetic resonance imaging (MRI), could be applied to next medical studies. Furthermore, molecularly targeted probes which could be identified by more than three imaging modalities are possible. In conclusion, nanotechnologies promise to extend the limitations of current molecular imaging techniques, and nanomedicine may play an important role in the future.

Y. Kim (✉)
Department of Nuclear Medicine, Asan Medical Center,
University of Ulsan College of Medicine, Seoul 05505, Republic of Korea
e-mail: kyi821209@naver.com

D. S. Lee
Department of Nuclear Medicine, Seoul National University
College of Medicine, Seoul 03080, Republic of Korea
e-mail: dsl@snu.ac.kr

D. S. Lee
Department of Molecular Medicine and Biopharmaceutical Sciences,
Graduate School of Convergence Science and Technology,
Seoul National University, Seoul 03080, Republic of Korea

D. S. Lee (ed.), *Radionanomedicine*, Biological and Medical Physics,
Biomedical Engineering, https://doi.org/10.1007/978-3-319-67720-0_22

22.1 Molecular Imaging by Nanotechnology

Nanotechnology has great potential for the detection and diagnosis of cancers and nanoparticles (NPs) can be used in the personalized treatment of various diseases [1]. In general, the diameter of a NP is between one to hundreds nanometers. NPs can interact with biomolecules both on the surface of and inside cells, which could be helpful in the diagnosis and treatment of disease. One major application of nanotechnology is in medicine [2].

Molecular imaging is defined as in vivo characterization and measurement of biological processes at the cellular or molecular level [3] (Table 22.1). In contrast to diagnostic imaging, molecular imaging attempts to determine the molecular abnormalities that underlie diseases. A key feature of molecular imaging is utilization of biomarkers, which are defined as measuring quantitative parameters of biological processes that serve as indicative endpoints [4]. Biomarkers can be generically depicted as the molecular signatures of biological systems. The difficulty in molecular imaging depends on identifying targets that are suitable for sensitive and accurate imaging.

Nuclear medicine is one of the most important fields in which molecular imaging techniques are applied using radioisotopes. The workflow of molecular imaging with radioisotopes includes (1) the design of target-specific molecules, (2) the attachment of radioisotopes without changing the biological properties of the target

Table 22.1 Characteristics of molecular imaging modalities (modified from Table 1 of [87])

Modality	Form of energy used	Spatial resolution (mm)	Advantages	Clinical translation
PET	Annihilation photons	1–2 (microPET)	High sensitivity Quantitative Tracer amount of probe	Yes
SPECT	Gamma rays	0.5–2 (microSPECT)	High sensitivity Quantitative Tracer amount of probe	Yes
MRI	Radiofrequency waves	0.01–0.1 (small-animal MRI)	High spatial resolution Superb soft tissue discrimination	Yes
Fluorescence imaging	Visible to infrared light	<1 (fluorescence reflectance imaging)	High sensitivity Multiplexed imaging	Yes
Bioluminescence imaging	Visible to infrared light	3–5	High sensitivity Multiplexed imaging	No
Ultrasonography (US)	High frequency waves	0.04–0.1 (small-animal US)	High sensitivity Portable	Yes

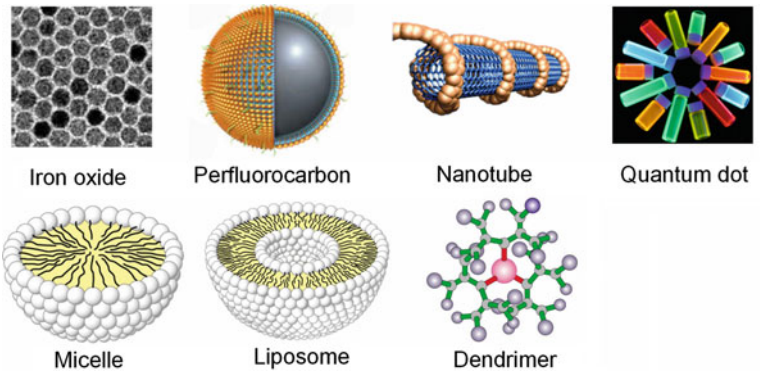

Fig. 22.1 Several types of nanoparticles for molecular imaging. Adapted from [84] with permission

molecules, and (3) in vivo imaging with both high resolution and sensitivity. The techniques are single-photon emission computed tomography (SPECT) or positron emission tomography (PET). The main advantages of nuclear molecular imaging (i.e., SPECT or PET) over other imaging (for example, optical or magnetic resonance imaging [MRI]) are that they are highly sensitive, quantitative, and not limited in tissue penetration [5].

This chapter focuses on the use of NPs in the field of medicine, including radiolabeled NPs. Various types of NPs (Fig. 22.1), targeting groups, multiplex imaging, radiolabeled NP imaging, and multimodal imaging are reviewed.

22.2 Nanomaterials and Targeting Groups

22.2.1 Nanomaterials

22.2.1.1 Gold Nanoparticles (GNPs)

GNPs are suitable for production of imaging probes because of several attractive characteristics, for example, size controllability, excellent biocompatibility, and simple surface modification [6]. In addition, GNPs show special optical properties, for example, distinctive extinction bands in the visible region [7]. Using GNPs as probes with multiple functions, such as X-ray absorption, optical quenching, and surface-enhanced Raman scattering (SERS), requires modifying the characteristics of GNPs by altering size, shape, or surface chemistry. The major concerns of medical imaging applications are the toxicity and biodistribution. Several previous studies have suggested that particle size could be a key parameter in defining the

biological characteristics of GNPs. GNPs of size between 10 and 100 nm are mainly accumulated in the reticuloendothelial system (RES), and the distribution homogeneity increases as the particle size decreases [8]. GNPs of size between 15 and 20 nm could pass through the blood–retinal barrier or blood–brain barrier [9]. Small sized GNPs with diameter between 1 and 2 nm have higher toxicity potential due to the possibility that they irreversibly bind to some important biopolymers [10].

22.2.1.2 Quantum Dots (QDs)

QDs are semiconductor particles which emit light by stimulation [11]. The color or wavelength of the light emitted from a QD depends on the crystal's size. QDs with smaller size (less than 2 nm in diameter) exhibit blue fluorescence (380 in diameter) exhibit red fluorescence (605 in diameter) [12]. QDs are made of a metalloid crystalline core and shell, which protects the core and gives bioavailability [13]. QDs have distinct electronic and optical characteristics, for instance, large absorption coefficients, and high levels of photostability and brightness. The broad excitation wavelength range and the narrow and symmetric emission spectra mean that QDs are appropriate for multiplex imaging using several intensities and colors by combination of encoded proteins/genes to image tumors [14].

22.2.1.3 Iron Oxide Nanoparticles (IONPs)

IONPs categorized according to size as standard superparamagnetic iron oxide (SPIO) (60–150 nm), ultra-small superparamagnetic iron oxide (USPIO) (5–40 nm), or monocrystalline iron oxide (MION)—a part of USPIO (10–30 nm). Superparamagnetic iron oxide nanoparticles (SPIONPs) have distinctive properties, for instance, biocompatibility and easy surface modification, making them attractive as tumor imaging probes. SPIONPs are made of ferric iron and ferrous iron. SPIONPs can make a T2 relaxation effect, which results in T2-weighted MRI images signal reduction. This T2 relaxation effect is due to the heterogeneity of the magnetic field surrounding the NPs, thus results in proton magnetic moments dephasing [15]. As SPIONPs are dissolved under acidic conditions, SPIONPS are considered benign in the body [16]. Although some IONPs have toxicity problems, coated SPIONPs have been investigated and identified as relatively nontoxic [17]. When used for MRI contrast agents, SPIONPs are usually covered with synthetic polymers, for example, silicone or sugars [18].

22.2.1.4 Dendrimers

Dendrimers are repetitively branched molecules. Imaging moieties can be encapsulated in the internal side or on the surface, and the degree of polymerization control allows dendrimers to be made with diverse sizes with different weights and chemical components. Their payload capacity and ability to form various polymer structures mean that dendrimers are attractive probes for the construction of multimodal imaging [19]. The large number of attachment position which are accessible on a dendrimer's surface can be exploited by various dendrimer-based imaging probes that have been developed using novel synthetic chemistry strategies for multimodal tumor imaging methods [20].

22.2.1.5 Liposomes

Liposome is a spherical vesicle with at least one lipid bilayer. NPs that enclose an aqueous area that can accommodate hydrophilic/lipophilic drugs. Liposomes can passively accumulate in tumors via cell-specific targeting or through extravasation of abnormal leaky tumor vasculature. In addition, liposomes have versatile modifiability as they can encapsulate, insert, or attach functional molecules to the inner membrane, the membrane bilayer, and the membrane surface, respectively. Several ways have been made for liposome preparation with different sizes, structures, and distributions [21]. Several liposome formulations have been approved by the FDA or are being actively tested in clinical trials [22]. The biodistribution of liposomes is a major concern in clinical applications. Similar to other NPs, conventional liposomes are susceptible to eliminate by the cells of the RES from systemic circulation [23]. Many articles have verified that 50–80% of liposomes are absorbed by RES, within first 15 min after their intravenous administration [24]. Nevertheless, it has been found that and modulation of the surface charge and reduction of the size of liposomes could diminish their uptake by the RES. Therefore, for imaging and therapeutic applications, liposomes with smaller diameters (80–200 nm) that are composed of negatively charged or neutral lipids and cholesterol have been developed [21].

22.2.2 Targeting Groups

22.2.2.1 Antibody Molecules

Antibodies, which are commonly used in immunohistochemistry, are ideal targeting agents. The potential of antibodies was suggested by Ehrlich [25], who described that they could serve as "magic bullets" as they can specifically recognize epitopes with high binding affinity. Antibody molecules have been enhanced via genetic engineering. Furthermore, the potential of making human antibodies and antibody

fragments without a human host, and the generation of entirely new and clinically relevant antibodies without immunization have been studied. Antibody molecules have been used to target NPs; however, relatively large size (approximately 12 nm) and Fc region immunogenicity of antibody molecules necessitate the utilization of antibody fragments rather than intact antibody molecules.

22.2.2.2 Antibody Fragments

Antibodies are about 150 kDa in size, so they clear slowly from the blood pool. This characteristics lead to significant accumulation of antibody molecules in normal organs and restrict their conveyance to target lesions [26]. The effective penetration of monoclonal antibodies (mAbs) into a bulky solid tumor is rarely reported [27]. The utilization of the antibody fragments could improve their entry to target area. And single-chain fragments (scFvs) could not activate immune function. Intact IgG molecules have two Fv chains, whereas scFvs have only one single binding area; thus, binding affinity of scFvs is less than intact IgG molecules. Compared to divalent IgG molecules, scFvs with faster clearance and lower affinity can result in there being a lower effective dose at the target site; it should be compensated by using a higher signal production in the functional site. Because scFvs generated by phage display can be engineered to function without inducing an immune response, it is likely that they will be utilized in the future to lead NPs to the targets.

22.2.2.3 Oligonucleotides (Aptamers)

Aptamers are oligonucleotide or peptide molecules with molecular weights about 5–10 kDa that can act as ligands that bind to proteins [28] or small molecules including metabolites [29]. They can be screened rapidly and efficiently to select the sequences that are optimal for binding to a specific target [30]. In addition, aptamers can recognize single protein in complex compound that are originated from cells. [31]. Therefore, they are excellent for both cancer research and therapy [32] and cardiovascular research and therapy [33]. Their advantages as targeting agents include inexpensiveness and rapid synthesis with homogeneity. Aptamers are also secure for long-term storage at room temperature. Unlike peptides, their conjugation chemistry can be simplified via hybridization or co-synthesis, and unlike lipids, they can target specific cell types [34]. Furthermore, low molecular weights of aptamers promote their entry to cells. Since they are tiny, they should be attached to NPs with sufficiently long linkers to ensure that their interactions with their specific targets are not sterically hindered.

22.2.2.4 Peptides

Oligopeptides have various functions; some could be used as NP production templates, and others could be utilized as charged molecules for NP production, especially homo-oligomers [35]. Small peptides are usually the type of drugs that are incorporated into NPs. Many other peptides are utilized as targeting groups, such as RGD [36], NC-1900, which is an active fragment analog of arginine vasopressin [37], and hexa-L-aspartic acid, which targets bone tissues [38]. Oligopeptides have similar advantages to aptamers when used as targeting groups.

22.3 In Vitro, Ex Vivo, and In Vivo Multiplex Molecular Imaging by SERS

22.3.1 SERS Nanoparticles (SERS NPs)

SERS NPs can cause a plasmonic effect that adsorbs molecules onto a noble metal surface (gold or silver), enhancing the Raman signal as much as 10^{14}-fold to 10^{15}-fold [39]. These NPs have multiplex capability and high sensitivity [40]. Furthermore, the low autofluorescence and photobleaching of SERS NPs can increase the diagnostic accuracy in SERS NP-based imaging.

22.3.2 In Vitro Cell Analysis

The gold standard of identifying tumor cells has been histopathology based on hematoxylin and eosin (H&E) staining in clinical study. However, this classification method provides no or little data about the cells' chemical and immunologic components.; So, Raman spectroscopy has the potential to complement H&E staining. Raman spectroscopy's high diagnostic value to identify tumor cells has been proven over the years. Chan et al. [41] demonstrated sensitivity of more than 98% when they categorize hematopoietic immortalized cell lines as normal or neoplastic through laser tweezers confocal Raman spectroscopy and principal component analysis from the Raman spectra. The results showed that distinction between normal and tumor cells could be quantified based on the differences of DNA and protein concentration.

Although the variation in immortalized cell lines may have been lower than that in potential samples from patients, the same group further verified that individual leukemia cells could be identified in blood that were acquired from cancer patients [42].

22.3.3 Ex Vivo Tissue Analysis

At the tissue level, great efforts have been done to confirm and quantify the chemical differences between normal and cancer tissues via Raman spectroscopy. The main advantage of Raman spectroscopy is its greatest shortcoming as well. As each spectrum includes a lot of information, it is sometimes hard to extract exact information. Despite this shortcoming, many previous studies have successfully proved the ability to analyze diseased tissue. Taking Raman spectra at defined points on excised parathyroid tissue allowed Das et al. [43] to demonstrate that Raman spectroscopy could discriminate between parathyroid adenomas and hyperplasia with 95% sensitivity. In addition, quantification of the chemical differences between normal and diseased tissues is crucial to improve the sensitivity and specificity. In addition, quantification of the chemical differences between normal and diseased tissues is crucial to improve the sensitivity and specificity. De Jong et al. [44] utilized Raman spectroscopy in conjunction with numerous multivariate data analysis to discriminate cells in bladder tissues. As differentiation between normal and cancer is pivotal, Chowdary et al. [45] demonstrated that Raman spectroscopy could be utilized to discern between benign and cancer in breast tissues.

22.3.4 In Vivo SERS Imaging

Several techniques have recently been developed for the rapid in vivo acquisition of multiple Raman signals. As expected, the most straightforward approach is targeting the skin. Raman spectroscopy has been conducted at very early stages to assess pigments and antioxidant levels. In recent years, near-infrared Raman spectroscopy [46] has been used to diagnose skin cancers. Compared to histopathological analysis, Raman spectroscopy of skin lesions has consistently demonstrated high diagnostic performance while performing studies, thus showed potential for clinical applicability. Interestingly, if only data from the high wavenumber area of the Raman spectra (>2800 cm^{-1}) are evaluated, a similar diagnostic performance was achieved when compared with the fingerprint region (approximately 400rformanc^{-1}). Therefore, the probe's design can be considerably simplified because there is no need to build high-performance filters into the probe head [47].

Raman spectroscopy data acquisition typically requires second range; however, recent progress of camera and spectrometer technology make data acquisition time to be the millisecond range, which could facilitate the real-time assessment of in vivo lesions [48]. Several applications of in vivo spectroscopy have been shown, including the various type of cancer diagnosis (Fig. 22.2). A recent in vivo Raman study of atherosclerosis proved that Raman spectroscopy can detect vulnerable plaques [49]. In another study, the same group found that in vivo Raman

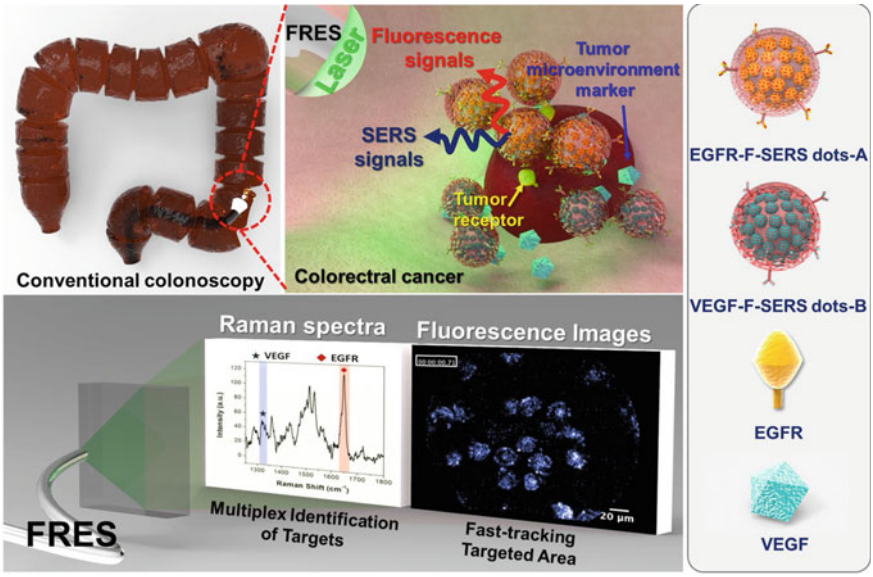

Fig. 22.2 Dual-modal, multiplex molecular diagnosis of colorectal cancer using surface enhanced Raman scattering (SERS) nanoparticles. Adapted from [85] with permission

spectroscopy allowed the assessment of the breast cancer tissue margin after operation; they also found and categorized cancer tissue which was ignored during operation, important data to recommend additional treatment [50].

22.4 Molecular Imaging Using Radiolabeled NPs

22.4.1 SPECT

Gamma ray emissions are the source of SPECT images [51]. Radioisotopes decay and emit gamma rays, which could be identified by a gamma camera to acquire three-dimensional images. An emitted gamma photon meets collimator, which permits gamma photons traveling along certain directions to correctly express the source of gamma ray. Commonly used radioisotopes for SPECT are ^{99m}Tc, ^{67}Ga, ^{111}In, and radioiodine (e.g., ^{131}I) (Table 22.2).

The generator-produced SPECT radiotracer, ^{99m}Tc, permits nuclear imaging when cyclotron is not available. ^{99m}Tc ($t1/2$ = 6 h) permits SPECT imaging up to 1 day after injection, and it is the most commonly utilized radiotracer. ^{99m}Tc has been labeled to IONPs [52], silver NPs (AgNPs) [53], GNPs [54], and silica

Table 22.2 Representative radioisotopes and radiolabeling methods of NPs (modified from Table 2 of [87])

Radioisotopes	Half life	Emission	Energy (KeV)	Radiolabeling methods
PET				
^{18}F	109.8 min	β^+	634	Direct (nucleophilic or electrophilic) or indirect (prosthetic) labeling
^{68}Ga	67.7 min	β^+	770, 1890	Coordination chemistry
^{64}Cu	12.7 h	β^-, β^+	579, 653	Coordination chemistry
^{124}I	4.18 days	β^+, γ	820, 1543, 2146	Nucleophilic halogen exchange chemistry
SPECT				
^{99m}Tc	6.0 h	γ	141	Coordination chemistry
^{111}In	2.8 days	γ, Auger electrons	172, 245	Coordination chemistry
^{67}Ga	3.3 days	γ	93, 185, 296	Coordination chemistry

nanoparticles (SNPs) [55]. Another example of a ^{99m}Tc tracer is the FDA-approved formulation of filtered ^{99m}Tc-sulfur nanocolloid (<100 nm) for the imaging of sentinel lymph nodes (SLNs) in prostate cancer [56]. In addition, SLN mapping with ultra-small SNPs has been studied [57].

For longer duration imaging, ^{67}Ga, ^{111}In, and various iodine species can be used. ^{67}Ga ($t1/2$ = 2.2 days) and ^{111}In ($t1/2$ = 2.8 days) have been utilized for radiolabel NPs using chelator-free methods [58, 59] (Fig. 22.3). Certain isotopes release both therapeutic electrons and gamma photons, enabling the use of the same isotope for both therapy and SPECT imaging (e.g., ^{131}I [$t1/2$ = 8 days] and ^{177}Lu [$t1/2$ = 6.7 days]). Nontherapeutic uses of ^{131}I often serve as ^{124}I analogs in preclinical studies because of the lower cost. ^{125}I-labeled albumin and transferrin ($t1/2$ = 50 days) have been utilized to investigate the protein corona of ^{59}Fe-SPIOs [60].

Since lead collimators are used to check the angle of incidence, SPECT imaging has a low efficiency of detection ($<10^{-4}$ times from emitted gamma rays) [61]. Recently, SPECT have been evolving with higher sensitivity and spatial resolution [62]. In addition to superior spatial resolution, the main strength of SPECT over PET is that simultaneous imaging of several radioisotope is possible, as the emitted gamma rays from different radioisotopes can be discerned according to their energy [63]. Whereas PET has higher detection efficiency than SPECT (up to 10%) [64]. PET was first invented in the mid-1970s [65], and micro-PET for small animal was first emerged in the late-1990s [66]. Until now, PET imaging is widely used in preclinical and clinical studies.

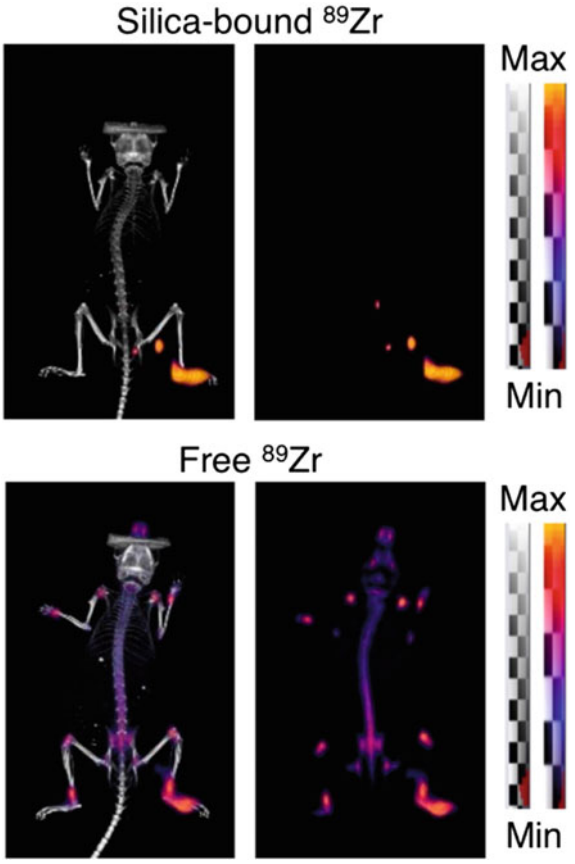

Fig. 22.3 PET/CT imaging using intrinsic radiolabeled, chelator-free silica nanoparticles for lymph node evaluation. Adapted from [58] with permission

22.4.2 PET

PET utilizes positron emitting radioisotopes for imaging and measurement of biological processes [67]. With the development of micro-PET scanners dedicated to small-animal imaging studies, knowledge and molecular measurements can be readily transferred between species, thus facilitating the clinical translation of newly developed PET agents [68]. PET imaging is feasible because of the annihilation process of an emitted positron with its counterpart, the electron. Annihilation process releases two 511-keV photons at an angle of nearly 180°. Most of the released photons are identified by detectors around the subject. Importantly, the more matter these photons get through, the greater the attenuation or absorption of the photons are induced [69]. When combined with CT or MRI, quantitation of the PET images (e.g., standard uptake values [SUVs]) could be easily done by CT- or MRI-based attenuation correction [70]. Common radioisotopes for PET imaging are ^{11}C, ^{68}Ga, ^{18}F, ^{64}Cu, ^{89}Zr, and ^{124}I (Table 22.2).

Typically, ^{11}C ($t1/2$ = 20 min) is not commonly utilized with NPs due to its short half-life. Nevertheless, a study showed its possibility. ^{11}C-methyl iodide was used as a methylation agent to react with carboxylic acid and amine functional groups bound to NPs, which was finally used as a PET/MRI imaging agent [71]. Similar, ^{13}N ($t1/2$ = 9.97 min) requires the direct bombardment of Al_2O_3 NPs, thus nullify a radiolabeling step for in vivo usage and allow imaging until 68 min after injection [72]. The isotope ^{68}Ga ($t1/2$ = 68 min) has a half-life that is sufficient for the in vivo imaging of small and short-circulating NPs. PEGylated IONPs was used for SLN imaging, thus allowing PET/MRI/Cherenkov luminescence imaging (CLI) [73]. ^{18}F ($t1/2$ = 110 min) is attached to NPs via synthetic methods and imaging is feasible until 8 h after injection. A substitution to synthetic methods is the usage of a proton beam to bombard TiO_2 NPs, providing ^{18}F-intrinsically radiolabeled NP.

If a longer in vivo time is needed, ^{64}Cu ($t1/2$ = 12.7 h) permits imaging until 48 h after injection. ^{64}Cu can be included into porphysomes until 48 h after injection. Most importantly, radiolabeled porphysomes can retain their size and optical properties, and have a nearly same biological properties of cold liposomes, thus demonstrating that radiolabeling does not alter the characteristics of the particles [74]. The PET isotopes with the longest half-lives utilized for NP imaging are ^{89}Zr ($t1/2$ = 78.4 h) and ^{124}I ($t1/2$ = 4.18 days). Mesoporous SNPs have been labeled with deferoxamine (DFOA) and demonstrated stability in vivo. Although DFOA is mainly used for ^{89}Zr radiolabeling, a study with SNPs [75] has shown that the chelator-free radiolabeling of various isotopes is possible with SNPs (Fig. 22.4).

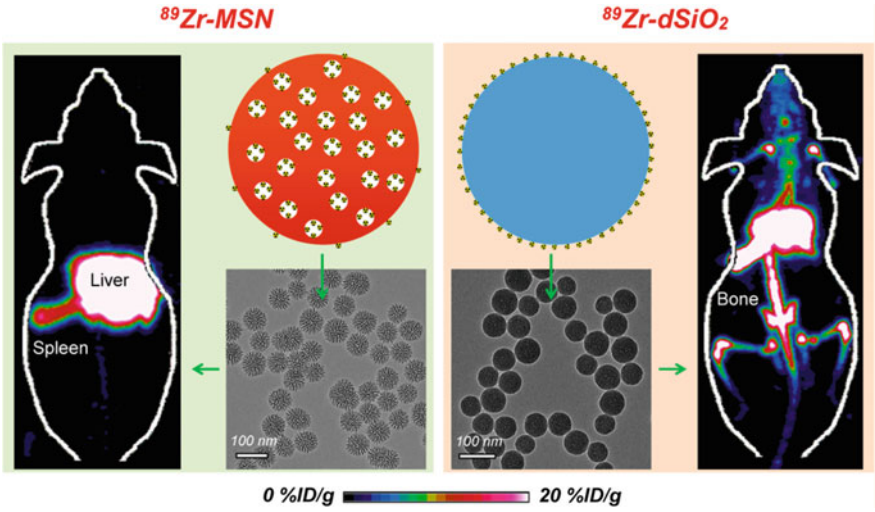

Fig. 22.4 PET biodistribution imaging using ^{89}Zr-labeled mesoporous silica nanoparticles (MSN). Adapted from [75] with permission

22.5 Multimodal Molecular Imaging

The multimodal probes development has been progressing rapidly due to advancements in hybrid imaging. Radiolabeled NPs have many strengths as multimodal probes, for example, the injection of a single agent for multimodal imaging. In addition, the signal is constant at the target region and no difference is found in biodistribution, which may arise when more than two agents are utilized.

Among several molecular imaging modalities, single modality is not enough for obtaining all the needed information [5]. For example, fluorescence signal quantification is difficult in vivo, especially in deep tissues. MRI has good resolution but relatively low sensitivity, whereas nuclear imaging has good sensitivity but comparatively low resolution. A combined utilization of several imaging modalities can offer synergistic benefits. Combination of optical imaging with three-dimensional tomography, such as PET, SPECT, or MRI, can facilitate noninvasive imaging in vivo with higher diagnostic value. NPs have large surface areas where multiple functional moieties can be used for multimodal molecular imaging (Table 22.3).

Cai et al. have developed a QD-based probe for both PET and near-infrared fluorescence (NIRF) imaging [76]. QD surface modification with RGD peptides facilitates integrin αvβ3 targeting, and DOTA (1,4,7,10-tetraazacyclododecane-1,4,7,10-tetraacetic acid, a highly effective chelator for various metal ions) conjugation enables PET imaging by ^{64}Cu labeling. The PET/NIRF dual-modality probe can confer sufficient tumor contrast at a much reduced concentration than that required for in vivo NIRF imaging [77], thus significantly lower the potential

Table 22.3 Representative examples of radiolabeled NPs and imaging methods (modified from Table 1 of [88])

Radioisotope	Nanoparticles	Chelator	Therapy	Imaging method
^{18}F	Lanthanide doped NP	N	N	PET/ULI (upconversion luminescence imaging)
^{68}Ga	Quantum dot	DOTA	N	PET/CT
^{64}Cu	Iron oxide	N	Y	PET/MRI
	Quantum dot	DOTA	N	PET/NIRF (near-infrared fluorescence)
	Gold nanoshell	DOTA	Y	PET/CT
	Liposome	DOTA	N	PET/CT
^{124}I	Iron oxide	Iodo-bead	N	PET/MRI/CL (Cerenkov luminescence)
^{99m}Tc	Gold	DTPA	N	SPECT/CT
	Iron oxide	DTPA	N	SPECT/MRI
^{111}In	Iron oxide	N	N	SPECT/CT
	Carbon nanotube	DTPA or DOTA	N	SPECT/CT
^{68}Ga	Quantum dot	DOTA	N	PET/CT

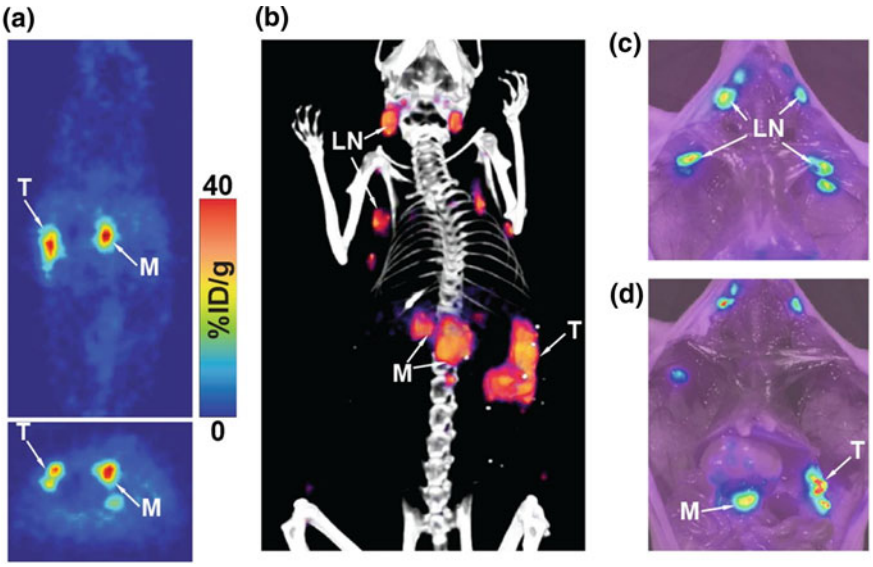

Fig. 22.5 Multimodal in vivo PET (**a**, **b**) and ex vivo NIRF (**c**, **d**) imaging using ^{89}Zr- and fluorescence-labeled nanoparticles in pancreatic cancer [86]

toxicity of cadmium-based QDs and contributing to future biomedical applications [78]. In another study, liposomes have been labeled with both radionuclides and gadolinium for SPECT imaging and MRI in vitro [79].

Most of the aforementioned studies demonstrated the possibility of dual-modality imaging in vivo. However, as the two modalities are not equally effective, the less sensitive modality is usually used for the ex vivo validation of the in vivo results obtained from the more sensitive imaging modality (Fig. 22.5). It was not until very recently that noninvasive dual-modality imaging was developed using a nanoplatform-based approach [80]. Gene silencing with short interfering RNA (siRNA) has become an attractive method to identify gene function in mammalian cells [81, 82]. A study has reported a multifunctional probe for the in vivo transfer of siRNA and simultaneous imaging of its accumulation in tumors by both MRI and NIRF imaging [80]. Additionally, the NP has been modified with a membrane translocation peptide for intracellular delivery [83].

22.6 Conclusion

In recent years, NPs have attracted great interest as tools for biomedical applications with the increasing use of multiplex, multimodal components. Molecular-targeted, radiolabeled NPs have several strengths over usual molecular imaging probes. Strengths of radiolabeled NPs are their high sensitivity and the quantification.

Multimodal imaging probes that unite nuclear imaging, which is highly sensitive and quantitative, with non-nuclear imaging (e.g., optical imaging for ex vivo identification of in vivo study; or MRI for anatomical localization) could be available in future biomedical applications. Molecular-targeted agents which can be detected by more than three imaging modalities are also possible. Advancements in nanotechnology could extend the limits of current molecular imaging techniques and facilitate point-of-care diagnosis, diagnostics/therapeutics integration, and personalized medicine development.

References

1. W. Cai, X. Chen, Nanoplatforms for targeted molecular imaging in living subjects. Small **3**, 1840–1854 (2007)
2. S.K. Sahoo, S. Parveen, J.J. Panda, The present and future of nanotechnology in human health care. Nanomedicine **3**, 20–31 (2007)
3. R. Weissleder, U. Mahmood, Molecular imaging. Radiology **219**, 316–333 (2001)
4. N. Beckmann, R. Kneuer, H.U. Gremlich, H. Karmouty-Quintana, F.X. Ble, M. Muller, In vivo mouse imaging and spectroscopy in drug discovery. NMR Biomed. **20**, 154–185 (2007)
5. T.F. Massoud, S.S. Gambhir, Molecular imaging in living subjects: seeing fundamental biological processes in a new light. Genes Dev. **17**, 545–580 (2003)
6. D.E. Lee, H. Koo, I.C. Sun, J.H. Ryu, K. Kim, I.C. Kwon, Multifunctional nanoparticles for multimodal imaging and theragnosis. Chem. Soc. Rev. **41**, 2656–2672 (2012)
7. M.A. El-Sayed, Some interesting properties of metals confined in time and nanometer space of different shapes. Acc. Chem. Res. **34**, 257–264 (2001)
8. L. Dykman, N. Khlebtsov, Gold nanoparticles in biomedical applications: recent advances and perspectives. Chem. Soc. Rev. **41**, 2256–2282 (2012)
9. N. Khlebtsov, V. Bogatyrev, L. Dykman, B. Khlebtsov, S. Staroverov, A. Shirokov et al., Analytical and theranostic applications of gold nanoparticles and multifunctional nanocomposites. Theranostics **3**, 167–180 (2013)
10. N. Khlebtsov, L. Dykman, Biodistribution and toxicity of engineered gold nanoparticles: a review of in vitro and in vivo studies. Chem. Soc. Rev. **40**, 1647–1671 (2011)
11. M. Cheki, M. Moslehi, M. Assadi, Marvelous applications of quantum dots. Eur. Rev. Med. Pharmacol. Sci. **17**, 1141–1148 (2013)
12. M. Bruchez Jr., M. Moronne, P. Gin, S. Weiss, A.P. Alivisatos, Semiconductor nanocrystals as fluorescent biological labels. Science **281**, 2013–2016 (1998)
13. R. Hardman, A toxicologic review of quantum dots: toxicity depends on physicochemical and environmental factors. Environ. Health Perspect. **114**, 165–172 (2006)
14. X. Gao, Y. Cui, R.M. Levenson, L.W. Chung, S. Nie, In vivo cancer targeting and imaging with semiconductor quantum dots. Nat. Biotechnol. **22**, 969–976 (2004)
15. Y. Ling, K. Wei, Y. Luo, X. Gao, S. Zhong, Dual docetaxel/superparamagnetic iron oxide loaded nanoparticles for both targeting magnetic resonance imaging and cancer therapy. Biomaterials **32**, 7139–7150 (2011)
16. E. Amstad, M. Textor, E. Reimhult, Stabilization and functionalization of iron oxide nanoparticles for biomedical applications. Nanoscale **3**, 2819–2843 (2011)
17. N. Lewinski, V. Colvin, R. Drezek, Cytotoxicity of nanoparticles. Small **4**, 26–49 (2008)
18. C.W. Jung, P. Jacobs, Physical and chemical properties of superparamagnetic iron oxide MR contrast agents: ferumoxides, ferumoxtran, ferumoxsil. Magn. Reson. Imaging **13**, 661–674 (1995)

19. M. Longmire, P.L. Choyke, H. Kobayashi, Dendrimer-based contrast agents for molecular imaging. Curr. Top. Med. Chem. **8**, 1180–1186 (2008)
20. H. Xu, C.A. Regino, Y. Koyama, Y. Hama, A.J. Gunn, M. Bernardo et al., Preparation and preliminary evaluation of a biotin-targeted, lectin-targeted dendrimer-based probe for dual-modality magnetic resonance and fluorescence imaging. Bioconjug. Chem. **18**, 1474–1482 (2007)
21. T.A. Elbayoumi, V.P. Torchilin, Current trends in liposome research. Methods Mol. Biol. **605**, 1–27 (2010)
22. A. Puri, K. Loomis, B. Smith, J.H. Lee, A. Yavlovich, E. Heldman et al., Lipid-based nanoparticles as pharmaceutical drug carriers: from concepts to clinic. Crit. Rev. Ther. Drug Carrier Syst. **26**, 523–580 (2009)
23. J.H. Senior, Fate and behavior of liposomes in vivo: a review of controlling factors. Crit. Rev. Ther. Drug Carrier Syst. **3**, 123–193 (1987)
24. P. Laverman, M.G. Carstens, O.C. Boerman, E.T. Dams, W.J. Oyen, N. van Rooijen et al., Factors affecting the accelerated blood clearance of polyethylene glycol-liposomes upon repeated injection. J. Pharmacol. Exp. Ther. **298**, 607–612 (2001)
25. P. Ehrlich, Croonian lecture: on immunity with special reference to cell life. Proc. R. Soc. Lond. **66**, 424–448 (1899)
26. D. Colcher, G. Pavlinkova, G. Beresford, B.J. Booth, A. Choudhury, S.K. Batra, Pharmacokinetics and biodistribution of genetically-engineered antibodies. Q. J. Nucl. Med. **42**, 225–241 (1998)
27. A.M. Scott, F.T. Lee, R. Jones, W. Hopkins, D. MacGregor, J.S. Cebon et al., A phase I trial of humanized monoclonal antibody A33 in patients with colorectal carcinoma: biodistribution, pharmacokinetics, and quantitative tumor uptake. Clin. Cancer Res. **11**, 4810–4817 (2005)
28. E.N. Brody, L. Gold, Aptamers as therapeutic and diagnostic agents. J. Biotechnol. **74**, 5–13 (2000)
29. K. Ohsawa, T. Kasamatsu, J. Nagashima, K. Hanawa, M. Kuwahara, H. Ozaki et al., Arginine-modified DNA aptamers that show enantioselective recognition of the dicarboxylic acid moiety of glutamic acid. Anal. Sci. **24**, 167–172 (2008)
30. H. Tian, Combinatorial selection of RNA ligands for complex cellular targets: the RNA liagands-based proteomics. Mol. Cell. Proteomics **1**, 99–103 (2002)
31. D.A. Daniels, H. Chen, B.J. Hicke, K.M. Swiderek, L. Gold, A tenascin-C aptamer identified by tumor cell SELEX: systematic evolution of ligands by exponential enrichment. Proc. Natl. Acad. Sci. U.S.A. **100**, 15416–15421 (2003)
32. D. Shangguan, Y. Li, Z. Tang, Z.C. Cao, H.W. Chen, P. Mallikaratchy et al., Aptamers evolved from live cells as effective molecular probes for cancer study. Proc. Natl. Acad. Sci. U.S.A. **103**, 11838–11843 (2006)
33. A.D. Keefe, R.G. Schaub, Aptamers as candidate therapeutics for cardiovascular indications. Curr. Opin. Pharmacol. **8**, 147–152 (2008)
34. T.C. Chu, K.Y. Twu, A.D. Ellington, M. Levy, Aptamer mediated siRNA delivery. Nucleic Acids Res. **34**, e73 (2006)
35. P.E. Kish, Y. Tsume, P. Kijek, T.M. Lanigan, J.M. Hilfinger, B.J. Roessler, Bile acid-oligopeptide conjugates interact with DNA and facilitate transfection. Mol. Pharm. **4**, 95–103 (2007)
36. R.M. Schiffelers, A. Ansari, J. Xu, Q. Zhou, Q. Tang, G. Storm et al., Cancer siRNA therapy by tumor selective delivery with ligand-targeted sterically stabilized nanoparticle. Nucleic Acids Res. **32**, e149 (2004)
37. Y.L. Xie, W. Lu, X.G. Jiang, Improvement of cationic albumin conjugated pegylated nanoparticles holding NC-1900, a vasopressin fragment analog, in memory deficits induced by scopolamine in mice. Behav. Brain Res. **173**, 76–84 (2006)
38. H. Hirabayashi, J. Fujisaki, Bone-specific drug delivery systems: approaches via chemical modification of bone-seeking agents. Clin. Pharmacokinet. **42**, 1319–1330 (2003)

39. S. Nie, S.R. Emory, Probing single molecules and single nanoparticles by surface-enhanced Raman scattering. Science **275**, 1102–1106 (1997)
40. M. Vendrell, K.K. Maiti, K. Dhaliwal, Y.T. Chang, Surface-enhanced Raman scattering in cancer detection and imaging. Trends Biotechnol. **31**, 249–257 (2013)
41. J.W. Chan, D.S. Taylor, T. Zwerdling, S.M. Lane, K. Ihara, T. Huser, Micro-Raman spectroscopy detects individual neoplastic and normal hematopoietic cells. Biophys. J. **90**, 648–656 (2006)
42. J.W. Chan, D.S. Taylor, S.M. Lane, T. Zwerdling, J. Tuscano, T. Huser, Nondestructive identification of individual leukemia cells by laser trapping Raman spectroscopy. Anal. Chem. **80**, 2180–2187 (2008)
43. K. Das, N. Stone, C. Kendall, C. Fowler, J. Christie-Brown, Raman spectroscopy of parathyroid tissue pathology. Lasers Med. Sci. **21**, 192–197 (2006)
44. B.W. de Jong, T.C. Schut, K. Maquelin, T. van der Kwast, C.H. Bangma, D.J. Kok et al., Discrimination between nontumor bladder tissue and tumor by Raman spectroscopy. Anal. Chem. **78**, 7761–7769 (2006)
45. M.V. Chowdary, K.K. Kumar, J. Kurien, S. Mathew, C.M. Krishna, Discrimination of normal, benign, and malignant breast tissues by Raman spectroscopy. Biopolymers **83**, 556–569 (2006)
46. C.A. Lieber, S.K. Majumder, D.L. Ellis, D.D. Billheimer, A. Mahadevan-Jansen, In vivo nonmelanoma skin cancer diagnosis using Raman microspectroscopy. Lasers Surg. Med. **40**, 461–467 (2008)
47. A. Nijssen, K. Maquelin, L.F. Santos, P.J. Caspers, T.C. Bakker Schut, J.C. den Hollander et al., Discriminating basal cell carcinoma from perilesional skin using high wave-number Raman spectroscopy. J. Biomed. Opt. **12**, 034004 (2007)
48. J.T. Motz, S.J. Gandhi, O.R. Scepanovic, A.S. Haka, J.R. Kramer, R.R. Dasari et al., Real-time Raman system for in vivo disease diagnosis. J. Biomed. Opt. **10**, 031113 (2005)
49. J.T. Motz, M. Fitzmaurice, A. Miller, S.J. Gandhi, A.S. Haka, L.H. Galindo et al., In vivo Raman spectral pathology of human atherosclerosis and vulnerable plaque. J. Biomed. Opt. **11**, 021003 (2006)
50. A.S. Haka, Z. Volynskaya, J.A. Gardecki, J. Nazemi, J. Lyons, D. Hicks et al., In vivo margin assessment during partial mastectomy breast surgery using raman spectroscopy. Cancer Res. **66**, 3317–3322 (2006)
51. K. Peremans, B. Cornelissen, B. Van Den Bossche, K. Audenaert, C. Van de Wiele, A review of small animal imaging planar and pinhole spect Gamma camera imaging. Vet. Radiol. Ultrasound. **46**, 162–170 (2005)
52. S. Xue, C. Zhang, Y. Yang, L. Zhang, D. Cheng, J. Zhang et al., ^{99m}Tc-labeled iron oxide nanoparticles for dual-contrast (T1/T2) magnetic resonance and dual-modality imaging of tumor angiogenesis. J. Biomed. Nanotechnol. **11**, 1027–1037 (2015)
53. E. Locatelli, M. Naddaka, C. Uboldi, G. Loudos, E. Fragogeorgi, V. Molinari et al., Targeted delivery of silver nanoparticles and alisertib: in vitro and in vivo synergistic effect against glioblastoma. Nanomedicine (Lond). **9**, 839–849 (2014)
54. E. Morales-Avila, G. Ferro-Flores, B.E. Ocampo-Garcia, L.M. De Leon-Rodriguez, C.L. Santos-Cuevas, R. Garcia-Becerra et al., Multimeric system of ^{99m}Tc-labeled gold nanoparticles conjugated to c[RGDfK(C)] for molecular imaging of tumor alpha(v)beta(3) expression. Bioconjug. Chem. **22**, 913–922 (2011)
55. M. Tsuchimochi, K. Hayama, M. Toyama, I. Sasagawa, N. Tsubokawa, Dual-modality imaging with 99mTc and fluorescent indocyanine green using surface-modified silica nanoparticles for biopsy of the sentinel lymph node: an animal study. EJNMMI Res. **3**, 33 (2013)
56. Y. Seo, C.M. Aparici, C.P. Chen, C. Hsu, N. Kased, C. Schreck et al., Mapping of lymphatic drainage from the prostate using filtered ^{99m}Tc-sulfur nanocolloid and SPECT/CT. J. Nucl. Med. **52**, 1068–1072 (2011)

57. M.S. Bradbury, M. Pauliah, P. Zanzonico, U. Wiesner, S. Patel, Intraoperative mapping of sentinel lymph node metastases using a clinically translated ultrasmall silica nanoparticle. Wiley Interdiscip. Rev. Nanomed. Nanobiotechnol. **8**, 535–553 (2016)
58. T.M. Shaffer, M.A. Wall, S. Harmsen, V.A. Longo, C.M. Drain, M.F. Kircher et al., Silica nanoparticles as substrates for chelator-free labeling of oxophilic radioisotopes. Nano Lett. **15**, 864–868 (2015)
59. H. Zhu, J. Zhao, X. Lin, Y. Hong, C. Li, Z. Yang, Design, synthesis and evaluation of dual-modality glyco-nanoparticles for tumor imaging. Molecules **18**, 6425–6438 (2013)
60. D. Hoffman, M. Sun, L. Yang, P.R. McDonagh, F. Corwin, G. Sundaresan et al., Intrinsically radiolabeled [^{59}Fe]-SPIONs for dual MRI/radionuclide detection. Am. J. Nucl. Med. Mol. Imaging **4**, 548–560 (2014)
61. A.F. Chatziioannou, Instrumentation for molecular imaging in preclinical research: micro-PET and micro-SPECT. Proc. Am. Thorac. Soc. **2**(533–6), 10–11 (2005)
62. F. Beekman, F. van der Have, The pinhole: gateway to ultra-high-resolution three-dimensional radionuclide imaging. Eur. J. Nucl. Med. Mol. Imaging **34**, 151–161 (2007)
63. D.S. Berman, H. Kiat, K. Van Train, J.D. Friedman, F.P. Wang, G. Germano, Dual-isotope myocardial perfusion SPECT with rest thallium-201 and stress Tc-99m sestamibi. Cardiol. Clin. **12**, 261–270 (1994)
64. E.P. Visser, J.A. Disselhorst, M. Brom, P. Laverman, M. Gotthardt, W.J. Oyen et al., Spatial resolution and sensitivity of the Inveon small-animal PET scanner. J. Nucl. Med. **50**, 139–147 (2009)
65. M.E. Phelps, E.J. Hoffman, N.A. Mullani, M.M. Ter-Pogossian, Application of annihilation coincidence detection to transaxial reconstruction tomography. J. Nucl. Med. **16**, 210–224 (1975)
66. S.R. Cherry, Y. Shao, R. Silverman, K. Meadors, S. Siegel, A. Chatziioannou et al., MicroPET: a high resolution PET scanner for imaging small animals. IEEE Trans. Nucl. Sci. **44**, 1161–1166 (1997)
67. M.E. Phelps, PET: the merging of biology and imaging into molecular imaging. J. Nucl. Med. **41**, 661–681 (2000)
68. Z. Liu, W. Cai, L. He, N. Nakayama, K. Chen, X. Sun et al., In vivo biodistribution and highly efficient tumour targeting of carbon nanotubes in mice. Nat. Nanotechnol. **2**, 47–52 (2007)
69. V. Schulz, I. Torres-Espallardo, S. Renisch, Z. Hu, N. Ojha, P. Bornert et al., Automatic, three-segment, MR-based attenuation correction for whole-body PET/MR data. Eur. J. Nucl. Med. Mol. Imaging **38**, 138–152 (2011)
70. M. Wiesmuller, H.H. Quick, B. Navalpakkam, M.M. Lell, M. Uder, P. Ritt et al., Comparison of lesion detection and quantitation of tracer uptake between PET from a simultaneously acquiring whole-body PET/MR hybrid scanner and PET from PET/CT. Eur. J. Nucl. Med. Mol. Imaging **40**, 12–21 (2013)
71. R. Sharma, Y. Xu, S.W. Kim, M.J. Schueller, D. Alexoff, S.D. Smith et al., Carbon-11 radiolabeling of iron-oxide nanoparticles for dual-modality PET/MR imaging. Nanoscale **5**, 7476–7483 (2013)
72. C. Perez-Campana, V. Gomez-Vallejo, M. Puigivila, A. Martin, T. Calvo-Fernandez, S.E. Moya et al., Biodistribution of different sized nanoparticles assessed by positron emission tomography: a general strategy for direct activation of metal oxide particles. ACS Nano **7**, 3498–3505 (2013)
73. R. Madru, T.A. Tran, J. Axelsson, C. Ingvar, A. Bibic, F. Stahlberg et al., ^{68}Ga-labeled superparamagnetic iron oxide nanoparticles (SPIONs) for multi-modality PET/MR/Cherenkov luminescence imaging of sentinel lymph nodes. Am. J. Nucl. Med. Mol. Imaging. **4**, 60–69 (2013)
74. T.W. Liu, T.D. MacDonald, J. Shi, B.C. Wilson, G. Zheng, Intrinsically copper-64-labeled organic nanoparticles as radiotracers. Angew. Chem. Int. Ed. Engl. **51**, 13128–13131 (2012)

75. F. Chen, S. Goel, H.F. Valdovinos, H. Luo, R. Hernandez, T.E. Barnhart et al., In vivo integrity and biological fate of chelator-free zirconium-89-labeled mesoporous silica nanoparticles. ACS Nano **9**, 7950–7959 (2015)
76. W. Cai, K. Chen, Z.B. Li, S.S. Gambhir, X. Chen, Dual-function probe for PET and near-infrared fluorescence imaging of tumor vasculature. J. Nucl. Med. **48**, 1862–1870 (2007)
77. W. Cai, D.W. Shin, K. Chen, O. Gheysens, Q. Cao, S.X. Wang et al., Peptide-labeled near-infrared quantum dots for imaging tumor vasculature in living subjects. Nano Lett. **6**, 669–676 (2006)
78. C. Kirchner, T. Liedl, S. Kudera, T. Pellegrino, A. Munoz Javier, H.E. Gaub et al., Cytotoxicity of colloidal CdSe and CdSe/ZnS nanoparticles. Nano Lett. **5**, 331–338 (2005)
79. S.W. Zielhuis, J.H. Seppenwoolde, V.A. Mateus, C.J. Bakker, G.C. Krijger, G. Storm et al., Lanthanide-loaded liposomes for multimodality imaging and therapy. Cancer Biother. Radiopharm. **21**, 520–527 (2006)
80. Z. Medarova, W. Pham, C. Farrar, V. Petkova, A. Moore, In vivo imaging of siRNA delivery and silencing in tumors. Nat. Med. **13**, 372–377 (2007)
81. C.C. Mello, D. Conte Jr., Revealing the world of RNA interference. Nature **431**, 338–342 (2004)
82. A. Fire, S. Xu, M.K. Montgomery, S.A. Kostas, S.E. Driver, C.C. Mello, Potent and specific genetic interference by double-stranded RNA in *Caenorhabditis elegans*. Nature **391**, 806–811 (1998)
83. M. Mae, U. Langel, Cell-penetrating peptides as vectors for peptide, protein and oligonucleotide delivery. Curr. Opin. Pharmacol. **6**, 509–514 (2006)
84. H. Hong, Y. Zhang, J. Sun, W. Cai, Molecular imaging and therapy of cancer with radiolabeled nanoparticles. Nano Today **4**, 399–413 (2009)
85. Y.I. Kim, S. Jeong, K.O. Jung, M.G. Song, C.H. Lee, S.J. Chung et al., Simultaneous detection of EGFR and VEGF in colorectal cancer using Fluorescence-Raman Endoscopy. Sci. Rep. **7**, 1035 (2017)
86. J.L. Houghton, B.M. Zeglis, D. Abdel-Atti, R. Aggeler, R. Sawada, B.J. Agnew et al., Site-specifically labeled CA19.9-targeted immunoconjugates for the PET, NIRF, and multimodal PET/NIRF imaging of pancreatic cancer. Proc. Natl. Acad. Sci. U.S.A. **112**, 15850–15855 (2015)
87. Y. Xing, J. Zhao, P.S. Conti, K. Chen, Radiolabeled nanoparticles for multimodality tumor imaging. Theranostics **4**, 290–306 (2014)
88. D.S. Lee, H.J. Im, Y.S. Lee, Radionanomedicine: widened perspectives of molecular theragnosis. Nanomedicine **11**, 795–810 (2015)

Chapter 23
Therapeutic/Theranostic Use of Radionanomedicine

So Won Oh and Dong Soo Lee

Abstract Radionanomedicine is a newly emerged field of medicine extending nuclear medicine by means of nanomaterial technology and platforms. Radionanomedicine utilizes versatility of nanoparticles (NP) and avoids inherent toxic effect of NPs. This is mainly due to the fact that NPs are used in trace amounts for targeting. The therapeutic effect of radionanomedicine comes from ionizing radiation of labeled radionuclides. The core concept of radionanomedicine depends on both characteristics of radionuclides and properties of NPs. The characteristics of NPs including multifunctionality, intrinsic properties are exploited to enhance the therapeutic effect of radiolabeled NPs. In addition, various strategies have been developed to deliver sufficient amount of radiolabeled NPs, such as local administration and co-application of thermal stimuli. In an attempt to improve the therapeutic effect of radionuclides, several approaches have been investigated, such as utilizing intrinsic radioactive properties of NPs or labeling with alpha emitters. The emergence of radionanomedicine is expected to restore of the essence of nuclear medicine as well as to enhance the clinical applicability of nanomedicine.

S. W. Oh (✉) · D. S. Lee
Department of Nuclear Medicine, Seoul National University College of Medicine, Seoul 03080, Republic of Korea
e-mail: mdosw@snu.ac.kr

D. S. Lee
e-mail: dsl@snu.ac.kr

S. W. Oh
Department of Nuclear Medicine, Seoul National University Boramae Medical Center, Seoul 07061, Republic of Korea

D. S. Lee
Department of Molecular Medicine and Biopharmaceutical Sciences, Graduate School of Convergence Science and Technology, Seoul National University, Seoul 03080, Republic of Korea

D. S. Lee (ed.), *Radionanomedicine*, Biological and Medical Physics, Biomedical Engineering, https://doi.org/10.1007/978-3-319-67720-0_23

23.1 Introduction

Radionanomedicine is a newly coined word that indicates the combined use of nuclear medicine and nanomedicine [1]. This new field of medicine can be considered as the extension of nuclear medicine utilizing nanomaterial technology and platforms. Nuclear medicine is often considered as a branch of medical imaging, but the core of nuclear medicine consists in the utilization of radioactive substances whether it deals with the diagnosis or treatment of disease. For the treatment of cancer, nuclear medicine can be versatile not only for its imaging capability but also for its therapeutic capacity (Fig. 23.1). The clinical nuclear medicine started from the therapeutic use of radionuclide, i.e. radioactive iodine administration for thyroid cancer treatment, and concomitant imaging revealed the success of this treatment, i.e. therapeutic radioiodine scan. Now, nuclear medicine is about to take advantage of the characteristics of nanomaterials for imaging and therapy. The emergence of radionanomedicine is expected to restore of the essence of nuclear medicine as well as to enhance the clinical applicability of nanomedicine.

Radionanomedicine is intended to be radio-theranostics, because the core concept of radionanomedicine depends both on the characteristics of labeled radionuclides and the properties of nanomaterial platforms. Nanomedicine has got the limelight in various fields of medicine, but in vivo theranostics using nanotechnology meets objections or concerns regarding nanomaterials possible hazards to humans and the environment [2–4]. Therefore, we need to develop methods to overcome these concerns about the toxic effects of in vivo use of nanomaterials. In radionanomedicine, nanomaterials are used in trace amounts for targeting purpose,

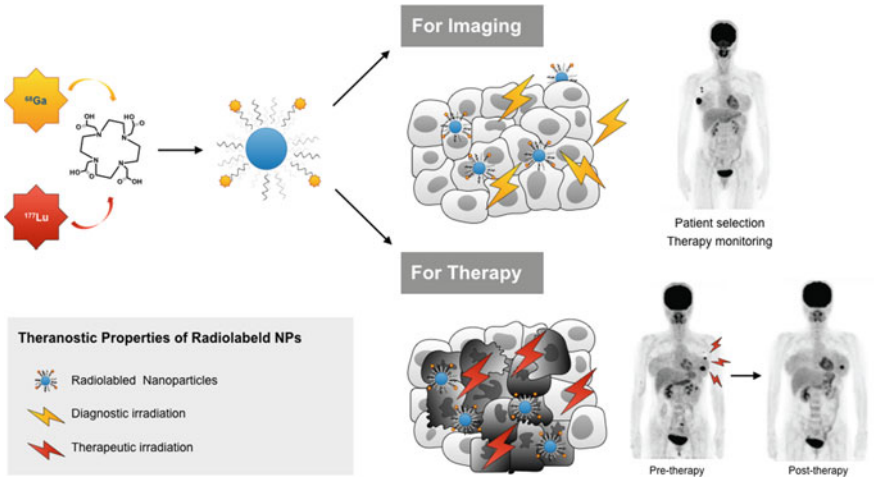

Fig. 23.1 Therapeutic properties of radiolabeled nanoparticles (NPs). The radiolabeled nanoparticles can be used for both imaging and therapy, according to the intrinsic properties of radionuclides

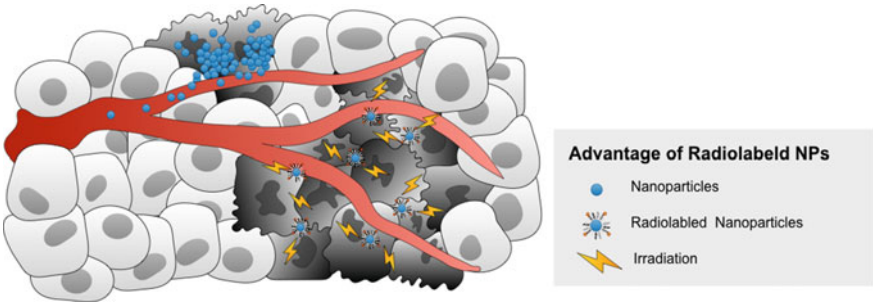

Fig. 23.2 Advantage of radiolabeled nanoparticles (NPs). Concerns about potential hazards of nanoparticles to human and environment are avoidable in radionanomedicine. Nanoparticles are used in trace amount for targeting specific markers on the tumor cells, and main therapeutic effect is produced by ionizing radiation

and their therapeutic effect comes from the ionizing radiation emitted from radionuclides (Fig. 23.2). Nanomaterials are toxic when they are used in pharmacologic amount, but use of trace amount of nanomaterials obviates their inherent toxic effects of nanomaterials out of concern in radionanomedicine. The adoption of nanomedicine to nuclear medicine will be accompanied by successful clinical application, or otherwise be dormant for a long time in the phase of basic research without translation into clinics.

23.2 Selection of Radionuclides for Therapy/Theranostics

Several factors should be considered when developing in vivo nano therapeutics labeled with radionuclide. Characteristics of nanoparticles (NPs) such as size, shape, intrinsic biologic effects, chemical functionality may affect biodistribution and therapeutic effects of radiolabeled NPs, and convenience of synthesis, etc. For appropriate selection of radionuclide, not only physical and chemical properties of radiolabeled NPs but also tumor characteristics to be treated with the radiolabeled NPs are also taken into account, since radionuclide exerts therapeutic effects after being delivered to the target cells through locoregional or systemic administration into the body. Tumor factors are also important to yield successful outcome in the treatment using radiolabeled NPs. The biological response to internal radiation therapy of individual cells within a tumor or organ might depend on cell-specific radiosensitivity and distribution of the radiopharmaceuticals at the macroscopic, multicellular, and subcellular levels [5]. In this regard, radionuclide therapy, also known as internal radiation therapy, differs from conventional external beam radiation therapy.

Internal radiation therapy causes cell death via several different mechanisms. Firstly, ionizing radiation can induce various damages in the cells, which lead to

either cell death or survival depending on the extent of given damage and the repair capability of the cells. Generally, the main target for the biologic effects by ionizing radiation in the cells is DNA. According to the physical properties of ionizing radiation, several DNA damages are induced by deposition of radioactivity; single-strand and double-strand DNA breaks, DNA base damage, and DNA-protein crosslinks [6]. Second, ionizing radiation that has a long range in tissues allows killing tumor cells located adjacent to the cells harnessing the target. So, even cells that lack targets can be affected by ionizing radiation, when they are placed within the particles' range. This collateral damage caused by ionizing radiation is as known as 'cross-fire effect', and it is helpful to overcome heterogeneity of expression of targets within a cancer [7]. Next, there is another mechanism that ionizing radiation can render damage to cells located far from the target cells. Often cells receive damages that are not directly traversed by ionizing radiation. This is defined as 'bystander effect', and it occurs when damaged cells release cytokines and free radicals [8]. In addition, radiation can activate various cell death pathways, since radiation causes damage not only to DNA but also to cell membranes and organelles including mitochondria that could initiate signaling of apoptosis [8, 9].

Internal radiation therapy generates heterogeneous, low-dose rate and continuous irradiation over hours and days. Irradiation at low-dose rate provides a window of opportunity for the cells to repair radiation-induced sub-lethal damages and to proliferate after recovery from the damage. In addition, the physical characteristics of particle-emitting radionuclides can affect biological effect of internal radiation therapy. For example, linear energy transfer (LET) means the energy that is released by ionizing radiation over a certain distance, and it depends on the nature of the emitted radiation from the radionuclides. Low LET radiation mainly causes sub-lethal damage that can be easily repaired, such as sparse ionization and individual DNA lesions, and high LET radiation are more cytotoxic than low LET radiation at the equivalent absorbed doses [7].

The most commonly used radionuclides in the clinical trials are beta-particle emitters such as lutetium-177 (^{177}Lu), yttrium-90 (^{90}Y), rhenium-188 (^{188}Re), copper-64 (^{64}Cu) and iodine-131 (^{131}I). They emit low LET radiation ($\sim$0.2 keV/μm) in the form of beta particles, internal conversion electrons, as well as gamma-rays or x-rays [10]. It might be undesirable since low LET radiation causes sub-lethal damages to cancer cells. However, beta emitters are often considered ideal for treating large tumors because of their long range and relatively long physical half-life. Beta emitter with a long range enables to deliver radiation damage not only tumor cells harboring targets but also neighboring cells without targets on their cell surfaces, thus it helps overcoming heterogeneous target expression within a tumor. So called 'cross-fire irradiation' is particularly advantageous, when not all the tumor cells can be reached by radiopharmaceuticals owing to the heterogeneous distribution of targets in the tumor tissues. Alpha emitters such as ^{213}Bi, ^{212}Bi, ^{211}At, and ^{225}Ac that produce high LET radiation (50–230 keV/μm) have desirable characteristics as cancer therapeutics, since they produce clusters of DNA damage that are difficult to repair. Moreover, the high cytotoxicity of high

LET radiation was found to be independent of the dose rate and also independent of oxygenation [11, 12]. Alpha emitters have high energy, but their path length are intermediate, merely corresponding to the diameter of several cells [12]. Therefore, their intermediate particle range and high LET radiation make alpha emitters suitable candidates for the treatment of blood or bone marrow malignancies, as well as for small solid tumors and metastases. Lastly, Auger electron emitters have relatively high LET radiation presenting with low toxicity compared with alpha emitters, but they are only suited for hitting a blow to single tumor cell. To exert radiobiological effects of Auger electrons, they must penetrate the cytoplasm and then reach the nucleus since their ranges in tissues are very short. For this reason, Auger electron emitters are not desirable as therapeutics in clinical practice.

23.3 Radiolabeled Nanoparticles for Therapeutic/ Theranostic Use

Nanoparticles are defined as materials that have at least one dimension in the range of 10–100 nm. NPs have novel properties that distinguish them from the bulk material. In addition to intrinsic properties of NPs, chemical and physical versatility of NPs could also be exploited to develop drugs for diagnostics and therapeutics. NPs could even be designed as multimeric systems to produce multivalent effects, because functionalization of NPs by conjugating biomolecules to their surfaces makes them target the receptors on the cancer cell surfaces. Moreover, functionalized NPs with various linkers are able to function as carriers for drugs, genes, and others. Micelles and liposomes, potential platforms for carrying therapeutics such as cytotoxic drugs, genes, or radionuclides, have already been used for cancer treatment in clinical practice. Various NPs such as gold nanoparticles, single-walled carbon nanotubes, quantum dots or iron oxide nanoparticles once labeled with beta-particle emitters, represent unique, multifunctional and target-specific radiopharmaceuticals functioning simultaneously as radiotherapy, thermal ablation and multimodal imaging systems. In this regard, NPs have emerged as clinically relevant platforms, and NPs labeled with therapeutic radionuclides can also be used as in vivo theranostics.

NPs labeled with therapeutic radionuclides have been proposed as a new class of therapeutics. In particular, multifunctionalized NP platforms are useful for taking advantages of already established radionuclide therapy (Fig. 23.3). The multifunctional NPs have the potential to carry high levels of radioactivity per particle by using various linkers and functionalization. Utilizing this advantage, the therapeutic effect of radiolabeled NPs could be maximized via multimeric receptor-specific biomolecules interactions. Utilizing this multifunctionality, the radiolabeled NPs conjugated with different targeting probes could be useful, since it can maximize therapeutic effects through targeted radiotherapy as well as other type of therapeutics.

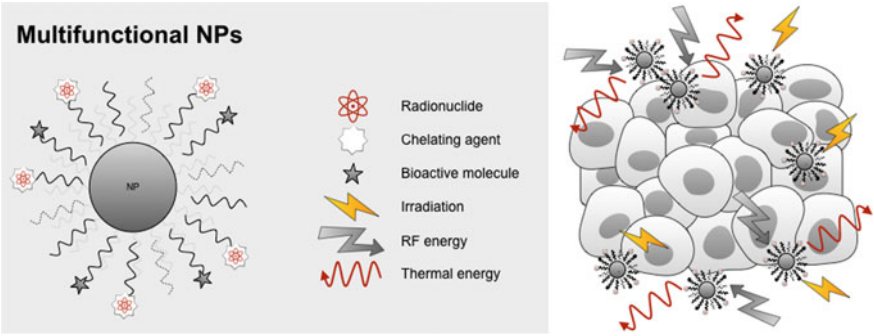

Fig. 23.3 Multifunctional nanoparticles (NPs). The multifunctional NPs can load high levels of radioactivity per particle by using various linkers and functionalization. Therapeutic effect of the multifunctional NPs can be maximized via multimetric interactions and different targeting probes

The multifunctional NPs can be designed to utilize multiple therapeutic modalities. The most commonly used radionuclides emitting beta-particles are ^{177}Lu and ^{90}Y, and they can be labeled with the multifunctional NPs in clinical trials. Clinical trials have proven that the multifunctional NPs labeled with radionuclides are promising for the treatment of malignant tumors. Large numbers of antibodies, peptides or any molecule with biological activity can be linked to the surface of a single radiolabeled nanocrystal, metal NP, or single-walled carbon nanotube, which enables both imaging and therapy of tumors over-expressing those specific antigens or receptors [13]. Soundararajan et al. evaluated NPs labeled with a beta-particle emitter (^{186}Re) and combined with radiofrequency (RF) ablation and liposomal doxorubicin in a xenograft rat model [14]. This combination of triple cancer therapeutics increased retention of the ^{186}Re-liposomal doxorubicin, which led to the effective reduction of tumor size, compared with those of single or dual therapies. The exact mechanism responsible for the synergistic effect of the triple combination therapies remains insufficiently understood, but it might be due to beneficial effects of internal radiation therapy of ^{186}Re such as cross-fire effects stemming from a long-ranged beta-particle.

Various factors including radiolabeling techniques, chemical functionalization, cost, and availability affect the successful clinical application of the radiolabeled NPs. In the clinical setting, it is highly recommended that NPs be efficiently labeled with radionuclides and the radiolabeled NPs keep stable for a sufficient time before use. Radionuclides should stay within the NPs before being delivered to yield sufficient therapeutic effects to the tumor. However, radiolabeled NPs must go through multiple unexpected biological processes before reaching tumor when administered systemically. The interaction of NPs with serum proteins influences the targeted delivery of the NPs, and then the NPs' interaction with the tumor microenvironment affects the penetration into the tumor tissues. As well as these biological processes in vivo, intrinsic properties of NPs such as size, surface characteristics, and radionuclides have an impact on the therapeutic outcome of

radiolabeled NPs. Thus, meticulous and comprehensive understanding chemistry and biology of NPs is required to develop successful radionanomedicine therapeutics.

23.4 Enhancement of Radiolabeled Nanoparticles for Effective Therapy

Gold nanoparticles (AuNPs) are one of the most actively investigated NPs for cancer treatment, and modification was suggested to enhance therapeutic effects of AuNPs. AuNPs have been proposed as localized heat sources for cancer treatment utilizing two relevant properties of gold; resistance to oxidation and plasmon resonance with light [15]. Another beneficial property of gold is thermo-ablation, which is produced by non-ionizing radiation such as microwaves or radiofrequency (RF). AuNPs released heat to destroy malignant cells by means of absorbing RF energy [16]. Besides AuNPs, several NPs such as iron oxide NPs or carbon NPs can generate thermal heat. For example, iron oxide NPs released heat when they were activated by an external alternating magnetic field, and then they induced necrosis of the tumor microenvironment [17].

As well as utilizing intrinsic properties of AuNPs, various attempts have been performed to modify AuNPs for efficient cancer theranostics. AuNPs can be conjugated with peptides targeting a specific receptor on tumor cells, e.g. tumor angiogenesis. Tumor angiogenesis is a well-known biologic process essential to tumor growth. As an imaging biomarker and a promising therapeutic tactic targeting tumor angiogenesis, arginine-glycine-aspartate (RGD) peptides have been actively investigated, since it antagonize $\alpha v\beta 3$ integrin thereby effectively inhibiting angiogenesis. The conjugation of RGD peptides to radiolabeled gold nanoparticles (^{177}Lu–RGD–AuNP) was evaluated for the treatment of glioma, and it induced significantly less tumor progression in vivo [18]. Radiolabeled bombesin can also be used for cancer treatment. Bombesin is a tetradecapeptide that has a high binding affinity to the gastrin-releasing peptide receptor (GRP). The overexpression of GRP was imaged by radiolabeled bombesin on primary prostate cancer and their metastatic lymph nodes in xenografts [19]. Bombesin conjugated with ^{177}Lu–AuNP was investigated for the treatment of prostate cancer, utilizing combination of photothermal therapy and radiation therapy [20]. This study also demonstrated that the radiolabeled NPs exhibited properties that are suitable for both plasmonic photothermal therapy and targeted radiotherapy in the treatment of prostate cancer.

23.5 Administration Methods of Radiolabeled Nanoparticles for Therapy

Therapeutic nanoparticles are usually delivered to solid tumor in a non-specific way, when they are administered systemically. NP accumulation in the solid tumor is mainly dependent on the non-specific mechanism as known as the enhanced permeability and retention (EPR) effect. The EPR effect is mainly contributed to leaky tumor vasculature and poor lymphatic drainage [21, 22]. However, the EPR effect is often inefficient to achieve a sufficient therapeutic effect, compared with specific drug delivery. Thus, various strategies have been developed, so as to adequately treat solid tumors by delivering sufficient amount of NPs to the tumor. For example, thermal stimuli can be given before systemic administration of the NPs to enhance the EPR effect. Local application of RF damage prior to NPs injection greatly increased the accumulation of NPs in the thermal ablation site [23]. This enhancement of the EPR effect seemed as the leakage of NPs expanded into the tumor and the NPs retained within a wide range of the region associated with the thermally induced inflammation.

In addition to this efficiency problem of the targeted delivery, there are several limitations in the systemic administration of the NPs. Nanosized materials are mainly eliminated by the mononuclear phagocytic system (or reticuloendothelial systems), and thus liver and spleen uptake could be a major obstacle to the use of systemically administered NPs for cancer treatment [24]. To overcome this problem, various strategies were proposed to improve pharmacokinetic profiles and enhance the therapeutic efficacy, e.g. changing the administration route. Direct image-guided intratumoral administration of therapeutic agents is currently undergoing evaluation. Intratumorally administered radiotherapeutic NPs seem to be a viable option for the use in cancer patients.

Locally administered radionuclide therapy can be considered as brachytherapy that is a localized and precise form of therapy delivering radiation in a short distance. Brachytherapy using radiolabeled NPs is different from the current typical brachytherapy in several aspects. Radiolabeled NPs are well dispersed and retained in solid tumors, giving a high radiation dose to the tumor while reducing the radiation exposure to the surrounding healthy tissues. A metallofullerene-based nanoplatform carrying ^{177}Lu was developed as brachytherapy for brain tumor [24]. This radiolabeled NPs successfully reduced tumor growth rate in a mice tumor model, and it remained in the brain tumor region. ^{177}Lu-DOTA administered alone was not effective in comparison to radiolabeled NPs conjugated with nanoplatforms, because it rapidly cleared from the brain tumor [25, 26]. Phillips et al. reported that gliomas of a rat model were treated with absorbed doses as high as 1700 Gray (Gy) by intratumoral administration of ^{186}Re-liposome NPs without significant toxicity to adjacent normal brain tissues [27]. In addition, their nanometer size permitted diffusion from the injection site to all over the tumor, giving further homogeneous radiation dose to the entire tumor. Long range of

beta-particles also contributes to generating further therapeutic effects probably due to the cross-fire and bystander effects.

It will be advantageous that brachytherapy using radiolabeled NPs of one kind are conjugated with another, as they are able to target multiple cancer specific markers. This multifunctionality of radiolabeled NPs enables them to localize more precisely and to give higher radiation dose than the conventional brachytherapy. Yook et al. suggested brachytherapy using ^{177}Lu–AuNP as a local treatment for locally advanced breast cancer [28, 29]. They designed AuNPs conjugated with ^{177}Lu and panitumumab targeting epidermal growth factor receptor (EGFR), which were delivered to breast cancer via local intratumoral injection. This EGFR-targeting NP (^{177}Lu–T–AuNP) was more efficiently bound to EGFR-positive tumor cells and more cytotoxic in vitro than non-targeting nanoseeds (^{177}Lu–NT–AuNP) [28]. However, this superiority of targeting NPs in the therapeutic efficacy was not reproduced in in vivo experiments. In the comparison experiment of ^{177}Lu–T–AuNP and ^{177}Lu–NT–AuNP in vivo, both different types of AuNPs arrested tumor growth effectively without causing cytotoxicity to adjacent normal cells, but they failed to show significant difference in therapeutic efficacy [29]. This is in the same line with disputes over the superiority (or non-inferiority) issue of active targeting versus passive targeting (or non-targeting). It is interesting in that the superiority of targeting strategy was not reproduced in vivo and by intratumoral injection of radiolabeled NPs. So, many variables would have intervened as confounders.

23.6 Therapeutic Effect of Intrinsic Radioactivity of Nanoparticles

Nanoparticles can utilize their intrinsic (core) radiotherapeutic properties. In this regard, ^{198}Au/^{199}Au is one good example. Both isotopes of gold possess intrinsic radioactive properties that are available for theranostic applications; ^{198}Au (β ray = 0.96 meV, γ ray = 411 keV) and ^{199}Au (β ray = 0.46 meV, γ ray = 158 keV). Khan et al. developed ^{198}Au dendrimer composite nanodevices, and confirmed therapeutic effects of the ^{198}Au NPs in the treatment of a mouse melanoma model by intratumoral injection [30]. The therapeutic effects of ^{198}Au NPs via intratumoral injection were also assessed in a mouse prostate cancer model. Chanda et al. designed ^{198}Au NPs functionalized with epigallocatechin-gallate (^{198}Au NP–EGCg) specifically targeting the laminin receptors that were overexpressed on prostate cancer cells, and they showed the therapeutic effects of ^{198}Au NP–EGCg in a mouse prostate cancer model [31]. Shukla et al. confirmed the therapeutic effects of ^{198}Au NP–EGCg in a mouse prostate cancer model, too [32]. In this study, approximately 72% of ^{198}Au NP–EGCg retained in the tumor after 24 h, and 80% of the tumor volume reduced after 28 days.

23.7 Therapy with Alpha Emitter-Labeled Nanoparticles

Alpha emitters have also been investigated as therapeutic radionuclides for the conjugation with nanoparticles. Alpha emitters have desirable characteristics for cancer therapy, and they are best suited for the therapy of invasive tumor cells. NPs labeled with ^{213}Bi were intratumorally injected in 5 patients for the treatment of glioma [33]. In this clinical trial, sufficient intratumoral distribution was achieved in patients with rather small tumors, whereas the intratumoral distribution of radioactivity was less homogenous in larger tumors. Other alpha emitters with relatively longer half-life such as ^{225}Ac have been investigated for the treatment of large tumors. In addition to the longe half-life, ^{225}Ac is advantageous that it emits 4 alpha-particles in the decay chain: ^{221}Fr, ^{217}At and ^{213}Bi. Therefore, ^{225}Ac could be a good candidate to improve the efficacy in treating large tumors, since it has a longe half-life and a cascading nature of decay. However, an appropriate strategy, i.e. encapsulation is required to keep the radionuclides within NPs, because ^{225}Ac has such a long half-life of 10 days.

The cascading decay of alpha emitters could be a limitation in the clinical application of radionanomedicine therapeutics. The potential release of daughter radionuclides should be considered in the biodistribution of NPs radiolabeled with alpha emitters. The possibility of chemical complex formation with daughter radionuclides should also be taken into consideration. In particular, daughter radionuclides are of concern to their off-target effect, especially when the chelation cannot retain daughter radionuclides sufficiently. The recoil can also occur when the heavy alpha particles break the chemical bonds, to leave the nucleus, to change the chemical properties of the daughter radionuclide [34]. In reality, daughter radionuclides could be retained poorly, though a variety of chelators have been investigated for ^{225}Ac complex [35, 36]. In addition to these disadvantages, the insufficient supply of ^{225}Ac could limit their vigorous use in the clinical application of ^{225}Ac labeled NPs. To overcome these limitations, McLaughlin et al. designed a core-shell NP using $GdPO_4$ to sequester the daughters within the NPs [37]. In this study, the $GdPO_4$ shell was able to retain the majority of the decay-chain daughter radionuclides (88% of the ^{221}Fr) while reducing the energy of the alpha-particles emitted by only 0.2%.

References

1. D.S. Lee, H.J. Im, Y.S. Lee, Radionanomedicine: widened perspectives of molecular theragnosis. Nanomedicine **11**(4), 795–810 (2015)
2. V.E. Kagan, H. Bayir, A.A. Shvedova, Nanomedicine and nanotoxicology: two sides of the same coin. Nanomedicine **1**(4), 313–316 (2005)
3. M.C. Garnett, P. Kallinteri, Nanomedicines and nanotoxicology: some physiological principles. Occup. Med. (Lond.) **56**(5), 307–311 (2006)
4. M.A. Maurer-Jones, K.C. Bantz, S.A. Love, B.J. Marquis, C.L. Haynes, Toxicity of therapeutic nanoparticles. Nanomedicine (Lond.) **4**(2), 219–241 (2009)

5. D. Rajon, W.E. Bolch, R.W. Howell, Survival of tumor and normal cells upon targeting with electron-emitting radionuclides. Med. Phys. **40**, 014101 (2013)
6. K.M. Prise, G. Schettino, M. Folkard, K.D. Held, New insights on cell death from radiation exposure. Lancet. Oncol. **6**, 520–528 (2005)
7. J.P. Pouget, I. Navarro-Teulon, M. Bardiès, N. Chouin, G. Cartron, A. Pèlegrin et al., Clinical radioimmunotherapy–the role of radiobiology. Nat. Rev. Clin. Oncol. **8**(12), 720–734 (2011)
8. M.C. Hernandez, S.J. Knox, Radiobiology of radioimmunotherapy: targeting CD20 B-cell antigen in non-Hodgkin's lymphoma. Int. J. Radiation Oncol. Biol. Phys. **59**, 1274–1287 (2004)
9. C. LA Friesen, J. Kotzerke, I. Buchmann, S.N. Reske, K.M. Debatin, Beta-irradiation used for systemic radioimmunotherapy induces apoptosis and activates apoptosis pathways in leukaemia cells. Eur. J. Nucl. Med. Mol. Imaging **30**, 1251–1261 (2003)
10. D.E. Milenic, E.D. Brady, M.W. Brechbiel, Antibody-targeted radiation cancer therapy. Nat. Rev. Drug Discov. **3**, 488–499 (2004)
11. J.P. Pouget, S.J. Mather, General aspects of the cellular response to low- and high-LET radiation. Eur. J. Nucl. Med. **28**(4), 541–561 (2001)
12. G. Sgouros, J.C. Roeske, M.R. McDevitt, S. Palm, B.J. Allen, D.R. Fisher et al., MIRD Pamphlet No. 22 (abridged): radiobiology and dosimetry of alpha-particle emitters for targeted radionuclide therapy. J. Nucl. Med. **51**(2), 311–328 (2010)
13. G. Ferro-Flores, B.E. Ocampo-García, C.L. Santos-Cuevas, E. Morales-Avila, E. Azorín-Vega, Multifunctional radiolabeled nanoparticles for targeted therapy. Curr. Med. Chem. **21**(1), 124–138 (2014)
14. A. Soundararajan, G.D. Dodd 3rd, A. Bao, W.T. Phillips, L.M. McManus, T.J. Prihoda et al., Chemoradionuclide therapy with ^{186}Re-labeled liposomal doxorubicin in combination with radiofrequency ablation for effective treatment of head and neck cancer in a nude rat tumor xenograft model. Radiology **261**, 813–823 (2011)
15. D.V.S. Pissuwan, M.B. Cortie, Therapeutic possibilities of plasmonically heated gold nanoparticles. Trends Biotechnol. **24**, 62–67 (2006)
16. R.M. Sharkey, D.M. Goldenberg, Novel radioimmunopharmaceuticals for cancer imaging and therapy. Curr. Opin. Investig. Drugs **9**, 1302–1316 (2008)
17. P. Cherukuri, E.S. Glazer, S.A. Curley, Targeted hyperthermia using metal nanoparticles. Adv. Drug Del. Rev. **62**, 339–345 (2010)
18. A. Vilchis-Juárez, G. Ferro-Flores, C. Santos-Cuevas, E. Morales-Avila, B. Ocampo-García, L. Díaz-Nieto et al., Molecular targeting radiotherapy with cyclo-RGDFK(C) peptides conjugated to ^{177}Lu-labeled gold nanoparticles in tumor-bearing mice. J. Biomed. Nanotechnol. **10**(3), 393–404 (2014)
19. M. de Visser, W.M. van Weerden, C.M. de Ridder, S. Reneman, M. Melis, E.P. Krenning et al., Androgen-dependent expression of the gastrin-releasing peptide receptor in human prostate tumor xenografts. J. Nucl. Med. **48**(1), 88–93 (2007)
20. N. Jiménez-Mancilla, G. Ferro-Flores, C. Santos-Cuevas, B. Ocampo-García, M. Luna-Gutiérrez, E. Azorín-Vega et al., Multifunctional targeted therapy system based on ^{99m}Tc/^{177}Lu-labeled gold nanoparticles-Tat(49-57)-Lys(3) -bombesin internalized in nuclei of prostate cancer cells. J. Label. Comp. Radiopharm. **56**(13), 663–671 (2013)
21. N. Bertrand, J. Wu, X. Xu, N. Kamaly, O.C. Farokhzad, Cancer nanotechnology: the impact of passive and active targeting in the era of modern cancer biology. Adv. Drug Deliv. Rev. **66**, 2–25 (2014)
22. H. Maeda, Toward a full understanding of the EPR effect in primary and metastatic tumors as well as issues related to its heterogeneity. Adv. Drug Deliv. Rev. **91**, 3–6 (2015)
23. H. Maeda, J. Wu, T. Sawa, Y. Matsumura, K. Hori, Tumor vascular permeability and the EPR effect in macromolecular therapeutics: a review. J. Control Release. **65**, 271–284 (2000)
24. M.D. Shultz, J.D. Wilson, C.E. Fuller, J. Zhang, H.C. Dorn, P.P. Fatouros, Metallofullerene-based nanoplatform for brain tumor brachytherapy and longitudinal imaging in a murine orthotopic xenograft model. Radiology **261**(1), 136–143 (2011)
25. H. Xie, B. Goins, A. Bao, Z.J. Wang, W.T. Phillips, Effect of intratumoral administration on biodistribution of ^{64}Cu-labeled nanoshells. Int. J. Nanomed. **7**, 2227–2238 (2012)

26. J.T. French, B. Goins, M. Saenz, S. Li, X. Garcia-Rojas, W.T. Phillips et al., Interventional therapy of head and neck cancer with lipid nanoparticle-carried rhenium 186 radionuclide. J. Vasc. Interv. Radiol. **21**, 1271–1279 (2010)
27. W.T. Phillips, B. Goins, A. Bao, D. Vargas, J.E. Guttierez, A. Trevino et al., Rhenium-186 liposomes as convection-enhanced nanoparticle brachytherapy for treatment of glioblastoma. Neuro. Oncol. **14**, 416–425 (2012)
28. S. Yook, Z. Cai, Y. Lu, M.A. Winnik, J.P. Pignol, R.M. Reilly, Radiation nanomedicine for EGFR-positive breast cancer: panitumumab-modified gold nanoparticles complexed to the β-particle-emitter, ^{177}Lu. Mol. Pharm. **12**(11), 3963–3972 (2015)
29. S. Yook, Z. Cai, Y. Lu, M.A. Winnik, J.P. Pignol, R.M. Reilly, Intratumorally injected ^{177}Lu-labeled gold nanoparticles: Gold nanoseed brachytherapy with application for neoadjuvant treatment of locally advanced breast cancer. J. Nucl. Med. **57**(6), 936–942 (2016)
30. M.K. Khan, L.D. Minc, S.S. Nigavekar, M.S. Kariapper, B.M. Nair, M. Schipper et al., Fabrication of 198Au0 radioactive composite nanodevices and their use for nanobrachytherapy. Nanomedicine **4**(1), 57–69 (2008)
31. N. Chanda, P. Kan, L.D. Watkinson, R. Shukla, A. Zambre, T.L. Carmack et al., Radioactive gold nanoparticles in cancer therapy: therapeutic efficacy studies of GA-^{198}AuNP nanoconstruct in prostate tumor-bearing mice. Nanomedicine **6**(2), 201–209 (2010)
32. R. Shukla, N. Chanda, A. Zambre, A. Upendran, K. Katti, R.R. Kulkarni et al., Laminin receptor specific therapeutic gold nanoparticles (^{198}AuNP-EGCg) show efficacy in treating prostate cancer. Proc. Natl. Acad. Sci. U.S.A. **109**(31), 12426–12431 (2012)
33. D. Cordier, F. Forrer, F. Bruchertseifer, A. Morgenstern, C. Apostolidis, S. Good et al., Targeted alpha-radionuclide therapy of functionally critically located gliomas with 213Bi-DOTA-[Thi8, Met(O2)11]-substance P: a pilot trial. Eur. J. Nucl. Med. Mol. Imaging **37**(7), 1335–1344 (2010)
34. R.M. de Kruijff, H.T. Wolterbeek, A.G. Denkova, A critical review of alpha radionuclide therapy-how to deal with recoiling daughters? Pharmaceuticals Basel. **8**(2), 321–336 (2015)
35. M.R. McDevitt, D. Ma, J. Simon, R.K. Frank, D.A. Scheinberg, Design and synthesis of ^{225}Ac radioimmunopharmaceuticals. Appl. Radiat. Isot. **57**, 841–847 (2002)
36. L.L. Chappell, K.A. Deal, E. Dadachova, M.W. Brechbiel, Synthesis, conjugation, and radiolabeling of a novel bifunctional chelating agent for ^{225}Ac. Radioimmunotherapy applications. Bioconjug. Chem. **11**, 510–519 (2000)
37. M.F. McLaughlin, J. Woodward, R.A. Boll, J.S. Wall, A.J. Rondinone, S.J. Kennel et al., Gold coated lanthanide phosphate nanoparticles for targeted alpha generator radiotherapy. PLoS One **8**(1), e54531 (2013)

Index

D. S. Lee (ed.), *Radionanomedicine*, Biological and Medical Physics, Biomedical Engineering, https://doi.org/10.1007/978-3-319-67720-0